IEMB
Institute of Evolution & Marine Biodiversity
2010 OUC

海洋生物多样性与进化研究所，中国海洋大学
Institute of Evolution & Marine Biodiversity, OUC

2015 年度工作报告

2015-12

海洋生物多样性与进化研究所

所长：　宋微波

副所长：张士璀

海洋生物多样性与进化研究所学术委员会

主　任：孟安明

副主任：宋微波

委　员：徐存拴　王金星　黄晓航　孙　黎　黄　倢

李　琪　包振民　张士璀　池振明　孙世春

地址：青岛市鱼山路5号 中国海洋大学达尔文馆
邮编：266003
电话：0532 -82031982
传真：0532 -82031982

目　录

海洋生物多样性与进化研究所年报

——2015 年度

在过去的一年，本着“致力于完成一批标志性原创成果，建设一支具有国际竞争力的研究团队，建设成为我国该领域具有国际地位和国际号召力、对外交流合作的展示窗口和创新人才培育的核心基地”这一目标，在各级领导和朋友的关爱、支持下，经过全体成员的共同努力，我们在科学研究、人才培养、实验室建设等诸多方面都取得了建设性进展。

在全所各团队师生的辛勤努力下，我们在多样性与进化-发育两个主流方向上均取得了良好进展。在科研项目的申报中，本年度国家自然科学基金成果丰硕，组织申报的 6 个项目全部获得批准，包括 1 项“优秀青年基金项目”、3 个面上项目和 2 个青年基金项目。作为成果产出，我们在纤毛虫的分子系统学、多样性与个体发育、文昌鱼免疫与内分泌系统演化、纤毛发育、蠕形动物的线粒体基因组与系统发育、鱼类免疫系统的进化等领域形成了一批有显示度的新成果。主要包括：● 继续扩展了我们对中国南海多种生境纤毛虫的区系、多样性研究，完成了对 30 余种 90 余种群纤毛虫的全基因组 DNA 提取、130 余条基因序列的获得和提交；同时，基于细胞学和基因序列信息，完成对褶纤虫科等多个科属级阶元的分子系统学分析和对异毛纲、核残迹纲等高级类群的系统重构建；● 完成了对喙纤虫的单细胞全基因组、多个细胞全转录组的提取以及柠檬类瘦尾虫的大核基因组的高通量测序；● 以纤毛虫模式生物-四膜虫为材料研究表观遗传调控，发现转座子通过非编码 RNA 与编码 RNA 之间的转换达到转录和抑制的平衡、以及核小体分布受顺式和反式作用元件共同调控；● 发现文昌鱼存在类似脊椎动物抗病毒免疫系统：在文昌鱼中首次发现了 RIG-I-like 受体分子 LGP2，文昌鱼 LGP2 能够和 Poly(I:C)结合，并且能够显著上调干扰素和 *Mx* 基因以及 RLRs 信号通路相关基因 *MAVS*, *NF-κB* 和 *IRF-3* 的表达，抑制淋巴囊肿病毒在 FG 细胞中的复制和石斑鱼虹彩病毒在 GS 细胞中的转录，同时证明文昌鱼存在脊椎动物样 viperin 抗病毒蛋白；● 证明唐氏综合症关键区基因 DSCR6 能够和 PcG 复合体蛋白-Ezh2 和 BMI1 结合，中和 PcG 对基因的抑制作用，将 PcG 从染色质解离，激活中胚层和体轴形成基因的表达；● 分离鉴定出多个影响运动纤毛发育的关键基因，发现 Ankrd45 蛋白在肝脏肿瘤形成中的新功能，同时深入研究了 Kinesin2 蛋白在感光细胞凋亡过程中的作用机制；● 完成了广分布、形态同质、鉴定困难的奇异拟纽虫种复合体、喙纽虫等纽形动物类群的物种界定研究，勾画了相关物种在世界海洋的地理分布格局；● 研究了大菱鲆天然免疫模式识别受体 TLR3 和 TLR22、TLR 信号通路接头蛋白 MyD88 与干扰素系统效应分子 ISG15 的结构、转录调控规律、配体识别途径、免疫应答表达模式等，对鱼类特异模式识别受体 tlr22 基因结构的进化规律提出了新见解；● 开展了长蛸等 14 种蛸科头足类的 DNA 提取、线粒体基因测序及相关序列提交；其中首次完成了中国小乳蛸等 8 个物种的线粒体全基因组测序工作，填补了头足类分子信息的部分空白，同时为

蛸科头足类的形态学分类及鉴定工作提供了参考；● 完成了刻肋海胆科细雕刻肋海胆等 5 种海胆的线粒体全基因组测定工作，丰富了海胆线粒体基因组数据库，初步完成了刻肋海胆科、属级阶元分子系统学的分析与系统地位探讨；● 发现并证明 Alpha 2 macroglobulin 在文昌鱼中是一种母源性免疫因子存在于卵子中，在胚胎早期发育阶段发挥重要的免疫防御作用；● 研究了墨西哥钝口螈趾部再生的生物学过程,初步阐明了 MMP 家族基因在趾部再生过程中的功能及其作用机制。

上述成果分别发表在遗传学、发育与进化、系统学与多样性等领域的多家国际主流刊物上，包括《PLOS Genet.》、《P. Nat. Acad. Sci.》、《Curr. Opin. Genet. Dev.》、《mBio》、《Eur. J. Immunol.》、《Mol. Phylogenet. Evol.》、《Development》、《Dev. Comp. Immunol.》、《Sci. Rep.》、《BMC Genomics》、《J. Nat. Prod.》、《J. Eukaryot. Microbiol.》、《Nutrients》等主流刊物。

研究所在队伍建设和人才培养方面均取得了丰硕成果。围绕主干研究领域中“基因进化”团队的强化建设，我们新近完成了对苏颖博士（英才一岗）的引入，另有发育团队一位师资博士后高瞻应聘上岗。

本年度王长云教授教授成果获得山东省科技进步奖二等奖，张士璀教授成果获得青岛市自然科学奖二等奖；赵呈天、高珊教授入选青岛海洋科学与技术国家实验室“鳌山人才计划”；王长云教授入选“泰山学者特聘专家”。此外，作为研究生培养的成果，本年度研究所共毕业博士研究生 18 人。其中，博士毕业生高凤获本年度“山东省优秀博士学位论文奖”。

开放、交流得到了进一步的加强。与国内外有关科研机构形成了更加密切的合作与交流，先后接待国内外来访专家 13 人次、组织了 9 人次出国参加国际学术会议等；主持、举办多项学术会议，包括：10 月主办“纤毛虫多样性与合作”国际学术研讨会，5 月主办 “第一届海洋微生物学国际研讨会”，11 月主办“第一届全国纤毛生物学会议”，为扩大研究所的学术影响产生了积极的效果。

我们愿借此机会，表达对各级领导、国内外同仁和朋友的衷心感谢之情，感谢您对研究所建设和发展给予的关爱与支持。我们深知，研究所筹建至今，仍处于起航阶段，未来任重道远。我们也期盼各级领导和朋友们的继续支持，并将继续秉持“国际前沿、国际视野、国际标准、国际影响”的建所理念，不断取得新的进步！

2015 年度大事记

- 所长宋微波教授当选中国科学院院士
- 研究所新引进“青年英才工程”岗位第一层次苏颖教授；发育团队新增一位师资博士后应聘上岗
- 研究所专职成员申报“国家自然科学基金”获得丰硕成果，6 个申报项目全部获准，其中高珊教授获“优秀青年科学基金”资助；赵呈天教授获 2015 年度山东省“杰出青年基金”资助
- 赵呈天、高珊教授入选青岛海洋科学与技术国家实验室“鳌山人才计划”；王长云教授入选“泰山学者特聘专家”
- 本年度各团队成员先后在《PLOS Genetics》、《mBio》和《Sci. Rep.》等领域主流刊物发表研究论文 70 余篇；董波教授有关生物管腔形态调控的特邀评述文章在《Cur. Opin. Gen. & Devel.》上在线发表
- 王长云教授主持成果获山东省科技进步成果二等奖；张士璀教授主持成果获青岛市自然科学二等奖
- 胡晓钟教授应邀担任国际主流刊物《Sci. Rep.》微生物领域编委
- 宋微波教授受聘担任《中国大百科全书》第三版-生态学领域及《中国动物志》副主编；国际刊物《真核微生物学报》编委
- 研究所本年度毕业博士研究生 18 人，7 名毕业生获中国海洋大学“优秀研究生学位论文奖”；原生动物学团队 2 名毕业生分获 2015 年山东省优秀学位论文、研究生优秀科技创新成果奖
- 顺利主办“纤毛虫多样性与合作”国际学术研讨会 (2015.10.19 -21)和 “第一届海洋微生物学国际研讨会” (2015.5.22 -25)
- 研究所本年度先后邀请 11 位国外专家学者来访和学术交流
- 各团队成员累计参加各类国际学术会议 9 人次、特邀大会报告 3 人次
- 研究所学术委员会第二次会议召开（9 月 23 日）

一　研究所工作纪要

（一）科研项目

2015 年度新申请及在研国家、省部级课题项目共计 56 项，经费总额度达 3803 万元。

上述项目中包括国家“973”计划课题 1 项、国家自然科学基金重点项目 2 项、国家自然科学基金优秀青年基金项目 2 项、国家自然科学基金联合项目 1 项、国家自然科学基金国际合作与交流项目 1 项、国家自然科学基金项目 25 项、国家自然科学基金青年项目 6 项、山东省杰出青年基金项目 1 项、教育部新世纪人才项目 1 项等（附表 1）。

（二）科技成果

2015 年度本所各团队共发表论文 78 篇，其中 SCI 收录论文 73 篇 (附表 2)。

本年度王长云教授等主持完成的成果“中国海洋药用生物资源调查、挖掘与开发应用”获得山东省科技进步奖二等奖、张士璀教授等主持完成的成果“鱼类卵黄蛋白原和卵黄蛋白免疫功能以及母源性免疫研究”获得青岛市自然科学奖二等奖。研究所博士毕业生获本年度“山东省优秀博士学位论文奖”1 项、 “山东省研究生优秀科技创新成果奖”二等奖 1 项（附表 3）。

（三）队伍建设与人才培养

1. 队伍建设

2015 年引入“英才工程”第一层次教授一名，吸收 1 名师资博士后青年教师。目前有专职人员 16 名，含博士生导师 6 名，教授 8 名。其中 4 人分别担任各自所属相关国家一、二级学会（如国际原生动物学会、亚洲原生动物学会、中国动物学会、中国细胞生物学学会、山东省细胞生物学学会等）理事或以上职务。研究所另有与研究所主流研发方向相关的校内双聘人员 10 人（附表 4）。本年度赵呈天、高珊教授入选青岛海洋科学与技术国家实验室“鳌山人才计划”；王长云教授入选“泰山学者特聘专家”。

此外，实验室把博士后培养制度当作实验室的重要工作之一，从博士后人员的筛选到平时的管理都坚持高标准。这些措施的实施极大地促进了青年学术骨干学术水平的提高。

2. 人才培养

本研究所涵盖 1 个博士后流动站（海洋生物学）、2 个博士点（发育生物学、动物学）和 1 个“泰山学者特聘教授”岗位。

2015 年研究所共毕业博士生 18 人，拥有在站博士后 18 名；目前本所在读研究生 71 名，其中博士研究生 25 名、硕士研究生 46 名（附表 5）。

研究所招收来自伊朗、巴基斯坦等 5 名外国留学生攻读博士学位，选派 5 名博士生公派出国进行合作交流。同时 2015 年度研究所接受了多名国内外同行及研究生前来进修、培养或合作研究。

（四）开放与交流

我们与国内外有关科研院所形成了广泛和密切的合作和交流关系，先后接待国内外来访专家 13 人次；主持、举办多项学术会议，如 10 月主办“纤毛虫多样性与合作”国际学术研讨会，5 月主办“第一届海洋微生物学国际研讨会”，11 月主办“第一届全国纤毛生物学会议”，为扩大研究所的学术影响产生了积极的效果。本年度先后组织了 9 人次出国参加国际学术会议、学术交流（附表 6）。

主要学术会议和交流情况如下：

1）进化所主办第四届“纤毛虫多样性与合作”国际研讨会顺利闭幕

海洋生物多样性与进化研究所主办的第四届“纤毛虫多样性与合作”国际学术研讨会于 2015 年 10 月 19 日至 21 日在鱼山校区顺利举行。本次为中美双边国际合作项目“纤毛虫多样性的国际合作网络建立”（IRCN-BC）的年度研讨会，由美国国家自然科学基金（NSF）和中国国家自然科学基金（NSFC）联合资助。该合作项目为期 5 年（2012-2016），核心目的为促进该分支领域广泛的国际合作与交流、扶持和推动年轻学者的参与和提高、整合全球该领域的研究团队以构建一个纤毛虫学领域内资源共享的信息合作平台。

本次会议由海洋生物多样性与进化研究所原生动物学团队主办,来自美国、英国、加拿大、俄罗斯、日本、乌克兰、阿塞拜疆、沙特、墨西哥、印度等国的近 30 位国际同行以及香港、台湾和大陆的 16 家科研院所和高校的 30 余位国内同行参加了此次研讨会。会议期间，与会专家作了 28 场口头报告，在纤毛虫的模式生物、生理、分类、遗传、寄生虫学与生态等多样性泛领域内多个方向进行了交流和讨论并就纤毛虫学研究国际合作的未来发展、方向建设和组织框架构建达成了初步共识。

根据 IRCN-BC 执行委员会的决定，2016 年将在美国关岛承办下届研讨会。

2）第一届海洋微生物学国际研讨会顺利举办

2015 年 5 月 22 日至 25 日，第一届海洋微生物学国际研讨会在青岛黄海饭店举行。本次会议由中国海洋大学张晓华教授实验室主办，邀请到来自美国、加拿大、英国、日本等海内外 22 位专家做特邀报告，并有三十余位专家学者做专题报告，共有 300 余位学者参会。

开幕式上，中国海洋大学副校长李华军对来访的各位专家学者表示欢迎，并肯定了这次会议的必要性，鼓励大家在会议期间充分进行交流。随后，联合国教科文组织（UNESCO）的官员 Dr. Ahmed Fahmi 作了题目为“UNESCO’s biotechnology program in the post-2015sustainable development agenda”的报告，对 UNESCO 的历史及现状进行了详细介绍。本次会议的另一议题是纪念海洋微生物学专家、“联合国教科文组织海洋生物技术中心”(UNESCO Marine Biotechnology Centre)的创始人徐怀恕先生。会议设立了由前美国国家自然基金主席、马里兰大学 Rita Cowell 教授资助的徐怀恕奖励基金，旨在鼓励优秀青年学者积极参加学术活动。会议同时宣布中国海洋大学张晓华教授（海洋生物多样性与进化研究所双聘教师）为新一任联合国教科文组织海洋生物技术中心主任。

开幕式结束后，进入学术报告环节，会议共分为六个分主题：1. 海洋微生物在全球生物地球化学循环中的作用；2. 微生物海洋学；3. 深海及极地海洋微生物； 4. 水产养殖中的海洋微生物；5. 生物工程中的海洋微生物；6. 物种间和物种内的信号传递-未被开发的治疗靶点。各位专家的精彩汇报引起了参会者的共鸣，会场讨论热烈，专家学者们各抒己见，对当今海洋微生物方面的研究热点及难点发表了自己的看法。

海洋微生物学是近几十年来发展最快的学科之一，本次国际会议为该领域的学者提供了很好的交流平台，也为今后的学术合作提供了契机。

3）进化所承办首届全国纤毛生物学学术会议

我校海洋生物多样性与进化研究所承办的“第一届全国纤毛生物学会议”于 2015 年 11 月 13 日至 14 日在鱼山校区学术交流中心顺利举行。来自北京大学、清华大学、南开大学、中国科学院等 18 个科研院所和来自北京 301 医院、同仁医院等多家医疗结构的近 70 名师生参加了此次研讨会。与会期间，来自各个研究团队的专家学者作了二十余场口头报告，以小鼠、斑马鱼、果蝇、线虫、衣藻等模式生物，对纤毛的结构、发生以及人类纤毛疾病等多方面进行了交流讨论，本次研讨会代表了我国纤毛生物学研究领域的最高水平。

纤毛是细胞表面突起形成的毛发状亚结构，在细胞运动，信号转导及发育过程中发挥关键作用，其功能缺陷可导致肾脏、眼睛等多种器官的发育异常，是多囊肾，视网膜色素变性，不孕不育等多种遗传疾病的重要诱因。我国的纤

毛生物学研究在国际上已经占据的重要地位，本次会议是研究所赵呈天老师召集的我国纤毛研究领域的第一次全国性学术研讨会，对促进我国纤毛生物学的研究及合作具有重要的意义。

4）进化所承办中国动物学名词审定会议

2015 年 4 月 20 日，由进化所承办的中国动物学会动物学名词审定会议在鱼山校区召开，郑守仪院士等来自全国科学技术名词审定委员会、中国海洋大学、华东师范大学、浙江农林大学、中国科学院海洋研究所的 10 名动物学资深专家参加本次会议。会议就原生动物、海绵动物、轮虫、纽形动物、帚形动物、腕足动物等相关动物学名词进行讨论，对相关学科门类名词的收词、定名、定义等进行审定，给予规范性、系统性的把关。各位专家以科学严谨的态度对待动物学名词审定工作，以期为我国动物学研究的发展提升奠定基础及提供支撑。

另外，张士璀教授为《中国动物学学科史研究》编写“我国胚胎学/发育生物学发展史”；为《水产大百科》编写鱼类免疫学部分条目。

5）进化所宋微波教授团队参加“第七届欧洲原生生物学大会”

四年一届的欧洲原生生物学家学会第 7 届学术大会(ECOP VII)于 9 月 5 至 10 日在西班牙的塞维利亚召开。本次会议由塞维利亚大学（US）承办，300 余位来自全球 33 个国家的同行学者参会。本所宋微波教授等一行 4 人参加。会上宋老师作了题为“Ciliate researches in China: Active groups, chance for collaboration and the on-going studies”的大会报告。胡晓钟老师和高珊老师分别就各自的研究方向作了分组口头报告。

6）本所原生动物学团队参加中国原生动物学分会第十八次学术讨论会

两年一度的中国动物学会原生动物学分会第十八次学术讨论会于 8 月 24 至 27 日在山东省烟台市召开，来自台湾、香港和大陆各科研院所、大学的代表 270 余人参加了本次大会。会议设“自由生活原生动物、寄生原生动物”两个分会，研讨范围覆盖了包括基因组学、生理学、多样性与进化、细胞生物学、原生生物的生物化学、分子生物学、发育与进化、生态学、免疫学、寄生虫学等领域。这也是国内同行对本领域过去两年来在上述各分支领域内所取得学术成果的一次集中学习和交流。

进化所所原生动物学团队宋微波教授带领师生 20 人参加了本次会议。高珊教授做了题为“表观遗传信息对基因表达何复制的调控—四膜虫视角”的大会报告。本次大会为 11 名优秀的年轻原生动物学工作者颁发了学会首届“青年科技奖”，高珊教授位列其中。大会评选出 8 名报告人作为优秀学术大会奖，本所博士生陈晓同学获得一等奖。

7）美国密歇根大学刘一凡博士访问海洋生物多样性与进化研究所

2015 年 6 月 25 日上午，受海洋生物多样性与进化研究所的邀请，美国密歇根大学病理学系刘一凡博士到访达尔文馆并为师生做了题为《多梳蛋白对生殖系-体细胞分化的表观遗传调控—纤毛虫视角》的主题学术报告。

报告中介绍了 RNA 干扰通路和 PRC 抑制通路对四膜虫大小核分化以及转座子表达的调控机制；其中对转座子的研究，解释了转座子的沉默与激活这一看似矛盾的现象，为研究转座子与宿主的协同进化提供了重要理论支持。报告会之后师生们也就四膜虫等纤毛虫原生动物复杂独特的生物学特性、表观遗传学领域的最新进展、表观遗传学研究在其他模式生物中的开展等同刘一凡博士展开了交流和讨论。

刘一凡博士现供职于美国密歇根大学病理学系，作为当今最活跃的四膜虫研究学者之一，带领团队在四膜虫的 Polycomb 抑制通路与 RNA 干扰通路的耦合、表观遗传信息对基因复制的调控等分支领域做出了大量优异的工作并在同行中享有较高声誉，他的学术成果先后发表在 PNAS、Genes &Development 等国际顶尖杂志上。

8）英国 Sheffield 大学 Malicki 教授来访

2015 年 11 月 6 日，受研究所赵呈天老师的邀请，来自英国著名常春藤学府 Sheffield 大学的 Jarema Malicki 教授来研究所进行了学术访问，并为研究所师生做了《The Cilium-a Unique Subcellular Compartment that Functions as a Signal Detection Device》的主题报告，受到了研究所师生的高度关注和热烈欢迎。

Malicki 教授在报告中阐述了纤毛这一研究领域的研究历史、背景、意义及近期的研究热点和突破，并着重阐述了斑马鱼作为模式动物对纤毛研究的贡献。在报告中，Malicki 教授详细讲述了纤毛相关基因所编码蛋白在分子细胞层面的作用机理和对信号通路的影响,并总结了自己近些年来的研究成果和未来的工作展望。报告之后，得到了师生们的高度评价和热烈的掌声，各位老师和同学积极提出自己的问题和想法，学术讨论气氛十分热烈。

Malicki 教授在纤毛领域的研究处于国际领先地位，曾在哈佛大学、塔夫斯大学做科学研究，其主要从事纤毛内转运复合体和眼睛感光细胞中原初纤毛的研究，其所做出的研究成果得到了同行的高度评价和赞誉，其学术论文发表在 Nature、Cell、Nature Genetics、Nature cell biology 等著名杂志上。

9）澳大利亚昆士兰大学 Robert Parton 教授到访进化所

2015 年 5 月 30 日—6 月 1 日，应海洋生物多样性与进化研究所董波教授的邀请，澳大利亚科学院院士、昆士兰大学 Robert Parton 教授到进化所进行学术

交流和访问。6 月 1 日上午，Parton 博士做了题为”New insights into the formation and function of caveolae”的学术报告，详细介绍了细胞膜小窝结构（Caveolae）形成的分子机制以及它们生物机体中功能的最近研究成果。会后，Robert 参观了进化所实验室并同相关师生进行了进一步交流，并就进一步开展合作进行了探讨。

Robert 的主要研究领域为细胞质膜的动态和表面结构，是这个领域最重要的科学家之一，他目前已经发表包括 Nature、Cell、Science 在内的百余篇高水平文章，其 H-index is 97。目前担任澳大利亚昆士兰大学正教授。2009 年被选为澳大利亚科学院院士。2014 年开始任 NHMRC（澳大利亚国家健康和医学研究委员会）资深成员专家。

10）美国耶鲁大学孙朝霞教授来访

受研究所赵呈天老师的邀请，来自耶鲁大学的孙朝霞教授于 9 月初来我校进行了学术访问，并作为特邀嘉宾参加了研究所参与承办的第四届全国斑马鱼大会。孙朝霞教授分别与 2015 年 9 月 6 日和 7 日上午做了两场题为《From Genetic Screen to Calcium Imaging: Searching for Mechanism and Treatment of Polycystic Kidney Disease》和《Intraciliary Calcium Oscillations Initiate Vertebrate Left-Right Development》的精彩报告。在这两场报告中，孙朝霞教授深入浅出的介绍了其课题组的最新研究成果：以斑马鱼为模型，利用多种转基因手段阐述了钙离子信号在脊椎动物体轴左右不对称发育过程中的作用。同时，孙教授也介绍了多囊肾研究的一些最新进展。孙教授的报告引起了在场学生的热烈讨论。

11）加拿大哥伦比亚大学 Curtis Suttle 教授来访

2015 年 5 月 18 日，应海洋生物多样性与进化研究所汪岷教授的邀请，美国微生物科学院院士、加拿大哥伦比亚大学 Curtis Suttle 教授来我校进行学术交流和访问。5 月 19 日上午，Suttle 教授开设名人讲堂，做了题为“Unravelling the virosphere”的学术报告，围绕浮游病毒学等热点话题与参会 30 余位师生开展了讨论。另外，Suttle 教授还作为 keynote speaker 参加了我校主办的第一届海洋微生物学国际研讨会，做了题为“Probing the diversity of virus in the ocean”的大会报告，期间与校内外参会专家进行了深入交流。

Curtis Suttle 教授是国际著名病毒学家，对环境微生物学、微生物生态学、病毒学和原生生物学等诸多领域均有较为深入的研究，主要研究领域为病毒多样性及其在全球循环中的作用，其研究不仅揭示了病毒是海洋系统生物量以遗传多样性最丰富的群体，还表明病毒作为分解者对海洋系统中的营养循环和能量流动起着至关重要的作用。发表了包括 Nature、Science 和 Proceedings of the U.S. National Academy of Sciences 等顶尖学术刊物在内的科学论文 150 余篇。

12）英国东英吉利大学 Gill Malin 教授和美国马里兰大学陈峰教授来访

2015 年 5 月 17 日，应海洋生物多样性与进化研究所汪岷教授的邀请，英国东英吉利大学 Gill Malin 教授到我校进行了为期一月的学术交流合作。Gill Malin 教授 1983 获得英国利物浦大学博士学位，2009 年至今在东英吉利大学环境学院做生物海洋学研究。在浮游植物生态学、DMSP、 生物海洋学、 生物地球化学循环、藻类、海洋中的微量气体等方面都有深入的研究，发表论文专著 100 余篇。5 月 19 日上午 Gill Malin 教授做了题为“studies at the biological oceanography-biogeochemistry interface”的学术报告，并就师生互访事宜进行探讨。另外，Gill Malin 教授还作为 keynote speaker 参加了我校主办的第一届海洋微生物学国际研讨会，做了题为“Phytoplankton functional types and production of dimethylsulphoniopropionate (DMSP)”的大会报告，与参会专家进行了合作探讨。

2015 年 7 月 14 日，应海洋生物多样性与进化研究所汪岷教授的邀请，美国马里兰大学陈峰教授来我校进行学术交流和访问。陈峰教授 1995 年博士毕业于德克萨斯州大学奥斯汀分校，现在马里兰大学海洋与环境科学学院从事浮游病毒和微微型浮游生物的研究，近十年发表相关学术论文 40 余篇。7 月 15 日上午，陈峰教授做了题为“Picocyanobacteria and Cyanoviruses in the Chesapeake Bay - from Isolation, Ecology to Omics ”的学术报告，报告内容丰富，在场 20 余名师生进行了热烈讨论，并探讨了今后的合作方向。

13）同济大学施威扬教授和中科院海洋所王昊博士来访

2015 年 1 月 22 日，应海洋生物多样性与进化研究所董波教授的邀请，同济大学生命科学与技术学院施威扬教授和中国科学院海洋研究所王昊博士来我校进行访问并进行了学术交流，海洋生物多样性与进化研究所、海洋生命学院和中科院海洋所多位专家、师生以“海洋模式动物基因组学及遗传学“为主题进行了交流研讨。

同济大学生命科学与技术学院施威扬教授做了题为“Exploring marine invertebrates as new models for genomics studies”的报告。施博士 1997 年毕业于清华大学生物系，2003 年在美国 Washington University in St. Louis 获得发育生物学博士，后在 University of California, Berkeley 从事博士后研究，现任同济大学生命科学与技术学院特聘教授。会上，施教授主要介绍了以模式动物海鞘为模型研究脊索动物早期胚胎发育的分子调控机制及对海鞘基因组中非编码 RNA 的发掘和分析的最新研究进展；他同时分享了其团队对牡蛎基因组解析的结果以及利用目前已发表的贝类基因组数据进行冠轮动物发育沙漏模型验证的尝试。

海洋所的王昊博士做了题为“Forward and reversed genetics in ascidian”的报告。王博士 2003 年毕业中国海洋大学，2011 年于香港科技大学获得博士学位，后在 University of California, Santa Barbara 从事博士后研究，现入选中科院海洋所“优青计划”。主要从事海洋无脊椎动物的分子免疫、幼虫变态发育以及遗传学方面的研究。在其报告中，王博士主要介绍了其如何利用正向和反向遗传学手段研究特定功能基因对海鞘胚胎发育的影响和机制；重点介绍基因组编辑技术 CRISPR/Cas9 在海洋动物中的应用及操作。

两位专家的精彩报告内容丰富，涉及当今遗传、进化和发育生物学研究的最前沿及最新的基因组编辑技术，引发了与会师生的热烈讨论。会后，大家就共同感兴趣的问题进行了更深入的讨论和交流，并探讨了今后合作的可能性。

14）研究所“2015 系列学术报告会”

“海洋生物多样性与进化研究所—2015 年系列学术报告会Ⅰ”于 6 月 13 日下午 2:00 在达尔文举行。会议由研究所赵呈天教授主持，研究所成员及来自鱼山校区各院系相关领域的 40 余位师生参加。本次报告会共安排了 3 个报告，主要围绕“胚胎与器官发育的分子机制研究”为主题展开。进化所双聘教授董波教授做了题为“Control of notochord lumen expansion by the balance between actomyosin contraction and lumen pressure”的报告；分子发育研究室博士后荣小至做了题为“斑马鱼 rspo 基因体内功能和作用机制的研究”的报告；进化与发育研究室博士毕业生王霞做了题为“保护斑马鱼（*Danio rerio*）胚胎免受细菌感染的新型母源性 LPS 结合蛋白 ZRANB2 的鉴定”的报告。引发了全场的踊跃提问和深入探讨。

“海洋生物多样性与进化研究所—2015 年系列学术报告会Ⅱ”于 11 月 20 日下午 2:00 在达尔文馆举行。会议由研究所赵呈天教授主持，研究所成员及来自鱼山校区各院系相关领域的 50 余位师生参加。本次报告会共安排了 4 个报告，主要围绕“发育生物学研究”为主题展开。其中特邀清华大学欧光朔教授做了题为“Mechanisms of C.elegans Neuroblast Development”的报告，欧光朔教授为国家青年千人计划学者，国家杰出青年基金获得者，主要从事线虫发育生物学研究，论文发表在 Science，Nature，PNAS, Dev. Cell, Current Biology，JCB 等著名期刊上。随后进化所刘振辉教授做了题为“Fat taste and regulation of obesity”的报告；梁宇君博士做了题为“蝾螈趾部再生”的报告；张宇博士做了题为“青岛文昌鱼(*Branchiostoma japonicum*) viperin 鉴定和功能分析---揭示 viperin 介导的抗病毒应答的起源”的报告。引发了全场的踊跃提问和深入探讨。

二　年度重要成果介绍

（一）中国南海沿岸带纤毛虫的区系分类与分子系统学研究

本年度开展了对中国南海多种生境纤毛虫的采集和鉴定，建立和发表30余个新阶元；完成了对30余种90余种群纤毛虫的全基因组DNA提取、130余条基因序列的获得和提交；基于细胞学和基因序列信息，完成对赭纤虫科、旋口虫科、颈毛虫科、殖口虫科、施氏毛虫科、尖毛虫科、小双虫科等多个科属级阶元的分子系统学分析和对异毛纲和核残迹纲等高级类群的系统重构建；完成了对喙纤虫的单细胞全基因组、多个细胞全转录组的提取以及柠檬类瘦尾虫的大核基因组的高通量测序。代表性成果包括：

1. 缘毛亚纲、核残迹纲、排毛亚纲、叶咽纲普遍被认为是纤毛门中研究较为欠缺的几大类群。共鉴定和发表了多个新阶元，包括4个新属、29个新种及郎当异列虫和前毛异列虫等8个国内新纪录种。利用核糖体小亚基基因构建系统进化树，完成对具钩虫属、全列虫属、拉姆虫属、多毛虫属、戴维虫属、伪腹柱虫属、平游虫属、*Sinistrostrombidium*、*Antestrombidium*、突口虫属等30余种的分子系统学分析。

2. 通过对柠檬类瘦尾虫的大核基因组的高通量测序数据的分析，获得大核基因23178条，其中完整染色体5932条，具有单端粒染色体10683条，且85%以上的序列与转录组数据匹配。同时研究发现该种ABC转运蛋白基因家族在在小核中不存在基因乱序现象。该工作为纤毛虫独特的基因组重组的研究增加新的参考，同时增加人们对真核生物染色体重组的认识。

3. 利用多基因序列信息系统探讨了异毛纲和核残纲内科属间的亲缘关系。同时证实了两纲在纤毛门内较近的亲缘关系。

（二）四膜虫表观遗传学研究

本年度的工作主要集中在对转座子表达及核小体占位的表观遗传调控机制研究。主要研究进展包括：

1. 利用纤毛虫独有的双核特征，证实顺式作用元件（DNA序列信息）和反式作用元件（转录活性及转录酶占位）共同决定四膜虫中核小体的占位及丰度，为深度解析核小体对生物过程的调控机制提供了新视角。

2. 证实四膜虫转座子的表达受表观遗传信息（RNA干扰通路和多梳蛋白抑制通路）调控。转座子通过非编码RNA与编码RNA之间的转换达到转录和抑制的平衡，为解释转座子的沉默与激活这一看似矛盾的现象提供了新的突破点。

（三）文昌鱼存在脊椎动物样抗病毒免疫系统

主要成果包括：1.在文昌鱼中首次发现了LGP2受体分子；2. Poly(I:C)能够上调文昌鱼LGP2的表达，文昌鱼LGP2能够和Poly(I:C)相结合；3.文昌鱼LGP2在FG细胞中过表达能够加强干扰素和干扰素诱导基因的表达，并且能够显著上调干扰素和Mx基因以及RLRs信号通路相关基因MAVS, NF-κB和IRF-3的表达；4.文昌鱼LGP2抑制淋巴囊肿病毒在FG细胞中的复制，并抑制石斑鱼虹彩病毒在GS细胞中的转录；5.首次报道了在文昌鱼中与脊椎动物结构和功能相似的LGP2蛋白；6.发现文昌鱼中存在脊椎动物样viperin蛋白。

（四）斑马鱼纤毛发育生物学研究

本年度的工作主要集中在对纤毛发育缺陷与胚胎体轴发育、肝脏发育及眼睛发育的功能研究。目前主要研究进展包括：

1. 继续深入研究的体轴发育与纤毛缺陷的关系，明确纤毛的运动性能与Hh信号及细胞运动之间的联系，并发现Myosin动力蛋白在胚胎体轴发育中的作用机制，本研究成果正在整理中，近期将投稿。

2. 继续深入探讨Kinesin动力蛋白在视网膜发育过程中的功能，并发现Kinesin蛋白与IFT蛋白在调控感光细胞凋亡方面存在不同的作用机制。

3. 对运动纤毛相关基因的研究有进一步的进展，发现E2F5基因在精子发生过程中的作用机理，同时研究了Ankrd45蛋白在肝脏肿瘤细胞中的功能，其具体作用机制仍在深入探讨中。

4. 参与撰写了综述3篇，一篇关于纤毛的研究方法（MCB），一篇探讨斑马鱼作为模式生物研究纤毛疾病的优缺点（JGG），一篇探讨Kinesin的功能（中文）。上述文章将于近期发表。

（五）纽形动物多样性与进化研究

由于纽形动物门形态同质性高、缺乏有效的外部形态特征，内部形态的研究需要进行连续切片，且早期文献对物种的描述过于简单等原因，其物种鉴定和分类非常困难。特别是对一些世界广布且常见的种类，一些学者根据不同地区的标本命名了不同的物种，另一些学者则根据形态相似相似性将他们归为是同物异名，导致这些类群学名的使用和分类十分混乱。我们选取了形态一致性高、世界广分布、鉴定困难的喙纽虫-红纵沟纽虫-绿纵沟纽虫组群、细卷曲纽虫等为研究对象，通过与国际同行合作，采集了这些类群世界范围内样品，开展了形态与分子相结合的物种界定研究。确定了喙纽虫-红纵沟纽虫-绿纵沟纽虫组群包含9个形态相似的物种，其中欧洲沿岸分布有8种，血色喙纽虫为南北半球温带广布种，绿纵沟纽虫分布于太平洋和大西洋，红纵沟纽虫分布于北冰洋和大西洋；具螺旋

吻针的奇异拟纽虫复合体可能包含5-6个物种，分布于太平洋东、西海岸；细卷曲纽虫实际包括三个物种，其中一种世界广分布，另外两种分别分布于太平洋和大西洋沿岸研究。研究结果为这些类群的物种鉴定和分类系统修订提供了客观标准，为探讨纽形动物的生物地理、物种形成和系统进化提供了依据。

（六）海洋微生物的多样性、环境适应机制及生物地球化学作用

1.狭长海水菌的寡营养适应机制。南太平洋环流区是世界上最干净的海域，营养物质非常匮乏。狭长海水菌分离自南太平洋环流区的表层海水。为搞清狭长海水菌是如何适应于南太平洋环流区这样极度寡营养环境及其生物地球化学作用，我们进行了全基因组测序及分析，并对分析结果进行了试验验证。研究结果表明，狭长海水菌是一种能适应于寡营养环境的富营养细菌。该菌株具有较大的基因组及丰富的转运蛋白以适应于富营养生活；同时，该菌株还可通过狭长的形状来附着于颗粒物质，通过滑行运动来寻找营养物质，并对多种有机物具有强降解能力，使之在寡营养环境中也能够存活。研究成果发表于BMC Genomics。

2.中国北部边缘海表层沉积物微生物群落结构特征。边缘海作为陆地与大洋之间的过渡，是近岸生态系统生源要素循环的主要载体。本研究从渤海、北黄海、南黄海及东海北部四个海域各采集三个站位的表层沉积物样品，对微生物的丰度和群落结构进行了研究。发现无论是细菌还是古菌，四个海域均具有各自独特的群落组成（图3）。纬度和底层水温度是影响微生物群落结构变化的最重要因素；沉积物粒径与叶绿素能显著影响古菌群落组成，而对细菌却无影响，说明古菌群落对这两种环境因素更加敏感。此外，细菌是沉积物中的主要微生物类型，比古菌高2-3个数量级。研究成果发表于Microb Ecol。

3.细菌密度感应在颗粒有机碳降解中的控制作用。密度感应是细菌通过信号分子的积累感知细胞密度，从而调控细菌生物发光和生物膜形成等多种行为相关基因表达的一种调控机制。海洋中颗粒有机物的沉降是碳从海洋表面运输到海底的重要过程。本研究鉴定了颗粒有机碳及其附着细菌中的密度感应信号分子，同时探讨了外源信号分子对细菌胞外水解酶产生的影响。研究发现，从我国边缘海颗粒有机碳及分离菌株中均能检测到密度感应信号分子（图7），而且发现外源信号分子的添加可控制分离菌株的碱性磷酸酶分泌，说明细菌密度感应对颗粒有机碳降解具有调控作用。研究成果发表于FEMS Microbiol Ecol。

（七）鱼类特异模式识别受体基因结构进化规律的新发现

Toll 样受体 22（TLR22）是仅见于鱼类中的一种天然免疫模式识别受体。不同于 Toll 样受体家族其他成员的是，它可以同时利用 MyD88 和 TRIF 依赖途径启动抗病原微生物天然免疫应答，因此具有非常广泛的 PAMP（病原相关分子模式）识别谱，在鱼类对抗微生物感染中扮演十分重要的角色。不同鱼类 tlr22

基因的内含子数目不一样，从无到 5 个不等。先前学术界认为，tlr22 基因结构与鱼类的生境相关：淡水和半咸水鱼类 tlr22 无内含子，咸水鱼类 tlr22 则为断裂基因。我们通过基因克隆和数据挖掘，系统地分析了鲤形目、鲇形目、鲑形目、鳕形目、鲻形目、刺鱼目、鲈形目、鲽形目和鲀形目等涵盖淡水、半咸水和咸水 20 多种鱼类的 tlr22 基因结构，发现 tlr22 基因内含子是伴随距今 1.7~1.9 亿年前新真骨鱼的出现而产生的，其数目与鱼类进化地位密切相关而与生境无关。因此，tlr22 基因内含子的产生极可能是非编码序列随机插入读框中的结果，其数目决定于物种的进化时间。这一发现不支持 tlr22 基因通过内含子调节其表达的观点。

（八）对虾细胞的体外培养与永生性转化研究

本年度在 2 项国家自然科学基金和 1 项 863 项目的资助下，本团队在对虾体细胞和胚胎细胞的原代培养及其永生性转化技术方面取得了重要进展，包括：1.筛选得到适于对虾细胞的虾源启动子（Ptctp）和虾病毒来源启动子（Pie1），并成功构建双启动子驱动的 GFP 和 mCherry 表达载体；2.改进并建立了嗜对虾细胞的报告基因病毒基因转移系统；3.克隆得到一系列与对虾细胞生长和转化相关的基因包括对虾 TERT、TCTP、Bcl2、Lin28、Survivin、POU3 和 Cyclin E 等基因，构建表达载体并开展了对虾细胞的转染和永生性转化分析；4.解决了对虾胚胎细胞原代培养中的细胞解离与污染问题，成功得到原代培养胚胎细胞单层，并分化得到自主跳动的心肌细胞，初步建立了对虾胚胎细胞原代培养方法。有关成果已申请国家发明专利 3 项（授权 1 项）和实用新型专利 1 项（授权）。

（九）棘皮类动物的分类学及系统学研究

本年度开展了棘皮动物门海胆、海星以及海参的形态分类的系统研究，并完成对拱齿目刻肋海胆科细雕刻肋海胆、芮氏刻肋海胆、哈氏刻肋海胆、疏棘角孔海胆和杂色角孔海胆共 5 种海胆的线粒体全基因组测定工作，其分子信息为国际首次获得，在一定程度上丰富了海胆线粒体基因组数据库，为探讨海胆分类地位提供了分子依据，为该类海胆的系统演化和中国海洋动物多样性研究提供了基础资料和重要科学数据。

1.分别对刻肋海胆科、海盘车科、刺参科和海参科进行了系统的形态学分类研究，通过传统形态学研究结合扫描电子显微镜等新方法，讨论了各属种之间的形态区别以及分类学中存在的问题，为各自的分类学提供了形态上的基础资料和分类依据。

2.利用 long-PCR 结合常规 PCR 方法测得 5 种刻肋海胆线粒体基因组全序，对 2 种刺冠海胆的线粒体基因组测定工作已进入尾声，目前正进行对海参的 16S 和

cox1 的测定工作。

3.新测的刻肋海胆科海胆线粒体全序列全长在 15710bp-15767bp 之间，其平均长度为 15731bp。基因组结构与棘皮动物门的大多数已知种一致，包括 22 个 tRNA、2 个核糖体 RNA、13 个蛋白质编码基因以及非编码区，排列顺序与已知海胆纲线粒体基因组特征相一致。刻肋海胆科的线粒体基因排列较为保守，13 同源蛋白质基因的长度和顺序相同，不同种类线粒体基因组长度的差异主要是由非编码区中的串联重复产生。

4.基于 13 种拱齿目海胆线粒体基因组全序，采用贝叶斯推断法对拱齿目线粒体全序列进行联合模型分析，并分别基于蛋白质编码基因、tRNA 基因及 rRNA 基因构建 ML 系统发育树。结果与形态学分类结果基本一致，刻肋海胆科海胆彼此近缘关系最近，且与球形海胆的遗传距离相对都较远。

（十）海洋浮游病毒和微微型浮游生物多样性及噬菌体分离鉴定研究

1.浮游病毒多样性研究。采用宏基因组技术研究了研究渤海、黄海（包括胶州湾）、东海、南海（已建立 23 个宏基因组数据库），北欧海（正在构建 12 个宏基因组数据库）、南极普利兹湾及邻近海域（正在构建 7 个宏基因组数据库）病毒的群落结构。研究发现：1）黄海和渤海 DNA 数据与 CAMERA 库比对显示，主要的病毒大类为 dsDNA 病毒（79.1%），主要病毒科为肌尾病毒科（31.1%）、短尾病毒科（19.6%）、长尾病毒科（20.4%）、藻病毒科（6.7%）。病毒种中，远洋杆菌噬菌体（SAR11）Pelagibacter phage HTVC008M 所占比例最高。黄渤海藻 DNA 病毒 mcp 基因序列与已知藻 DNA 病毒的亲缘关系较远。2）其中对渤海 1 个站位两个时间点的病毒宏基因组数据分析显示，双链 DNA 病毒占绝对优势，其中有尾噬菌体目下的肌尾噬菌体，短尾噬菌体，长尾噬菌体占据优势地位。比例最高的功能基因大类为复制，结合和修复基因。另外系统进化分析显示，渤海病毒组与 T4-like 噬菌体大类亲缘关系较近；3）在秦皇岛扇贝养殖区，研究结果表明赤潮前该海域病毒以噬菌体为主要组成部分（67.691%），藻类 DNA 病毒仅占 1.570%。伴随赤潮爆发，噬菌体占比下降至 47.439%，藻类 DNA 病毒含量急剧提高，达 20.298%。其中，一种新的病毒 DNA 被检测出来。赤潮前后浮游病毒物种多样性的变化从侧面有力论证了赤潮期间水体生态群落的变化趋势。

2.微微型浮游生物多样性研究。秦皇岛扇贝养殖区是典型的富营养养殖水体，利用 Illumina’s MiSeq 高通量测序技术对养殖区的微微型真核生物的群落组成及多样性进行了研究，相应的选取远海贫营养水域监测点作为对照。对比之下发现从两个站点得到的群落，养殖区与对比站位群落组成相似，但相对丰度与物种结构均存在显著差异。其中养殖区的微微型真核生物的群落多样性明显较高，并发现秦皇岛养殖区出现丰度极高的“褐潮”藻种，抑食金球藻。影响

养殖区群落组成结构。本实验总结出了水产养殖区在微微型真核生物多样性方面的独到之处。

3. 海洋噬菌体的分离纯化和鉴定。构建了实验室海洋病毒分离纯化与鉴定研究平台，使用双层平板法发现并分离纯化了 7 株新型海洋噬菌体，开展了噬菌体生物学特性的测定，已完成其中 4 株噬菌体的全基因组测序与分析等方面的工作，测序结果显示四株已测序的噬菌体基因组中，未知功能的 ORFs 比例均超过 50 %，有待进一步深入研究。本实验的研究结果为海洋噬菌体基因库贡献了 2 株新的长尾噬菌体和 2 株肌尾噬菌体全基因组信息，为进一步研究海洋噬菌体的基因结构、功能提供重要的基础信息，对进一步探究宿主一噬菌体之间的相互作用关系提供了理论基础。

三　下年度计划

1. 积极准备 2016 年度国家基金等各项研究课题的申报；

2. 积极争取国内、省内及学校的人才计划支持，进行高层次人才引进；

3. 借助新项目启动等机制，认真规划、促进研究所内各团队研究目标的整合、交流和协同攻关；

4. 完善配套硬件平台，充分利用大型仪器设备共享平台，提高设备利用率；

5. 继续加强对外的合作与交流：包括 2016 年度邀请 4-5 批次的国际同行的来访；积极参加高水平的国际会议；博士研究生、研究人员赴国外的双边培养、进修及学术交流；

6. 积极组织申报各种科技奖励；

7. 完善研究所管理体系、网站建设，使之更好地为研究生培养和科研工作服务，发挥其宣传窗口功能。

我们将参照《高等学校重点实验室建设与管理暂行办法》的有关要求，做好研究所的建设和管理工作，进一步重视对年轻学术骨干的培养，充分发挥学术委员会的作用，把握好研究所的研究方向，围绕探索和解决海洋生物多样性与进化研究存在的焦点问题，通过硬件建设与高水平的人才工程构筑等措施，进一步强化优势突出的研究平台，强化代表我国本领域研究前沿水平的集团优势，引领和推动国内相关应用学科的发展，使海洋生物多样性与进化研究所的综合能力得到进一步提升，成为学校培养和凝聚创新人才的重要基地。

四　附表、附件

（一）附表：

附表 **1**　新申请及在研项目清单

附表 **2**　发表论文目录

附表 **3**　在职人员及博士毕业生获奖情况

附表 **4**　研究所组成人员名单

附表 **5**　研究生及博士后名单

附表 **6**　学术交流与合作

附表 **7**　学术委员会名单

（二）附件：**2015** 年—研究论文摘要集

附表 1 新申请及在研项目清单（10 万元以上项目）

序号	项目名称及编号	项目来源	负责人	资助经费（万元）	项目起止期限
1	鱼类应对虹彩病毒感染的免疫反应与调控网络 2012CB114404	“973”计划	张士璀	194	2012-2016
2	南中国海纤毛虫原生动物的区系与多样性研究 31430077	国家自然科学基金重点项目	宋微波	323	2015-2019
3	珊瑚礁生态系统中药用生物的化学防御物质及其化学生态效应 41130858	国家自然科学基金重点项目	王长云	280	2012-2016
4	免疫增强剂促进石斑鱼免疫分子和免疫力亲子传递之基础研究 U1401211	国家自然科学基金联合基金项目	张士璀	260	2015-2018
5	利用纤毛虫模式动物四膜虫对表观遗传学的研究 31522051	国家自然科学基金优秀青年基金项目	高　珊	150	2016-2018
6	利用模式生物研究纤毛发生及相关疾病 31422051	国家自然科学基金优秀青年基金项目	赵呈天	100	2015-2017
7	纤毛虫多样性研究的合作网络建立 31111120437	国家自然科学基金国际合作交流项目	宋微波	75	2012-2016
8	PSCAL 在视网膜感光细胞形成中的功能和作用机理研究 31572219	国家自然科学基金	李红岩	79	2016-2019
9	以斑马鱼为模式研究脂肪酸受体CD36在鱼类脂味觉感知中的作用 31572259	国家自然科学基金	刘振辉	79	2016-2019
10	黄海近岸厌氧环境纤毛虫的生物多样性研究 41576134	国家自然科学基金	胡晓钟	84	2016-2019
11	中国单针类纽虫四科的分类学研究 31471957	国家自然科学基金	孙世春	82	2015-2018
12	我国边缘海颗粒有机碳中细菌密度感应及其对有机碳降解的调控作用 41476112	国家自然科学基金	张晓华	100	2015-2018
13	嗜对虾细胞的高效报告基因病毒表达系统研究及其在转基因对虾上的应用31472274	国家自然科学基金	郭华荣	85	2015-2018
14	以纤毛虫原生动物-嗜热四膜虫为模式:DNA 复制延伸相关的表观遗传学研究 31470064	国家自然科学基金	高　珊	30	2015-2016
15	鱼类新母源性免疫因子的分离、鉴定与作用机理 31372505	国家自然科学基金	张士璀	77	2014-2017

16	斑马鱼纤毛动力蛋白 Kinesin2 的功能研究 31372274	国家自然科学基金	赵呈天	83	2014-2017
17	柳珊瑚内生真菌中抗藤壶附着大环内酯化合物构效关系及其作用机制 41376145	国家自然科学基金	王长云	82	2014-2017
18	南中国海叶咽纲和前口纲纤毛虫原生动物的研究 41376141	国家自然科学基金	胡晓钟	79	2014-2017
19	黄海沿岸的核残亚纲纤毛虫原生动物研究 41276139	国家自然科学基金	宋微波	88	2013-2016
20	Zfp3612 在胚胎体轴形成中的作用机理研究 31272395	国家自然科学基金	李红岩	82	2013-2016
21	微拟球藻生长相变分子机制研究 31270408	国家自然科学基金	杨官品	82	2013-2015
22	南太平洋环流区洋底沉积物及海水的微生物群落演化及功能活性研究 41276141	国家自然科学基金	张晓华	87	2013-2016
23	温带海区排毛亚纲纤毛虫无性生殖期间的皮层演化模式 41176119	国家自然科学基金	胡晓钟	71	2012-2015
24	白洋淀湿地腹毛类纤毛虫的区系与多样性研究 31172063	国家自然科学基金	李凤超	60	2012-2015
25	垂体-肝脏轴起源探索：文昌鱼生长激素受体（GHR）样基因克隆、表达及其配体分离、鉴定和功能分析 31172071	国家自然科学基金	张士璀	61	2012-2015
26	一种西沙柳珊瑚及其共附生微生物中次级代谢产物的生物活性与协同作用 81172977	国家自然科学基金	王长云	60	2012-2015
27	中国沿海寄生/共栖纽虫区系及典型类群进化研究 31172046	国家自然科学基金	孙世春	60	2012-2015
28	对虾细胞的分子重编程与永生性转化研究 31172391	国家自然科学基金	郭华荣	59	2012-2015
29	基于线粒体全序列的蛸科头足类系统发育与分类学研究 31172058	国家自然科学基金	郑小东	62	2012-2015
30	黄渤海贝类寄生桡足类的分类学研究 31501842	国家自然科学基金青年项目	董　超	23	2016-2018
31	从文昌鱼化学防御系统分析、鉴定探索脊椎动物肝脏与化学防御系统起源 31501856	国家自然科学基金青年项目	张　宇	23	2016-2018

32	海洋纤毛虫具沟急游虫的基因组重组过程与进化探讨 41406135	国家自然科学基金青年项目	高　凤	26	2015-2017
33	硬骨鱼特有的 NOD 样受体在抗菌免疫中的功能与调控机制 31402030	国家自然科学基金青年项目	孙　晨	25	2015-2017
34	抑癌基因 blu 与纤毛发生、细胞周期的关系研究 81301718	国家自然科学基金青年项目	赵呈天	23	2014-2016
35	山东沿海寡毛亚纲纤毛虫的分类学研究 31201696	国家自然科学基金青年项目	刘炜炜	24	2013-2015
36	发育生物学 JQ201506	山东省杰出青年基金	赵呈天	60	2015-2018
37	西太平洋中南部水体综合调查冬季航次 GASI-02-PAC-ST-MSwin	国家海洋局专项	汪　岷	50	2015-2017
38	南极周边海域海洋生物多样性和生态考察 CHINARE-01-05	国家海洋局极地专项	汪　岷	40	2012-2015
39	基于生态系统的海洋功能区划关键技术研究与应用 201505001	海洋公益专项	胡国斌	52	2015-2018
40	我国南海近岸纤毛虫原生动物研究：区系构成、物种与基因多样性 201562029	中央高校基本科研业务费	高　珊	200	2015-2018
41	蛋白质翻译后修饰在信号转导过程中的功能研究 201564011	中央高校基本科研业务费	赵呈天	38	2015-2016
42	纤毛虫大小核基因的重组与模式解析：对物种分化与基因组进化机制的探讨 201564022	中央高校基本科研业务费	高　凤	33	2015-2016
43	发育生物学 NCET-13-0537	教育部新世纪优秀人才支持计划	赵呈天	50	2014-2016
44	盾纤类纤毛虫的系统学及线粒体基因组图谱绘制 2015T80746	中国博士后科学基金（特别资助）	高　凤	15	2015-2016
45	柠檬瘦尾虫的大小核基因分化初探	山东省博士后创新项目专项资金	高　凤	15	2015-2016
46	海鞘软骨调节素调控脊索管腔发育的分子机理及其应用研究 ZR2015DM003	山东省自然科学基金	董　波	16	2015-2017
47	文昌鱼肝盲囊化学防御基因的表达调控与通路分析 ZR2015CQ004	山东省自然科学基金	张　宇	13	2015-2017
48	表观遗传信息对复制延伸过程及脆性位点表达的调控研究 ZR2014CQ011	山东省自然科学基金	高　珊	12	2014-2017

附表 2 发表论文目录

序号	成果名称	作者及位次	刊名	年、卷(期)、页	收录情况
1	A cortical instability drives periodic supracellular actin pattern formation in epithelial tubes	Hannezo E., Dong B., Recho P., Joanny J.F. & Hayashi S.	P. Natl. Acad.of Sci. USA	2015, 142: 1639-1650	SCI IF=9.81
2	Shaping of biological tubes by mechanical interaction of cell and extracellular matrix	Dong B. & Hayashi S.	Curr. Opin. Genet. Dev.	2015, 32: 129-134	SCI IF=8.57
3	Genome Sequencing of the Perciform Fish Larimichthys crocea Provides Insights into Molecular and Genetic Mechanisms of Stress Adaptation	Ao J., Mu Y., Xiang L., Fan D., Feng M., Zhang S. et al.	PLOS. Genet.	2015, DOI:10.1371	SCI IF=7.53
4	Analyses of alternatively processed genes in ciliates provide insights into the origins of scrambled genomes and may provide a mechanism for speciation.	Gao F., Roy S.W. & Katz L. A.	MBio	2015, 6: 1-8	SCI IF=6.8
5	Regulation by a TGFβ-ROCK-actomyosin axis secures a non-linear lumen expansion that is essential for tubulogenesis	Denker E., Sehring I., Dong B., Audisso J., Mathiesen B. & Jiang D.	Development	2015, 142: 1639-1650	SCI IF=6.27
6	Bioinformatical analysis of the sequences, structures and functions of fungal polyketide synthase product template domains	Liu L., Zhang Z., Shao C., Wang J., Bai H. & Wang C.	Sci. Rep.	2015, 5(10463): 1−12	SCI IF=5.58
7	Evolutionary conservation of molecular structure and antiviral function of a viral receptor, LGP2, in amphioxus Branchiostoma japonicum	Liu S., Liu Y., Yang S., Huang Y., Qin Q. & Zhang S.	Eur. J. Immunol.	2015，DOI: 10.1002	SCI IF=4.0
8	Construction of a high density SNP linkage map of kelp (Saccharina japonica) by sequencing *Taq* I site associated DNA and mapping of a sex determining locus	Zhang N., Zhang L., Tao Y., Guo L., Sun J., Li X., Zhao N., Peng J., Li X., Zeng L., Chen J. & Yang G.	BMC Genomics	2015, 16: 189	SCI IF=4.0
9	Genomic insight into Aquimarina longa SW024T: its ultra-oligotrophic adapting mechanisms and biogeochemical functions	Xu T., Yu M., Lin H., Zhang Z., Liu J. & Zhang X.	BMC Genomics	2015, 16:772	SCI IF=3.99
10	Phylogenetic framework of the systematically confused *Anteholosticha-Holosticha* complex (Ciliophora, Hypotrichia) based on multigene analysis	Zhao X., Gao S., Fan Y., Strueder-Kypke M. & Huang J.	Mol. Phylogen. Evol.	2015, 91: 238-247	SCI IF=3.9
11	Chromone derivatives from a sponge-derived strain of the fungus *Corynespora cassiicola*	Zhao D., Shao C., Gan L., Wang M. & Wang C.	J. Nat. Prod.	2015, 78, 286-293	SCI IF=3.80
12	Azaphilone and diphenyl ether derivatives from a gorgonian-derived strain of the fungus *Penicillium pinophilum*	Zhao D., Shao C., Zhang Q., Wang K., Guan F., Shi T. & Wang C.	J. Nat. Prod.	2015, 78: 2310–2314.	SCI IF=3.80
13	Phylogenetic diversity and antibacterial activity of culturable fungi derived from the Zoanthid *Palythoa haddoni* in the South China Sea	Qin X., Yang K., Li J., Wang C. & Shao C.	Mar. Biotech.	2015, 17(1): 99-109	SCI IF=3.27
14	Immune-Relevant and Antioxidant Activities of Vitellogenin and Yolk Proteins in Fish	Sun C. & Zhang S.	Nutrients	2015, 7, 8818–8829	SCI IF=3.27
15	Immune-Relevant and Antioxidant Activities of Vitellogenin and Yolk Proteins in Fish	Sun C. and Zhang S. C.	Nutrients	2015, 7(10), 8818-8829	SCI IF=3.27
16	Phylogenomics of non-model ciliates based on transcriptomic analyses	Chen X., Zhao X, Liu X., Warren A., Zhao F.Q. & Miao M.	Prot. Cell	2015，DOI 10.1007/s13238-015-0147-3	SCI IF=3.2

17	Two new genera of planktonic ciliates and insights into the evolution of the family Strombidiidae (Protista, Ciliophora, Oligotrichia)	Liu W.W., Yi Z., Xu D., Clamp J. C., Li J., Lin X, & Song W.	Plos One	2015，DOI:10.1371/journal.pone.0131726.	SCI IF=3.2
18	A case study to estimate the applicability of secondary structures of SSU-rRNA gene in taxonomy and phylogenetic analyses of ciliates	Wang P., Gao F., Huang J., Struder-Kypke M. & Yi Z.	Zool. Scr.	2015, 44: 574-585	SCI IF=3.2
19	New considerations on the phylogeny of cyrtophorian ciliates (Protozoa, Ciliophora): expanded sampling to understand their evolutionary relationships	Chen X., Pan H., Huang J., Warren A., Al-Rasheidd K.A.S. & Gao S.	Zool. Scr.	2015，DOI:10.1111/zsc.12150	SCI IF=3.2
20	Morphology and molecular phylogeny of three cyrtophorid ciliates (Protozoa, Ciliophora) from China, including two new species, Chilodonella parauncinata sp. n. and Chlamydonella irregularis sp. n.	Qu Z., Pan H., Hu X., Li J., Al-Farraj S. A, Al-Rasheidd K.A.S. & Yi Z.	J. Eukaryotic Microbiol.	2015, 62: 267-279	SCI IF=3.2
21	Morphology and phylogeny of two species of *Loxodes* (Ciliophora, Karyorelictea), with description of a new subspecies, *Loxodes striatus orientalis* subsp. n.	Xu Y., Pan H.B., Miao M., Hu X., Al-Rasheid K. A.S. & Song W.	J. Eukaryot. Microbiol.	2015, 62: 206-216	SCI IF=3.2
22	Morphology and phylogeny of three trachelocercid ciliates, with description of a new species, *Trachelocerca orientalis* spec. nov. (Ciliophora, Karyorelictea)	Yan Y., Gao F., Xu Y., Al-Rasheid K. A. S. & Song W.	J. Eukaryot. Microbiol.	2015, 62: 157-166	SCI IF=3.2
23	Phycoerythrins in phycobilisomes from the marine red alga Polysiphonia urceolata	Zhao M., Sun L., Sun S., Gong X., Fu X. & Chen M.	Int. J. Biol. Macromol.	2015, 73: 58–64	SCI IF=3.10
24	Molecular cloning and expression studies of the adapter molecule myeloid differentiation factor 88 (MyD88) in turbot (*Scophthalmus maximus*)	Lin J., Hu G., Yu C., Li S., Liu Q. & Zhang S.	Dev. Comp. Immunol.	2015, 52:166-171	SCI IF=2.82
25	Morphology and molecular phylogeny of three marine *Condylostoma*species from China, including two new ones (Ciliophora, Heterotrichea)	Yan Y., Chen X.M., Chen X.R., Gao F., Al-Farrah S.A. & Al-Rasheid K.A.S.	Eur. J. Protistol.	2015, 51: 66-78	SCI IF=2.8
26	Morphology of three *Litonotus* species (Ciliophora: Pleurostomatida) from China seas, with brief notes on their SSU rDNA-based phylogeny	Pan H., Li L., Wu L., Miao M., Al-Rasheid K.A. & Song W.	Eur. J. Protistol.	2015, 51: 494-506	SCI IF=2.8
27	Taxonomy and molecular phylogeny of two novel ciliates, withestablishment of a new genus, *Pseudogastrostyla* n. g. (Ciliophora,Hypotrichia, Oxytrichidae)	Fan Y., Zhao X., Hu X., Miao M., Warren A. & Song W.	Eur. J. Protistol.	2015, 51: 374–385	SCI IF=2.8
28	Taxonomic studies on seven species of *Dysteria* (Ciliophora, Cyrtophoria), including a description of *Dysteria paraprocera* sp. n.	Qu, Z., Wang, C., Gao, F., Li, J., Al-Rasheid, K.A.S. & Hu, X.	Eur. J. Protistol.	2015,51: 241–258	SCI IF=2.8
29	Morphology of three new colonial sessile peritrich ciliates, *Pseudepistylis paramphora* n. sp., *Zoothamnium paranii* n. sp. and *Z. hartwigi* n. sp., with notes on *Epicarchesium variabile* (Ciliophora, Peritrichia)	Sun P., Warren A., Al-Farraj S.A. & Song W.	Eur. J. Protistol.	2015, 51: 186-195	SCI IF=2.8
30	Morphology, morphogenesis and molecular phylogeny of a soil ciliate, *Pseudouroleptus caudatus caudatus* Hemberger, 1985 (Ciliophora,Hypotricha), from Lhalu Wetland, Tibet	Chen L., Zhao X., Ma H., Warren A., Shao C. & Huang J.	Eur. J. Protistol.	2015, 51: 1-14	SCI IF=2.8
31	Biodiversity of marine scuticociliates (Protozoa, Ciliophora) from China: description of nine morphotypes including a new species, Philaster sinensis spec. nov.	Pan X.M., Yi Z.Z., Li J.Q., Ma H.G., Al-Farraj S.A., & Al-Rasheid K.A.S.	Eur. J. Protistol.	2015, 51：142-157	SCI IF=2.8

32	Molecular cloning, expression, purification and characterization of vitellogenin in scallop Patinopecten yessoensis with special emphasis on its antibacterial activity	Wu B., Liu Z., Zhou L., Ji G. & Yang A.	Dev. Comp. Immunol.	2015, 49：249-258	SCI IF=2.8
33	Identification and functional characterization of viperin of amphioxus Branchiostoma japonicum: Implications for ancient origin of viperin-mediated antiviral response	Lei M., Liu H., Liu S., Zhang Y. & Zhang S.	Dev. Comp. Immunol.	2015, 53：293e302	SCI IF=2.8
34	Morphology and molecular phylogeny of three new oligotrich ciliates (Protozoa, Ciliophora) from the South China Sea	Liu W., Yi Z., Lin X., Li J., Al-Farraj S. A., Al-Rasheid K. A.S. & Song W.	Zool. J. Linn. Soc.	2015, 174: 653-665	SCI IF=2.7
35	Molecular cloning and expression analysis of interferon stimulated gene 15 (ISG15) in turbot, *Scophthalmus maximus*.	Lin J., Hu G., Liu D., Li S., Liu Q. & Zhang S.	Fish Shellfish Immunol.	2015, 45:895-900	SCI IF=2.67
36	Cloning and expression analysis of a Toll-like receptor 22 (TLR22) gene from turbot, *Scophthalmus maximus*	Hu G., Zhang S., Yang X., Liu D., Liu Q. & Zhang S.	Fish Shellfish Immunol.	2015, 44:399-409	SCI IF=2.67
37	Subergorgiaols A–L, 9,10-secosteroids from the South China Sea gorgonian *Subergorgia rubra*	Sun X., Cao F., Shao C., Chen M., Liu H., Zheng C. & Wang C.	Steroids	2015, 94: 7–14.	SCI IF=2.64
38	*Leucothrix pacifica* sp. nov., isolated from seawater of South Pacific Gyre and emended description of the genus *Leucothrix*	Zhang Z., Gao X., Wang L. & Zhang X.	Int. J. Syst .Evol. Microbiol.	2015, DOI: 10.1099/ijs.0.000270	SCI IF=2.51
39	*Muricauda pacifica* sp. nov., isolated from seawater of the South Pacific Gyre	Zhang Z., Gao X., Qiao Y., Wang Y. & Zhang X.	Int. J. Syst .Evol. Microbiol.	2015, DOI: 10.1099/ijsem.0.000542	SCI IF=2.51
40	*Celeribacter manganoxidans* sp. nov., a manganese-oxidizing bacterium isolated from deep-sea sediment of polymetallic nodule province	Wang L., Liu Y., Wang Y., Dai X. & Zhang X.	Int. J. Syst .Evol. Microbiol.	2015, DOI: 10.1099/ijsem.0.000751	SCI IF=2.51
41	*Jiella aquimaris* gen. nov., sp. nov., isolated from offshore surface seawater of the East China Sea	Liang J., Liu J. & Zhang X-H	Int. J. Syst .Evol. Microbiol.	2015,65: 1127–1132	SCI IF=2.51
42	*Spongiibacterium pacificum* sp. nov., isolated from seawater of South Pacific Gyre and emended description of the genus *Spongiibacterium*	Gao X., Zhang Z., Dai X. & Zhang X.	Int. J. Syst .Evol. Microbiol.	2015, 65: 154–158	SCI IF=2.51
43	*Hyunsoonleella pacifica* sp. nov., isolated from seawater of South Pacific Gyre	Gao X., Zhang Z., Dai X. & Zhang X.	Int. J. Syst .Evol. Microbiol.	2015, 65: 1155–1159	SCI IF=2.51
44	Morphology and morphogenesis of a novel mangrove ciliate, *Sterkiella subtropica* sp. nov. (Protozoa, Ciliophora, Hypotrichia), with phylogenetic analyses based on small-subunit rDNA sequence data	Chen X.M., Gao F., Al-Farraj S.A., Al-Rasheid K.A.S., Xu K & Song W.	Int. J. Syst .Evol. Microbiol.	2015, 65: 2292-2303	SCI IF=2.5
45	New record of *Apoholosticha sinica* (Ciliophora, Urostylida) from the UK: morphology, 18S rRNA gene phylogeny and notes on morphogenesis	Hu X., Fan Y. & Warren A.	Int. J. Syst .Evol. Microbiol.	2015, 65: 2549-2561	SCI IF=2.5
46	Reconsideration of the 'well-known' hypotrichous ciliate Pleurotricha curdsi (Shi et al., 2002) Gupta et al., 2003 (Ciliophora, Sporadotrichida), with notes on its morphology, morphogenesis and molecular phylogeny	Lu X., Shao C., Yu Y., Warren A. & Huang J.	Int. J. Syst .Evol. Microbiol.	2015, 65: 3216–3225	SCI IF=2.5
47	Identification and expression of an uncharacterized Ly-6 gene cluster in zebrafish Danio rerio	Guo Q., Ji D., Wang M. & Zhang S. & Li H.	Funct. Integr. Genomics	2015, 15(5):577-85.	SCI IF=2.48

48	Identification, expression and regulation of amphioxus G6Pase gene withan emphasis on origin of liver	Wang Y., Wang H., Li M., Gao Z. & Shicui Zhang	Gen. Comp.e Endocr.	2015,214 : 9–16	SCI IF=2.47
49	Identification of a Ly-6 superfamily gene expressed in lateral line neuromasts in zebrafish	Ji D., Li L., Zhang S. & Li H.	Dev. Genes Evol.	2015, 225(1):47-53.	SCI IF=2.44
50	Taxonomy and molecular phylogeny of four *Strombidium* species, including description of *S. pseudostylifer* sp. nov. (Ciliophora, Oligotrichia)	Song W., Li J., Liu W., Al-Rasheid K., Hu X. & Lin X.	Syst. Biodivers.	2015, 13: 76-92	SCI IF=2.2
51	Redefinition of the hypotrichous ciliate Uncinata, with descriptions of the morphology and phylogeny of three urostylids (Protista, Ciliophora)	Luo X.,Gao F., Al-Rasheid K., Warren A., Hu X. & Song W.	Syst. Biodivers	2015, 13: 455-471	SCI IF=2.2
52	Zebrafish phosvitin is an antioxidant with non-cytotoxic activity	Hu L., Sun C., Luan J., Lu L. & Zhang S.	Acta Bioch. Bioph. Sin.	2015,47(5):349–354	SCI IF=2.19
53	Identification and biochemical characterization of polyamine oxidases in amphioxus: Implications for emergence of vertebrate-specific spermine and acetylpolyamine oxidases	Wang H., Liu B., Li H. & Zhang S.	Gene	2016，575：429－437	SCI IF=2.14
54	Identification and expression of lypc, a novel dark-inducible member of Ly6 superfamily in zebrafish Danio rerio	Li L., Ji D., Teng L., Zhang S. & Li H.	Gene	2015, 574(1):69-75	SCI IF=2.14
55	A Toll-like receptor 3 homolog that is up-regulated by poly I:C and DNA virus in turbot, *Scophthalmus maximus*	Hu G., Li X., Liu D., Liu Q. & Zhang S.	J. Fish Biol.	2015, 86:431-447.	SCI IF=1.66
56	Complete Genome of a Novel *Pseudoalteromonas* Phage PHq0	Wang D., Li Y., Sun M., Huang J., Shao H., Xin Q. & Wang M.	Curr. Microbiol.	DOI:10.1007/s00284-015-0919-2	SCI IF=1.42
57	Mitochondrial genome of Micrura bella (Nemertea: Heteronemertea), the largest mitochondrial genome known to phylum Nemertea	Shen C. & Sun S..	Mitochondr. DNA	2015, DOI: 10.3109/19401736.2015.1060429	SCI IF=1.21
58	DNA Taxonomy of Paranemertes (Nemertea: Hoplonemertea) with Spirally Fluted Stylets	Hao Y., Kajihara H., Chernyshev A., Okazaki R. & Sun S.	Zool.Sci.	2015, 32: 571–578	SCI IF=0.88
59	Species Diversity of Ramphogordius sanguineus / Lineus ruber Like Nemerteans (Nemertea: Heteronemertea) and Geographic Distribution of R. sanguineus	Kang X., Fernández-Álvarez FÁ, Alfaya JEF, Machordom A., Strand M., Sundberg P. &Sun S.	Zool. Sci.	2015, 32: 579–589	SCI IF=0.88
60	Special Issue: Proceedings of the 8th International Conferenceon Nemertean Biology	Sun S., Kajihara H. & Chernyshev A.	Zool. Sci.	2015, 32: 499–500	SCI IF=0.88
61	Problems with the use of liposome- and retrovirus-mediated gene transfer methods in the primary lymphoid cells of the Oka organs of the greasyback shrimp, *Metapenaeus ensis* (De Haan, 1844)	Han Q., Dong D., Zhang X., Liang C., Lu Q. &Guo H.	Crustaceana	2015，DOI 10.1163/15685403-00003498	SCI IF=0.47
62	Morphology of two novel species of *Chaenea* (Ciliophora, Litostomatea): *Chaenea paucistriata* spec. nov. and *C. sinica* spec. nov.	Fan X., Xu Y., Gu F., Li J., Al-Farraj S., Al-Rasheid K. & Hu X.	Acta. Protozool.	2015, 54: 97-106	SCI IF=0.8
63	Two oxytrichids from the ancient Lake Biwa, Japan, with notes on morphogenesis in *Notohymena australis* (Ciliophora, Sporadotrichida)	Hu X. & Kusuoka Y.	Acta. Protozool.	2015, 54: 107-122	SCI IF=0.8
64	Morphological and morphogenetic redescriptions and SSU rRNA gene-based phylogeny of the poorly-known species *Euplotes amieti* Dragesco, 1970 (Ciliophora, Euplotida)	Liu M., Fan Y., Miao M., Hu X., Al-Rasaheid K., Al-Farraj S. & Ma H.	Acta. Protozool.	2015, 54: 173-184	SCI IF=0.8

65	Morphology and phylogeny of four marine scuticociliates (Protista, Ciliophora), with descriptions of two new species: *Pleuronema elegans* spec. nov. and *Uronema orientalis* spec. nov.	Pan X., Huang J., Gao F., Fan X., Ma H., Al-Rasheid K. & Miao M.	Acta. Protozool.	2015, 54: 31-43	SCI IF=0.8
66	Two new and two rarely known species of *Ancistrum* (Scuticociliatia, Thigmotrichida) parasitizing marine molluscs	Xu K., Song W. & Warren A.	Acta. Protozool.	2015, 2015, 54: 195-208	SCI IF=0.8
67	Data on ten new myxosporean parasites (Myxozoa, Myxosporea, Bivalvulida) from the Yellow Sea, China	Zhao Y., Al-Farraj S., Al-Raseheid K. & Song W.	Acta. Protozool.	2015, 54: 305-323	SCI IF=0.8
68	High-density cultivation of the marine ciliate *Uronema marinum* (Ciliophora, Oligohymenophorea) in axenic medium	Zheng W., Gao F. & Warren A.	Acta. Protozool.	2015, 54: 325–330	SCI IF=0.8
69	Molecular Phylogenetic Lineage of Plagiopogon and Askenasia (Protozoa, Ciliophora) Revealed by Their Gene Sequences	Liu A., Yi Z., Lin X., Hu X., Saleh A.& Al-Rasheid K.	J. Ocean Univ. China	2015, 14 (4): 724-730	SCI IF=0.56
70	A General Overview of the Typical 18 Frontal-Ventral-Transverse Cirri Oxytrichidae s. l. Genera(Ciliophora, Hypotrichia)	Shao C., Lu X. & Ma H.	J. Ocean Univ. China	2015, 14 (3): 522-532	SCI IF=0.56
71	Monophyly or polyphyly? Possible confl ict between morphological and molecular interpretations of the wellknown genus Zoothamnium (Ciliophora, Peritrichia)	Li L., Ma H. & Al-Rasheid K.	J. Ocean Univ. China	2015, 14 (3): 522-532	SCI IF=0.56
72	Evaluation of cytotoxicity and genotoxicity of insecticide carbaryl to flounder gill cells and its teratogenicity to zebrafish embryos	Manish Raj Pandey & Guo H.	J. Ocean Univ. China	2015，14 (2): 362-374	SCI IF=0.56
73	Problems with the use of liposome- and retrovirus-mediated gene transfer methods in the primary lymphoid cells of the Oka organs of the greasyback shrimp, Metapenaeus ensis (De Haan, 1844)	Han Q., Dong D., Zhang X., Liang C., Lu Q. & Guo H.	Crustaceana	2015，DOI: 10.1163/1568 5403-000034 98	SCI IF=0.47
74	The molecular data suggests that the ciliate *Mesodinium* (Protista, Ciliophora) might represent an undescribed taxon at class level	Chen X., Ma H., Al-Rasheid K. & Miao M.	Zool. Syst.	2015, 40: 31-40	
75	纤毛虫两型核之间的基因组重组.	郑维波，高凤	生命科学	2015, 27: 486-494	
76	海洋模式动物海鞘及其脊索发育与调控	董波	科学通报	2015，60: 1167-1179.	
77	马粪海胆不同地区群体形态学比较研究	刘成龙，曾晓起	中国海洋大学学报	2015,45（4）: 40-45	
78	基于棘的显微结构的海盘车属鉴别研究	徐思嘉，肖宁，曾晓起	中国海洋药物	2015,34（3）: 53-58	

附表 3　在职人员及博士毕业生获奖情况

附表 3-1 2015 年在职人员获奖情况一览表

序号	获奖名称	获奖人	授奖单位	时间
1	山东省科技进步二等奖	王长云	山东省	2015 年 1 月
2	青岛市自然科学二等奖	张士璀	青岛市	2015 年 6 月

附表 3-2　2015 年硕博士毕业生获奖情况一览表

序号	获奖名称	获奖人/获奖成果	导师	授奖单位	时间
1	山东省优秀博士学位论文奖	高　凤	宋微波	山东省教育厅 山东省人民政府学位委员会	2015
2	山东省研究生优秀科技创新成果奖	樊阳波	宋微波	山东省教育厅 山东省人民政府学位委员会	2015
3	山东省优秀博士毕业生	沈春阳	孙世春	山东省教育厅	2015

附表 4 研究所组成人员名单

姓 名	性别	出生年月	最后学位	研究方向	技术职称	备注
宋微波	男	1958.12	博士	原生动物多样性与进化	院士 教授	
张士璀	男	1957.1	博士	脊索动物发育与进化	教授	
孙世春	男	1965.10	博士	无脊椎动物多样性与进化	教授	
胡晓钟	男	1970.10	博士	原生动物多样性与进化	教授	
赵呈天	男	1978.12	博士	脊索动物发育与进化	教授	
刘振辉	男	1971.10	博士	脊索动物发育与进化	教授	
高 珊	女	1983.2	博士	原生动物多样性与进化	教授	
苏 颖	女	1979.7	博士	脊索动物发育与进化	教授	
杨官品	男	1963.6	博士	藻类遗传多样性与进化	教授	校内双聘
张晓华	女	1962.6	博士	微生物多样性与进化	教授	校内双聘
王长云	男	1965.2	博士	海洋药用生物多样性	教授	校内双聘
曾晓起	男	1963.3	硕士	无脊椎动物生物多样性	教授	校内双聘
汪 岷	女	1969.11	博士	微生物学多样性	教授	校内双聘
胡国斌	男	1971.10	博士	脊椎动物发育与进化	教授	校内双聘
郭华荣	女	1970.1	博士	无脊椎动物发育	教授	校内双聘
郑小东	男	1971.7	博士	无脊椎动物多样性与进化	教授	校内双聘
董 波	男	1973.10	博士	发育生物学	教授	校内双聘
李红岩	女	1975.10	博士	脊索动物发育与进化	副教授	
孙 晨	男	1983.9	博士	脊索动物发育与进化	副教授	
汲广东	男	1976.9	博士	脊索动物发育与进化	讲师	
高 凤	女	1985.7	博士	原生动物发育与进化	讲师	
张 宇	女	1984.4	博士	脊索动物发育与进化	讲师	
高 瞻	男	1988.9	博士	脊索动物发育与进化	讲师	
梁宇君	男	1973.10	博士	脊索动物发育与进化	讲师	校内双聘
马洪钢	男	1976.10	硕士	原生动物发育与进化	工程师	
张 川	女	1982.2	硕士	行政管理	秘书	

附表 5 研究生及博士后名单

（一）2015 年在读研究生名单

序号	姓　名	专业方向	年级	硕士/博士
1	郑维波	水生生物学	2015 级	博士
2	刘铭鉴	水生生物学	2015 级	博士
3	黄洁	发育生物学	2015 级	博士
4	呼景阔	水生生物学	2015 级	博士
5	杜鑫	无脊椎动物系统学	2015 级	博士
6	王鹏	海洋生物学	2015 级	博士
7	杜小媛	海洋生物学	2015 级	博士
8	王愫	海洋生物学	2015 级	博士
9	曲志帅	原生动物系统分类学	2014 级	博士
10	罗晓甜	纤毛虫细胞发生学	2014 级	博士
11	陈晓	原生动物系统分类学	2014 级	博士
12	蒋成砚	发育生物学	2014 级	博士
13	Muhammad Mohsin	无脊椎动物进化	2014 级	博士
14	冯东	发育生物学	2014 级	博士
15	张海峰	发育生物学	2014 级	博士
16	王志杨	渔业资源	2014 级	博士
17	张晓萌	渔业资源	2014 级	博士
18	刘璐	渔业资源	2014 级	博士
19	阎莹	原生动物系统分类学	2013 级	博士
20	宋雯	原生动物分类学	2013 级	博士
21	赵晓璐	原生动物系统学与进化	2013 级	博士
22	董渊	发育生物学	2013 级	博士
23	李萌阳	发育生物学	2013 级	博士
24	崔鹏飞	发育生物学	2013 级	博士
25	武瑾	无脊椎动物进化	2013 级	博士
26	陈凌云	动物学	2011 级	博士
27	张滕滕	动物学	2015 级	硕士

28	连春禹	水生生物学	2015 级	硕士
29	盛亚岚	水生生物学	2015 级	硕士
30	王锐	动物学	2015 级	硕士
31	王伦	海洋生物学	2015 级	硕士
32	贾硕	发育生物学	2015 级	硕士
33	褚延延	无脊椎动物系统学	2015 级	硕士
34	钟慎杰	生物工程	2015 级	硕士
35	马增钰	海洋生物学	2015 级	硕士
36	白玉	海洋生物学	2015 级	硕士
37	程潇	海洋生物学	2015 级	硕士
38	冯铄淇	海洋生物学	2015 级	硕士
39	李嵩	原生动物分类学	2014 级	硕士
40	王春荻	原生动物分子系统学	2014 级	硕士
41	董婧怡	原生动物分类学	2014 级	硕士
42	王媛媛	原生动物分子生物学	2014 级	硕士
43	王玉蕊	原生动物分子生物学	2014 级	硕士
44	徐丛梅	无脊椎动物进化	2014 级	硕士
45	许苹	无脊椎动物进化	2014 级	硕士
46	郭晓敏	海洋生物学	2014 级	硕士
47	曲宝臻	海洋生物学	2014 级	硕士
48	胡玉	海洋生物学	2014 级	硕士
49	辛佳静	海洋生物学	2014 级	硕士
50	刘学敏	发育生物学	2014 级	硕士
51	曹绪文	发育生物学	2014 级	硕士
52	张钰博	发育生物学	2014 级	硕士
53	王雅硕	发育生物学	2014 级	硕士
54	王萌	生物工程	2014 级	硕士
55	刘海洋	生物工程	2014 级	硕士
56	谢海波	发育生物学	2014 级	硕士
57	康云思	发育生物学	2014 级	硕士
58	朱盼盼	发育生物学	2014 级	硕士
59	韩霄	发育生物学	2014 级	硕士
60	卢晓腾	纤毛虫分类学	2013 级	硕士

61	郭紫薇	海洋生物	2013 级	硕士
62	段楚楚	遗传学	2013 级	硕士
63	刘圆圆	生化与分子生物学	2013 级	硕士
64	赵晓婷	海洋生物	2013 级	硕士
65	王颖	生物工程	2013 级	硕士
66	肖红彦	生物工程	2013 级	硕士
67	梁雪	海洋生物	2013 级	硕士
68	苗珊珊	海洋生物学	2013 级	硕士
69	王雅冬	海洋生物学	2013 级	硕士
70	张晓丽	海洋生物学	2013 级	硕士
71	宋著	发育生物学	2013 级	硕士

（二）本年度博士研究生公派出国双边联合培养情况

序号	学生姓名	国家	境外学校
1	阎莹	美国	Smith College
2	宋雯	美国	University of Connecticut
3	赵晓璐	美国	Michigan University
4	马媛媛	德国	University of Kiel
5	陈凌云	美国	North Carolina Central University

（三）在站博士后名单

序号	姓名	研究方向	入站时间
1	王　霞	海洋生物学	2015 年
2	高　瞻	海洋生物学	2015 年
3	Alireza Asem	遗传学	2015 年
4	刘　璐	药学	2015 年
5	王开玲	药学	2015 年
6	隗健凯	基因组学与发育生物学	2015 年
7	张晓明	细胞发育生物学	2015 年
8	高　凤	原生动物分子生物学	2014 年
9	李　静	原生动物分子生物学	2014 年
10	孙　晨	进化与发育	2014 年
11	张　宇	进化与发育	2014 年
12	白　虹	药物化学	2014 年
13	汤开浩	海洋微生物学	2014 年
14	荣小至	发育生物学	2014 年
15	姜 勇	微型生物生态	2014 年
16	窦娜莎	海洋生物学	2013 年
17	逄朝霞	海洋生物学	2013 年
18	董　超	甲壳动物分类与多样性	2013 年

附表 6 学术交流与合作

附表 6-1 出访、参加学术会议一览表

序号	会议名称	主办单位名称	时间地点	内容与成果
1	第四届“纤毛虫多样性与合作”国际研讨会	海洋生物多样性与进化研究所	2015 年 10 月 19-21 日 青岛	来自美国等近 30 位国际同行以及 30 余位国内同行参会。与会专家作了 28 场口头报告，在纤毛虫的模式生物、生理、分类、遗传、寄生虫学与生态等多样性泛领域内多个方向进行了交流和讨论并就纤毛虫学研究国际合作的未来发展、方向建设和组织框架构建达成了初步共识
2	海洋微生物学国际研讨会	中国海洋大学	2015 年 5 月 22-25 日 青岛	海洋微生物学团队为主办方，参会人员 300 余人，来自于美国、英国、加拿大、日本、埃及、南非、孟加拉、中国香港等国家和地区，本课题组有 3 个口头报告
3	首届全国纤毛生物学学术会议	海洋生物多样性与进化研究所	2015 年 11 月 13-14 日 青岛	来自北京大学等 18 个科研院所和来自北京 301 医院、同仁医院等多家医疗结构的近 70 名师生参会。对纤毛的结构、发生以及人类纤毛疾病等多方面进行了交流讨论，本次研讨会代表了我国纤毛生物学研究领域的最高水平
4	第七届欧洲原生生物学大会	欧洲原生生物学家学会	2015 年 9 月 5-10 日 西班牙 塞维利亚	300 余位来自全球 33 个国家的同行学者参会。本所宋微波教授等一行 4 人参加。会上宋老师作了题为“Ciliate researches in China: Active groups, chance for collaboration and the on-going studies”的大会报告。胡晓钟老师和高珊老师分别就各自的研究方向作了分组口头报告
5	中国原生动物学分会第十八次学术讨论会	中国动物学会原生动物学分会	2015 年 8 月 24 -27 日 山东 烟台	进化所所原生动物学团队宋微波教授带领师生 20 人参加了本次会议。高珊教授做了题为“表观遗传信息对基因表达何复制的调控—四膜虫视角”的大会报告。大会为 11 名优秀的年轻原生动物学工作者颁发了学会首届“青年科技奖”，高珊教授位列其中

6	Gordon Research Conference	香港科技大学	2015 年 8 月 2-7 日 香港	海洋微生物学团队 2 人参会，并有 2 个 poster
7	第四届全国斑马鱼大会	中国海洋大学	2015 年 9 月 6-8 日 青岛	研究所参与承办本次会议,参会 500 人
8	FASEB 纤毛研讨会	FASEB summer conference	2015 年 7 月 19-24 日 美国 科罗拉多	赵呈天教授参加会议
9	纤毛虫分子生物学会议	卡美日诺大学	2015 年 7 月 10-16 日 意大利 卡美日诺	高珊教授参会并做口头报告
10	中国细胞生物学学学会 2015 年全国学术大会	中国细胞生物学学学会	2015 年 4 月 1-4 日 深圳	郭华荣参会，墙报交流：Study on the in vitro culture and immortalization of penaeus shrimp cells
11	Aquaculture 2015 - Cutting Edge Science in Aquaculture	Elsevier 出版社	2015 年 8 月 23-26 日 法国 蒙彼利埃	郭华荣参会，并作大会口头报告：Study on the in vitro culture and immortalization of penaeus shrimp cells
12	中国动物学会▪中国海洋湖沼学会贝类学分会第十次会员代表大会暨第十七次学术讨论会	中国海洋湖沼学会	2015 年 10 月 14-16 日 湖南 长沙	头足类生物学团队 2 人参会，在会上做了“中国东南沿海一种未定短腿蛸的形态学和分子学鉴定”主题的口头报告
13	第四届国际基因组学大会	中国科学院北京基因组研究所	2015 年 10 月 23-25 日 西安	汪岷教授做了题为“Seasonal variation and distribution of viruses in the North Yellow Sea by metagenomic analysis”的大会报告
14	2015 第三届非编码 RNA 学术研讨会	生物谷	2015 年 10 月 29-30 日 上海	郭华荣教授参会
15	2015 亚太发育生物学国际研讨会	中国科学院动物研究所	2015 年 9 月 11-14 日 西安	梁宇君博士提交了会议论文摘要；展示了墙报

附表 6-2　来访人员一览表

序号	来访人员姓名	职称	国家	工作单位	在室工作期限
1	Robert Parton	教授	澳大利亚	昆士兰大学	5 月 30 日-6 月 1 日
2	刘一凡	副教授	美国	密歇根大学	6 月 24-27 日
3	罗海伟	助理教授	香港	香港中文大学	9 月 13-16 日
4	Stephen Giovannoni	教授	美国	美国俄勒冈州立大学	7 月 24 日
5	Tomer Ventura	助理教授	澳大利亚	University of the Sunshine Coast	11 月 6-8 日
6	Sun Zhaoxia	教授	美国	耶鲁大学	9 月 5-8 日
7	Malicki Jarema	教授	英国	Sheffied University	11 月 5-8 日
8	Curtis Suttle	美国微生物学院院士，教授	加拿大	哥伦毕业大学	5 月 19-25 日
9	Gill Malin	教授	英国	东英吉利大学	5 月 18-31 日
10	陈峰	教授	美国	马里兰大学	7 月 14-15 日
11	Jonnathan Todd	资深讲师	英国	东英吉利大学	12 月 4-6 日
12	欧光朔	教授	中国	清华大学	11 月 20 日
13	施威扬	教授	中国	同济大学	1 月 22 日
14	王昊	研究员	中国	中科院海洋所	1 月 22 日

附表 7　学术委员会名单

姓　名	职　称	工作单位	研究方向	学术委员会职务
孟安明	院士，教授	清华大学	发育生物学	主任委员
宋微波	院士，教授	中国海洋大学	原生动物多样性与进化	副主任委员
徐存拴	教　授	河南师范大学	发育生物学	委员
王金星	教　授	山东大学	动物学、免疫学	委员
黄晓航	研究员	海洋局一所	海洋生物	委员
孙　黎	研究员	中科院海洋所	海洋微生物学	委员
黄　倢	研究员	黄海水产研究所	病毒学	委员
李　琪	教　授	中国海洋大学	遗传多样性	委员
包振民	教　授	中国海洋大学	贝类学、遗传学	委员
张士璀	教　授	中国海洋大学	脊索动物发育与进化	委员
池振明	教　授	中国海洋大学	微生物多样性与进化	委员
孙世春	教　授	中国海洋大学	无脊椎动物多样性与进化	委员

附件:

2015-研究论文摘要集

2015-12

RESEARCH ARTICLE

Analyses of Alternatively Processed Genes in Ciliates Provide Insights into the Origins of Scrambled Genomes and May Provide a Mechanism for Speciation

Feng Gao,[a,b] Scott W. Roy,[c] Laura A. Katz[a,d]

Department of Biological Sciences, Smith College, Northampton, Massachusetts, USA[a]; Laboratory of Protozoology, Institute of Evolution and Marine Biodiversity, Ocean University of China, Qingdao, China[b]; Department of Biology, San Francisco State University, San Francisco, California, USA[c]; Program in Organismic and Evolutionary Biology, UMass-Amherst, Amherst, Massachusetts, USA[d]

ABSTRACT **Chromosome rearrangements occur in a variety of eukaryotic life cycles, including during the development of the somatic macronuclear genome in ciliates. Previous work on the phyllopharyngean ciliate *Chilodonella uncinata* revealed that macronuclear β-tubulin and protein kinase gene families share alternatively processed germ line segments nested within divergent regions. To study genome evolution in this ciliate further, we characterized two additional alternatively processed gene families from two cryptic species of the ciliate morphospecies *C. uncinata*: those encoding histidine acid phosphatase protein (*Hap*) and leishmanolysin family protein (*Lei*). Analyses of the macronuclear *Hap* and *Lei* sequences reveal that each gene family consists of three members in the macronucleus that are marked by identical regions nested among highly divergent regions. Investigation of the micronuclear *Hap* sequences revealed a complex pattern in which the three macronuclear sequences are derived either from a single micronuclear region or from a combination of this shared region recombined with additional duplicate micronuclear copies of *Hap*. We propose a model whereby gene scrambling evolves by gene duplication followed by partial and reciprocal degradation of the duplicate sequences. In this model, alternative processing represents an intermediate step in the evolution of scrambled genes. Finally, we speculate on the possible role of genome architecture in speciation in ciliates by describing what might happen if changes in alternatively processed loci occur in subdivided populations.**

IMPORTANCE **Genome rearrangements occur in a variety of eukaryotic cells and serve as an important mechanism for generating genomic diversity. The unusual genome architecture of ciliates with separate germline and somatic nuclei in each cell, provides an ideal system to study further principles of genome evolution. Previous analyses revealed complex forms of chromosome rearrangements, including gene scrambling and alternative processing of germ line chromosomes. Here we describe more complex rearrangements between germ line and somatic chromosomes than previously seen in alternatively processed gene families. Drawing on the present and previous findings, we propose a model in which alternative processing of duplicated micronuclear regions represents an intermediate stage in the evolution of scrambled genes. Under this model, alternative processing may provide insights into a mechanism for speciation in ciliates. Our data on gene scrambling and alternative processing also enhance views on the dynamic nature of genomes across the eukaryotic tree of life.**

Received 16 December 2014 **Accepted** 18 December 2014 **Published** 3 February 2015

Citation Gao F, Roy SW, Katz LA. 2015. Analyses of alternatively processed genes in ciliates provide insights into the origins of scrambled genomes and may provide a mechanism for speciation. mBio 6(1):e01998-14. doi:10.1128/mBio.01998-14.

Editor Patricia J. Johnson, UCLA

Address correspondence to Laura A. Katz, lkatz@smith.edu.

This article is a direct contribution from a Fellow of the American Academy of Microbiology.

Genomes are incredibly dynamic within diverse lineages across the tree of life (1, 2). Dynamic genomes differ not only in terms of extensive intra- and interspecific variation in genome content and structure but also in genome processing (e.g., DNA elimination and reorganization). Genome rearrangements occur in a variety of eukaryotic cells and serve as an important mechanism for generating genomic diversity. For example, the switching of variant surface glycoprotein (VSG) to generate antigenic variation in *Trypanosoma brucei* occurs in part by DNA rearrangements involving >1,000 VSG genes (3). Similarly, recombination of V(D)J regions generates diversity in immunoglobulins in humans and other vertebrates (4). Moreover, different chromosomal rearrangements of the supergene locus *P*, which contains a cluster of several genes that control different aspects of wing patterning, result in various wing pattern morphs in the polymorphic mimetic butterfly *Heliconius numata* (5). Finally, rearrangements of a single locus underlie the expression of seven mating types in *Tetrahymena thermophila* (6). Here, mating type is determined through a stochastic process in which the macronuclear copy of the mating gene is alternatively assembled from sequences in the micronuclear mating type locus (6).

Although developmentally regulated chromosome rearrangement occurs in a variety of eukaryotes, genome rearrangements may be most pronounced in ciliates. Ciliates are a very diverse

clade of microbial eukaryotes that segregate germ line and somatic functions into two types of nuclei with distinct genome structures: the diploid micronucleus (germ line) and the polyploid macronucleus (soma). Micronuclei and macronuclei differentiate from a genetically novel zygotic nucleus following sexual conjugation. The new zygotic nucleus divides by mitosis. The two descendant nuclei then take on distinct roles, with one developing into a germ line micronucleus and the other into a somatic macronucleus. During development, the macronuclear genome is transformed through a series of chromosomal rearrangements, including fragmentation, DNA elimination, and DNA amplification (7–15).

The types of DNA elimination during macronuclear development are quite diverse, both within a given ciliate species and among different ciliates (9, 12). Precise excision of internal eliminated sequences (IESs) occurs in *Paramecium*, *Oxytricha*, and *Chilodonella*. A more complex form of genome reorganization (termed gene scrambling) is observed in some ciliates, such as *Chilodonella*, *Oxytricha*, and other stichotrichous ciliates: not only must IESs be removed, but also the intervening macronucleus-destined sequences (MDSs) must be reordered. Gene scrambling has been well characterized in genes encoding actin I, telomere end-binding protein subunit α, and DNA polymerase α in spirotrichs (16–19) and actin and β-tubulins in *Chilodonella uncinata* (20).

The mechanism underlying gene scrambling is not well understood, but MDS boundary motifs, macronuclear RNA templates and small RNAs appear to be important. First, splicing appears to involve homologous recombination between pairs of identical short sequence motifs (called pointers) at the 3′ end of one MDS and the 5′ end of the subsequent MDS (15, 21). Second, RNA transcripts from the parental macronucleus have important roles in guiding creation of new macronuclear chromosomes, and small RNAs determine which sequences to retain in the macronucleus (22, 23). These transcripts serve as templates for splicing and also have a role in proofreading of spliced DNAs (24). The importance of the parental macronuclear genome for development of the new somatic genome is underscored by two observations. First, introducing novel chromosomal sequences in the form of new templates into the macronucleus leads to the presence of these novel chromosomal arrangements in the macronucleus in subsequent generations (9, 24, 25). Second, a high frequency of aberrant nanochromosomes appears to be created in the process of macronuclear creation; however, these aberrant nanochromosomes are not found in the mature macronucleus, indicating that they are discarded and/or corrected by a proofreading mechanism (26). Thus, the presence/absence of a sequence in the preceding macronucleus promotes presence/absence in the new macronucleus.

A previous study on the ciliate *Chilodonella uncinata* revealed a highly complex form of chromosome rearrangement, in which some micronuclear segments are used to generate multiple macronuclear sequences (20), a process called alternative processing. For example, the macronuclear β-tubulin genes P1 and P2 are assembled by alternative processing of several micronuclear loci: MIC P1, MIC P2, and MIC SP1 (20). Previous analyses of transcriptome data revealed more than 100 candidate alternatively processed gene families, indicating that alternative processing may be extensive among gene families within *C. uncinata* (27). Alternative processing in the spirotrichous ciliate *Oxytricha trifallax* was subsequently reported (26, 28, 29).

In the present study, we explored two gene families that were previously identified as possibly alternatively processed on the basis of transcriptome data (27, 30): that encoding histidine acid phosphatase family protein (*Hap*) and that encoding leishmanolysin family protein (*Lei*). *Hap* encodes a member of a large functionally diverse group of proteins that play key roles in such varied biological processes as metabolism, development, and intracellular signaling (31). Leishmanolysin was identified as an important virulence factor that was found in the parasite *Leishmania*, where it contributes to a variety of functions allowing host immune evasion (32, 33). The function of these genes in ciliates is as yet unknown. We found that both gene families have three macronuclear copies that are marked by patterns of regions of identity intermingled with divergent regions. We characterized the micronuclear *Hap* sequences, which revealed a complex pattern of alternative processing to produce the three macronuclear sequences. We propose a model in which alternative processing of duplicated micronuclear sequences represents an intermediate stage in the evolution of scrambled genes. Finally, we speculate on the possibility that alternative processing can contribute to high rates of speciation in ciliates.

RESULTS

***Hap* and *Lei* have multiple macronuclear sequences marked by alternating regions of nucleotide divergence and identity.** We identified three macronuclear sequences for both *Hap* (Acc. no. KJ000273-KJ000278) and *Lei* genes (see Table S1 in the supplemental material). For each gene family, comparison between different macronuclear sequences revealed a combination of identical and diverged sequences (Fig. 1). For the *Hap* genes, comparison of two macronuclear sequences (termed MAC P1 and MAC P2) showed three identical regions (indicated by a π value of 0) (Fig. 1) alternating with more divergent regions. Comparison between MAC P1 and the third sequence (MAC P3) also showed three identical regions, but these regions were in different locations (Fig. 1A). For the *Lei* gene, MAC P1 and MAC P2 share four identical regions alternating with more divergent regions, while MAC P1 and MAC P3 share five identical regions with some varying boundaries as compared to MAC P2 (Fig. 1B).

We sought to time the duplication events that led to the different macronuclear sequences relative to the divergence of the Pol and USA strains (Fig. 1C and D). We found that there was more nucleotide divergence between different macronuclear sequences than there was between the two strains' copies of the same macronuclear sequence (see Fig. S1 and S2 in the supplemental material), indicating that for both gene families the duplication events predate the divergence between the strains.

Macronuclear *Hap* sequences are assembled from alternatively processed MDSs from a single micronuclear locus containing duplicated *Hap* genes. To assess the processing between the germ line micronucleus and somatic macronucleus, we used traditional PCR to characterize the micronuclear sequences of *Hap* genes for the Pol strain (ca. 3.6 kb in length) (Fig. 2), using a MAC P2-specific forward primer and a shared reverse primer. This revealed a single micronuclear locus containing three duplicated *Hap* gene sequences. Based on the comparison with the macronuclear sequences, we term these P2 specific (blue in Fig. 2), P3 specific (purple in Fig. 2), and shared (black in Fig. 2).

Comparison of micronuclear and macronuclear sequences of *Hap* gene revealed a complex pattern of alternative processing and gene scrambling. Pointer sequences ranging from 4 to 8 bp were

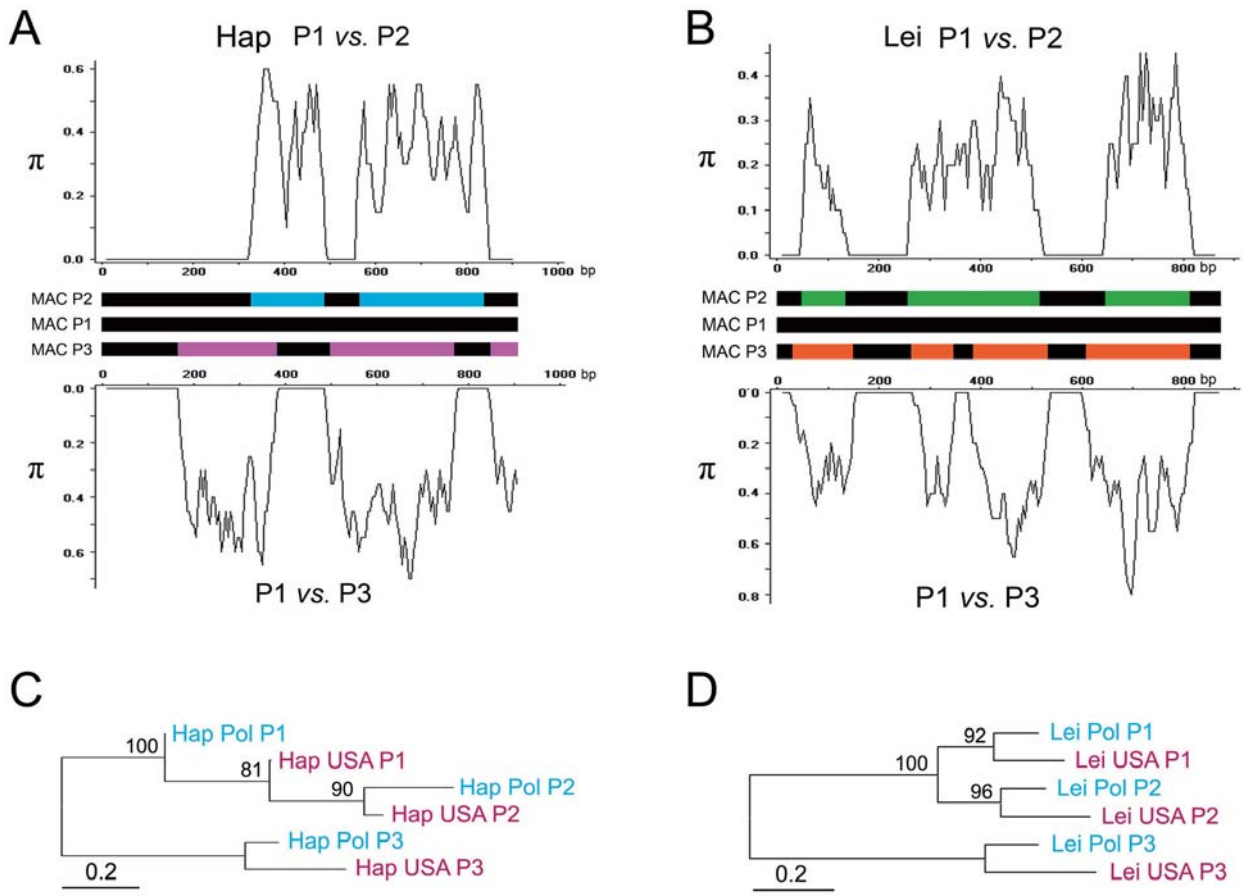

FIG 1 Sequence comparisons among gene family members of *Hap* (A) and *Lei* (B) and genealogies of gene family members from Pol and USA strains for *Hap* (C) and *Lei* (D). (A and B) Graphs are sliding-window analyses of pairwise divergence (π) calculated using DnaSP (59). The top comparison is of macronuclear (MAC) P1 and P2, and the bottom comparison is of MAC P1 and P3. Regions in black at identical positions correspond to shared sequences. (C and D) Topologies were estimated by PhyML (58) as implemented in SeaView (57). Numbers at nodes represent the bootstrap values of maximum likelihood analysis out of 1,000 replicates. Scale bars show substitutions per site.

found at the boundaries of MDSs and IESs (Table 1), supporting the alternative processing of *Hap* gene. The MAC P1 has the simplest pattern and is made up of four MDSs that are located sequentially in a single micronuclear copy (shared) and are separated by three rapidly evolving IESs (see Fig. S3 in the supplemental material). In contrast, both MAC P2 and P3 are scrambled in the micronucleus and are generated by combination of interdigitated sequences from the single micronuclear region. MAC P2 contains sequence from both the shared and P2-specific copies: interestingly, two of the shared MDSs found in MAC P1 are also found in MAC P2 (first and fourth), whereas the other two (second and third) undergo alternative processing with P2-specific sequences. MAC P3 is generated from the shared sequence and yet another sequence (P3 specific) and is more complex yet: (i) no full MDS is shared with either MAC P1 or MAC P2, with only partial shared MDSs being present, and (ii) three of the five P3-specific MDSs are present in the opposite orientation (i.e., on the reverse strand).

We used information on the structure of *Hap* in the Pol micronuclear sequence to design USA-specific primers for characterizing micronuclear copies in this strain. The organization of the USA micronuclear sequence shows a structure similar to that of Pol, except that the fourth MDS of MAC P3 is divided into two MDSs by a 35-bp IES (see Fig. S4 in the supplemental material), implying that this IES was either gained in the USA strain or lost in the Pol strain. The pointer sequences in the USA strain range from 2 to 8 bp, with some MDS-IES junction shifts compared to the Pol strain (Table 1; also, see Table S2 and Fig. S3 in the supplemental material).

Using a similar approach, we were not able to characterize the micronuclear copy(ies) corresponding to the *Lei* gene. Walking PCR for the *Lei* gene yielded sequences that are identical to the macronuclear sequences, indicating that the primers are interrupted by IESs in the micronucleus (we had macronuclear contamination in our micronuclear preps), the gene is highly fragmented or scrambled, and/or the region we characterized does not contain IESs in the micronucleus.

DISCUSSION

This study of two gene families in two strains of the ciliate morphospecies *C. uncinata* leads to three main insights: (i) macronuclear *Hap* and *Lei* gene family members show a combination of regions of identity and highly divergent regions that are suggestive of alternative processing; (ii) the three macronuclear *Hap* members are generated by alternative processing of a single micronuclear region that contains duplicated and decayed *Hap* genes; and (iii) alternative processing is more complex than previously be-

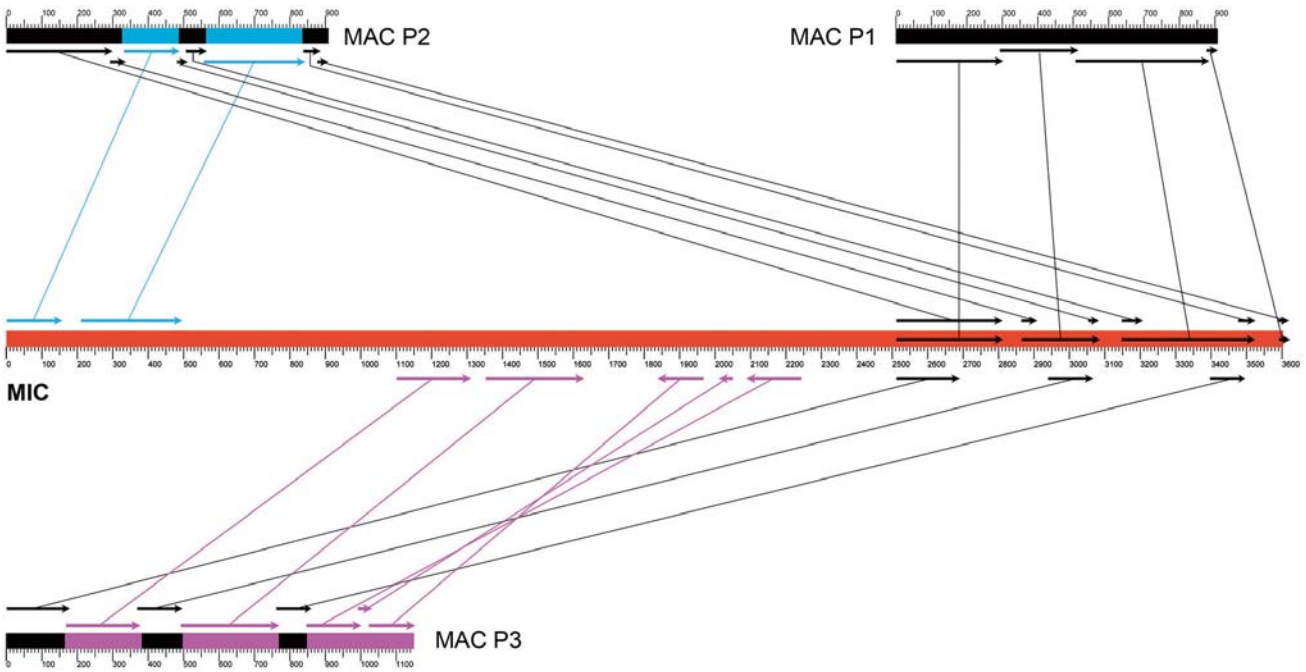

FIG 2 Schematic maps of the somatic and corresponding germ line sequences of *Hap*. The three diverse *Hap* genes are alternatively spliced together from a single micronuclear locus. Colors correspond to macronuclear loci in Fig. 1. MDSs for each macronuclear locus are marked with arrows, and their corresponding sites in the micronuclear locus are also indicated with the same arrows linked with lines. The directions of the arrows indicate the sequence directions in the macronuclear locus.

lieved, as the sharing of micronuclear regions can vary in generating macronuclear products. Drawing on these findings, we hypothesize that alternative processing of duplicated micronuclear sequences may be an intermediate step in the evolution of gene scrambling and may play a role in speciation in ciliates.

Complex processing of Hap and Lei gene family members. Sliding-window analyses of divergence among *Hap* and *Lei* gene family members revealed stretches of identity nested within highly divergent regions. The identical regions are flanked by highly divergent stretches where pairwise differences (π) can be up to 0.60 (*Hap*) or 0.80 (*Lei*), values that are likely underestimates due to multiple hits/saturation (Fig. 1). Previous studies of β-tubulin and protein kinase domain-containing gene families in *C. uncinata* showed similar patterns, with islands of identity within highly divergent macronuclear gene family members (20, 27).

TABLE 1 Characteristics of pointers of the *Hap* gene family from strain Pol of *C. uncinata*

Pointer	Sequence	Start and end	Haplotype(s)
1	TGACAAC	2786-2792/2846-2852	P1/P2
2	CAGAAAC	3059-3065/3130-3136	P1/P2
3	TACCCAAG	3499-3506/3572-3579	P1/P2
4	GATCTTC	133-139/3035-3041	P2
5	AAGATGGA	3182-3189/191-198	P2
6	TTTGCTT	471-476/3458-3464	P2
7	GGTTGCA	2663-2669/1083-1089	P3
8	AGAA	1286-1289/2926-2929	P3
9	GAAACC	3045-3050/1333-1338	P3
10	TCACT	1607-1611/3384-3388	P3
11	TTCG	3466-3469/2223-2220	P3
12	ATTCAAA	2078-2072/2031-2025	P3
13	CCAGAAAG	2002-1995/1949-1942	P3

Analyses of the transcriptome data from *C. uncinata* Pol strain revealed more than 100 gene families that also show similar patterns, suggesting that alternative processing could be common (27).

Three macronuclear *Hap* members are generated by alternative processing of a single micronuclear region that contains duplicated and decayed *Hap* genes. Several lines of evidence support this conclusion: (i) the sharing of identical regions among macronuclear sequences; (ii) the recovery of only one micronuclear sequence containing regions identical to all regions of the macronuclear *Hap* genes; (iii) the presence of pointer sequences at appropriate locations between the micronuclear regions that need to be joined to form macronuclear sequences; and (iv) the fact that the two strains of *C. uncinata* show the same alternative processing patterns. Based on the pattern observed here, we hypothesize that the original *Hap* gene duplicated twice, followed by decay of some of the coding regions and subsequent replacement by recombination of intact homologous regions during macronuclear development (see cartoons in Fig. 3 and 4). The processing of the *Hap* micronuclear locus leads to the three alternatively processed macronuclear sequences in which identical macronuclear regions come from shared micronuclear regions.

Alternative processing is more complex than previously believed, as the sharing of micronuclear regions can vary in generating macronuclear products. Our *Hap* MIC locus adds to the list of alternatively processed genes in *C. uncinata*, which includes β-tubulin gene family (20) and a protein kinase domain containing protein (PKc) gene family (27). Previous analyses of the β-tubulin gene family showed that two members, MAC P1 and MAC P2, are generated using the same alternatively processed MIC SP1 regions (20). The analyses of the PKc gene family also

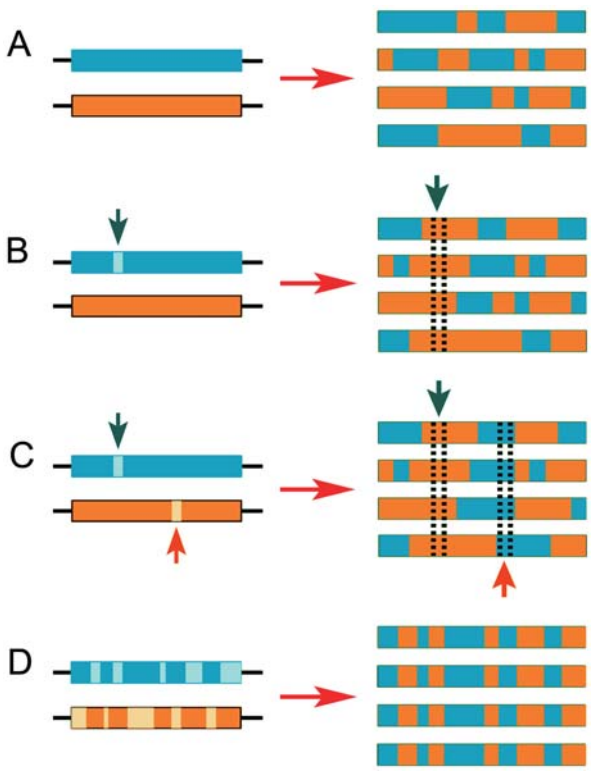

FIG 3 Model for the origins of scrambled micronuclear genes. (A) Following an initial micronuclear duplication, DNA splicing could use a variety of sequences as pointers, leading to identical spliced molecules deriving from various combinations of the two micronuclear duplicates. Blue and orange boxes on the left indicate the two duplicates. Mixed blue/orange boxes on the right indicate various spliced DNAs generated by using a variety of spliced sites. (B) Due to RNA template proofreading, a mutation in one duplicate (arrow) leads to the mutated region becoming restricted to the micronucleus (light color), leading to constitutive usage of sequence from the nonmutated duplicate at that site (all spliced DNAs use orange in the mutated region). (C) A second mutation in the other duplicate leads to constitutive usage of sequence from the other (blue) duplicate at a second site. (D) Accumulation of mutations in the duplicates leads to a scrambled gene.

showed that the shared identical regions are processed using the same MIC regions (27). The present study of *Hap* gene revealed a different pattern in that *Hap* macronuclear gene family members MAC P2 and MAC P3 are generated using different alternatively processed (i.e., shared) MIC P1 regions. This complex pattern of sharing indicates that there must be a controlled and precise rearrangement mechanism to guide the macronucleus-destined sequences into the correct linear order and orientation, as has been found in other ciliates (24, 34).

On the origins and consequences of genome scrambling. Our analyses of patterns among *Hap* and *Lei* gene family members leads to a model on the evolution of gene scrambling whereby duplication of micronuclear regions is followed by a transient period of alternative processing, which is later resolved as gene scrambling (Fig. 3 and 4). The cases of alternative processing reported here and elsewhere (20, 27, 29, 35) share the observation that macronuclear gene family members are generated by recombination between duplicated micronuclear sequences. Such a system may arise through constructive neutral evolution (36, 37), though we recognize the challenges of disentangling the evolutionary forces (e.g., genetic drift and natural selection) at play in the origin of this system (38–42). Hence, we focus on the role of gene duplication in enabling the evolution of alternative processing and, ultimately, gene scrambling.

Following duplication of micronuclear regions, the existence of long stretches of identical sequences provides redundancy in the pointer pairs that direct rearrangements during macronuclear development (Fig. 3A). Alternative usage of various combinations of these nascent pointers could lead to production of macronuclear sequences from diverse combinations of the micronuclear duplicates. Over time, the redundancy in pointer sequences and duplicated coding regions could allow an inactivating mutation in a region of one duplicate to become fixed with no negative fitness effect (i.e., decay) (Fig. 3B). Such mutated regions could be excluded from the macronucleus by scanning during macronuclear development, which ensures that sequences in the newly formed macronucleus reflect those in the previous macronucleus (34, 43, 44); thus, a mutated region of one duplicate could become restricted to the micronucleus. A similar inactivating mutation in the other duplicate could then lead to restriction of that region to the micronucleus, at which point all functional macronuclear regions would be assembled from multiple micronuclear sequences, constituting a newly scrambled gene (Fig. 3C). Further mutations could eventually lead to a pattern of nearly complete reciprocal degradation, with the pointer sequences representing the only remaining regions of sequence redundancy (Fig. 3D). For instance an inactivating mutation within remaining paralogous regions in the black duplicate on the right of Fig. 2 would abolish MAC P1, in which case all remaining macronuclear sequences would be the result of scrambling.

In this scenario, alternative processing could represent a transient stage on the road to full gene scrambling (Fig. 4). This model mirrors classic duplicate gene pseudogenization (45, 46), in which one of a pair of duplicate genes degrades by mutation, though in the case of alternative processing in ciliates, different regions of the duplicates could reciprocally degrade. Another possibility is that some parts of the duplicated gene could be retained in duplicate due to evolution of new functions (neofunctionalization) or partitioning of ancestral functions between the two regions (subfunctionalization) (45, 46). In this case, alternative processing could be evolutionarily stable, with further degradation opposed by purifying selection. In the examples reported here, the persistence of some gene regions in duplicates despite significant sequence divergence suggests that purifying selection is acting to oppose inactivating regions, and thus that they are not simply functionally redundant.

We further speculate that our model of differential degradation of duplicates leading to gene scrambling may provide a mechanism for speciation in ciliates (Fig. 4). If the degradation of regions occurs multiple times in subdivided populations, then this could create a barrier to successful reproduction between resulting strains as offspring between such crosses would not be capable of generating functional gene family members (Fig. 4D and E). In other words, differing patterns of alternative processing of scrambled "options" in subdivided populations would lead to incompatibility in subsequent matings between members, resulting in incipient species. In this scenario, it is possible that reproductive barriers may occur more rapidly than predicted by the accumulation of point mutations, which would explain the disconnect between the rates of morphological and molecular evolution that underlie ciliate species (47–55).

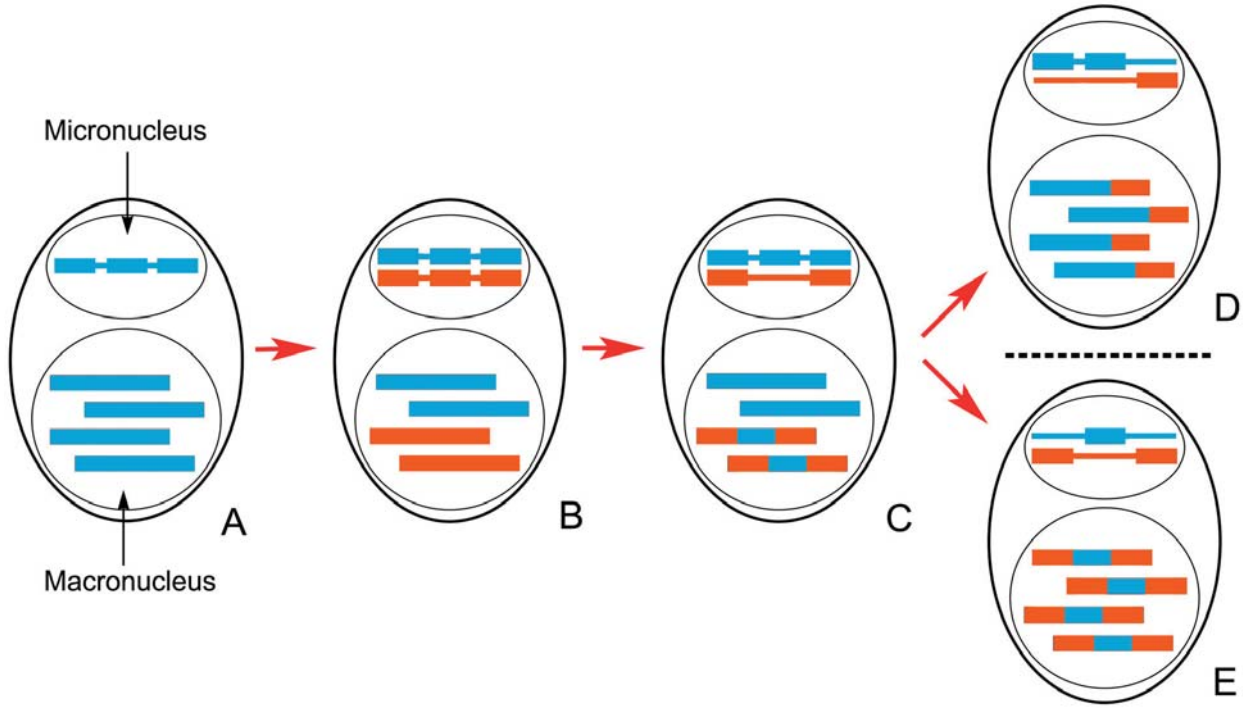

FIG 4 Genome architecture drives evolution in ciliates, resulting in gene scrambling and perhaps even speciation. (A) Each ciliate contains a germ line micronucleus with a canonical eukaryotic genome and a somatic macronucleus represented by a large polyploid nucleus. A single gene with IESs is shown in the micronucleus, and multiple copies of the processed gene are present in the macronucleus. (B) The gene duplicates in the micronucleus followed by divergence, and both copies are processed during macronuclear development. (C) A coding region in the micronucleus degrades and is replaced by recombination of homologous regions from the intact copy, leading to alternatively processed macronuclear chromosomes. Further decay can happen, so that no duplicate homologous regions remain and only one haplotype will be generated during macronuclear development, resulting in gene scrambling. (D and E) Populations that become fixed for different scrambling "options" may become incompatible (i.e., incipient species).

MATERIALS AND METHODS

Ciliate culturing and DNA extraction. We maintained two previously characterized cryptic species (referred to here as strains, as they have not been described formally) of the ciliate morphospecies *C. uncinata*, Pol (ATCC PRA-256) and USA-Sc2, following protocols described by Katz et al. (48). To isolate total DNA, cultures were treated overnight with penicillin-streptomycin-amphotericin B (17-745 H; Lonza, Allendale, NJ), and cells were pelleted by spinning at 5,000 rpm for 20 min. Genomic DNA was extracted using phenol-chloroform following standard protocols (56). Micronuclear DNA was isolated according to Katz and Kovner (20). Briefly, micronuclear DNA was gel isolated by gel electrophoresis using low-melting-point UltraClean agarose (15005-50; Mobio, Carlsbad, CA) after digestion with Bal 31 nuclease (M02135; New England Biolabs, Ispwich, MA) to enrich micronuclear DNA. Gel-isolated micronuclear DNA was purified using β-agarase (M03925; New England Biolabs).

Traditional PCR and cloning. We chose two gene families, encoding histidine acid phosphatase family protein (*Hap*) and leishmanolysin family protein (*Lei*), for which multiple RNA transcripts sharing some sequences are present in the assembled *C. uncinata* transcriptome. Primers for both *Hap* and *Lei* genes were designed from these shared regions. The primers were then used on two *C. uncinata* strains, Pol and USA, to amplify the macronuclear sequences. Haplotype-specific primers were designed to amplify the micronuclear sequences. PCR was performed using Phusion Hot Start high-fidelity DNA polymerase (F 540 L; Finnzymes, Finland). Amplified products were cloned using Zero Blunt TOPO kits (K2800; Invitrogen, CA), and screened using the polymerase TaqGold (Applied Biosystems, CA).

Genome walking PCR and cloning. We used Seegene's DNA walking SpeedUp kit (K1052; Seegene, Rockville, MD) to amplify additional regions of *Lei*. PCR amplification was performed following Seegene kit protocol using kit primers and gene-specific primers designed for this study. Genome walking PCR products were cloned using TA TOPO cloning kits (45-0641; Invitrogen) and screened using the polymerase TaqGold (Applied Biosystems, CA).

Sequencing and data analysis. Sequences were generated using the BigDye terminator v3.1 cycle sequencing kit (no. 4337455) from PE Applied Biosystems (Wellesley, MA). Reaction products were cleaned using gel filtration columns (no. 42453) from Edge Biosystems (Gaithersburg, MD) and analyzed on a PerkinElmer ABI-3100 automated sequencer at the Center for Molecular Biology (Smith College, Northampton, MA). Contigs were assembled in SeqMan (DNASTAR), and all polymorphisms were confirmed by eye. SeaView v. 4.2.4 (57) and MegAlign (DNASTAR) were used to create alignments. Genealogies based on nucleotide alignments were estimated using PhyML (58) as implemented in SeaView v. 4.2.4 with the model GTR+gamma. DnaSP (59) was used to perform sliding-window analysis to calculate average pairwise differences (π). Sliding-window analyses were performed with a 20-bp window and a 5-bp step.

Nucleotide sequence accession numbers. The macronuclear sequences for *Lei* genes have been deposited in GenBank database under accession no. KJ000279 to KJ000284. The micronuclear sequence of *Hap* genes for the Pol strain has been deposited under accession no. KJ626297. The micronuclear sequence of *Hap* genes for the USA strain has been deposited under accession no. KJ626298.

SUPPLEMENTAL MATERIAL

Supplemental material for this article may be found at http://mbio.asm.org/lookup/suppl/doi:10.1128/mBio.01998-14/-/DCSupplemental.

Figure S1, PDF file, 0.5 MB.

Figure S2, PDF file, 0.1 MB.
Figure S3, PDF file, 0.3 MB.
Figure S4, PDF file, 1.2 MB.
Table S1, PDF file, 0.04 MB.
Table S2, PDF file, 0.05 MB.

ACKNOWLEDGMENT

This work was supported by the AREA award from the National Institutes of Health (1R15GM097722) to L.A.K.

REFERENCES

1. **Parfrey LW, Lahr DJ, Katz LA.** 2008. The dynamic nature of eukaryotic genomes. Mol Biol Evol **25:**787–794. http://dx.doi.org/10.1093/molbev/msn032.
2. **Zufall RA, Robinson T, Katz LA.** 2005. Evolution of developmentally regulated genome rearrangements in eukaryotes. J Exp Zool B Mol Dev Evol **304:**448–455. http://dx.doi.org/10.1002/jez.b.21056.
3. **Stockdale C, Swiderski MR, Barry JD, McCulloch R.** 2008. Antigenic variation in *Trypanosoma brucei*: joining the DOTs. PLoS Biol **6:**e185. http://dx.doi.org/10.1371/journal.pbio.0060185.
4. **Nemazee D.** 2006. Receptor editing in lymphocyte development and central tolerance. Nat Rev Immunol **6:**728–740. http://dx.doi.org/10.1038/nri1939.
5. **Joron M, Frezal L, Jones RT, Chamberlain NL, Lee SF, Haag CR, Whibley A, Becuwe M, Baxter SW, Ferguson L, Wilkinson PA, Salazar C, Davidson C, Clark R, Quail MA, Beasley H, Glithero R, Lloyd C, Sims S, Jones MC, Rogers J, Jiggins CD, ffrench-Constant RH.** 2011. Chromosomal rearrangements maintain a polymorphic supergene controlling butterfly mimicry. Nature **477:**203–206. http://dx.doi.org/10.1038/nature10341.
6. **Cervantes MD, Hamilton EP, Xiong J, Lawson MJ, Yuan D, Hadjithomas M, Miao W, Orias E.** 2013. Selecting one of several mating types through gene segment joining and deletion in *Tetrahymena thermophila*. PLoS Biol **11:**e1001518. http://dx.doi.org/10.1371/journal.pbio.1001518.
7. **Heyse G, Jönsson F, Chang WJ, Lipps HJ.** 2010. RNA-dependent control of gene amplification. Proc Natl Acad Sci U S A **107:**22134–22139. http://dx.doi.org/10.1073/pnas.1009284107.
8. **Katz LA, Lasek-Nesselquist E, Snoeyenbos-West OL.** 2003. Structure of the micronuclear alpha-tubulin gene in the phyllopharyngean ciliate *Chilodonella uncinata*: implications for the evolution of chromosomal processing. Gene **315:**15–19. http://dx.doi.org/10.1016/j.gene.2003.08.003.
9. **Nowacki M, Shetty K, Landweber LF.** 2011. RNA-mediated epigenetic programming of genome rearrangements. Annu Rev Genomics Hum Genet **12:**367–389. http://dx.doi.org/10.1146/annurev-genom-082410-101420.
10. **Goldman AD, Landweber LF.** 2012. *Oxytricha* as a modern analog of ancient genome evolution. Trends Genet **28:**382–388. http://dx.doi.org/10.1016/j.tig.2012.03.010.
11. **Katz LA.** 2001. Evolution of nuclear dualism in ciliates: a reanalysis in light of recent molecular data. Int J Syst Evol Microbiol **51:**1587–1592.
12. **Chalker DL, Yao MC.** 2011. DNA elimination in ciliates: transposon domestication and genome surveillance. Annu Rev Genet **45:**227–246. http://dx.doi.org/10.1146/annurev-genet-110410-132432.
13. **Riley JL, Katz LA.** 2001. Widespread distribution of extensive chromosomal fragmentation in ciliates. Mol Biol Evol **18:**1372–1377. http://dx.doi.org/10.1093/oxfordjournals.molbev.a003921.
14. **Chalker DL.** 2008. Dynamic nuclear reorganization during genome remodeling of *Tetrahymena*. Biochim Biophys Acta **1783:**2130–2136. http://dx.doi.org/10.1016/j.bbamcr.2008.07.012.
15. **Prescott DM.** 1994. The DNA of ciliated protozoa. Microbiol Rev **58:**233–267.
16. **Landweber LF, Kuo TC, Curtis EA.** 2000. Evolution and assembly of an extremely scrambled gene. Proc Natl Acad Sci U S A **97:**3298–3303. http://dx.doi.org/10.1073/pnas.040574697.
17. **Mitcham JL, Lynn AJ, Prescott DM.** 1992. Analysis of a scrambled gene: the gene encoding alpha-telomere-binding protein in *Oxytricha nova*. Genes Dev **6:**788–800. http://dx.doi.org/10.1101/gad.6.5.788.
18. **Chang WJ, Kuo S, Landweber LF.** 2006. A new scrambled gene in the ciliate *Uroleptus*. Gene **368:**72–77. http://dx.doi.org/10.1016/j.gene.2005.10.008.
19. **Prescott DM, Greslin AF.** 1992. Scrambled actin I gene in the micronucleus of *Oxytricha nova*. Dev Genet **13:**66–74. http://dx.doi.org/10.1002/dvg.1020130111.
20. **Katz LA, Kovner AM.** 2010. Alternative processing of scrambled genes generates protein diversity in the ciliate *Chilodonella uncinata*. J Exp Zool B Mol Dev Evol **314:**480–488. http://dx.doi.org/10.1002/jez.b.21354.
21. **DuBois ML, Prescott DM.** 1997. Volatility of internal eliminated segments in germ line genes of hypotrichous ciliates. Mol Cell Biol **17:**326–337.
22. **Fang W, Wang X, Bracht JR, Nowacki M, Landweber LF.** 2012. Piwi-interacting RNAs protect DNA against loss during *Oxytricha* genome rearrangement. Cell **151:**1243–1255. http://dx.doi.org/10.1016/j.cell.2012.10.045.
23. **Zahler AM, Neeb ZT, Lin A, Katzman S.** 2012. Mating of the stichotrichous ciliate *Oxytricha trifallax* induces production of a class of 27 nt small RNAs derived from the parental macronucleus. PLoS One **7:**e42371. http://dx.doi.org/10.1371/journal.pone.0042371.
24. **Nowacki M, Vijayan V, Zhou Y, Schotanus K, Doak TG, Landweber LF.** 2008. RNA-mediated epigenetic programming of a genome-rearrangement pathway. Nature **451:**153–158. http://dx.doi.org/10.1038/nature06452.
25. **Nowacki M, Landweber LF.** 2009. Epigenetic inheritance in ciliates. Curr Opin Microbiol **12:**638–643. http://dx.doi.org/10.1016/j.mib.2009.09.012.
26. **Möllenbeck M, Zhou Y, Cavalcanti AR, Jönsson F, Higgins BP, Chang WJ, Juranek S, Doak TG, Rozenberg G, Lipps HJ, Landweber LF.** 2008. The pathway to detangle a scrambled gene. PLoS One **3:**e2330. http://dx.doi.org/10.1371/journal.pone.0002330.
27. **Gao F, Song W, Katz LA.** 2014. Genome structure drives patterns of gene family evolution in ciliates, a case study using *Chilodonella uncinata* (Protista, Ciliophora, Phyllopharyngea). Evolution **68:**2287–2295. http://dx.doi.org/10.1111/evo.12430.
28. **Zhou Y, Wubneh H, Schwarz C, Landweber LF.** 2011. A chimeric chromosome in the ciliate *Oxytricha* resulting from duplication. J Mol Evol **73:**70–73. http://dx.doi.org/10.1007/s00239-011-9464-1.
29. **Swart EC, Bracht JR, Magrini V, Minx P, Chen X, Zhou Y, Khurana JS, Goldman AD, Nowacki M, Schotanus K, Jung S, Fulton RS, Ly A, McGrath S, Haub K, Wiggins JL, Storton D, Matese JC, Parsons L, Chang WJ, Bowen MS, Stover NA, Jones TA, Eddy SR, Herrick GA, Doak TG, Wilson RK, Mardis ER, Landweber LF.** 2013. The *Oxytricha trifallax* macronuclear genome: a complex eukaryotic genome with 16,000 tiny chromosomes. PLoS Biol **11:**e1001473. http://dx.doi.org/10.1371/journal.pbio.1001473.
30. **Grant JR, Lahr DJG, Rey FE, Burleigh JG, Gordon JI, Knight R, Molestina RE, Katz LA.** 2012. Gene discovery from a pilot study of the transcriptomes from three diverse microbial eukaryotes: *Corallomyxa tenera*, *Chilodonella uncinata*, and *Subulatomonas tetraspora*. Protist Genomics **1:**3–18. http://dx.doi.org/10.2478/prge-2012-0002.
31. **Rigden DJ.** 2008. The histidine phosphatase superfamily: structure and function. Biochem J **409:**333–348. http://dx.doi.org/10.1042/BJ20071097.
32. **Etges R, Bouvier J, Bordier C.** 1986. The major surface protein of *Leishmania promastigotes* is a protease. J Biol Chem **261:**9098–9101.
33. **Bouvier J, Etges RJ, Bordier C.** 1985. Identification and purification of membrane and soluble forms of the major surface protein of *Leishmania promastigotes*. J Biol Chem **260:**15504–15509.
34. **Bracht JR, Fang W, Goldman AD, Dolzhenko E, Stein EM, Landweber LF.** 2013. Genomes on the edge: programmed genome instability in ciliates. Cell **152:**406–416. http://dx.doi.org/10.1016/j.cell.2013.01.005.
35. **Ardell DH, Lozupone CA, Landweber LF.** 2003. Polymorphism, recombination and alternative unscrambling in the DNA polymerase alpha gene of the ciliate *stylonychia lemnae* (Alveolata; class Spirotrichea). Genetics **165:**1761–1777.
36. **Stoltzfus A.** 1999. On the possibility of constructive neutral evolution. J Mol Evol **49:**169–181. http://dx.doi.org/10.1007/PL00006540.
37. **Stoltzfus A.** 2012. Constructive neutral evolution: exploring evolutionary theory's curious disconnect. Biol Direct **7:**35. http://dx.doi.org/10.1186/1745-6150-7-35.
38. **Doolittle WF, Lukes J, Archibald JM, Keeling PJ, Gray MW.** 2011. Comment on "Does constructive neutral evolution play an important role in the origin of cellular complexity?". Bioessays **33:**427–429.
39. **Keeling PJ, Leander BS, Lukes J.** 2010. Constructive neutral evolution cannot explain current kinetoplastid panediting patterns reply. Proc Natl Acad Sci U S A **107:**E26. http://dx.doi.org/10.1073/pnas.0911933107.
40. **Lukeš J, Archibald JM, Keeling PJ, Doolittle WF, Gray MW.** 2011. How

a neutral evolutionary ratchet can build cellular complexity. IUBMB Life **63:**528–537. http://dx.doi.org/10.1002/iub.489.
41. **Speijer D.** 2010. Constructive neutral evolution cannot explain current kinetoplastid panediting patterns. Proc Natl Acad Sci U S A **107:**E25. http://dx.doi.org/10.1073/pnas.0909867107.
42. **Speijer D.** 2011. Does constructive neutral evolution play an important role in the origin of cellular complexity? Making sense of the origins and uses of biological complexity. Bioessays **33:**344–349. http://dx.doi.org/10.1002/bies.201100010.
43. **Chalker DL, Meyer E, Mochizuki K.** 2013. Epigenetics of ciliates. Cold Spring Harb Perspect Biol **5:**a017764. http://dx.doi.org/10.1101/cshperspect.a017764.
44. **Fuhrmann G, Swart E, Nowacki M, Lipps HJ.** 2013. RNA-dependent genome processing during nuclear differentiation: the model systems of stichotrichous ciliates. Epigenomics **5:**229–236. http://dx.doi.org/10.2217/epi.13.15.
45. **Force A, Lynch M, Pickett FB, Amores A, Yan YL, Postlethwait J.** 1999. Preservation of duplicate genes by complementary, degenerative mutations. Genetics **151:**1531–1545.
46. **Lynch M, Conery JS.** 2000. The evolutionary fate and consequences of duplicate genes. Science **290:**1151–1155. http://dx.doi.org/10.1126/science.290.5494.1151.
47. **Gao F, Katz LA, Song W.** 2013. Multigene-based analyses on evolutionary phylogeny of two controversial ciliate orders: Pleuronematida and Loxocephalidae (Protista, Ciliophora, Oligohymenophorea). Mol Phylogenet Evol **68:**55–63. http://dx.doi.org/10.1016/j.ympev.2013.03.018.
48. **Katz LA, DeBerardinis J, Hall MS, Kovner AM, Dunthorn M, Muse SV.** 2011. Heterogeneous rates of molecular evolution among cryptic species of the ciliate morphospecies *Chilodonella uncinata*. J Mol Evol **73:**266–272. http://dx.doi.org/10.1007/s00239-011-9468-x.
49. **Hall MS, Katz LA.** 2011. On the nature of species: insights from *Paramecium* and other ciliates. Genetica **139:**677–684. http://dx.doi.org/10.1007/s10709-011-9571-3.
50. **Simon EM, Nanney DL, Doerder FP.** 2008. The "*Tetrahymena pyriformis*" complex of cryptic species. Biodivers Conserv **17:**365–380. http://dx.doi.org/10.1007/s10531-007-9255-6.
51. **McManus GB, Xu D, Costas BA, Katz LA.** 2010. Genetic identities of cryptic species in the *Strombidium stylifer/apolatum/oculatum* cluster, including a description of *Strombidium rassoulzadegani* n. sp. J Eukaryot Microbiol **57:**369–378. http://dx.doi.org/10.1111/j.1550-7408.2010.00485.x.
52. **Esteban GF, Finlay BJ.** 2003. Cryptic freshwater ciliates in a hypersaline lagoon. Protistologica **154:**411–418. http://dx.doi.org/10.1078/143446103322454149.
53. **Huang J, Chen Z, Song W, Berger H.** 2014. Three-gene based phylogeny of the Urostyloidea (Protista, Ciliophora, Hypotricha), with notes on classification of some core taxa. Mol Phylogenet Evol **70:**337–347. http://dx.doi.org/10.1016/j.ympev.2013.10.005.
54. **Li J, Liu W, Gao S, Warren A, Song W.** 2013. Multigene-based analyses of the phylogenetic evolution of oligotrich ciliates, with consideration of the internal transcribed spacer 2 secondary structure of three systematically ambiguous genera. Eukaryot Cell **12:**430–437. http://dx.doi.org/10.1128/EC.00270-12.
55. **Zhang Q, Yi Z, Fan X, Warren A, Gong J, Song W.** 2014. Further insights into the phylogeny of two ciliate classes Nassophorea and Prostomatea (Protista, Ciliophora). Mol Phylogenet Evol **70:**162–170. http://dx.doi.org/10.1016/j.ympev.2013.09.015.
56. **Ausubel FM, Brent R, Kingston RE, Moore DD, Seidman JG, Smith JA, Struhl K.** 1993. Current protocols in molecular biology. Wiley-Liss, New York, NY.
57. **Gouy M, Guindon S, Gascuel O.** 2010. SeaView version 4: a multiplatform graphical user interface for sequence alignment and phylogenetic tree building. Mol Biol Evol **27:**221–224.
58. **Guindon S, Gascuel O.** 2003. A simple, fast, and accurate algorithm to estimate large phylogenies by maximum likelihood. Syst Biol **52:**696–704. http://dx.doi.org/10.1080/10635150390235520.
59. **Librado P, Rozas J.** 2009. DnaSP V5: a software for comprehensive analysis of DNA polymorphism data. BioInformatics **25:**1451–1452. http://dx.doi.org/10.1093/bioinformatics/btp187.

APTARA | EJI | eji201545860 | Dispatch: October 13, 2015 | CE:
Journal | MSP No. | No. of pages: 13 | PE: XXXXX

Eur. J. Immunol. 2015. 00: 1–13 DOI: 10.1002/eji.201545860 Innate immunity

European Journal of Immunology

Evolutionary conservation of molecular structure and antiviral function of a viral receptor, LGP2, in amphioxus *Branchiostoma japonicum*

Shousheng Liu[1], *Yuanyuan Liu*[1], *Shuangshuang Yang*[1], *Youhua Huang*[2], *Qiwei Qin*[2] *and Shicui Zhang*[1]

[1] Laboratory for Evolution and Development, Department of Marine Biology, Institute of Evolution and Marine Biodiversity, Ocean University of China, Qingdao, China
[2] Key Laboratory of Tropical Marine Bio-resources and Ecology, South China Sea Institute of Oceanology, Chinese Academy of Sciences, Guangzhou, China

RIG-I-like (where RIG-I is retinoic acid inducible gene I) receptor LGP2 (where LGP2 is laboratory of genetics and physiology) is an important intracellular receptor that recognizes viral RNAs in innate immunity, but its origin and evolution remains unknown. Here we clearly demonstrate the presence of a RIG-I-like receptor, BjLGP2, in the basal chordate amphioxus. It is predominantly expressed in the hepatic caecum and hindgut, and is upregulated following challenge with poly(I:C). BjLGP2 is distributed in the cytoplasm of both grouper spleen and flounder gill (FG) cells, and the recombinant BjLGP2 interacts with poly(I:C). BjLGP2 can enhance the expression of IFN and IFN-inducible genes in FG cells upon poly(I:C) challenge. It also significantly induces the expression of the antiviral genes *ifn-i* and *Mx* as well as the signal transduction relevant genes *MAVS*, *NF-κB*, and *IRF-3* in FG cells upon lymphocystis disease virus challenge. Moreover, BjLGP2 inhibits the replication of lymphocystis disease virus in FG cells and the gene transcription of Singapore grouper iridovirus in grouper spleen cells. This is the first report showing that a LGP2 protein in invertebrate species (amphioxus) is structurally conserved and plays an antiviral role similar to that of vertebrate LGP2 proteins.

Keywords: Amphioxus · Antiviral activity · *Branchiostoma* · Lancelet · LGP2

Additional supporting information may be found in the online version of this article at the publisher's web-site

Introduction

The innate immune response of host begins with the recognition of nonself by PRRs that interact with PAMPs, signature molecules associated with groups of pathogens. Four different PRRs families have been identified: TLRs, RNA helicase family of retinoic acid inducible gene I (RIG-I) like receptors (RLRs), NOD-like receptors (NLRs), and C-type lectin receptors (CLRs) [1, 2]. Among them, RLRs in humans consists of three members: RIG-I, melanoma differentiation associated receptor 5 (MDA5), and laboratory of genetics and physiology 2 (LGP2). These receptors possess a central DExD/H-box helicase domain that shows intrinsic RNA binding and ATP hydrolysis functions, and a C-terminal repressor domain (RD) [3, 4]. RIG-I and MDA5 also contain two N-terminal caspase recruitment domains (CARDs) that are essential for mediating interactions with downstream signaling pathway, but LGP2 does not [5, 6]. They are all cytosolic sensors that recognize viral RNA and induce signal transduction, upon binding to exogenous

Correspondence: Dr. Shicui Zhang
e-mail: sczhang@ouc.edu.cn

RNA, via the interaction with the mitochondrial antiviral signaling protein (MAVS or IPS-1), ultimately resulting in NF-κB- and IRF-3-dependent production of type I IFN and proinflammatory cytokines [7].

RLRs have been identified in a variety of vertebrate species, including rabbit [8], duck [9], and many teleost fishes such as zebrafish, Atlantic salmon, grass carp, flounder, rainbow trout, and fathead minnow [10–15]. These orthologues are highly conserved from fish to mammals [16], although they have been evolving in mammals under strong selective pressure probably due to an innate species-specific resistance/susceptibility to diverse viral pathogens [17, 18]. Like their mammalian counterparts, duck and fish RLRs play an important role in the recognition of viral RNA to induce the antiviral activity by the production of IFN-stimulated proteins [9, 13, 19, 20]. Notably, identification and functional characterization of RLRs have so far been exclusively restricted to vertebrates; little information is available regarding invertebrate RLRs. Recently, our search of the completed draft assembly and automated annotation of the Florida amphioxus *Branchiostoma florida* genome database (http://genome.jgi-psf.org//Brafl1/Brafl1.home.html) led to the identification of LGP2 (Protein ID: 249510), MDA5 (Protein ID: 76000), and RIG-I-like receptor (Protein ID: 106572), implicating the presence of a vertebrate-like cytoplasmic viral sensing system in this evolutionarily important animal, a basal chordate. However, functional characterization of RLRs remains completely lacking in amphioxus. In this study, we reports the functional characterization of a member of RLR family, LGP2, from the amphioxus *Branchiostoma japonicum*, designated BjLGP2, highlighting its evolutionary conservation of molecular structure and antiviral function.

Results

Sequence, structure, and phylogeny of amphioxus LGP2

A cDNA fragment of approximately 1748 bp was obtained by PCR. Based on this partial sequence, a fragment of 649 bp was cloned by 5′ RACE, and a fragment of 1061 bp cloned by 3′ RACE. The full-length cDNA of BjLGP2 was obtained by assembling the overlapped cDNA fragments (GenBank accession Number: KR560072). The assembled cDNA was 2751 bp long and contained an opening reading frame (ORF) of 2241 bp, a 5′-untranslated region (UTR) of 159 bp, and a 3′-UTR of 351 bp. The ORF of the cDNA encoded a deduced protein of 746 amino acids with a calculated molecular weight of about 84.6 kDa and an isoelectric point of 6.17. The protein possessed an N-terminal DExD/H-box RNA helicase domain, an intermediate HELICc domain, and a C-terminal RD domain that are all typical of human LGP2 (Fig. 1A). Sequence comparison showed that BjLGP2 was approximately 33.2–35.3% and 34.8–36.3% identical to mammalian and fish counterparts at amino acid level, and the important motifs of LGP2 such as ATP-binding motif, ATPase motif, RNA-binding motif, two

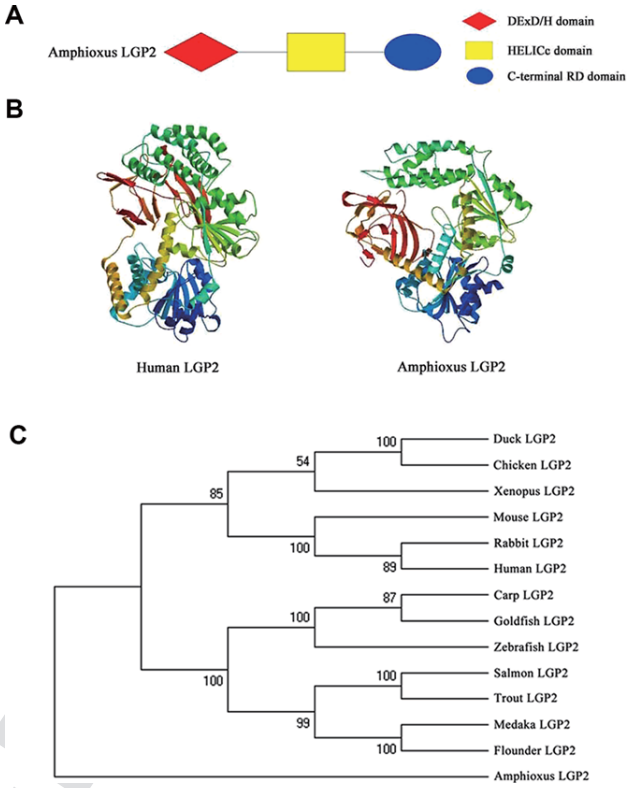

Figure 1. Sequence, predicted 3D structure, and phylogeny of amphioxus LGP2. (A) The domain structure of amphioxus LGP2 predicted by SMART program. (B) The 3D structure of human LGP2 and amphioxus LGP2 generated by SWISS-MODEL online software. (C) The phylogenetic tree constructed with the amino acid sequences of LGP2 proteins available, including BjLGP2, by MEGA (version 5.0) using the neighbor-joining method, and the reliability of each node was estimated by bootstrapping with 1000 replications.

Zn^{2+}-binding motifs, and RNA-binding loop were highly conserved in all LGP2 proteins including BjLGP2 (Supporting Information Fig. 1). Molecular modeling revealed that the 3D structure of BjLGP2 consists of 22 α-helice and 21 β-sheets, which is closely similar to that of human LGP2 containing 23 α-helice and 22 β-sheets (Fig. 1B). Moreover, the phylogenetic tree conducted demonstrated that BjLGP2 was located at the base of vertebrate LGP2 proteins (Fig. 1C), well reflecting the phylogeny of chosen organisms. These data suggest that BjLGP2 may represent the archetype of vertebrate LGP2.

Tissue-specific and poly(I:C)-induced expression of *Bjlgp2*

Expression of *Bjlgp2* in the different tissues of *B. japonicum* was examined by quantitative real-time PCR (qRT-PCR). It was found that BjLGP2 mRNA was predominantly present in the hepatic caecum and hindgut, and at a low level present in the testis and ovary, but it was barely detectable in the gill, notochord, and muscle (Fig. 2A). It is clear that *Bjlgp2* is expressed in a tissue-specific manner.

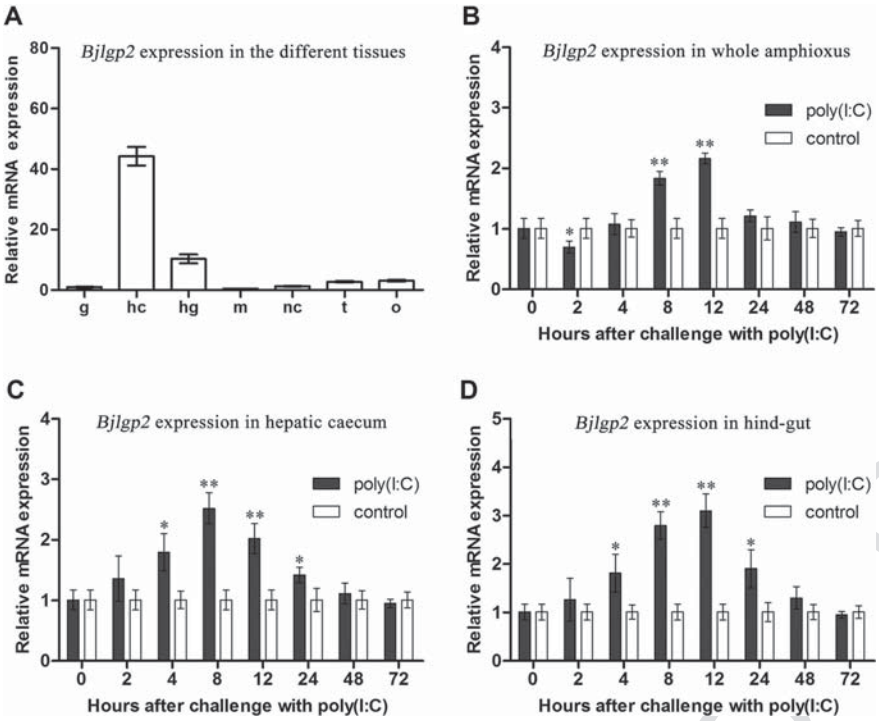

Figure 2. Tissue-specific and poly(I:C)-induced expression of *Bjlgp2*. (A) Total RNA was extracted from various tissues of *B. japonicum*, and the expression profiles of *Bjlgp2* were determined in the different tissues by qRT-PCR. g, gill; hc, hepatic caecum; hg, hindgut; m, muscle; nc, notochord; t, testis; o, ovary. The results shown are mean values ± SD, $n = 3$ replicates per tissue, and are pooled from three experiments. Data were normalized to the EF1α gene as internal control. (B–D) *Branchiostoma japonicum* were sampled at 0, 2, 4, 8, 12, 24, 48, and 72 h after exposure to sterilized seawater containing poly(I:C) (10 μg/mL), or sterilized seawater as a control, and total RNA was extracted from whole animals and the hepatic caecum and hindgut. The expression profiles of *Bjlgp2* were determined by qRT-PCR. The results shown are mean values ± SD, $n = 3$ replicates per group, and are pooled from three experiments per time point. Asterisks indicate statistically different (*$p < 0.05$, **$p < 0.01$) compared to control. Data were normalized to the EF1α gene as internal control. Unpaired Student's *t*-test was used for statistical analysis.

We then examined the effects of poly(I:C) on *Bjlgp2* in the whole amphioxus as well as in the hepatic caecum and hindgut. As shown in Figure 2B, challenge with poly(I:C) induced a temporary decrease in BjLGP2 mRNA in the whole animal at 2 h postchallenge, whereas it caused an increase in BjLGP2 mRNAs at 8–12 h. Similarly, challenge with poly(I:C) also resulted in an upregulation of *Bjlgp2* in the hepatic caecum at 4–8 h and in the hindgut at 4–12 h, followed by a decrease (Fig. 2C and D). The reason for the initial temporary decrease of *Bjlgp2* mRNA in whole amphioxus is not clear at the moment, and may be rather complex. One possible explanation is that the challenge with poly(I:C) induces an immediate response in amphioxus, which leads to quick translation of existing *Bjlgp2* mRNA into protein necessary for the action against poly(I:C), thereby resulting in temporary decrease of *Bjlgp2* mRNA in the whole animal. To test if BjLGP2 mRNA is specifically upregulated by poly(I:C), the effect of LPS on *Bjlgp2* expression was also tested. It was found that challenge with LPS-induced upregulation of BjLGP2 mRNA in amphioxus (Supporting Information Fig. 2), indicating BjLGP2 mRNA was not specifically induced by poly(I:C), consistent with the results reported by [13, 21]. These data together suggest that BjLGP2 may be associated with the immune responses induced by poly(I:C) and LPS as well.

Interaction of rBjLGP2 with poly(I:C)

Recombinant BjLGP2 with the His tag expressed in *Escherichia coli* was purified by chromatography on Ni-NTA resin column. The purified protein rBjLGP2 was analyzed by SDS-PAGE, and yielded a single band of approximately 88.5 kDa (Fig. 3A), corresponding to the expected size. Western blotting showed that rBjLGP2 reacted with anti-His tag Ab, indicating that BjLGP2 was correctly expressed (Fig. 3A).

To determine if rBjLGP2 could bind to poly(I:C), pull-down assays were performed using poly(C) or poly(I:C)-conjugated agarose. As shown in Figure 3B, rBjLGP2 was detected from the poly(I:C)-conjugated agarose, indicating that rBjLGP2 is able to bind to poly(I:C). In addition, the binding of rBjLGP2 to poly(I:C) was partially inhibited by coincubation of poly(I:C)-conjugated agarose with soluble poly(I:C). By contrast, no rBjLGP2 was detected from the poly(C) conjugated agarose or the sample buffer alone (blank control). These show that rBjLGP2 is able to interact with poly(I:C).

Subcellular localization of amphioxus LGP2

Protein subcellular localization is tightly linked to its function. To examine the subcellular localization of amphioxus LGP2, the plasmids *pcDNA3.1/V5/egfp* and *pcDNA3.1/V5/Bjlgp2/egfp* were transfected into grouper spleen (GS) and flounder gill (FG) cells and then cultured for 48 h. As shown in Figure 4, the green fluorescence was observed throughout the cytoplasm of GS and FG cells transfected with *pcDNA3.1/V5/Bjlgp2/egfp*. By contrast, the green fluorescence was seen in both the cytoplasm and nucleus of GS and FG cells transfected with *pcDNA3.1/V5/egfp*. These show that amphioxus LGP2 is distributed in the cytoplasm of GS and FG cells, agreeing with the cytosolic localization of RLRs as viral RNA sensors.

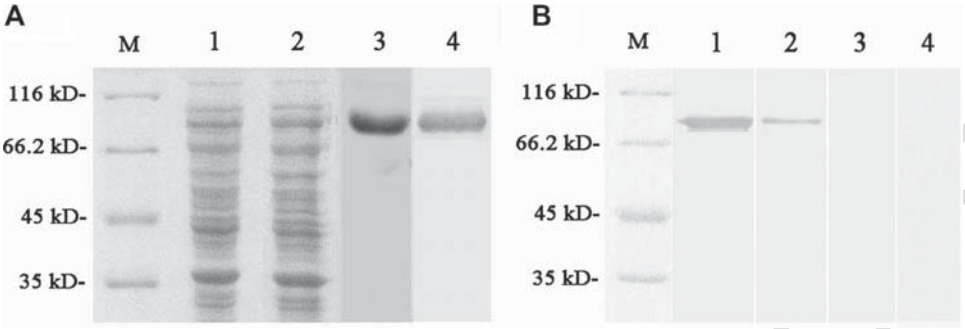

Figure 3. Pull-down assays combined with Western blotting to show the interaction of rBjLGP2 with poly(I:C). (A) *Branchiostoma japonicum* LGP2 was expressed in *E. coli* and purified, the rBjLGP2 was analyzed by 12% SDS-PAGE and identified by Western blotting. Lane M, marker; lane 1, total cellular extracts from *E. coli* transetta (DE3) containing *pET-28a/Bjlgp2* before induction; lane 2, total cellular extracts from IPTG-induced *E. coli* transetta (DE3) containing *pET-28a/Bjlgp2*; lane 3, recombinant BjLGP2 purified on Ni-NTA resin column; lane 4, Western blotting of corresponding purified rBjLGP2 immunostained with anti-His-tag Ab. One representative blot out of three independent experiments is shown. (B) Purified recombinant protein was incubated with poly(C)- or poly(I:C)-conjugated agarose beads. After being washed, the supernatants were subjected to Western blot analysis using anti-His-tag mAb. Competition of poly(I:C) binding to rBjLGP2 was conducted by inclusion of 50 μg/mL soluble poly(I:C) in the reaction. Lane M, marker; lane 1, rBjLGP2 pulled down from poly(I:C)-conjugated agarose; lane 2, rBjLGP2 pulled down from poly(I:C)-conjugated agarose that was coincubated with soluble poly(I:C); lane 3, sample pulled down from poly(C)-conjugated agarose; lane 4, sample buffer for blank control. One representative blot out of three independent experiments is shown.

Upregulation of IFN-I, Mx, ISG15, and ISG56 genes by BjLGP2 upon poly(I:C) challenge

To determine the effects of BjLGP2 on the expression of type I IFN gene and IFN-inducible genes following challenge with poly(I:C), the mixtures consisting of poly(I:C) and *pcDNA3.1/V5-His*, or poly(I:C) and *pcDNA3.1/V5/Bjlgp2*, were solved in Lipofectamine 2000 and transfected into FG cells. Figure 5 shows the expression of *ifn-i*, *Mx*, *ISG15* (where ISG15 is stimulated gene 15), and *ISG56* in the cells at 48 h after transfection. It was found that

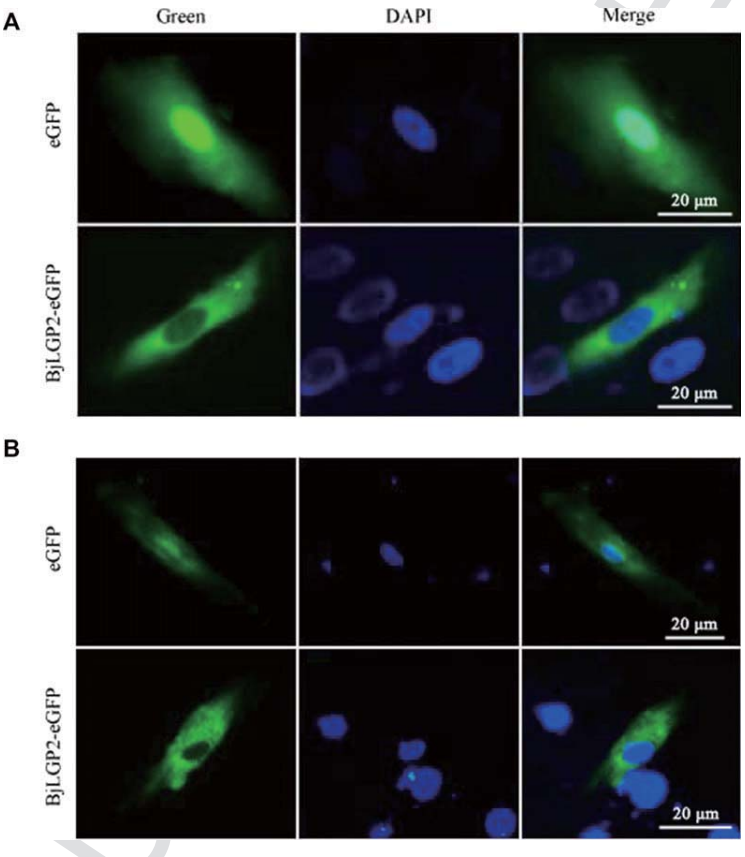

Figure 4. Subcellular localization of BjLGP2 in (A) GS cells and (B) FG cells. The GS cells and FG cells were transiently transfected with *pcDNA3.1/V5/egfp* or *pcDNA3.1/V5/Bjlgp2/egfp*. After 48 h, the cells were imaged by fluorescence microscopy. The nucleus was stained by DAPI. One representative image for each out of three independent experiments is shown. Scale bar: 20 μm.

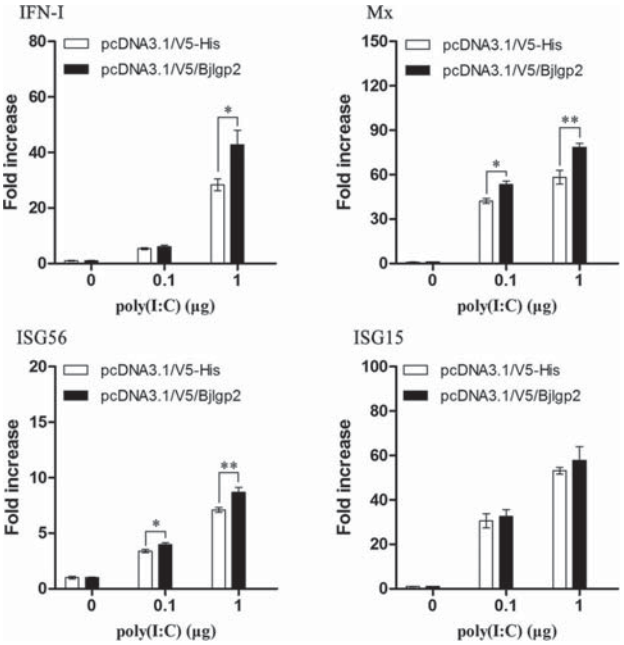

Figure 5. Effects of amphioxus LGP2 on the expression of type I IFN and IFN-inducible genes in FG cells upon poly(I:C) challenge. FG cells were transfected with 1 μg *pcDNA3.1/V5-His* or *pcDNA3.1/V5/Bjlgp2* with 0, 0.1, or 1 μg poly(I:C). Forty-eight hours after transfection, the expression profiles of type I *ifn* (*ifn-i*), *Mx*, *ISG15*, and *ISG56* were measured by qRT-PCR. The flounder β-*actin* gene was chosen as the reference for internal standardization. Gene expression levels are expressed as fold increase values relative to the *pcDNA3.1/V5-His*-transfected cells in the absence of poly(I:C). The data shown are mean values ± SD, $n = 3$ replicates per group, and are pooled from three experiments. Asterisks indicate significant differences of the expression levels between *pcDNA3.1/V5-His*- and *pcDNA3.1/V5/Bjlgp2*-transfected cells in the presence of poly(I:C) ($^*p < 0.05$, $^{**}p < 0.01$). Unpaired Student's *t*-test was used for statistical analysis.

intracellular poly(I:C) induced a conspicuous increase in the expression of *ifn-i*, *Mx*, *ISG15*, and *ISG56* in a dose-dependent manner, and the poly(I:C)-inducing expression of *ifn-i*, *Mx*, and *ISG56* was further increased by BjLGP2 that was expressed in the cells, although the expression of *ISG15* was only slightly upregulated (Fig. 5). These indicate that BjLGP2 is able to enhance the expression of IFN and IFN-inducible genes, including *ifn-i*, *Mx*, and *ISG56*, upon poly(I:C) challenge.

Stimulation of MAVS, NF-κB, IRF-3, IFN-I, and Mx genes by BjLGP2 upon LCDV challenge

The RLR members RIG-I and MDA5 usually induce signal transduction, upon binding to viral RNA, via the interaction with MAVS, and ultimately results in NF-κB- and IRF-3-dependent production of type I IFN and proinflammatory cytokines [7]. To test the effects of BjLGP2 on the expression of MAVS, NF-κB, and IRF-3, type I IFN and Mx genes, upon challenge with virus, the FG cells were transfected with *pcDNA3.1/V5-His* or *pcDNA3.1/V5/Bjlgp2*, and then infected with lymphocystis disease virus (LCDV). Figure 6 shows the expression profiles of *MAVS*, *NF-κB*, *IRF-3*, *ifn-i*, and *Mx* measured by qRT-PCR at 48 h postchallenge. It was found that infection with LCDV induced an increased expression of *MAVS*, *NF-κB*, *IRF-3*, *ifn-i*, and *Mx* genes, and the expression of all the genes was remarkably enhanced by BjLGP2 that was expressed in the cells (Fig. 6). These show that BjLGP2 is able to stimulate the expression of the antiviral genes *ifn-i* and *Mx* as well as the signal transduction relevant genes *MAVS*, *NF-κB*, and *IRF-3*, upon LCDV challenge.

Antiviral activity of amphioxus LGP2

To test if BjLGP2 has any antiviral role, we examined the effects of BjLGP2 on the replication of LCDV in FG cells, and the viral gene transcription of Singapore grouper iridovirus (SGIV) in GS cells. As shown in Figure 7A, the replication of LCDV was significantly inhibited in *pcDNA3.1/V5/Bjlgp2*-transfected FG cells compared to *pcDNA3.1/V5-His*-transfected FG cells, at 48 h and 72 h postinfection with LCDV. Similarly, the viral gene transcripts, as evidenced by *mcp* and *vp16* transcription, were markedly downregulated in *pcDNA3.1/V5/Bjlgp2*-transfected GS cells compared to *pcDNA3.1/V5-His*-transfected GS cells, at 48 h postinfection with SGIV. These show that amphioxus LGP2 is able to inhibit the replication of LCDV and the gene transcription of SGIV, suggesting it has antiviral activity against LCDV and SGIV.

Discussion

Identification and functional characterization of LGP2 have so far been exclusively restricted to vertebrate species [9, 13, 19, 20], and nothing is known regarding invertebrate LGP2 to date. The present study reports the identification, expression, and functional characterization of LGP2 in the amphioxus *B. japonicum*. To our knowledge, this is the first such data in invertebrates. The deduced 746 amino acid long protein, BjLGP2, displays features in common with those in rabbit [8], duck [9], and teleost fishes [10–15]; it is structurally characterized by the presence of an N-terminal DExD/H-box RNA helicase domain with ATP-binding motif and ATPase motif, an intermediate HELICc domain with RNA-binding motif and a C-terminal RD domain with RNA binding loop and two Zn^{2+}-binding motifs. Moreover, the predicted 3D structure of BjLGP2 is highly similar to that of human LGP2 homologue. Additionally, phylogenetic analyses show that BjLGP2 is the archetype of vertebrate LGP2 homologues. All these features implicate a high degree of conservation and essential function of amphioxus LGP2, resembling vertebrate LGP2 proteins.

In flounder, LGP2 gene is highly expressed in the head kidney, which is inducible by poly(I:C) stimulation and VHSV infection [13]. In mammals, LGP2 expression is also induced by poly(I:C) [22]. In accordance, *Bjlgp2* exhibits a tissue-specific expression with abundant expression in the immune-relevant tissues, hepatic caecum, and hindgut, and its expression is remarkably elevated

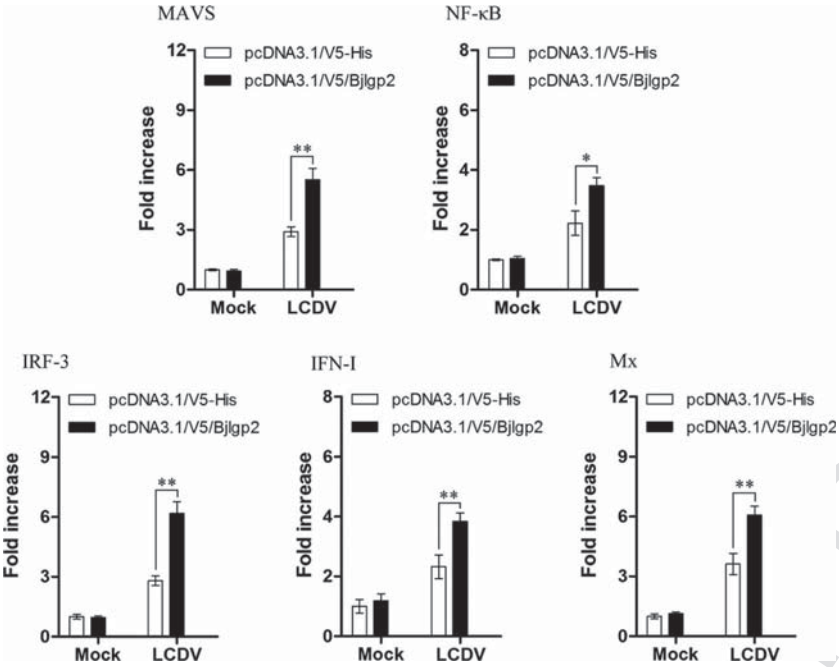

Figure 6. Effects of amphioxus LGP2 on the expression of MAVS, NF-κB, IRF-3, IFN-I, and Mx genes in FG cells upon LCDV challenge. FG cells were transfected with *pcDNA3.1/V5-His* or *pcDNA3.1/V5/Bjlgp2*. Twenty-four hours after transfection, FG cells were infected with LCDV for 48 h. Expression of *MAVS*, *nf-κB*, *irf-3*, *ifn-i*, and *Mx* was assayed by qRT-PCR. The flounder β-*actin* gene was chosen as the reference for internal standardization. Gene expression levels are expressed as fold increase values relative to the mock in the *pcDNA3.1/V5-His*-transfected cells. The data shown are mean values ± SD, $n = 3$ replicates per group, and are pooled from three experiments. Asterisks indicate significant differences of the expression levels between *pcDNA3.1/V5-His*- and *pcDNA3.1/V5/Bjlgp2*-transfected cells after challenged with LCDV ($^{*}p < 0.05$, $^{**}p < 0.01$). Unpaired Student's *t*-test was used for statistical analysis.

by stimulation with poly(I:C). This suggests that BjLGP2, like vertebrate LGP2, is also involved in immune response of amphioxus against viral infection.

Vertebrate RLRs act as cytosolic sensors that recognize viral RNA and induce signal transduction, upon binding to exogenous RNA, via the interaction with the MAVS or IPS-1, ultimately resulting in NF-κB- and IRF-3-dependent production of type I IFN and proinflammatory cytokines [7]. The roles of RIG-I and MDA5 were shown to be a canonical pattern of PRRs in innate immunity, however, the function of LGP2 in antiviral immunity is contradictory due to its lack of the CARDs at the N-terminal region that are necessary to interact with MAVS [15]. Some studies showed that LGP2 was a negative mediator in RIG-I/MDA5-activited antiviral responses, and overexpression of LGP2 inhibited IFN-stimulated regulatory element and NF-kB-dependent pathways after induced by paramyxovirus Sendai (SV) and Newcastle disease virus in a TLR-independent way [23]. However, the positive role of LGP2 in antiviral signaling transduction has also been reported. LGP2-dificient mice exhibited a defect in type I IFN production and unable to mount efficient antiviral responses against the infection by the encephalomyocarditis virus [24]. LGP2 was also shown to facilitate RIG-I and MDA5 recognition of viral dsRNA or 5′-triphosphorylated RNA, and both of $LGP2^{-/-}$ and Lys-30 to Ala mutant ($LGP2^{K30A/K30A}$ in the LGP2 helicase domain) mice were

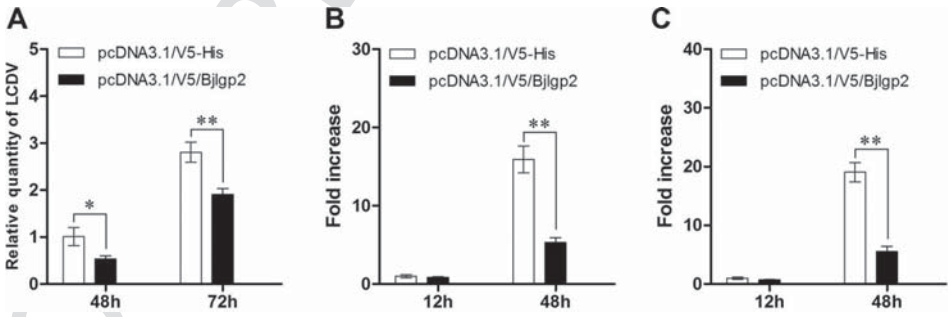

Figure 7. The effects of BjLGP2 on viral replication and transcription. (A) FG cells were transfected with *pcDNA3.1/V5-His* or *pcDNA3.1/V5/Bjlgp2*. Twenty-four hours after transfection, FG cells were infected with LCDV for 48 and 72 h. The relative quantity of LCDV in each sample was measured by qRT-PCR. The flounder β-*actin* was chosen as the reference for internal standardization. The relative quantity of LCDV was shown relative to that in the *pcDNA3.1/V5-His*-transfected cells at 48 h postinfection with LCDV. (B, C) GS cells were transfected with *pcDNA3.1/V5-His* or *pcDNA3.1/V5/Bjlgp2*. Twenty-four hours after transfection, GS cells were infected with SGIV for 12 and 48 h. The relative expression levels of the major capsid protein *mcp* (B) and the envelope protein *vp16* (C) of SGIV were measured by qRT-PCR. The grouper β-actin was chosen as the reference for internal standardization. The expression levels were expressed as folds increase relative to that in the *pcDNA3.1/V5-His*-transfected cells at 12 h postinfection with SGIV. Data shown are mean values ± SD, $n = 3$ replicates per group, and are pooled from three experiments. Asterisks indicate significant differences of the relative quantity of LCDV or the expression levels of *mcp* and *vp16* between *pcDNA3.1/V5/Bjlgp2*-transfected cells and *pcDNA3.1/V5-His*-transfected cells ($^{*}p < 0.05$, $^{**}p < 0.01$). Unpaired Student's *t*-test was used for statistical analysis.

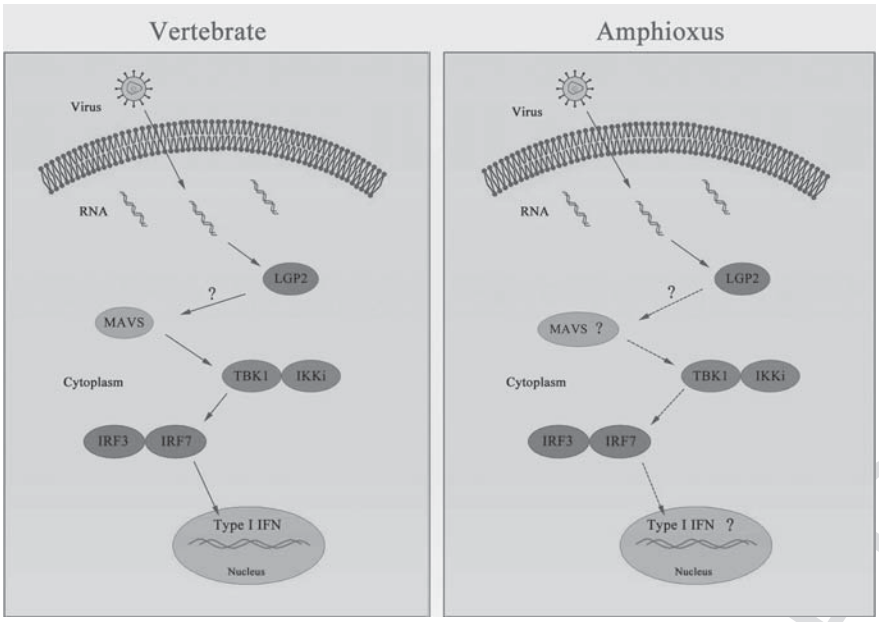

Figure 8. Signaling pathway and possible regulatory manners of vertebrate LGP2 and amphioxus LGP2. Viral dsRNA was recognized by LGP2, triggering signal transduction to nucleus through the TBK1/IKKi and IRF3/IRF7 pathway and inducing the production of type I IFN. It is currently unclear how the LGP2 interacts with the MAVS protein as the lack of caspase recruitment domains (CARD) in LGP2. No canonical type I IFN homologue has been identified in amphioxus.

highly susceptible to encephalomyocarditis virus [25]. In this study, we first show that BjLGP2 is distributed in the cytoplasm of both GS and FG cells, and rBjLGP2 is able to interact with poly(I:C), a synthetic mimic of ds RNA, indicating that amphioxus LGP2 is a cytosolic sensor capable of identifying viral RNA. Second, we show that the expression of IFN and IFN-inducible genes, including *ifn-i*, *Mx*, and *IGS56*, is enhanced in FG cells expressing BjLGP2, upon poly(I:C) challenge, although the expression of *ISG15* was only slightly upregulated, well agreeing with the observations that in vertebrates, LGP2 expression is induced by poly(I:C) stimulation [13, 22]. Third, we show that the expression of the antiviral genes *ifn-i* and *Mx* as well as the signal transduction relevant genes *MAVS*, *NF-κB*, and *IRF-3* is upregulated in FG cells expressing BjLGP2 upon LCDV challenge, suggesting that amphioxus LGP2 has the capacity to induce a vertebrate-like RLRs signaling pathway, upon binding to viral RNA, via the interaction with MAVS, and eventually to lead to NF-κB- and IRF-3-dependent production of type I IFN and proinflammatory cytokines [7]. Finally, we demonstrate that the replication of LCDV in FG cells and the gene transcription of SGIV in GS cells are considerably suppressed by BjLGP2 expressing in the cells, indicating that amphioxus LGP2 has also antiviral activity against LCDV and SGIV. Collectively, these data suggest that amphioxus LGP2 is highly likely to play an antiviral role via a RLRs signal transduction pathway similar to that of vertebrate RLRs signaling pathway (Fig. 8). This seems further corroborated by the searching of Florida amphioxus genome database (http://genome.jgi-psf.org//Brafl1/Brafl1.home.html) that resulted in the identification of all RLR members and the downstream elements MAVS-like protein (Protein ID: 106569), TBK1 (Protein ID: 123253), IKKi (Protein ID: 74350), IRF3 (where IRF3 is IFN regulatory factor) (Protein ID: 118813), and IRF7 (Protein ID: 68560) in *B. floridae*, although canonical type I IFN was not identified in amphioxus [26]. However, it must be pointed out that the viruses (LCDV and SGIV) tested in this study are both DNA viruses. Although Pollpeter et al. observed that the response to dsDNA viruses is suppressed in cells lacking LGP2, RLRs are considered to be mainly involved in detection of viral RNA [27]. Therefore, an RNA virus, for example, VHSV would have been more suitable for these experiments, and probably produced a better result. In summary, this study reports the molecular cloning and functional characterization of an ancient viral receptor: an LGP2 orthologue in the basal chordate amphioxus. Our results demonstrate that the expression of amphioxus LGP2 is induced by poly(I:C) and virus, and that LGP2 binds to poly(I:C), inhibits LCDV and SGIV infection, and simultaneously induces type I IFN and IFN-inducible gene expression. These findings highlight the evolutionarily high conservation of molecular structure and antiviral function of LGP2 throughout the period of chordate evolution, that is, for about 5.5 hundred million years.

Materials and methods

Animal, cell, and virus

All amphioxus experiments in this paper conformed to the ethical guidelines established by the Institutional Animal Care and Use Committee of the Ocean University of China. Amphioxus *B. japonicum* used were collected from the vicinity of Qingdao, China. The FG cells derived from the gills of flounder (*Paralichthys olivaceus*) were established in our laboratory, and cultured in minimal essential medium (MEM, HyClone) supplemented with 10% FBS (Life Technologies), 100 IU/mL penicillin, and 100 mg/mL streptomycin at 22°C as described previously [28]. The GS cells

were grown and maintained in Leibovitz's L-15 medium containing 10% FBS (Life Technologies) at 25°C [29]. LCDV was isolated from diseased flounder with symptom of lymphocystis as described previously [30], and SGIV was kept in the key laboratory of Tropical Marine Bio-resources and Ecology, South China Sea Institute of Oceanology, Chinese Academy Sciences, and propagated in GS cells. Virus stocks were stored at −80°C until used.

Cloning and sequencing of BjLGP2 cDNA

Total RNAs were extracted from *B. japonicum* with RNAiso plus (TaKaRa) according to the manufacturer's instructions. The first-strand cDNA was synthesized with reverse transcription kit (TaKaRa) using oligo (dT) primer after digestion with recombinant DNase I (RNase free) (TaKaRa) to eliminate the genomic contamination. A partial cDNA fragment of BjLGP2 was amplified by PCR with the primer pairs P1 and P2 (Table 1) that were designed on the basis of LGP2 gene sequence found in *B. floridae* genome database (http://genome.jgi-psf.org//Brafl1/Brafl1.home.html). To obtain a full-length cDNA sequence, 3′ and 5′ RACE were performed using the BD SMART™ RACE cDNA amplification kit (Clontech, China) according to the manufacturer's instructions, with the gene-specific primer pairs P3 and P4, and P5 and P6 (Table 1), respectively. The clones obtained were sequenced and the overlapping sequences were assembled. Based on the cDNA sequence assembled, the full-length ORF of BjLGP2 was obtained by PCR with the primer pairs P7 and P8 (Table 1) and verified by sequencing.

Sequence analysis

Sequence comparison against the GenBank protein database was performed using the BLAST network server at NCBI. The protein domains were analyzed using the SMART program (http://smart.embl-heidelberg.de/). The molecular mass and isoelectronic point of the protein were determined using ProtParam (http://www.expasy.ch/tools/protparam.html). The 3D structures of BjLGP2 as well as human LGP2 were established using the SWISS-MODEL online software at the Expert Protein Analysis System (http://swissmodel.expasy.org/interactive). Multiple alignments of the protein sequences were generated using the ClustalW program. The phylogenetic tree was constructed using the amino acid sequences of LGP2 proteins available, including BjLGP2, by MEGA (version 5.0) based on the neighbor-joining method, and the reliability of each node was estimated by bootstrapping with 1000 replication.

qRT-PCR

qRT-PCR was used to determine the expression profile of *Bjlgp2* in the different tissues of *B. japonicum*, including the gill, hepatic caecum, hindgut, muscle, notochord, testis, and ovary. Total RNAs were extracted with RNAiso plus (TaKaRa) from the tissues, and digested with recombinant DNase I (RNase free). cDNAs were synthesized as described above, and used as template for qRT-PCR. The gene *ef1*-α was chosen as the reference for internal standardization [31]. The primers P9 and P10 specific of *Bjlgp2*, and P11 and P12 specific of *ef1*-α (Table 1) were designed to amplify the specific fragments of both genes. qRT-PCR was performed on ABI 7500 real-time PCR system (Applied Biosystems) as described previously [32]. Reaction of each sample was performed in triplicate. At the end of each PCR reaction, dissociation analysis was performed to confirm the amplification specificity. Data were analyzed with the comparative *Ct* method ($2^{-\Delta\Delta Ct}$) based on *Ct* values for *Bjlgp2* and *ef1*-α in order to calculate the relative mRNA expression level [33].

To test the effect of the viral mimic poly(I:C), a synthetic ds RNA [34–36] and the bacterial signature molecule (LPS) on *Bjlgp2* expression, adult *B. japonicum* were exposed to sterilized seawater with 10 μg/mL of poly(I:C) (Sigma), 10 μg/mL of LPS (Sigma), or sterilized seawater alone (control), respectively, as described previously [37], and sampled at 0, 2, 4, 8, 12, 24, 48, and 72 h after the exposure. Total RNAs were prepared from the whole body as well as the hepatic caecum and hindgut with Trizol. The cDNA synthesis and qRT-PCR were processed as above.

Construction of expression vector

For prokaryotic expression vector construction, the full-length ORF of *Bjlgp2* was amplified by PCR using the primers P13 and P14 (Table 1). The PCR product was digested with *EcoR* I and *Sal* I and subcloned into the plasmid expression vector pET-28a (Novagen) previously cut with the same restriction enzymes. The identity of insert was verified by sequencing and the plasmid was designated *pET-28a/Bjlgp2*. For eukaryotic expression vector construction, the full-length ORF of *Bjlgp2* was amplified by PCR using the primers P15 with *BamH* I site and P16 with *EcoR* I site (Table 1), and subcloned into the plasmid expression vector pcDNA3.1/V5-His (Invitrogen), and the plasmid was designated *pcDNA3.1/V5/Bjlgp2*. In parallel, the full length of eGFP gene was amplified by PCR using the primers P17 with *Xba* I site and P18 with *Apa* I site (Table 1), and subcloned into the plasmid expression vector pcDNA3.1/V5-His, designated *pcDNA3.1/V5/egfp*, or into the *pcDNA3.1/V5/Bjlgp2*, designated *pcDNA3.1/V5/Bjlgp2/egfp*.

Expression, purification, and refolding of recombinant BjLGP2 (rBjLGP2)

The plasmid *pET-28a/Bjlgp2* was transformed into *E. coli* transetta (DE3), and the cells were cultured overnight in LB broth containing 50 μg/mL kanamycin. When OD_{600} reached about 1.0, isopropyl β-D-thiogalactoside was added to the cultures at a final

Table 1. Sequences of the primers used in this study

Primer	Sequence (5'-3')	Sequence information
P1 (S)	GAACACCATCATCTGTGCACCTAC	cDNA fragment primer
P2 (AS)	CGTGATGATTCTCCTTGATCTTGCG	cDNA fragment primer
P3 (S)	TTCCGCTATGACTATGTGGGC	3′-RACE PCR primer
P4 (S)	ATGTGGGCAACGAGATAGGC	3′-RACE PCR primer
P5 (AS)	TGGTCATGATGGAATTGTACGG	5′-RACE PCR primer
P6 (AS)	CGTCAAAGATGAGCATAGAGAAGG	5′-RACE PCR primer
P7 (S)	ATGTACGGCGATCTCGCAGACCAGT	ORF primer
P8 (AS)	CTAATACATCATCAGTTCTTCTTCC	ORF primer
P9 (S)	ACATTCTACCCCTCAGTGGCGAG	Real-time PCR primer
P10 (AS)	TTCTGGCAGTAGTGACACTCGTCAA	Real-time PCR primer
P11 (S)	TGCTGATTGTGGCTGCTGGTACTG	Real-time PCR primer
P12 (AS)	GGTGTAGGCCAGCAGGGCGTG	Real-time PCR primer
P13 (S)	CCGGAATTCATGTACGGCGATCTCGCAGACCAGT	Recombinant primer
P14 (AS)	ACGCGTCGACCTAATACATCATCAGTTCTTCTTCC	Recombinant primer
P15 (S)	CGCGGATCCACATGTACGGCGATCTCGCAGACCAGT	Recombinant primer
P16 (AS)	CCGGAATTCATACATCATCAGTTCTTCTTCC	Recombinant primer
P17 (S)	GCTCTAGAATGGTGAGCAAGGGCG	Recombinant primer
P18 (AS)	AGAGGGCCCGATTACTTGTACAGCT	Recombinant primer
P19 (S)	ATGCTTAACAGGATCTTCTTCGTTT	Real-time PCR primer
P20 (AS)	GTCTGAATTTATGATCCATCCATCT	Real-time PCR primer
P21 (S)	CCGCACGGGACACAACTTTAACATG	Real-time PCR primer
P22 (AS)	TGGTTCTCCAGCTTGTTTCATCTGC	Real-time PCR primer
P23 (S)	CACCTACGACATCACACCTGACGAG	Real-time PCR primer
P24 (AS)	TCTCAGACGCAGTAACAGGTCCATG	Real-time PCR primer
P25 (S)	CACCAGCACCAGGAGGACAGC	Real-time PCR primer
P26 (AS)	AACACGTGACTGGACTTCAGCTCTA	Real-time PCR primer
P27 (S)	GAATATTGGCCCCACTGACCAGGAC	Real-time PCR primer
P28 (AS)	TGGAAAGGAAAGCCTCCCTCACG	Real-time PCR primer
P29 (S)	GAGAAGACCGAACCTCCGATTACAC	Real-time PCR primer
P30 (AS)	GCAGAGCACGCAGGAACTGTATC	Real-time PCR primer
P31 (S)	GACGGCACATAAGCACAGCACG	Real-time PCR primer
P32 (AS)	GGCTGATTGAATGAGTAGGAGGGCT	Real-time PCR primer
P33 (S)	ATCAAACTCAAGCCAAACTGACCCG	Real-time PCR primer
P34 (AS)	CAGTCTCTCCCATTGATGAAGTCCA	Real-time PCR primer
P35 (S)	TTATGGTCGTTTGTCCAATGTCAGT	Real-time PCR primer
P36 (AS)	TTACGTTGTGATTCACTGCCATTGT	Real-time PCR primer
P37 (S)	GCACGCTTCTCTCACCTTCA	Real-time PCR primer
P38 (AS)	AACGGCAACGGGAGCACTA	Real-time PCR primer
P39 (S)	TCATGCTGTACGAAGACGACC	Real-time PCR primer
P40 (A)	TGACATATCAACGCTGGAAGG	Real-time PCR primer
P41 (S)	TACGAGCTGCCTGACGGACA	Real-time PCR primer
P42 (AS)	GGCTGTGATCTCCTTCTGCA	Real-time PCR primer

a)S and AS represent sense and antisense, respectively.
ORF, open reading frame.

concentration of 1 mM, and the cultures were allowed to shake for 12 h at 28°C. The recombinant protein that was expressed in inclusion bodies was purified and refolded according to the method described previously [38] with the exception of dialysis pH value being 8.5. The refolded protein was analyzed by 12% SDS-PAGE, and immunostained using anti-His-tag mAb (CWBIO, China) as the primary Ab, according to the method described previously [28]. The concentration of the refolded protein was determined by BCA method.

Assay for binding of rBjLGP2 with poly(I:C)

Assay for binding of rBjLGP2 with poly(I:C) was performed as described previously [15, 39] with a slight modification. In brief, poly(C)-conjugated agarose beads (Sigma) and poly(I) (Sigma) were resuspended in 50 mM Tris-HCl (pH 7.0) containing 150 mM NaCl, respectively, and adjusted to a concentration of 2 mg/mL. The poly(C)-conjugated agarose bead solution and poly(I) solution were mixed at a ratio of 1:2 v/v. The mixture was incubated

Table 2. Sequences used in this study (all the sequences are from GenBank). Q6

Species	Common name	Gene	Accession no.
Homo sapiens	Human	LGP2	NM_024119.2
Mus musculus	Mouse	LGP2	NM_030150.2
Bos taurus	Cow	LGP2	NM_001015545.1
Oryctolagus cuniculus	Rabbit	LGP2	XM_002719391.2
Cairina moschata	Duck	LGP2	KC422351.1
Gallus gallus	Chicken	LGP2	HQ845773.1
Xenopus tropicalis	Xenopus	LGP2	XM_004918712.1
Danio rerio	Zebrafish	LGP2	NM_001257157.1
Paralichthys olivaceus	Flounder	LGP2	HM070372.1
Oncorhynchus mykiss	Trout	LGP2	FN396358.1
Salmo salar	Altlantic salmon	LGP2	BT045378.1
Cyprinus carpio	Carp	LGP2	KM374816.1
Oryzias latipes	Medaka	LGP2	XM_004071291.2
Branchiostoma japonicum	Amphioxus	LGP2	KR560072
Paralichthys olivaceus	Flounder	Mx	AB110446.1
Paralichthys olivaceus	Flounder	ISG15	AB519717.1
Paralichthys olivaceus	Flounder	ISG56	AU260972
Paralichthys olivaceus	Flounder	Type I IFN	AB511962.1
Paralichthys olivaceus	Flounder	MAVS	HM070252.1
Paralichthys olivaceus	Flounder	IRF3	GU017417.1
Paralichthys olivaceus	Flounder	NF-κB	HM771267.1
Paralichthys olivaceus	Flounder	β-actin	HQ386788.1
Epinephelus coioides	Grouper	β-actin	AY510710.2

at 4°C overnight to form poly(I:C), then centrifuged at 1000 × *g* for 1 min, and washed with 50 mM Tris-HCl (pH 7.0) with 150 mM NaCl. The pellets, that is, poly(I:C)-conjugated agarose beads, were suspended in 50 mM Tris-HCl (pH 7.0) with 150 mM NaCl as a 50% slurry and stored at 4°C till used. For pull-down assay, aliquots of 50 μL of poly(C)- and poly(I:C)-coated beads were resuspended in 200 μL of the binding buffer consisting of 50 mM Tris-HCl (pH7.5), 150 mM NaCl, 1 mM EDTA, and 1% NP-40, mixed with 50 μL of 0.1 mg/mL purified rBjLGP2 and incubated at 4°C for 1 h. For competition experiment, pull-down reactions was supplemented with soluble poly(I:C) at a final concentration of 50 μg/mL. The beads were centrifuged at 1000 × *g* at room temperature for 1 min, rinsed three times with the binding buffer, and resuspended in three volumes of 1× SDS-PAGE sample buffer. The samples were incubated at 100°C for 5 min, and centrifuged at 13 000 × *g* for 30 s. The supernatants were collected, analyzed on 12% SDS-PAGE, and immunostained as above. In parallel, the sample buffer was loaded for SDS-PAGE and immunostained as blank control.

Cell transfection and fluorescent microscopy

To examine the subcellular localization of BjLGP2, both GS and FG cells were seeded in six-well plates and transfected with the different plasmids using Lipofectamine 2000 Reagent (Invitrogen). Briefly, *pcDNA3.1/V5/egfp* and *pcDNA3.1/V5/Bjlgp2/egfp* plasmids were mixed with Lipofectamine 2000, and the mixtures were added into GS cells or FG cells and incubated at 25°C (for GS cells) or 22°C (for FG cells) for 48 h. The transfected cells were washed with PBS, fixed with 4% paraformaldehyde, and stained with 1 mg/mL DAPI as described previously [40]. The samples were observed under a fluorescence microscopy (Leica, Germany).

Assay for effects of BjLGP2 on gene expression upon intracellular poly(I:C) challenge

Effects of intracellular poly(I:C) on induction of type I IFN and IFN-inducible genes were assayed as described previously [13] with a slight modification. In brief, FG cells were adjusted to a density of 5 × 10^5 cells/mL, seeded onto a 12-well plate with each well containing 1 mL of the cell suspension, and cultured at 22°C for 24 h. For intracellular stimulation with poly(I:C), aliquots of 1 μg *pcDNA3.1/V5-His* and *pcDNA3.1/V5/Bjlgp2* were mixed with different amounts (0, 0.1, and 1 μg) of poly(I:C), respectively; the mixtures were then solved in 4 μL Lipofectamine 2000 with 1.6 μg of total nucleic acids, and transfected into the cells in each well. Six hours after transfection, culture media were replaced with MEM containing 10% FBS, and the cells were cultured and harvested at 48 h after transfection. Total RNAs were extracted and cDNA synthesized as described above. Expression of type I *ifn* (*ifn-i*), *Mx*, *ISG15*, and *ISG56* was measured by qRT-PCR upon poly(I:C) stimulation. The flounder β-*actin* gene was chosen as the reference for internal standardization. Specific primers P19

and P20 for *ifn-i*, P21 and P22 for *Mx*, P23 and P24 for *ISG15*, P25 and P26 for *ISG56*, P27 and P28 for β-*actin* were designed based on the sequences of respective flounder genes available at NCBI. qRT-PCR was performed as above.

Assay for effects of BjLGP2 on gene expression upon LCDV challenge

qRT-PCR was also used to assay the effects of amphioxus LGP2 on the expression of immune-relevant genes in FG cells challenged with LCDV. In brief, FG cells were adjusted to a density of 5×10^5 cells/mL, seeded onto a 12-well plate with each well containing 1 mL of the cell suspension, and cultured at 22°C for 24 h. A total of 1.6 μg plasmid *pcDNA3.1/V5-His* or *pcDNA3.1/V5/Bjlgp2* was mixed with 4 μL Lipofectamine 2000, and transfected into the cells according to manufacturer's instructions. Twenty-four hours after transfection, culture media were removed from the cell monolayer, and the cells were washed with PBS and infected with 200 μL LCDV suspension with a titer of 2.7×10^4 $TCID_{50}$/mL (where TCID is tissue culture infective dose) per well. After 3 h of virus adsorption, the cells were washed with PBS and cultured in MEM containing 2% FBS for 48 h, and harvested. Both total RNAs extraction and cDNA synthesis were conducted as above. Expression of *MAVS*, *NF-κB*, *IRF-3*, *ifn-i,* and *Mx* was assayed by qRT-PCR. The flounder β-*actin* gene was chosen as the reference for internal standardization. Specific primers P29 and P30 for *MAVS*, P31 and P32 for *NF-κB*, P33 and P34 for *IRF-3* were designed based on the sequences of respective flounder genes available at NCBI. qRT-PCR was performed as described above.

Assay for antiviral activity of BjLGP2

To evaluate the effects of BjLGP2 on virus infection, viral replication and transcription were detected using qRT-PCR in the BjLGP2-expressing cells. To assay the antiviral activity of BjLGP2 against LCDV, the FG cells were adjusted to a density of 5×10^5 cells/mL, seeded onto a 12-well plate with each well containing 1 mL of the cell suspension, and cultured at 22°C for 24 h. A total of 1.6 μg plasmid *pcDNA3.1/V5-His* or *pcDNA3.1/V5/Bjlgp2* was mixed with 4 μL Lipofectamine 2000, and transfected into the cells according to manufacturer's instructions. Twenty-four hours after transfection, culture media were removed from the cell monolayers and washed with PBS, and then the cells in each well were infected with 200 μL of LCDV suspension with a titer of 2.7×10^4 $TCID_{50}$/mL. After 3 h of virus adsorption, the virus suspension was removed, and the cells were washed with PBS and cultured in MEM containing 2% FBS for 48–72 h. The cells in each well were harvested, and genomic DNAs were extracted from the cells harvested with a DNA purification kit (CWBIO, China) according to manufacturer's instruction. qRT-PCR was employed to analyze the relative quantity of LCDV in each sample. A pair of primers specific of LCDV, P35, and P36 were designed according to the sequence of the major capsid protein gene *mcp* of LCDV. The flounder β-*actin* was chosen as the reference for internal standardization. For the antiviral activity of BjLGP2 against SGIV, the GS cells were similarly processed as above, except that the GS cells were Leibovitz's L-15 containing 2% FBS, and the cells in each well were infected with 200 μL of SGIV suspension with a titer of 4.6×10^5 $TCID_{50}$/mL. The cells were harvested for RNA extraction at 12 and 48 h postinfection. qRT-PCR was performed to measure the relative expression levels of *mcp* and the envelope protein 16 gene (*vp16*) of SGIV. The grouper β-actin was chosen as the reference for internal standardization. The primers P37 and P38 specific of *mcp* of SGIV, P39 and P40 specific of *vp16* of SGIV, and P41 and P42 specific of grouper β-*actin* (Table 1) were designed on the gene sequences available.

Statistical analysis

All the experiments were performed in triplicate and repeated at least three times. Data were subjected to statistical evaluation with unpaired *t*-test, $p < 0.05$ was considered as significant. All the data were expressed as mean ± SD.

Acknowledgments: This work was supported by grants of the National Science Foundation of China (31172071) and the Ministry of Science and Technology of China (2012CB114404). The authors thank Dr. Qinghua Liu (Center of Biotechnology R&D, Institute of Oceanology, Chinese Academy of Sciences, Qingdao, China) for the gift of diseased flounder with symptom of lymphocystis. We also thank Dr. Chen Sun for aids in cell culture.

Conflict of interest: The authors declare no commercial or financial conflict of interest.

References

1 **Takeuchi, O. and Akira, S.**, Pattern recognition receptors and inflammation. *Cell* 2010. **140**: 805–820.

2 **Zhu, Z. X., Zhang, X. L., Wang, G. Q. and Zheng, H. X.**, The laboratory of genetics and physiology 2: emerging insights into the controversial functions of this RIG-I-like receptor. *Biomed. Res. Int.* 2014.

3 **Takahasi, K., Kumeta, H., Tsuduki, N., Narita, R., Shigemoto, T., Hirai, R., Yoneyama, M. et al.**, Solution structures of cytosolic RNA sensor MDA5 and LGP2 C-terminal domains identification of the rna recognition loop in RIG-I-like receptors. *J. Biol. Chem.* 2009. **284**: 17465–17474.

4 **Takeuchi, O. and Akira, S.**, Innate immunity to virus infection. *Immunol. Rev.* 2009. **227**: 75–86.

Q8

5 **Bruns, A. M., Leser, G. P., Lamb, R. A. and Horvath, C. M.**, The innate immune sensor LGP2 activates antiviral signaling by regulating MDA5-RNA interaction and filament assembly. *Mol. Cell* 2014. **55**: 771–781.

6 **Yoneyama, M., Kikuchi, M., Natsukawa, T., Shinobu, N., Imaizumi, T., Miyagishi, M., Taira, K. et al.**, The RNA helicase RIG-I has an essential function in double-stranded RNA-induced innate antiviral responses. *Nat. Immunol.* 2004. **5**: 730–737.

7 **Loo, Y. M. and Gale, M.**, Immune signaling by RIG-I-like receptors. *Immunity* 2011. **34**: 680–692.

8 **de Matos, A. L., McFadden, G. and Esteves, P. J.**, Evolution of viral sensing RIG-I-like receptor genes in Leporidae genera Oryctolagus, Sylvilagus, and Lepus. *Immunogenetics* 2014. **66**: 43–52.

9 **Jiao, P. R., Wei, L. M., Song, Y. F., Cui, J., Zhang, S., Han, F., Yuan, R. Y. et al.**, Molecular cloning and immune responsive expression of LGP2 gene, a pivotal member of the RLR gene family from Muscovy duck *Cairina moschata*. *Poult. Sci.* 2015. **94**: 1170–1176.

10 **Zou, J., Chang, M. X., Nie, P. and Secombes, C. J.**, Origin and evolution of the RIG-I like RNA helicase gene family. *BMC Evol. Biol.* 2009. **9**.

11 **Huang, T., Su, J. G., Heng, J. F., Dong, J., Zhang, R. F. and Zhu, H. M.**, Identification and expression profiling analysis of grass carp Ctenopharyngodon idella LGP2 cDNA. *Fish Shellfish Immunol.* 2010. **29**: 349–355.

12 **Yang, C. R., Su, J. G., Huang, T., Zhang, R. F. and Peng, L. M.**, Identification of a retinoic acid-inducible gene I from grass carp (*Ctenopharyngodon idella*) and expression analysis in vivo and in vitro. *Fish Shellfish Immunol.* 2011. **30**: 936–943.

13 **Ohtani, M., Hikima, J., Kondo, H., Hirono, I., Jung, T. S. and Aoki, T.**, Evolutional conservation of molecular structure and antiviral function of a viral RNA receptor, LGP2, in Japanese flounder, *Paralichthys olivaceus*. *J. Immunol.* 2010. **185**: 7507–7517.

14 **Ohtani, M., Hikima, J., Kondo, H., Hirono, I., Jung, T. S. and Aoki, T.**, Characterization and antiviral function of a cytosolic sensor gene, MDA5, in Japanese flounder, *Paralichthys olivaceus*. *Dev. Comp. Immunol.* 2011. **35**: 554–562.

15 **Chang, M. X., Collet, B., Nie, P., Lester, K., Campbell, S., Secombes, C. J. and Zou, J.**, Expression and functional characterization of the RIG-I-like receptors MDA5 and LGP2 in Rainbow trout (*Oncorhynchus mykiss*). *J. Virol.* 2011. **85**: 8403–8412.

16 **Rajendran, K. V., Zhang, J. R., Liu, S. K., Peatman, E., Kucuktas, H., Wang, X. L., Liu, H. et al.**, Pathogen recognition receptors in channel catfish: II. Identification, phylogeny and expression of retinoic acid-inducible gene I (RIG-I)-like receptors (RLRs). *Dev. Comp. Immunol.* 2012. **37**: 381–389.

17 **Cagliani, R., Forni, D., Tresoldi, C., Pozzoli, U., Filippi, G., Rainone, V., De Gioia, L. et al.**, RIG-I-like receptors evolved adaptively in mammals, with parallel evolution at LGP2 and RIG-I. *J. Mol. Biol.* 2014. **426**: 1351–1365.

18 **de Matos, A. L., McFadden, G. and Esteves, P. J.**, Positive evolutionary selection on the RIG-I-like receptor genes in mammals. *PLoS One* 2013. **8**.

19 **Biacchesi, S., LeBerre, M., Lamoureux, A., Louise, Y., Lauret, E., Boudinot, P. and Bremont, M.**, Mitochondrial antiviral signaling protein plays a major role in induction of the fish innate immune response against RNA and DNA viruses. *J. Virol.* 2009. **83**: 7815–7827.

20 **Su, J. G., Huang, T., Dong, J., Heng, J. F., Zhang, R. F. and Peng, L. M.**, Molecular cloning and immune responsive expression of MDA5 gene, a pivotal member of the RLR gene family from grass carp *Ctenopharyngodon idella*. *Fish Shellfish Immunol.* 2010. **28**: 712–718.

21 **Chen, L. J., Li, Q. M., Su, J. G., Yang, C. R., Li, Y. Q. and Rao, Y. L.**, Trunk kidney of grass carp (*Ctenopharyngodon idella*) mediates immune responses against GCRV and viral/bacterial PAMPs in vivo and in vitro. *Fish Shellfish Immunol.* 2013. **34**: 909–919.

22 **Cowled, C., Baker, M. L., Zhou, P., Tachedjian, M. and Wang, L. F.**, Molecular characterisation of RIG-I-like helicases in the black flying fox, *Pteropus alecto*. *Dev. Comp. Immunol.* 2012. **36**: 657–664.

23 **Rothenfusser, S., Goutagny, N., DiPerna, G., Gong, M., Monks, B. G., Schoenemeyer, A., Yamamoto, M. et al.**, The RNA helicase Lgp2 inhibits TLR-independent sensing of viral replication by retinoic acid-inducible gene-I. *J. Immunol.* 2005. **175**: 5260–5268.

24 **Venkataraman, T., Valdes, M., Elsby, R., Kakuta, S., Caceres, G., Saijo, S., Iwakura, Y. et al.**, Loss of DExD/H box RNA helicase LGP2 manifests disparate antiviral responses. *J. Immunol.* 2007. **178**: 6444–6455.

25 **Satoh, T., Kato, H., Kumagai, Y., Yoneyama, M., Sato, S., Matsushita, K., Tsujimura, T. et al.**, LGP2 is a positive regulator of RIG-I- and MDA5-mediated antiviral responses. *Proc. Natl. Acad. Sci. USA* 2010. **107**: 1512–1517.

26 **Li, G., Zhang, J. Y., Sun, Y., Wang, H. and Wang, Y. Q.**, The evolutionarily dynamic IFN-inducible GTPase proteins play conserved immune functions in vertebrates and cephalochordates. *Mol. Biol. Evol.* 2009. **26**: 1619–1630.

27 **Pollpeter, D., Komuro, A., Barber, G. N. and Horvath, C. M.**, Impaired cellular responses to cytosolic DNA or infection with *Listeria monocytogenes* and Vaccinia virus in the absence of the murine LGP2 protein. *PLoS One* 2011. **6**.

28 **Liu, S. S., Hu, G. B., Sun, C. and Zhang, S. C.**, Anti-viral activity of galectin-1 from flounder *Paralichthys olivaceus*. *Fish Shellfish Immunol.* 2013. **34**: 1463–1469.

29 **Huang, Y. H., Huang, X. H., Cai, J., OuYang, Z. L., Wei, S. N., Wei, J. G. and Qin, Q. W.**, Identification of orange-spotted grouper (*Epinephelus coioides*) interferon regulatory factor 3 involved in antiviral immune response against fish RNA virus. *Fish Shellfish Immunol.* 2015. **42**: 345–352.

30 **Cheng, S. F., Zhan, W. B., Xing, J. and Sheng, X. Z.**, Development and characterization of monoclonal antibody to the lymphocystis disease virus of Japanese flounder *Paralichthys olivaceus* isolated from China. *J. Virol. Methods* 2006. **135**: 173–180.

31 **Wang, Y. and Zhang, S.**, EF1alpha is a useful internal reference for studies of gene expression regulation in amphioxus *Branchiostoma japonicum*. *Fish Shellfish Immunol.* 2012. **32**: 1068–1073.

32 **Xu, N., Pan, J. L., Liu, S. S., Xue, Q. G. and Zhang, S. C.**, Three in one: identification, expression and enzymatic activity of lysozymes in amphioxus. *Dev. Comp. Immunol.* 2014. **46**: 508–517.

33 **Livak, K. J. and Schmittgen, T. D.**, Analysis of relative gene expression data using real-time quantitative PCR and the 2(T)(-Delta Delta C) method. *Methods* 2001. **25**: 402–408.

34 **Feng, C. Y. and Rise, M. L.**, Identification and molecular cloning of Atlantic cod (*Gadus morhua*) activating transcription factor 3 (ATF3) transcript and its induction in spleen following intraperitoneal polyriboinosinic polyribocytidylic acid injection. *Fish Shellfish Immunol.* 2011. **31**: 475–481.

35 **Hori, T. S., Gamperl, A. K., Booman, M., Nash, G. W. and Rise, M. L.**, A moderate increase in ambient temperature modulates the Atlantic cod (*Gadus morhua*) spleen transcriptome response to intraperitoneal viral mimic injection. *BMC Genomics* 2012. **13**: 431.

36 **Rise, M. L., Hall, J., Rise, M., Hori, T., Gamperl, A. K., Kimball, J., Hubert, S. et al.**, Functional genomic analysis of the response of Atlantic cod (*Gadus*

morhua) spleen to the viral mimic polyriboinosinic polyribocytidylic acid (pIC). *Dev. Comp. Immunol.* 2008. **32**: 916–931.

37 **Yuan, S., Huang, S., Zhang, W., Wu, T., Dong, M., Yu, Y., Liu, T. et al.**, An amphioxus TLR with dynamic embryonic expression pattern responses to pathogens and activates NF-kappaB pathway via MyD88. *Mol. Immunol.* 2009. **46**: 2348–2356.

38 **Xu, N. and Zhang, S. C.**, Identification, expression and bioactivity of a chitotriosidase-like homolog in amphioxus: dependence of enzymatic and antifungal activities on the chitin-binding domain. *Mol. Immunol.* 2012. **51**: 57–65.

39 **Stumper, R., Loo, Y. M., Foy, E., Li, K., Yoneyama, M., Fujita, T., Lemon, S. M. and Gale, M.**, Regulating intracellular antiviral defense and permissiveness to hepatitis C virus RNA replication through a cellular RNA helicase, RIG-I. *J. Virol.* 2005. **79**: 2689–2699.

40 **Wei, S. N., Huang, Y. H., Huang, X. H. and Qin, Q. W.**, Characterization of c-Jun from orange-spotted grouper, *Epinephelus coioides* involved in SGIV infection. *Fish Shellfish Immunol.* 2015. **43**: 230–240.

Abbreviations: **FG**: flounder gill · **GS**: grouper spleen · **IRF3**: IFN regulatory factor 3 · **ISG15**: IFN-stimulated gene 15 · **LCDV**: lymphocystis disease virus · **LGP2**: laboratory of genetics and physiology 2 · **MAVS**: mitochondrial antiviral signaling protein · **MDA5**: melanoma differentiation associated receptor 5 · **MEM**: minimal essential medium · **ORF**: opening reading frame · **qRT-PCR**: quantitative real-time PCR · **RIG-I**: retinoic acid inducible gene I · **RLRs**: retinoic acid inducible gene I (RIG-I) like receptors · **SGIV**: Singapore grouper iridovirus · **TCID**: tissue culture infective dose

Full correspondence: Dr. Shicui Zhang, Room 205, Ke Xue Guan, 5 Yushan Road, Ocean University of China, Qingdao 266003, China
e-mail: sczhang@ouc.edu.cn

Received: 11/6/2015
Revised: 7/8/2015
Accepted: 30/9/2015

Cortical instability drives periodic supracellular actin pattern formation in epithelial tubes

Edouard Hannezo[a,b,1,2], Bo Dong[c,d,1,2], Pierre Recho[a,e], Jean-François Joanny[a,f], and Shigeo Hayashi[c]

[a]Physicochimie Curie (Institut Curie/CNRS–UMR168/Université Pierre et Marie Curie), Institut Curie, Paris Sciences et Lettres, Centre de Recherche, 75248 Paris Cedex 05, France; [b]Cavendish Laboratory, University of Cambridge, Cambridge CB3 0HE, United Kingdom; [c]Laboratory for Morphogenetic Signaling, RIKEN Center for Developmental Biology, Kobe, Hyogo 650-0047, Japan; [d]Ministry of Education Key Laboratory of Marine Genetics and Breeding, College of Marine Life Sciences, Institute of Evolution and Marine Biodiversity, Ocean University of China, Qingdao 266003, China; [e]Mathematical Institute, University of Oxford, Oxford OX2 6GG, United Kingdom; and [f]École Supérieure de Physique et de Chimie Industrielles de la Ville de Paris, 75005 Paris, France

Edited by Thomas D. Pollard, Yale University, New Haven, CT, and approved May 19, 2015 (received for review March 9, 2015)

An essential question of morphogenesis is how patterns arise without preexisting positional information, as inspired by Turing. In the past few years, cytoskeletal flows in the cell cortex have been identified as a key mechanism of molecular patterning at the subcellular level. Theoretical and in vitro studies have suggested that biological polymers such as actomyosin gels have the property to self-organize, but the applicability of this concept in an in vivo setting remains unclear. Here, we report that the regular spacing pattern of supracellular actin rings in the *Drosophila* tracheal tubule is governed by a self-organizing principle. We propose a simple biophysical model where pattern formation arises from the interplay of myosin contractility and actin turnover. We validate the hypotheses of the model using photobleaching experiments and report that the formation of actin rings is contractility dependent. Moreover, genetic and pharmacological perturbations of the physical properties of the actomyosin gel modify the spacing of the pattern, as the model predicted. In addition, our model posited a role of cortical friction in stabilizing the spacing pattern of actin rings. Consistently, genetic depletion of apical extracellular matrix caused strikingly dynamic movements of actin rings, mirroring our model prediction of a transition from steady to chaotic actin patterns at low cortical friction. Our results therefore demonstrate quantitatively that a hydrodynamical instability of the actin cortex can trigger regular pattern formation and drive morphogenesis in an in vivo setting.

actomyosin | biophysics | pattern formation | *Drosophila* | biological tubes

Self-organization is one of the principal mechanisms of biological pattern formation at the molecular, cellular, and tissue scale. Although the pioneering work of Turing (1) has suggested reaction–diffusion as a generic route toward pattern generation (2), a concrete biomolecular or mechanical understanding of how this might occur in vivo remains elusive, except in a few specific cases (3–5). For instance, Kondo and coworkers (6) demonstrated that pigment patterning on the skin of the *Pomocanthus imperator* can be understood quantitatively from the simple attraction–repulsion kinetics of two cell types.

At the cellular level, active structures, such as the cytoskeleton, are generically expected to display a large variety of structures from a theoretical perspective (7–12), many of which have been reproduced in elegant in vitro studies (13–15). In the case of actomyosin gels, the contractile stresses arising from molecular motors have been shown to create large actin flows that can reorganize the cortex (16, 17). Because actin filaments and motors are "self-advected," or transported, by their own flow (18), there is a self-reinforcing loop in gel density, capable of creating patterns. Nevertheless, most theoretical studies do not consider the cross-effects of polymerization and diffusion, which resist pattern formation. Interestingly, in the past years, several groups have reported in vivo examples of actin patterns: mammalian axons (19), *Caenorhabditis elegans* embryo (20), and *Drosophila* trachea (21) are all cellular cylinders that display a regular array of concentric actin rings on their cortex.

In this article, we study the example of ring formation in the *Drosophila* trachea and propose a generic mechanism for stable actin pattern formation, arising from the interplay of actin turnover and myosin activity. The model makes clear predictions, which we test through fly genetics and drug experiments.

Formation of Supracellular Actin Rings

In *Drosophila* tracheal tubules, actin filaments concentrate at the apical cortex. Using Lifeact-mEGFP, which binds actin filaments, we performed time-lapse imaging to characterize the dynamics of actin in the fly tracheal system. At stage 15 of embryogenesis, we observed de novo formation of circumferential supracellular actin rings, from an initially uniform apical cortex, with different actin markers: Lifeact-mEGFP (Fig. 1*A* and Movie S1) and moesin-GFP (movie S3 of ref. 22). These structures, which face the extracellular matrix (ECM)-filled lumen, became prominent at stage 16 and showed a well-defined period (0.5 ± 0.1 μm; $n > 150$ rings). There are between 15 and 20 rings in one cell, and this pattern is later used as a template to deposit a ring pattern of cuticle (taenidial folds) (21). Using immunostaining, we also detected that nonmuscle myosin II (myosin heavy chain Zip) was enriched at the apical cortex and colocalized with actin filaments (Fig. 1*B*), although the pattern was not as clear. Rings were also present later at the third-instar larval stage (21, 23), in the air-filled trachea, with a larger, but still regular wavelength period (1.2 ± 0.1 μm; $n > 150$) (Fig. 1*C* and *SI Appendix*, Fig. S1). The appearance of actin rings coincided precisely with a 60% increase in filamentous actin concentration, referred to simply as actin in the rest of the manuscript (Fig. 1*A*), as measured through Lifeact-mEGFP. As increased actomyosin concentrations correspond to increased contractility (18), we therefore proposed a minimal model of the actomyosin cortex, where a contractility-driven advection–reaction instability drives regular actin pattern formation (Fig. 1*D*).

Significance

Robust pattern formation is a ubiquitous question of developmental biology. In 1952, Turing proposed in a seminal paper that this could be achieved by a hydrodynamical instability of two diffusing species reacting with each other, but direct experimental evidence of how a mechanism is implemented biologically is still lacking. In this paper, we show by a combina-tion of experiment and theory that the actin cytoskeleton, one of the main force-producing mechanisms in biology, has the property to self-organize into regular supracellular patterns in vivo in *Drosophila*. We show that the wavelength of the pattern depends on the physical properties of the gel and can be modified experimentally.

Author contributions: E.H. and B.D. designed research; E.H., B.D., P.R., J.F.J., and S.H. performed research; E.H., B.D., P.R., J.F.J., and S.H. analyzed data; and E.H., B.D., and P.R. wrote the paper.

The authors declare no conflict of interest.

This article is a PNAS Direct Submission.

[1]E.H. and B.D. contributed equally to this work.

[2]To whom correspondence may be addressed. Email: eh508@cam.ac.uk or bodong@ouc.edu.cn.

This article contains supporting information online at www.pnas.org/lookup/suppl/doi:10.1073/pnas.1504762112/-/DCSupplemental.

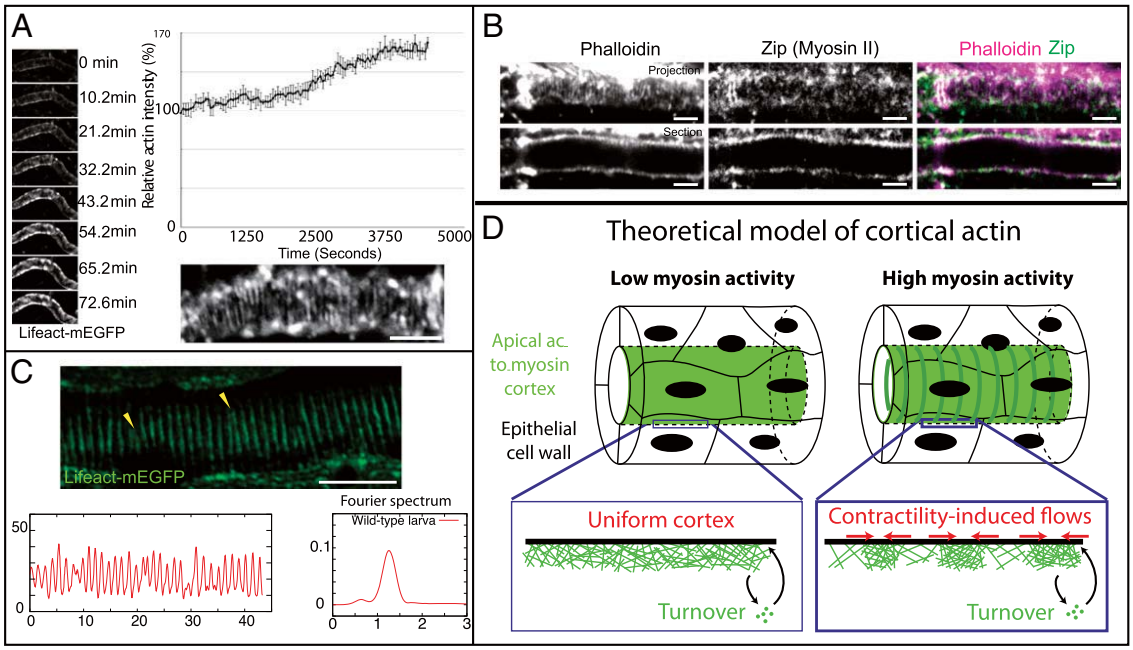

Fig. 1. Periodic supracellular actin rings in tracheal tubular system. (*A*) Live imaging of actin dynamics during the formation of the pattern, using Lifeact-mEGFP. Actin intensity increases by 70% at the onset of ring formation. (*Bottom Right*) Enlargement of actin ring structure (phalloidin) at embryonic stage 16. (*B*) Actin (phalloidin) and myosin II heavy chain (Zip) in the tracheal tubular system at stage 16. (*C*) At third-instar larval stage, the actin rings (in green, fixed sample) are very regularly spaced, as can be seen in the intensity profile and in the Fourier spectrum, with a period of 1.2 μm. (*D*) Theoretical model of an actomyosin cortex as a viscous and contractile gel, undergoing turnover and in frictional contact with an ECM. An instability into periodic patterns in actin concentration is very generically expected due to myosin contractility. (Scale bars: 10 μm.)

Theory of Actin Pattern Formation

We first concentrate on understanding the formation of actin stripes within a single cell and restrict ourselves to patterns displaying radial symmetry. We thus consider the cell cortex as a finite one-dimensional (1D) (of length L, in the axial direction x), compressible, viscous, and contractile actomyosin gel, in frictional contact with a rigid substrate. The conservation equation for the actin gel of density ρ reads as follows:

$$\partial_t \rho = \frac{\rho_0 - \rho}{\tau} - \partial_x(\rho v) + D\partial_{xx}\rho, \qquad [1]$$

where τ is the turnover time of actin treadmilling around a reference density ρ_0, and D is an effective diffusion coefficient, whose physical origin we discuss in *SI Appendix*. This equation expresses that changes in actin concentration over time (left-hand term) arise from three contributions (from left to right in the right-hand term): actin turnover, advection by cortical flows, and effective diffusion of filaments.

Momentum balance in the gel and constitutive behavior at linear order in the gel density around the reference state, respectively, read as follows (8):

$$\partial_x \sigma = \xi v \quad \sigma = \chi^0 \rho/\rho_0 + \eta \partial_x v, \qquad [2]$$

where σ is axial stress in the network and v is velocity. ξ is the friction coefficient with respect to the substrate; χ^0, the contractility arising from myosin motors; and η, the gel viscosity. As detailed in *SI Appendix*, we assume that myosin is in excess, with fast turnover, and therefore simply follows actin concentration. Starting from an initially uniform density ρ, a patterning instability occurs when myosin contractility reaches a threshold $\chi_c = (\sqrt{\eta/\tau} + \sqrt{D\xi})^2$ and forms a stationary pattern at a wavelength:

$$\lambda_c = 2\pi \left(\frac{D\tau\eta}{\xi}\right)^{1/4}. \qquad [3]$$

Therefore, as expected, high diffusion, friction, viscosity, or a low turnover time τ all stabilize a uniform cortex, by increasing the contractility threshold for pattern formation. The influence of each parameter on the wavelength is more complex: higher diffusion, viscosity, and turnover time favor large wavelengths, whereas a higher friction favors small wavelengths. These criteria are similar to ref. 24, which investigates in a different setting the temporal size oscillations of apical cell areas. The case $\tau \to \infty$ has been studied theoretically previously (10, 11) and yields to actin accumulation in a single region. We can therefore define two characteristic length scales crucial for the patterning:

- $l_h = \sqrt{\eta/\xi}$ is the hydrodynamic wavelength, i.e., it quantifies the length at which contractile stresses are propagated in the cortex. For lengths larger (respectively, smaller) than l_h, the flow is dissipated by friction (respectively, viscosity).
- $l_t = \sqrt{D\tau}$ compares the range at which diffusion and turnover act. On lengths larger (respectively, smaller) than l_t, a change in concentration is relaxed dominantly through turnover (respectively, diffusion).

We adimensionalize the equations (*SI Appendix*). Our model then involves only three nondimensional parameters: $\alpha = l/l_h$, which reflects the size of a cell with respect to the hydrodynamic length scale, $\chi = \rho_0\chi^0/\xi D$, which measures the importance of contractility-induced flows favoring the localization of the gel and $\phi = \eta/D\tau\xi$, which is the ratio of viscous stress created by actin turnover over frictional stress created by random diffusive motion. We performed a detailed analysis of the bifurcation diagram (*SI Appendix*, Figs. S9–S12) of this system, which demonstrates the pertinence of the linear analysis, as well as a numerical analysis confirming our analytical predictions (*SI Appendix*, Figs. S13–S15).

We also incorporated in our model the 2D geometry of the cortex, neglecting the effect of curvature as a first approximation and modeling the tube as a 2D periodic strip. In the absence of any polarizing, isotropic labyrinth patterns are formed as expected. Nevertheless, as the ECM is composed of chitin fibers oriented predominantly in the axial direction (25), and as cells themselves elongate preferentially in the axial direction as well (26, 27), we examine the effect of an anisotropic friction coefficient ξ_i. For orthoradial frictions slightly larger than axial frictions ($\xi_\theta > 1.1\xi_z$), circumferential actin rings are formed (Fig. 2*E*). We observe that defects remain in the simulation at steady state, closely mirroring the actual ring reconnections (Fig. 1*C*), and causing the formation of local spirals on small step size, instead of rings. Interestingly, the isotropic labyrinth patterns resembles closely the actin organization in DAAM mutants as reported in ref. 21.

Testing the Model

Validation of the Model Hypothesis. First, we performed fluorescence recovery after photobleaching (FRAP) experiments to measure some of the parameters that we use, and validate our hypothesis of the cortex as a viscous, active gel undergoing turnover. When we bleached a large region in the cortex at the embryonic state, we observed a rapid and uniform recovery of fluorescence, which can be well fitted by a single exponential (Fig. 2*A* and Movie S2), which is what is predicted by Eq. **1** (see *SI Appendix* for details). This allowed us to estimate the turnover time $\tau = 15 \pm 7$ s ($n = 10$), which is consistent with previously reported cortical turnover times (28). The immobile fraction is typically small (<20% in our experiments).

To extract the diffusion coefficient as well, we monitored the variance of the concentration profile after photobleaching (29) and showed that it increased linearly in time (Fig. 2*A*, *Bottom Right*), as predicted quantitatively by Eq. **1** (see *SI Appendix* for details). The diffusion coefficient that we extracted is $D = 0.04 \pm 0.03$ $\mu m^2 \cdot s^{-1}$ ($n = 10$). Therefore, these experiments allow us to calculate the characteristic length $l_t \approx 0.8 \pm 0.5$ μm in this system, close to the measured ring wavelength of 0.5 ± 0.1 μm.

Estimating the hydrodynamic length l_h is more difficult in this system, and can be considered as the one fitting parameter to match the observed wavelength. Assuming a friction $\xi = 10^9$ Pa·s·m^{-1} (30), a cortical thickness of 100 nm (28), and a viscosity $\eta_{3D} = \eta/h = 10^2$ Pa·s, as reported in ref. 31, we can then estimate the hydrodynamic length to $l_h \approx 0.1$ μm. This predicts a wavelength for the pattern near the threshold of $\lambda_c = 1.8$ μm, which is slightly larger, although of the same order of magnitude, than the data for embryonic and larval trachea. One should note that this is only the wavelength at the threshold, as the ring spacing is predicted to decrease as contractility increases (*SI Appendix*).

Now that we validated the basic hypotheses of our model, we then tested its two main predictions: that the instability is contractility dependent, and that the wavelength of the pattern can be modified by modifying the physical properties of the gel described above.

Model Predictions. To verify the first prediction, we incubated the embryos with 250 μM Y-27632, a drug widely used to decrease myosin II contractility, by inhibiting the Rho-associated protein kinase (ROCK) (32). Strikingly, the actin ring pattern disappeared (Fig. 2*C*), indicating that myosin contractility is essential for its formation and maintenance. This also reinforced our hypothesis that the observed increase of actin intensity at stage 14–15 is the trigger of pattern formation.

For the second prediction, we can note from Eq. **3** that decreasing the friction coefficient ξ is predicted to increase the wavelength of the pattern, because cortical flows can propagate on larger scales. Friction can be expected to arise from several contributions, and in particular from the linkage of the cortex to the ECM via the adhesion complex. We therefore expected that genetically modifying cortical adhesion should modify the ring spacing.

We start by examining mutants for Src42A, which is involved in the stabilization of the adhesion complex (27), interacting with

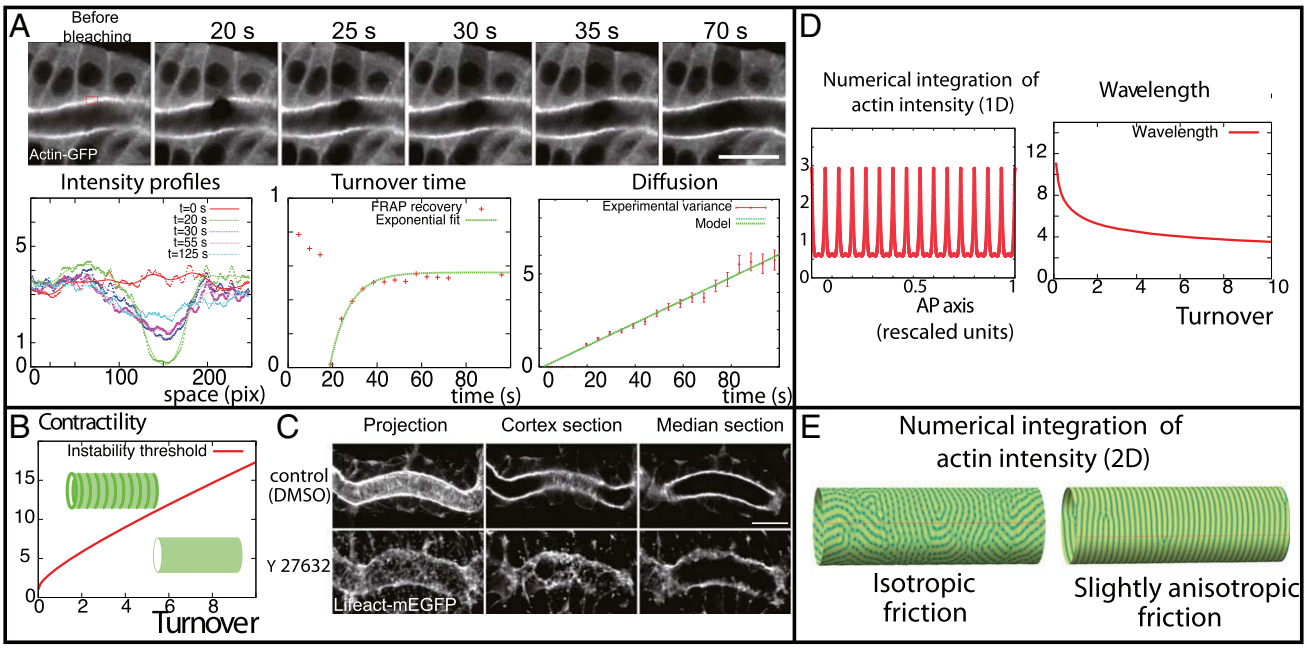

Fig. 2. Theoretical predictions and validation of the model's key assumptions. (*A*) Fluorescence recovery after photobleaching (FRAP) experiments on the apical cortex (marked by Actin-GFP) just before ring formation. We measure both the turnover time and the diffusion coefficient of the actin gel from the recovery curves. (*B*) Phase diagram of the instability. A cortex is predicted to organize into periodic patterns as soon as the rescaled contractility χ is above a critical value, which increases with the rescaled turnover ϕ. (*C*) Actin patterns at embryonic stage 16 disappear with contractility inhibition (through incubation of 250 μM Y27632), as predicted by our model. (*D*) Theoretical profiles of actin concentration for different values of our parameters in 1D. (*E*) In 2D, if all parameters are isotropic, labyrinth patterns are formed (*Left*), but circumferential rings are formed for small anisotropies (*Right*, where the friction coefficient ζ_θ is increased by 20% in the orthoradial direction). (Scale bars: 10 μm.)

E-Cadherin and β-catenin, being important for adhesion turnover and homeostasis. Src42A and its associated protein, formin family F-actin nucleator DAAM1, have also been shown to affect axial cortical tension and to induce aberrant phenotypes in tracheal development (26, 27, 33). In *Src42* mutants, the ring structure is still clearly visible (Fig. 3*A*), but the period is 0.8 ± 0.2 μm, a 70% increase compared with the wild type (Fig. 3*B*; $n > 110$ rings for each; $P < 10^{-10}$; counted on at least five different tracheas). Moreover, we examined the effect of down-regulation of moesin, the key linker between cortex and membrane in *Drosophila* (34), by expressing moesin RNAi in trachea. Actin patterns are severely in embryos and larvae (*SI Appendix*, Fig. S1 *A* and *B*). Because taenidial folds are precisely complementary with actin pattern (*SI Appendix*, Fig. S2), we measured the wavelength of taenidial folds in moesin RNAi larvae and found a 25% increase compared with wild type (1.8 ± 0.5 μm vs. 1.45 ± 0.3 μm; $P < 10^{-10}$; $n > 250$ patterns for at least four trachea in each condition), in agreement again with a decreased friction in moesin RNAi.

Moreover, the friction is dependent, not only on linkage molecules, but crucially on the presence of a solid ECM substrate to adhere on. In a previous work, we have indeed shown that, at that stage, a chitin/Dumpy matrix core is assembled at the center of the tube and behaved like an elastic solid on timescales of hours (25). In the absence of a solid ECM, we expect the friction coefficient to be drastically reduced, as only a small effective friction remains, arising from the viscous flow of the cytosol permeating through the gel, as discussed extensively in ref. 35. Moreover, for a finite-size system (i.e., one cell length L), the wavelength cannot be infinite, so as soon as it is larger than the cell size ($\lambda > L$), we expect that actin should accumulate in one single spot (i.e., one actin ring per cell).

To verify this prediction, we investigate the chitin synthase Krotzkopf verkehrt kkv^1 mutants, where the formation of the chitin/Dumpy matrix core is impaired (36) (Fig. 3). At stage 15, where rings should normally form, the tube develops an aberrant "pearling" phenotype, characterized by a series of large constrictions. We displayed on Fig. 3*C* examples of this phenotype, stained for phalloidin and DE-cadherin. The constrictions colocalize with rings containing both actin (Fig. 3*C*) and myosin II (*SI Appendix*, Fig. S3). We can therefore hypothesize that the actomyosin-generated stress in this region is large enough to locally constrict the tube, in a very similar manner to a cytokinetic ring in dividing cells (17) and nondividing notochord cells (37). This effect is amplified by the fact that there is no elastic chitin anymore in the center to resist the constriction. To test this quantitatively, we measure simultaneously along the length of the tube the local diameter, as well as the local average actin density (Fig. 3*C*). This reveals a robust anticorrelation between the two: constricted regions have large actin densities, whereas enlarged regions have low actin densities. Moreover, we incubated *kkv* mutant embryos in 250 μM Y-27632. The tube uniformly dilated, which is expected from Laplace law by reducing the tension (Fig. 3*D*). As expected, we also observed that most of the constriction disappears (except at the fusion points between the main trunk and the side branches), proving that the actomyosin rings we observe are contractile as assumed in the model. Although the actin rings are no longer as periodically arranged, we can still measure a characteristic distance of 4.5 ± 2 μm between each ring ($n > 40$; Fig. 3*B*) and observed that this corresponds indeed on average to one ring per cell (Fig. 3*C*).

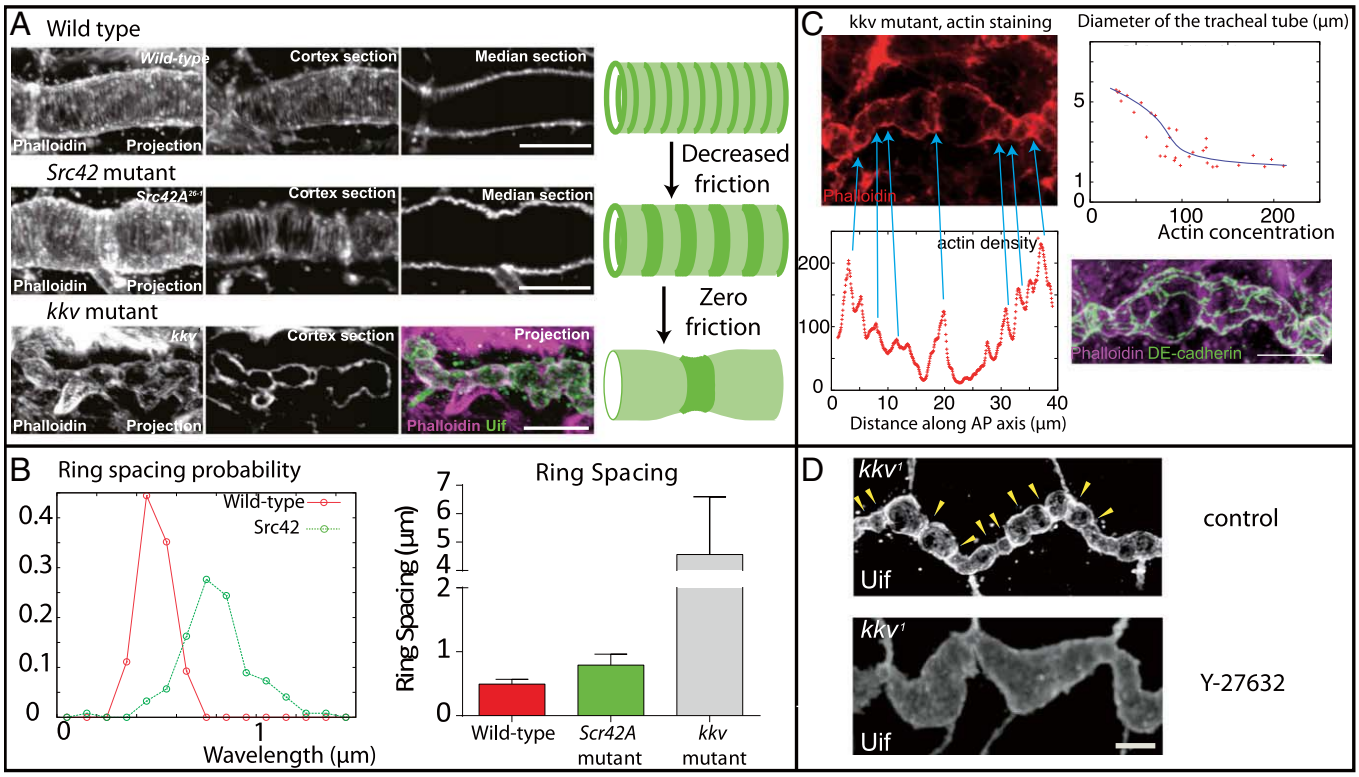

Fig. 3. Model predictions tested through pharmacological perturbation and fly genetics. (*A*) The period of the ring pattern increased by 70% in *Src42* mutants, and 10-fold by genetic removal of the extracellular matrix inside the tube (*kkv* mutant). One of our model's core predictions is that decreasing friction should increase the wavelength of the pattern. (*B*) Wavelength increases in *Src42* and *kkv* mutant ($P < 10^{-10}$), compared with wild type. (*C*) Local constrictions are observed in *kkv* mutants lacking an ECM substrate and colocalize with actin (phalloidin staining), and high actin concentration correlates with small tube radius, showing that the rings are contractile. (*Bottom Right*) Cadherin (green) and actin (purple) stating, showing that only one actin ring is present per cell on average. (*D*) Actomyosin constrictions in *kkv* mutant disappeared by lowering contractility through Y-27632 treatment. (Scale bars: 10 μm.)

Dynamical Properties of Actin Rings

Moreover, we took advantage of this *kkv* mutant, where the spacing is larger, to resolve better the live dynamics of the actomyosin rings. We took time-lapse images of tracheal tubes labeled by moesin-GFP, both in wild type and in *kkv* mutants. To our surprise, the live imaging revealed unexpected dynamics, with constrictions being extremely dynamical in time, and moving along the trachea in a disorderly manner (Fig. 4 *A* and *B*, and Movie S3).

To probe whether our physical model could reproduce this behavior, we examined the effect of simple nonlinearity to our equation. Surprisingly, adding a small nonlinearity in the turnover rate of actin caused a transition from stationary patterns to chaotic patterns (Fig. 4*C*), a previously unreported property of such a simple model of active fluid. We numerically drew a phase diagram of this secondary instability and showed that chaotic time oscillation of our patterns occurred only below a critical threshold in friction (*SI Appendix*, Figs. S5 and S6). Again, this is in agreement with the experiments: lowering friction causes both an increase in pattern wavelength, and a transition from stationary to nonstationary rings. Furthermore, we showed that the patterns in our simulations are truly chaotic (*SI Appendix*). Although a detailed nonlinear analysis is well beyond the aim of this article, we can give a simple physical argument for the transition at low friction: two neighboring rings can only interact with each other and merge if their distance is lower than the hydrodynamic wavelength. Otherwise, their interaction is screened. This gives a criteria, $\lambda = 2\pi(D\tau\eta/\zeta)^{1/4} < (\eta/\zeta)^{1/2}$, indicating that chaos can only occur if the friction is lower than a critical value, $\zeta < \zeta_c \propto \eta/D\tau$.

We now turn back to the question of the signal triggering actin and myosin recruitment on the apical cortex, which drives the instability. Because this recruitment is concomitant with diametric tube expansion, we hypothesized that this could be a mechanosensitive cue, as it was recently shown that tension on the adherens junctions via α-catenin caused a mechanosensitive recruitment of actin, through vinculin and Mena/VASP proteins (38, 39). We thus examined the small-diameter tube mutant γ-COP (40), which cannot enlarge due to impaired apical secretion. The phenotype is less severe for the heterozygous mutant ($cop^{+/-}$) than homozygous ($cop^{-/-}$) (Fig. 4 *D* and *E*). Neither mutants display a clear structure of actin rings, which is consistent with the previous report (41) that in mosaic mutants for sec24, encoding a cargo-binding subunit of the COPII complex, the thin part of the tube lacks actin rings. Crucially, we looked at cortical actin levels in wild-type, $cop^{+/-}$ and $cop^{-/-}$ embryos (*SI Appendix*, Fig. S4), and showed a progressive decrease in actin levels as the tube expansion is impaired: $cop^{+/-}$ tracheas are 20% smaller than wild type and had 40% less actin, and $cop^{-/-}$ tracheas are 45% smaller than wild type and had 65% less actin (Fig. 4*F*). This reinforces our hypothesis that actin recruitment is the driver of the instability and is connected with the widening of the tracheal tube. Interestingly, periodic actin rings were also observable on the side branches of the wild-type trachea (Fig. 4*G′*) and had the same period as on the main trunk, even though the diameter of the side branches is about three times lower. This argues against a direct influence of tube radius itself on the pattern (12) in this system.

Discussion

By a combination of modeling, genetics, and pharmacological experiments, we have shown that cortical actin patterns can arise de novo through a contractility-dependent physical instability. Because myosin motors are contractile, imbalances in their distribution create hydrodynamical actin flows; and because the motors are advected, a self-reinforcing loop exists, which can generate a sustained steady state of actomyosin flows from an initially uniform distribution. Interestingly, such a mechanism has been theoretically predicted and experimentally shown to be at play to drive amoeboid cell migration in zebrafish embryonic progenitor cells (11, 42). This corresponds to our low-friction limit, where only one actin accumulation forms in the cell.

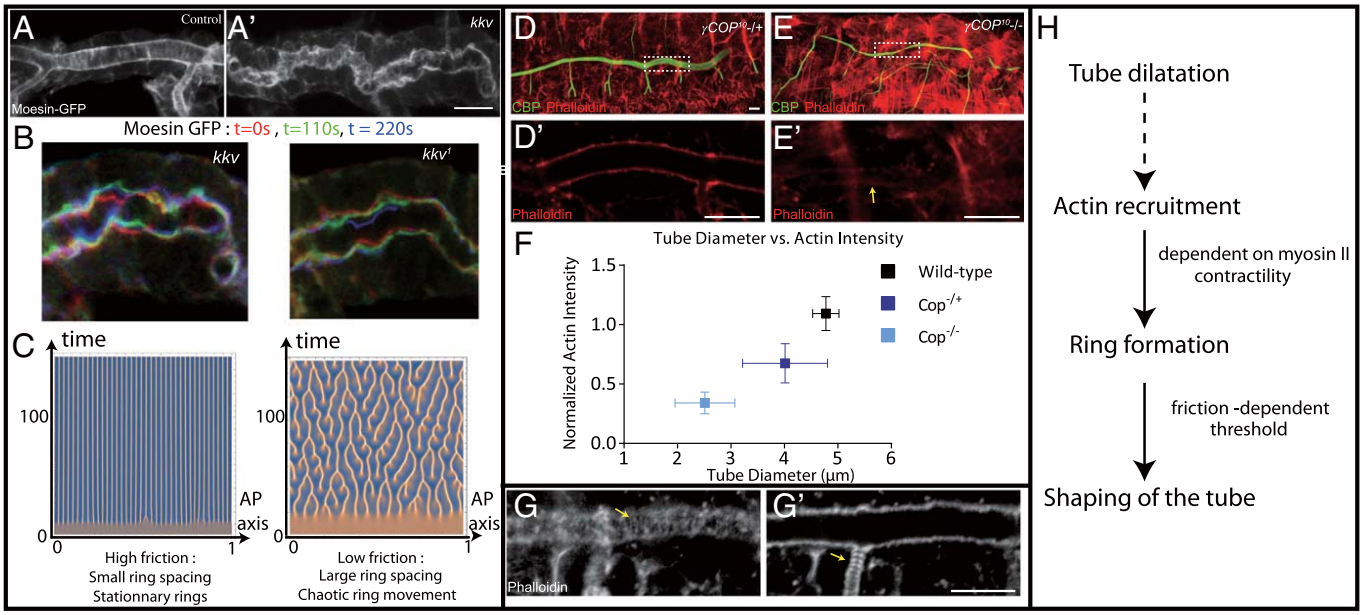

Fig. 4. (*A*) Live imaging of rings in control tracheas using moesin-GFP. (*A′*) Live imaging of rings in kkv mutants using moesin-GFP. (*B*) Moesin-GFP in *kkv* mutants. We show three superimposed time steps: $t = 0$ (green), $t = 90$ s (red), and $t = 180$ s (blue), showing that, in *kkv* mutants, the constrictions are not stationary. (*C*) Kymograph of patterns in the high- and low-friction regimes, in the case of a nonlinear turnover. A transition toward chaos is observed. (*D* and *E*) Heterozygous and homozygous γ-COP mutants. (*D′* and *E′*) Longitudinal section of tracheal tube in heterozygous (*D′*) and homozygous (*E′*) γ-COP mutants. (*F*) COP mutants show a decreased tube diameter, compared with wild type, as well as a decreased cortical actin level. Both phenotypes are stronger for homozygous mutants. (*G*) Fixed samples of actin (phalloidin) rings in wild type. One can observe that rings form both in the main trunk (*G*) and in side branches (*G′*), at the same wavelength. (*H*) Summary of the proposed model. (Scale bars: 10 μm.)

Nevertheless, our analysis proves that, generically, other modes of the instability can be seen, for high frictions or lower turnover rate for instance, and result in a patterned actin cortex of well-defined wavelength. Although this instability is qualitatively different from Turing's original ideas, it demonstrates the increasing relevance of hydrodynamical approaches to study developmental (5) and biological problems in general (7). A strength of our model is that it provides a clear physical basis for pattern formation, as the wavelength of the pattern is dictated by the physical properties of the actin gel, which are a priori all measurable experimentally in a variety of conditions (18). A key question that remains, however, is how the orientation of the pattern is regulated, to form rings in the circumferential direction, given that several mutants can cause formation of other types of pattern orientation, at constant wavelength (21). Curvature in particular could be a geometrical cue that cells are able to read and adapt to. Another aspect that deserves future attention will be the supracellular coordination between actin rings. As long as a pattern exists in individual cells, we show (*SI Appendix*, Fig. S16) for very small couplings, for instance a dependency of junction maturation on stress, as reported in ref. 38, is enough for robust supracellular coupling.

Our live imaging also revealed an intriguing dynamical property of the actin rings, which move around and coalesce without apparent steady state. Our model reproduces this finding, although other contributions could be in play, in particular a coupling between the actin dynamics and the local axial curvature, which is high in the constriction region, similar to the dynamics of FtsZ proteins on cylindrical membranes (43, 44).

Interestingly, several other instances of such periodic cortical patterns have been reported in *C. elegans* embryos (20) and in mammalian axons (19) through superresolution microscopy. Given the generality of our model, one expects that more examples should be found, provided that the friction is large enough that several patterns can fit in one cell size. In the future, it will be very interesting to study whether our biophysical mechanism applies to them.

Materials and Methods

Fly Strains and Genetics. UAS-actin-GFP was from Hiroki Oda, Kyoto Research Park, Kyoto, Japan and UAS-lifeact-mEGFP has been described previously (25). UAS-Zip-GFP was from Dan Kiehart, Duke University, Durham, NC. *kkv*^{1} was from the *Drosophila* Genetic Resource Center in Kyoto. *src42*$^{A26-1}$/CyO was from Kaoru Saigo, University of Tokyo, Tokyo. Moesin RNAi strains (P[TRiP.JF01610]; no. 31135) were from Bloomington *Drosophila* Stock Center, *Drosophila* RNAi Project (Transgenic RNAi Project).

Immunofluorescence. The primary antibodies used in this study were as follows: guinea pig anti-Uif (1:500; a gift from Robert E. Ward, University of Kansas, Lawrence, KS); phalloidin (1:100; Sigma); rat anti–DE-cadherin (DCAD 2) (1:20; Developmental Studies Hybridoma Bank); rabbit anti-zip2 (1:200; a gift from Fumio Matsuzaki, RIKEN CDB, Kobe, Japan); and chitin-binding probe (CBP) (1:50).

ACKNOWLEDGMENTS. We thank H. Oda, R. E. Ward, K. Saigo, T. Nishimura, D. Pinheiro, Y. Bellaiche, the Bloomington Stock Center, *Drosophila* Genetic Resource Center (Kyoto), and the Developmental Studies Hybridoma Bank for generously providing antibodies and fly stocks; A. Hayashi for sharing phalloidin staining samples; Y. H. Zhang for plasmid and protocol for CBP preparation; and T. Kondo and J. Prost for suggestions and discussion. This work was supported by the Taishan Scholar Program of Shandong and the Fundamental Research Funds for the Central Universities in China (3005000-841412019) (to B.D.) and a Grant-in-Aid for Scientific Research on Innovative Areas from Ministry of Education, Culture, Sports, Science and Technology of Japan (to S.H.). E.H. acknowledges support from the Young Researcher Prize of the Bettencourt-Schueller Foundation.

1. Turing AM (1952) The chemical basis of morphogenesis. *Philos Trans R Soc Lond B Biol Sci* 237(641):37–72.
2. Keller EF, Segel LA (1971) Model for chemotaxis. *J Theor Biol* 30(2):225–234.
3. Howard J, Grill SW, Bois JS (2011) Turing's next steps: The mechanochemical basis of morphogenesis. *Nat Rev Mol Cell Biol* 12(6):392–398.
4. Maini PK (2004) The impact of Turing's work on pattern formation in biology. *Math Today* 40(4):140–141.
5. Economou AD, et al. (2012) Periodic stripe formation by a Turing mechanism operating at growth zones in the mammalian palate. *Nat Genet* 44(3):348–351.
6. Inaba M, Yamanaka H, Kondo S (2012) Pigment pattern formation by contact-dependent depolarization. *Science* 335(6069):677.
7. Cates ME, Marenduzzo D, Pagonabarraga I, Tailleur J (2010) Arrested phase separation in reproducing bacteria creates a generic route to pattern formation. *Proc Natl Acad Sci USA* 107(26):11715–11720.
8. Marchetti MC, et al. (2013) Hydrodynamics of soft active matter. *Rev Mod Phys* 85(3): 1143–1189.
9. Backouche F, Haviv L, Groswasser D, Bernheim-Groswasser A (2006) Active gels: Dynamics of patterning and self-organization. *Phys Biol* 3(4):264–273.
10. Bois JS, Jülicher F, Grill SW (2011) Pattern formation in active fluids. *Phys Rev Lett* 106(2):028103.
11. Recho P, Putelat T, Truskinovsky L (2013) Contraction-driven cell motility. *Phys Rev Lett* 111(10):108102.
12. Srivastava P, Shlomovitz R, Gov NS, Rao M (2013) Patterning of polar active filaments on a tense cylindrical membrane. *Phys Rev Lett* 110(16):168104.
13. Schaller V, Weber C, Semmrich C, Frey E, Bausch AR (2010) Polar patterns of driven filaments. *Nature* 467(7311):73–77.
14. Sumino Y, et al. (2012) Large-scale vortex lattice emerging from collectively moving microtubules. *Nature* 483(7390):448–452.
15. Surrey T, Nédélec F, Leibler S, Karsenti E (2001) Physical properties determining self-organization of motors and microtubules. *Science* 292(5519):1167–1171.
16. Mayer M, Depken M, Bois JS, Jülicher F, Grill SW (2010) Anisotropies in cortical tension reveal the physical basis of polarizing cortical flows. *Nature* 467(7315):617–621.
17. Turlier H, Audoly B, Prost J, Joanny JF (2014) Furrow constriction in animal cell cytokinesis. *Biophys J* 106(1):114–123.
18. Prost J, Jülicher F, Joanny JF (2015) Active gel physics. *Nat Phys* 11(2):111–117.
19. Xu K, Zhong G, Zhuang X (2013) Actin, spectrin, and associated proteins form a periodic cytoskeletal structure in axons. *Science* 339(6118):452–456.
20. Priess JR, Hirsh DI (1986) *Caenorhabditis elegans* morphogenesis: The role of the cytoskeleton in elongation of the embryo. *Dev Biol* 117(1):156–173.
21. Matusek T, et al. (2006) The *Drosophila* formin DAAM regulates the tracheal cuticle pattern through organizing the actin cytoskeleton. *Development* 133(5):957–966.
22. Kondo T, et al. (2007) Small peptide regulators of actin-based cell morphogenesis encoded by a polycistronic mRNA. *Nat Cell Biol* 9(6):660–665.
23. Glasheen BM, Robbins RM, Piette C, Beitel GJ, Page-McCaw A (2010) A matrix metalloproteinase mediates airway remodeling in *Drosophila*. *Dev Biol* 344(2):772–783.
24. Dierkes K, Sumi A, Solon J, Salbreux G (2014) Spontaneous oscillations of elastic contractile materials with turnover. *Phys Rev Lett* 113(14):148102.
25. Dong B, Hannezo E, Hayashi S (2014) Balance between apical membrane growth and luminal matrix resistance determines epithelial tubule shape. *Cell Rep* 7(4):941–950.
26. Nelson KS, et al. (2012) *Drosophila* Src regulates anisotropic apical surface growth to control epithelial tube size. *Nat Cell Biol* 14(5):518–525.
27. Förster D, Luschnig S (2012) Src42A-dependent polarized cell shape changes mediate epithelial tube elongation in *Drosophila*. *Nat Cell Biol* 14(5):526–534.
28. Salbreux G, Charras G, Paluch E (2012) Actin cortex mechanics and cellular morphogenesis. *Trends Cell Biol* 22(10):536–545.
29. de Beco S, Gueudry C, Amblard F, Coscoy S (2009) Endocytosis is required for E-cadherin redistribution at mature adherens junctions. *Proc Natl Acad Sci USA* 106(17):7010–7015.
30. Marcy Y, Joanny JF, Prost J, Sykes C (2007) Probing friction in actin-based motility. *New J Phys* 9(11):431–438.
31. Evans E, Yeung A (1989) Apparent viscosity and cortical tension of blood granulocytes determined by micropipet aspiration. *Biophys J* 56(1):151–160.
32. Ishizaki T, et al. (2000) Pharmacological properties of Y-27632, a specific inhibitor of rho-associated kinases. *Mol Pharmacol* 57(5):976–983.
33. Shindo M, et al. (2008) Dual function of Src in the maintenance of adherens junctions during tracheal epithelial morphogenesis. *Development* 135(7):1355–1364.
34. Jankovics F, Sinka R, Lukácsovich T, Erdélyi M (2002) MOESIN crosslinks actin and cell membrane in *Drosophila* oocytes and is required for OSKAR anchoring. *Curr Biol* 12(23):2060–2065.
35. Callan-Jones AC, Julicher F (2011) Hydrodynamics of active permeating gels. *New J Phys* 13(9):093027.
36. Tonning A, et al. (2005) A transient luminal chitinous matrix is required to model epithelial tube diameter in the *Drosophila* trachea. *Dev Cell* 9(3):423–430.
37. Dong B, Deng W, Jiang D (2011) Distinct cytoskeleton populations and extensive crosstalk control *Ciona* notochord tubulogenesis. *Development* 138(8):1631–1641.
38. Yonemura S, Wada Y, Watanabe T, Nagafuchi A, Shibata M (2010) α-Catenin as a tension transducer that induces adherens junction development. *Nat Cell Biol* 12(6):533–542.
39. Leerberg JM, et al. (2014) Tension-sensitive actin assembly supports contractility at the epithelial zonula adherens. *Curr Biol* 24(15):1689–1699.
40. Norum M, et al. (2010) Trafficking through COPII stabilises cell polarity and drives secretion during *Drosophila* epidermal differentiation. *PLoS One* 5(5):e10802.
41. Förster D, Armbruster K, Luschnig S (2010) Sec24-dependent secretion drives cell-autonomous expansion of tracheal tubes in *Drosophila*. *Curr Biol* 20(1):62–68.
42. Ruprecht V, et al. (2015) Cortical contractility triggers a stochastic switch to fast amoeboid cell motility. *Cell* 160(4):673–685.
43. Osawa M, Anderson DE, Erickson HP (2008) Reconstitution of contractile FtsZ rings in liposomes. *Science* 320(5877):792–794.
44. Shlomovitz R, Gov NS (2009) Membrane-mediated interactions drive the condensation and coalescence of FtsZ rings. *Phys Biol* 6(4):046017.

Molecular Phylogenetics and Evolution 91 (2015) 238–247

Contents lists available at ScienceDirect

Molecular Phylogenetics and Evolution

journal homepage: www.elsevier.com/locate/ympev

Phylogenetic framework of the systematically confused *Anteholosticha–Holosticha* complex (Ciliophora, Hypotrichia) based on multigene analysis ☆

Xiaolu Zhao [a,b,1], Shan Gao [b,1], Yangbo Fan [b], Michaela Strueder-Kypke [c], Jie Huang [a,b,*]

[a] Key Laboratory of Aquatic Biodiversity and Conservation of Chinese Academy of Sciences, Institute of Hydrobiology, Chinese Academy of Sciences, Wuhan 430072, China
[b] Laboratory of Protozoology, Institute of Evolution and Marine Biodiversity, Ocean University of China, Qingdao 266003, China
[c] Department of Molecular and Cellular Biology, University of Guelph, Guelph, Ontario N1G 2W1, Canada

ARTICLE INFO

Article history:
Received 9 February 2015
Accepted 27 May 2015
Available online 4 June 2015

Keywords:
Anteholosticha
Arcuseries
Holosticha
Molecular phylogeny
Multigene analysis

ABSTRACT

The *Anteholosticha–Holosticha* complex is an extremely divergent group within the urostylids, especially because the genus characterization lacks suitable synapomorphies. Previous studies have shown that morphological classification of species within this group often conflicts with SSU-rDNA data, that is this complex is not recovered as a monophyletic group and *Anteholosticha* spp. are widely dispersed throughout the urostylid assemblage in SSU-rDNA trees. In this study, we provided 38 new sequences (including the type species of *Anteholosticha*) of SSU-rDNA, ITS1-5.8S-ITS2 and LSU-rDNA genes to infer molecular phylogenies of all available taxa in the *Anteholosticha–Holosticha* complex. The results show that: (1) *Holosticha* is monophyletic in all trees, suggesting it is a well-defined genus; (2) *Anteholosticha* is polyphyletic and distinctly separated from *Holosticha* in all single-gene based and concatenated phylogenies; (3) the monophyly of *Arcuseries*, a recently established genus split from *Anteholosticha*, is strongly supported by all molecular data; (4) *Anteholosticha multicirrata*, *Anteholosticha manca*, *Anteholosticha paramanca* and *Bakuella subtropica* may share a most recent common ancestor; (5) multi-gene analyses receive higher support values than the single-gene analyses.

1. Introduction

The subclass Hypotrichia is characterized by the highly developed ciliature pattern, a diverse morphology and a very complicated division process (Adl et al., 2012; Berger, 2006, 2008; Corliss, 1979; Jiang et al., 2013; Lynn, 2008; Song et al., 2009; Vďačný et al., 2014). They inhabit wide range of marine, estuarine and fresh waters, sometimes with great abundance and biomass. Although numerous studies have been performed on the assignments and phylogenetic relationships of species within this group (Berger, 2006, 2008; Chen et al., 2013a; Corliss, 1979; Fan et al., 2013; Foissner and Stoeck, 2011; Gao et al., 2010, 2013; Kim et al., 2013; Lynn, 2008; Pan et al., 2013; de Puytorac, 1994; Singh and Kamra, 2013), incongruences between morphological and gene sequence data have always existed especially in morphologically diverse taxa (Gentekaki et al., 2014; Huang et al., 2012; Lahr et al., 2013; Li et al., 2013; Moreira et al., 2007; Simpson et al., 2006; Zhang et al., 2014). According to Lynn's system (2008), the order Urostylida comprises four families (Pseudokeronopsidae, Pseudourostylidae, Urostylidae, Epiclintidae). Yi et al. (2008) proposed a fifth family, Psammomitridae. Urostylida is considered as one of the most confounded groups of hypotrichs due to the lack of some important morphogenetic data and the convergent evolution of some diagnostic morphological features (Berger, 2006; Liu et al., 2010). Thus, the classification of the urostylids is difficult in practice, and phylogenetic relationships within this group are largely unresolved.

The genus *Holosticha* Wrześniowski, 1877 originally included all hypotrichs with three frontal cirri, transverse cirri, and a midventral complex composed of cirri arranged in a zigzag pattern (Borror, 1972; Borror and Wicklow, 1983; Kahl, 1932). Following a detailed revision by Berger (2003), most species were transferred out of *Holosticha* and were tentatively assigned either to *Caudiholosticha* (with caudal cirri) or *Anteholosticha* (without caudal cirri). Berger (2003, 2006) inferred, however, that neither of

☆ This paper was edited by the Associate Editor J.B. Dacks.

* Corresponding authors at: Key Laboratory of Aquatic Biodiversity and Conservation of Chinese Academy of Sciences, Institute of Hydrobiology, Chinese Academy of Sciences, Wuhan 430072, China (J. Huang). Fax: +86 27 68780816.
E-mail address: jhuang@ihb.ac.cn (J. Huang).

[1] These authors contributed equally.

http://dx.doi.org/10.1016/j.ympev.2015.05.021
1055-7903/

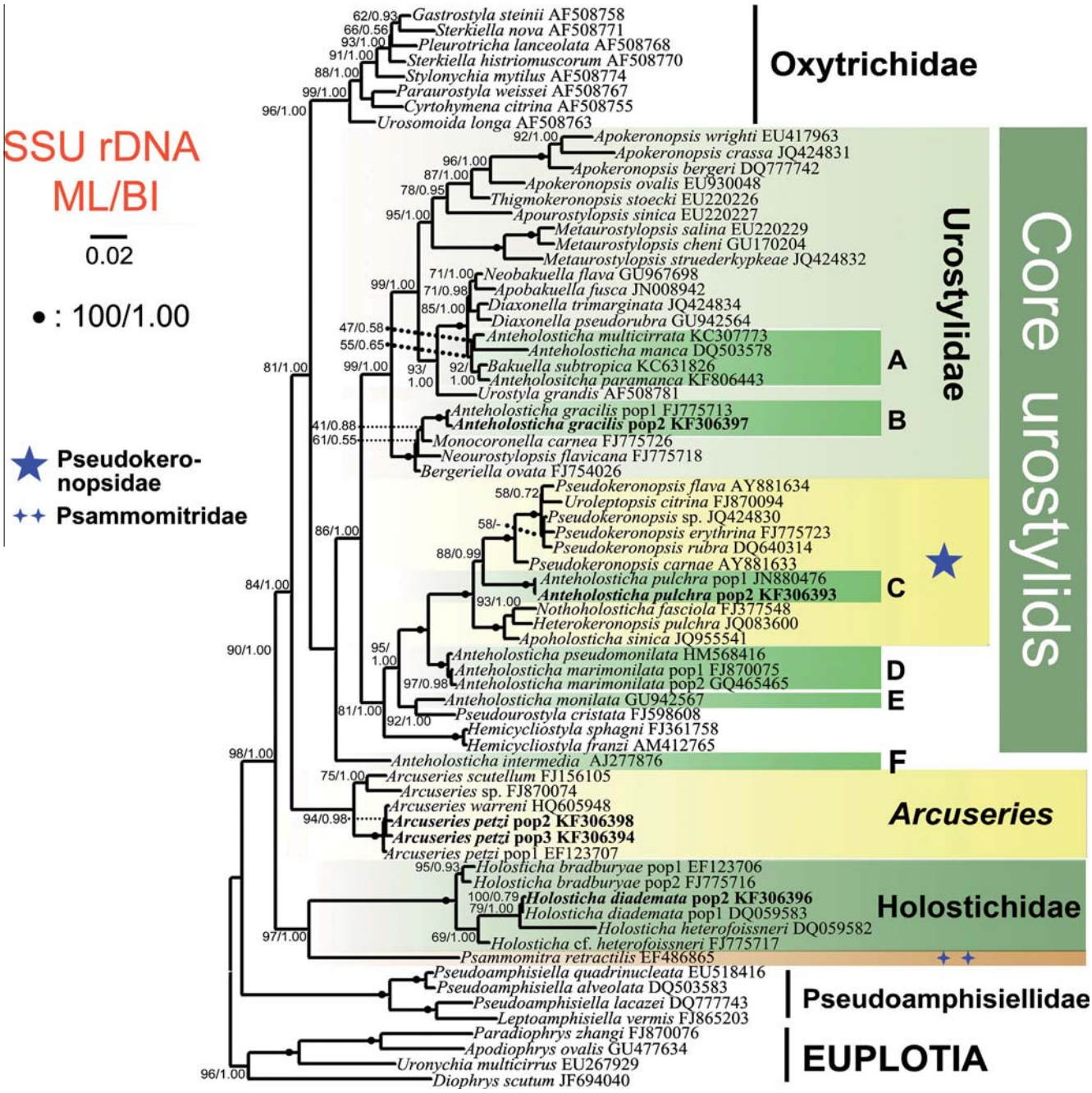

Fig. 1. Maximum likelihood (ML) tree inferred from SSU-rRNA gene sequences of representative taxa and species newly sequenced (bold) in this study (71 taxa and 1767 nucleotide characters). Numbers at nodes represent the bootstrap values of ML and the posterior probabilities of Bayesian analysis (BI), respectively. Fully supported branches are marked with solid circles at the nodes. "–" indicates the disagreement between BI tree and the reference ML tree. The scale bar corresponds to two substitutions per 100 nucleotide positions. A–F represents the different subgroups of *Anteholosticha* species.

monilata (subgroup E) shows a close relationship to *Pseudourostyla cristata* (92% ML, 1.00 BI). Moreover, the basal position of *Anteholosticha multistilata* (subgroup F) to the well-supported core group of urostylids (referred to as "core urostylids") is highly supported by both ML and BI analyses (90% ML, 1.00 BI).

3.3. LSU-rDNA (Dataset 2, Table 2, Fig. 2) and ITS1-5.8S-ITS2 (Dataset 3, Table 2, Fig. 3) phylogeny

In this study, we added 14 new sequences of ITS1-5.8S-ITS2 and 19 of LSU-rDNA, expanding the total taxa in our phylogenetic analyses to 52 and 49, respectively. Analyses inferred from LSU-rDNA sequences showed similar topologies to that of the SSU-rDNA tree. The sister relationship between oxytrichids and the core group of urostylids is well supported by BI analysis (0.91), but only poorly supported by ML analysis (66%). Basal to this large group is a strongly supported monophyletic cluster of *Arcuseries* (99% ML, 1.00 BI). Similarly, the close relationship of *Holosticha* and *Psammomitra* received maximal support (100% ML, 1.00 BI), occupying the basal position of the in-group in the phylogenetic tree. The position of *Anteholosticha pulchra* differed from that in the SSU-rDNA tree: it clusters with the *Nothoholosticha-Apoholosticha* clade instead of the *Pseudokeronopsis-Uroleptopsis* clade. However, this relationship may vary when more LSU-rDNA data are available as the support values from both methods are poor (47% ML, 0.58 BI).

The Journal of Eukaryotic Microbiology

Published by the International Society of Protistologists

Journal of Eukaryotic Microbiology ISSN 1066-5234

ORIGINAL ARTICLE

Morphology and Phylogeny of Three Trachelocercid Ciliates, with Description of a New Species, *Trachelocerca orientalis* spec. nov. (Ciliophora, Karyorelictea)

Ying Yan[a], Feng Gao[a], Yuan Xu[b], Khaled A. S. Al-Rasheid[c] & Weibo Song[a]

a Laboratory of Protozoology, Institute of Evolution & Marine Biodiversity, Ocean University of China, Qingdao, 266003, China
b State Key Laboratory of Estuarine and Coastal Research, East China Normal University, Shanghai, 200062, China
c Zoology Department, King Saud University, Riyadh, 11451, Saudi Arabia

Keywords
Marine ciliates; SSU rRNA gene; trachelocercids.

Correspondence
F. Gao, Laboratory of Protozoology, Institute of Evolution & Marine Biodiversity, Ocean University of China, Qingdao 266003, China
Telephone number: +86 532 8203 1676;
FAX number: +86 532 8203 1676;
e-mail: gaof@ouc.edu.cn

Y. Xu, State Key Laboratory of Estuarine and Coastal Research, East China Normal University, Shanghai 200062, China
Telephone number: +86 21 5434 5473;
FAX number: +86 21 5434 5473;
e-mail: hdxy8626@163.com

Received: 29 March 2014; revised 2 July 2014; accepted July 4, 2014.

doi:10.1111/jeu.12154

ABSTRACT

Three trachelocercid ciliates, *Trachelocerca orientalis* spec. nov., *Prototrachelocerca fasciolata* (Sauerbrey, 1928) Foissner, 1996 and *Tracheloraphis huangi* Xu et al., 2011, isolated from marine coastal habitats at Qingdao, China, were taxonomically studied using observation in vivo and silver staining methods. The new species *T. orientalis* spec. nov. can be recognized by the combination of its size (600–1,200 μm in vivo), 15–21 somatic kineties and about 13 groups of macronuclear nodules forming a strand and the colorless globular cortical granules. Together with the sequence data of the small subunit ribosomal RNA (SSU rRNA) gene, the information of a new isolate of *P. fasciolata* and three populations of *T. huangi* is also documented based on the present work. According to the molecular data, the phylogeny of three species is estimated and the analyses show that they are all found within the trachelocercid assemblage though *T. huangi* does not cluster with its congeners but with *Trachelocerca* species. Nonetheless, the monophyly of *Trachelocerca* is not rejected by the approximately unbiased test ($p = 0.345 > 0.05$), while that of *Tracheloraphis* is not confirmed ($p = 0.0002 < 0.05$).

THE karyorelictean family Trachelocercidae Kent 1881 were found commonly all over the world, which play significant ecological roles in marine habitats (Al-Rasheid 1996, 1997, 1998, 2001; Carey 1992; Dragesco and Dragesco-Kernéis 1986; Foissner 1996). Since the first species was described over 200 yr ago, definition and classification of members within the family were extremely confused due to the highly similar morphology until more reliable characters (somatic and oral ciliary patterns) were applied to distinguish them (Dragesco 1960; Foissner and Dragesco 1996a; Kahl 1933). Of more than 70 species reported within Trachelocercidae, there is detailed information for only nine (Alekperov et al. 2007; Andreoli et al. 2009; Carey 1992; Foissner 1996, 1997a,b; Foissner and Al-Rasheid 1999; Foissner and Dragesco 1996a,b; Mazei et al. 2009; Song et al. 2009; Wilbert 1986).

In last few years, studies on the fauna of trachelocercids have been performed in China seas (Gao et al. 2010; Xu et al. 2011b, 2012, 2013a,b; Yan et al. 2013). In this study, we investigated three trachelocercids isolated from coastal area at Qingdao, China, with regard to their live morphology, ciliature, and SSU rRNA gene based phylogenetic, as a new contribution, the results are documented here.

MATERIALS AND METHODS

Sampling and morphological investigations

Trachelocerca orientalis spec. nov. was isolated on 8 April 2012 from the intertidal zone in Qingdao, China (36°05′N, 120°27′E), where the water temperature was 15 °C and salinity was 14‰ (Fig. 1C, S1).

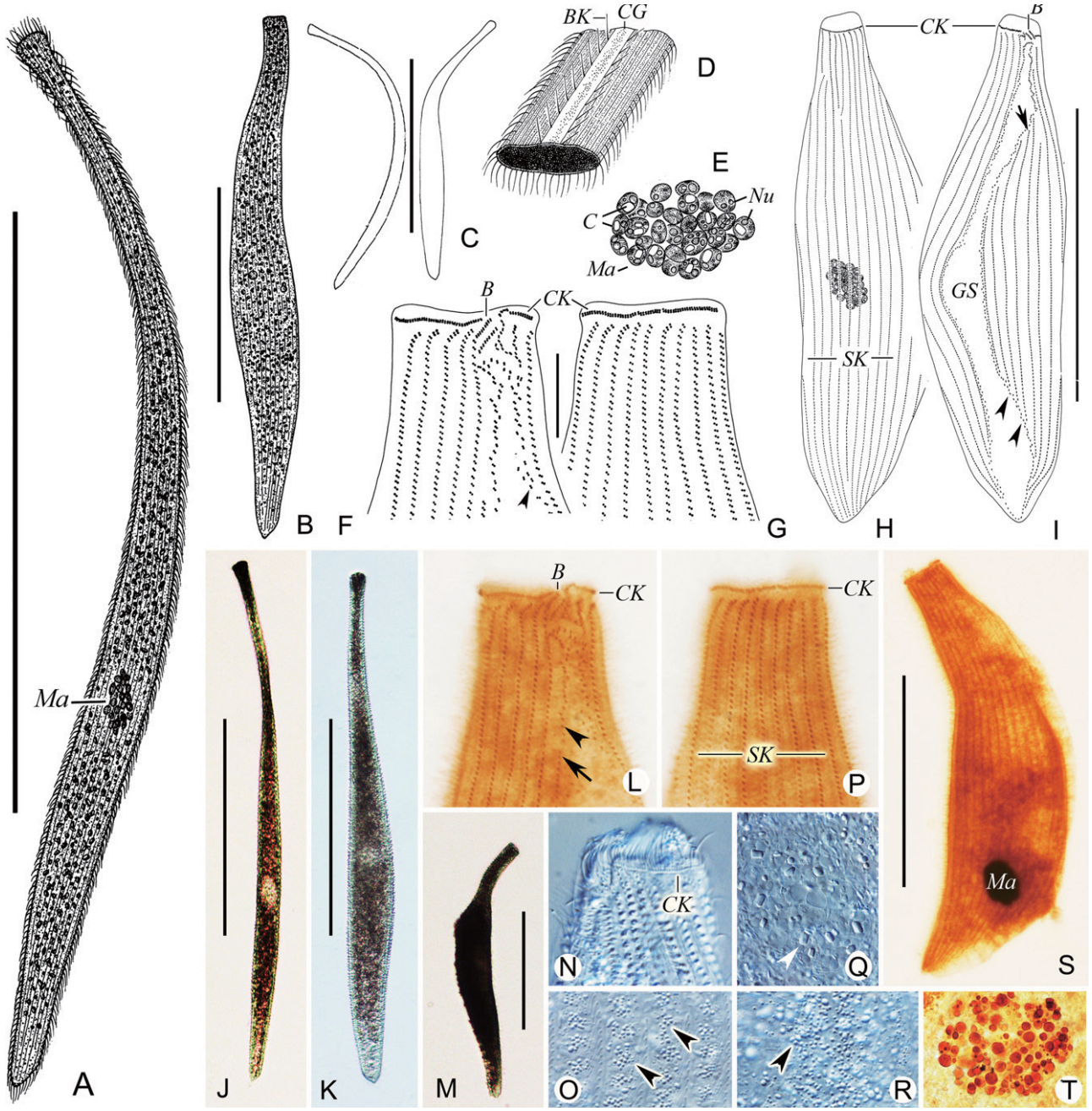

Figure 4 *Tracheloraphis huangi* from life (A–E) and after protargol impregnation (F–I). **A.** Typical individual; **B**. contracted individual; **C**. shape variants; **D**. transverse section of cell marking bristle kinety and cortical granules; **E.** nuclear group; **F, G**. left (F) and right (G) side of anterior body region, indicating bristle kinety (arrowhead), brosse and interrupted circumoral kinety; **H, I**. ciliary pattern of left (I) and right (H) side, showing glabrous stripe occupying the width of about three ciliary rows, and anterior (arrow in I) and posterior secant system (arrowheads in I); **J, K**. extended gliding individual; **L, P**. ciliary pattern in anterior body end of left (L) and right (P) side, noting brosse, circumoral kinety, bristle kineties (arrowhead in L) and anterior secant system (arrow in L); **M**. contracted individual; **N**. anterior body region showing circumoral kinety; **O, R**. distribution of cortical granules between ciliary rows (O) and in glabrous stripe (R) (arrowheads); **Q**. macronuclei indicating (protein?) crystals (arrowhead); **S.** Overview showing ciliary pattern and the single nuclear group; **T.** macronuclei forming a single nuclear group. B = brosse, BK = bristle kinety, C = crystal, CK = circumoral kinety, CG = cortical granules, GS = glabrous stripe, Ma = macronuclei, NG = nuclear group, SK = somatic kineties. Bars: 300 μm (A, J, K), 200 μm (C, H, I), 150 μm (M, S), 100 μm (B), 30 μm (F, G).

with high support values (99% ML, 1.00 BI). Therefore, both *Trachelocerca* and *Tracheloraphis* are not monophyletic. However, the AU test shows that the monophyly of *Trachelocerca* could not be rejected ($p = 0.345 > 0.05$), while the hypothesis that *Tracheloraphis* is monophyletic is rejected ($p = 0.0002 < 0.05$).

The Journal of Eukaryotic Microbiology

Published by the International Society of Protistologists

Journal of Eukaryotic Microbiology ISSN 1066-5234

ORIGINAL ARTICLE

Morphology and Phylogeny of Two Species of *Loxodes* (Ciliophora, Karyorelictea), with Description of a New Subspecies, *Loxodes striatus orientalis* subsp. n.

Yuan Xu[a,b], Hongbo Pan[c], Miao Miao[d], Xiaozhong Hu[b], Saleh A. Al-Farraj[e], Khaled A. S. Al-Rasheid[e] & Weibo Song[b]

a State Key Laboratory of Estuarine and Coastal Research, East China Normal University, Shanghai, 200062, China
b Laboratory of Protozoology, Institute of Evolution & Marine Biodiversity, Ocean University of China, Qingdao, 266003, China
c College of Fisheries and Life Science, Shanghai Ocean University, Shanghai, 201302, China
d College of Life Sciences, University of Chinese Academy of Sciences, Beijing, 100049, China
e Zoology Department, College of Science, King Saud University, Riyadh, 11451, Saudi Arabia

Keywords
Ciliates; freshwater; infraciliature; *Remanella*; SSU rRNA gene.

Correspondence
M. Miao, College of Life Sciences, University of Chinese Academy of Sciences, Beijing 100049, China
Telephone number: +86 010 88256167;
FAX number: +86 010 88256079;
e-mail: doublemiao@126.com
X. Hu, Laboratory of Protozoology, Institute of Evolution & Marine Biodiversity, Ocean University of China, Qingdao 266003, China
Telephone number/FAX number: +86 532 82031610;
e-mail: xiaozhonghu@ouc.edu.cn

Received: 10 March 2014; revised 30 June 2014; accepted July 21, 2014.

doi:10.1111/jeu.12162

ABSTRACT

The morphology and phylogeny of *Loxodes vorax* and *L. striatus orientalis* subsp. n. were investigated based on infraciliature and small subunit (SSU) rRNA gene sequence data. *Loxodes striatus orientalis* subsp. n. was separated from *L. striatus striatus* stat. n. by having fewer dikinetids in the intrabuccal kinety (35–55 vs. 50–70) and a variable number of macronuclei (2–4 vs. 2). In addition, the SSU rRNA gene sequence of the new subspecies differs in 13 and 11 nucleotides from that of two populations of the nominotypic subspecies. We also summarized the morphological differences between *Loxodes* and *Remanella* based on the data available. Phylogenetic analyses revealed that the genus *Loxodes* was monophyletic and nested within *Remanella* species. This study might, therefore, support the hypothesis that the freshwater genus *Loxodes* evolved from the marine genus *Remanella*.

RECENTLY, several marine karyorelictid groups, including trachelocercids, *Geleia*, *Kentrophoros* and *Remanella*, have been studied using the protargol staining method and phylogenetic analysis based on the small subunit (SSU) rRNA gene (Gao et al. 2010; Xu et al. 2011a,b,c, 2012, 2013a; Yan et al. 2013). The sole freshwater genus, *Loxodes,* has been widely used as material for studying a wide range of different aspects of karyorelictids, including their nuclear division (Bobyleva et al. 1980; Raikov 1982, 1994, 1996), cytology, e.g. nitrate respiration, structure and function of Müller vesicles (Fenchel and Finlay 1986a; Finlay 1985), phylogenetic position (Andreoli et al. 2009; Hammerschmidt et al. 1996), behaviour, e.g. predatory behaviour, defensive behaviour, geotaxis, and photo-behaviour (Buonanno 2005; Buonanno et al. 2005; Fenchel and Finlay 1984, 1986b; Goulder 1972) and the adaptation of ciliates to suboxic environments (Fenchel and Bernard 1996; Finlay et al. 1986). Since its initial establishment by Ehrenberg in 1830, six species have been assigned to this genus, namely, *Loxodes kahli*, *Loxodes magnus*, *Loxodes rex*, *Loxodes rostrum*, *Loxodes striatus,* and *L. vorax*, but detailed information on the oral ciliature is only available for two of these species (Foissner and Rieder 1983; Kim et al. 2009). In addition, detailed reinvestigation of *Loxodes* is required to separate it from *Remanella* (Foissner 1996). Indeed, since it was first established, the validity of the genus *Remanella* has long been questioned because the difference between it and *Loxodes* has not been shown at the

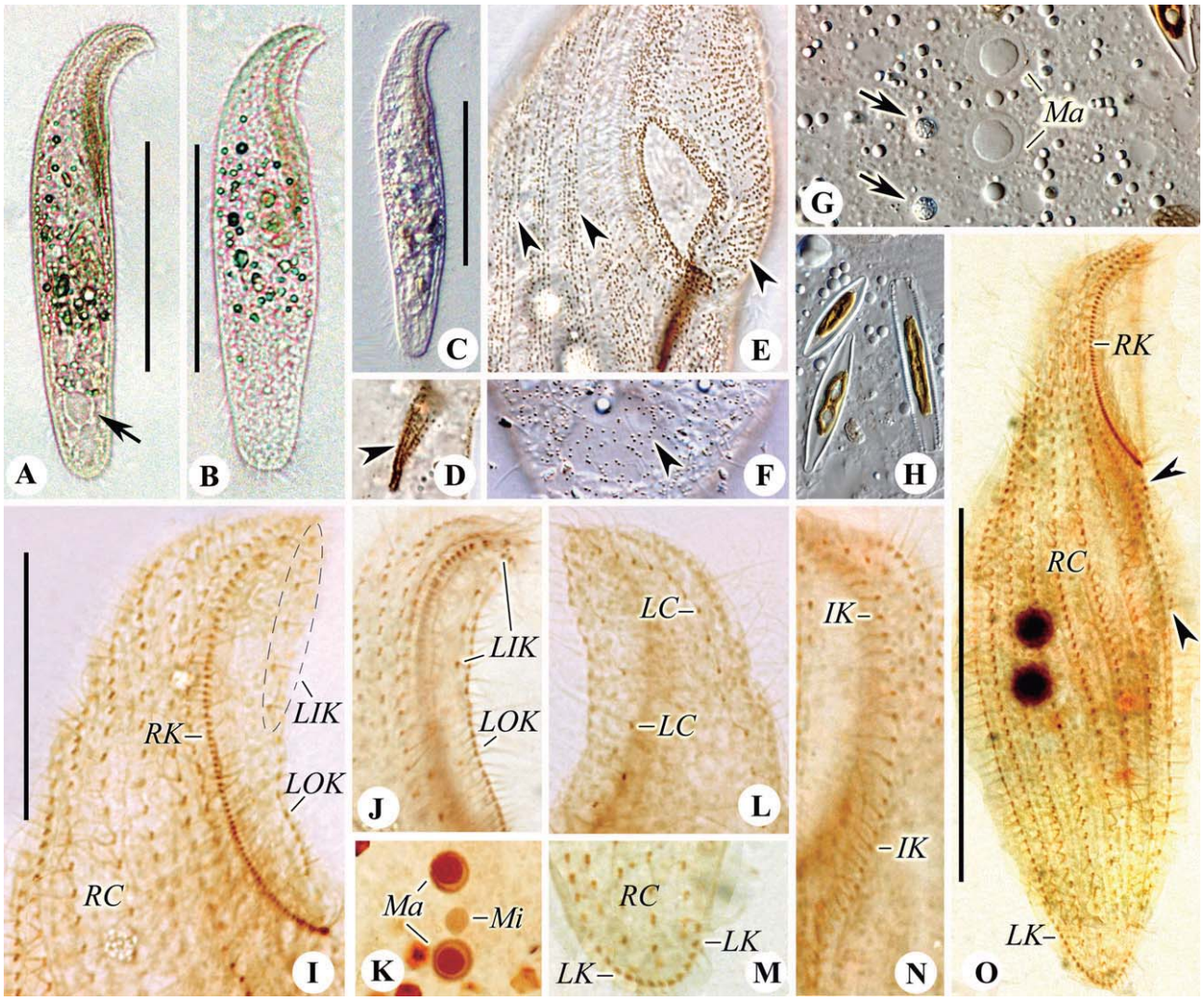

Figure 3 *Loxodes vorax* in vivo (**A**–**H**) and after protargol impregnation (**I**–**O**). **A**. Right side of a typical individual; arrow marks vacuole at posterior end. **B, C**. Different body shape. **D**. Cortical granules (arrowhead) densely packed in pharyngeal tube. **E, F**. Right (**E**) and left side (**F**), noting cortical granules (arrowheads) packed in oral area, between ciliary rows and scattered on left side. **G**. Detailed view of mid-body region, indicating Müller vesicles (arrows) and macronuclei. **H**. Digested algae. **I, J.** Infraciliature of buccal area, showing the right buccal kinety, left outer buccal kinety, left inner buccal kinety and right lateral ciliary row. **K.** Macronuclei and micronucleus. **L.** Left side of anterior region, showing left lateral ciliary row. **M.** Right side of posterior region, marking dorsolateral kinety and right lateral ciliary rows. **N.** Intrabuccal kinety. **O.** Infraciliature of right side, noting several dikinetids behind the buccal area (arrowheads). IK = intrabuccal kinety; LC = left lateral ciliary row; LIK = left inner buccal kinety; LK = dorsolateral kinety; LOK = left outer buccal kinety; Ma = macronuclei; Mi = micronucleus; RC = right lateral ciliary rows; RK = right buccal kinety. Scale bars 75 μm (A–C), 25 μm (I) and 50 μm (O).

Other *Loxodes* forms have many more macronuclei and right lateral ciliary rows, and thus cannot be confused with *L. striatus* (Table 2).

The two subspecies of *L. striatus* differ from each other in the number of dikinetids in the intrabuccal kinety (35–55 in *L. striatus orientalis* subsp. n. vs. 50–70 in *L. striatus striatus* stat. n.) and the number of macronuclei (2–4 in *L. striatus orientalis* vs. constant 2 in *L. striatus striatus* stat. n.) (Foissner and Rieder 1983). In addition, the SSU rRNA gene sequence of *L. striatus orientalis* subsp. n. differs in 13 and 11 nucleotides, respectively, from that of the two populations of *L. striatus* in Genbank (Fig. 6). Unfortunately, there is no morphological description of these two populations of *L. striatus* and *L. magnus* in the original reports (Andreoli et al. 2009; Hammerschmidt et al. 1996; Hirt et al. 1995). According to personal communications, however, there is no evidence these species could be misidentified. Therefore, we think the two sequences of *L. striatus* were from *L. striatus striatus* stat. n., which explains the difference between the SSU rRNA gene sequences of *L. striatus orientalis* subsp. n. and *L. striatus striatus* stat. n.

The Journal of Eukaryotic Microbiology

Published by the International Society of Protistologists

Journal of Eukaryotic Microbiology ISSN 1066-5234

ORIGINAL ARTICLE

Morphology and Molecular Phylogeny of Three Cyrtophorid Ciliates (Protozoa, Ciliophora) from China, Including Two New Species, *Chilodonella parauncinata* sp. n. and *Chlamydonella irregularis* sp. n.

Zhishuai Qu[a], Hongbo Pan[b], Xiaozhong Hu[a], Jiqiu Li[c], Saleh A. Al-Farraj[d], Khaled A. S. Al-Rasheid[d] & Zhenzhen Yi[c]

a Laboratory of Protozoology, Institute of Evolution & Marine Biodiversity, Ocean University of China, Qingdao, 266003, China
b College of Fisheries and Life Science, Shanghai Ocean University, Shanghai, 201306, China
c Laboratory of Protozoology, College of Life Science, South China Normal University, Guangzhou, 510631, China
d Zoology Department, College of Science, King Saud University, P.O. Box 2455, Riyadh, 11451, Saudi Arabia

Keywords
Chlamydodontida; ciliate; infraciliature; small subunit rRNA gene; taxonomy.

Correspondence
Xiaozhong Hu, Laboratory of Protozoology, Institute of Evolution & Marine Biodiversity, Ocean University of China, Qingdao 266003, China
Telephone number/FAX number: +86-0532-8203-1610;
e-mail: xiaozhonghu@ouc.edu.cn

Received: 5 April 2014; revised 18 June 2014; accepted July 21, 2014.

doi:10.1111/jeu.12175

ABSTRACT

This study investigated the morphology and molecular characteristics of three interesting free-living cyrtophorid ciliates, including two new species, isolated from China: *Chilodonella parauncinata* sp. n. can be identified by its elongated body shape, with a sharp protrusion in the left anterior part, cell size ca. 60 × 25 μm in vivo, five right and 6–7 left kineties with kinetosomes densely arranged, and a curved cyrtos. *Chlamydonella irregularis* sp. n. differs from its congeners by the oval body shape, cell size 50–60 × 25–40 μm in vivo, irregular shape of macronucleus, 30–40 club-shaped ventral protuberances, and 17 somatic kineties. Two isolates of *Chlamydonella derouxi* Song, 2003, collected from an intertidal area in Shandong and a mangrove wetland in Guangdong respectively, correspond well with two previous descriptions, but differ in comprising more basal bodies in left and right equatorial fragments and in having more finger-like protuberances on the ventral side. Phylogenetic analyses based on the small subunit rRNA gene sequences showed that *C. parauncinata* sp. n. clustered with *Chilodonella uncinata*, but was a well-outlined species of the genus, and *C. irregularis* sp. n. and *C. derouxi* grouped in the family Lynchellidae with their congeners to form the monophyletic genus *Chlamydonella*.

CYRTOPHORID ciliates are a highly specialised and divergent group of ciliates, which include more than 150 nominal morphotypes so far, with most of these being marine free-living species (Chen et al. 2011; Deroux 1976a,b,c; Dragesco 1966; Fauré-Fremiet 1965; Foissner 1979a; Gao et al. 2012; Gong and Song 2006a,b, 2009; Gong et al. 2005, 2007, 2008; Kahl 1931; Pan et al. 2011, 2012, 2013a,b). Because there are few reliable morphological features in vivo which can be used to distinguish different species, accurate identification of cyrtophorids must rely on infraciliature information. In previous studies, however, many species in this group have only been described based on live observation, and this has resulted both in inefficiency in identifying species and, inevitably, many problems with synonyms (Gong and Song 2009). Descriptions based on infraciliature are therefore needed to clarify species circumference.

During the past decade, there has been extensive investigation of cyrtophorid ciliates in China, with more than 40 species reported. In particular, the most recent studies tend to suggest that the species richness of this group in China is even higher than previously thought, with various new taxa being successively reported (Chen et al. 2012; Gong and Song 2004; Pan et al. 2012, 2013a,b; Song et al. 2009).

This paper presents morphological descriptions of two new species, *Chilodonella parauncinata* sp. n. and *Chlamydonella irregularis* sp. n., and two populations of *Chlamydonella derouxi* Song 2003, particularly with

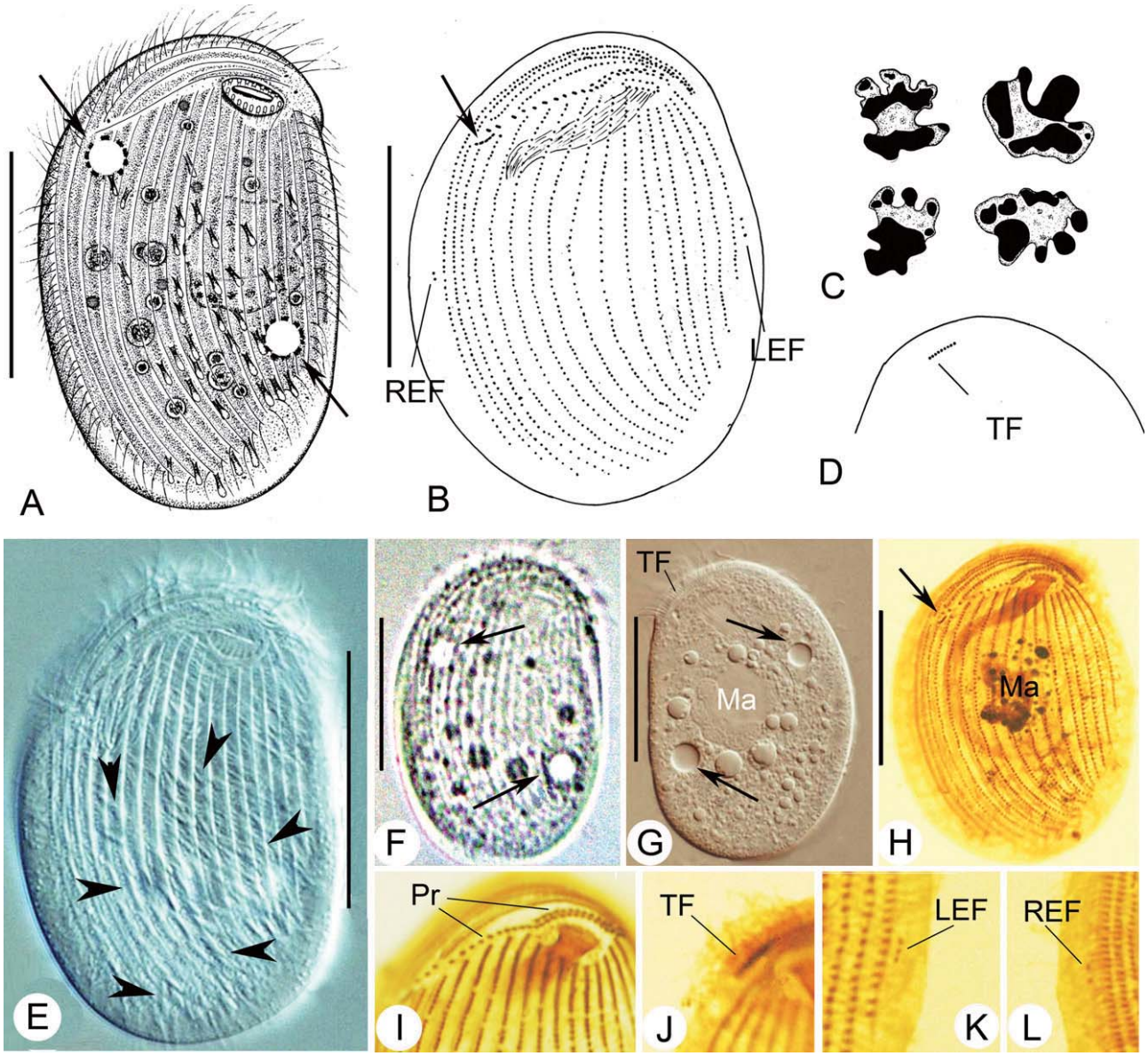

Figure 5 *Chlamydonella irregularis* sp. n. from life (**A**, **E**–**G**) and after protargol impregnation (**B**–**D**, **H**–**L**). **A, E, F.** Ventral views, arrowheads show the protuberances on the ventral side, arrows mark the contractile vacuoles. **B, H.** Ventral views, arrows mark the fragment separated from preoral kinety on the right. **C.** Variable shapes of macronucleus after protargol impregnation. **D, J.** Dorsal view, showing the terminal fragment. **I.** Shows the oral kineties. **K, L.** Shows the left and right equatorial fragments. LEF = left equatorial fragment; Ma = macronucleus; Pr = preoral kinety; REF = right equatorial fragment; TF = terminal fragment. Bars: 30 μm.

sp. n. and *C. uncinata*, with a sequence identity of 96.5%. The SSU rRNA gene sequences of *C. derouxi*, *C. irregularis* sp. n., and *C. pseudochilodon* differ from each other in 79–88 nucleotides with sequence identities ranging from 94.4% to 95.1% (see Table 4).

Maximum likelihood and BI trees have similar topologies, and were therefore combined into a single tree (Fig. 2). The monophyly of the Subclass Cyrtophorida is fully supported. As shown in Fig. 2, *C. parauncinata* sp. n. is sister to *C. uncinata* with full support, and is positioned inside the monophyletic family Chilodonellidae. *Chlamydonella* is a monophyletic genus: *C. derouxi* clusters with the *Chlamydonella pseudochilodon* with full support values, forming a parallel clade to *C. irregularis* sp. n. with high support values (BI/ML, 1.00/97).

DISCUSSION

Comparison of *C. parauncinata* sp. n. with congeners (Table 5 and Fig. 7, 8A–H)

Kahl (1931) recorded more than 30 nominal *Chilodonella* species in his epic work. After that, only four new species have been suggested (Jankowski 2007; Kidder and Sum-

Zoologica Scripta

New considerations on the phylogeny of cyrtophorian ciliates (Protozoa, Ciliophora): expanded sampling to understand their evolutionary relationships

Xiao Chen*, Hongbo Pan*, Jie Huang, Alan Warren, Saleh A. Al-Farraj & Shan Gao

Submitted: 14 May 2015
Accepted: 11 October 2015
doi:10.1111/zsc.12150

Chen, X., Pan, H., Huang, J., Warren, A., Al-Farraj, S.A., & Gao, S. (2015). New considerations on the phylogeny of cyrtophorian ciliates (Protozoa, Ciliophora): expanded sampling to understand their evolutionary relationships. — *Zoologica Scripta*, *00*, 000–000.

To rationalize the confusing relationships among the cyrtophorian ciliates, we expanded the taxon sampling by sequencing the small subunit ribosomal RNA (SSU rRNA) gene of representatives of 12 genera (20 species, 23 new sequences). The SSU rRNA sequences of *Spirodysteria*, *Agnathodysteria*, *Brooklynella* and *Odontochlamys* are reported for the first time. Phylogenetic trees were constructed, and secondary structures of variable region 4 (V4) of all genera for which SSU rRNA gene sequence data are available were predicted. The results indicate that (i) *Brooklynella* is likely an intermediate taxon between Dysteriidae and Hartmannulidae; (ii) the genus *Dysteria* is paraphyletic with *Spirodysteria* and *Mirodysteria* nested within it; (iii) the genus *Agnathodysteria* is well separated from *Dysteria* based on both molecular and morphological data; *and* (iv) *Trithigmostoma* is a basal genus of Chilodonellidae, based on both the morphological and molecular data.

Corresponding author: *Shan Gao, Laboratory of Protozoology, Institute of Evolution & Marine Biodiversity, Ocean University of China, Qingdao 266003, China and Laboratory for Marine Biology and Biotechnology, Qingdao National Laboratory for Marine Science and Technology, Qingdao 266003, China. E-mail: shangao@ouc.edu.cn*

Xiao Chen, Laboratory of Protozoology, Institute of Evolution & Marine Biodiversity, Ocean University of China, Qingdao 266003, China. E-mail: seanchen607@gmail.com

Hongbo Pan, College of Fisheries and Life Science, Shanghai Ocean University, Shanghai 201306, China. E-mail: panhongbobio@sina.com

Jie Huang, Laboratory of Protozoology, Institute of Evolution & Marine Biodiversity, Ocean University of China, Qingdao 266003, China. E-mail: hjbx152@163.com

Alan Warren, Department of Life Sciences, Natural History Museum, Cromwell Road, London SW7 5BD, UK. E-mail: a.warren@nhm.ac.uk

Saleh A. Al-Farraj, Zoology Department, College of Science, King Saud University, Riyadh 11451, Saudi Arabia. E-mail: salfarraj@hotmail.com

Shan Gao, Laboratory of Protozoology, Institute of Evolution & Marine Biodiversity, Ocean University of China, Qingdao 266003, China and Laboratory for Marine Biology and Biotechnology, Qingdao National Laboratory for Marine Science and Technology, Qingdao 266003, China. E-mail: shangao@ouc.edu.cn

**These authors contributed equally to the study.*

Introduction

As the main component of the class Phyllopharyngea de Puytorac *et al*., 1974, the subclass Cyrtophoria Fauré-Fremiet in Corliss, 1956 is a highly divergent ciliate group with numerous morphotypes (Figs 1 and 2) (Corliss 1979; Small & Lynn 1985; de Puytorac 1994; Lynn & Small 2002; Gong 2005; Lynn 2008). The membership of the Cyrtophoria has experienced several changes since its establishment. It contained one order, eight families and 43 genera in Corliss (1979). De Puytorac (1994) recognized three orders, that is Chilodonellida Deroux, 1970, Chlamydodontida Deroux, 1976 and Dysteriida Deroux, 1976. Lynn & Small (2002) assigned phyllopharyngeans with subclass rank and recognized two orders, namely Chlamydodontida and Dysteriida, with the order Chilodonellida being assigned to the order Chlamydodontida as the family

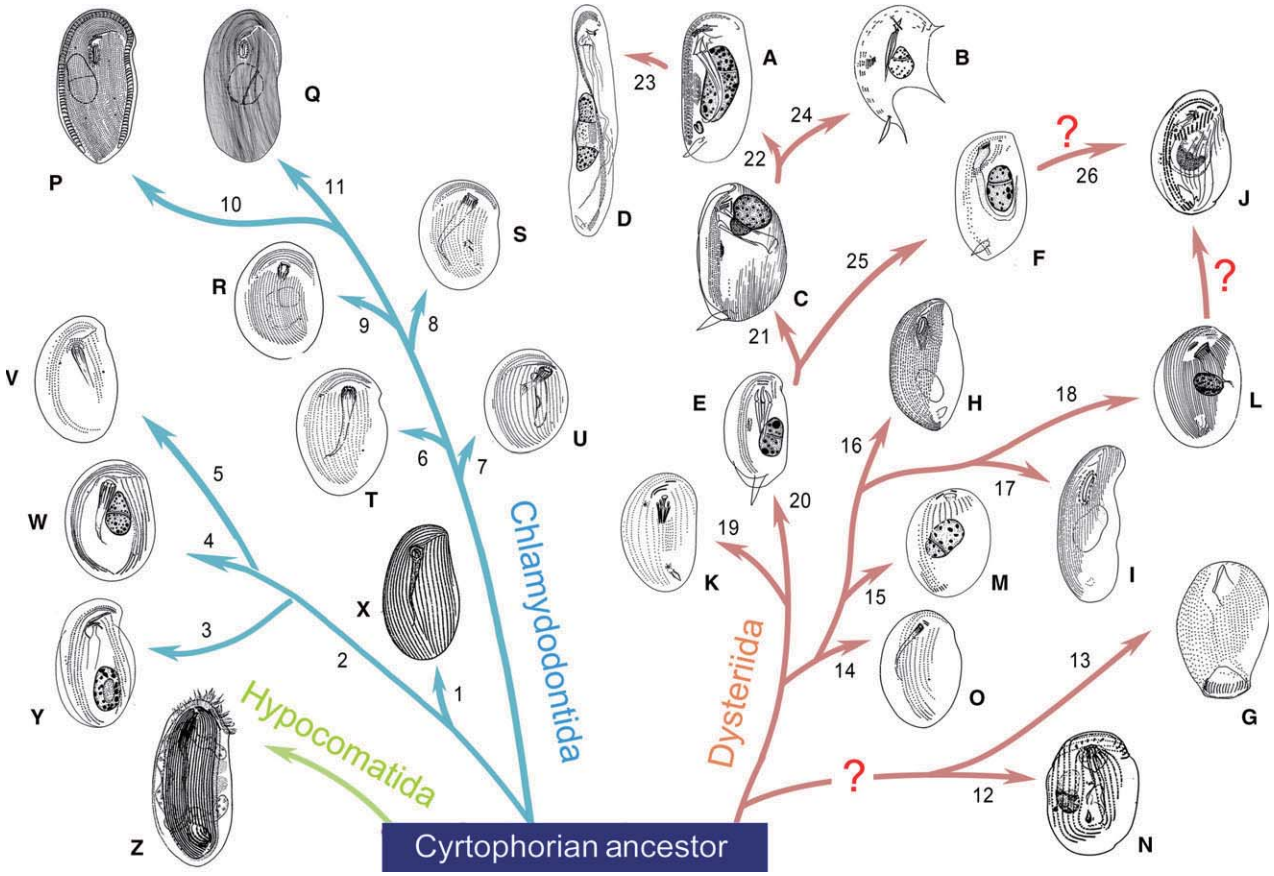

Fig. 2 Diagrammatic representations and suggested evolutionary relationships among the currently recognized cyrtophorian genera. Roman letters in the diagrams correspond to those in parentheses in Fig. 1, referring to each genus. Numbers label the morphological generic features: 1. cell usually with pronounced anterior projection or 'beak' to left; macronucleus centric and heteromerous; all ventral kineties continuous (*Trithigmostoma*); 2. right kineties separated from left kineties; the presence of glabrous region in the middle of ventral side; 3. preoral kinety continuous; terminal fragment apically positioned (*Odontochlamys*); 4. preoral kinety segmented (*Pseudochilodonopsis*); 5. preoral kinety continuous; terminal fragment subapically positioned (*Chilodonella*); 6. oral ciliature comprises only one kinety (*Chlamydonellopsis*); 7. three oral kineties forming a Y-shape (*Chlamydonella*); 8. the presence of cross-striated band around perimeter between ventral and dorsal surfaces; pre- and postoral kineties completely separated; perioral kineties consisting one continuous anterior and two detached posterior rows (*Coeloperix*); 9. the presence of non-cross-striated grooves around perimeter between ventral and dorsal surfaces; pre- and postoral kineties completely separated; perioral kineties consisting one continuous anterior and two detached posterior rows (*Lynchella*); 10. the presence of cross-striated band; oral ciliature consisting two circumoral kineties and one preoral kinety (*Chlamydodon*); 11. the absence of cross-striated band; oral ciliature consisting two circumoral kineties and one preoral kinety (*Paracyrtophoron*); 12. right kineties separated from left kineties; oral kinety segmented; with non-ciliated adhesive region (*Pithites*); 13. right and left kineties continuous with each other; oral kinety segmented; posterior glandular region conspicuously depressed (*Trichopodiella*); 14. right kineties separated from left kineties posteriorly; oral ciliature consisting only two circumoral kineties; podite absent (*Trochochilodon*); 15. oral kineties consisting two fragments; postoral kineties strongly shortened posteriad; terminal fragments consisting several parallel arranged fragments; podite present (*Aporthotrochilia*); 16. left kineties shortened posteriad; podite present; oral kineties consisting two circumoral kineties and one preoral kinety (*Harmannula*); 17. oral kineties consisting obliquely arranged fragments (*Heterohartmannula*); 18. podite surrounded by kineties; circumoral kineties consisting more than two parallel fragments (*Aegyriana*); 19. postoral kineties considerably shorter than right kineties and terminating at the same postequatorial level; podite present (*Brooklynella*); 20. body laterally compressed but no ventral groove; two nematodesmal rods; constantly two left frontal kineties (*Trochilia*); 21. six nematodesmal rods; three left frontal kineties (*Agnathodysteria*); 22. body laterally compressed with ventral groove; two nematodesmal rods (*Dysteria*); 23. body twisted; right kineties shortened posteriad (*Spirotdysteria*); 24. right kineties reduced to several sparsely arranged fragments; spines present on dorsal margin (*Mirodysteria*); 25. four nematodesmal rods; postoral and left kineties extremely short, positioned anterior of equator (*Microxysma*); 26. six nematodesmal rods; postoral and left kineties short, positioned anterior of equator (*Trochilioides*).

Zoologica Scripta

A case study to estimate the applicability of secondary structures of SSU-rRNA gene in taxonomy and phylogenetic analyses of ciliates

Pu Wang* Feng Gao* Jie Huang, Michaela Strüder-Kypke & Zhenzhen Yi

Submitted: 10 February 2015
Accepted: 9 May 2015
doi:10.1111/zsc.12122

Wang, P., Gao, F., Huang, J., Strüder-Kypke, M. & Yi, Z. (2015). A case study to estimate the applicability of secondary structures of SSU-rRNA gene in taxonomy and phylogenetic analyses of ciliates. — *Zoologica Scripta*, *44*, 574–585.

Phylogenetic studies of ciliates are mainly based on the primary structure information of the nuclear genes. Some regions of the small subunit ribosomal RNA (SSU-rRNA) gene have distinctive secondary structures, which have demonstrated value as phylogenetic/taxonomic characters. In the current work, we predict the secondary structures of four variable regions (V2, V4, V7 and V9) in the SSU-rRNA gene of 45 urostylids. Structure comparisons indicate that the V4 region is the most effective in revealing interspecific relationships, while the V9 region appears suitable at the family level or higher. The V2 region also offers some taxonomic information, but is too conserved to reflect phylogenetic relationships at the family or lower level, at least for urostylids. The V7 region is the least informative. We constructed several phylogenetic trees, based on the primary sequence alignment and based on an improved alignment according to the secondary structures. The results suggest that including secondary structure information in phylogenetic analyses provides additional insights into phylogenetic relationships. Using urostylid ciliates as an example, we show that secondary structure information results in a better understanding of their relationships, for example generic relationships within the family Pseudokeronopsidae.

Corresponding authors: *Jie Huang, Laboratory of Protozoology, Institute of Evolution & Marine Biodiversity, Ocean University of China, Qingdao 266003, China and Key Laboratory of Aquatic Biodiversity and Conservation of Chinese Academy of Sciences, Institute of Hydrobiology, Chinese Academy of Sciences, Wuhan 430072, China. E-mail: jhuang@ihb.ac.cn*
and
Zhenzhen Yi, Laboratory of Protozoology, Institute of Evolution & Marine Biodiversity, Ocean University of China, Qingdao 266003, China and Laboratory of Protozoology, Key Laboratory of Ecology and Environmental Science in Guangdong Higher Education, College of Life Science, South China Normal University, Guangzhou 510631, China. E-mail: zyi@scnu.edu.cn
Pu Wang and Feng Gao, Laboratory of Protozoology, Institute of Evolution & Marine Biodiversity, Ocean University of China, Qingdao, China. E-mail: wp0537@126.com, gaof@ouc.edu.cn
Jie Huang, Laboratory of Protozoology, Institute of Evolution & Marine Biodiversity, Ocean University of China, Qingdao, China and Key Laboratory of Aquatic Biodiversity and Conservation of Chinese Academy of Sciences, Institute of Hydrobiology, Chinese Academy of Sciences, Wuhan, China. E-mail: jhuang@ihb.ac.cn
Michaela Strüder-Kypke, Department of Molecular and Cellular Biology, University of Guelph, Guelph, ON, Canada. E-mail: michaela.strueder.kypke@uoguelph.ca
Zhenzhen Yi, Laboratory of Protozoology, Institute of Evolution & Marine Biodiversity, Ocean University of China, Qingdao, China and Laboratory of Protozoology, Key Laboratory of Ecology and Environmental Science in Guangdong Higher Education, College of Life Science, South China Normal University, Guangzhou, China. E-mail: zyi@scnu.edu.cn
**Co-first authors.*

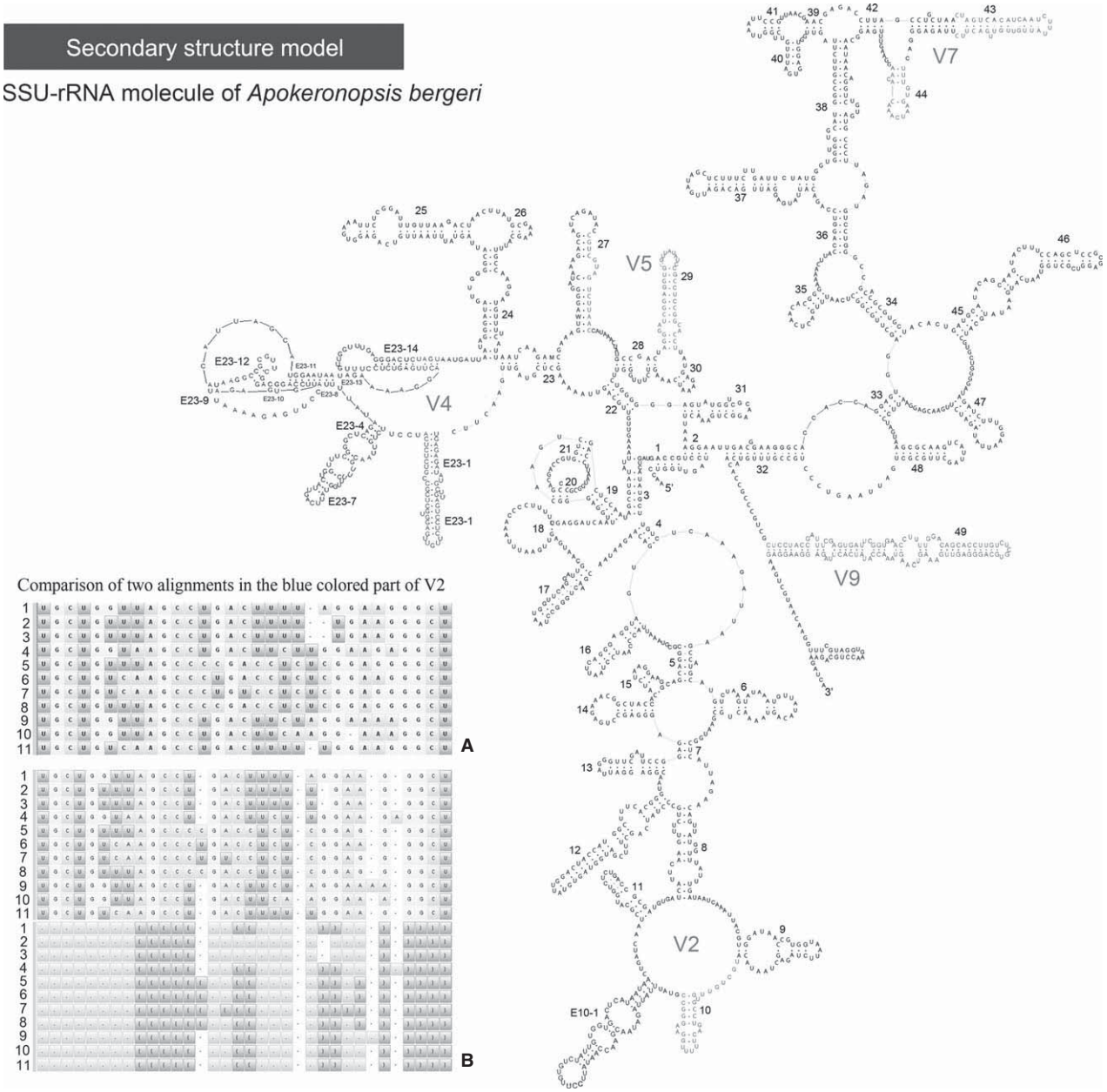

Fig. 3 Secondary structure model of the SSU-rRNA molecule of *Apokeronopsis bergeri* with an example of comparison of ambiguously aligned loci in V2. Nucleotides highlighted in blue show the ambiguously aligned loci: (A) primary sequence alignment and (B) sequence–structure alignment. Numbers represent taxa: 1 *Antebolosticha monilata*, 2 *Antebolosticha pseudomonilata*, 3 *Antebolosticha marimonilata*, 4 *Holosticha heterofoissneri*, 5 *Arcuseries petzi*, 6 *Arcuseries* sp., 7 *Arcuseries scutellum*, 8 *Arcuseries warren*, 9 *Antebolosticha intermedia*, 10 *Urostyla grandis* and 11 *Uroleptopsis citrina*.

yield consistent topologies, with the sequence–structure tree receiving higher support values (Fig. 1). However, incongruities exist for poorly supported nodes. Hence, for taxa of poorly supported branches, the sequence–structure tree can improve the resolution of the inferred relationships and shows a more robust result than the primary sequence tree. In addition to the robust secondary structure information, employing other gene markers and increased taxon sampling are needed to produce more informative phylogenies.

Comparison of the secondary structures

The complete secondary structure of SSU-rRNA is predicted for the first time for a large number of taxa in the

International Journal of Systematic and Evolutionary Microbiology (2015), **65**, 2292–2303 **DOI** 10.1099/ijs.0.000253

Morphology and morphogenesis of a novel mangrove ciliate, *Sterkiella subtropica* sp. nov. (Protozoa, Ciliophora, Hypotrichia), with phylogenetic analyses based on small-subunit rDNA sequence data

Xumiao Chen,[1,2] Feng Gao,[2] Saleh A. Al-Farraj,[3] Khaled A. S. Al-Rasheid,[3] Kuidong Xu[1] and Weibo Song[2]

Correspondence
Kuidong Xu
kxu@qdio.ac.cn
Weibo Song
wsong@ouc.edu.cn

[1]Institute of Oceanology, Chinese Academy of Sciences, Qingdao 266071, PR China

[2]Laboratory of Protozoology, Institute of Evolution & Marine Biodiversity, Ocean University of China, Qingdao 266003, PR China

[3]Zoology Department, College of Science, King Saud University, Riyadh 11451, Saudi Arabia

A novel marine hypotrichous ciliate, *Sterkiella subtropica* sp. nov., was recently isolated from a mangrove wetland in Hong Kong. Its morphology, morphogenesis and systematic position have been investigated. The novel species is diagnosed by combined features of morphology, ciliature and nuclear apparatus, while its ontogenetic events present a stable pattern: (i) the six streaks of the undulating membrane (UM) and cirral anlagen are segmented in a 1 : 3 : 3 : 3 : 4 : 4 pattern from left to right, and form three frontal, four frontoventral, one buccal, five ventral and five transverse cirri; (ii) the dorsal structure is similar to most other oxytrichids; that is, in a '4 + 2' pattern with three caudal cirri being formed. Based on the small-subunit rDNA sequence, the novel species is different from its congeners by between 21 and 35 bp, with sequence identities from 0.978 to 0.987. All molecular trees exhibited a similar topology: the monophyly of species of the genus *Sterkiella* is not completely supported in our analyses, and approximately unbiased tests (both including and excluding the novel species) also reject the possibility that *Sterkiella* is a monophyletic lineage, as indicated by the morphology-based classification.

INTRODUCTION

Based on their morphological and morphogenetic characteristics, the hypotrichous ciliates are considered to be one of the most confusing and divergent groups of protists (Berger, 1999, 2006, 2008, 2011; Chen *et al.*, 2013a; Fan *et al.*, 2014; Jiang *et al.*, 2013; Küppers & Claps, 2013; Li *et al.*, 2013; Park *et al.* 2013). The ontogenetic processes of hypotrichids reveal highly diversified patterns, which provide information that is indispensable for a better understanding of their complex evolutionary and systematic relationships (Foissner, 1996; Foissner *et al.*, 2014; Jung *et al.*, 2014; Küppers *et al.*, 2011; Lu *et al.*, 2014; Lv *et al.*, 2013; Shao *et al.*, 2013, 2014a, b, c; Singh & Kamra, 2013; Singh *et al.* 2013).

Abbreviations: AU, approximately unbiased; AZM, adoral zone of membranelles; BI, Bayesian inference; ML, maximum-likelihood; SSU, small subunit; UM, undulating membrane.

The GenBank/EMBL/DDBJ accession number for the SSU rDNA sequence of *Sterkiella subtropica* sp. nov. is KM924307.

Based on cladistics analyses using mainly morphological and morphogenetic information, a new subfamily, Stylonychinae, was suggested by Berger & Foissner (1997), which includes the 18-cirri oxytrichids with a rigid body, no cortical granules and an adoral zone of membranelles (AZM) usually more than 40 % of the body length. Subsequently, phylogenetic research based on molecular data has strongly supported the monophyly of the subfamily Stylonychinae (Bernhard *et al.*, 2001; Chen *et al.*, 2013b; Foissner *et al.*, 2004; Hu *et al.*, 2011; Schmidt *et al.*, 2007). The evolutionary relationships between the genera in the subfamily Stylonychinae are complex and confusing, however, since some genera still appear to be non-monophyletic, despite their well-outlined morphological characteristics and highly stable ontogenetic processes.

In the present work, we describe the morphology and ontogeny of *Sterkiella subtropica* sp. nov. isolated from a mangrove wetland in Hong Kong, southern China. Its morphological characteristics correspond well with those of its congeners, and its ontogenetic process conforms to the

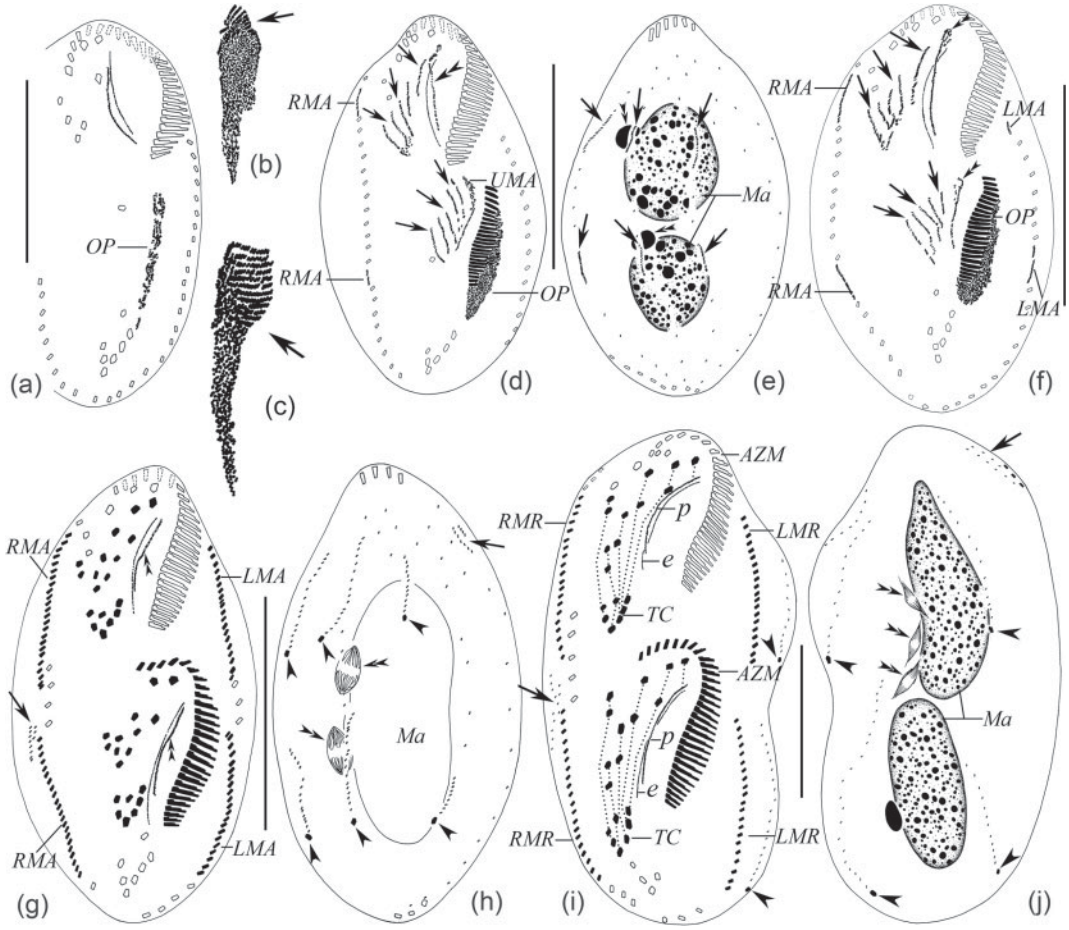

Fig. 3. Infraciliature of *Sterkiella subtropica* sp. nov. during the ontogenetic process after protargol impregnation. The parental cirri are shown in outline, whereas new ones are shown in solid black. (a–c) Ventral views of early dividers. Note that the basal bodies in the oral primordium (OP) form an elongated field (a), and then develop and differentiate new membranelles posteriad from the anterior end. (d, e) Ventral (d) and dorsal (e) views of the same specimen in the middle stage. Arrows show the fronto-ventral-transverse (FVT) cirral anlagen (d) and the anlagen of the dorsal kineties (e); double-arrowheads indicate how the old paroral membrane dedifferentiates into the UMA (d) and the micronuclei (e). (f) Ventral view of a middle divider. Arrows and double arrowheads show the FVT cirral anlagen forming and the UMA giving rise to one frontal cirrus, in both proter and opisthe. (g, h) Ventral (g) and dorsal (h) views of a late divider. Arrows mark the anlagen for dorsomarginal kineties formed near the anterior ends of the RMA, double-arrowheads show the UMA splitting into endoral and paroral membranes (g) and dividing micronuclei (h), and arrowheads indicate the caudal cirri formed at the ends of anlagen of dorsal kineties. (i, j) Ventral (i) and dorsal (j) views of a late divider. Arrows and arrowheads respectively mark the newly formed dorsomarginal kineties and caudal cirri, and double arrowheads indicate the dividing micronuclei; dashed lines connect the cirri differentiated from the same streak of anlagen. e, Endoral membrane; LMA, anlagen of left marginal row; LMR, row of left marginal cirri; Ma, macronuclear nodules; OP, oral primordium; p, paroral membrane; RMA, anlagen of right marginal row; RMR, row of right marginal cirri; TC, transverse cirri; UMA, anlagen of undulating membranes. Scale bars=60 μm.

lengthens, widens and differentiates new adoral membranelles posteriad, with a proliferation of basal bodies (Figs. 3b, c and 4b, c). Meanwhile, the old frontoventral cirri and undulating membranes remain intact (Fig. 3a).

In the middle stage, the fronto-ventral-transverse cirral anlagen (FVT anlagen) form five streaks in both the proter and opisthe, in which the two posterior-most frontoventral cirri are involved. At the same time, the old paroral membrane dedifferentiates in the proter to form one frontal cirrus anteriad; in the opisthe, the undulating membranes anlage appears *de novo* to the left of the FVT-anlagen with one frontal cirrus then originating from its anterior part. The opisthe's oral primordium differentiates into more and more new membranelles (Figs. 3d, f and 4d, e).

During the late stages, in the opisthe, the new AZM extends and bends towards the right, while the parental adoral zone remains entirely in the proter. The anlage of undulating

International Journal of Systematic and Evolutionary Microbiology (2015), **65**, 3216–3225 **DOI** 10.1099/ijs.0.000377

Reconsideration of the 'well-known' hypotrichous ciliate *Pleurotricha curdsi* (Shi *et al.*, 2002) Gupta *et al.*, 2003 (Ciliophora, Sporadotrichida), with notes on its morphology, morphogenesis and molecular phylogeny

Xiaoteng Lu,[1,2] Chen Shao,[3] Yuhe Yu,[1] Alan Warren[4] and Jie Huang[1]

Correspondence
Jie Huang
jhuang@ihb.ac.cn

[1]Key Laboratory of Aquatic Biodiversity and Conservation of Chinese Academy of Sciences, Institute of Hydrobiology, Chinese Academy of Sciences, Wuhan 430072, PR China

[2]Laboratory of Protozoology, Institute of Evolution & Marine Biodiversity, Ocean University of China, Qingdao 266003, PR China

[3]The Key Laboratory of Biomedical Information Engineering, Ministry of Education, School of Life Science and Technology, Xi'an Jiaotong University, Xi'an 710049, PR China

[4]Department of Life Sciences, Natural History Museum, London SW7 5BD, UK

The oxytrichid species *Pleurotricha curdsi* (Shi *et al.*, 2002) Gupta *et al.*, 2003, isolated from a tributary of the Yangtze River in the Mudong district of Chongqing, southern China, was reinvestigated with emphasis on its morphology, morphogenesis and small-subunit (SSU) rDNA-based phylogeny. Compared with three previously described populations, the Mudong population of *P. curdsi* is characterized by its large body size, 170–295 × 65–110 μm *in vivo*, and by having a variable number of right marginal rows, either two or three. Likewise, the number of right marginal rows anlagen (RMA) is also variable, i.e. usually two, but sometimes several small extra anlagen that give rise to the formation of the third row, are present to the left of the RMAs. We posit that the Mudong population is an intermediate form between the three previously described populations. Phylogenetic analyses based on the SSU rDNA sequence data show that all populations of *P. curdsi* cluster with the type species of the genus, *Pleurotricha lanceolata*, in a clade nested within the Oxytrichidae.

INTRODUCTION

Hypotrichs, with their highly diverse cirral and morphogenetic patterns, play a major role in understanding the systematics and evolutionary relationships among ciliates (Foissner *et al.*, 2014; Heber *et al.*, 2014). Recent molecular and morphological investigations have contributed significantly to understanding the evolution and phylogeny of hypotrichous ciliates (Chen *et al.*, 2013a, b, 2014; Fan *et al.*, 2014a, b, c; Huang *et al.*, 2014; Jiang *et al.*, 2013; Jung *et al.*, 2014; Kim *et al.*, 2014; Kumar *et al.*, 2014; Küppers, 2014; Li *et al.*, 2013, 2014; Lv *et al.*, 2013; Paiva *et al.*, 2014; Park *et al.*, 2013; Shao *et al.*, 2013a, b, 2014a, b, c; Singh & Kamra, 2013, 2014; Singh *et al.*, 2013). Species identification and separation among oxytrichids remains problematic, however, because many have not been sufficiently studied.

The oxytrichid genus *Pleurotricha* Stein, 1895 has *Pleurotricha lanceolata* (basionym *Stylonychia lanceolata* Ehrenberg, 1835) as the type species. Three other species have since been described, namely *Pleurotricha grandis* Stein, 1859, *Pleurotricha planensis* Fernandez-Leborans, 1984, and *Pleurotricha curdsi* (Shi *et al.*, 2002) Gupta *et al.*, 2003, although, according to Berger (1999), *P. planensis* is insufficiently described and is considered *species indeterminata* pending a detailed redescription.

P. curdsi was first reported by Shi *et al.* (2002) as *Allotricha curdsi*. Gupta *et al.* (2003) investigated an Indian population of this species and, based on their findings, transferred it to the genus *Pleurotricha*. Recently, Xu *et al.* (2015) isolated a population of *P. curdsi* from Shanghai, China, and reported its morphology and small-subunit (SSU) rDNA sequence.

Abbreviations: BI, Bayesian inference; FVT, frontoventral-transverse; ML, maximum-likelihood; RMA, right marginal rows anlagen; SSU, small-subunit.

The GenBank/EMBL/DDBJ accession numbers of four clones of the SSU rDNA sequence of *Pleurotricha curdsi* are KP262048–KP262051.

A supplementary figure and a sequence alignment are available with the online Supplementary Material.

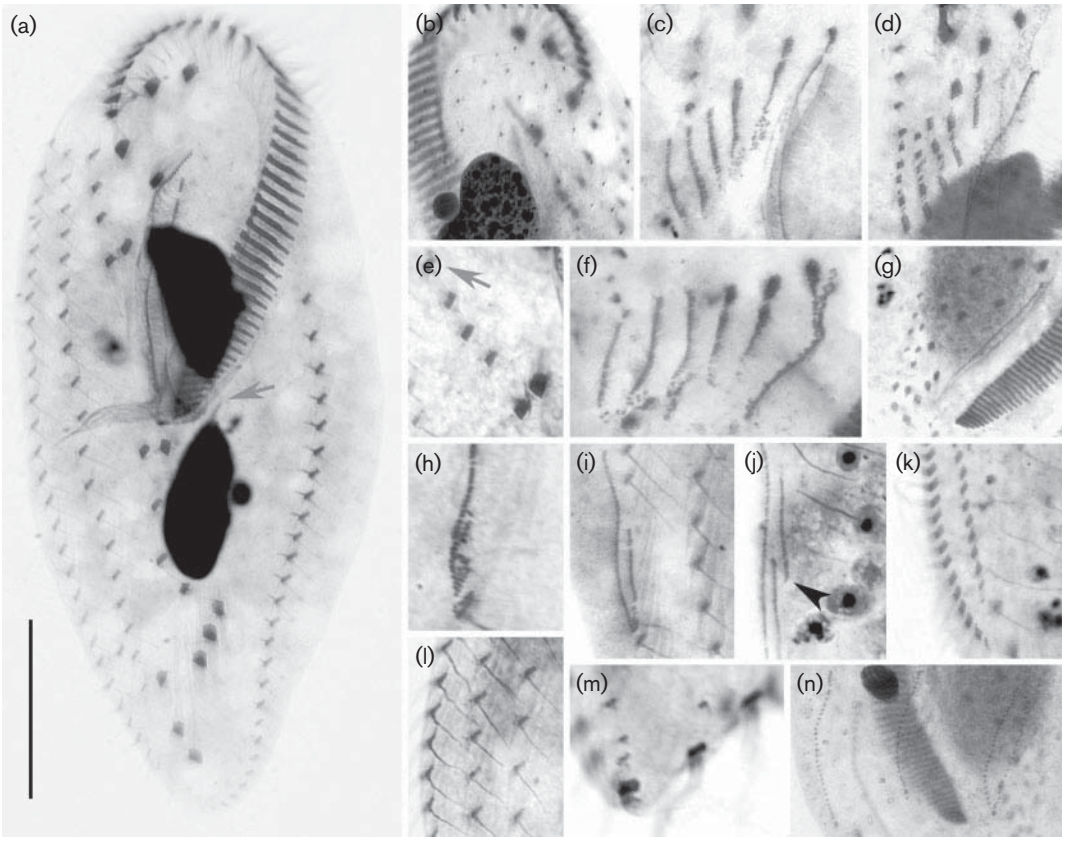

Fig. 3. Photomicrographs of *P. curdsi* after protargol staining. (a) Ventral views of the infraciliature; arrow marks the inconspicuous strand between the macronuclear nodules. (b) Dorsal view of the infraciliature to show the dorsal kineties. (c, f) Ventral views of the same middle divider to show the FVT anlagen in the proter (c) and opisthe (f). (d) Ventral view of a slightly later divider to show the FVT anlagen in the proter. (e) Ventral view to show the additional frontoventral cirri (arrow). (g) Ventral view of a late divider to show the differentiated FVT anlagen in the opisthe. (h–j) Ventral views showing the development of the right marginal rows: (h) shows that the right marginal anlagen originate from the parental cirri within the outermost right marginal row; (i) a later divider, showing the right marginal anlage splitting into two; arrowhead in (j) shows the small fragment left of the right marginal anlagen. (k) Ventral view of a late divider to show that the right marginal anlagen have differentiated into two right marginal rows. (l) Ventral view to show three right marginal rows. (m) Dorsal view to show the three caudal cirri. (n) Dorsal view of a late divider to show the dorsal kineties anlagen. Bar, 60 μm.

Molecular data and phylogenetic analyses

We sequenced the SSU rDNA of four clones of *P. curdsi*. As shown in Fig. S1 (available in the online Supplementary Material), the sequences of clones 1 and 4 are identical, and differ at three and two positions from the sequences of the other two clones and from the Shanghai population of *P. curdsi*, respectively. It should be noted that all four detected polymorphic sites are located in the conserved region of the SSU rDNA; the two mutations of clones 1 and 4 from T to C and T to A (sites 309 and 442 in Fig. S1) are only found in these two sequences out of the 62 taxa included in the present analyses. To exclude the possibility of sequencing error, all four samples were resequenced. The four sequences have been deposited in the GenBank database with lengths and accession numbers as follows: clone 1 (1768 bp, accession no. KP262048), clone 2 (1768 bp, KP262049), clone 3 (1768 bp, KP262050) and clone 4 (1768 bp, KP262051). The DNA G+C contents of the four clones are 44.97, 44.85, 44.97 and 44.97 % respectively. Within the genus *Pleurotricha*, there are eight sites of nucleotide variation in total (Fig. S1).

The topologies of the ML and BI trees were similar: therefore, we present only the ML tree (Fig. 4). These analyses reveal that the genus *Pleurotricha* is monophyletic, with high support values (ML/BI, 87 %/0.99). Within the *Pleurotricha* assemblage, three populations of the type species *P. lanceolata* form a well-supported clade (ML/BI, 94 %/0.99), whereas the relationships between the Mudong and Shanghai populations of *P. curdsi* are less resolved, as they form a polytomy in both the ML and BI analyses.

Protein Cell
DOI 10.1007/s13238-015-0147-3

Protein & Cell

RESEARCH ARTICLE

Phylogenomics of non-model ciliates based on transcriptomic analyses

Xiao Chen[1,2], Xiaolu Zhao[2], Xiaohui Liu[1], Alan Warren[3], Fangqing Zhao[4]✉, Miao Miao[1]✉

[1] College of Life Sciences, University of Chinese Academy of Sciences, Beijing 100049, China
[2] Institute of Evolution & Marine Biodiversity, Ocean University of China, Qingdao 266003, China
[3] Department of Life Sciences, Natural History Museum, Cromwell Road, London SW7 5BD, UK
[4] Beijing Institutes of Life Science, Chinese Academy of Sciences, Beijing 100101, China
✉ Correspondence: zhfq@mail.biols.ac.cn (F. Zhao), miaomiao@ucas.ac.cn (M. Miao)

Received December 25, 2014 Accepted January 21, 2015

ABSTRACT

Ciliates are one of the oldest living eukaryotic unicellular organisms, widely distributed in the waters around the world. As a typical marine oligotrich ciliate, *Strombidium sulcatum* plays an important role in marine food webs and energy flow. Here we report the first deep sequencing and analyses of RNA-Seq data from *Strombidium sulcatum*. We generated 42,640 unigenes with an N50 of 1,451 bp after *de novo* assembly and removing rRNA, mitochondrial and bacteria contaminants. We employed SPOCS to detect orthologs from *S. sulcatum* and 17 other ciliates, and then carried out the phylogenomic reconstruction using 127 single copy orthologs. In phylogenomic analyses, concatenated trees have similar topological structures with concordance tree on the class level. Together with phylogenetic networks analysis, it aroused more doubts about the placement of *Protocruzia*, *Mesodinium* and *Myrionecta*. While epiplasmic proteins are known to be related to morphological characteristics, we found the potential relationship between gene expression of epiplasmic proteins and morphological characteristics. This work supports the use of high throughput approaches for phylogenomic analysis as well as correlation analysis between expression level of target genes and morphological characteristics.

KEYWORDS *Strombidium*, protozoa, transcriptome, non-model ciliate, phylogenomic analysis

INTRODUCTION

Ciliates are unique among unicellular organisms in having two types of nuclei thus separating the germline and somatic functions and are therefore commonly used to study genome structure and gene expression (Aury et al., 2006). Over the last ten years, high throughput sequencing has made ciliate genomic research available on a large scale, and the genomes of several species have been sequenced and analyzed, e.g. *Tetrahymena thermophila* (Eisen et al., 2006), *Paramecium tetraurelia* (Auryet al., 2006), *Ichthyophthirius multifiliis* (Coyne et al., 2011) and *Oxytricha trifallax* (Swart et al., 2013). In addition, the transcriptomes of 13 ciliate species representing 10 genera and five classes are now available (Table S1) including those of *Tetrahymena thermophila* (Xiong et al., 2012) and *Chilodonella uncinata* (Grant et al., 2012).

Strombidium sulcatum Claparède & Lachmann, 1859 (Fig. 1 A–F) is an oligotrich ciliate that plays an important role in food webs and energy flow in marine pelagic waters (Bernard & Rassoulzadegan, 1990, Montagnes et al., 1990). Since Claparède & Lachmann described *S. sulcatum* as the type species for the genus *Strombidium*, there have been numerous reports on its trophic status and diversity (Wiadnyana & Rassoulzadegan, 1989, e.g. Bernard & Rassoulzadegan, 1990, Allali et al., 1994, Christaki et al., 1998, Dolan et al., 2003). With the development of molecular sequencing technology, the taxonomic status of *S. sulcatum* and other species of *Strombidium* have been reassessed (Modeo et al., 2003, McManus et al., 2010, Li et al., 2013).

Ciliates are characterized by having basal bodies and associated appendages bounded to a submembrane

Xiao Chen and Xiaolu Zhao have contributed equally to this work

Electronic supplementary material The online version of this article (doi:10.1007/s13238-015-0147-3) contains supplementary material, which is available to authorized users.

Published online: 02 April 2015

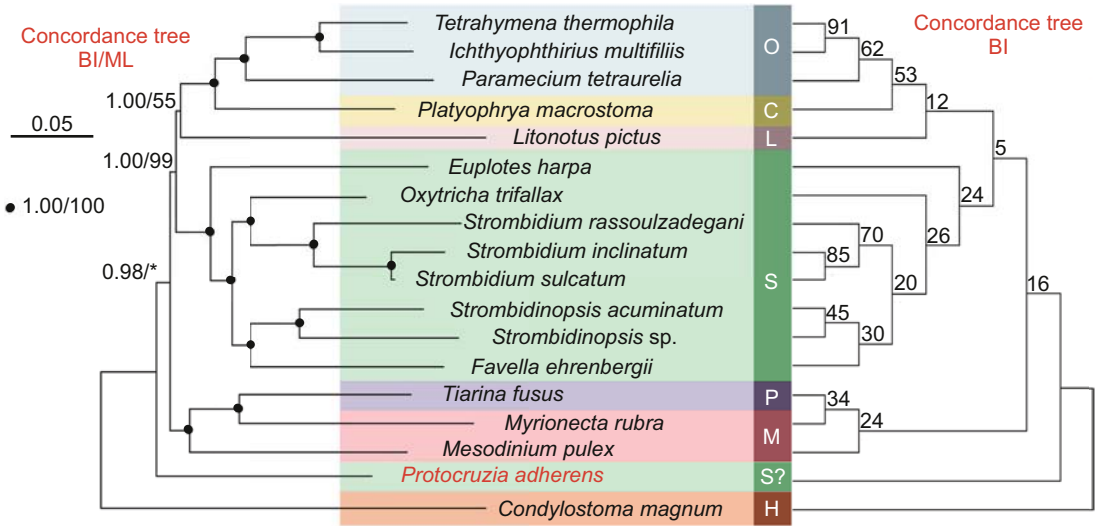

Figure 4. Comprehensive maximum likelihood phylogenomic tree based on 127 orthologs from 18 ciliates. Asterisks indicate bootstrap values less than 50% at a given node. The scale bar corresponds to five substitutions per one hundred nucleotide positions in the concatenated tree (left). The numbers depict the concordance factors in the concordance tree (right).

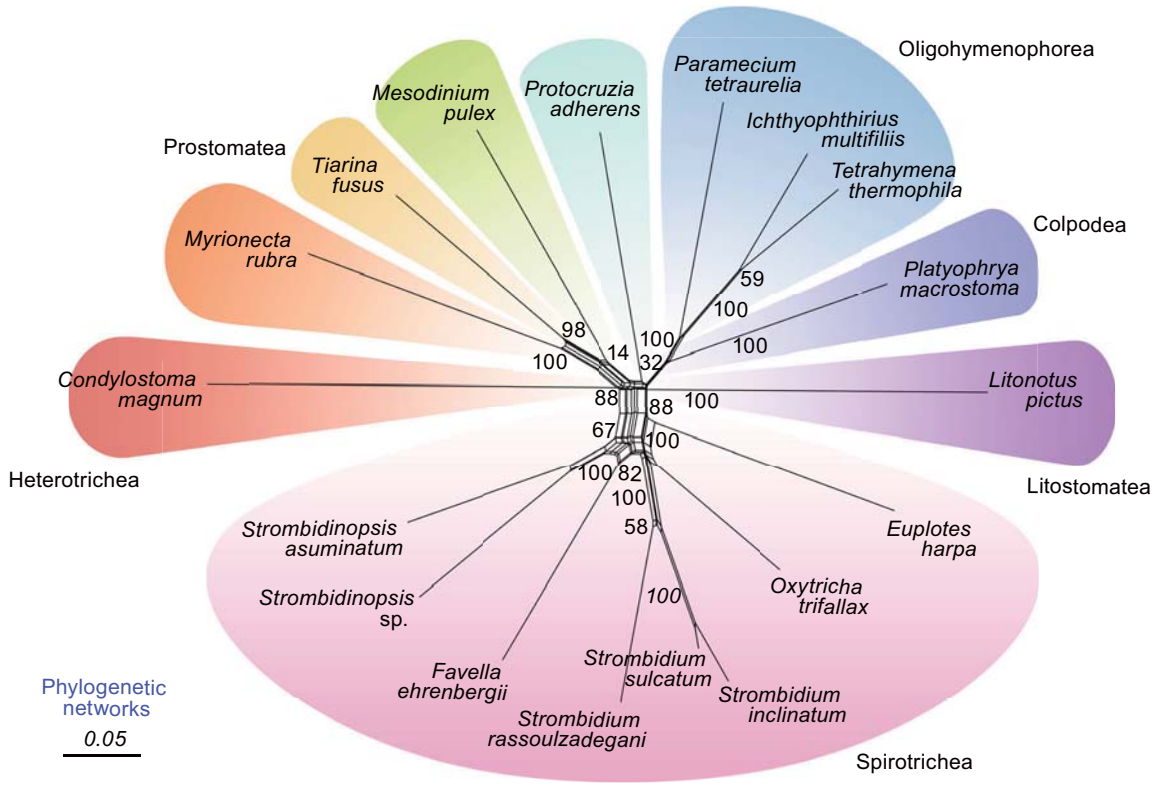

Figure 5. Phylogenetic network computed from the concatenated orthologs alignment dataset using the neighbornet algorithm and the uncorrected distances. Numbers along edges are bootstrap support values coming from 1000 replicates. Values <50% are not shown. The scale bar indicates five substitutions per one hundred nucleotide positions.

Available online at www.sciencedirect.com

ScienceDirect

European Journal of Protistology 51 (2015) 1–14

European Journal of PROTISTOLOGY

www.elsevier.com/locate/ejop

Morphology, morphogenesis and molecular phylogeny of a soil ciliate, *Pseudouroleptus caudatus caudatus Hemberger*, 1985 (Ciliophora, Hypotricha), from Lhalu Wetland, Tibet

Lingyun Chen[a,b,1], Xiaolu Zhao[a,1], Honggang Ma[a], Alan Warren[c], Chen Shao[b,*], Jie Huang[d,*]

[a]*Laboratory of Protozoology, Institute of Evolution & Marine Biodiversity, Ocean University of China, Qingdao 266003, China*
[b]*The Key Laboratory of Biomedical Information Engineering Ministry of Education, Department of Biology and Engineering, School of Life Science and Technology, Xi'an Jiaotong University, Xi'an 710049, China*
[c]*Department of Life Sciences, Natural History Museum, London SW7 5BD, UK*
[d]*Key Laboratory of Aquatic Biodiversity and Conservation of Chinese Academy of Sciences, Institute of Hydrobiology, Chinese Academy of Sciences, Wuhan 430072, China*

Received 16 December 2013; received in revised form 1 August 2014; accepted 1 September 2014
Available online 6 September 2014

Abstract

Pseudouroleptus caudatus caudatus Hemberger, 1985, a soil ciliate isolated from Tibet, was studied in vivo and after protargol impregnation. The Tibetan population is mainly characterized by: elongate body with narrowly rounded anterior end and tapered posterior end; length of buccal area relative to body length ca. 20–25%; cortical granules colourless, round, densely distributed throughout sub-pellicular layer of cell; one parabuccal cirrus; post-peristomial cirrus lacking in 75% of specimens analyzed; left and right ventral rows commence at same level; four dorsal kineties; 3–6 inconspicuous caudal cirri; two macronuclear nodules; 2–7 micronuclei; contractile vacuole located at about 33% of body length near left margin. Morphogenesis is characterized by: (1) parental adoral zone of membranelles retained completely; (2) anterior segments of streaks VI and IV and the whole of streak V form the anterior, middle, posterior segments of the mixed row, respectively; (3) right ventral row originates de novo in both daughter cells; (4) marginal rows develop intrakinetally; (5) dorsal kinety anlage 3 develops de novo in the proter and intrakinetally in the opisthe; and (6) the two macronuclear nodules fuse into a single mass which then divides. Molecular phylogenies corroborate the morphological identification and support the close relationship between *Pseudouroleptus* and *Strongylidium*.

Keywords: Hypotricha; Morphogenesis; Phylogeny; *Pseudouroleptus caudatus caudatus*; Taxonomy

Introduction

The Hypotricha Stein, 1859 is a speciose and morphologically diverse group that inhabits a wide range of biotopes (Berger 2008; Chen et al. 2013a,b; Fan et al. 2014; Foissner 2012; Jiang et al. 2013; Kahl 1932; Küppers and Claps 2013; Li et al. 2010a,b, 2013; Liu et al. 2010; Lv et al. 2013; Paiva

*Corresponding authors.
E-mail addresses: andrews1201@hotmail.com (C. Shao), jhuang@ihb.ac.cn (J. Huang).
[1]Co-first authors.

http://dx.doi.org/10.1016/j.ejop.2014.09.001
0932-4739/

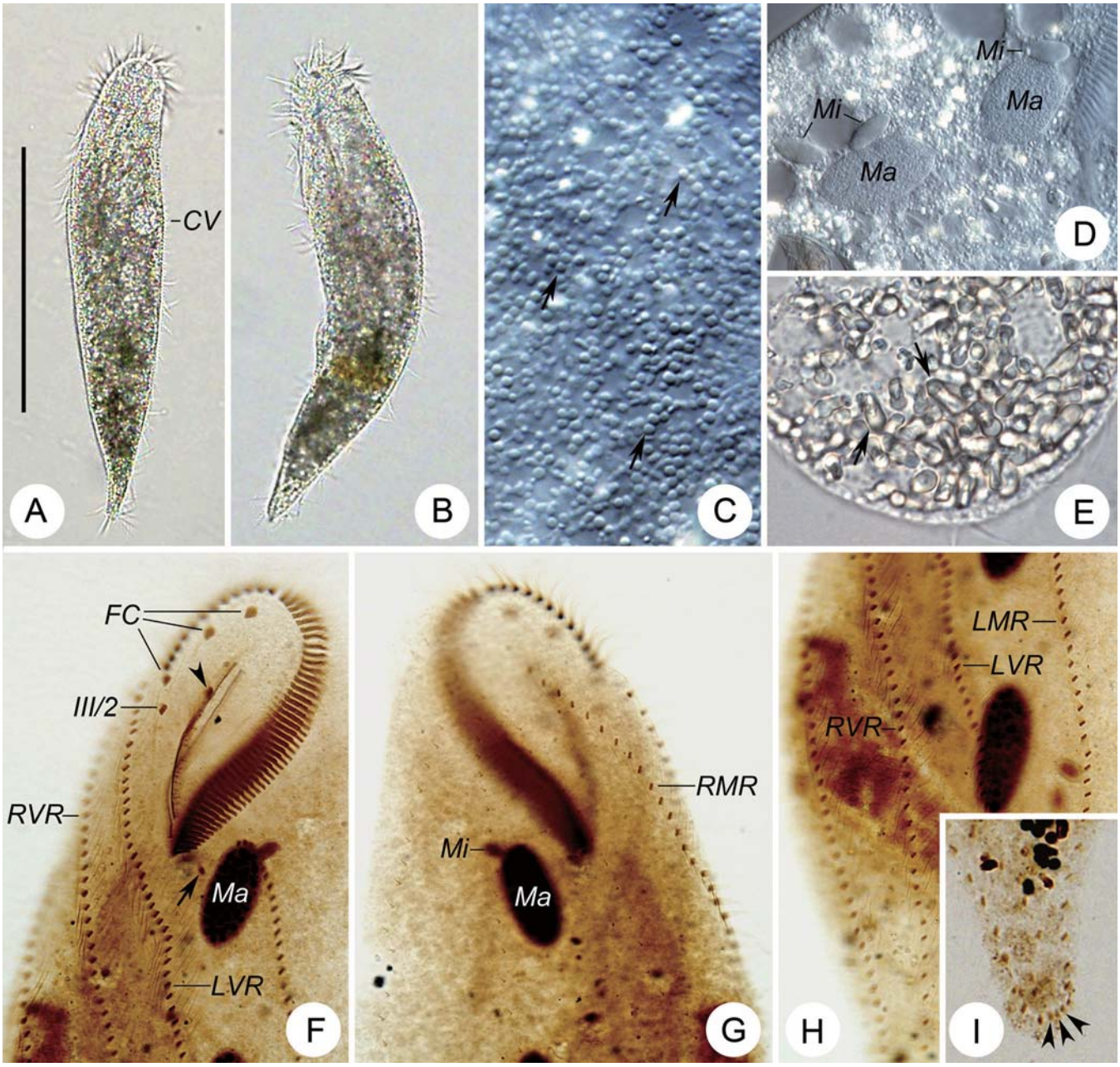

Fig. 3. ((A)–(I)). Photomicrographs of *Pseudouroleptus caudatus caudatus* from life ((A)–(E)) and after protargol staining ((F)–(I)). (A) Ventral view of a representative specimen. (B) Showing a bending specimen. (C) Detail of cell surface in dorsal view, to show the distribution of cortical granules, possibly mitochondria (arrows). (D) Nuclear apparatus. (E) Posterior body region, to show the food vacuoles (arrows). (F) Ventral view of anterior portion of cell, to show, inter alia, the buccal cirrus (arrowhead) and the post-peristomial cirrus (arrow). (G) Dorsal view of anterior portion of cell, to show the macronuclear nodules and micronuclei. (H) Ventral view of the midbody region. (I) Posterior region of cell showing the caudal cirri (arrowheads). CV, contractile vacuole; FC, frontal cirrus; III/2, cirrus III/2; LMR, left marginal row; LVR, left ventral row; Ma, macronuclear nodules; Mi, micronuclei; RMR, right marginal row; RVR, right ventral row. Bar, 150 μm.

more flexible and contractile than the rest of the cell; length to width ratio about 5:1 in vivo on average, 2.5:1 in protargol-stained cells; right margin sigmoidal, curving to right in posterior region, left margin varying from almost straight to sigmoidal (Figs 2A, C 3A, B). Cytoplasm colourless to greyish, usually with numerous lipid droplets ca. 3–5 μm in diameter, and food vacuoles 5–10 μm in diameter containing algae that render cell dark when observed at low magnification (Fig. 3A, E). Contractile vacuole about 20 μm across, located at about 33% of body length near left cell margin (Figs 2A, 3A). Cortical granules (possibly mitochondria) colourless, round, about 1.5 μm in diameter, and densely distributed in the sub-pellicular layer throughout the entire cell (Figs 2B, 3C). Invariably two macronuclear nodules in anterior half

Available online at www.sciencedirect.com

ScienceDirect

European Journal of Protistology 51 (2015) 494–506

European Journal of PROTISTOLOGY

www.elsevier.com/locate/ejop

Morphology of three *Litonotus* species (Ciliophora: Pleurostomatida) from China seas, with brief notes on their SSU rDNA-based phylogeny

Hongbo Pan[a,b], Lifang Li[c,*], Lei Wu[d], Miao Miao[e,**], Khaled A.S. Al-Rasheid[f], Weibo Song[b]

[a] *College of Fisheries and Life Science, Shanghai Ocean University, Shanghai 201306, China*
[b] *Institute of Evolution and Marine Biodiversity, Ocean University of China, Qingdao 266003, China*
[c] *Marine College, Shandong University at Weihai, Weihai 264209, China*
[d] *Key Laboratory of Ecology and Environment Science in Guangdong Higher Education, South China Normal University, Guangzhou 510631, China*
[e] *College of Life Sciences, University of Chinese Academy of Sciences, Beijing 100049, China*
[f] *Zoology Department, College of Science, King Saud University, Riyadh 11451, Saudi Arabia*

Received 13 July 2015; received in revised form 28 August 2015; accepted 28 August 2015
Available online 16 September 2015

Abstract

The morphology and ciliary pattern of three brackish pleurostomatid ciliates, *Litonotus gracilis* spec. nov., *L. tropicus* spec. nov., and *L. duplostriatus*, were investigated. *Litonotus gracilis* differs from its congeners by body size (200–400 × 15–40 μm in vivo), body shape (slenderly spindle-shaped, long neck), the number of somatic kineties (6–7 left and 11–17 right somatic kineties), long bar-shaped extrusomes arranged along oral slit, tiny cortical granules arranged like honeycomb, one subterminally located contractile vacuole and, usually, four macronuclear nodules. *Litonotus tropicus* is characterized by four contractile vacuoles dorsally located, 8–11 right and four or five left somatic kineties. *Litonotus duplostriatus* is lanceolate-shaped, with 11–14 right and five or six left somatic kineties, one subterminally located contractile vacuole, fusiform-shaped extrusomes distributed along oral slit. *Litonotus dragescoi* Pan et al., 2013 is not a valid name, it still be named as *Litonotus fasciolatus* (basionym *Loxophyllum fasciolatus* Dragesco, 1966). Molecular phylogenetic analyses based on SSU rDNA sequence data indicate that neither the family Litonotidae nor the genus *Litonotus* is monophyletic, and *L. gracilis* has a closer relationship with the genus *Kentrophyllum* than with other *Litonotus* species.

Keywords: *Litonotus*; Morphology; New species; Pleurostomatida; SSU rDNA

Introduction

The ciliate genus *Litonotus* Wrzesniowski, 1870 belongs to the order Pleurostomatida Schewiakoff, 1896, a ubiquitous and diverse group of periphytic ciliates that sometimes play an important role in sewage plants and can be used to monitor the water quality (Foissner et al. 1995; Gong et al. 2005; Vd'ačný and Rajter 2014). It is diagnosed by right somatic kineties terminating anteriorly along perioral kineties and the absence of dorsally positioned extrusomes (Foissner 1984; Lynn 2008).

Among over 75 nominal species in this genus, fewer than half have been adequately studied with standard taxonomic

*Corresponding author. Tel.: +86 0631 5688303.
**Corresponding author.
E-mail addresses: qd_liliy@sina.com (L. Li), doublemiao@126.com (M. Miao).

http://dx.doi.org/10.1016/j.ejop.2015.08.003
0932-4739/

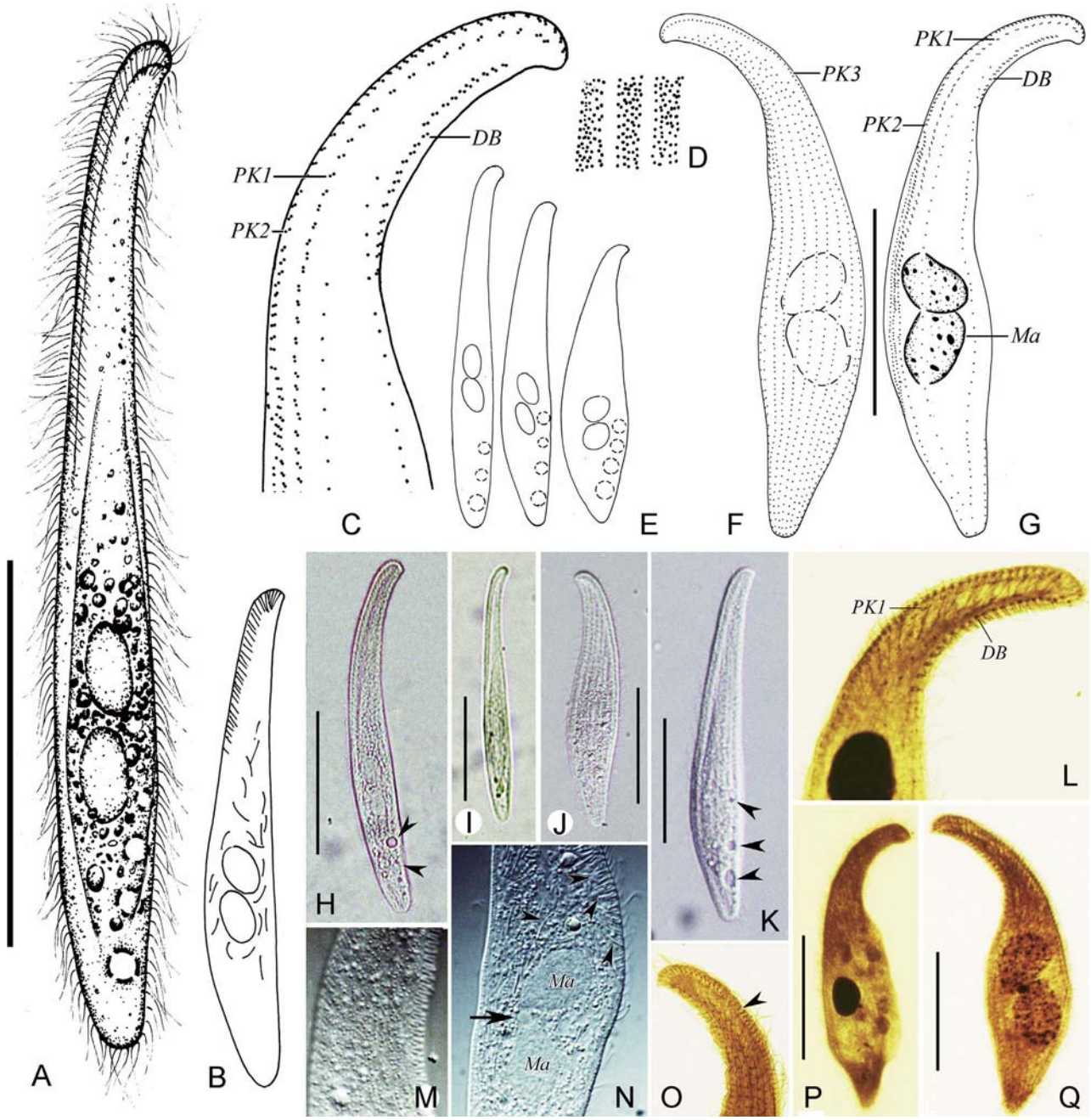

Fig. 3. **(A–Q)**. *Litonotus tropicus* spec. nov. from life (A, B, D, E, H–K, M, N) and after protargol staining (C, E, F, G, L, O–Q). **(A)** Left view. **(B)** Distribution of extrusomes. **(C)** Anterior portion. **(D)** Cortical granules. **(E)** Variants of cell shape. **(F, G)** Left (G) and right (F) view of the holotype. **(H)** Left view of a typical individual, arrowheads indicate contractile vacuoles. **(I–K)** Shape variants, arrowheads in (K) show contractile vacuoles. **(L)** Anterior portion. **(M)** Cortical granules. **(N)** Details of cytoplasm, arrow points to micronucleus. **(O)** Anterior portion, arrowhead refers to perioral kinety 3. **(P)** Left view of an individual with single macronucleus. **(Q)** Right view. DB, dorsal brush; Ma, macronucleus; PK1–3, perioral kineties 1–3. Bars, 50 μm.

lanceolate in outline with typical beak-like anterior end and bluntly pointed posterior end (Figs 4A, E, 5A–C, E, F). Margins of body proper convex. Bilaterally flattened about 1:3; right side flat, left side usually bulged with two inconspicuous ridges (Figs 4A, C, 5A, B, D). Two oval macronuclear nodules, about 20 × 10 μm in vivo, centrally positioned; in four out of 20 individuals, three macronuclear nodules detected (Fig. 5I). Micronuclei undetected. One contractile vacuole subterminally located (Fig. 5G). Extrusomes fusiform, about 8 μm long, densely arranged along oral slit and scattered in cytoplasm (Figs 4B, D, 5H, K). Cortex thin and flexible, underneath numerous tiny (<0.5 μm) cortical granules. Colourless cytoplasm often containing many differently sized, greasily shining globules rendering main

Available online at www.sciencedirect.com

ScienceDirect

European Journal of Protistology 51 (2015) 66–78

European Journal of PROTISTOLOGY

www.elsevier.com/locate/ejop

Morphology and molecular phylogeny of three marine *Condylostoma* species from China, including two new ones (Ciliophora, Heterotrichea)

Ying Yan[a,1], Xumiao Chen[a,b,1], Xiangrui Chen[c,*], Feng Gao[a], Saleh A. Al-Farraj[d], Khaled A.S. Al-Rasheid[d]

[a] *Laboratory of Protozoology, Institute of Evolution & Marine Biodiversity, Ocean University of China, Qingdao 266003, China*
[b] *Institute of Oceanology, Chinese Academy of Sciences, Qingdao 266071, China*
[c] *School of Marine Science, Ningbo University, Ningbo 315211, China*
[d] *Zoology Department, College of Science, King Saud University, Riyadh 11451, Saudi Arabia*

Received 29 May 2014; received in revised form 3 November 2014; accepted 4 November 2014
Available online 11 November 2014

Abstract

The present study investigates the morphologic and molecular characteristics of three *Condylostoma* species isolated from brackish and marine tropical habitats of China, including *Condylostoma tropicum* spec. nov., *Condylostoma elongatum* spec. nov. and *Condylostoma curvum* Burkovsky, 1970. The two new species have slender and elongated bodies with the posterior portion distinctly narrowed, forming long tails, thus they obviously differ from most congeners. In addition, *Condylostoma tropicum* spec. nov. is characterized by its small buccal cavity, single frontal cirrus, 26–33 somatic kineties, and moniliform macronucleus composed of 8–22 nodules. *Condylostoma elongatum* spec. nov. is distinguished by its huge body size (1000–1200 μm long in vivo), the prominent buccal cavity, 5–7 frontal cirri and 37–43 somatic kineties. *Condylostoma curvum* is also reinvestigated in this paper using both protargol impregnation and molecular techniques. Phylogenetic analyses based on SSU rDNA sequence data indicate that the three organisms are located within the genus *Condylostoma*; the genus *Condylostoma* fails to form a monophyletic branch in both Maximum-likelihood tree and Bayesian inference analysis. Nonetheless, the AU test shows that the monophyly of *Condylostoma* could not be rejected.

Keywords: *Condylostoma*; Morphology; New species; Phylogeny

Introduction

The genus *Condylostoma* Bory de St. Vincent, 1824 is a well-known heterotrichous taxon including more than 30 nominal species, most of which are large and elongated, free-living, densely ciliated and with a moniliform macronucleus. They are common members of the periphyton, benthos, and psammon in marine and limnetic habitats (e.g., Al-Rasheid 1999; Burkovsky 1970; Corliss 1979; Dragesco 1960; Dragesco and Dragesco-Kernéis 1986; Fauré-Fremiet 1958; Kahl 1932; Song and Wilbert 1997; Spiegel 1926; Wilbert and Kahan 1981). The species identification in this genus is one of the hardest work. This is partly because many forms share very similar morphological features observed in vivo and relatively few characters can be reliably used for

*Corresponding author. Tel.: +86 574 8760 0161.
E-mail addresses: xiangruichen@26.com, xiangruichen@126.com (X. Chen).
[1] Contributed equally to this work.

http://dx.doi.org/10.1016/j.ejop.2014.11.001
0932-4739/

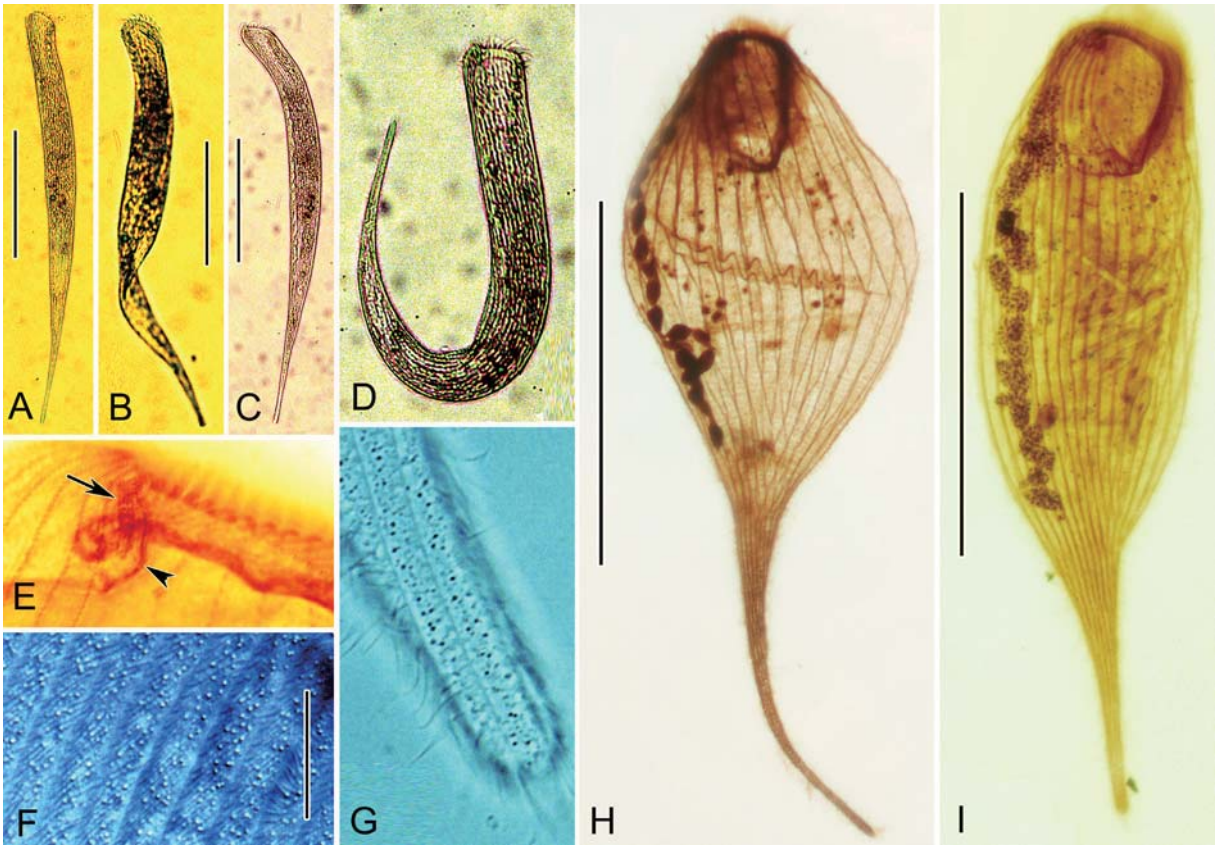

Fig. 2. (A–I) Photomicrographs of *Condylostoma tropicum* spec. nov. from life (A–D, F and G) and after protargol impregnation (E, H and I). (A–D) Ventral views, to show different body shape. (E) Buccal apparatus, to show the frontal cirrus (arrow) and the distal end of paroral membrane (arrowhead). (F) Cortical granules. (G) Posterior region of cell. (H) Ventral view, note the slim tail and moniliform macronucleus. (I) Ventral view of infraciliature of holotype specimen. Scale bars = 200 μm (A, B, C, H, I); 30 μm (F).

Etymology. The species-group name *elongatum* (Latin adjective; elongate) alludes to the elongate body outline.

Description. Fully extended cell 1000–1200 μm × 50–60 μm in vivo. Folded and flexible body laterally flattened and ribbon-like, with anterior three quarters of cell almost of same width and posterior quarter rapidly narrowed forming a slim tail (Figs 3A, B, 4A, D).

Round and colourless cortical granules about 1.5 μm in diameter, scattered between ciliary rows (Figs 3E, 4K). Cytoplasm colourless and transparent except for opaque middle part, packed with large number of colourless and ellipsoid cytoplasmic granules and several huge food vacuoles (Figs 3A, 4A, B). Food vacuoles filled with yellowish diatoms and greyish organic matter, about 30–60 μm in diameter. Macronucleus moniliform, composed of 12–22 nodules, located along right margin of cell (Figs 3A, B, 4H). Contractile vacuole not observed. Locomotion by gliding, winding between sand grains and organic debris.

Transparent buccal area prominent with a huge cavity, bottom of which leading into a well-defined cytopharynx (Figs 3C, 4E). Ratio of buccal area to body length about 20% in vivo. Oral apparatus as shown in Figs 3D, 4I, J. Adoral zone comprising 94–171 membranelles, with cilia about 35 μm in length. Proximal portion of adoral zone extending spirally into cytopharynx. Paroral membrane highly developed as in other congeners and terminating near cytopharynx (Fig. 3D). Five to seven frontal cirri at distal end of adoral zone, arranged longitudinally and parallel with anterior end of paroral membrane (Figs 3D, 4G, I, J, arrowheads). Frontal cirri sometimes not easily detectable because of contraction and invagination of this part of cell. 37–43 longitudinal somatic kineties including 30–36 shortened rows on both ventral and dorsal side, each composed of densely arranged dikinetids, that is, only seven or eight kineties extending complete length of cell (Fig. 3F, G). Typical suture not easily observed on ventral side of body.

Comments and comparison. Condylostoma elongatum spec. nov. can be distinguished from most congeners by its huge body size and the long tail. Only two other species, namely *C. longicaudatum* Dragesco, 1996 and *C. reichi* Wilbert and Kahan, 1981, exhibit these characters and should therefore be compared with the new species.

Condylostoma elongatum differs from *C. longicaudatum* by the following combination of characters: (1) shorter body (1000–1200 μm vs. >1600 μm); (2) having more somatic kineties (37–43 vs. 20–32), and fewer frontal cirri (5–7 vs. 8) (Fig. 6A, C; Dragesco 1996).

Available online at www.sciencedirect.com

ScienceDirect

European Journal of Protistology 51 (2015) 186–195

European Journal of PROTISTOLOGY

www.elsevier.com/locate/ejop

Morphology of three new colonial sessile peritrich ciliates, *Pseudepistylis paramphora* n. sp., *Zoothamnium paranii* n. sp. and *Z. hartwigi* n. sp., with notes on *Epicarchesium variabile* (Ciliophora, Peritrichia)

Ping Sun[a,d], Alan Warren[b], Saleh A. Al-Farraj[c], Weibo Song[d,*]

[a] *Key Laboratory of the Ministry of Education for Coastal and Wetland Ecosystem, College of the Environment and Ecology, Xiamen University, Xiamen 361102, China*
[b] *Department of Life Sciences, Natural History Museum, London SW7 5BD, UK*
[c] *Zoology Department, King Saud University, Riyadh 11451, Saudi Arabia*
[d] *Laboratory of Protozoology, Institute of Evolution & Marine Biodiversity, Ocean University of China, Qingdao 266003, China*

Received 13 October 2014; received in revised form 8 January 2015; accepted 16 January 2015
Available online 3 February 2015

Abstract

Four colonial sessile peritrichs were discovered during a survey of ciliate diversity of coastal waters of the Yellow Sea, Shandong Province, China. Following studies of their living morphology, infraciliature and silverline system, three were identified as new members of the genera *Pseudepistylis* and *Zoothamnium. Pseudepistylis paramphora* n. sp. is the second species assigned to the genus, which is characterized by its rigid, dichotomously branched stalk, reticulate silverline system and marine habitat. *Zoothamnium paranii* n. sp. was isolated from brackish water and *Z. hartwigi* n. sp. was collected from marine water. *Zoothamnium paranii* is characterized largely by its highly variable zooid size and having an extremely long infundibular polykinety 3. *Zoothamnium hartwigi* is separated from its congeners by having two types both of peristomial lip and infundibular polykinety 3. We also supply supplementary morphometric data and photomicrographs of *Epicarchesium variabile* based on examinations of specimens in vivo and after silver staining.

Keywords: Colonial peritrichs; *Epicarchesium*; New species; *Pseudepistylis*; Taxonomy; *Zoothamnium*

Introduction

Sessile peritrichs of the order Sessilida are a large, distinctive assemblage of ciliates that are commonly found in a wide variety of marine, freshwater and terrestrial habitats (Corliss 1979; Foissner et al. 1992; Ji and Kusuoka 2009; Shi et al. 2014; Sun et al. 2013; Wang et al. 2011; Wu et al. 2011). Due to their prodigious abilities as suspension feeders, sessilid peritrichs are a major component of most microbial periphyton communities in both natural and artificial water bodies, especially eutrophic environments, e.g. aquaculture farming areas and sewage treatment plants (Azam et al. 1983; Finley, 1969; Ji et al. 2009a; Sun et al. 2012). Colonial peritrichs are particularly conspicuous and can be differentiated by

Abbreviations: P1–3, infundibular polykinety 1–3.

*Corresponding author. Tel.: +86 53282032283; fax: +86 53282032283.
E-mail address: wsong@ouc.edu.cn (W. Song).

http://dx.doi.org/10.1016/j.ejop.2015.01.001
0932-4739/

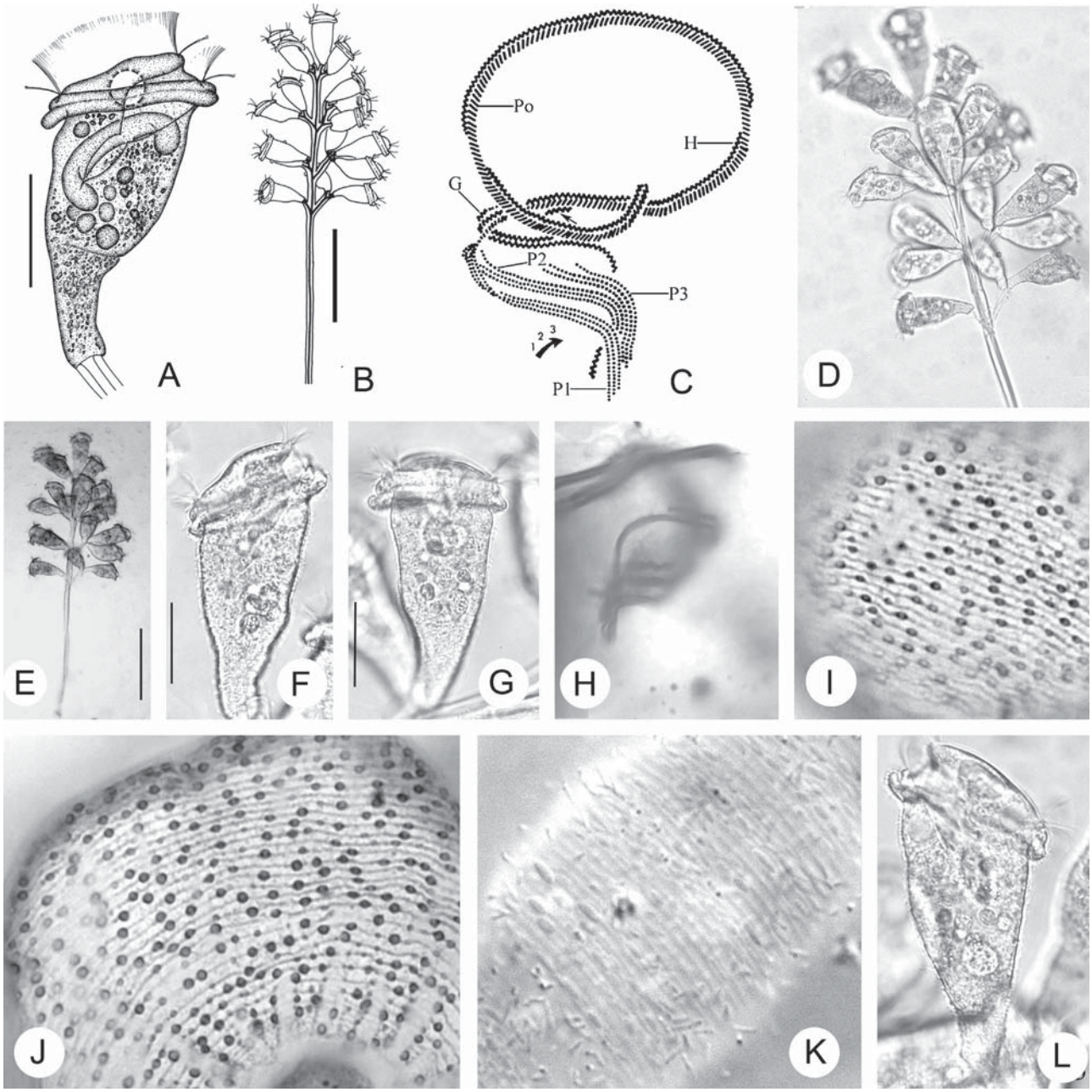

Fig. 2. *Zoothamnium paranii* n. sp. from life (A, B, D–G, K, L) and after staining with protargol (C, H) and silver nitrate (I, J). **A**, **F**–**G**, **L** – living zooids at high magnification; **B**, **D**, **E** – colony form in vivo; **C** – entire oral infraciliature in ventral view, arrow marks epistomial membrane and arrow with numerals indicates numbering convention for polykineties and rows of kinetosomes within each polykinety; **H** – detailed arrangement of infundibular polykineties; **I**, **J** – silverline system; **K** – living zooid at high magnification focused to show the pellicular striations. G, germinal kinety; H, haplokinety; P1–3, infundibular polykinety 1–3; Po, polykinety. Scale bars: 40 μm in A, F, G; 100 μm in B, E.

3 at abstomal end and clearly separated from them. All three rows of P3 converge with row 3 of P1 at adstomal end.

Type locality. A brackish-water pond connected with marine coastal water, just behind No. 2 Middle School of Qingdao (36°03′30″N, 120°19′21″E), Shandong Province, China.

Ecological conditions. Brackish water, salinity 17‰, temperature 15 °C.

Deposition of slides. A protargol slide (registration number SP-2005-1016-01) containing the holotype specimen (Fig. 1H; Table 1) is deposited in the Laboratory of Protozoology, Ocean University of China, China. One paratype

Available online at www.sciencedirect.com

ScienceDirect

European Journal of Protistology 51 (2015) 241–258

European Journal of PROTISTOLOGY

www.elsevier.com/locate/ejop

Taxonomic studies on seven species of *Dysteria* (Ciliophora, Cyrtophoria), including a description of *Dysteria paraprocera* sp. n.

Zhishuai Qu[a], Chundi Wang[a], Feng Gao[a], Jiqiu Li[b], Khaled A.S. Al-Rasheid[c], Xiaozhong Hu[a,*]

[a]*Laboratory of Protozoology, Institute of Evolution & Marine Biodiversity, Ocean University of China, Qingdao, 266003, China*
[b]*Laboratory of Protozoology, College of Life Science, South China Normal University, Guangzhou, 510631, China*
[c]*Zoology Department, College of Science, King Saud University, PO Box 2455, Riyadh, 11451, Saudi Arabia*

Received 23 December 2014; received in revised form 21 April 2015; accepted 24 April 2015
Available online 2 May 2015

Abstract

The living morphology and infraciliature of seven *Dysteria* species isolated from the seas around China were investigated by observation of both living cells and specimens after protargol impregnation. *Dysteria paraprocera* sp. n. is characterized as follows: cell size 110–150 × 30–40 μm in vivo; body elongate rectangular and slender; a yellow-brown to dark red coloured pigment spot located at anterior end of body; three right kineties, with rightmost two extending apically to dorsal margin and innermost one starting at level of cytostome; eight or nine short left kineties at equatorial area. *Dysteria nabia*, *D. proraefrons*, *D. brasiliensis*, *D. cristata*, *D. derouxi* and *D. crassipes* basically correspond well with previous studies and therefore only brief descriptions are presented. Discussions of these species are helpful, however, in understanding the circumscription of *Dysteria* morphotypes. After careful comparison, *Dysteria procera* sensu Liu et al. (2008, Acta Hydrobiol. Sin. 32 (suppl.), 84–89 (in Chinese with English abstract)) was verified as a new species, *D. subtropica* sp. n., mainly because the innermost right kinety starts at mid-body. Small-subunit (SSU) rRNA genes were sequenced for four species of *Dysteria*, namely, *D. paraprocera* sp. n., *D. subtropica* sp. n., *D. proraefrons* and *D. nabia*. Sequence comparisons and phylogenetic analyses indicate that these species are well outlined and cluster with their congeners.

Keywords: *Dysteria*; Dysteriidae; Marine ciliates; Morphology; Phylogeny; SSU rRNA gene

Introduction

The cyrtophorids are a group of highly specialized and divergent ciliates with dorsoventrally or laterally flattened bodies (Gao et al. 2012; Kahl 1931). More than 150 cyrtophorid species have been reported to date, with most of these being free-living marine forms (e.g. Foissner et al. 1991; Gong and Song 2009; Park and Min 2014; Song et al. 2009; Zhao et al. 2014). Over the last two decades a taxonomical survey of ciliates in marine biofilm environments in China has reported more than 40 new or poorly-known cyrtophorids, meaning that this group is more species rich than had previously been thought (Chen et al. 2012; Fan et al. 2014; Gong and Song 2006a, b; Gong et al. 2005, 2008; Pan et al. 2012, 2013a,b; Qu et al. 2015).

The species-rich genus *Dysteria*, a group of cyrtophorids with highly bilaterally compressed bodies and cilia restricted

*Corresponding author. Tel.: +86 0532 8203 1610; fax: +86 0532 8203 1610.
E-mail address: xiaozhonghu@ouc.edu.cn (X. Hu).

http://dx.doi.org/10.1016/j.ejop.2015.04.005
0932-4739/

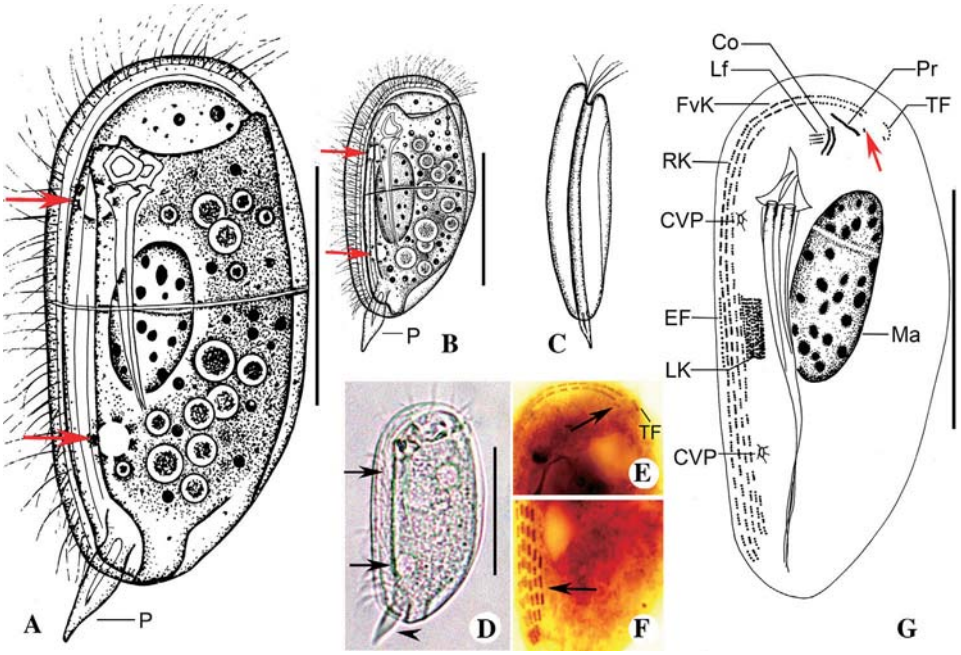

Fig. 5. *Dysteria nabia* from life (A–D) and after protargol impregnation (E–G). (A) Left lateral view of a representative individual, arrows show contractile vacuoles. (B) A different shaped individual, arrows point to contractile vacuoles. (C) Ventral view. (D) Representative individual, arrows show contractile vacuoles and arrowhead marks podite. (E) Anterior portion of cell, arrow indicates pair of kinetosomes near anterior end of frontoventral kineties. (F) Posterior end of ventral groove, arrow marks innermost right kinety. (G) General view of infraciliature, arrow points to pair of kinetosomes near anterior end of frontoventral kineties. Co, circumoral kineties; CVP, contractile vacuole pore; EF, equatorial fragment; FvK, frontoventral kineties; Lf, left frontal kineties; LK, left kineties; Ma, macronucleus; P, podite; Pr, preoral kinety; RK, right kineties; TF, terminal fragment. Scale bars: 30 μm. (For interpretation of the references to color in this figure legend, the reader is referred to the web version of this article.)

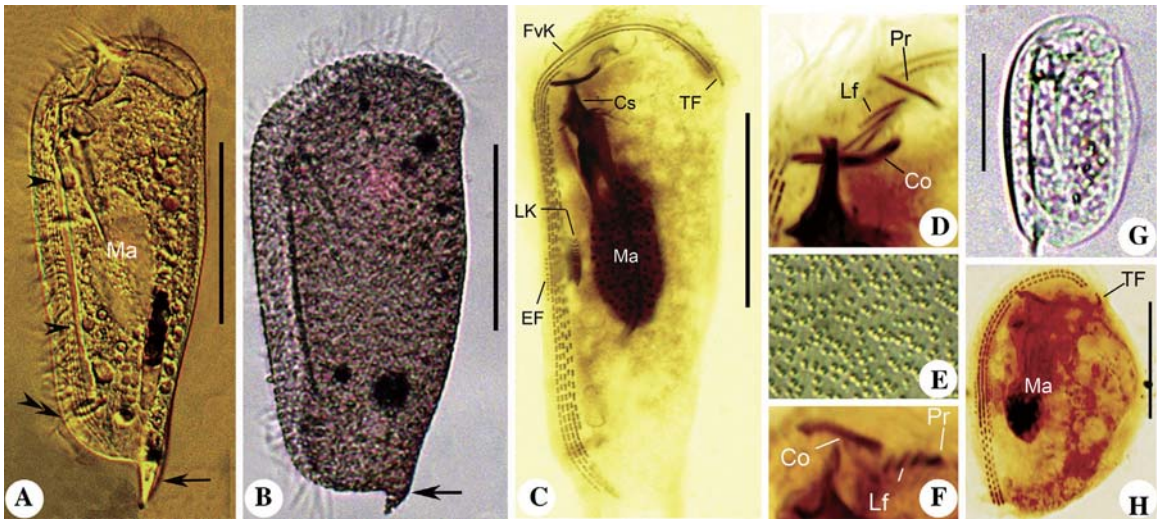

Fig. 6. Photomicrographs of *Dysteria brasiliensis* ((A), (C) and (D), Yantai population; (B) and (E), Zhanjiang population) and *D. cristata* (F–H) from life (A, B, E and G) and after protargol impregnation (C, D, F and H). (A) Left lateral view under differential interference contrast, arrow shows dorsal spine, arrowheads mark contractile vacuoles and double-arrowhead points to podite. (B) Left lateral view, arrow marks podite. (C) General view of infraciliature. (D) Oral infraciliature. (E) Spherical ectosymbiotic bacteria on surface of cell. (F) Oral infraciliature. (G) Left lateral view. (H) General view of infraciliature. Co, circumoral kineties; Cs, cytostome; EF, equatorial fragment; FvK, frontoventral kineties; Lf, left frontal kineties; LK, left kineties; Ma, macronucleus; Pr, preoral kinety; TF, terminal fragment. Scale bars: 30 μm (A–C), 20 μm (G and H).

Available online at www.sciencedirect.com

ScienceDirect

European Journal of Protistology 51 (2015) 142–157

European Journal of PROTISTOLOGY

www.elsevier.com/locate/ejop

Biodiversity of marine scuticociliates (Protozoa, Ciliophora) from China: Description of seven morphotypes including a new species, *Philaster sinensis* spec. nov.

Xuming Pan[a,b], Zhenzhen Yi[a,*], Jiqiu Li[a], Honggang Ma[b], Saleh A. Al-Farraj[c], Khaled A.S. Al-Rasheid[c]

[a]*Key Laboratory of Ecology and Environmental Science in Guangdong Higher Education, South China Normal University, Guangzhou 510631, China*
[b]*Laboratory of Protozoology, Institute of Evolution & Marine Biodiversity, Ocean University of China, Qingdao 266003, China*
[c]*Zoology Department, King Saud University, Riyadh 11451, Saudi Arabia*

Received 21 August 2014; received in revised form 17 February 2015; accepted 18 February 2015
Available online 25 February 2015

Abstract

Seven marine scuticociliates, *Philaster sinensis* spec. nov., *Pseudocohnilembus hargisi* Evans and Thompson, 1964. J. Protozool. 11, 344, *Parauronema virginianum* Thompson, 1967. J. Protozool. 14, 731, *Uronemella filificum* (Kahl, 1931. Tierwelt. Dtl. 21, 181) Song and Wilbert, 2002. Zool. Anz. 241, 317, *Cohnilembus verminus* Kahl, 1931, *Parauronema longum* Song, 1995. J. Ocean Univ. China. 25, 461 and *Glauconema trihymene* Thompson, 1966. J. Protozool. 13, 393, collected from Chinese coastal waters, were investigated using live observations, silver impregnation methods, and, in the case of the new species, SSU rDNA sequencing. *Philaster sinensis* spec. nov. can be recognized by the combination of the following characters: body cylindrical, approximately 130–150 × 35–55 μm in vivo; apical end slightly to distinctly pointed, posterior generally rounded; 19–22 somatic kineties; M1 triangular, consisting of 13 or 14 transverse rows of kinetosomes; M2 comprising 10–12 longitudinal rows; CVP positioned at end of SK1; marine habitat. We also provide improved diagnoses for *Pseudocohnilembus hargisi*, *Parauronema virginianum*, *Uronemella filificum* and *Parauronema longum* based on their original descriptions as well as the present work. Phylogenetic analyses support the monophyly of the genus *Philaster*.

Keywords: Marine habitat; *Philaster sinensis* spec. nov.; Phylogeny; Scuticociliates

Introduction

Ciliates in the subclass Scuticociliatia Small, 1967 are commonly found in ecosystems worldwide and exhibit both a great biological and morphologic diversity (Foissner and Wilbert 1981; Fan et al. 2011a,b; Foissner et al., 1994, 2013; Pan et al. 2011; 2013c; Seo et al. 2013; Song and Wilbert 2002; Thompson and Kaneshiro, 1968; Whang et al. 2013).

Abbreviations: AIC, Akaike information criterion; BI, Bayesian inference; CV, contractile vacuole; CVP, contractile vacuole pore; MCMC, Markov chain Monte Carlo; ML, maximum-likelihood; M1, membranelle 1; M2, membranelle 2; M3, membranelle 3; PM, paroral membrane; SK1, first somatic kinety; SK2, second somatic kinety.

*Corresponding author.
E-mail address: zyi@scnu.edu.cn (Z. Yi).

http://dx.doi.org/10.1016/j.ejop.2015.02.005
0932-4739/

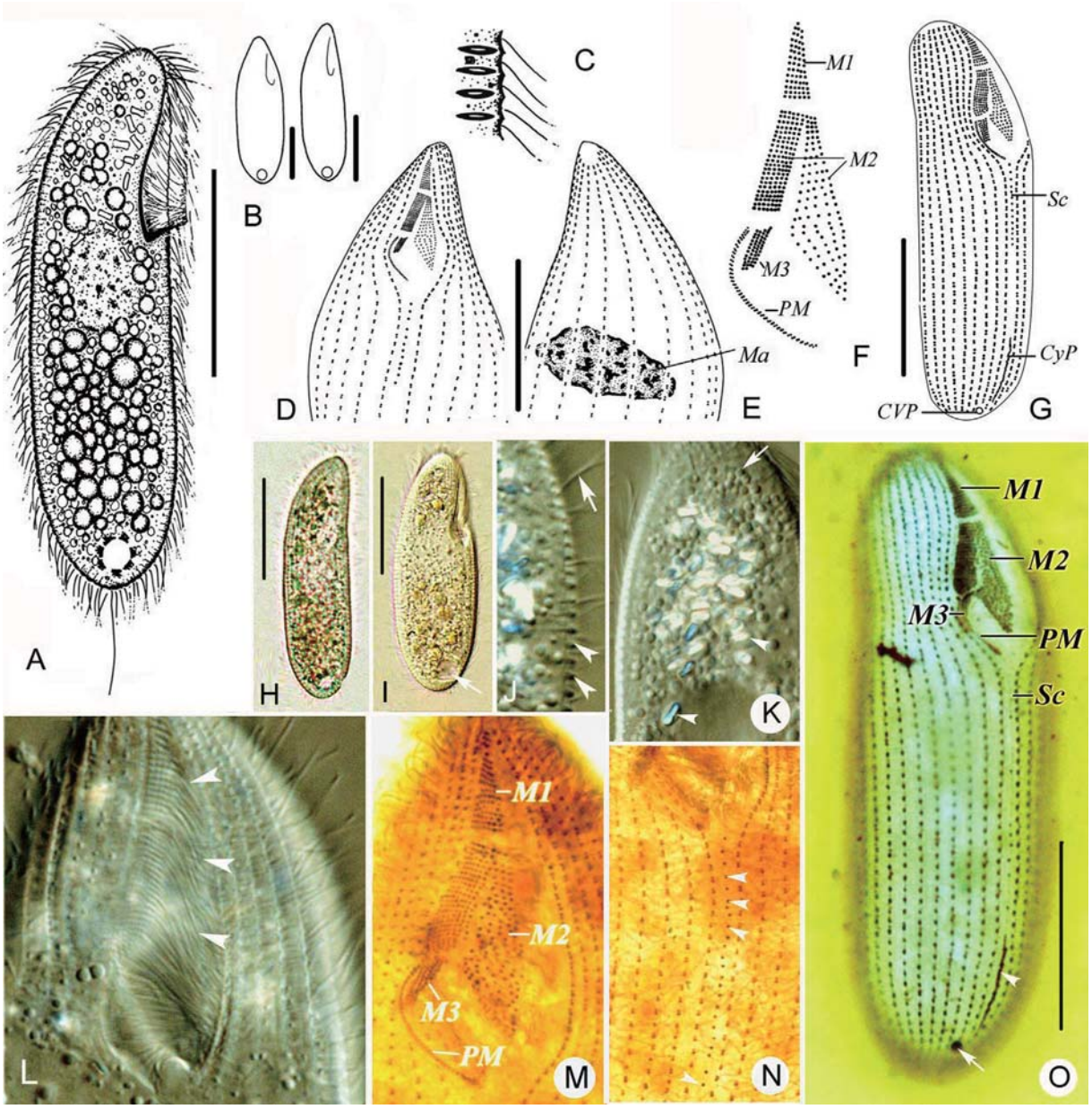

Fig. 2. *Philaster sinensis* spec. nov. in vivo (A–C, H–L), after protargol (D–F, M, N) and silver nitrate staining (G, O). (A, H) Right lateral view of a representative individual. (B) Different body shapes. (C) Detailed view of cortex to demonstrate arrangement of extrusomes. (D, E) Ventral (D) and dorsal (E) views of holotype specimen, showing infraciliature and nuclear apparatus. (F) Detailed structure of buccal area. (G, O) Ventral view, showing infraciliature, arrow in (O) refers to CVP and arrowhead marks cytoproct. (I) Ventral view, arrow marks CV. (J) Ventral view, arrowheads show extrusomes, arrow exhibits somatic cilia. (K) Ventral view, arrowheads show irregularly-shaped crystals, arrow marks extrusomes. (L) Ventral view, arrowheads mark PM. (M) Infraciliature of buccal area. (N) Posterior region, arrowheads show scutica whose basal bodies are serially arranged. CVP, contractile vacuole pore; CyP, cytoproct; M1, 2, 3, membranelles 1, 2, and 3; Ma, macronucleus; PM, paroral membrane; Sc, scutica. Bars, 50 μm (D–G, O), 55 μm (A), 60 μm (B, H, I).

posterior generally rounded; length of buccal field approximately 35% of body. Extrusomes bar-shaped. 19–22 somatic kineties; membranelle 1 triangular, consisting of 13 or 14 transverse rows of kinetosomes; membranelle 2 comprising 10–12 longitudinal rows. One spherical to oval macronucleus centrally located. CV caudally positioned; CVP positioned at end of SK1. Marine habitat.

Type locality: A sand beach at Nanyao, Qingdao, northern China (36°06′39″N; 120°35′26″E).

Habitat: Coastal water and sand, salinity 31‰, pH 8.0

Deposition of slides: A protargol slide containing the holotype specimen (Fig. 2D, E), and a silver nitrate slide containing paratype specimens are deposited in the Laboratory of Protozoology, Ocean University of China with registration

Systematics and Biodiversity (2015), **13(5)**: 455–471

Taylor & Francis
Taylor & Francis Group

Research Article

Redefinition of the hypotrichous ciliate *Uncinata*, with descriptions of the morphology and phylogeny of three urostylids (Protista, Ciliophora)

XIAOTIAN LUO[1], FENG GAO[1], KHALED A. S. AL-RASHEID[2], ALAN WARREN[3], XIAOZHONG HU[1] & WEIBO SONG[1]

[1]Laboratory of Protozoology, Institute of Evolution and Marine Biodiversity, Ocean University of China, Qingdao 266003, China
[2]Zoology Department, College of Science, King Saud University, P.O. Box 2455, Riyadh 11451, Saudi Arabia
[3]Department of Life Sciences, Natural History Museum, London SW7 5BD, UK

(Received 2 December 2014; accepted 24 March 2015)

We investigated the morphology, morphogenesis and small subunit rRNA gene-based phylogeny of three marine urostylids, *Uncinata gigantea* Bullington, 1940, *Holosticha heterofoissneri* Hu & Song, 2001, and *Holosticha* cf. *heterofoissneri*. The dorsal morphogenesis of *Uncinata gigantea* shows *de novo* formation of two groups of anlagen near the marginal rows. *Holosticha* cf. *heterofoissneri* demonstrates fragmentation of the first dorsal kinety anlage as in *Holosticha heterofoissneri*. Our population of *H. heterofoissneri* corresponds well with previously described populations in terms of its general morphology and ciliary pattern. *Uncinata gigantea* can be recognized by its large and highly contractile body, yellowish to brownish cell colour, two types of cortical granules, and 20–30 transversely oriented and densely arranged cirri in the left marginal row, which often overlie the buccal vertex. Based on the new data, especially infraciliature, the genus *Uncinata* is here redefined. Both the morphology and phylogenetic analyses suggest that the genus *Uncinata* should be classified within the family Urostylidae. In addition, both morphological and morphogenetic data suggest that *Holosticha bradburyae* Gong et al., 2001 should be transferred to *Uncinata* as *U. bradburyae* (Gong et al., 2001) comb. nov., due to its possession of a characteristically prominent beak-like, leftwards curved projection and the developmental mode of the dorsal kineties. This assignment is supported by the phylogenetic analyses, which placed *Uncinata gigantea* in a clade with *U. bradburyae* (Gong et al., 2001) comb. nov., and revealed only 1.13% (19 bp) difference in their SSU-rDNA gene sequence.

Key words: *Holosticha*, mangrove wetland, marine ciliates, phylogeny, systematics, *Uncinata*

Introduction

The hypotrichs are among the most speciose and diverse groups of ciliates with about 700 valid species so far described (Berger, 1999, 2006, 2008, 2011). However, many nominal species are poorly known and their systematic positions are uncertain (Berger, 1999, 2006; Chen, Zhao, Ma, Warren, Shao & Huang, 2015; Chen, W., Chen, Li, Warren, & Lin, 2015; Kumar, Bharti, Marinsalti, Insom, & Terza, 2014; Küppers, 2014; Li et al., 2014; Shao, Chen, Pan, Warren, & Miao, 2014a; Singh & Kamra, 2015; Song, Warren, & Hu, 2009). This is mainly because early studies of hypotrichs tended only to provide descriptions of their living morphology, and to omit data on their infraciliature. This situation has been greatly improved as a result of the application of silver staining techniques to reveal the infraciliature, which has led to a better understanding both of morphology and morphogenesis in hypotrichs and the development of molecular techniques for phylogenetic analyses. Consequently, many species have been transferred to their correct taxonomic group, many of which have been redefined or newly erected (Berger, 2008, 2011). The investigation of previously undersampled or unexplored habitats has also led to the discovery of an unknown hypotrich diversity (Chen, L., Liu, Liu, Al-Rasheid, & Shao, 2013; Chen, X., Shao, Lin, Clamp, & Song, 2013b; Fan et al., 2014a, Fan, Hu, Gao, Al-Farraj, & Al-Rasheid, 2014b; Foissner, Filker, & Stoeck, 2014; Heber, Stoeck, & Foissner, 2014; Jung, Park, & Min, 2014; Kim, Vdacny, Shazib, & Shin, 2014; Kumar et al., 2015; Lu, Gao, Shao, Hu, & Warren, 2014; Shao, Li, Zhang, Song, & Berger, 2014b; Shao, Lv, Pan, Al-Rasheid, & Yi, 2014c).

Correspondence to: Xiaozhong Hu. E-mail: xiaozhonghu@ouc.edu.cn

ISSN 1477-2000 print / 1478-0933 online

http://dx.doi.org/10.1080/14772000.2015.1046967

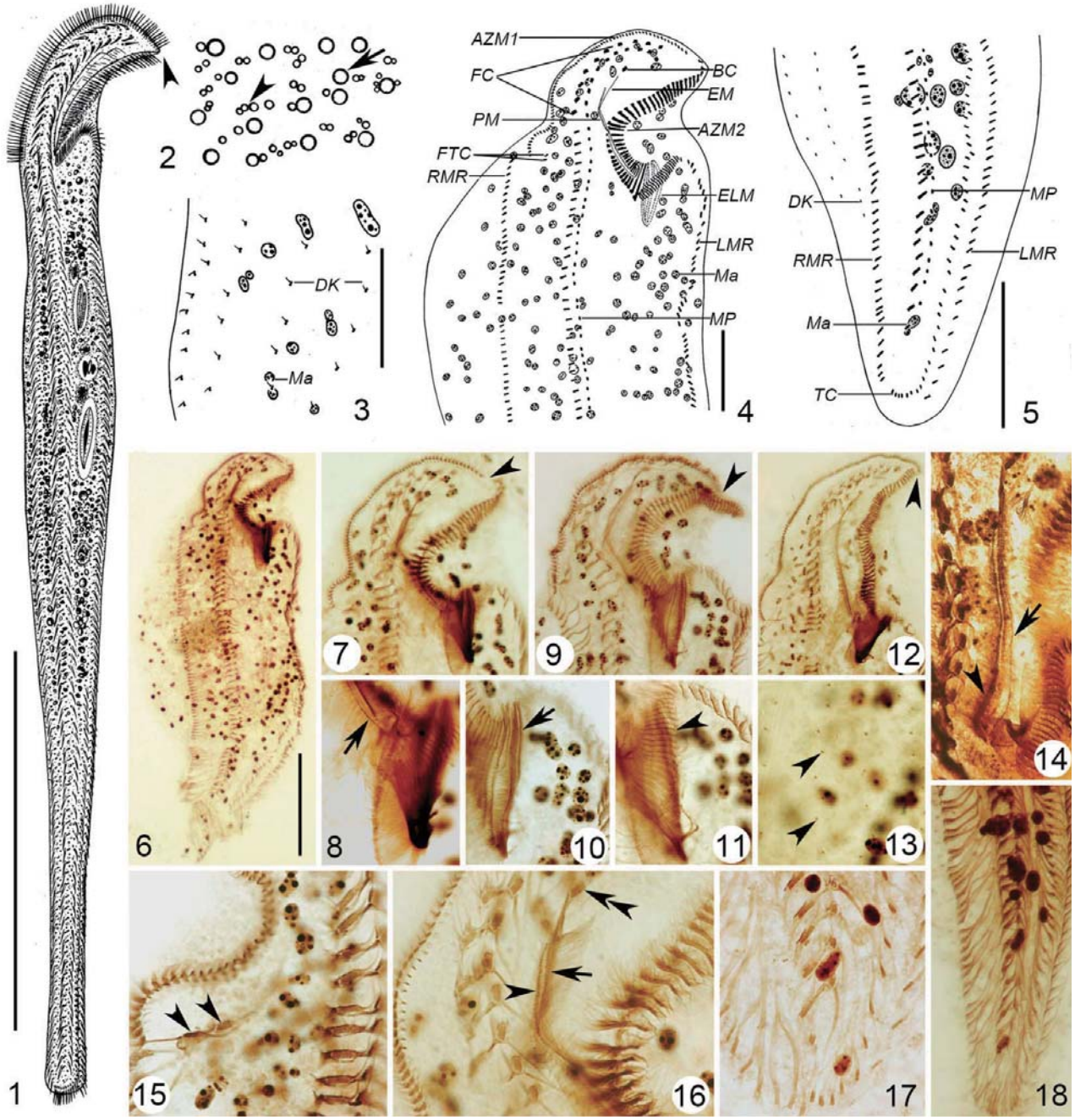

Fig. 1–18. *Uncinata gigantea* from live material (1, 2) and after protargol staining (3–18). (1) ventral view of a representative specimen, arrowhead marks the prominent characteristic beak-like, leftwards curved projection; (2) distribution of cortical granules on dorsal side, arrowhead marks an example of the small type, arrow indicates an example of the large type; (3–6) dorsal (3) and ventral (4–6) views of infraciliature and nuclear apparatus of typical individuals; (7, 8) ventral views of the same specimen as (6), arrowhead marks the conspicuous gap in the adoral zone, arrow indicates the strongly curved endoral membrane; (9–11) ventral views of the same specimen, arrowhead in (9) marks the conspicuous gap in the adoral zone, arrowhead in (11) marks the transversely oriented anterior region of the left marginal cirri row, arrow indicates the distinctly elongated proximalmost membranelles; (12) ventral view, showing bicorona of frontal cirri and the zigzag pattern of midventral rows, arrowhead marks the conspicuous gap of the adoral zone; (13) dorsal view, arrowheads show dikinetids; (14) ventral view, showing undulating membranes, arrowhead marks the multiple-rowed paroral membrane, arrow indicates the long, strongly curved, single-rowed endoral membrane; (15, 16) ventral views of anterior part, arrowheads in (15) indicate two relatively fine frontoterminal cirri, arrowhead in (16) indicates the multiple-rowed paroral membrane, arrow marks the long, single-rowed endoral membrane, double arrowheads show the anteriorly located buccal cirrus; (17, 18) ventral views showing infraciliature and strong fibres associated with cirri. AZM1, distal part of adoral zone of membranelles; AZM2, proximal part of adoral zone of membranelles; BC, buccal cirrus; DK, dorsal kineties; ELM, elongated membranelles; EM, endoral membrane; FC, frontal cirri; FTC, frontoterminal cirri; LMR, left marginal cirri row; Ma, macronuclear segments; MP, midventral pairs; PM, paroral membrane; RMR, right marginal cirri row; TC, transverse cirri. Scale bars: Fig (1), 300 μm; Figs (3, 4), 50 μm; Figs (5, 6), 100 μm.

Systematics and Biodiversity (2015), **13(6)**: 608–623

Research Article

Biodiversity of oligotrich ciliates in the South China Sea: description of three new *Strombidium* species (Protozoa, Ciliophora, Oligotrichia) with phylogenetic analyses

WEN SONG[1], XIAOLU ZHAO[1], WEIWEI LIU[2], XIAOZHONG HU[1], SALEH A. AL-FARRAJ[3], KHALED A. S. AL-RASHEID[3], WEIBO SONG[1] & ALAN WARREN[4]

[1]Laboratory of Protozoology, Institute of Evolution and Marine Biodiversity, Ocean University of China, Qingdao 266003, China
[2]Key Laboratory of Tropical Marine Bio-resources and Ecology, South China Sea Institute of Oceanology, Chinese Academy of Science, Guangzhou 510301, China
[3]Zoology Department, College of Science, King Saud University, Riyadh 11451, Saudi Arabia
[4]Department of Life Sciences, Natural History Museum, London SW7 5BD, UK

(Received 21 December 2014; accepted 16 July 2015)

The morphology and small subunit ribosomal RNA (SSU rRNA) gene sequences of three new species of ciliates in the genus *Strombidium* are recorded: *S. paracapitatum* sp. nov., *S. cuneiforme* sp. nov., and *S. caudispina* sp. nov. *Strombidium paracapitatum* sp. nov. is characterized by having a prominent and transparent apical protrusion and two types of extrusomes. *Strombidium cuneiforme* sp. nov. differs from its congeners in the combination of its long conical body shape, eyespot and elongated tail. *Strombidium caudispina* sp. nov. is recognized by its posterior spine and short ventral kinety. In SSU rRNA gene trees, all members of the genus *Strombidium* cluster into three separate groups. The first group is composed of nine *Strombidium* species including *S. cuneiforme* sp. nov., plus *Williophrya maedai.* The second group consists of *S. paracapitatum* sp. nov., *S. caudispina* sp. nov. and three congeners. The third group comprises *S. conicum* and *S. chlorophilum*.

http://zoobank.org/urn:lsid:zoobank.org:pub:25871A6B-772A-4D26-9940-ACE2B5F1EA07

Key words: ciliates, new species, oligotrich, South China Sea, SSU rRNA gene, Strombidiidae, *Strombidium*

Introduction

The South China Sea is located in the northern tropics and possesses a range of habitats along its Chinese coastline, including mangrove wetlands, estuaries, and bays, all of which contribute to a high diversity of planktonic ciliated protozoa (Liu et al., 2009, 2010; Tsai, Chen, & Chiang, 2010; Tsai, Xu, Chung, & Chiang, 2008; Wang et al., 2014). Recent studies on the diversity of ciliates from this area have observed ~20 oligotrich species, including a new family and a new genus (Liu et al., 2013; Liu, Yi, Lin, & Al-Rasheid, 2011a; Liu, Yi, Lin, Warren, & Song, 2012; Liu et al., 2011b, 2015a, 2015b; Song et al., 2013, 2015; Zhang, Zhang, & Xiao, 2010).

Strombidium is a speciose oligotrich genus comprising >60 nominal species. Of these only about half have been described using currently accepted techniques (e.g. Agatha, 2014; Agatha & Riedel-Lorjé, 1997; Lei, Xu, & Song, 1999; Lynn & Montagnes, 1988; Martin & Montagnes, 1993; Montagnes, Lynn, Stoecker, & Small, 1988; Montagnes, Taylor, & Lynn, 1990; Petz, Song, & Wilbert, 1995; Song, Wang, & Warren, 2000). During the past decade, eight new *Strombidium* species have been reported, which indicates that there is still much to learn about the diversity of this genus (Agatha, Strüder-Kypke, Beran, & Lynn, 2005; McManus, Xu, Costas, & Katz, 2010; Song, 2005; Song et al., 2015; Wilbert & Song, 2005; Xu, Sun, Song, & Warren, 2008; Xu, Warren, & Song, 2009). In addition, the systematics of *Strombidium* remains poorly understood, although previous studies have strongly argued for its monophyly (Agatha, 2014; Agatha & Strüder-Kypke, 2014; Gao, Gong, Lynn, Lin, & Song, 2009; Li, Liu, Gao, Warren, & Song, 2013; Liu et al., 2011a, 2011b; Song et al., 2013, 2015; Tsai, Chen,

Correspondence to: Xiaozhong Hu. E-mail: xiaozhonghu@ouc.edu.cn

ISSN 1477-2000 print / 1478-0933 online

http://dx.doi.org/10.1080/14772000.2015.1081992

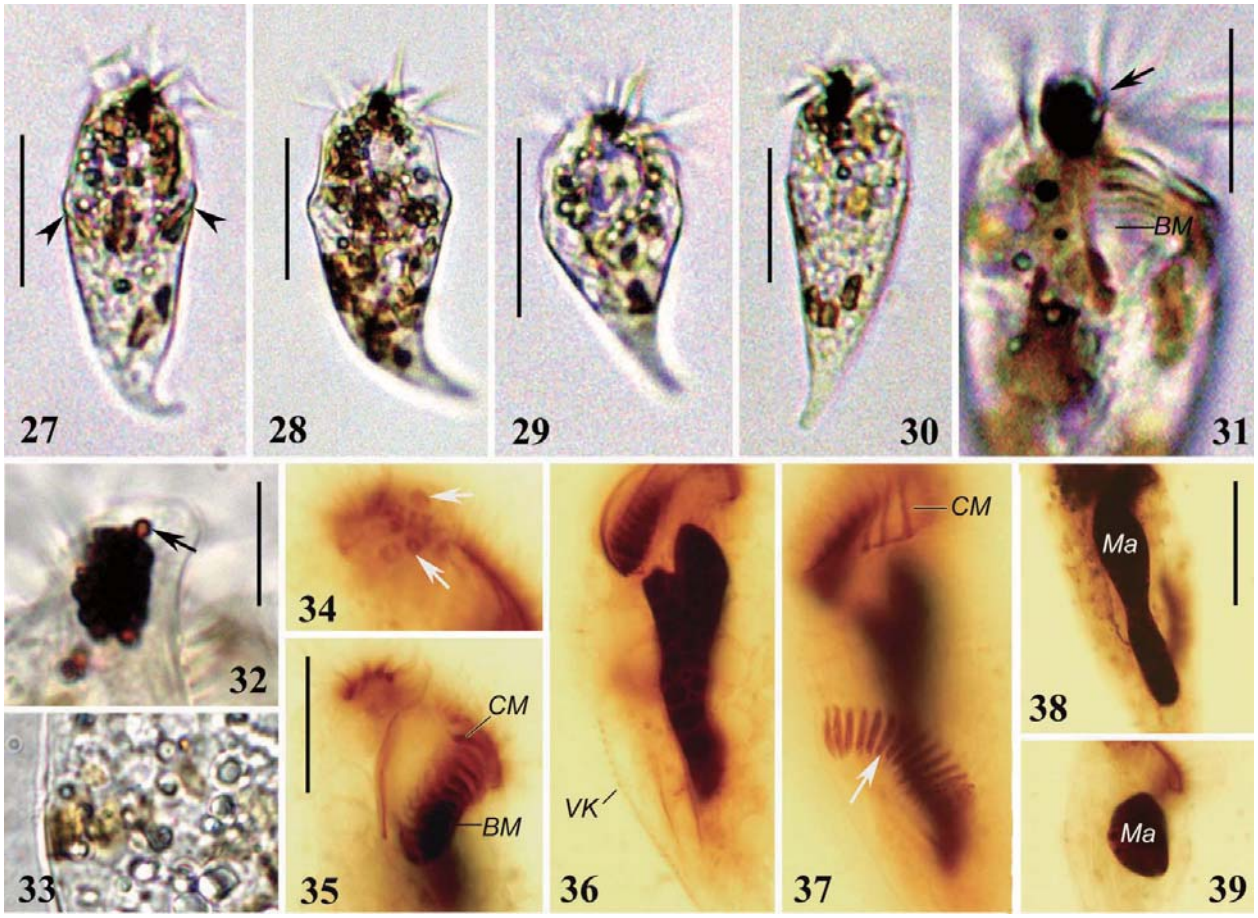

Fig. 27–39. Photomicrographs of *Strombidium cuneiforme* sp. nov. from life (27–33) and after protargol staining (34–39). (27–29) ventral views of three individuals, arrowheads mark the extrusomes; (30) lateral view; (31) anterior ventral view, arrow marks apical protrusion; (32) detail of eyespot, arrow marks a red pigment granule; (33) detail showing cytoplasmic inclusions; (34) apical protrusion, arrows mark pigment granules; (35) buccal apparatus; (36) ventral view of a specimen; (37) early divider: arrow marks oral primordium; (38, 39) different shapes of macronucleus. BM, buccal membranelles; CM, collar membranelles; Ma, macronucleus; VK, ventral kinety. Scale bars: Figs 27–30: 35 μm; Figs 31, 35: 10 μm; Fig. 32: 5 μm; Fig. 38: 30 μm.

containing prominent eyespot, posterior cell tapering and elongated. Buccal field occupies ~1/4 of cell length. Extrusomes needle-shaped, ~12 × 0.5 μm in size. Macronucleus ovoidal or elongate-ovoid. AZM composed of 10–14 collar and 10–13 buccal membranelles. Girdle kinety pre-equatorial and ostensibly continuous, composed of 46–65 dikinetids. Ventral kinety composed of 24–33 dikinetids.

Type locality and habitat. A mangrove wetland near Zhanjiang (21°22′N, 110°25′E), Guangdong Province, southern China: salinity 17.0‰, temperature 24.5°C, and pH 6.8.

Deposition of slides. A slide with the holotype specimen (registration number: SW2013102402-1) is deposited in the Laboratory of Protozoology, Ocean University of China. A slide with paratype specimens (registration number: NHMUK 2015.1.2.2.) is deposited in the Natural History Museum, London.

Etymology. The Latin 'cuneiforme' means wedge-shaped, referring to the wedge-like body shape of this species.

SSU rRNA gene sequence. The length of the SSU rRNA gene sequence of *Strombidium cuneiforme* sp. nov. (GenBank accession number: KP260512) is 1728 bp and the G + C content is 45.54%.

Description. Cell 50–90 × 20–30 μm *in vivo*, 52–91 × 19–32 μm after protargol staining. Shape elongate conical, with posterior portion bluntly pointed, sometimes curved to left or dorsal side. Widest at anterior 1/3, with ratio of length: width 2.5–3:1. Anterior end domed and with ~5 μm-high apical protrusion on right side of peristome; apical protrusion not visible in protargol-stained

Systematics and Biodiversity (2015), **13(1)**: 76–92

Research Article

Taxonomy and molecular phylogeny of four *Strombidium* species, including description of *S. pseudostylifer* sp. nov. (Ciliophora, Oligotrichia)

WEN SONG[1,2], JIAMEI LI[2], WEIWEI LIU[3], KHALED A. S. AL-RASHEID[4], XIAOZHONG HU[2] & XIAOFENG LIN[1]

[1]Laboratory of Protozoology, Key Laboratory of Ecology and Environment Science in Guangdong Higher Education, South China Normal University, Guangzhou 510631, China
[2]Laboratory of Protozoology, Institute of Evolution and Marine Biodiversity, Ocean University of China, Qingdao 266003, China
[3]Key Laboratory of Tropical Marine Bio-resources and Ecology, South China Sea Institute of Oceanology, Chinese Academy of Science, Guangzhou 510301, China
[4]Zoology Department, College of Science, King Saud University, P.O. Box 2455, Riyadh 11451, Saudi Arabia

(Received 18 July 2014; accepted 23 September 2014)

Oligotrich ciliates are important components of marine microplankton and have a high biodiversity. In the present paper, the morphology and small subunit rRNA (SSrRNA) gene sequence of four *Strombidium* species are recorded, including a new species, *S. pseudostylifer* sp. nov. that was sampled from a mangrove wetland. This new species is characterized by its prominent apical protrusion, long constant tail and large number of ventral dikinetids. In addition, the morphology of two poorly known species, *S. chlorophilum* Montagnes et al., 1988 and *S. oculatum* Gruber, 1884 are redescribed based on the Chinese populations and their diagnoses are improved. The morphology of three populations of *S. stylifer* Levander, 1894 collected from three sampling sites in China are also compared, revealing that the only difference between them are the sizes of their cells and macronuclei. Finally, the phylogenetic analyses of the above four *Strombidium* species, as inferred from their SSrRNA gene sequence data, show that *S. oculatum*, *S. stylifer* and *S. pseudostylifer* cluster within the main *Strombidium* branch while *S. chlorophilum* clusters with *S. conicum* and branches from the main *Strombidium* group.

http://zoobank.org/urn:lsid:zoobank.org:pub:E869E485-8F29-4B2B-8BB2-D3A039AA6403

Key words: ciliates, mangrove wetland, new species, SSrRNA gene sequence, Strombidiidae, *Strombidium chlorophilum*, *Strombidium oculatum*, *Strombidium pseudostylifer*, *Strombidium stylifer*

Introduction

The oligotrich ciliates are a large group of planktonic protozoa and recent studies have demonstrated that they exhibit great biodiversity (Agatha, 2011a; Liu, Yi, Lin, & Al-Rasheid, 2011a; Liu et al., 2011b). As representatives of this group, *Strombidium* species are most familiar to taxonomists because of their horizontal girdle kinety, longitudinal ventral kinety and oral primordium posterior to the girdle kinety as that in the type species, *Strombidium sulcatum* Claparède & Lachmann, 1859 (Agatha, 2011b; Claparède & Lachmann, 1859; Maeda & Carey, 1985; Montagnes, Taylor, & Lynn, 1990). Up to now, there are about 65 species of *Strombidium*, with some of these having been described and redescribed using modern techniques (Agatha, 2011a; Agatha & Riedel-Lorjé, 1997; Agatha, Strüder-Kypke, Beran, & Lynn, 2005; Lei, Xu, & Song, 1999; Lynn & Montagnes, 1988; Montagnes, Lowe, Poulton, & Jonsson, 2002; Montagnes, Lynn, Stoecker, & Small, 1988; Montagnes et al., 1990; Petz, 1994; Petz, Song, & Wilbert, 1995; Song, 2005; Song, Wang, & Warren, 2000). There remain, however, many poorly known members of this genus and there is a clear need for further taxonomic investigations using a combination of morphological and molecular data. Furthermore, previous studies using molecular phylogeny have not supported the monophyly of the genus *Strombidium* since *S. conicum* always groups with other genera of Strombidiidae (Agatha & Strüder-Kypke, 2014; Gao, Gong, Lynn, Lin, & Song,

Correspondence to: Xiaofeng Lin. E-mail: xlin@scnu.edu.cn

ISSN 1477-2000 print / 1478-0933 online

http://dx.doi.org/10.1080/14772000.2014.970674

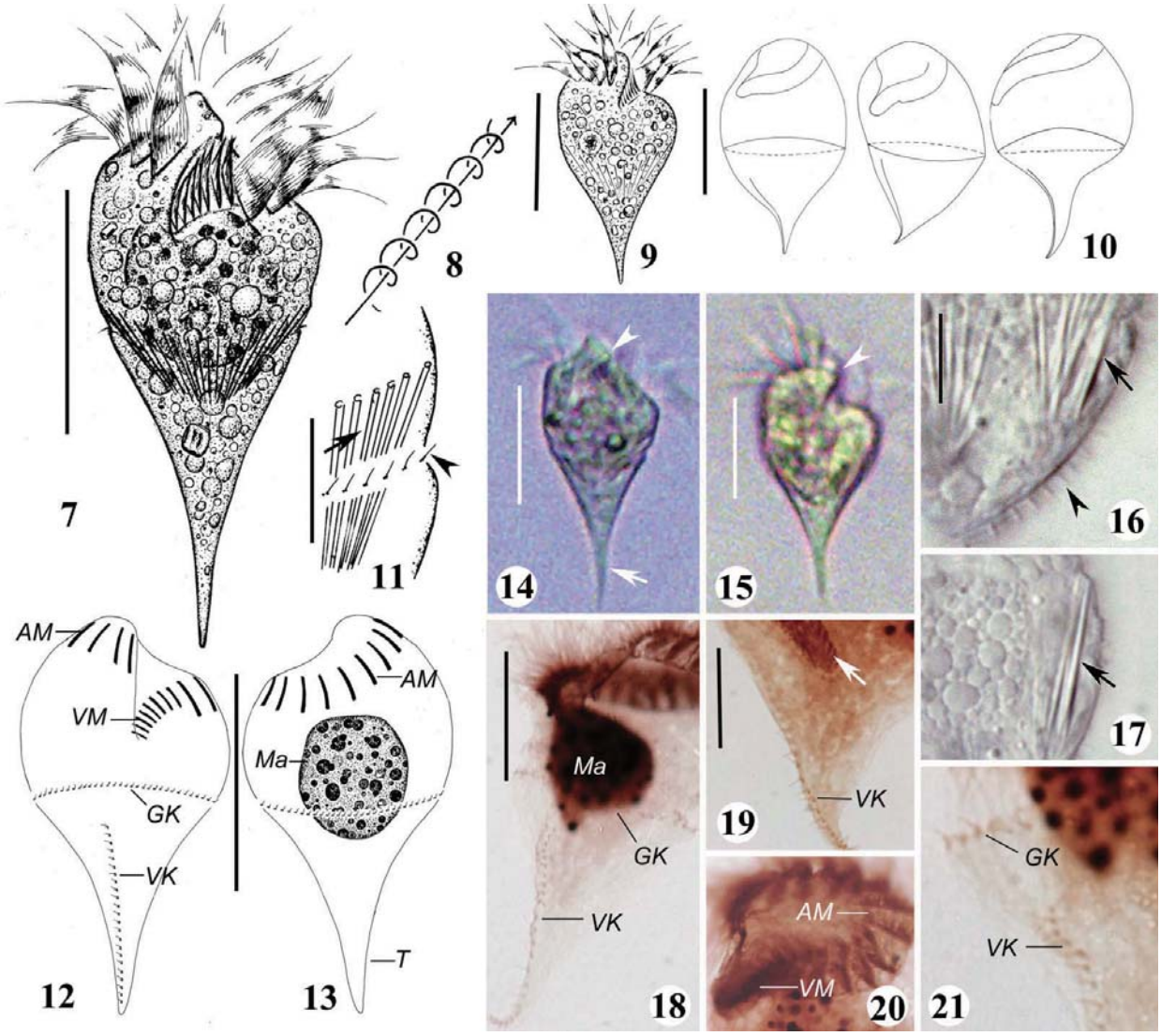

Figs. 7−21. *Strombidium pseudostylifer* sp. nov. from life (7−9, 11, 14−17) and after protargol impregnation (10, 12, 13, 18−21). (7, 9) Ventral views of normal and short individuals with short tail; (8) swimming trace; (10) variety of tail shapes due to distension after protargol impregnation; (11) detail of extrusomes (arrow) and cilia of girdle kinety (arrowhead); (12, 13) ventral and dorsal views of ciliary pattern; (14, 15) ventral views of specimens with different shapes, arrowheads mark apical protrusion, arrow marks the constant tail; (16) detail of cilia of ventral kinety (arrowhead) and extrusomes (arrow); (17) detail of macronucleus and extrusomes (arrow); (18) somatic ciliature of cell; (19) ventral posterior of cell, arrow marks the oral primordium; (20) oral ciliature; (21) ventral mid portion of cell. AM, anterior membranelles; GK, girdle kinety; Ma, macronucleus; T, tail; VK, ventral kinety; VM, ventral membranelles. Scale bars: Figs 7, 9, 10, 14, 15: 20 μm; Figs 11, 16, 19: 10 μm; Figs 12, 13: 40 μm; Fig 18: 20 μm.

Cell rotating in spirals about main body axis when swimming, sometimes circling around irregularly (Fig. 8).

Buccal cavity deep, occupying about one third of the body length. Anterior part of the adoral zone composed of 14−17 membranelles with bases about 9 μm wide, and with cilia up to 25 μm long *in vivo*. The ventral part composed of about 7−9 membranelles, with bases about 3−5 μm wide and with cilia about 5−8 μm in length, decreasing in width towards the cytostome. Ventral membranelles are continuous with the anterior membranelles (Figs 12, 13, 20). Endoral membrane composed of a row of kinetosomes and located on inner wall of right buccal lip.

Somatic ciliature arranged in girdle and ventral kineties. Girdle kinety continuous, located posterior to equator and composed of about 45 horizontally oriented dikinetids. Each girdle dikinetid possesses a cilium of about 2 μm long with left basal bodies (Figs 12, 13, 21). Ventral kinety longitudinally oriented, about 30 μm long, starting about 10−15 μm below the girdle kinety and

PLOS ONE

RESEARCH ARTICLE

Two New Genera of Planktonic Ciliates and Insights into the Evolution of the Family Strombidiidae (Protista, Ciliophora, Oligotrichia)

Weiwei Liu[1,2,3☯], Zhenzhen Yi[1☯], Dapeng Xu[4], John C. Clamp[5], Jiqiu Li[1], Xiaofeng Lin[1]*, Weibo Song[2]*

1 Laboratory of Protozoology, Key Laboratory of Ecology and Environmental Science in Guangdong Higher Education, South China Normal University, Guangzhou, China, **2** Laboratory of Protozoology, Institute of Evolution and Marine Biodiversity, Ocean University of China, Qingdao, China, **3** Key Laboratory of Tropical Marine Bio-resources and Ecology, South China Sea Institute of Oceanology, Chinese Academy of Science, Guangzhou, China, **4** State Key Laboratory of Marine Environmental Science, Institute of Marine Microbes and Ecosphere, Xiamen University, Xiamen, China, **5** Department of Biology, North Carolina Central University, Durham, United States of America

☯ These authors contributed equally to this work.
* xlin@scnu.edu.cn (XL); wsong@ouc.edu.cn (WS)

OPEN ACCESS

Citation: Liu W, Yi Z, Xu D, Clamp JC, Li J, Lin X, et al. (2015) Two New Genera of Planktonic Ciliates and Insights into the Evolution of the Family Strombidiidae (Protista, Ciliophora, Oligotrichia). PLoS ONE 10(6): e0131726. doi:10.1371/journal.pone.0131726

Editor: Peter Prentis, Queensland University of Technology, AUSTRALIA

Received: March 6, 2015

Accepted: June 4, 2015

Published: June 29, 2015

Data Availability Statement: SSrDNA sequences files are available from the GenBank database (accession number(s) JX310365, JX310366). The remaining relevant data may be found within the paper and its Supporting Information files.

Funding: Financial support was provided by the National Natural Science Foundation of China (projects numbers: 31222050, 31172060, 31201696, 31430077, 31471973), Research Fund for the Outstanding Young Teachers Program of Higher Education in Guangdong (Yq2013052), and the International Research Coordination Network for Biodiversity of Ciliates funded jointly by the U.S.

Abstract

Oligotrich ciliates are common marine microplankters, but their biodiversity and evolutionary relationships have not been well-documented. Morphological descriptions and small subunit rRNA gene sequences of two new species representing two new strombidiid genera, *Sinistrostrombidium cupiformum* gen. nov., sp. nov. and *Antestrombidium agathae* gen. nov., sp. nov. are presented, and their taxonomy and molecular phylogeny are analyzed. *Sinistrostrombidium* gen. nov. is characterized by a sinistrally spiraled girdle kinety and a longitudinal ventral kinety. *Antestrombidium* gen. nov. is distinguished by tripartite somatic kineties (circular and ventral kineties plus dextrally spiraled girdle kinety). *Sinistrostrombidium* and *Antestrombidium* branched separately from one another in phylogenetic trees, clustering with different clades of strombidiids. The new genera added to the diversities of ciliary patterns and small subunit rRNA gene sequences in strombidiids leads to presentation of a new hypothesis about evolution of the 12 known strombidiid genera, based on ciliary pattern and partly supported by molecular evidence. In addition, our new morphological and molecular analyses support establishment of a new order Lynnellida ord. nov., characterized by an open adoral zone of membranelles without differentiation of anterior and ventral membranelles, for *Lynnella*, but we remain unable to assign the genus to a subclass with confidence.

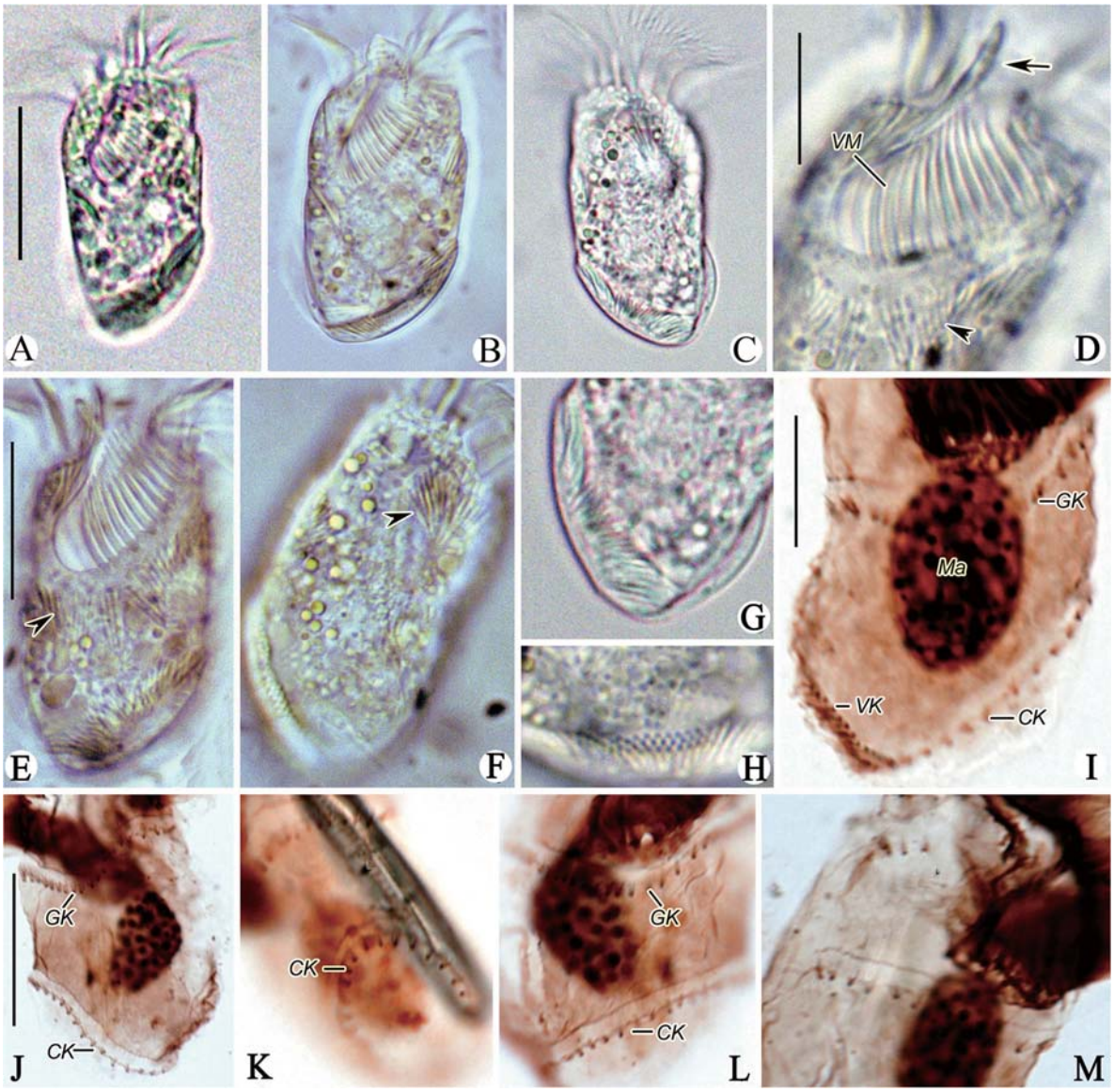

Fig 5. Photomicrographs of *Antestrombidium agathae* gen. nov., sp. nov. from life (A-H) and after staining with protargol (I-M). A, B. Ventral views of two individuals; C. Dorsal view; D. Ventral view of anterior part of cell, arrow marks the apical protrusion and arrowhead indicates the extrusomes; E, F. Ventral (E) and Dorsal (F) views showing the distribution of extrusomes (arrowheads); G, H. Posterior portion of cell showing the distribution of extrusomes; I, J. Ventral and dorsal views of posterior portion of cell, showing the somatic kineties; K, L. Left and ventral views showing the GK and CK; M. Right lateral view showing the GK. Legend: CK-circular kinety; GK-girdle kinety; Ma-macronucleus; VK-ventral kinety; VM-ventral membranelles. Scale bars: A-C. 30 μm; D, G-I, L, M. 10 μm; E, F, J, K. 20 μm.

doi:10.1371/journal.pone.0131726.g005

surface is elevated to form conspicuous ridges (Fig 4A and 4B, arrow; 5D-H, arrowheads). Undischarged extrusomes rod-shaped, measuring approximately 6 × 0.6 μm (Fig 4C). Macronucleus ovoid, located in posterior half of cell, and measuring approximately 10 × 15 μm after staining with protargol (Figs 4G and 4H; 5I). Micronucleus, contractile vacuole and cytopyge not observed. In Petri dish with *in situ* water at room temperature, cell normally moves by crawling over debris but swims away by rotation about longitudinal axis in spirals (about 70 μm across) when disturbed (Fig 4D).

The LINNEAN SOCIETY of London ZOOLOGICAL Journal of the Linnean Society

Zoological Journal of the Linnean Society, 2015, **174**, 653–665. With 4 figures

Morphology and molecular phylogeny of three new oligotrich ciliates (Protozoa, Ciliophora) from the South China Sea

WEIWEI LIU[1,2,3]†, ZHENZHEN YI[2]†, XIAOFENG LIN[2]*, JIQIU LI[2], SALEH A. AL-FARRAJ[4], KHALED A. S. AL-RASHEID[4] and WEIBO SONG[3]*

[1]*Key Laboratory of Tropical Marine Bio-resources and Ecology, South China Sea Institute of Oceanology, Chinese Academy of Science, Guangzhou 510301, China*
[2]*Laboratory of Protozoology, Key Laboratory of Ecology and Environmental Science in Guangdong Higher Education, South China Normal University, Guangzhou 510631, China*
[3]*Laboratory of Protozoology, Institute of Evolution & Marine Biodiversity, Ocean University of China, Qingdao 266003, China*
[4]*Zoology Department, College of Science, King Saud University, Riyadh 11451, Saudi Arabia*

Received 21 November 2014; revised 30 January 2015; accepted for publication 1 February 2015

The present paper documents the morphology and systematic positions of three new oligotrich ciliates, ***Parallelostrombidium obesum* sp. nov.**, ***Parallelostrombidium ellipticum* sp. nov.**, and ***Strombidium tropicum* sp. nov.**, which were sampled from habitats with different salinities in southern China. ***Parallelostrombidium obesum* sp. nov.** is characterized by a fat body and the posterior portions of the girdle and ventral kineties extending transversely on the dorsal side. ***Parallelostrombidium ellipticum* sp. nov.** is recognizable by the anterior ends of the girdle and ventral kineties being close to each other and the posterior ends of the girdle and ventral kineties intersecting on the dorsal side. ***Strombidium tropicum* sp. nov.** is distinguished by a ventrally opened girdle kinety that is slightly spiralled with the right end shifted posteriad. *Small subunit rRNA* gene trees show that ***P. obesum* sp. nov.** and ***P. ellipticum* sp. nov.** fall into a mixed group composed of *Parallelostrombidium* and some *Novistrombidium* species, and that ***S. tropicum* sp. nov.** branches at the base of the clade containing non-*Strombidium* species. The relationships of *Parallelostrombidium* species and that of *Strombidium* species are both not resolved considering their low support values in our phylogenetic analysis.

doi: 10.1111/zoj.12257

ADDITIONAL KEYWORDS: ***Parallelostrombidium ellipticum* sp. nov.** – ***Parallelostrombidium obesum* sp. nov.** – *small subunit rRNA* – Strombidiidae – ***Strombidium tropicum* sp. nov.**

INTRODUCTION

Oligotrich ciliates, which are commonly found in marine, brackish, and freshwater habitats, are a species-rich group of ciliates and have been of great interest to protozoologists working in ecological fields because of their important role in the pelagic microbial food loop (Song, Wang & Warren, 2000; Fenchel, 2008; Caron *et al*., 2012). Recent research, however, has indicated that this assemblage is much more diverse than previously supposed (Song, Warren & Hu, 2009; Kim *et al*., 2010; Agatha, 2011, 2014; Lee *et al*., 2012; Liu *et al*., 2013; Tsai, Chen & Chiang, 2015), and there is a pressing need for thorough taxonomic investigations of the large number of previously unknown species. For these unknown taxa, analyses that combine traditional methods (e.g. living observations, silver impregnation, statistical analyses, and morphogenetic investigations) with molecular methods are more likely to yield reliable results (Modeo *et al*., 2003; Gao *et al*., 2009; McManus *et al*., 2010; Liu *et al*., 2011a, b, 2012; Agatha & Strüder-Kypke, 2012; Song *et al*., 2013, 2015; Xu *et al*., 2013).

*Corresponding authors. E-mails: xlin@scnu.edu.cn and wsong@ouc.edu.cn
†These authors contributed equally.

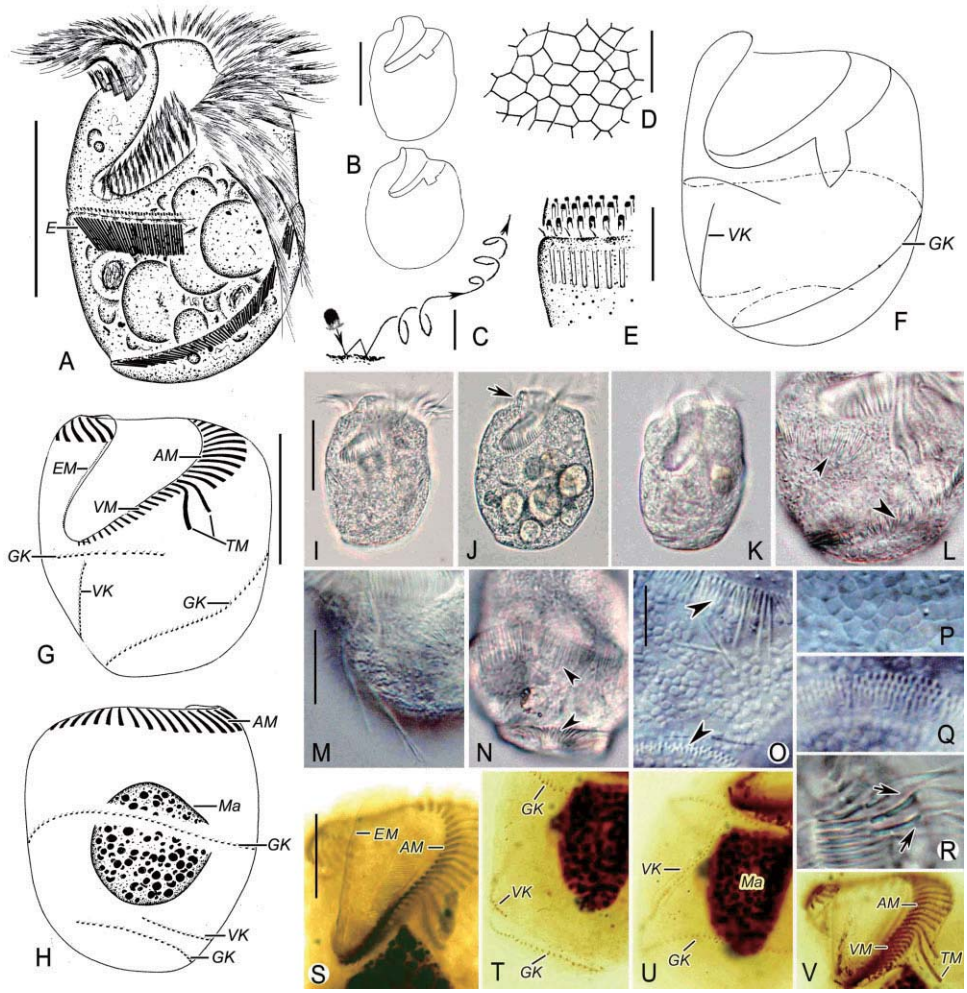

Figure 1. ***Parallelostrombidium obesum*** **sp. nov.** from life (A–E, I–R) and after protargol impregnation (F–H, S–V). A, ventral view of typical specimen. B, I, J, different body shapes, arrow marks the apical protrusion. C, swimming trace. D, P, pattern of cortical platelets. E, O, Q, detail of extrusomes attached above the girdle kinety. F, pattern of somatic ciliature. G, H, ventral (G) and dorsal (H) views of the same specimens showing the ciliary pattern and the macronucleus. K, lateral view. L, N, ventral (L) and dorsal (N) views showing the distribution of extrusomes (arrowheads). M, two thigmotactic membranelles. R, detail of bases of thigmotactic membranelles (arrows). S, V, ventral views of anterior portion of cell showing oral membranelles. T, U, dorsal (T) and ventral (U) views showing the girdle and ventral kineties. AM, anterior membranelles; E, extrusomes; EM, endoral membrane; GK, girdle kinety; Ma, macronucleus; TM, thigmotactic membranelles; VK, ventral kinety; VM, ventral membranelles. Scale bars: 120 μm (C); 40 μm (A, B, F–K); 20 μm (L–N, S–V); 10 μm (D, E, O–R).

posterior ends transversely truncated with conspicuous apical protrusion; macronucleus ovoid; ~30 anterior, ~17 ventral, and consistently two conspicuous thigmotactic membranelles; girdle kinety comprising ~130 dikinetids, spiralling around cell with one and a half whorls and the anterior end of the girdle kinety extending to the left of the ventral kinety and located far away from the ventral kinety; ventral kinety with ~35 dikinetids; the posterior portions of girdle and ventral kineties crossing the right margin of cell and extending transversely on the posterior dorsal side. Marine form.

Type locality: A mangrove wetland near Shenzhen (22°37′N, 114°04′E), Guangdong, China. Water temperature was 27.0 °C, salinity 17.0‰, and pH 8.2.

Etymology: The Latin adjective obesum [neuter gender] (fat) refers to the fat body of the species.

Deposition of slides: A protargol slide containing the holotype specimen (marked with a black circle) has been deposited at the Natural History Museum, London, with registration number NHMUK 2014.5.7.1. One protargol slide with paratype specimens has been deposited in

Chinese Journal of Oceanology and Limnology

http://dx.doi.org/10.1007/s00343-015-4083-0

Monophyly or polyphyly? Possible conflict between morphological and molecular interpretations of the well-known genus *Zoothamnium* (Ciliophora, Peritrichia)*

LI Lifang (李丽芳)[1, 2, **], MA Honggang (马洪钢)[2], AL-RASHEID Khaled A. S.[3]

[1] *Marine College, Shandong University, Weihai 264209, China*

[2] *Institute of Evolution & Marine Biodiversity, Ocean University of China, Qingdao 266003, China*

[3] *Zoology Department, King Saud University, Riyadh 11451, Saudi Arabia*

Received Apr. 18, 2014; accepted in principle May 29, 2014; accepted for publication Jul. 19, 2014

Abstract In this paper, we explore possible conflict between morphological and molecular interpretations of phylogenetic relationships within the well-known peritrichous genus *Zoothamnium*. On the basis of morphological evidence, for a long time this genus has been believed to be a well-defined monophyletic taxon. Nonetheless, *Zoothamnium* exhibits higher genetic diversity than the gross morphology of its species. Here, we used all available genetic information for the small subunit of ribosomal RNA (SSU rRNA) and internal transcribed spacer region (ITS1-5.8S-ITS2) for this genus to reconstruct phylogenies for four datasets (SSU rRNA, ITS1, ITS2, and ITS1-5.8S-ITS2) and a combined dataset (SSU rRNA+ITS1-5.8S-ITS2) using different phylogenetic methods and with consideration of the secondary structure of the genes. Confidence in phylogenetic tree selection was assessed with the approximately unbiased test. The molecular results showed both that *Zoothamnium* is more likely to be polyphyletic, and morphologically similar genera *Zoothamnopsis* and *Myoschiston* were always nested among *Zoothamnium* species. Accordingly, as with some other groups of ciliates, to understand more fully the correct phylogeny of *Zoothamnium* there remains a need for additional data from both morphological and molecular studies, covering additional *Zoothamnium* spp. and members of closely related genera (e.g. *Zoothamnopsis*, *Myoschiston*, and *Epistylis*).

Keyword: peritrichous ciliates; *Zoothamnium*; phylogenetic analyses; monophyly; polyphyly

1 INTRODUCTION

The peritrichous ciliates are common in nature and remarkable for their species richness, living in freshwater, brackish water, and salt water (Kahl, 1933; Stiller, 1971; Foissner et al., 1992; Song et al., 2002; Ji et al., 2005, 2006, 2009; Ji and Kusuoka, 2009; Song et al., 2009; Foissner et al., 2010; Zhan et al., 2013).

It is commonly accepted that, morphologically, the peritrichous genus *Zoothamnium* Bory de St. Vincent, 1826 is characterized by a continuous spasmoneme within a branching stalk (vs. *Myoschiston*: lacking a spasmoneme in the basal stalk in the mature stage), thus leading to a contraction of the entire colony and a transverse silverline pattern (vs. *Zoothamnopsis*: reticulate pattern). *Zoothamnium* is a unique taxon compared with other taxa and has been recognized without question as a well-defined clade for nearly two centuries (Kahl, 1933; Bauer-Nebelsick et al., 1996; Song, 1997; Lynn, 2008; Ji et al., 2009; Sun et al., 2012b). The characteristics usually used to identify or characterize species of *Zoothamnium* include the size, body shape, features of the pellicle surface and stalk, appearance of the peristomial lip, pattern of infraciliature and number of silverlines.

During the last decade, progress in molecular

* Supported by the National Natural Science Foundation of China (Nos. 31071898, 31111120437), the Scientific Research Foundation for the Returned Overseas Chinese Scholars, State Education Ministry of China, the Key Laboratory of Mariculture (KLM), Ministry of Education, Ocean University of China, the Research Group Project (No. RGP-VPP-083), and the King Saud University Deanship of Scientific Research

** Corresponding author: qd_liliy@sina.com

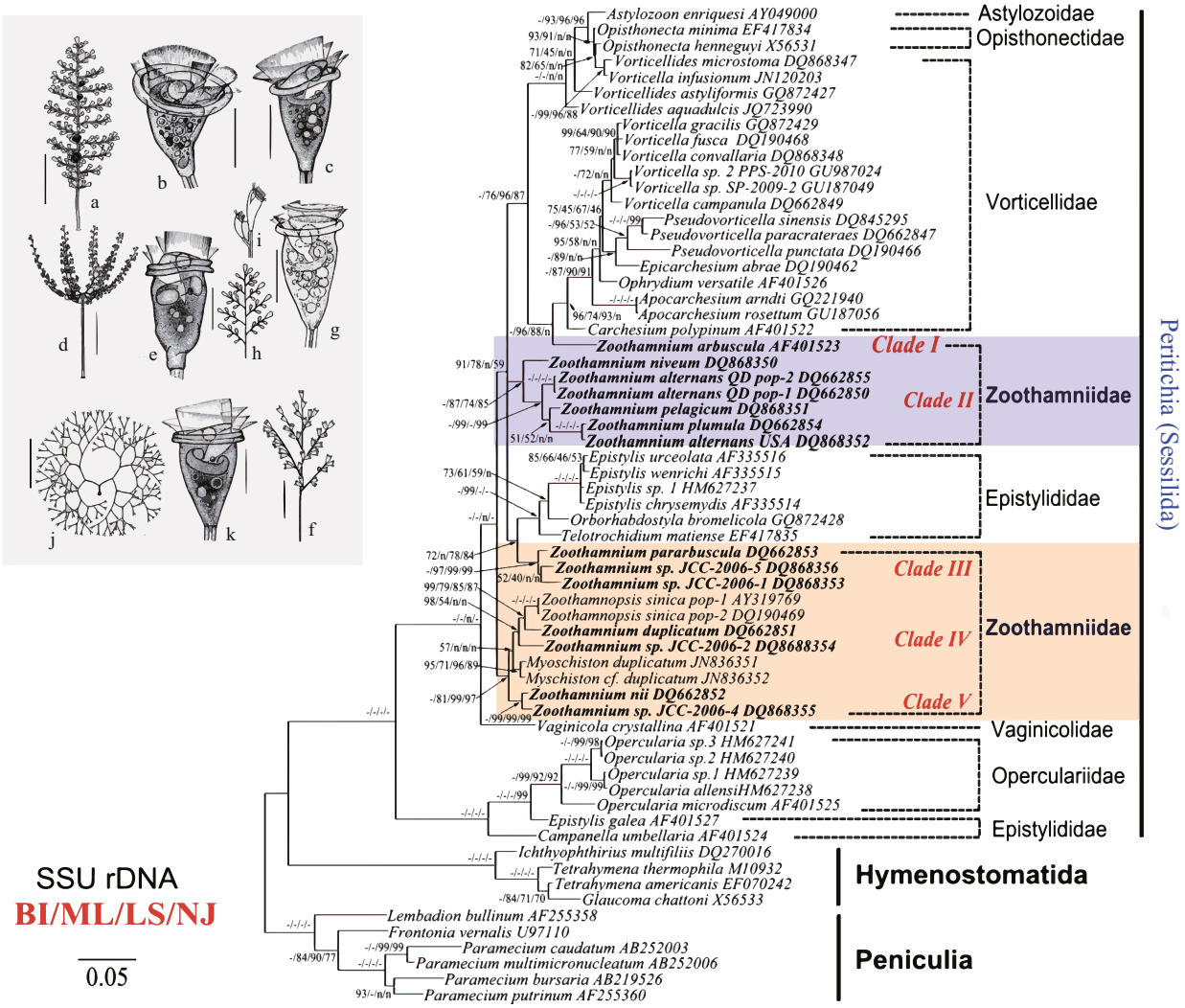

Fig.1 Bayesian inference tree inferred from the nucleotide sequences of small subunit rDNA (SSU rDNA) showing the phylogeny of the peritrichous genus *Zoothamnium*

Numbers at nodes represent bootstrap values (in %) out of 1 000 replicates: the first number is the Bayesian credibility value using the MrBayes (BI) algorithm, the second number is from the maximum likelihood (ML) method, the third and fourth numbers are derived from the distance matrix based on the least-squares (LS) and neighbor joining (NJ) methods. Evolutionary distance is represented by the branch length to separate the species in the figure. The scale bar corresponds to five substitutions per 100 nucleotide positions. Regions are separated by double lines, and positions of nucleotides at the beginning and end of each region are given at the top of each column. Deletions are indicated by introduction of alignment gaps (-). Homologous groups of nucleotides are indicated by boxes. Species in different clades are separated by a beeline in the list of taxa. Insets: morphology of five *Zoothamnium* spp. a, b (from Ji et al., 2006): colony (a) and microzooid (b) of *Z. alternans*; c, d (from Ji et al., 2005b): *Z. pararbuscula*; e, f: *Z. nii* (from Ji et al., 2005a); g–i: *Z. plumula*; j, k: *Z. duplicatum* (from Ji et al., 2005c). Scale bars: 30 μm (b, c, e, g, k), 300 μm (a, f), 500 μm (d, j).

The following results reconfirmed those from previous molecular studies:

1) The BI, LS, and NJ analyses supported a sister-group relationship between Clade III (*Zoothamnium pararbuscula* - *Z.* sp. JCC-2006-1 - *Z.* sp. JCC-2006-5) and *Epistylis-Orborhabdostyla-Telotrochidium*, which was also supported by Foissner et al. (2010), although their analysis did not include *Zoothamnium* sp. JCC-2006-1 and *Z.* sp. JCC-2006-5;

2) *Zoothamnium arbuscula* was associated more closely with *Carchesium polypinum* and other vorticellids than with zoothamniids (Clamp and Williams, 2006; Li et al., 2008a; Foissner et al., 2010);

3) The distinct morphological similarity of *Zoothamnopsis*, *Zoothamnium* and *Myoschiston* was supported by the molecular data. In the phylogenetic trees presented here, *Zoothamnopsis* and *Myoschiston* were nested within the unresolved *Zoothamnium* species (except *Z. arbuscula*). Similarities in the secondary structure (i.e. the Helix E10-1 and Helix 23-1 regions) provided further evidence for the close relationship between these three genera and suggested that they belong to the same family (figure not shown) (Li et al., 2008a, b; Sun et al., 2012b).

Available online at www.sciencedirect.com

ScienceDirect

European Journal of Protistology 51 (2015) 374–385

European Journal of PROTISTOLOGY

www.elsevier.com/locate/ejop

Taxonomy and molecular phylogeny of two novel ciliates, with establishment of a new genus, *Pseudogastrostyla* n. g. (Ciliophora, Hypotrichia, Oxytrichidae)

Yangbo Fan[a], Xiaolu Zhao[a,1], Xiaozhong Hu[a,*], Miao Miao[b,*], Alan Warren[c], Weibo Song[a]

[a]*Laboratory of Protozoology, Institute of Evolution and Marine Biodiversity, Ocean University of China, Qingdao 266003, China*
[b]*College of Life Sciences, Graduate University of Chinese Academy of Sciences, Beijing, China*
[c]*Department of Life Sciences, Natural History Museum, London SW7 5BD, United Kingdom*

Received 19 December 2014; received in revised form 12 June 2015; accepted 12 June 2015
Available online 7 July 2015

Abstract

Two novel hypotrichous ciliates, *Pseudogastrostyla flava* n. g., n. sp. and *Urosomoida subtropica* n. sp., isolated from Daya Bay Mangrove Park, Huizhou, southern China, were observed in vivo and after protargol staining. *Pseudogastrostyla* n. g. is diagnosed by having more than 18 frontal-ventral-transverse cirri, an indistinct frontoventral row, undulating membranes in *Oxytricha*-pattern and dorsomarginal kinety, but lacking dorsal kinety fragmentation during morphogenesis. The monotypic species, *P. flava* n. sp., is characterized by its brownish body colour, brown-yellowish cortical granules mostly arranged in groups, frontoventral row terminating near mid-body, and one caudal cirrus. *Urosomoida subtropica* n. sp. can be recognized by having one micronucleus located between two macronuclear nodules, four transverse cirri, pretransverse ventral cirrus (V/2) anteriorly located, four dorsal kineties and three caudal cirri. Phylogenetic analyses based on SSU rRNA gene sequence data indicate that *Pseudogastrostyla* n. g. is nested within the oxytrichids and is most closely related to *Rubrioxytricha ferruginea*, and that *Urosomoida subtropica* n. sp. clusters with *Oxytricha elegans* rather than the type species, *U. agilis*. Nodal support values are, however, too low to draw any conclusions about the molecular systematics of the genus *Urosomoida*.

Keywords: Phylogeny; *Pseudogastrostyla flava* n. g., n. sp.; SSU rDNA; Taxonomy; *Urosomoida subtropica* n. sp.

Introduction

Oxytrichids are one of the largest groups of hypotrichous ciliates and exhibit an extremely high degree of adaptive evolution (Berger 1999; Berger and Foissner 1997; Chen et al. 2013; Dragesco and Dragesco-Kernéis 1986; Hemberger 1982; Hu and Kusuoka 2015). In his comprehensive guide to the oxytrichids, Berger (1999) recognized about 170 valid species. Recent investigations of oxytrichid diversity have increased this total to nearly 200 valid morphospecies (Berger 2011; Heber et al. 2014; Jung et al. 2014; Kim et al. 2014; Kumar et al., 2014; Kumar et al., 2015; Küppers 2014; Lv et al. 2013; Shao et al., 2013a; Shao et al., 2013b; Shao et al., 2014; Singh and Kamra 2013; Singh and Kamra, 2015; Singh et al. 2013; Weisse et al. 2013). Most oxytrichids

*Corresponding authors.
E-mail addresses: xiaozhonghu@ouc.edu.cn (X. Hu), doublemiao@126.com (M. Miao).
[1]Co-first author.

http://dx.doi.org/10.1016/j.ejop.2015.06.007
0932-4739/

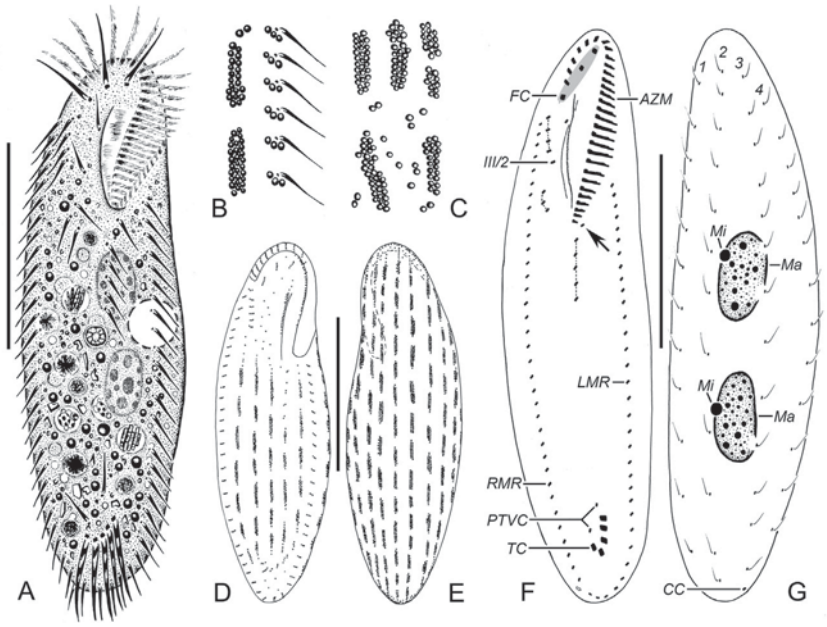

Fig. 1. *Pseudogastrostyla flava* n. g., n. sp. from life (A–E) and after protargol staining (F, G). (A) Ventral view of a representative individual. (B–E) Ventral (B, D) and dorsal (C, E) views to show the arrangement of cortical granules. (F, G) Ventral (F) and dorsal (G) view of the holotype specimen to show the infraciliature and nuclear apparatus, shaded area denotes the frontal cirri and arrow marks cirrus IV/2. The cirri connected by broken lines are from the same cirral anlage. AZM, adoral zone of membranelles; CC, caudal cirri; FC, frontal cirri; LMR, left marginal row; Ma, macronuclear nodules; Mi, micronuclei; PTVC, pretransverse ventral cirri; RMR, right marginal row; TC, transverse cirri; 1–4, dorsal kineties 1–4. Scale bars = 50 μm.

cell midline; nodules ellipsoidal, about 13 × 8 μm in vivo (Figs 1G, 2G). Usually two micronuclei, one closely associated with each macronuclear nodule; micronuclei spherical, about 2 μm in diameter in vivo. Contractile vacuole about 10 μm in diameter, positioned in mid-body near left margin, contracting at intervals of about 10 s (Fig. 1A). Locomotion by continuous, moderately fast crawling on bottom of Petri dish.

Adoral zone about 30% of body length in vivo, composed of 23–29 membranelles; distal portion extending posteriorly

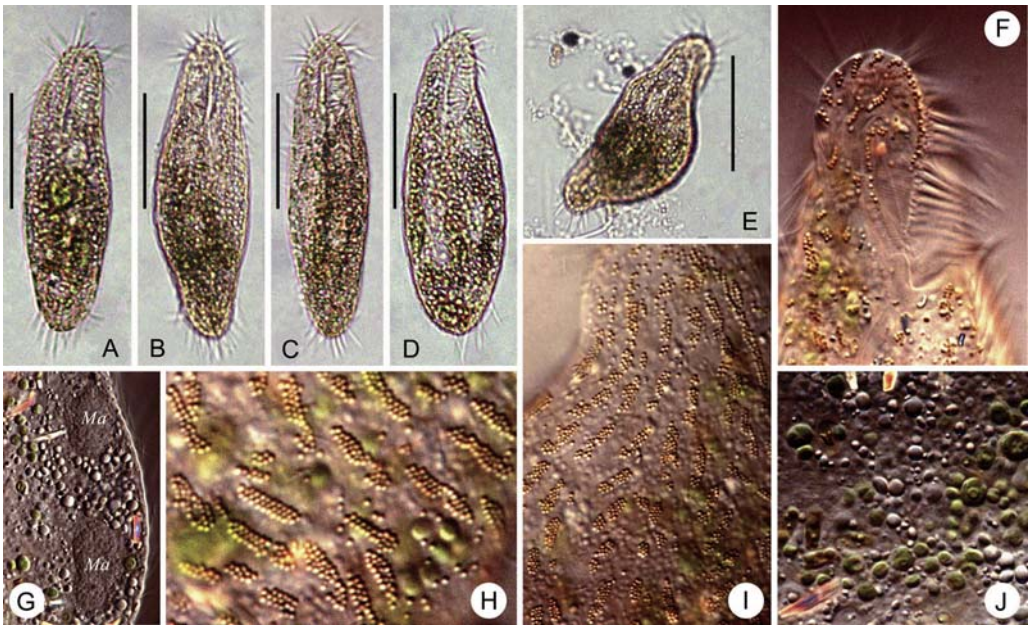

Fig. 2. Photomicrographs of *Pseudogastrostyla flava* n. g., n. sp. from life. (A–E) Ventral views of different individuals showing variation in body shape. (F) Anterior portion of ventral side to show the buccal field and arrangement of cortical granules. (G) Macronuclear nodules. (H, I) Dorsal views to show the arrangement of cortical granules. (J) Cytoplasmic inclusions. Ma, macronuclear nodules. Scale bars = 50 μm.

ACTA
PROTOZOOLOGICA

Acta Protozool. (2015) 54: 171–182
www.ejournals.eu/Acta-Protozoologica
doi:10.4467/16890027AP.15.014.3211

Morphological and Morphogenetic Redescriptions and SSU rRNA Gene-based Phylogeny of the Poorly-known Species *Euplotes amieti* Dragesco, 1970 (Ciliophora, Euplotida)

Mingjian LIU[1], Yangbo FAN[1], Miao MIAO[2], Xiaozhong HU[1], Khaled A. S. AL-RASHEID[3], Saleh A. AL-FARRAJ[3], Honggang MA[1]

[1] Laboratory of Protozoology, Institute of Evolution & Marine Biodiversity, Ocean University of China, Qingdao 266003, China; [2] College of Life Sciences, University of Chinese Academy of Sciences, Beijing 100049, China; [3] Zoology Department, College of Science, King Saud University, Riyadh 11451, Saudi Arabia

Abstract. This paper investigates the morphology and morphogenesis during binary fission of a Chinese population of *Euplotes amieti* Dragesco, 1970, a fresh water form which has previously not been well defined. This organism is morphologically very similar to the well-known *Euplotes eurystomus* but differs from the latter both in the number of dorsal kineties and the molecular data. According to the information obtained, it is characterized by a combination of features including nine frontoventral cirri, ca. 60 membranelles, 12–15 dorsal kineties, a macronucleus in the shape of the number 3, and a 'double-*eurystomus*' type of silverline system. Its morphogenesis proceeds broadly in the same pattern as in its congeners. In this study, the SSU rRNA gene was sequenced for the first time, and phylogenetic analyses indicated that it is closely related to the *eurystomus-aediculatus-woodruffi-* complex. Considering the extreme similarities in morphology between *E. amieti* and *E. eurystomus*, we believe that the four sequences (four isolates) under the name of *Euplotes eurystomus* (No. FR873716; FR873717; EF193250; AJ310491 deposited in GenBank) are very likely from misidentified material; that is, they represent different populations of *Euplotes amieti*.

Key words: Euplotidae, fresh water ciliate, ontogenesis, phylogenetic analysis, taxonomy.

INTRODUCTION

The ciliate family Euplotidae is one of the most complicated and confused taxa with a huge variety of species, worldwide distribution and strong adaptability in marine, freshwater and terrestrial biotopes (Tuffrau 1960, Carter 1972, Curds and Wu 1983, Song *et al*. 2009). With the improvement in impregnation methods during the last few decades, some new and poorly known euplotids have been discovered and well-defined (Pan *et al.* 2012, Chen *et al.* 2013, Jiang *et al.* 2013). Borror and Hill (1995) split *Euplotes* into four genera: *Euplotes*, *Euplotopsis*, *Euplotoides*, and *Moneuplotes* based on characteristics of cortical structure, endosymbionts, morphometric data, morphoge-

Address for correspondence: Honggang Ma, Laboratory of Protozoology, Institute of Evolution and Marine Biodiversity, Ocean University of China, Qingdao 266003, China; E-mail: mahg@ouc.edu.cn; Miao Miao, College of Life Sciences, University of Chinese Academy of Sciences, Beijing 100049, China; E-mail: doublemiao@126.com

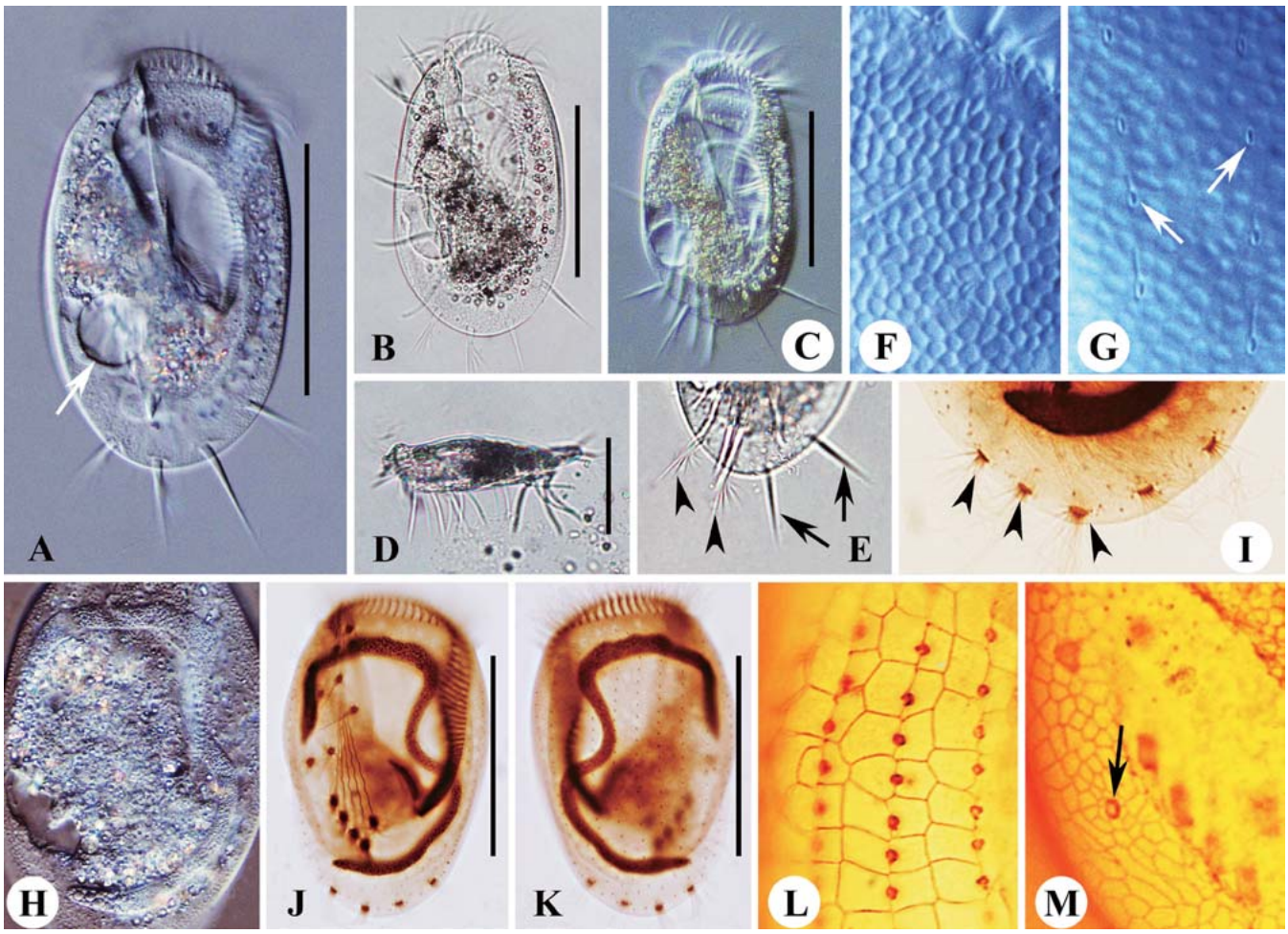

Fig. 2. Photomicrographs of *Euplotes amieti* Dragesco, 1970 *in vivo* (A–H), after protargol (I–K) and silver nitrate (L, M) impregnation. (**A**) Ventral view of a representative individual. Arrow points to the contractile vacuole. (**B, C**) Different body shapes. (**D**) Lateral view showing flattened body. (**E**) Posterior part of an individual, arrowheads show the caudal cirri and arrows indicate the left marginal cirri. (**F**) Numerous irregular ellipsoid to oval granules (possibly mitochondria) extremely densely packed beneath dorsal and ventral pellicle. (**G**) Detailed view, arrows point to the basal positions of dorsal cilia. (**H**) Showing the endoplasm and the typical 3-shaped macronucleus. (**I**) Individual with three caudal cirri (arrowheads). (**J, K**) Ventral (J) and dorsal (K) view of the same specimen, showing the infraciliature and nuclear apparatus. (**L, M**) Portion of dorsal (L) and ventral (M) silverline system. Arrow indicates the position of contractile vacuole pore. Scale bars: 100 μm.

the macronucleus. Silverline system on dorsal side of the double-*eurystomus* type (Figs 1E, F, 2L). One contractile vacuole pore positioned in the right part of the transverse cirri on ventral side (Fig. 1E).

Morphogenesis (Figs 3 and 4): Stomatogenesis starts with the appearance of a small patch of kinetosomes, which is the opisthe's oral primordium, within a pouch beneath the cortex of the ventral surface, positioned between the cytostome and the left marginal cirri (Figs 3A, 4C). As the pouch enlarges, kinetosomes proliferate rapidly and begin to align into membranelles from the anterior end and organize towards the posterior (Figs 3C, 4E).

An additional anlage, the primordium for the paroral membrane (UM-anlage), appears within the subcortical pouch, which is located close to the posterior end of the oral primordium (Figs 3C, 4E).

Following this, the UM-anlage begins to lengthen and becomes broader. Throughout the entire morphogenetic process, the parental adoral zone remains nearly intact (Figs 3C, E, 4E).

ACTA
PROTOZOOLOGICA

Acta Protozool. (2015) 54: 107–122
www.ejournals.eu/Acta-Protozoologica
doi:10.4467/16890027AP.15.009.2734

Two Oxytrichids from the Ancient Lake Biwa, Japan, with Notes on Morphogenesis of *Notohymena australis* (Ciliophora, Sporadotrichida)

Xiaozhong HU[1] and Yasushi KUSUOKA[2]

[1]Laboratory of Protozoology, Institute of Evolution and Marine Biodiversity & College of Fisheries, Ocean University of China, Qingdao, China; [2]Lake Biwa Museum, Oroshimo 1091, Kusatsu, Shiga, Japan

Abstract. Two oxytrichid freshwater ciliates, *Apoamphisiella tihanyiensis* (Gellért and Tamás, 1958) Foissner, 1997 and *Notohymena australis* (Foissner and O'Donoghue, 1990) Berger, 1999, were recorded for the first time in Lake Biwa, a 4-million-year-old lake located at the Shiga Prefecture in Japan. Their morphology was investigated based on observations of live and protargol-impregnated material. Based on the present observation and previous descriptions, *A. tihanyiensis* is characterized by having an elliptical body shape, yellowish cortical granules, two long frontoventral rows, enlarged frontal and transverse cirri, highly variable numbers of frontoventral, and postoral ventral cirri, and six to 11 caudal cirri arranged in three short rows. New data confirm the presence of pretransverse ventral cirri in this species. Morphologically, *N. australis* differs from its congeners in having the following combination of characters: greenish cortical granules, the cirrus V/2 located slight anterior to the leftmost transverse cirrus, dorsal kinety 3 almost as long as body, and seven to 10 caudal cirri arranged in three short rows. Morphogenesis in *N. australis* shows the same pattern as in *N. apoaustralis* but differs from that of other congeners in the origin of oral primordium and the formation of more than just three caudal cirri.

Key words: *Apoamphisiella*, freshwater ciliate, infraciliature, *Notohymena*, ontogenesis, Stichotrichia.

INTRODUCTION

The oxytrichids *s.l.* are a group of hypotrichs distributed in various biotopes worldwide (e.g. Kahl 1932; Berger 1999, 2006; Küppers and Claps 2013; Tirjaková and Vd'ačný 2013). Most species have a characteristic 18 frontal-ventral-transverse cirral pattern (Stiller 1974; Berger and Foissner 1997; Weisse *et al.* 2013). A recent comprehensive guide to this group of ciliates was provided by Berger (1999). According to this revision, the Oxytrichidae includes ca. 32 valid genera and 170 valid species. However, many of them were described on only a few occasions and from a limited geographical range, and intraspecific morphological variability remains unknown. In the last two decades, several new species were added to this family and ten more genera were reported or re-established, which suggests that the diversity of this group of ciliates is under-estimated (e.g. Foissner *et al.* 2002; Paiva *et al.* 2003, 2004; Küppers *et al.* 2007, 2011; Berger 2008, 2011; Li *et al.* 2010; Shao *et al.* 2011, 2013a, b; Lv *et al.* 2013; Singh and Kamra 2013).

Address for correspondence: Xiaozhong Hu, Laboratory of Protozoology, Institute of Evolution and Marine Biodiversity & College of Fisheries, Ocean University of China, Qingdao 266003, China; E-mail: xiaozhonghu@ouc.edu.cn

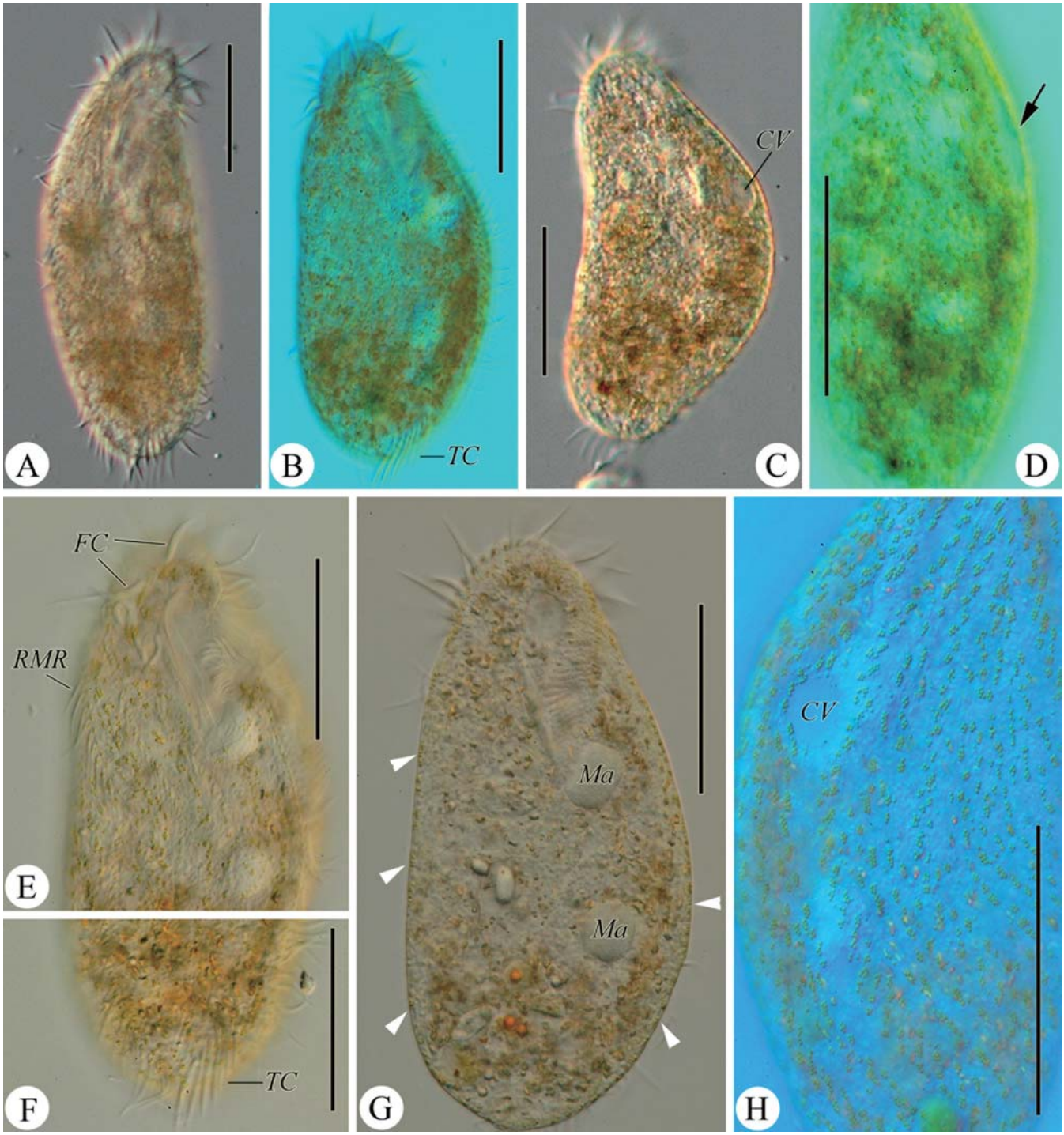

Figs 2A–H. *Apoamphisiella tihanyiensis* from life. **A, B** – ventral view of different cells; **C** – a contracted cell, showing contractile vacuole; **D** – part of cell in dorsal view, showing contractile vacuole with collecting canals (arrow); **E, F** – ventral views of anterior (E) and posterior (F) parts of the same cell, showing arrangement of cortical granules; **G** – plumper individual, showing cortical granules (arrowheads) and macronuclear nodules; **H** – part of cell in dorsal view showing spherical contractile vacuole and arrangement of cortical granules. CV – contractile vacuole, FC – frontal cirri, Ma – macronuclear nodule, RMR – right marginal row, TC – transverse cirri. Scale bars: 60 μm.

ACTA
PROTOZOOLOGICA

Acta Protozool. (2015) 54: 31–43
www.ejournals.eu/Acta-Protozoologica
doi:10.4467/16890027AP.15.003.2190

Morphology and Phylogeny of Four Marine Scuticociliates (Protista, Ciliophora), with Descriptions of Two New Species: *Pleuronema elegans* spec. nov. and *Uronema orientalis* spec. nov.

Xuming PAN[1†], Jie HUANG[2†], Xinpeng FAN[3], Honggang MA[1], Khaled A. S. AL-RASHEID[4], Miao MIAO[5] and Feng GAO[1]

[1]Laboratory of Protozoology, Institute of Evolution and Marine Biodiversity, Ocean University of China, Qingdao 266003, China; [2]Key Laboratory of Aquatic Biodiversity and Conservation of Chinese Academy of Science, Institute of Hydrobiology, Chinese Academy of Science, Wuhan 430072, China; [3]School of Life Sciences, East China Normal University, Shanghai 200062, China; [4]Zoology Department, King Saud University, Riyadh 11451, Saudi Arabia; [5]College of Life Sciences, University of Chinese Academy of Sciences, Beijing 100049, China
[†]Contributed equally

Abstract. The morphology and infraciliature of four marine scuticociliates, *Pleuronema elegans* spec. nov., *P. setigerum* Calkins, 1902, *P. grolierei* Wang *et al*., 2008 and *Uronema orientalis* spec. nov., collected from China seas, were investigated through live observation and protargol staining methods. *Pleuronema elegans* spec. nov. can be recognized by the combination of the following characters: size *in vivo* 90–115 × 45–60 μm, slender oval in outline with a distinctly pointed posterior end; about 10 prolonged caudal cilia; consistently two preoral kineties and 18 or 19 somatic kineties; membranelle 2a double-rowed with its posterior end straight; membranelle 3 three-rowed; one macronucleus; marine habitat. *Uronema orientalis* spec. nov. is distinguished by the following features: *in vivo* about 40–55 × 20–30 μm with a truncated apical plate; consistently twenty somatic kineties; membranelle 1 single-rowed and divided into two parts which comprise four and three basal bodies respectively; contractile vacuole pore positioned at the end of the second somatic kinety; marine habitat. We also provide improved diagnoses for *P. grolierei* Wang *et al*., 2008 and *P. setigerum* Calkins, 1902 based on current and previous reports. The small subunit rRNA gene of *U. orientalis*, *P. elegans*, *P. grolierei* and *P. puytoraci* were sequenced. Phylogenetic analyses indicate that *Uronema* and *Pleuronema* are not monophyletic.

Key words: Scuticociliates, *Pleuronema elegans* spec. nov., *Uronema orientalis* spec. nov., phylogeny.

INTRODUCTION

Investigations into scuticociliates have demonstrated that this assemblage is much more diverse than was previously assumed (Thompson and Kaneshiro 1968; Foissner and Wilbert 1981; Foissner *et al*. 1994, 2013; Song and Wilbert 2002; Long *et al*. 2007; Song *et al*. 2007; Miao *et al*. 2008, 2009; Wilbert and Song 2008; Yi *et al*. 2009; Budiño *et al*. 2011; Fan *et al*. 2011a, b; Lobban *et al*. 2011; Pan *et al*. 2011, 2013d; Salinas *et al*. 2011; Seo *et al*. 2013; Whang *et al*. 2013). Many nominal species are insufficiently described and/or lack gene sequence data, and, consequently, further investi-

Address for correspondence: Jie Huang, Key Laboratory of Aquatic Biodiversity and Conservation of Chinese Academy of Science, Institute of Hydrobiology, Chinese Academy of Science, Wuhan 430072, China; Feng Gao, Laboratory of Protozoology, Institute of Evolution and Marine Biodiversity, Ocean University of China, Qingdao 266003, China

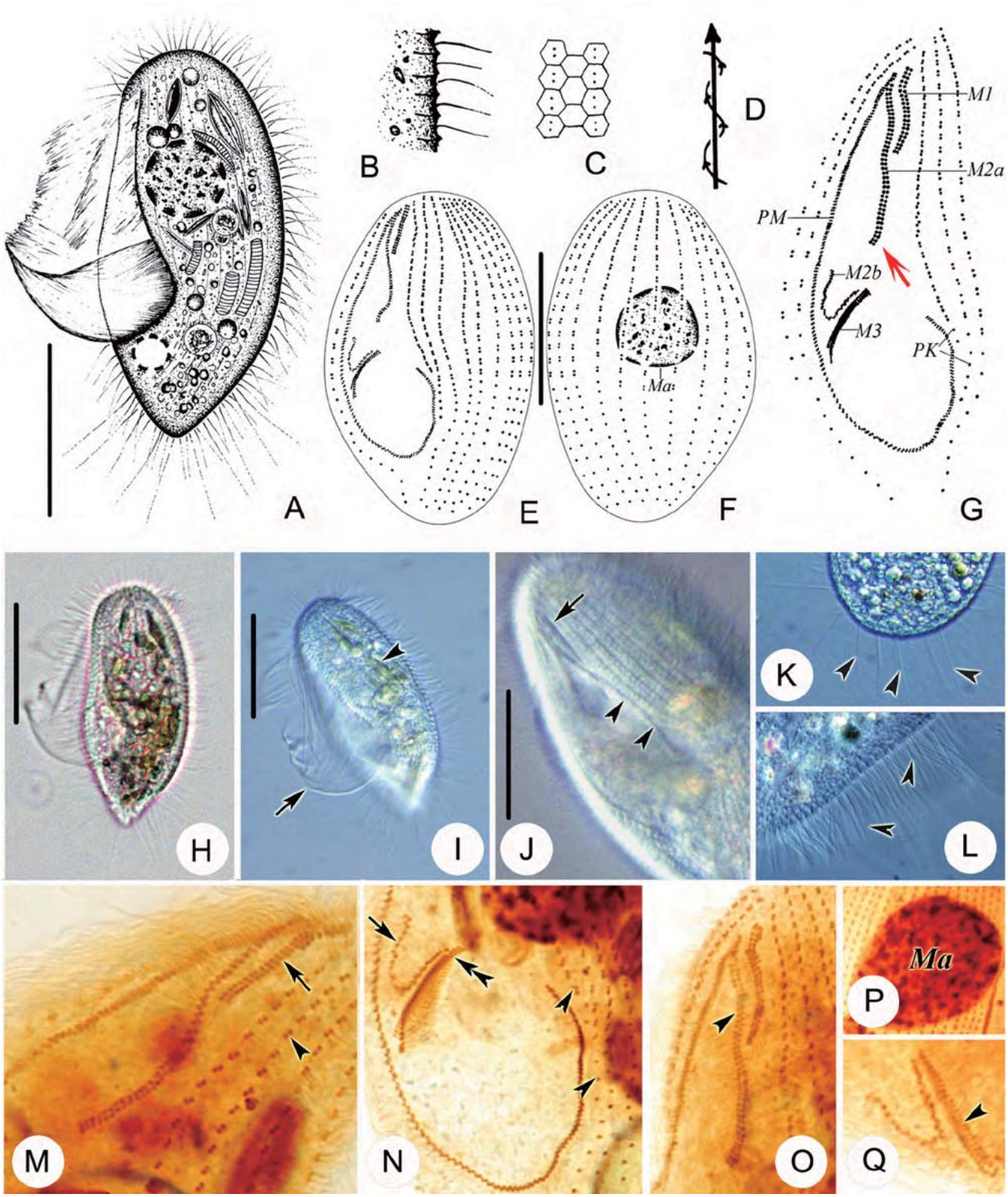
A
B
C
D
E
F
G
M1
M2a
PM
M2b
M3
PK
Ma
H
I
J
K
L
M
N
O
P
Q
Ma

ACTA
PROTOZOOLOGICA

Acta Protozool. (2015) 54: 305–323
www.ejournals.eu/Acta-Protozoologica
doi:10.4467/16890027AP.15.026.3540

Data on Ten New Myxosporean Parasites (Myxozoa, Myxosporea, Bivalvulida) from the Yellow Sea, China

Yuanjun ZHAO[1, 2], Saleh A. AL-FARRAJ[3], Khaled A. S. AL-RASHEID[3], Weibo SONG[2]

[1] Chongqing Key Laboratory of Animal Biology, Chongqing Normal University, 400047, China; [2] Laboratory of Protozoology, Institute of Evoulution and Marine Biodiversity, Ocean University of China 266003, China; [3] Zoology Department, College of Science, King Saud University, Riyadh 11451, Saudi Arabia

Abstract. Ten new species of myxosporeans found from marine fishes were collected from coastal waters off the Yellow Sea in China: *Sphaerospora sebasta* sp. n. coelozoic in the gall bladder of *Sebastes schlegeli*, *Ceratomyxa hemitriptera* sp. n. coelozoic in the gall bladder of *Hemitripterus villosus*, *Ceratomyxa kareus* sp. n. coelozoic in the gall bladders of *Kareius bicoloratus* and *Zebrias zebra*, *Ceratomyxa lateolabrax* sp. n. and *Ceratomyxa lomi* sp. n. coelozoic in the gall bladder of *Lateolabrax japonicus*, *Ceratomyxa qingdaoensis* sp. n. coelozoic in the urinary bladder of *Argyrosomus argentatus*, *Ceratomyxa saurida* sp. n. coelozoic in the gall bladder of *Saurida elongata*, *Ceratomyxa sebastisca* sp. n. coelozoic in the gall bladder of *Sebastiscus* sp., *Ceratomyxa simplex* sp. n. coelozoic in the gall bladder of *Chirolophis japonicus* and *Ceratomyxa triacantha* sp. n. coelozoic in the gall bladder and bile of *Triacanthus brevirostris*. All those forms were described in a book chapter cited as "known forms" several years ago, but have never been formally established as new taxa which are thus officially reported here. The present contribution only provided the morphology and geographic distribution of these organisms.

Key words: Myxosporea, *Sphaerospora*, *Ceratomyxa*, new species, marine fishes.

Abbreviations: T = thickness of spore, L = length of spore, D = diameter of polar capsule, PC = polar capsules.

INTRODUCTION

Myxosporeans are parasites widely dispersed among fishes and most of them have a fairly well-defined host location (Lom and Dyková 1992). Like all the other parasitic organisms, myxosporeans exert a certain pathogenic influence on their hosts, although the degree of pathogeny varies according to the parasite's biology, ecology and state of development, and the host's nutrition, stress level and immunological system (Lom and Dyková 2006). In myxozoan parasites, it is considered that *Sphaerospora* species could usually be the danger of the aquaculture (Lom and Dyková 2006) and most species of the genus *Ceratomyxa*, live in the gall bladders of marine fishes, is generally benign, however, *Ceratomyxa shasta* is an exception (Lom and Dyková 2006). Until recently little attention has been paid to myxosporean parasites from the Yellow Sea, despite the fact that there has been an enormous development in commercial fish farming in this region in recent decades (Zhao and Song 1999, 2001, 2003a, 2003b, 2009; Zhao *et al*. 2000, 2002). In

Address for correspondence: Yuanjun Zhao, Chongqing Key Laboratory of Animal Biology, Chongqing Normal University, 400047, China; E-mail: zhaoyuanjuncqnu@126.com

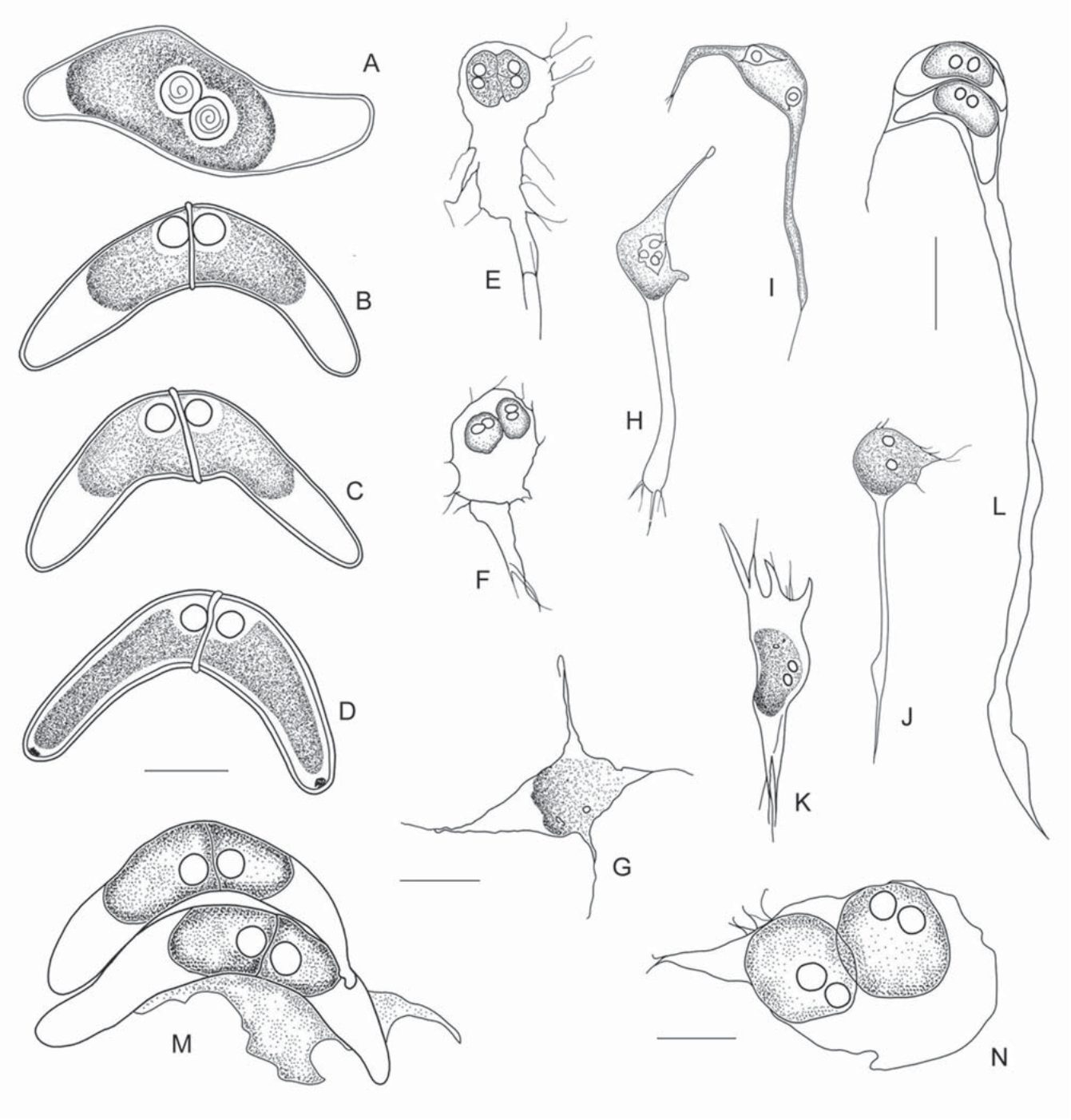

Fig. 2. Schematic illustrations of *Ceratomyxa kareus* sp. n. **A–L** – from *Kareius bicoloratus*; **M–N** – from *Zebrias zebra*; **A–D** – lateral view of mature spore; **E–F, N** – plasmodia with two spores; **G–J** – earlier stage plasmodia; **K** – plasmodium with one spore; **L–M** – plasmodia with mature spores. Scale bars: 10 μm.

ACTA
PROTOZOOLOGICA

Acta Protozool. (2015) 54: 195–208
www.ejournals.eu/Acta-Protozoologica
doi:10.4467/16890027AP.15.016.3213

Two New and Two Poorly Known Species of *Ancistrum* (Ciliophora, Scuticociliatia, Thigmotrichida) Parasitizing Marine Molluscs from Chinese Coastal Waters of the Yellow Sea

Kuidong XU[1, 2], Weibo SONG[2], Alan WARREN[3]

[1] Department of Marine Organism Taxonomy and Phylogeny, Institute of Oceanology, Chinese Academy of Sciences, Qingdao 266071, China; [2] Laboratory of Protozoology, Institute of Evolution and Marine Diversity, Ocean University of China, Qingdao 266003, China; [3] Department of Life Sciences, Natural History Museum, Cromwell Road, London SW7 5BD, U.K.

Abstract. The morphology and taxonomy of two new and two poorly known ciliate species of *Ancistrum*, found in the mantle cavity (mainly on gills) of marine molluscs from culture beds and pools along the Chinese coast of the Yellow Sea, were investigated using living observation and silver impregnation. *Ancistrum haliotis* n. sp. was isolated from the abalone *Haliotis discus hannai* Ino, *A. crassum* Fenchel, 1965 from the purple clam *Saxidomus purpuratus* (Sowerby), *A. acutum* n. sp. from the surf clam *Mactra veneriformis* Reeve, and *A. japonicum* Uyemura, 1937 from both the venus clam *Cyclina sinensis* (Gmelin) and from *Dosinia japonica* (Reeve). *Ancistrum haliotis* differs from its most similar relative *A. mytili* (Quennerstedt, 1867) by the body outline (anterior portion narrower vs. wider than the posterior portion), the macronuclear shape (broadly ellipsoidal vs. reniform or sausage-like), and by having fewer somatic kineties (28–32 vs. usually more than >40). *Ancistrum crassum* is characterized by the naked area at the apical end of the cell, the relatively short buccal field occupying about two thirds of the body length, and the posterior-dorsal cone-shaped prolongation. *Ancistrum acutum* n. sp. and *A. japonicum* are almost identical in morphometry, but differ distinctly in the live morphology (anterior end pointed and posterior end rounded vs. anterior end narrowly rounded and posterior-dorsal end protruded) and ciliary pattern (all right-side kineties extend to posterior body end vs. all right-side kineties excluding somatic kinety 1 distinctly shortened posteriad, forming a glabrous zone). We neotypify *Ancistrum japonicum* and discuss the taxonomic status of the four species. Based on an evaluation of all nominal species of *Ancistrum* and *Ancistrumina*, we recognize nine valid species of *Ancistrum* and provide a tabular guide to their identification. *Fenchelia* Raabe, 1970 is regarded as a junior synonym of *Ancistrum* Maupas, 1883. We synonymize *Ancistrumina nucellae* Khan, 1970 with *Ancistrum japonicum* Uyemura, 1937 and *Ancistrum edajimanum* Oishi, 1978 with *A. crassum* Fenchel, 1965.

Key words: *Ancistrum haliotis* n. sp., *Ancistrum crassum*, *Ancistrum acutum* n. sp., *Ancistrum japonicum*, marine parasitic ciliate, morphology, neotype, new species, taxonomy.

Address for correspondence: Weibo Song, Laboratory of Protozoology, Institute of Evolution and Marine Diversity, Ocean University of China, Qingdao 266003, China; E-mail: wsong@ouc.edu.cn

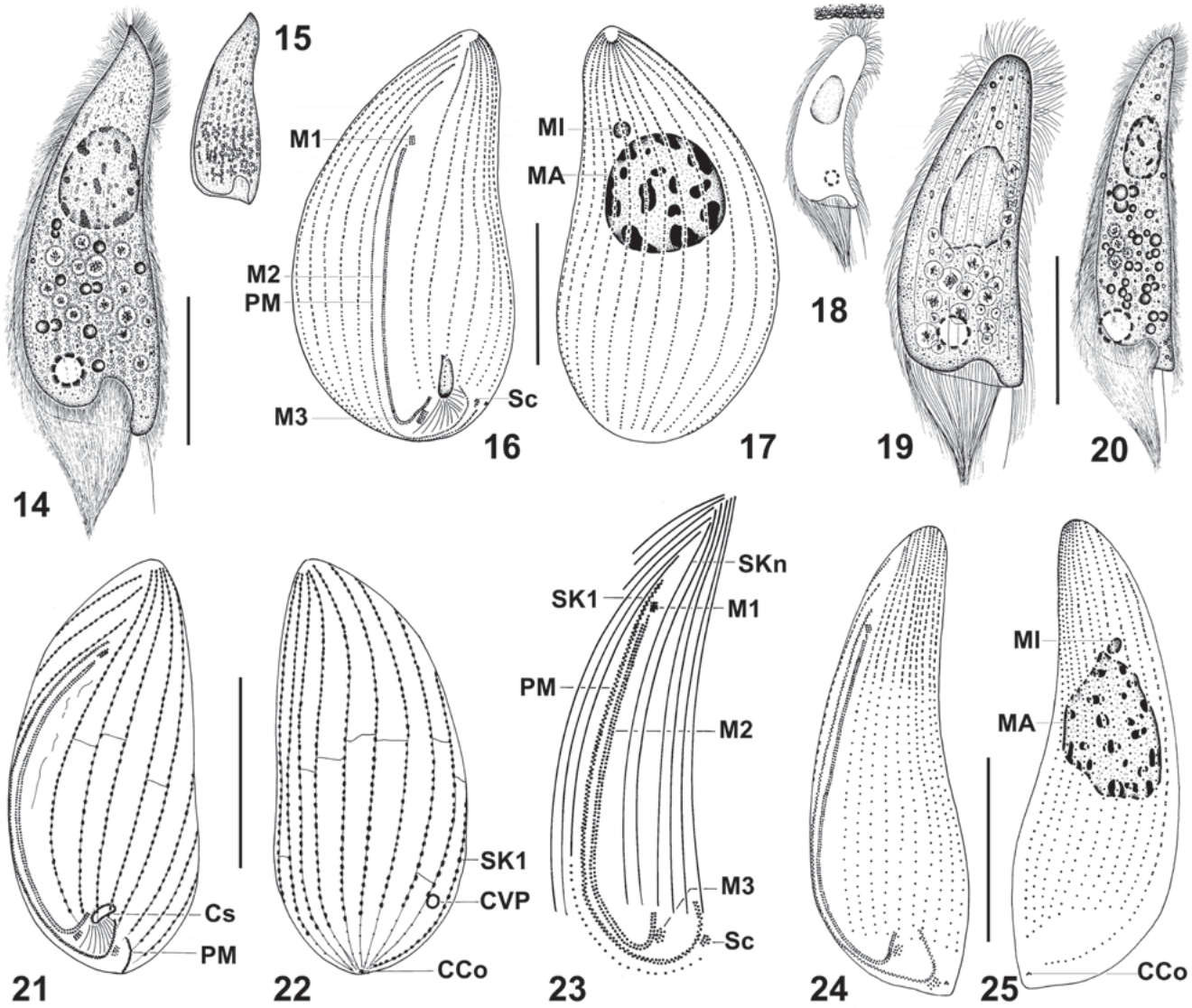

Figs 14–25. *Ancistrum acutum* n. sp. from the surf clam *Mactra veneriformis* (14–17) and *Ancistrum japonicum* Uyemura, 1937 from the Japanese dosinia *Dosinia japonica* (18, 19, 21, 22) and the clam *Cyclina sinensis* (20, 23–25), from life (14, 15, 18–20) and after protargol (23–25) and silver nitrate impregnation (16, 17, 21, 22). **14** – left lateral view of a representative specimen; **15** – body variant and cortical granules; **16, 17** – ventral and dorsal view of the holotype specimen; **18, 19** – lateral view of living cells; **20** – lateral view of a representative specimen; **21, 22** – lateral view of same specimen; **23** – ventral ciliature; **24, 25** – lateral view of the neotype specimen. CCo – caudal complex; Cs – cytostome; CVP – contractile vacuole pore; M1–3 – membranelles 1–3; MA – macronucleus; MI – micronucleus; PM – paroral membrane; Sc – scutica; SK1, n – somatic kineties 1, n. Scale bars: 30 µm.

registration number RZ-950428-32. A protargol slide with paratype specimens is deposited in the Natural History Museum, London with registration number NHMUK 2014.4.8.2. A voucher slide with protargol-stained specimens from the host mollusc *Mactra chinensis* is deposited in the Marine Biological Museum, Chinese Academy of Sciences (Qingdao) with registration number QD-971204.

Etymology: The Latin adjective *acutus* (acute) refers to the pointed anterior end of body, a main feature of the species. We have retained the species name originally designated by Xu *et al*. (2003) so as not to inflate the number of ciliate species names.

Description: Size *in vivo* 80–110 × 25–35 µm, usually about 90 × 30 µm, while on average 85 × 36 µm in protargol-stained specimens, suggesting a slight infla-

ACTA
PROTOZOOLOGICA

Acta Protozool. (2015) 54: 97–106
www.ejournals.eu/Acta-Protozoologica
doi:10.4467/16890027AP.15.008.2733

Morphology of Two Novel Species of *Chaenea* (Ciliophora, Litostomatea): *Chaenea paucistriata* spec. nov. and *C. sinica* spec. nov.

Xinpeng FAN[1], Yuan XU[2], Fukang GU[1], Jiqiu LI[3], Saleh A. AL-FARRAJ[4], Khaled A. S. AL-RASHEID[4] and Xiaozhong HU[5]

[1]School of Life Sciences, East China Normal University, Shanghai, PR China; [2]State Key Laboratory of Estuarine and Coastal Research, East China Normal University, Shanghai, PR China; [3]Laboratory of Protozoology, Guangdong Provincial Key Laboratory for Healthy and Safe Aquaculture, South China Normal University, Guangzhou, China; [4]Zoology Department, College of Science, King Saud University, Riyadh, Saudi Arabia; [5]Laboratory of Protozoology, Institute of Evolution and Marine Biodiversity, Ocean University of China, Qingdao, PR China

Abstract. During faunistic studies of ciliates in coastal waters of Daya Bay and Bohai Bay, China, two previously unknown ciliates were discovered and investigated using standard taxonomic methods. Morphological comparative analyses revealed that they represent two novel species in the genus *Chaenea*. *Chaenea paucistriata* spec. nov. can be distinguished from its congeners by the following traits: body length *in vivo* about 180–250 μm; eight somatic kineties; dorsal brush rows 1–4 consisting of three, five, seven, and two dikinetids, respectively; rod-like extrusomes, 8 μm long; 63–94 macronuclei; cortical granules minute and colourless. *Chaenea sinica* spec. nov. differs from its congeners in having: body length *in vivo* about 140–240 μm; 17–21 somatic kineties; dorsal brush rows 1–4 consisting of 3–7, 10 or 11, 11–13, and 3–6 dikinetids, respectively; rod-like extrusomes about 6–8 μm long; 71–164 macronuclei. A key is presented to assist the identification of all *Chaenea* species.

Key words: *Chaenea*, ciliary pattern, identification key, marine ciliates, new species, taxonomy.

INTRODUCTION

The widespread haptorid genus *Chaenea* Quennerstedt, 1867 has been found in marine sand, freshwater, brackish water and moist soil (Borror 1963; Carey 1992; Dragesco 1960, 1966; Dragesco and Dragesco-Kernéis 1986; Fauré-Fremiet and Ganier 1969; Foissner 1984; Fryd-Versavel *et al.* 1975; Gao *et al.* 2008; Kahl 1926, 1927, 1928, 1933; Kwon *et al.* 2014; Lipscomb and Riordan 1990; Song *et al.* 2009; Wang 1934). Its members are characterized by the following features: cell elongate and contractile; cytostome apically located and surrounded by dikinetid circumoral kinety; somatic kineties which are slightly spiralled when contracted and mainly composed of monokinetids; dorsal brush consisting of four dikinetidal rows; one permanent contractile vacuole located at the posterior end of the body; extrusomes rod-like or thorn-like, attached to the oral

Address for correspondence: Fukang Gu, School of Life Sciences, East China Normal University, Shanghai 200062, PR China; E-mail: fkgu@bio.ecnu.edu.cn

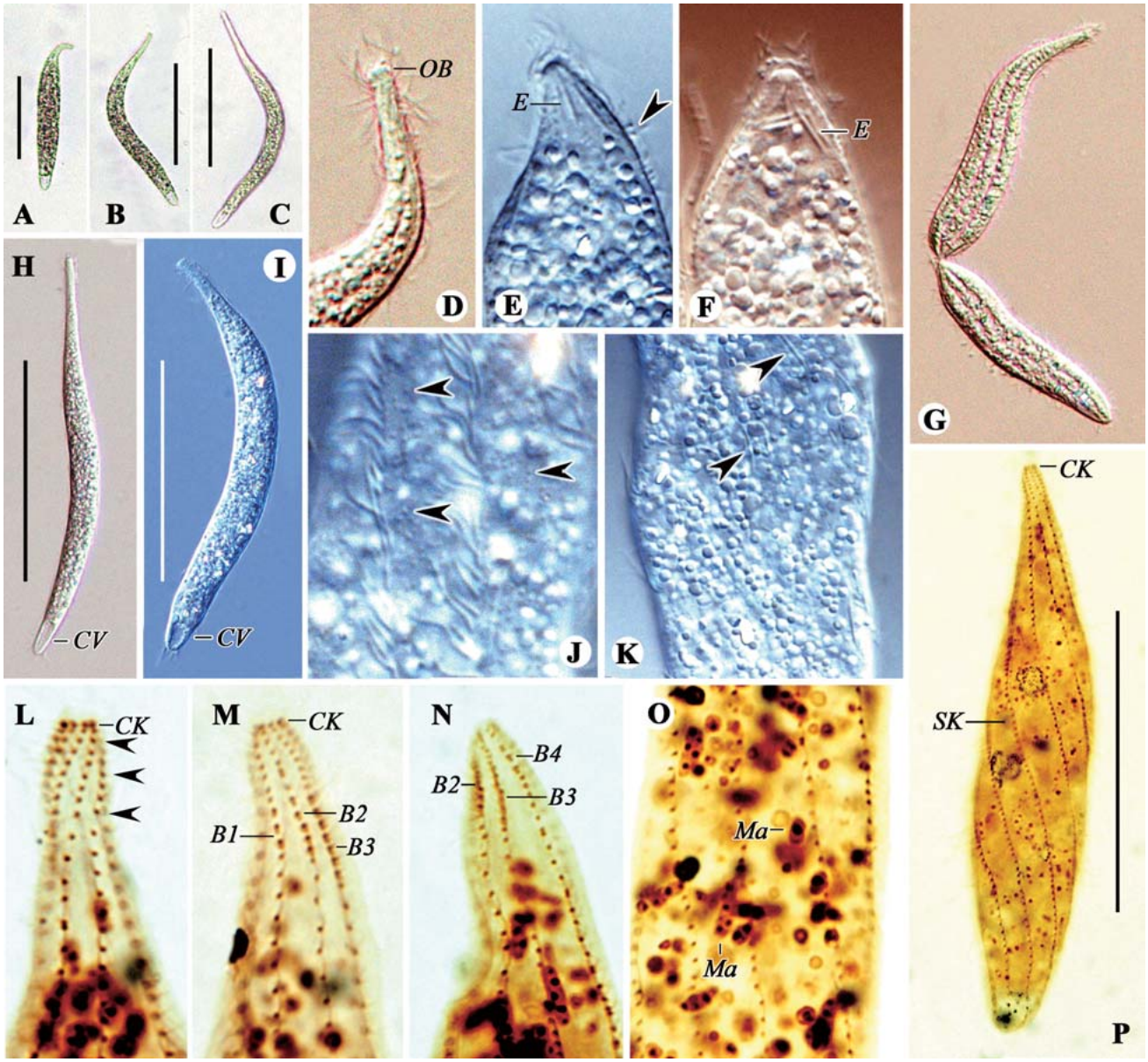

Figs 2A–P. *Chaenea paucistriata* spec. nov. *in vivo* (**A–K**) and after protargol impregnation (**L–P**). **A–C** – different body shapes; **D** – anterior body end to show the oral bulge; **E, F** – fine structure of anterior end to show rod-shaped extrusomes, arrowhead indicating cilia of the dorsal brush; **G** – dividing cell, showing cortical furrows along somatic kineties; **H, I** – typical individual, indicating contractile vacuole; **J** – cortical granules between somatic kineties (arrowheads); **K** – fine structure of the mid-body to show cytoplasmic granules and rod-shaped extrusomes (arrowheads); **L–N** – ciliary pattern of anterior body end, showing circumoral kinety narrowly spaces oralized somatic monokinetids (arrowheads), and dorsal brush rows 1–4; **O** – ciliary pattern in mid-body and many scattered macronuclei; **P** – overview showing circumoral kinety and somatic kineties. B1–4 – dorsal brush rows 1–4, CK – circumoral kinety, CV – contractile vacuole, E – extrusomes, Ma – macronuclei, OB – oral bulge, SK – somatic kinety. Scale bars: 90 µm (**A–C, H, I**), 70 µm (**P**).

comprising three, five, seven and two dikinetids respectively (number of specimens = 15) (Figs 1C, F, 2M, N). Cilia of dorsal brush about 3–4 µm long.

Oral bulge inconspicuous after protargol staining (Fig. 2L, M, P). Circumoral kinety inconspicuous and composed of dikinetids which are at the anterior end of each somatic kinety (Figs 1C, E, F, 2L, M, P).

Comparison: Considering the general morphology in terms of body length and the number of macronuclei, five species should be compared with *Chaenea paucis-*

ACTA
PROTOZOOLOGICA

Acta Protozool. (2015) 54: 325–330
www.ejournals.eu/Acta-Protozoologica
doi:10.4467/16890027AP.15.027.3541

Short Communication

High-Density Cultivation of the Marine Ciliate *Uronema marinum* (Ciliophora, Oligohymenophorea) in Axenic Medium

Weibo ZHENG[1], Feng GAO[1], Alan WARREN[2]

[1] Laboratory of Protozoology, Institute of Evolution and Marine Biodiversity, Ocean University of China, Qingdao 266003, China; [2] Department of Life Sciences, Natural History Museum, London SW7 5BD, UK

Abstract. *Uronema marinum* is a cosmopolitan marine ciliate. It is a facultative parasite and the main causative agent of outbreaks of scuticociliatosis in aquaculture fish. This study reports a method for the axenic cultivation of *U. marinum* in high densities in an artificial medium comprising proteose peptone, glucose and yeast extract powder as its basic components. The absence of bacteria in the cultures was confirmed by fluorescence microscopy of DAPI-stained samples and the failure to recover bacterial SSU-rDNA using standard PCR methods. Using this axenic medium, a maximum cell density of 420,000 ciliate cells/ml was achieved, which is significantly higher than in cultures using living bacteria as food or in other axenic media reported previously. This method for high-density axenic cultivation of *U. marinum* should facilitate future research on this economically important facultative fish parasite.

Key words: Axenic cultivation, ciliates, fish parasite, scuticociliatosis, *Uronema marinum.*

INTRODUCTION

Axenic cultures of ciliates have proved to be extremely valuable in a wide range of research fields including growth, nutrition, respiration, genetics, facultative parasitism, and molecular biology. The lack of efficient, cost-effective methods for axenic cultivation is a major constraint for research on most ciliates (Soldo and Merlin 1972). Nevertheless comparatively few ciliate species, mostly from fresh-waters, have been cultured axenically. The peniculine species *Paramecium caudatum* was the first ciliate to be successfully cultivated axenically and was grown in a medium containing dead yeast cells, liver extract and kidney tissue (Glaser *et al.* 1933). Pure cultures of strains belonging to the "*Colpidium-Glaucoma-Leucophrys-Tetrahymena* group" were subsequently established (Corliss 1952). In each case the main nutritional sources were proteose peptone and yeast extract. In such cultures, the cell densities of *Tetrahymena* and *Paramecium* can reach 75 cells/µl and 38 cells/µl, respectively (Martin *et al.* 1976, Thiele *et al.* 1980). The axenic cultivation of marine ciliates is far less common and is largely restricted to philasterid scuticociliates such as *Uronema nigricans, Parauronema virginiatum* and *Miamiensis avidus.* In these cultures, maximum populations are usually obtained after 4–5 days and range from several hundred to 3 or 4 × 10^3 cells/µl (Soldo *et al.* 1972, Lee *et al.* 2003).

Address for correspondence: Feng Gao, Laboratory of Protozoology, Institute of Evolution and Marine Biodiversity, Ocean University of China, Qingdao 266003, China; E-mail: gaof@ouc.edu.cn

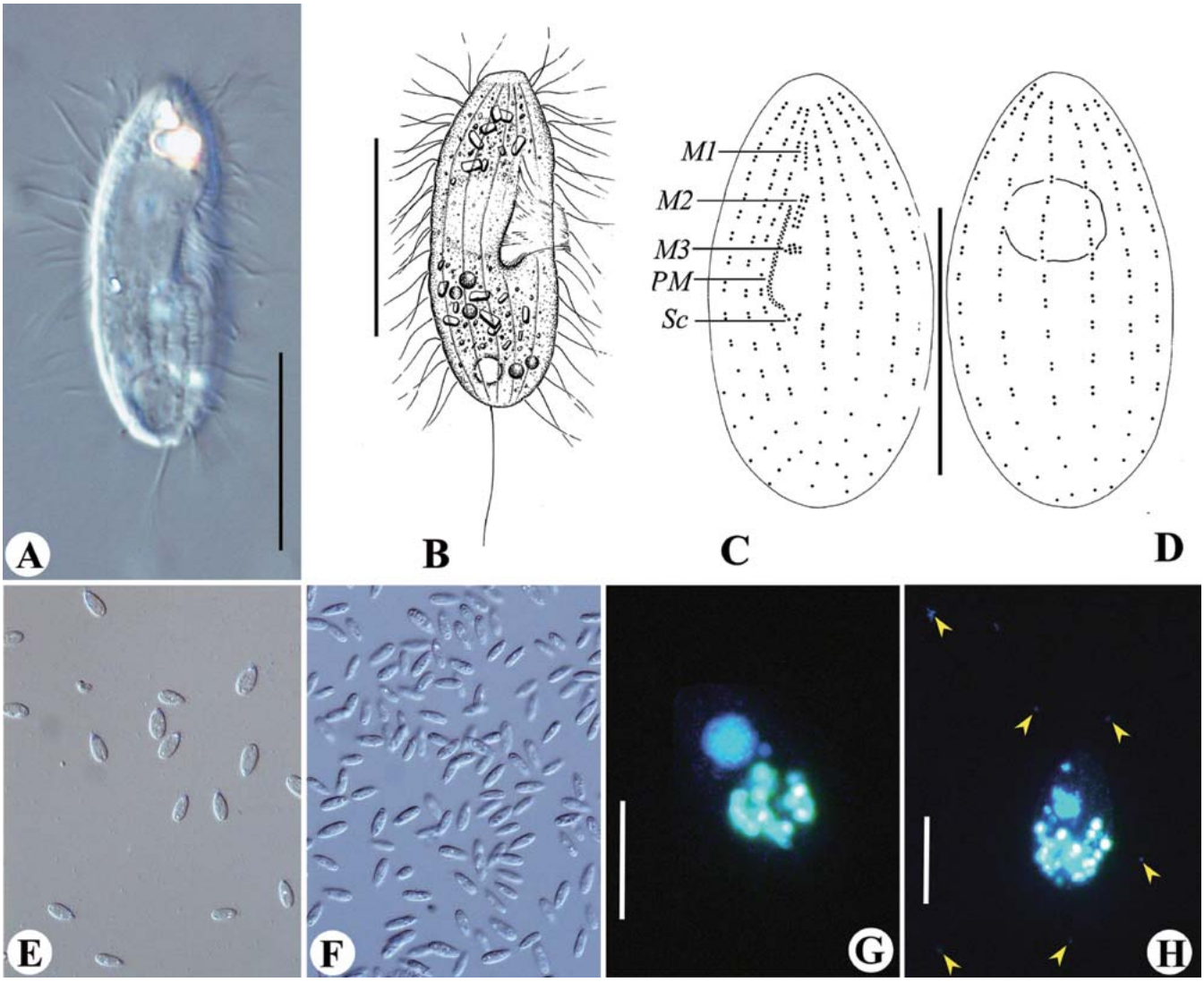

Fig. 1. *Uronema marinum* from life (A, B, E, F), after protargol (C, D) and DAPI-staining (G, H). **A, B** – lateral-ventral view of typical cell (B, from Pan *et al.* 2010); **C, D** – ventral and dorsal view of the same specimen (from Pan *et al.* 2010); **E** – 72 hours after inoculating into PGY medium; **F** – 168 hours after inoculating into PGY medium; **G** – *Uronema marinum* in axenic culture, demonstrating the absence of bacteria; **H** – *Uronema marinum* in bacterized filtered seawater cultivating system, arrowheads indicate bacteria that are active in the real-time viewing conditions; M1–3 – membranelles 1–3, PM – paroral membrane, Sc – scutica. Scale bars: 20 μm.

terized filtered seawater containing about 250 *U. marinum* individuals was inoculated into the medium. The flask was incubated at 25°C in the dark. The culture was observed every 24 hours with stereomicroscope.

Detection of the presence of bacteria

Both fluorescence microscopy and PCR were used to check for the presence of bacteria in the axenic cultures with three replicates when the axenic cultivating system was established. The bacterized filtered seawater culture system served as the positive control.

For fluorescence microscopy observations, DAPI stain was added to a sample of culture to give a final concentration of 10 μg/ml of DAPI (4'-6-diamidine-2-phenylindole, Sangon Biotech Co., Ltd., Shanghai, China, cat. no. D6584). Staining was carried out at room temperature for 30 min according to the manufacturer's protocol. Organisms were observed with a fluorescence microscope (DMR Leica Microsystems, Mannheim, Germany). Fluorochromes were visualized with an excitation wavelength of 350 nm.

For the PCR method, the bacterial small subunit ribosomal RNA gene (SSU-rDNA) was used as the target to detect the pres-

J. Ocean Univ. China (Oceanic and Coastal Sea Research)
DOI 10.1007/s11802-015-2559-3
ISSN 1672-5182, 2015 14 (4): 724-730
http://www.ouc.edu.cn/xbywb/
E-mail:xbywb@ouc.edu.cn

Molecular Phylogenetic Lineage of *Plagiopogon* and *Askenasia* (Protozoa, Ciliophora) Revealed by Their Gene Sequences

LIU An[1)], YI Zhenzhen[2), *], LIN Xiaofeng[2)], HU Xiaozhong[1)], Saleh A. AL-FARRAJ[3)], and Khaled A. S. AL-RASHEID[3)]

1) *Laboratory of Protozoology*, *Institute of Evolution & Marine Biodiversity*, *Ocean University of China*, *Qingdao* 266003, *P. R. China*
2) *Laboratory of Protozoology*, *School of Life Science*, *South China Normal University*, *Guangzhou* 510631, *P. R. China*
3) *Zoology Department*, *College of Science*, *King Saud University*, *Riyadh* 11451, *Saudi Arabia*

(Received December 10, 2013; revised January 21, 2014; accepted April 27, 2015)

Abstract Prostomates and haptorians are two basal groups of ciliates with limited morphological characteristics available for taxonomy. Morphologically, the structures used to identify prostomates and haptorians are similar or even identical, which generate heavy taxonomic and phylogenetic confusion. In present work, phylogenetic positions lineage of two rare genera, *Plagiopogon* and *Askenasia*, were investigated. Three genes including small subunit ribosomal RNA gene (hereafter SSU rDNA), internal transcribed spacer region (ITS region), and large subunit ribosomal RNA gene (LSU rDNA) were analyzed, 10 new sequences five species each. Our findings included 1) class Prostomatea and order Haptorida are multiphyletic; 2) it may not be appropriate to place order Cyclotrichiida in subclass Haptoria, and the systematic lineage of order Cyclotrichiida needs to be verified further; 3) genus *Plagiopogon* branches consistently within a clade covering most prostomes and is basal of clade Colepidae, implying its close lineage to Prostomatea; and 4) *Askenasia* is phylogenetically distant from the subclass Haptoria but close to classes Prostomatea, Plagiopylea and Oligohymenophorea. We supposed that the toxicyst of *Askenasia* may be close to taxa of prostomes instead of haptorians, and the dorsal brush is a more typical morphological characteristics of haptorians than toxicysts.

Key words *Plagiopogon*; *Askenasia*; multi-gene phylogeny; SSU rDNA; ITS region; LSU rDNA

1 Introduction

The ciliated protozoa are an important group of protists with important significance in the microbial food web and an exceeding diversity of approximately 8000 described species (Lynn, 2008). Among ciliated protozoa, species of class Prostomatea and subclass Haptoria are often found in both terrestrial and marine habitats, and even in red tided seawaters (Dale and Dahl, 1987; Gustafson *et al.*, 2000; Hansen and Fenchel, 2006; Lynn, 2008; Müller, 1989). Morphologically, prostomates and haptorians are very simple and have relatively limited characteristics available for taxonomy (Lynn, 2008). Because of these-simple structures, Prostomatea and Haptoria were once considered to be ancestral (Corliss, 1979; Lynn, 2008). However, the ultrastructural and molecular researches have shown that they are secondary species evolved from what (Bardele, 1989; Baroin-Tourancheau *et al.*, 1992; Hiller, 1993; Lynn *et al.*, 1999; Vd'acny *et al.*, 2010; Yi *et al.*, 2010). There are still some biases in whether a particular species should be placed in Prostomatea or Haptoria due to the discrepancy between morphological and molecular characteristics.

Plagiopogon has been less described morphologically, thus being absent of detailed scales and ciliary patterns (Corliss, 1979; Foissner *et al.*, 2008; Kahl, 1930; Lynn, 2008; Small and Lynn, 1985). Small and Lynn (1985) and Lynn (2008) placed it in family Colepidae (class Prostomatea, order Prorodontida) because both *Plagiopogon* and other members of Colepidae have calcium carbonate plates and caudal cilia (Lipscomb and Riordan, 2012). In contrast, Kahl (1930) and Corliss (1979) assigned *Plagiopogon* to order Haptorida. These differences cannot be resolved because of limited morphological descriptions at present.

Askenasia was previously assigned to Haptorida though it was placed in different families/orders in different systems (Corliss, 1979; Foissner and Foissner, 1988; Lynn, 2008). Based on small subunit ribosomal RNA gene (abbreviated as SSU rDNA) sequences; however, Zhang *et al.* (2012) revealed that *Askenasia* was related to Prostomatea and Plagiopylea instead of Litostomatea. This gene sequence (about 1200 bp in length) may not be appropriate for precisely assigning a species

* Corresponding author. Tel: 0086-20-85210644
E-mail: zyi@scnu.edu.cn

clade (ML 99, BI 1.00) adjacent to Oligohymenophorea and Colpodea.

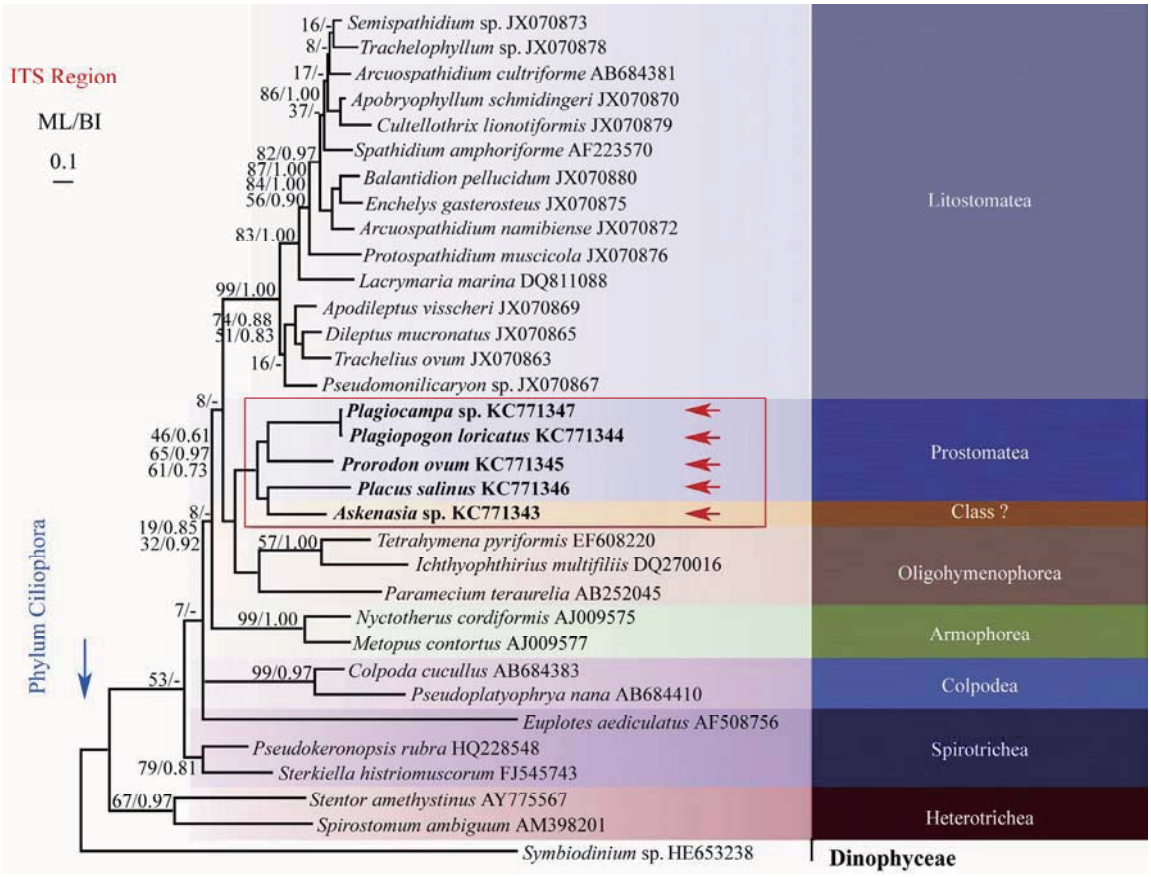

Fig.3 Maximum likelihood (ML) and Bayesian inference (BI) phylogenetic trees based on ITS region sequences. *Symbiodinium* sp. was selected as the outgroup taxon. New sequences are shown in bold and arrowed. Numbers near nodes represent ML non-parametric bootstrap values and BI posterior probabilities. Black circles indicate full support (100 ML, 1.00 BI). '–' indicates disagreement between ML and BI analyses. The scale bar corresponds to 10 substitutions per 100 nucleotide positions.

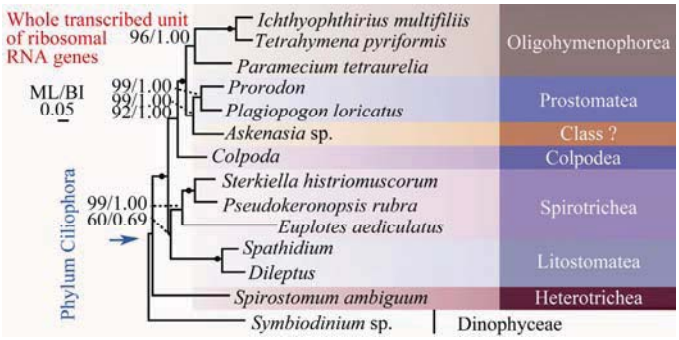

Fig.4 Maximum likelihood (ML) and Bayesian inference (BI) phylogenetic trees based on the transcribed unit of ribosomal RNA genes (SSU rDNA, ITS region and LSU rDNA). *Symbiodinium* sp. was selected as outgroup taxon. New sequences obtained in our work are shown in bold and arrowed. Numbers near nodes represent ML non-pa- rametric bootstrap values and BI posterior probabilities. Black dots indicate full support (100 ML, 1.00 BI). The scale bar corresponds to 5 substitutions per 100 nucleotide positions.

4 Discussion

4.1 Classification of Prostomes and Haptorians

Considering that *Urotricha* (Prorodontida, Urotrichidae) and *Balanion* (Prorodontida, Balanionidae) branch independent of the core prostome clade, the monophyly of Prostomatea is not supported. Further research is needed to resolve the phylogenetic positions of *Urotricha* and *Balanion*. Furthermore, our ITS region (Fig.3) and LSU rDNA (Fig.2) phylogenetic analyses also supported the contention that Prostomatea is a secondarily derived group of ciliates, which is congruent with previous works based on SSU rDNA analyses (Baroin-Tourancheau *et al.*, 1992; Lynn *et al.*, 1999).

The monophyly of haptorians is also rejected by our

J. Ocean Univ. China (Oceanic and Coastal Sea Research)

Review

DOI 10.1007/s11802-015-2482-7
ISSN 1672-5182, 2015 14 (3): 522-532
http://www.ouc.edu.cn/xbywb/
E-mail:xbywb@ouc.edu.cn

A General Overview of the Typical 18 Frontal-Ventral-Transverse Cirri Oxytrichidae *s. l.* Genera (Ciliophora, Hypotrichia)

SHAO Chen[1), *], LU Xiaoteng[1), 2)], and MA Honggang[2)]

1) *The Key Laboratory of Biomedical Information Engineering of Ministry of Education*, *School of Life Science and Technology*, *Xi'an Jiaotong University*, *Xi'an* 710049, *P. R. China*
2) *Laboratory of Protozoology*, *Institute of Evolution and Marine Biodiversity*, *Ocean University of China*, *Qingdao* 266003, *P. R. China*

(Received September 11, 2013; revised October 15, 2013; accepted July 10, 2014)

Abstract Oxytrichidae *s. l.* ciliates usually have 18 frontal-ventral-transverse cirri which are clustered to six distinct groups usually originating from six longitudinal primordia segregating 1, 3, 3, 3, 4, 4 cirri. During morphogenesis, three dorsal kineties anlagen are primarily formed. Fragmentation of kinety 3 usually present, while sometimes secondarily lost. Dorsomarginal kineties are formed, while sometimes lost. Oxytrichids tend to have overlapping characters, *e.g.* cell shape and size, infraciliature, pellicle features. This makes a great problem for genera separation. In the present work, all typical 18 frontal-ventral-transverse-cirri Oxytrichidae *s. l.* genera were revised systematically based on their living morphology, ciliature patterns and dorsal morphogenetic features. The outline of the genera, the schematic illustrations, and the key to typical 18 frontal-ventral-transverse-cirri genera of Oxytrichidae *s. l.* were clarified. Additionally, some morphological and morphogenetic patterns were summarized and compared.

Key words Oxytrichinae; Sporadotrichida; Stylonychinae; taxon

1 Introduction

Species of the well-known hypotrichous ciliates are of highly diverse regarding their structure, morphology and ontogenetic patterns, and are commonly found in various habitats including marine, limnetic and terrestrial biotopes (Chen *et al*., 2013a, b; Foissner, 2012; Foissner and Stoeck, 2011; Foissner *et al*., 2010; Hu and Song, 2002; Hu *et al*., 2012; Jiang *et al*., 2013a, b; Jung *et al*., 2011; Li *et al*., 2010a, b, 2013; Liu *et al*., 2010; Lv *et al*., 2013; Paiva *et al*., 2012; Pan *et al*., 2012, 2013; Song *et al*., 2009; Vďačný *et al*., 2010; Wang *et al*., 2011; Xu *et al*., 2011). Among these groups, many taxa have been investigated in detail using either morphological or molecular methods (Berger, 1999, 2008, 2011; Huang *et al*., 2012; Yi and Song, 2011; Yi *et al*., 2009a, b, c, d, 2012).

The family Oxytrichidae is species-rich and morphologically diverse, in which nearly 200 valid morphospecies have been described so far (Berger, 1999, 2011; Gupta *et al*., 2001; Kamra *et al*., 2008; Qin *et al*., 2011; Singh *et al*., 2013; Song, 1990, 2004; Song and Wilbert 2002; Weisse *et al*., 2012; Wilbert and Song, 2008), rendering Oxytrichidae one of the largest families of Sporadotrichida.

Systematic revision of 24 Oxytrichidae genera had been provided by Berger (1999). However, in the subsequent studies, 13 more have been reported or re-established, namely *Heterooxytricha* Shao *et al*., 2011, *Actinotricha* Cohn, 1866, *Ponturostyla* Jankowski, 1989, *Architricha* Gupta *et al*., 2006, *Heterotachysoma* Shao *et al*., 2013, *Paraurosomoida* Singh and Kamra, 2013, *Apogastrostyla* Li *et al*., 2010, *Rigidohymena* Berger, 2011, *Tetmemena* Eigner, 1999, *Parasterkiella* Küppers *et al*., 2011, *Erimophrya* Foissner *et al*., 2002, *Vermioxytricha* Foissner *et al*., 2002, *Hemiurosoma* Foissner *et al*., 2002 (Berger, 2008, 2011; Foissner *et al*., 2002; Gupta *et al*., 2003, 2006; Küppers *et al*., 2011; Li *et al*., 2010a; Shao *et al*., 2011, 2013a, b; Singh and Kamra, 2013; Song, 2001). The diagnoses of *Oxytricha* Bory De Saint-Vincent in Lamouroux, Bory De Saint-Vincent and Deslongchamps, 1824, *Urosomoida* Hemberger in Foissner, 1982, *Tachysoma* Stokes, 1887, *Actinotricha* Cohn, 1866 and *Coniculostomum* Njine, 1979 were also revised (Shao *et al*., 2011, 2013a; Song, 2001).

The aims of this study included 1) clarifying the outline of the typical 18 frontal-ventral-transverse-cirri genera; 2) summarizing the patterns of development and determining the amount of variability during morphogenesis in

* Corresponding author. Tel: 0086-29-82668463 Ext 423
E-mail: shaochen@mail.xjtu.edu.cn

***Oxytricha* pattern** (Berger, 1999): Kinety 3 fragments and dorsomarginal kineties are present (Fig.1g). Caudal cirri are present or absent. If present, usually three (sometimes more than three and arranged in three rows), one (or one row) each is present on kineties 1, 2, and 4. Apomorphy: Multiple fragmentation of kinety 3 is present or/and there are more than two dorsomarginal kineties (Fig.2c).

***Urosomoida* pattern** (Berger, 1999): Fragmentation of kinety 3 is lost and dorsomarginal kineties are present (Fig.1h). Caudal cirri are present or absent. If present, usually three, one each is present on kineties 1–3.

***Gonostomum* pattern** (Berger, 1999): Fragmentation of kinety 3 is lost and dorsomarginal kineties are absent (Fig.1i). Caudal cirri are present or absent. If present, usually three, one each is present on kineties 1–3.

***Tachysoma* pattern** (Berger, 1999): Two dorsal kineties fragment and dorsomarginal kineties are present (Fig.1j). Apomorphy: Multiple fragmentation of dorsal kineties is present or/and there are more than two dorsomarginal kineties (Fig.4j).

***Coniculostomum* pattern** (Berger, 1999): Kinety 3 fragments and dorsomarginal kineties are present. Some parental kineties are retained during morphogenesis (Fig.1k). Caudal cirri are present or absent. If present, usually three, one each is present on kineties 1, 2 and 4.

***Hemigastrostyla* pattern** (Shao *et al*., 2011): Two dorsal kineties fragment and dorsomarginal kineties are absent (Fig.1l).

2.2 Characterization of Genera in the Subfamily Oxytrichinae

Oxytricha Bory De Saint-Vincent in Lamouroux, Bory De Saint-Vincent and Deslongchamps, 1824: adoral zone

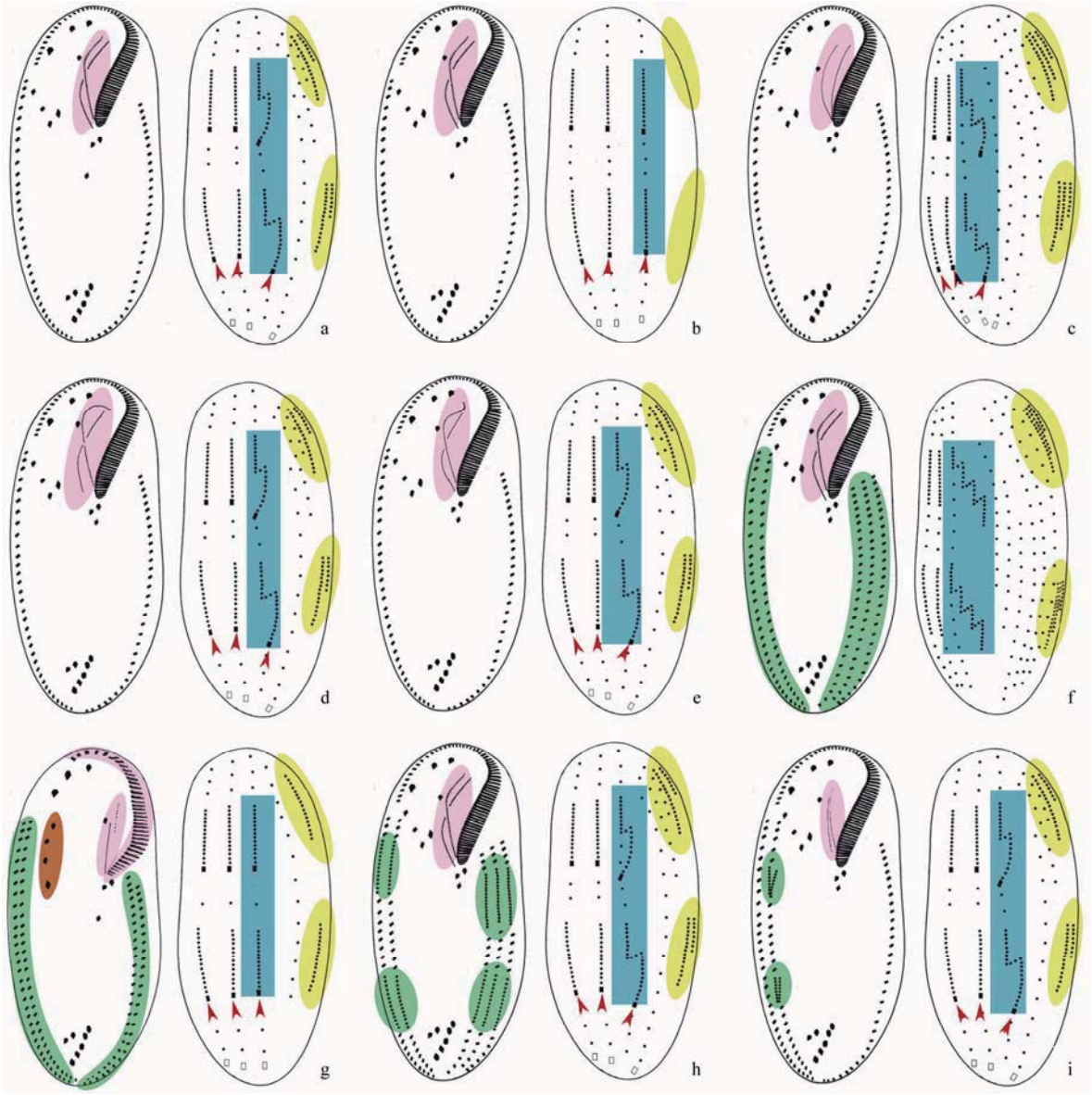

Fig.2 Diagram of the ventral and dorsal views of infraciliature and formation patterns of dorsal kineties anlagen and caudal cirri in Oxytrichidae *s. l.* genera. (a) *Oxytricha*; (b) *Heterooxytricha*; (c) *Australocirrus*; (d) *Cyrtohymena*; (e) *Notohymena*; (f) *Ponturostyla*; (g) *Parurosoma*; (h) *Architricha*; (i) *Allotricha*. Red arrows indicate caudal cirri. Oral apparatus, dorsal kinety 3, dorsomarginal kineties, multi-marginal rows/anlagen and some frontoventral cirri which are aligned in a row are shaded in violet, blue, yellow, green and brown, respectively.

nutrients

MDPI

Review

Immune-Relevant and Antioxidant Activities of Vitellogenin and Yolk Proteins in Fish

Chen Sun and Shicui Zhang *

Received: 15 July 2015 ; Accepted: 25 August 2015 ; Published: 22 October 2015

Laboratory for Evolution & Development, Institute of Evolution & Marine Biodiversity and Department of Marine Biology, Ocean University of China, Qingdao 266003, China; sunchen@ouc.edu.cn

* Correspondence: sczhang@ouc.edu.cn; Tel./Fax: +86-532-82032787

Abstract: Vitellogenin (Vtg), the major egg yolk precursor protein, is traditionally thought to provide protein- and lipid-rich nutrients for developing embryos and larvae. However, the roles of Vtg as well as its derived yolk proteins lipovitellin (Lv) and phosvitin (Pv) extend beyond nutritional functions. Accumulating data have demonstrated that Vtg, Lv and Pv participate in host innate immune defense with multifaceted functions. They can all act as multivalent pattern recognition receptors capable of identifying invading microbes. Vtg and Pv can also act as immune effectors capable of killing bacteria and virus. Moreover, Vtg and Lv are shown to possess phagocytosis-promoting activity as opsonins. In addition to these immune-relevant functions, Vtg and Pv are found to have antioxidant activity, which is able to protect the host from oxidant stress. These non-nutritional functions clearly deepen our understanding of the physiological roles of the molecules, and at the same time, provide a sound basis for potential application of the molecules in human health.

Keywords: vitellogenin; lipovitellin; phosvitin; immunity; antioxidant activity

1. Introduction

Most fishes are oviparous, with their eggs being fertilized externally [1]. Eggs or haploid reproductive cells, which develop into viable embryos after fertilization, are the final product of oocyte growth and differentiation [2]. Generally, several steps are involved in oocyte development: formation of primordial germ-cells (PGCs), and transformation of PGCs into oogonia and then to oocytes. Subsequently, massive maternal information and molecules needed for early embryo development are deposited in growing oocytes during vitellogenesis, including RNAs, proteins, lipids, vitamins, and hormones [2,3]. One of the most important proteins deposited in oocytes is vitellogenin (Vtg), a member of the large lipid transfer protein (LLTP) superfamily [3–5]. Vtg is a high molecular mass glycolipophosphoprotein, usually circulating in the blood (vertebrates)/hemolymph (invertebrates) as a homodimer [4,6–8]. There are usually several isoforms of Vtg in a given species, which are encoded by a multigene family [9,10]. For instance, three *vtg* genes have been identified in chicken *Gallus gallus* [11,12], four in Africa frog *Xenopus laevis* [13,14], and six in nematode *Caenorhabditis elegans* [15]. Multiple *vtg* genes are also common in teleosts. It has been documented that there are seven *vtg* genes in zebrafish *Danio rerio* [16,17], two *vtg* genes in carp *Cyprinus carpio* [18], four *vtg* genes in medaka *Oryzias latipes* [10], three *vtg* genes in striped bass *Morone saxatilis* [19], and three *vtg* genes in white perch *Morone americana* [20]. All vitellogenins (Vtgs) encoded by multiple genes display a similar structure in vertebrates, such as fish, and invertebrates, particularly insects [21,22]. In most cases, Vtg contains three conserved domains, the LPD_N (also known as vitellogenin_N or LLT domain), which is identified at the *N*-terminus, the domain of unknown function (DUF) 1943, and the von Willebrand factor type D domain (vWD), which is located at the

an immune-relevant role was the observation by Zhang *et al.*, that Vtg purified from the ovaries of the protochordate amphioxus (*Branchiostoma japonicum*) exhibited hemagglutinating activity against chick, toad and grass carp erythrocytes as well as antibacterial activity against the Gram-negative bacterium *E. coli* [59]. Soon after that, Vtg purified from the rosy barb *Puntius conchonius* was found to be capable of inhibiting the growth of the Gram-negative bacteria *E. coli*, *E. aerogenes* and *Pseudomonas putida* as well as the Gram-positive bacteria *Staphylococcus aureus*, *Bacillus subtilis* and *Streptococcus pyogenes* [60], and Vtg from the carp capable of suppressing the growth of *E. coli* and *S. aureus* in a dose dependent-manner [61]. Interestingly, Vtgs from protostomes also appear to have antibacterial activity. Vtg from the scallop (*Patinopecten yessoensis*) was recently shown to have antibacterial activity against Gram-positive and Gram-negative bacteria [62]. In addition, Vtg in the nematode *C. elegans* seems also involved in its antibacterial defense. A reduced survival was observed in the *vtg*-knockdown *C. elegans* after pathogen infection [63]. Another evidence for a role of invertebrate Vtg associated with resistance against bacteria was provided by the enhancement of resistance of nematode against the pathogen *Photorhabdus luminescens*, when the production of Vtg was stimulated by estrogen 17β-estradiol and phytoestrogen daidzein. However, reduction of Vtg caused by soy isoflavone genistein diminished the host resistance to *P. luminescens* [64]. Taken together, it appears that the antibacterial activity is a universal property of Vtgs from both vertebrates and invertebrates.

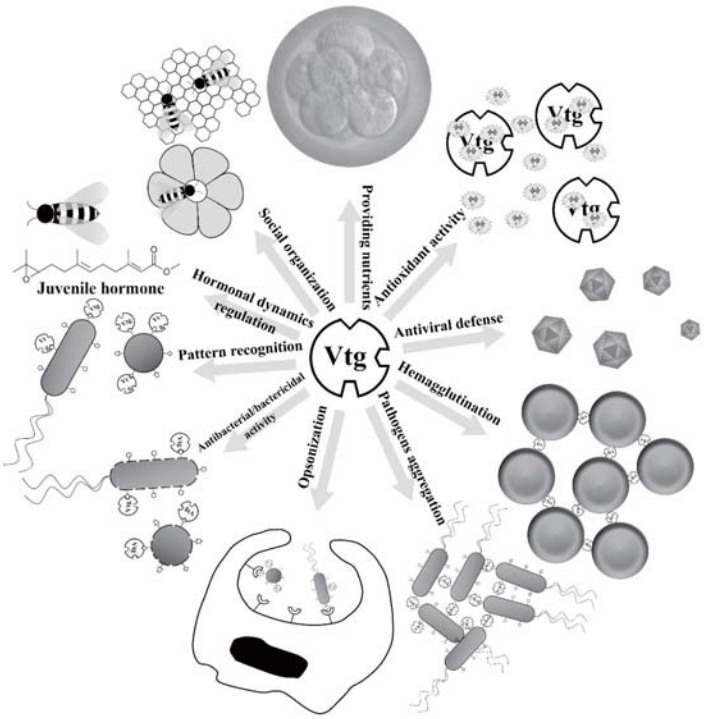

Figure 2. Multiple roles of vitellogenin (Vtg). Vtg is traditionally thought to provide protein- and lipid-rich nutrients for developing embryos and larvae. However, accumulating data demonstrate that its roles extend beyond the nutritional function. In the advanced eusocial insect honeybee, Vtgs were shown to be associated with the social organization, temporal division of labor and foraging specialization, regulation of hormonal dynamics and change in gustatory responsiveness. Recent studies show that Vtgs also play immune-relevant roles. Vtg is able to recognize the invading microbes as a multivalent pattern recognition receptor, kill bacteria or neutralize virus as an effector molecule as well as enhance phagocytosis as an opsonin. Besides, Vtg also exhibits activities to hemagglutinate erythrocytes and aggregate pathogens. In addition to immune roles, Vtg plays another novel role as an antioxidant.

Fish & Shellfish Immunology 46 (2015) 710–715

Contents lists available at ScienceDirect

Fish & Shellfish Immunology

journal homepage: www.elsevier.com/locate/fsi

Vitellogenin is an immunocompetent molecule for mother and offspring in fish

Shicui Zhang*, Yuan Dong, Pengfei Cui

Laboratory for Evolution & Development, Institute of Evolution & Marine Biodiversity and Department of Marine Biology, Ocean University of China, Qingdao 266003, China

ARTICLE INFO

Article history:
Received 21 May 2015
Received in revised form
8 August 2015
Accepted 12 August 2015
Available online 14 August 2015

Keywords:
Vitellogenin
Phosvitin
Lipovitellin
Vg-derived peptide

ABSTRACT

Our understanding of the function of vitellogenin (Vg) in reproduction has undergone a transformation over the past decade in parallel with new insights into the role of Vg in immunity. Initially, Vg was regarded as a female-specific reproductive protein, which is cleaved into yolk proteins such as phosvitin (Pv) and lipovitellin (Lv), stored in egg, providing the nutrients for developing embryos. Recently, Vg is shown to be an immune-relevant molecule involved in the defense of the host against the microbes including bacterium and virus. Furthermore, Pv and Lv, that both are proteolytically cleaved products of Vg, play a defense role in developing embryos. Importantly, yolk protein-derived small peptides also display antimicrobial activity. These data together indicate that Vg, in addition to being involved in yolk protein formation, plays a non-reproductive role via functioning as an immune-relevant molecule in both parent fishes and their offspring. It also shows that yolk proteins and their degraded peptides are novel players in maternal immunity, opening a new avenue to study the functions of reproductive proteins.

1. Introduction

Vitellogenin (Vg, from latin *vitellus*, yolk, and *gener*, to produce) was initially proposed by Pan et al. [1] to describe female-specific insect hemolymph protein precursor of egg yolk, regardless of its amino acid sequence and structure. Vg is now known as a high molecular mass glycolipophosphoprotein usually circulating in the blood (vertebrates)/hemolymph (invertebrates) as a homodimer, which is usually encoded by multiple *vg* genes in several species including insects, fish and frog [2]. Vg displays a similar structural characteristic in vertebrates, such as fish, and invertebrates, particularly insects. In most cases, Vg contains three conserved domains, the LPD_N (also known as vitellogenin_N or LLT domain) which is identified at the N-terminus, the domain of unknown function (DUF) 1943, and the von Willebrand factor type D domain (vWD) which is located at the C-terminus and distributed over a wide range of proteins (Fig. 1). Occasionally, a domain of unknown function called DUF1944 is found to be present in between DUF1943 and vWD in some Vg proteins from vertebrates such as chicken and fish [3]. Beginning at the N-terminus, a complete fish Vg consists of a signal peptide, a lipovitellin heavy chain (LvH), a phosphorylated serine-rich phosvitin (Pv), a lipovitellin light chain (LvL), and a β-component (β-C) plus a C-terminal coding region (CT) comprising the vWD. Notably, Pv can be absent, as observed in zebrafish Vg3 and most invertebrate Vg [4,5].

Vg, as an egg yolk protein precursor, is present in the females of nearly all oviparous species including fish, amphibians, reptiles, birds, most invertebrates and the platypus. Vg is usually synthesized extra-ovarianly (in the liver of vertebrates, the hepatopancreas of crustaceans and the fat body of insects) and transported by the circulation system to the ovary, where it is internalized into growing oocytes via receptor-mediated endocytosis and proteolytically cleaved by the aspartic protease cathepsin D [6–8] to generate yolk proteins, such as Lv subunits, Pv and β-C. Lv subunits and Pv are stored in yolk globules or platelets, while β-C remains in cytoplasm as a soluble fraction [9–11]. These yolk proteins are later used as the nutrients by developing embryos [12,13].

Vg was once regarded as a female-specific protein; however, synthesis, albeit in smaller quantities, has been shown to occur in male and even sexually immature animals [14,15]. This suggests that Vg presumably fulfills a more general role independent of gender. In recent years, both Vg and its derived yolk proteins have been shown to be connected with the immune defense in fish, challenging the traditional view that Vg and its derived yolk

* Corresponding author.
E-mail address: sczhang@ouc.edu.cn (S. Zhang).

http://dx.doi.org/10.1016/j.fsi.2015.08.011
1050-4648/

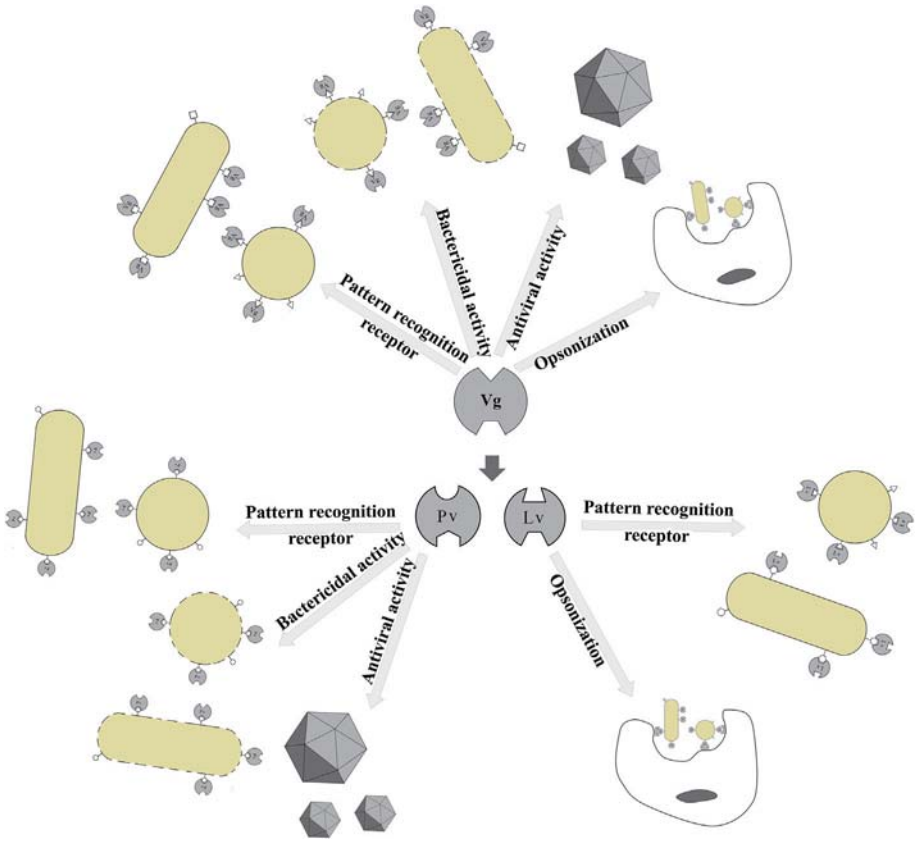

Fig. 3. Defense roles of Vg and Vg-cleaved yolk proteins in fish. Vitellogenin (Vg) is an immunocomponent molecule functioning as a pattern recognition receptor capable of identifying bacteria, an effector molecule capable of killing bacteria and neutralizing virus, and an opsonin capable of enhancing phagocytosis. Phosvitin (Pv) is a pattern recognition receptor and an effector molecule, whereas lipovitellin (Lv) is pattern recognition receptor and an opsonin.

scanning electron microscopy that Pv was able to cause lysis of both *E. coli* and *S. aureus* [64], and by phagocytosis test that coating of *E. coli* and *S. aureus* with Lv facilitated the phagocytosis of these bacteria by macrophages [67]. These show that Pv is an effector molecule capable of killing bacteria directly, whereas Lv is an opsonin capable of enhancing macrophage phagocytosis.

4. Defense roles of Vg-derived peptides

Yolk proteins stored inside eggs of oviparous organisms supply the developing embryos with nutrients. Egg fertilization triggers the activity of several enzymes such as aspartic and cysteine cathepsins and serine peptidases [7,68,69] to catalyze proteolysis of yolk proteins into small peptides and/or free amino acids, which are an important source of nutrients for early embryos [14,70–73]. Such dependence of embryogenesis on degradation of yolk proteins to generate a supply of small peptides and amino acids is also widely demonstrated in fishes including salmon, winter flounder, rainbow trout and medaka [13,70,74,75]. Interestingly, our previous studies show that the C-terminal 55 residues (NH_2-SRMSKTATIIEPFRKFHKDRYLAHHSATKDTSSGSAAASFEQMQKQNRFLGNDIP-COOH) of zebrafish Pv exhibits a strong antimicrobial activity capable of protecting both adult fish and embryos from the assault of pathogenic *Aeromonas hydrophila* [64,76]. To test if the smaller peptides derived from yolk proteins like Pv play an antimicrobial role, we have tentatively synthesized three 15-amino acid peptides, peptide 1 (6TATIIEPFRKFHKDR20; numbering as the C-terminal 55 residue sequence), peptide 2 (9IIEPFRKFHKDRYLA23) and peptide 3 (34GSAAASFEQMQKQNR48), and performed colony forming unit assay against the Gram-negative bacterium *A. hydrophila* and the Gram-positive bacterium *S. aureus* (Our unpublished data). Bacteria *A. hydrophila* and *S. aureus* were each pre-incubated with the peptide 1, 2 or 3 solutions (25, 50 and 100 μg/ml in PBS) or combination of different peptides (V/V = 1:1) for 1 h, and plated onto 3 plates with LB agar. After incubation at 37 °C for 12 h, the resulting bacterial colonies in each plate were counted. The percent of bacterial growth inhabitation was inferred from the difference between the numbers of colonies in the test and control. The control was processed similarly except that PBS was used instead of the peptide solution. The results showed that peptides 1 and 3 both were able to inhibit the growth of *A. hydrophila* and *S. aureus* in a dose-dependent manner, while peptide 2 only inhibited *A. hydrophila* growth but not *S. aureus* growth (Fig. 2A and C). Additionally, combination of different peptides (V/V = 1:1) seemed to enhance their antimicrobial activity against both *A. hydrophila* and *S. aureus* (Fig. 2B and D). It appears that the smaller peptides derived from yolk proteins, in addition to supplying nutrient, also play an antimicrobial role during early embryogenesis. Notably, Li et al. [77] showed that lysophophatidic acid, a signaling molecule derived from phosphatidylcholines of Pv [78], is able to regulate hemangioblast formation and primitive hematopoiesis in zebrafish. These suggest that the smaller molecules derived from yolk proteins may play multiple roles in developing embryos, which need to be further studied.

5. Concluding remarks

As fish culture both for food and as pets is the fastest growing

Fish & Shellfish Immunology 46 (2015) 493–500

Contents lists available at ScienceDirect

Fish & Shellfish Immunology

journal homepage: www.elsevier.com/locate/fsi

Short communication

Expression of virus-responsive genes and their response to challenge with poly(I:C) at different stages of the annual fish *Nothobranchius guentheri*: Implications for an asymmetric decrease in immunity

Shousheng Liu [a], Chengyan Jiang [a, b], Chuchu Duan [a], Lili Hu [a], Shicui Zhang [a, *]

[a] *Laboratory for Evolution & Development, Institute of Evolution & Marine Biodiversity and Department of Marine Biology, Ocean University of China, Qingdao 266003, China*

[b] *College of Life Science and Technology, Hong He University, Mengzi, Yunnan 661100, China*

ARTICLE INFO

Article history:
Received 17 April 2015
Received in revised form
29 June 2015
Accepted 19 July 2015
Available online 21 July 2015

Keywords:
Annual fish
Nothobranchius guentheri
Aging
Anti-virus response

ABSTRACT

Aging deteriorates immunity. However, if aging affects immunity in an asymmetric or symmetric way remains largely unknown. In this study we clearly demonstrate that compared with adult fish, the anti-viral responses of aged annual fish *Nothobranchius guentheri*, as reflected by the expression levels of virus-responsive genes, including *lgp2* and *mda5* encoding sensor molecules, *ifn-i* and *viperin* encoding the effector molecules and *irf1*, *irf7*, *stat1* and *atf3* encoding the regulation elements, are either reduced remarkably or elevated markedly or show little difference depending upon the different tissues. Moreover, although challenge with poly(I:C) results in a significant decrease in the expression of virus-responsive genes in most tissues of aged *N. guentheri*, it also causes a considerable increase in the expression of the genes in other tissues of aged fish. Collectively, these data suggest that the anti-viral responses of the annual fish *N. guentheri* generally reduces with age in an asymmetric way among the most tissues.

1. Introduction

Aging, the process of becoming older, is a multifactorial action that is associated with a variety of impairments in the physiology of an organism, including immune function, triggering a progressive, irreversible deterioration that ultimately leads to its death [1,2]. Many studies of the effects of aging on the immune system have been carried out in humans or in rodent models, highlighting age-dependent deterioration of both the cellular and humoral immune responses. Immunological deterioration with age is related with a decline in the production of naïve T and B cells, defects in the production of high-affinity antibodies, and impaired CD4 T cell function [2–6]. The capacity to mount a primary humoral response is also reduced during aging [7–12]. As a result, elderly individuals are less able to mount an immune response after challenges with newly encountered pathogens than young adults and are more susceptible than young to microbial infections, autoimmune diseases and neoplasia that contribute to both morbidity and mortality [13–15]. Although not thoroughly examined, there also exist data to propose that aging may lead to diminished immune control over chronic viral infections. For example, the neutralizing activity of virus-specific antibodies declines with age though the antibody levels are maintained in aged mice [2], and the increased incidence of herpes zoster disease in elderly individuals is thought to be partly due to the waning of cell-mediated immune control over dormant varicella (chicken pox) virus reactivation [16].

Fishes show three patterns of aging. Migratory fishes such as lampreys, eels and Pacific salmon display rapid senescence and sudden death at first spawning, while long-lived species of colder regions including sturgeons, paddlefish, plaice, and flatfish as well as rockfish (e.g. *Sebastes aleutianus*) exhibit indeterminate growth with extremely slow or negligible aging [17–19]. By contrast, the guppy, red panchax, platyfish, Indian murrel and many other teleosts including some small laboratory fishes, such as zebrafish *Danio rerio*, medaka *Oryzias curvinotus* and annual fish *Nothobranchius furzeri*, share many hallmarks of aging similar to those observed in mammalian species [20–23]. Annual fishes, especially the genus Nothobranchius, have become a rising star for aging studies: they have a relatively short lifespan, are commercially available and are

* Corresponding author. Room 205, Ke Xue Guan, 5 Yushan Road, Ocean University of China, Qingdao 266003, China.
E-mail address: sczhang@ouc.edu.cn (S. Zhang).

http://dx.doi.org/10.1016/j.fsi.2015.07.010
1050-4648/

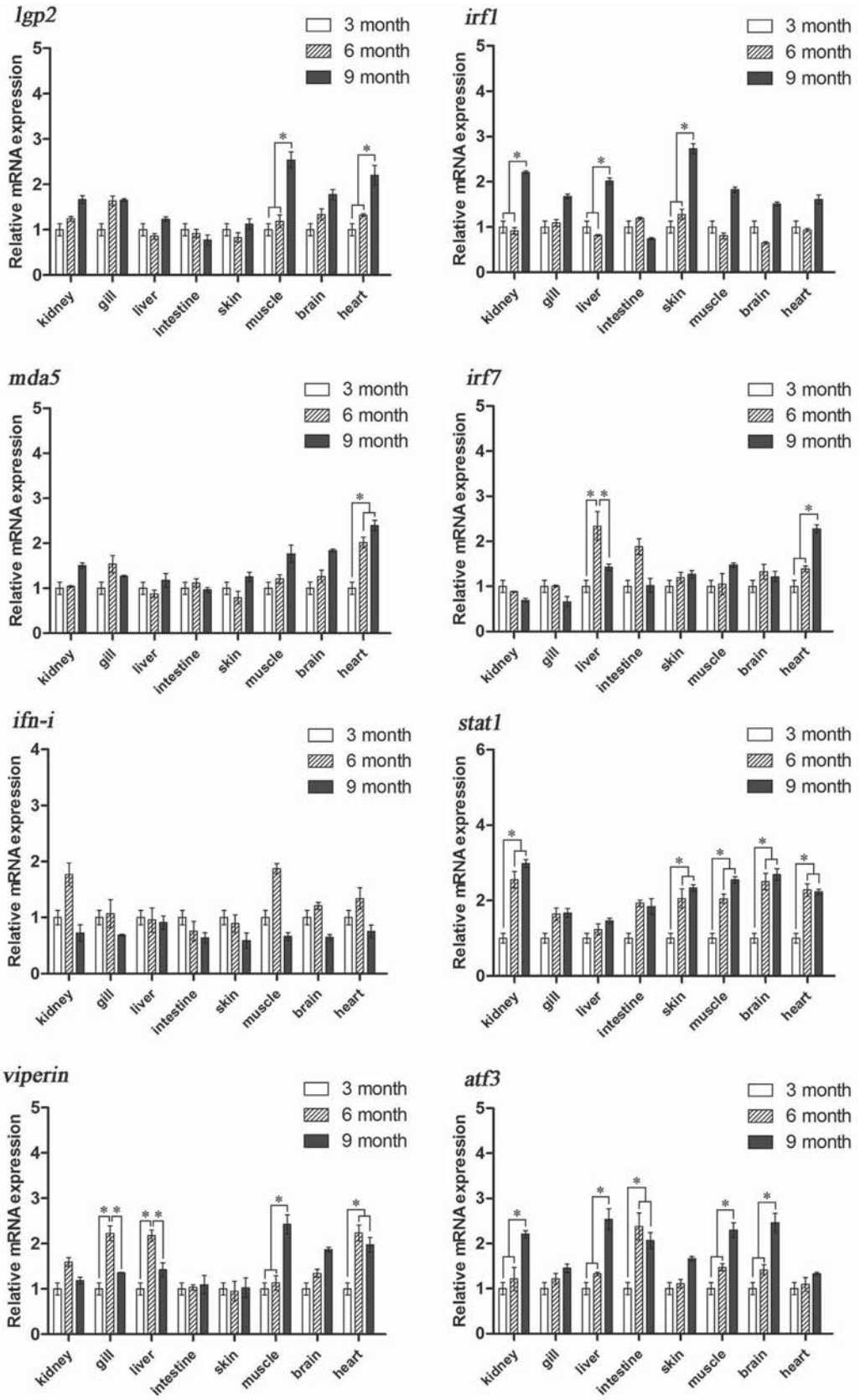

Fig. 1. Expression profiles of *lgp2*, *mda5*, *ifn-i*, *viperin*, *irf1*, *irf7*, *stat1* and *atf3* in the different tissues from young, adult and aged *N. guentheri*. Data are expressed mean ± SD from three replicates. The symbol * indicates a significant difference ($p < 0.05$).

General and Comparative Endocrinology 214 (2015) 9–16

Contents lists available at ScienceDirect

General and Comparative Endocrinology

journal homepage: www.elsevier.com/locate/ygcen

Identification, expression and regulation of amphioxus G6Pase gene with an emphasis on origin of liver

Yu Wang [a], Hui Wang [b], Mengyang Li [a], Zhan Gao [a], Shicui Zhang [a,*]

[a] Laboratory for Evolution & Development, Institute of Evolution & Marine Biodiversity and Department of Marine Biology, Ocean University of China, Qingdao 266003, China
[b] Key Laboratory of Nutrition and Metabolism, Institute for Nutritional Sciences, Shanghai Institutes for Biological Sciences, Chinese Academy of Sciences, Shanghai, China

ARTICLE INFO

Article history:
Received 10 November 2014
Revised 25 December 2014
Accepted 28 December 2014
Available online 5 March 2015

Keywords:
Amphioxus
Zebrafish
Glucose-6-phosphatase
Liver
Digestive diverticulum
Glucose homeostasis

ABSTRACT

Vertebrate glucose-6-phosphatase (G6Pase) consists of three isozymes: G6Pase-I, G6Pase-II and G6Pase-III. Despite extensive study on G6Pases in vertebrates, information regarding expression and regulation of G6Pase genes is rather limited in invertebrates. Here we report the identification of G6Pase gene in amphioxus *Branchiostoma japonicum*, which is abundantly expressed in the digestive diverticulum and ovary in a tissue-specific manner. The phylogenetic and genomic structure analyses reveal that amphioxus G6Pase bears close resemblance to vertebrate G6Pase-III and represents the archetype of vertebrate G6Pase from which the vertebrate G6Pase isoforms may be originated by 2 rounds of genome duplication during vertebrate evolution. We also demonstrate that GH treatment induces a closely similar expression pattern and trend of *g6pases* in both zebrafish and amphioxus, and that G6Pase activity in amphioxus digestive diverticulum is subjected to regulation of feeding and fasting as observed in vertebrates. Collectively, all these provide functional evidences supporting the notion that the digestive diverticulum is the liver homologue playing a key role in maintaining the glucose homeostasis in amphioxus.

1. Introduction

Glucose-6-phosphatase (EC3.1.3.9, G6Pase) is an enzyme that catalyzes the hydrolysis of glucose 6-phosphate (G6P) produced from glycogen or gluconeogenic precursors, resulting in the creation of free glucose (and a phosphate group, Pi), which is then released from the cell to blood via glucose transporter membrane proteins (Ghosh et al., 2002). This catalysis completes the final step in gluconeogenesis and glycogenolysis, and thus plays a crucial role in the mediation of blood glucose homeostasis.

In mammals, three genes encoding G6Pase-I, G6Pase-II and G6Pase-III, individually, are identified (Hutton and O'Brien, 2009). Different mammalian G6Pase genes show different expression patterns, with *g6pase-I* being expressed predominantly in liver and kidney and at lower levels in intestine (Foster et al., 1997; van Schaftingen and Gerin, 2002; van de Werve et al., 2000), *g6pase-II*, also known as islet-specific G6Pase-related gene, exclusively expressed in pancreatic islets (Arden et al., 1999; Ebert et al., 1999), and *g6pase-III* ubiquitously expressed in all the tissues examined, albeit at higher levels in brain, muscle, and kidney (Martin et al., 2002). In addition, G6Pase genes are subject to hormonal regulation. For example, growth hormone (GH) is found to elevate hepatic expression of G6Pase genes in both rats (Vidal et al., 1993) and sea bream (Leung and Woo, 2010). Similarly, nutrient status (e.g. starvation) also induces an increase in G6Pase activity in the liver (van Schaftingen and Gerin, 2002). By contrast, little information is available regarding the expression and regulation of G6Pase genes in lower animals, especially in invertebrates, though G6Pase was shown to be present in the muscles of insects such as silkworm, wasp, and honey bee (Surholt and Newsholme, 1981).

The cephalochordate amphioxus, which occupies a nodal position from invertebrate to vertebrate (Stach, 2008), has a digestive diverticulum, the pouch that protrudes forward as an outpocketing of the digestive tube and extends along the right side of the posterior part of the pharynx, which has long been considered to be the precursor homologue of vertebrate liver (Hammar, 1898; Welsch, 1975). Our recent studies have shown that the digestive diverticulum of the amphioxus *Branchiostoma japonicum* is capable of synthesizing the liver-specific proteins such as vitellogenin, Bf/C2, GST and hexokinases (Fan et al., 2007; Han et al., 2006; He et al., 2008; Li et al., 2014), reinforcing the homology of digestive diverticulum to vertebrate liver. However, information regarding the functional homology of the digestive diverticulum to liver remains largely lacking. The aim of the present study was therefore to address this issue by investigating the expression of G6Pase gene

* Corresponding author. Fax: +86 532 82032.
E-mail address: sczhang@ouc.edu.cn (S. Zhang).

http://dx.doi.org/10.1016/j.ygcen.2014.12.021
0016-6480/

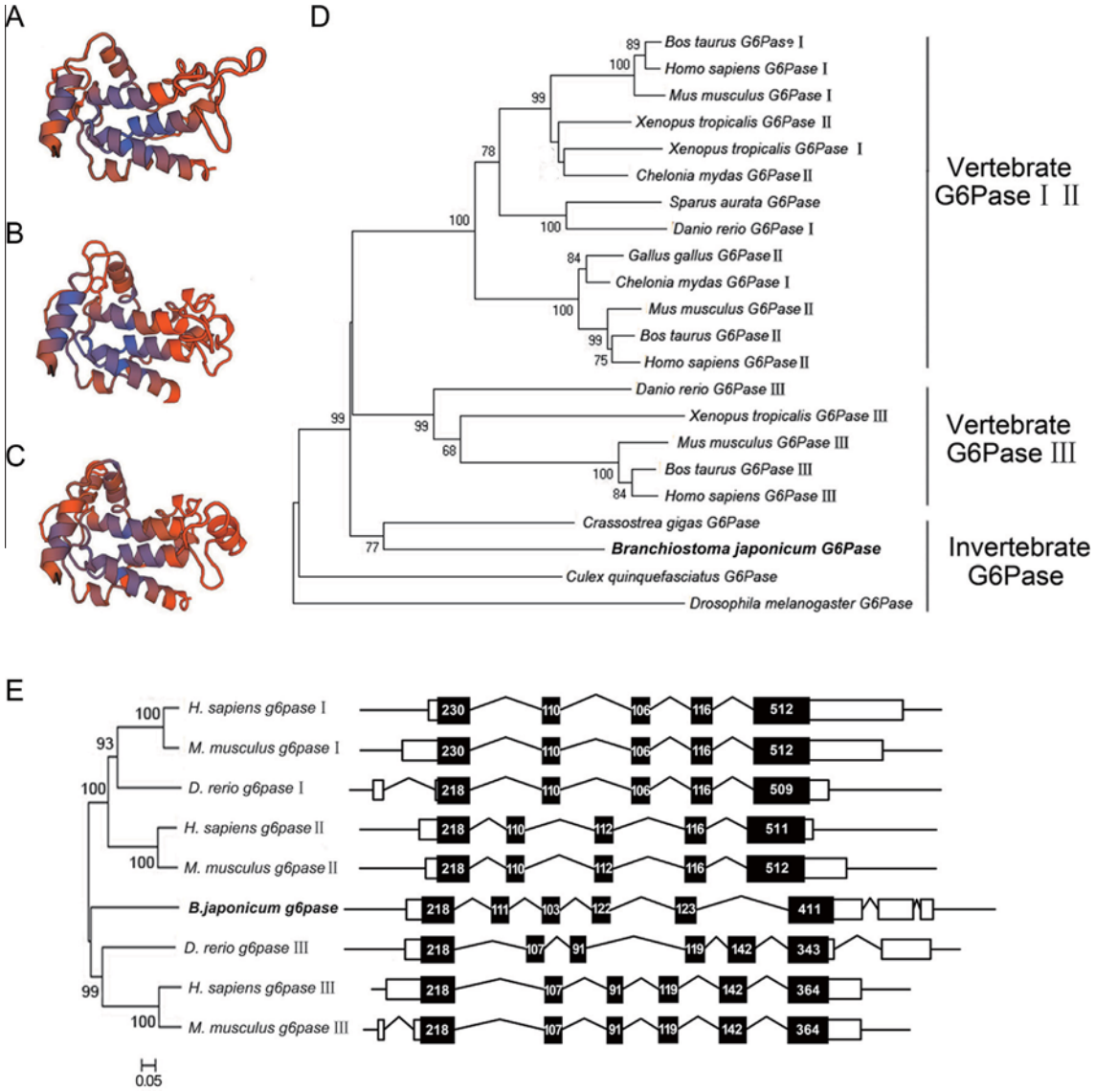

Fig. 1. Three-dimensional (3D) structure, phylogenetic tree and genomic structure. 3D structures of zebrafish G6Pase-I (A), zebrafish G6Pase-III (B) and amphioxus G6Pase (C) were generated by SWISS-MODEL online software using the same template model (PDB id: 1iw8). (D) Phylogenetic tree of glucose-6-phosphatase including amphioxus G6Pase, which was constructed by the MEGA 6.0 software package base on Neighbor-Joining method. (E) Genomic structures of *g6pase* genes. Open rectangles and black rectangles represent non-coding exons and coding exons, respectively. The broken lines between two rectangles represent introns. The horizontal lines represent flanking sequences. The numbers in the black rectangles represent the nucleotide number of each coding exon. The information of the exon–intron organization of vertebrate *g6pases* was obtained from Ensembl database (http://asia.ensembl.org/index.html) and the information of amphioxus *g6pase* obtained using the Gene Structure Display Server 2.0 (GSDS 2.0) (http://gsds.cbi.pku.edu.cn/).

of a single genomic DNA sequence (XM_002594668.1) of G6Pase (http://genome.jgi-psf.org//Brafl1/Brafl1.home.html). The *B. floridae* G6Pase cDNA encodes a protein with about 84.2% identity to *B. japonicum* G6Pase at amino acid level, suggesting that amphioxus G6Pase is highly conserved within the genus. Analysis of the genomic structure showed that amphioxus *g6pase* comprised 6 coding exons interspaced by 5 introns of 828, 668, 775, 2945 and 5957 bp, respectively. The introns all begin with GT and end with an AG dinucleotide, sequences thought necessary for correct RNA splicing of various eukaryotic genes (Breathnach et al., 1978). Notably, the vertebrate *g6pase-I* and *g6pase-II* both had 5 coding exons interspaced by 4 introns, while the *g6pase-III* had 6 coding exons interspaced by 5 introns, bearing similarity to that of amphioxus *g6pase* (Fig. 1E). Collectively, these data suggest that *g6pase-III* bears a close resemblance to amphioxus *g6pase*, which may represent the archetype of vertebrate G6Pase genes. Moreover, synteny analysis revealed that amphioxus *g6pase* was mapped on the scaffold 382 of *B. floridae* genome, and flanked by angiotensin-converting enzyme (ACE) gene downstream and Acyl CoA binding protein (ACBP) gene upstream. Notably, ACE gene was also located downstream of *g6pases* in the invertebrate such as mosquito and vertebrates including humans, mouse and zebrafish (Fig. 2), providing an additional evidence showing that amphioxus G6Pase is the archetype of G6Pases. The genomic structures of *g6pases* seemed highly conserved throughout vertebrate evolution as *g6pase-I* was all located upstream of AARSD1 gene, and *g6pase-II* was flanked by SPC25 and ABCB11genes, *g6pase-III* flanked by LSM12 and HDAC5 genes. Interestingly, all the *g6pases* (2 *g6pase-I* plus 1 *g6pase-III*) in zebrafish were positioned on a single chromosome, while *g6pase-I* and *g6pase-II* in frog *X. tropicalis* were mapped on the same chromosome, but *g6pase-III* on another one. By contrast, chickens and turtles had only two G6Pase genes,

PLOS | GENETICS

RESEARCH ARTICLE

Genome Sequencing of the Perciform Fish *Larimichthys crocea* Provides Insights into Molecular and Genetic Mechanisms of Stress Adaptation

Jingqun Ao[1☯], Yinnan Mu[1☯], Li-Xin Xiang[2☯], DingDing Fan[3☯], MingJi Feng[3☯], Shicui Zhang[4☯], Qiong Shi[3], Lv-Yun Zhu[2], Ting Li[1], Yang Ding[1], Li Nie[2], Qiuhua Li[1], Wei-ren Dong[2], Liang Jiang[5], Bing Sun[4], XinHui Zhang[3], Mingyu Li[1], Hai-Qi Zhang[2], ShangBo Xie[3], YaBing Zhu[3], XuanTing Jiang[3], Xianhui Wang[1], Pengfei Mu[1], Wei Chen[1], Zhen Yue[3], Zhuo Wang[3], Jun Wang[3]*, Jian-Zhong Shao[2]*, Xinhua Chen[1]*

1 Key Laboratory of Marine Biogenetics and Resources, Third Institute of Oceanography, State Oceanic Administration, Fujian Collaborative Innovation Center for Exploitation and Utilization of Marine Biological Resources, Key Laboratory of Marine Genetic Resources of Fujian Province, Xiamen, P. R. China, **2** College of Life Sciences, ZheJiang University, Key Laboratory for Cell and Gene Engineering of Zhejiang Province, Hangzhou, ZheJiang, P. R. China, **3** BGI-Tech, BGI-Shenzhen, Shenzhen, Guangdong, P. R. China, **4** Ocean University of China, Qingdao, Shandong, P. R. China, **5** College of Life Sciences, Shenzhen University, Shenzhen, Guangdong, P. R. China

☯ These authors contributed equally to this work.
* wangj@genomics.org.cn (JW); shaojz@zju.edu.cn (JS); chenxinhua@tio.org.cn (XC)

OPEN ACCESS

Citation: Ao J, Mu Y, Xiang L-X, Fan D, Feng M, Zhang S, et al. (2015) Genome Sequencing of the Perciform Fish *Larimichthys crocea* Provides Insights into Molecular and Genetic Mechanisms of Stress Adaptation. PLoS Genet 11(4): e1005118. doi:10.1371/journal.pgen.1005118

Editor: Manfred Schartl, University of Wuerzburg, GERMANY

Received: August 22, 2014

Accepted: March 3, 2015

Published: April 2, 2015

Data Availability Statement: The whole-genome sequences of *L. crocea* have been deposited in the DNA Data Bank of Japan (DDBJ), the European Molecular Biology Laboratory (EMBL) nucleotide sequencing database and GenBank under the accession JRPU00000000. The version described in this paper is the first version JRPU01000000. All short-read data of WGS and BAC have been deposited in the Short Read Archive (SRA) under accession SRA159210 and SRA159209 respectively. Raw sequencing data of transcriptomes have been deposited in the Gene Expression Omnibus under

Abstract

The large yellow croaker *Larimichthys crocea* (*L. crocea*) is one of the most economically important marine fish in China and East Asian countries. It also exhibits peculiar behavioral and physiological characteristics, especially sensitive to various environmental stresses, such as hypoxia and air exposure. These traits may render *L. crocea* a good model for investigating the response mechanisms to environmental stress. To understand the molecular and genetic mechanisms underlying the adaptation and response of *L. crocea* to environmental stress, we sequenced and assembled the genome of *L. crocea* using a bacterial artificial chromosome and whole-genome shotgun hierarchical strategy. The final genome assembly was 679 Mb, with a contig N50 of 63.11 kb and a scaffold N50 of 1.03 Mb, containing 25,401 protein-coding genes. Gene families underlying adaptive behaviours, such as vision-related crystallins, olfactory receptors, and auditory sense-related genes, were significantly expanded in the genome of *L. crocea* relative to those of other vertebrates. Transcriptome analyses of the hypoxia-exposed *L. crocea* brain revealed new aspects of neuro-endocrine-immune/metabolism regulatory networks that may help the fish to avoid cerebral inflammatory injury and maintain energy balance under hypoxia. Proteomics data demonstrate that skin mucus of the air-exposed *L. crocea* had a complex composition, with an unexpectedly high number of proteins (3,209), suggesting its multiple protective mechanisms involved in antioxidant functions, oxygen transport, immune defence, and osmotic and ionic regulation. Our results reveal the molecular and genetic basis of fish adaptation and response to hypoxia and air exposure. The data generated by this study will

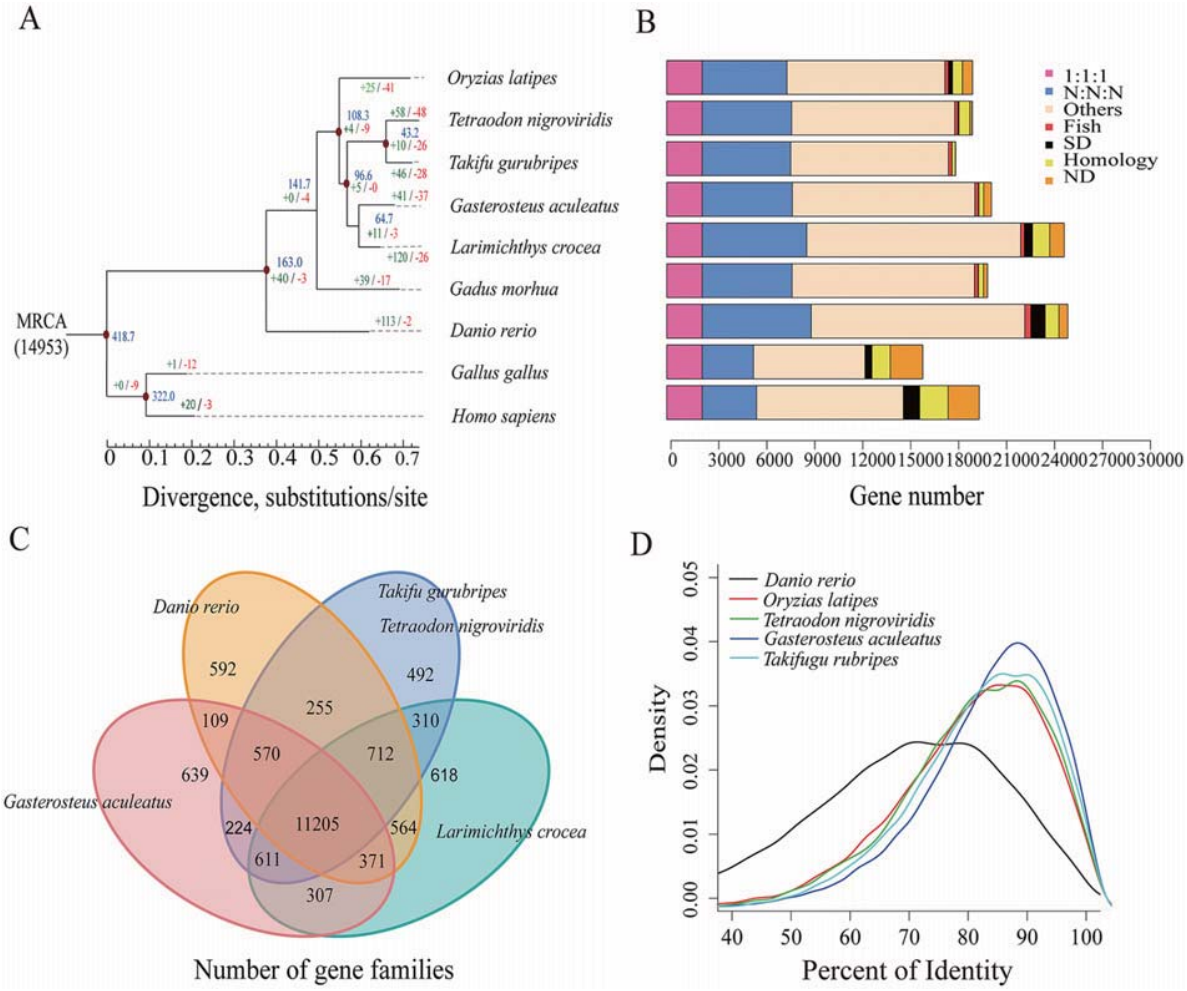

Fig 1. Phylogenetic tree of and orthologous genes in *L. crocea* and other vertebrates. (**A**) The phylogenetic tree was constructed from 2,257 single-copy genes with 3.18 M reliable sites by maximum likelihood methods. The red points on six of the internal nodes indicate fossil calibration times in the analysis. Blue numbers indicate the divergence time (Myr, million years ago), and the green and red numbers represent the expanded and extracted gene families, respectively, in *L. crocea*. (**B**) The different types of orthologous relationships are shown. "1:1:1" = universal single-copy genes; "N:N:N" = orthologues exist in all genomes; "Fish" = fish-specific genes; "SD" = genes that have undergone species-specific duplication; "Homology" = genes with an e-value less than 1e-5 by BLAST but do not cluster to a gene family; "ND" = species-specific genes; and "Others" = orthologues that do not fit into the other categories. (**C**) The shared and unique gene families in five teleost fish are shown in the Venn diagram. (**D**) Distribution of the identity values of orthologous genes is compared among *L. crocea* and other teleosts.

doi:10.1371/journal.pgen.1005118.g001

"delta" group, which is important for the perception of water-borne odorants [20]. *L. crocea* also possessed the highest number of genes that were classified into the "eta" group (30, $P < 0.001$), and these genes may contribute to the olfactory detection abilities, which could be useful for feeding and migration [21].

L. crocea is named for its ability to generate strong repetitive drumming sounds, especially during reproduction [8]. For good communication, fish have developed high sensitivities to environmental sound. Three important auditory genes, otoferlin (*OTOF*), *claudinj*, and otolin 1 (*OTOL1*), were significantly expanded in the *L. crocea* genome ($P < 0.01$, S19 Table). These expansions may contribute to the detection of sound signaling during communication, and thus to reproduction and survival [22].

Acta Biochim Biophys Sin, 2015, 47(5), 349–354
doi: 10.1093/abbs/gmv023
Advance Access Publication Date: 6 April 2015
Original Article

Original Article

Zebrafish phosvitin is an antioxidant with non-cytotoxic activity

Lili Hu[1], Chen Sun[1], Jing Luan[2], Linlin Lu[3], and Shicui Zhang[1,*]

[1]Laboratory for Evolution and Development, Institute of Evolution and Marine Biodiversity and Department of Marine Biology, Ocean University of China, Qingdao 266042, China, [2]Shandong Entry-Exit Inspection and Quarantine Bureau, Qingdao 266001, China, and [3]Center for Reproductive Medicine, Qingdao Women and Children Hospital, Qingdao 266034, China

*Correspondence address. Tel/Fax: +86-532-82032787; E-mail: sczhang@ouc.edu.cn

Received 8 October 2014; Accepted 20 February 2015

Abstract

Antioxidants, or anti-oxidant agents, have attracted a great deal of attention in recent years because of their roles in prevention of chronic diseases and utilization as preservatives in food and cosmetics. In this study, we clearly demonstrated that zebrafish recombinant phosvitin (rPv) is an antioxidant agent capable of inhibiting the oxidation of the linoleic acid, and scavenging the 2,2-diphenyl-1-picrylhydrazyl radical. We also showed that zebrafish rPv is a cellular antioxidant capable of protecting radical-mediated oxidation of cellular biomolecules. Importantly, zebrafish rPv is non-cytotoxic to murine macrophage RAW264.7 cells. It is the first report that showed the antioxidant activities of Pv in fishes, suggesting that zebrafish Pv can be an important antioxidant, which can be used as preservatives in food and cosmetics and even as supplementary mediator in different diseased states.

Key words: zebrafish, yolk protein, phosvitin (Pv), antioxidant, oxidation

Introduction

Oxidative stress refers to the effect of oxidation in which an abnormal level of reactive oxygen species (ROS) leads to damage to all components of the cell, including proteins, lipids, and DNAs. ROS produced in cells includes hydrogen peroxide (H_2O_2), hydroxyl radical (·OH), and superoxide anion (O_2^-), which has been implicated in aging and a number of human chronic diseases such as diabetes, arthritis, neurodegenerative disease, cardiovascular disease, and cancer [1]. All these disease conditions are believed to be directly or indirectly related to oxidation of cellular biomolecules by ROS generated excessively in tissues [2]. Specially, leukocytes have been identified to produce large amount of ROS during infections as a part of direct immune response. Thus, biomolecules in leukocytes have a great risk to get oxidized by ROS during inflammatory events.

Antioxidants, or anti-oxidant agents, are substances that neutralize ROS or their actions [3]. Within the human body there is a complex network of antioxidant metabolites and enzymes that work together to prevent oxidative damage to cellular components [4]. In general, antioxidant systems either prevent ROS from being formed or remove them before they damage vital biomolecules of the cell. However, during chronic disease conditions antioxidant system in human body can not function properly, and therefore, supplementary antioxidants are important mediators, which are capable of preventing and/or improving different diseased states [5]. Antioxidants are also widely used as preservatives to prevent deterioration of food and cosmetics. Therefore, antioxidants, especially their roles in prevention of disease, have attracted a great deal of attention in recent years.

Many antioxidative substances have been isolated from natural resources, including foods. For example, hen egg yolk phosvitin (Pv) has been isolated and its derived oligophosphopeptides show strong antioxidant activity owing to its high serine and phosphorus content, which makes this protein one of the strongest iron-chelating agents [6,7]. Hen egg Pv was also found to possess antithrombin activity [8], bactericidal activity against *Escherichia coli* [9], and endotoxin-neutralizing activity [10]. Similarly, fish Pv was also shown to be not only directly bactericidal but also able to bind the pathogen-associated molecular patterns such as lipopolysaccharide, lipoteichoic acid, and peptidoglycan [11]. In addition, fish Pv also displays an

[10,13], indicating that zebrafish rPv is non-cytotoxic to the murine cells *in vitro*.

Zebrafish rPv shows a strong antioxidant activity against oxidation of linoleic acid

The antioxidant activity of zebrafish rPv against the peroxidation of linoleic acid is shown in **Fig. 2**. Increasing the concentration of zebrafish rPv from 2.5 to 10 μM resulted in greater inhibition of linoleic acid oxidation. At 2.5 μM, VE showed little antioxidant activity against the oxidation of linoleic acid compared with blank ($P > 0.05$). By contrast, zebrafish rPv exhibited a significant antioxidant activity against the oxidation of linoleic acid at the same concentration, compared with that of both blank and VE control ($P < 0.05$), suggesting that zebrafish rPv is a stronger antioxidant than VE in the linoleic acid system. Notably, zebrafish rPv also displayed a markedly stronger antioxidant activity against the peroxidation of linoleic acid than hen egg Pv at the same concentration (5 μM or 100 μg/ml) [7]. These data demonstrated that zebrafish rPv is a strong antioxidant agent capable of inhibiting the oxidation of the linoleic acid system in a dose-dependent manner.

Zebrafish rPv is an antioxidant with prolonged radical-scavenging activity

As shown in **Fig. 3**, VC used as a reference compound had a strong effect as a radical scavenger, and the DPPH radical-scavenging capacity of VC reached ~96% after 1 h of reaction at all the three concentrations tested. In contrast, the radical-scavenging activity of zebrafish rPv was markedly lower than that of VC. In the initial 2.5 h of reaction, the DPPH radical-scavenging capacity of zebrafish rPv was only ~10% at both 5 and 10 μM, and remained to be ~15% even at 15 μM. However, the radical-scavenging capacity of zebrafish rPv increased with prolonged reaction time, in sharp contrast to VC. At 45 and 55 h, the radical-scavenging capacity of zebrafish rPv at 5, 10, and 15 μM reached ~33%, 41%, and 47% as well as 39%, 47%, and 52%, respectively (**Fig. 3**). Moreover, zebrafish rPv showed stronger radical-scavenging capacity than hen egg Pv [7]. These results suggested that zebrafish rPv is an antioxidant with a longer radical-scavenging capacity.

Table 1. The viability of RAW264.7 cells in the presence of zebrafish rPv

rPv concentration (μM)	Viability (%)
0 (control)	100
10	98 ± 13
150	101 ± 14
300	91 ± 7

Zebrafish rPv is able to inhibit cell membrane lipid peroxidation

Unsaturated fatty acids in cell membrane lipids are highly susceptible to free radical attack during oxidation. TBARS assay was used to study the effects of zebrafish rPv on the inhibition of cell membrane lipid peroxidation. In this assay, membrane lipid peroxidation was initiated by generating hydroxyl radicals (·OH) via Fenton's reaction. As shown in **Fig. 4**, zebrafish rPv displayed a significant inhibitory effect at 300 μM, with the inhibition rate of ~43.8% compared with control. This indicated that zebrafish rPv possesses the ability to inhibit the cell membrane lipid peroxidation.

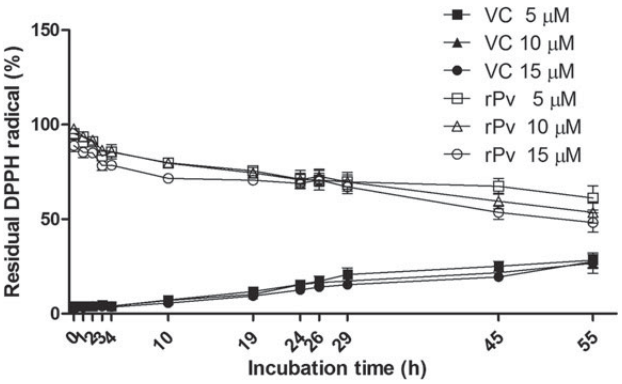

Figure 3. DPPH radical-scavenging activities of zebrafish rPv Aliquots of 2.5 ml of 10 mM PBS (pH 7.4) containing 5, 10, and 15 μM of rPv or L-ascorbic acid (VC) were mixed with 1.5 ml of 995 g/l ethanol and 1 ml of 995 g/l ethanol with 0.2 g/l DPPH. Data were expressed as the mean ± SEM ($n = 3$). The bars represent the standard error of mean values.

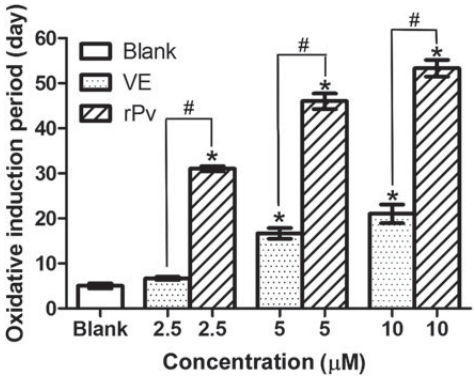

Figure 2. Antioxidant activities of zebrafish rPv in linoleic acid system Data were expressed as the mean ± SEM ($n = 3$). The bars represent the standard error of mean values. *$P < 0.05$ compared with the blank control group, and #$P < 0.05$ compared with the VE group.

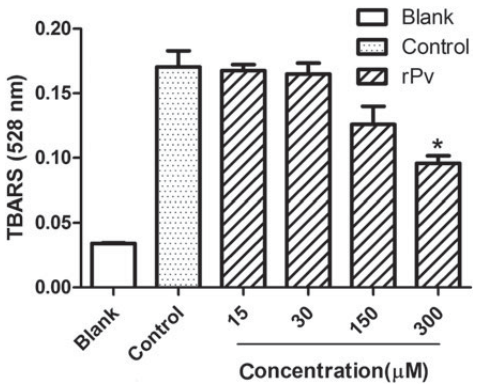

Figure 4. Membrane lipid peroxidation determination by TBARS method Data were expressed as the mean ± SEM ($n = 3$). The bars represent the standard error of mean values. *$P < 0.05$ compared with the control group.

Developmental and Comparative Immunology 53 (2015) 293–302

Contents lists available at ScienceDirect

Developmental and Comparative Immunology

journal homepage: www.elsevier.com/locate/dci

Identification and functional characterization of viperin of amphioxus *Branchiostoma japonicum*: Implications for ancient origin of viperin-mediated antiviral response

Miaomiao Lei, Haohan Liu, Shousheng Liu, Yu Zhang**, Shicui Zhang*

Laboratory for Evolution & Development, Institute of Evolution & Marine Biodiversity and Department of Marine Biology, Ocean University of China, Qingdao 266003, PR China

ARTICLE INFO

Article history:
Received 19 April 2015
Received in revised form
9 July 2015
Accepted 11 July 2015
Available online 17 July 2015

Keywords:
Amphioxus
Cephalochordate
Viperin
Interferons
Antiviral activity

ABSTRACT

Viperin, an antiviral protein, has been shown to be active against a wide range of DNA and RNA viruses, but no information is available regarding functional characterization of viperin in invertebrate species. In this study, we clearly demonstrate that amphioxus (*Branchiostoma japonicum*) viperin, BjVip, has features in common with those of vertebrate viperin, including the presence of the SAM superfamily domain with the characteristic CNYKCGFC motif, syntenic conservation, and predicted 3D structure. *Bjvip* exhibits a tissue-specific expression with abundant levels in the hepatic cecum, hind-gut, gill and muscle, and following challenge with the viral mimic poly I:C, its expression is significantly up-regulated, suggesting an involvement of BjVip in immune response of amphioxus against viral infection. Importantly, we show that the cells transfected with *Bjvip* is able to kill LCDV or inhibiting its propagation, and co-incubation of rBjVip with WSSV markedly attenuates its infectivity. Thus, we provide the first evidences that amphioxus viperin, like that of vertebrates, is capable of promoting resistance against viral infection *in vitro* and *in vivo*, indicating that viperin-mediated antiviral response already emerged in the primitive chordate. We also prove that amphioxus viperin has evolved under positive selection.

1. Introduction

Vertebrate interferon (IFNs) proteins, mainly comprising type I (IFN-α/β), type-II (IFN-γ) and type III (IFN-λ) IFNs, are rapidly induced following viral infection and subsequently activate thousands of interferon-regulated genes (IRGs) or interferon-stimulated genes (ISGs) (De Veer et al., 2001; Sen and Sarkar, 2007). ISGs encode proteins that generally display a range of antiviral activities against diverse pathogens (Sadler and Williams, 2008; Sen, 2001). Viperin (*v*irus *i*nhibitory *p*rotein, *e*ndoplasmic *r*eticulum-associated, *in*terferon-inducible) is one of ISGs-encoding proteins, which could inhibit many DNA and RNA viruses such as CHIKV, HCMV, HCV, DENV, WNV, SINV, influenza, and HIV LAI strain etc. Initially identified as cig5 in HCMV-infected primary human foreskin cells (Zhu et al., 1997), viperin is subsequently found in rainbow trout as the vig1 gene inducible by viral haemorrhagic septicaemia virus and in mouse as the vig1/cig5 homologue inducible by vesicular stomatitis virus and pseudorabies virus (Boudinot et al., 1999, 2000). Viperin has now been identified in various species of vertebrates. All viperin homologues are highly conserved in the primary sequence, which includes a relatively less conserved N-terminal amphipathic α-helix required for endoplasmic reticulum (ER) localization (Hinson and Cresswell, 2009a,b), a central radical S-adenosylmethionine (SAM) domain which contains a CxxxCxxC motif important for the formation of a [4Fe–4S] cluster (Frey et al., 2008), and a highly conserved C-terminal region that is known to be critical for antiviral activity against a number of viruses (Helbig and Beard, 2014; Helbig et al., 2013). Positive selection has been reported to drive rapid evolution of certain amino acid residues in the N-terminal regions of the highly conserved viperin proteins of fishes (Padhi, 2013).

Viperin could be induced in a variety of cell types by different cellular factors, such as type I, II and III IFNs, DNA and RNA viral proteins, viral mimic polyriboinosinic polyribocytidylic acid (poly I:C) and polysaccharide (Boudinot et al., 1999; Chin and Cresswell,

* Corresponding author. Room 205, Ke Xue Guan, 5 Yushan Road, Ocean University of China, Qingdao 266003, PR China.
** Corresponding author. Room 319, Darwin Building, 5 Yushan Road, Ocean University of China, Qingdao 266003, PR China.
E-mail addresses: yuzhang@ouc.edu.cn (Y. Zhang), sczhang@ouc.edu.cn (S. Zhang).

http://dx.doi.org/10.1016/j.dci.2015.07.008
0145-305X/

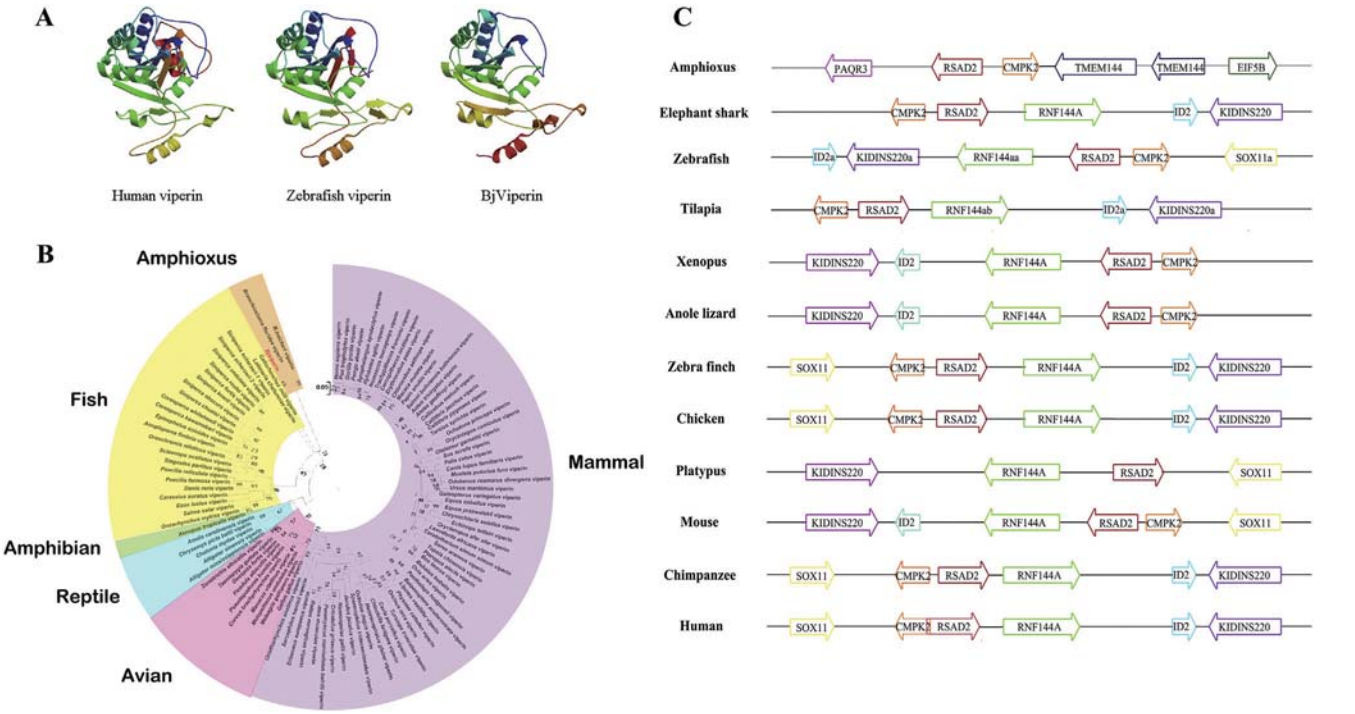

Fig. 1. Molecular modeling, phylogenetic tree and synteny. (A) Molecular model of BjVip predicted by fully-automated protein structure homology modeling. (B) Phylogenetic tree of viperin proteins constructed in the JTT model of MEGA 6.0 using the amino acid-based maximum likelihood (ML) algorithm. The reliability of each node was estimated by bootstrapping with 1000 replications. Accession numbers for sequences used are listed in Supplementary S3. (C) Syntenic analysis of viperin homologues of human, chimpanzee, mouse, platypus, chicken, zebra finch, anole lizard, frog, zebrafish, tilapia, elephant shark and Florida amphioxus. Abbrevation: PAQR3, progestin and adipoQ receptor family member 3-like; RSAD2, radical S-adenosyl methionine domain containing 2, viperin; CMPK2, cytidine monophosphate (UMP-CMP) kinase 2; TMEM144, transmembrane protein 144; EIF5B, eukaryotic translation initiation factor 5B; SOX11, SRY (sex determining region Y)-box11; SOX11a, SRY-box containing gene 11a; RNF144 A, ring finger protein 144 A; RNF144aa, ring finger protein 144aa; RNF144 ab, ring finger protein 144 ab; Kidins220, kinase D-interacting substrate, 220 kDa; Kidins220a, kinase D-interacting substrate of 220a; ID2, inhibitor of DNA binding 2, dominant negative helix-loop-helix protein, ID2a, inhibitor of DNA binding 2, dominant negative helix-loop-helix protein, a; DCDC2C, doublecortin domain containing 2C. Arrows show the direction of transcription of genes.

revealed that seven codon sites (sites 14 A, 20 T, 25 T, 26I, 28 S, 29 V and 31 P) were detected to evolve under positive selection (Supplementary S5). These seven positive selective sites were all located at the N-terminal amphipathic α-helix domain. The site 28 S was detected to evolve under strong positive selection with posterior probabilities ≥0.95. To test whether there was positive selection among different branches, branch-specific model test was performed. LRT from comparison of the free-ratio model with the one-ratio model ($P = 4.734 \times 10^{-5}$) showed that ω ratios were variable among lineages. Totally, three branches with $\omega > 1$ suggested positive selection during evolution (Fig. 2B), but the comparison of the two-ratio model with the one-ratio model revealed all branches with $P > 0.05$, indicating that there were no positive selection among branches.

3.3. Expression of Bjvip in normal and poly I:C-challenged tissues

qRT-PCR was used to examine the relative expression levels of *Bjvip* in the normal and poly I:C-challenged tissues of amphioxus. The dissociation curve of amplification product showed a single peak, indicating that the amplification was specific (Data not shown). As shown in Fig. 3A, *Bjvip* was predominantly expressed in the hepatic cecum, hind-gut, gill and muscle, and at a lower level in the ovary, testis and notochord, indicating that *Bjvip* is expressed in a tissue-specific fashion. Challenge with poly I:C resulted in a significantly enhanced expression of *Bjvip* in all the tissues tested, including the hepatic cecum, hind-gut, gill and muscle (Fig. 3B–E), implicating that the expression of *Bjvip* is subjected to the stimulation of the viral mimic poly I:C.

3.4. Antiviral activity of BjVip in cell culture

To examine the potential effect of BjVip on viral infection, the FG cells were transfected with the plasmids pcDNA3.1/GFP/*Bjvip* and pcDNA3.1/GFP (as negative control). As shown in Fig. 4A, BjVip was produced in the transfected cells. The cells were then infected with LCDV, and the relative amount of LCDV in the cells was determined by qRT-PCR at 24, 48 and 72 h. Compared with control group, the relative amount of LCDV in the cells transfected with pcDNA3.1/GFP/*Bjvip* plasmid was significantly lowered at 48 and 72 h post infection (Fig. 4C), suggesting that BjVip is capable of either killing LCDV or inhibiting its propagation.

3.5. Antiviral activity of rBjVip in shrimp

Recombinant BjVip (rBjVip) with the His tag expressed in *E. coli* was purified by chromatography on a Ni-NTA resin column. The rBjVip obtained was analyzed by SDS-PAGE, which yielded a single band of approximately 45 kDa (Fig. 5A), well matching the expected sizes (43.5 kDa calculated by Editseq). Western blotting showed that rBjVip reacted with rabbit anti-His tag antibody, indicating that it was correctly expressed (Fig. 5A).

Pilot experiments showed that no WSSV was detected in the hepatopancreas and muscles of the shrimps used in the experiments (Data not shown). The shrimps were injected intraperitoneally with Tris-NaCl alone or WSSV in Tris-NaCl or WSSV that had been co-incubated with rBjVip, and then the relative quantities of WSSV in the hepatopancreas and muscles were measured by qRT-PCR. No positive signals were detected in the hepatopancreas and

Gene 575 (2016) 429–437

Contents lists available at ScienceDirect

Gene

journal homepage: www.elsevier.com/locate/gene

Research paper

Identification and biochemical characterization of polyamine oxidases in amphioxus: Implications for emergence of vertebrate-specific spermine and acetylpolyamine oxidases

Huihui Wang [1], Baobao Liu [1], Hongyan Li *, Shicui Zhang **

[a] Laboratory for Evolution & Development, Institute of Evolution & Marine Biodiversity, Ocean University of China, Qingdao 266003, China
[b] Department of Marine Biology, Ocean University of China, Qingdao 266003, China

ARTICLE INFO

Article history:
Received 12 March 2015
Received in revised form 6 August 2015
Accepted 8 September 2015
Available online 12 September 2015

Keywords:
Amphioxus
Branchiostoma
Polyamine oxidase
Spermine oxidase
Acetylpolyamine oxidase

ABSTRACT

Polyamine oxidases (PAOs) have been identified in a wide variety of animals, as well as in fungi and plant. Generally, plant PAOs oxidize spermine (Spm), spermidine (Spd) and their acetylated derivatives, N^1-acetylspermine (N^1-Aspm) and N^1-acetylspermidine (N^1-Aspd), while yeast PAOs oxidize Spm, N^1-Aspm and N^1-Aspd, but not Spd. By contrast, two different enzymes, namely spermine oxidase (SMO) and acetylpolyamine oxidase (APAO), specifically catalyze the oxidation of Spm and N^1-Aspm/N^1-Aspd, respectively. However, our knowledge on the biochemical and structural characterization of PAOs remains rather limited, and their evolutionary history is still enigmatic. In this study, two amphioxus (*Branchiostoma japonicum*) PAO genes, named *Bjpao1* and *Bjpao2*, were cloned and characterized. Both *Bjpao1* and *Bjpao2* displayed distinct tissue-specific expression patterns. Notably, rBjPAO1 oxidized both spermine and spermidine, but not N^1-acetylspermine, whereas rBjPAO2 oxidizes both spermidine and N^1-acetylspermine, but not spermine. To understand structure-function relationship, the enzymatic activities of mutant BjPAOs that were generated by site-directed mutagenesis and expressed in *E. coli* were examined, The results indicate that the residues H64, K301 and T460 in rBjPAO1, and H69, K315 and T467 in rBjPAO2 were all involved in substrate binding and enzyme catalytic activity to some extent. Based on our results and those of others, a model depicting the divergent evolution and functional specialization of vertebrate SMO and APAO genes is proposed.

1. Introduction

Polyamines (PAs), occurring most often in nature as spermine (Spm), spermidine (Spd) and putrescine (Put), are polybasic hydrocarbon chain molecules found in all cells across all kingdoms. PAs are involved in many biological processes, including cell growth, differentiation and apoptosis, via reversible electrostatic interaction with acidic molecules (e.g. DNA, RNA, nucleotides and proteins) through their strong polybasic character, affecting nucleic acid and protein synthesis, gene expression, protein function and regulation of ion channels (Tavladoraki et al., 2011; Polticelli et al., 2012). Maintenance of homeostasis of PAs in cells is necessary for these processes, but excess PAs can be toxic (Toninello et al., 2004; Amendola et al., 2009; Pegg, 2013), and thus have to be catabolized. The PA-catabolizing enzymes are known as polyamine oxidases (PAOs), which are flavin adenine dinucleotide (FAD)-containing enzymes capable of catalyzing the oxidation of PAs.

The substrate specificity of PAOs depends upon the source of the enzymes. Generally, plant PAOs oxidize Spm, Spd and their acetylated derivatives, N^1-Aspm and N^1-Aspd (Fincato et al., 2011), while yeast PAOs oxidize Spm, N^1-Aspm and N^1-Aspd, but not Spd (Landry and Sternglanz, 2003; Huang et al., 2005). Recently, the recombinant Pacific oyster PAO, the first one reported in invertebrates, is shown to be able to oxidize both Spm and N^1-Aspm, albeit with different efficiency (Cervelli et al., 2015). By contrast, two specialized PAO subfamilies, spermine oxidase (SMO; EC 1.5.3.16) and N^1-acetylpolyamine oxidase (APAO; EC 1.5.3.11) are identified in vertebrates (Polticelli et al., 2012). SMO catalyzes the oxidation of Spm, whereas APAO catalyzes the oxidation of N^1-Aspm and N^1-Aspd (Polticelli et al., 2012). Despite these enormous

Abbreviations: APAO, N^1-acetylpolyamine oxidase; DNA, deoxyribonucleic acid; DTT, dithiothreitol; FAD, flavin adenine dinucleotide; h, hour; HRP, horseradish peroxidase; IPTG, isopropyl β-D-thiogalactoside; KDa, kilodalton(s); LB, Luria–Bertani (medium); M, mole per liter; MDL 72,527, N^1, N^4-bis (2, 3-butadienyl)-1, 4-butanediamine; Min, minute; N^1-Aspm, N^1-acetylspermine; N^1-Aspd, N^1-acetylspermidine; ORF, open reading frame; PAO, polyamine oxidase; PAGE, PA-gel electrophoresis; PBS, phosphate-buffered saline; PCR, polymerase chain reaction; pH, potential of hydrogen; Put, putrescine; pI, isoelectric point; qRT, PCR-quantitative real-time PCR; RACE, rapid-amplification of cDNA ends; RNA, ribonucleic acid; s, second; SMO, spermine oxidase; Spd, spermidine; Spm, spermine; SDS, sodium dodecyl sulfate; Tris, tris (hydroxymethyl) aminomethane.

* Correspondence to: H. Li, Room 211, Ke Xue Guan, 5 Yushan Road, Ocean University of China, Qingdao 266003, China.
** Correspondence to: S. Zhang, Room 205, Ke Xue Guan, 5 Yushan Road, Ocean University of China, Qingdao 266003, China.
E-mail addresses: hongyanli@ouc.edu.cn (H. Li), sczhang@ouc.edu.cn (S. Zhang).
[1] These authors contributed equally to this work.

http://dx.doi.org/10.1016/j.gene.2015.09.017
0378-1119/

progresses, however, our knowledge on the biochemical and structural characterization of metazoan PAOs is still rather limited.

Members of PAO gene family have been identified from a variety of animals, including vertebrates, arthropodes, mollusks, nematodes and placozoa, as well as from fungi and plants (Polticelli et al., 2012). Notably, the presence of two related PAOs has been found in all the vertebrates and the cephalochordate amphioxus, but only a single copy of PAO gene been documented thus far in the invertebrates, including urochordates. Collectively, these suggest that a duplication event of an ancestral PAO-like gene resulted in the emergence of SMO and APAO in the vertebrates (Polticelli et al., 2012; Cervelli et al., 2015). However, the molecular process leading to the functional specialization of the ancestral gene remains largely elusive.

Amphioxus, a cephalochordate, has a vertebrate-like body plan including dorsal neural tube, notochord, segmented somites and pharyngeal gill slits, but it is less complex than vertebrates, having a genome uncomplicated by extensive genomic duplication (Putnam et al., 2008). It represents a close relative to vertebrates, which is the best available stand-in for the proximate invertebrate ancestor of vertebrates, and thus an ideal model organism for gaining insights into origin and evolution of vertebrates (Zhang et al., 2010). However, biochemical characterization of PAOs is still lacking in this evolutionarily important animal. The aims of this study are therefore to clone the PAO genes from the amphioxus *Branchiostoma japonicum*, named *Bjpao1* and *Bjpao2*, to analyze their expression patterns, and to examine their enzymatic activities and structure-function relation. This will certainly deepen our understanding of the molecular process leading to the emergence of SMO and APAO during vertebrate evolution.

2. Materials and methods

2.1. Cloning and sequencing of Bjpao cDNAs

Total RNAs were extracted with TRIzol (TaKaRa, Dalian, China) from adult *B. japonicum* collected during the breeding season (mid-June to mid-July) in the vicinity of Qingdao, China, and digested with RNase-free DNase (TaKaRa) to eliminate the genomic contamination. The first-strand cDNA was synthesized with reverse transcription system (TaKaRa) using oligo d(T) primer. To amplify the complete cDNA fragments of *Bjpao1*, polymerase chain reaction (PCR) was performed using the first-strand cDNA as template, in a volume of 20 μl PCR mixture containing 1× PCR buffer, 0.5 unit of Ex Taq DNA polymerase (TaKaRa) and 0.4 μM of the PAO gene-specific primers P1 and P2 (Table 1), which were designed on the basis of the putative PAO sequence found in the Florida amphioxus *B. floridae* genome database (http://genome.jgi-psf.org//Brafl1/Brafl1.home.html). PCR was carried out at 94 °C for 5 min, followed by 34 cycles at 94 °C for 30 s, 60 °C for 30 s, 72 °C for 1 min 30 s, and a final extension step at 72 °C for 7 min. To amplify the initial fragment of *Bjpao2*, the primers P17 and P18 (Table 1) were designed on the basis of the putative PAO sequence found in *B. floridae* genome database and PCR was performed as follows: 1 cycle of 94 °C for 5 min, 30 cycles of 94 °C for 30 s, 58 °C for 30 s, and 72 °C for 40 s, followed by the final extension at 72 °C for 7 min. To get the full-length cDNA sequence, both 5′ RACE and 3′ RACE were performed using the gene-specific primers P19 and P21, and the gene-specific nested primers P20 and P22 (Table 1), respectively. The P19 and P21 as well as P20 and P22 were designed according to the initial region

Table 1
Sequences of the primers used in this study.

Primers	Sequence (5′-3′)	Sequence information
Primers for Bjpao1		
P1 (sense)	ATGACAACAGGGAGACCCCAGAT	Primer for *Bjpao1* cDNA
P2 (antisense)	TTACATTTTATACAAGTCTATAAGTCTAGAAGC	Primer for *Bjpao1* cDNA
P3 (sense)	TTCCAGCCTTCATTCCTCG	Primer for qRT-PCR
P4 (antisense)	CGGTGTTGGCGTACAGGTC	Primer for qRT-PCR
P5 (sense)	TTCCAGCCTTCATTCCTCG	Primer for qRT-PCR
P6 (antisense)	CGGTGTTGGCGTACAGGTC	Primer for qRT-PCR
P7 (sense)	CGGAATTCATGACAACAGGGAGACC	Primer for expression
P8 (antisense)	CCGCTCGAGTTACATTTTATACAAGTCT	Primer for expression
P9 (sense)	GCTC***CAA***GGCAACAAGGACAAC	Primer for mutation (H64Q)
P10 (sense)	GCTC***GAA***GGCAACAAGGACAAC	Primer for mutation (H64E)
P11(antisense)	CAGGTTGTCCCTAACTCAAGGTTGT	Primer for mutation (H64Q, H64E)
P12(sense)	GTTGAC***ATG***ATTTTTCTGAGATTTC	Primer for mutation (K301M)
P13(antisense)	AGTTCCGAAACCAAGACTACTTATT	Primer for mutation (K301M)
P14 (sense)	AACACCCTACATCACC***TAT***ACACAT	Primer for mutation (T460Y)
P15 (sense)	AACACCCTACATCACC***AGT***ACACAT	Primer for mutation (T460S)
P16(antisense)	ATAGTAGCCTCTCCTGCAAACAGC	Primer for mutation (T460Y, T460S)
Primers for Bjpao2		
P17 (sense)	GATGAGGTGAAGCCTGACGACT	Primer for *Bjpao2* initial region
P18 (antisense)	TGTGGTCGCCTTCAAGTTCAT	Primer for *Bjpao2* initial region
P19(antisense)	CAGAGGAGGCTGGAACAGAGTC	5′ RACE GSP PCR
P20 (antisense)	AGCAATACAGTCTGGAGGAATGG	5′ RACE GSP nested PCR
P21 (sense)	GAGGATGGGGTTTGGTGTAGTC	3′ RACE GSP PCR
P22 (sense)	GGACCAAGACCATAGCAACAGC	3′ RACE GSP nested PCR
P23 (sense)	TACATGGAAACGCTGAGTGAAGAGG	Primer for qRT-PCR
P24 (antisense)	TAAAAGAGTAGGAGCCGCAGGTC	Primer for qRT-PCR
P25 (sense)	CGGAATTCATGGCTTCCACGGGTCTG	Primer for expression
P26 (antisense)	CCGCTCGAGTCATGCTTACTAGCATACAGGTTA	Primer for expression
P27 (sense)	GATC***CAA***GGTACCATTGGGAAC	Primer for mutation (H69Q)
P28 (antisense)	CAGTTGGCACCAAACTCTAGAGTGTCTG	Primer for mutation (H69Q)
P29 (sense)	GATC***GAA***GGTACCATTGGGAACCC	Primer for mutation (H69E)
P30 (antisense)	CAGTTGGCACCAAACTCTAGAGTGTCTG	Primer for mutation (H69E)
P31 (sense)	GTCAAC***ATG***ATCTTCCTCACCTTCGAGC	Primer for mutation (K315M)
P32 (antisense)	TACACCAAACCCCATCCTCTCTATA	Primer for mutation (K315M)
P33 (sense)	CAGTGAGTTTTTCTCC***TAT***GTCCAT	Primer for mutation (T467Y)
P34 (antisense)	TGAGTGGCCTCCCCTGCAAACTGC	Primer for mutation (T467Y)
P35 (sense)	CAGTGAGTTTTTCTCC***AGT***GTCCAT	Primer for mutation (T467S)
P36 (antisense)	TGAGTGGCCTCCCCTGCAAACTGC	Primer for mutation (T467S)

Gene 574 (2015) 69–75

Contents lists available at ScienceDirect

Gene

journal homepage: www.elsevier.com/locate/gene

Research paper

Identification and expression of *lypc*, a novel dark-inducible member of Ly6 superfamily in zebrafish *Danio rerio*

Lingyi Li [a,b], Dongrui Ji [a,b], Lei Teng [c], Shicui Zhang [a,b], Hongyan Li [a,b,*]

[a] Institute of Evolution & Marine Biodiversity, Qingdao 266003, China
[b] Laboratory for Evolution & Development, Department of Marine Biology, Ocean University of China, Qingdao 266003, China
[c] Department of Biology, Medical College of Qingdao University, Qingdao 266071, China

ARTICLE INFO

Article history:
Received 14 November 2014
Received in revised form 26 June 2015
Accepted 28 July 2015
Available online 13 August 2015

Keywords:
Ly6 superfamily
Zebrafish
Pigment cells
lypc

ABSTRACT

Snake venom neurotoxins and lymphocyte antigen-6 (Ly6) family members identified in many metazoans possess conserved LU domain containing eight or ten conserved cysteine residues which form 4 to 5 conserved disulfide bonds. They are found to execute a wide variety of biological effects, but information regarding Ly6 superfamily in zebrafish remains rather limited. Here we identified a novel Ly6 gene located on the chromosome 15 in zebrafish, and named it *lypc* highlighting its predominant expression in the pigment cells. Both homology modeling and sequence comparison revealed that *lypc* has features typical of Ly6 family members. Whole mount *in situ* hybridization showed that *lypc* was expressed in the trunk pigment cells and retinal pigment cells. Moreover, real-time quantitative PCR demonstrated that the expression of *lypc* was subjected to diurnal variation regulation, i.e. the expression of *lypc* displays a clear rhythmic pattern, and dark exposure apparently stimulated its expression. Collectively, these data indicate that *lypc* is a novel dark-inducible Ly6 member with a predominant expression in the pigment cells of zebrafish, laying a foundation for further elucidation of its functions.

1. Introduction

The proteins of lymphocyte antigen 6 (Ly6) superfamily members, which are present in many metazoans, possess a conserved LU domain with 8 or 10 cysteine residues, forming 4 to 5 conserved disulfide bonds. Many members of Ly6 superfamily are glycosylphosphatidylinositol (GPI)-anchored cell surface proteins (Mallya et al., 2006) and implicated in a variety of biological processes. For example, human GPI-anchored CD59 not only protects host cells from complement-induced lysis but also binds to CD2, transducing activation signals within T cells (Deckert et al., 1995); murine Lynx protein dampens the activity of cholinergic system through direct interaction with nicotinic receptors (Kobayashi et al., 2014); zebrafish GPI-anchored Lypd6 physically interacts with the Wnt receptor Frizzled8 and the coreceptor Lrp6 (Ozhan et al., 2013); and the fruitfly protein encoded by *Boudin* (*bou*) is essential for tracheal morphogenesis in the embryo and contributes to the maintenance of the paracellular barrier and the organization of the septate junctions (Hijazi et al., 2009). Members of Ly6 superfamily, like the secreted Ly6/urokinase-type plasminogen activator receptor (uPAR)-related protein-1 (SLURP1) which is highly expressed in human cornea, are also present in secreted forms. SLURP1 is associated with the hyperkeratotic disorder Mal-de-Meleda and is able to modulate corneal homeostasis by serving as a soluble scavenger of uPA as well as regulating the uPA-dependent functions of uPAR (Swamynathan and Swamynathan, 2014). Moreover, SLURP1 is found to be a marker of cell differentiation, predominantly expressed in the granular layer of skin, notably in the acrosyringium (Favre et al., 2007). Despite the extensive studies on the members of Ly6 superfamily, functional identification of Ly6 family genes remains in infancy.

Zebrafish is a widely used model organism, and its embryogenesis and development (Kimmel et al., 1995) have been extensively studied. We have identified 20 uncharacterized LU domain-containing genes in zebrafish (Ji et al., 2012). Among them, one gene is found to be homologous to the Ly6/Neurotoxin superfamily and is expressed in the pigment cells in a tissue-specific manner (see below), and thus designated *lypc*. To our best knowledge, little information is available regarding *lypc* to date. Therefore, the aims of this study are to examine the expression profile of *lypc* and to explore its expression regulation during the embryonic development of zebrafish.

2. Materials and methods

2.1. Fish maintenance

Wild type zebrafish strain AB and the adult *casper* mutant line (White et al., 2008) were bred and maintained in salinity-controlled

Abbreviations: LU, domain Ly6 antigen/uPA receptor-like domain; *lypc*, Ly6 expressed in pigment cells; qRT-PCR, quantitative real-time polymerase chain reaction; BLAST, basic local alignment search tool; DIG, digoxigenin.

* Corresponding author at: Room 301, Darwin Building, Ocean University of China, 5 Yushan Road, Qingdao 266003, China.
E-mail address: hongyanli@ouc.edu.cn (H. Li).

http://dx.doi.org/10.1016/j.gene.2015.07.088
0378-1119/

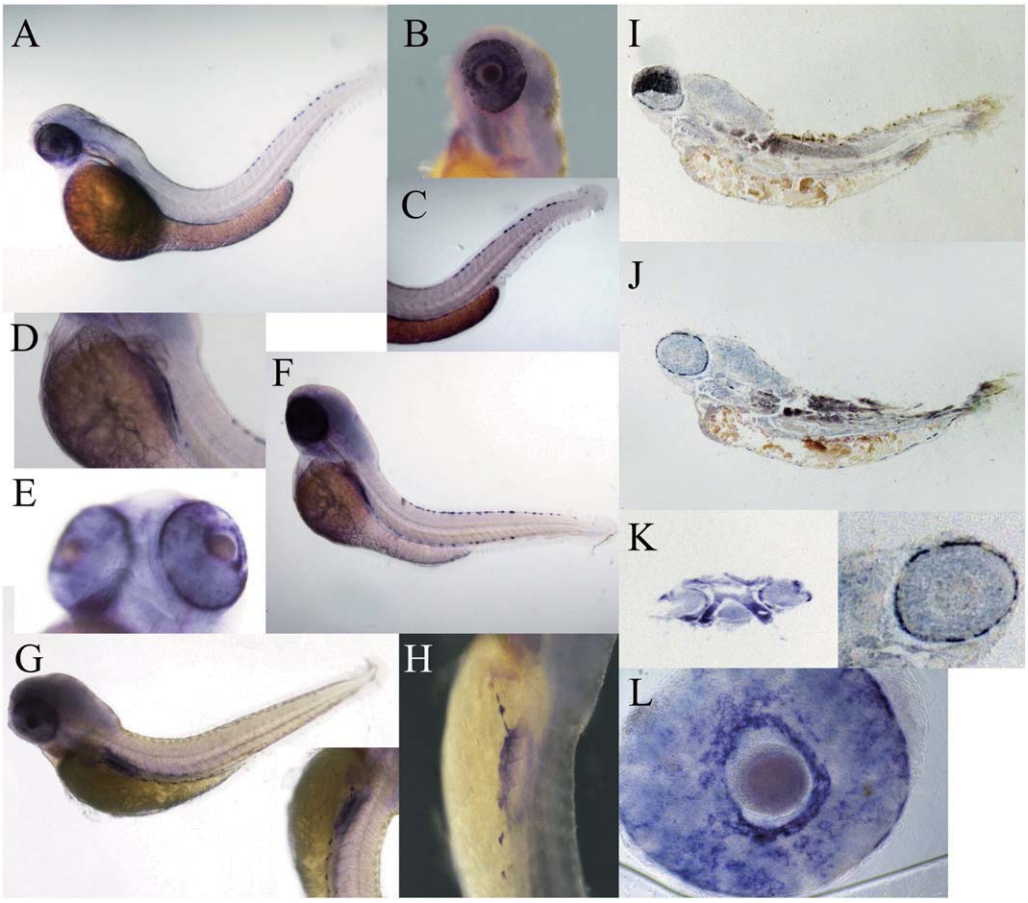

Fig. 3. The expression pattern of *lypc* in early development: (A): Long-pec embryo (48 hpf), pigment cells reach terminal differentiation along dorsal strip (arrows) (B): pigment cells in the retina of embryo (48 hpf) (C): pigment cells in tail (48 hpf). (D–F): By 72 h, *lypc* strongly expresses on ventral side of yolk sac. *Lypc* positive cells have organized along the dorsal, ventral and yolk stripes. Red arrow: dorsal stripe, ventral yolk stripes (G–H). Lateral view of larva of 96 hpf. The expression pattern of *lypc* was mainly restricted to the ventral yolk stripes. (I–J) The longitudinal section embryos at 72 hpf after in situ hybridization (K) is showing the traverse section of embryo at 72 hpf. Strong signal in epidermal cells in the trunk and tail reveals that *lypc* expresses in pigment cells. (L) The retina of zebrafish embryo at 72 hpf.

predominantly expressed in the dorsal and ventral pigment cells close to the urogenital pore (Fig. 3J) and the retinal pigment epithelium (RPE) cells (Fig. 3K), but little in the deep cells. Histological examination of 4-day-old larvae further revealed that *lypc* was expressed in the retinal pigment epithelium beyond the retinal outer nuclear layer (ONL; Fig. 4A–C). No signal was detected using sense riboprobe (Data not shown.). *mitfa* was expressed in melanocyte of both neural crest and optic cup pigmented epithelial cell, and in 20–25 somites to Prim-5, it was expressed in neural crest cells migrating in lateral pathway, trunk anterior region, trunk melanoblast (Thisse et al., 2004). The expression of *lypc* only partially overlaped with that of *mitfa*.

To pinpoint the pigment cell type in which *lypc* is expressed in the trunk, we investigated the expression pattern of *lypc* in the pigment cells of mutant *casper*, which is a *roy*, *mitfa* (*nacre*) double homozygous mutant with a transparent body due to loss of melanocytes and iridopore from 1-cell to adult and normal retinal pigment cells (White et al., 2008). It was found that the expression of *lypc* in the trunk disappeared in *casper* mutant compared to wild type (Fig. 5). This further proved that *lypc* is indeed expressed in the pigment cells, probably in the melanocytes and iridophores.

3.3. Lypc is rhythmically expressed in zebrafish

It has been shown that most genes expressed in the pigment cells are involved in the circadian clock (Li et al., 2013). We thus wonder if the expression of *lypc* is regulated by the environmental light–dark (LD) cycle. The results showed that *Lypc* mRNA levels increased steadily in the larvae aged 24 to 72 hpf. The first peak of *lypc* expression was observed at ZT21 (zeitgeber time 21) in the second day post fertilization (dpf). In the following days, the amplitude of this rhythm became stronger, with lower expression at zeitgeber time ZT0, which refers to the light time of the day, and second peak expression at ZT 21, which corresponds to the dark time of the day (Fig. 6). It has been shown that *mitfa* shows strong circadian rhythm expression and is dark induced, while the expression of *nfil3-5* (Li et al., 2013), a light-induced gene, is repressed during the dark period, but increased in the light period and reached peak level after lights-off (Li et al., 2013). In our study, *mitfa* and *nfil3-5* exhibited the same expression pattern as reported before, and notably, the expression of *lypc* was reduced in the light environment and elevated in dark place, which is similar to that of *mitfa* (Fig. 6). These data suggest that *lypc* is a circadian clock gene, and subjected to regulation by light–dark cycle with the darkness exerting a profound effect on its expression.

4. Discussion

A great number of Ly6 superfamily members have been identified to date in various species (Gumley et al., 1995; Galat, 2008; Hijazi et al., 2009). We have predicted the presence of about 20 putative LU domain

Funct Integr Genomics (2015) 15:577–585
DOI 10.1007/s10142-015-0449-9

ORIGINAL PAPER

Identification and expression of an uncharacterized Ly-6 gene cluster in zebrafish *Danio rerio*

Quanyang Guo[1,2] · **Dongrui Ji**[1,2] · **Man Wang**[1,2] · **Shicui Zhang**[1,2] · **Hongyan Li**[1,2]

Received: 31 December 2014 / Revised: 7 June 2015 / Accepted: 16 June 2015 / Published online: 26 June 2015

Abstract The Ly-6/uPAR/CD59/neurotoxin superfamily (Ly-6SF) identified in most metazoan has been shown to play important roles in different biological processes including immunity, cellular adhesion, and cell signaling. Members of this superfamily contain one or more conserved domains known as Ly-6/uPAR (LU) domain, which harbors 8 or 10 conserved cysteine residues forming 4–5 disulfide bonds. In this study, we reported the identification of a novel zebrafish *Ly-6* gene cluster on chromosome 21, which consists of seven genes *ly21.1*, *ly21.2*, *ly21.3*, *ly21.4*, *ly21.5*, *ly21.6*, and *ly21.7* and their spatiotemporal expression pattern during development. All the seven genes possess features typical of the *Ly-6/neurotoxin* superfamily, and phylogenetic analysis shows that these genes form a single cluster branching form other members of Ly-6 family, suggesting that the seven genes evolved by an event of intra-chromosome gene duplication. However, deduced Ly21.1-7 proteins share little homology with Ly-6 family proteins from other species, no orthologs are identified in vertebrates, including teleosts, hinting that *ly21.1-7* genes are evolutionarily a novel addition to zebrafish. Expression analyses show that maternal mRNAs of *ly21.1-7* genes are detected during early developmental stages, but later in development, they exhibit tissue-specific expression. Except for *ly21.2* which is expressed in the skin ionocytes, all the remaining six genes are mainly expressed in the developing brain.

Keywords *Ly-6* superfamily · Zebrafish · Gene cluster · Expression pattern

Introduction

Lymphocyte antigen-6 (Ly-6) proteins are characterized by a conserved Ly-6/uPAR (LU) domain initially identified in the sea-snake erabutoxin b by Tsernoglou and Petsko (1977), which is approximately 70 to 100 amino acids long, and possesses 8 to 10 highly conserved cysteine residues (Cys) in stereotyped positions that form a defined disulfide-bonding pattern (Galat 2008). Almost all *Ly-6* family members have an N-terminal signal peptide sequence. They are divided into two broad categories based on whether a C-terminal glycophosphatidyl inositol (GPI)-anchored sequence exists or not. The first family comprises secreted proteins, such as snake neurotoxin, SLURP-1, and rat-secreted urine protein (Fleming et al. 1993; Adermann et al. 1999; Southan et al. 2002), while the second family consists of GPI-anchored proteins, tethered to the membrane by GPI signal, including CD59, Lynx1, and uPAR (Davies et al. 1989; Miwa et al. 1999; Blasi and Carmeliet 2002).

A great number of *Ly-6* superfamily members have been identified to date in a variety of species such as fruit-fly and mammals (Gumley et al. 1995; Galat 2008; Hijazi et al. 2009). A total of 45 members of the *Ly-6* superfamily,

Electronic supplementary material The online version of this article (doi:10.1007/s10142-015-0449-9) contains supplementary material, which is available to authorized users.

✉ Hongyan Li
hongyanli@ouc.edu.cn

[1] Institute of Evolution & Marine Biodiversity, Ocean University of China, Room 301, Darwin Building, Qingdao 266003, China

[2] Laboratory for Evolution & Development, Department of Marine Biology, Ocean University of China, 5 Yushan Road, Qingdao 266003, China

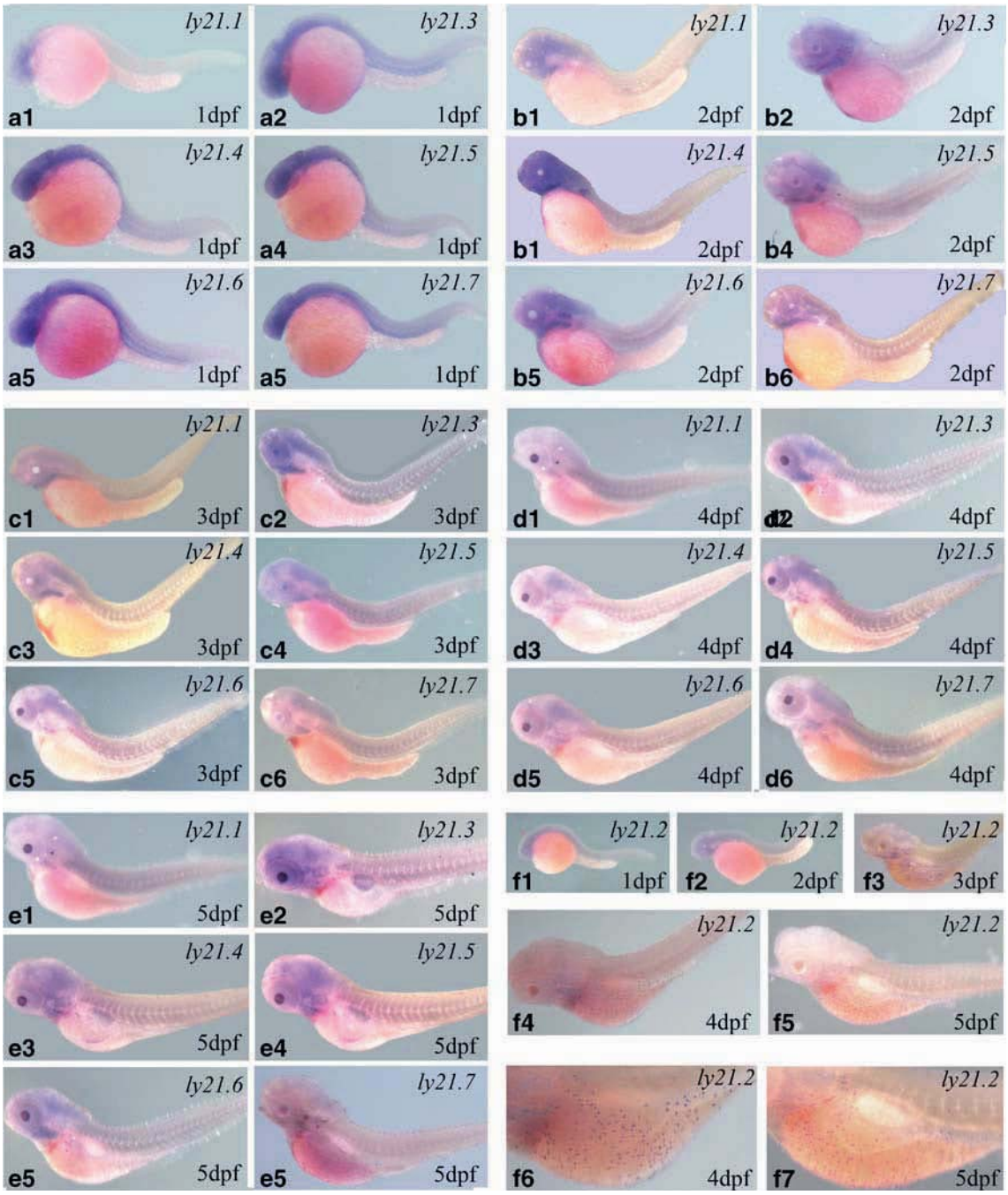

Fig. 4 Expression pattern of *ly21.1-7* in the zebrafish at 1–5 dpf by whole mount in situ hybridization. The probes used for in situ hybridization are listed in the *upper right corner of each panel*. Developmental stages are indicated in the *lower right corners*. **a1**–**f7** are lateral view with anterior to the left. **a1**–**e6** The six genes except for *ly21.2* expressed mainly in the developing brain. **f1**–**f5** *ly21.2* gene expression in the skin of the yolk sac from 3 to 5 dpf. **f6**–**f7** High magnification views of **f4** and **f5** respectively

events from other branches of teleosts (van der Aa et al. 2009), providing a support to the notion that the genes encoding a Ly-6 motif are prone to sudden phases of extensive duplication and diversification in different phylogenetic groups (Galat 2008; Hijazi et al. 2009; Bamezai 2004).

Maternal mRNAs of *ly21.1-7* genes are detected during early developmental stages, but later in development, they clearly show tissue-specific expression. Except for *ly21.2*, all the remaining six genes are mainly expressed in the developing brain. Among them, four genes *ly21.4*, *ly21.5*, *ly21.6*, and *ly21.7* are expressed specially in brain ventricular zone. It has been known that many members of Ly-6 superfamily genes are expressed in the developing and/or adult nervous system and always detected in both distinct and common neuronal populations, suggesting a specific function of Ly-6 members in the development/differentiation of nervous system (Heintz 2004;

Dev Genes Evol (2015) 225:47–53
DOI 10.1007/s00427-015-0487-2

SHORT COMMUNICATION

Identification of a Ly-6 superfamily gene expressed in lateral line neuromasts in zebrafish

Dongrui Ji · Lingyi Li · Shicui Zhang · Hongyan Li

Received: 14 June 2014 / Accepted: 5 January 2015 / Published online: 14 January 2015

Abstract Lymphocyte antigen-6 (Ly-6) superfamily members have been identified in zebrafish, but the expression and function of these Ly-6 genes remain largely unknown. Posterior lateral line (pLL) system is produced by migrating pLL primordium (pLLp). Chemokine signaling, Notch, Wnt, and fibroblast growth factor (FGF) signaling regulate migration of pLLp cells and formation of neuromasts. However, the mechanism of neuromast deposition remains to be explored. Identification of novel genes expressed in pLLp will certainly help the study of such a process. Here we identified a Ly-6 gene called *neuromast-expressed gpi-anchored lymphocyte antigen-6* (*negaly6*), which was specifically expressed in neuromast. Quantitative real-time PCR (qRT-PCR) analysis showed that *negaly6* started to be expressed at 24 hpf, and whole-mount in situ hybridization analysis indicated that *negaly6* was highly expressed in the trailing zone of pLLp and mature neuromast. Furthermore, *negaly6* expression was inhibited by FGF signaling antagonist but not by Wnt signaling agonist or antagonist. Collectively, these data indicate that *negaly6* may be associated with the regulation of neuromast deposition via FGF signaling pathway.

Keywords Lateral line · Ly-6 · Neuromast · Zebrafish

Communicated by: Matthias Hammerschmidt

D. Ji · L. Li · S. Zhang · H. Li
Institute of Evolution & Marine Biodiversity, Ocean University of China, Qingdao 266003, China

D. Ji · L. Li · S. Zhang · H. Li (✉)
Laboratory for Evolution & Development, Department of Marine Biology, Ocean University of China, Room 301, 5 Yushan Road, Qingdao 266003, China
e-mail: hongyanli@ouc.edu.cn

Introduction

The lateral line of fish is a sensory system that responds to surrounding water displacement and senses water electrical currents. The presence of lateral line system can help fish to achieve important behaviors such as schooling, prey capture, or predator escape. The lateral line consists of a set of sensory organs called neuromast, which comprises mechanosensory hair cells in the center, surrounded by supporting cells and mantle cells (Ghysen and Dambly-Chaudière 2004). Lateral line system comprises two branches, the neuromasts on the head forming the anterior lateral line system (aLL) and the neuromasts on the trunk and tail forming the posterior lateral line system (pLL). pLL is produced by the pLL primordium (pLLp) which is first identified as a group of cells located posterior to the otic vesicle. Neuromast precursors (protoneuromasts) are formed by the migrating pLL primordium and deposited subsequently on the trunk and tail along with pLLp migration (Nechiporuk and Raible 2008).

It has been shown that pLLp migration is mediated by chemokine signaling. Chemokine receptor *cxcr4b* is expressed in the leading zone of primordium, while the receptor *cxcr7* is expressed in the trailing zone. Sdf1a, the ligand of the CXCR4b and CXCR7 receptor, is expressed along the horizontal myoseptum and guides the primordium migration through the activation of CXCR4b and CXCR7 (David et al. 2002; Haas and Gilmour 2006; Valentin et al. 2007). Wnt/β-catenin signaling controls collective cell migration in the primordium by coordinating the expression of *cxcr4b* and *cxcr7*. In the leading zone of the primordium, Wnt/β-catenin signaling can inhibit the expression of *cxcr7*. In contrast, the expression of *cxcr4b* is inhibited in the trailing zone due to the lack of Wnt/β-catenin signaling (Aman and Piotrowski 2008). However, the mechanism underlying neuromast deposition is not clear; for example, genes expressed in the trailing zone of pLLp and those involved in the

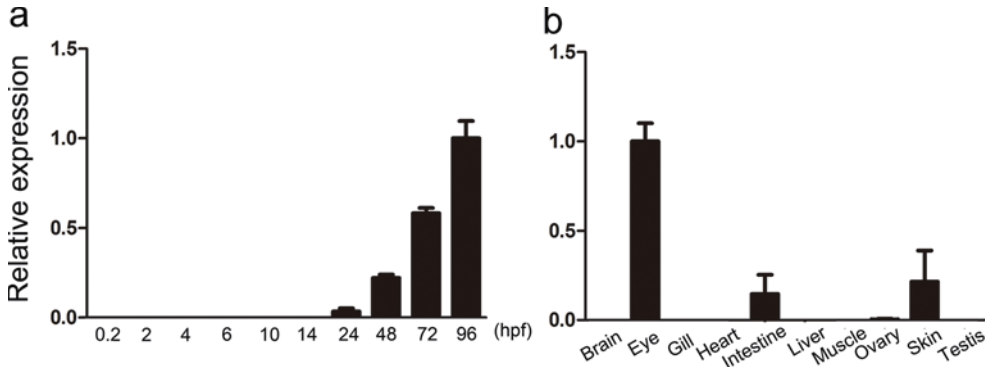

Fig. 3 The relative expression of *negaly6* mRNA in **a** zebrafish early development and **b** adult tissues. *hpf* hour post-fertilization. *β-actin* is used as a reference gene

fixed with 4 % paraformaldehyde overnight at 4 °C. Fixed embryos were rinsed with PBS and infiltrated with 30 % sucrose in PBS and cryosectioned. To label the nuclei of pLLp cells, fixed embryos were stained with SYTOX® green nucleic acid stain (Molecular Probes) for 10 min.

Results and discussion

Molecular characterization of zebrafish Ly-6 member *negaly6*

We have identified about 20 putative LU domain-containing genes which had not been characterized previously (Ji et al. 2012). In this study, we show that one of these Ly-6 genes was expressed in the neuromasts; thus, we designated this Ly-6 gene *neuromast-expressed gpi-anchored lymphocyte antigen-6* (*negaly6*), highlighting its expression in the neuromast.

negaly6 (XP_002664937) is located on the chromosome 16 and codes for a GPI-anchored protein of 211 amino acids including a signal peptide and two LU domains (Fig. 1a). Ly-6 protein usually contains 10 position-specific conserved cysteines, although other amino acid sequences are highly variable (Galat 2008). Alignments of amino acid sequences of LU domains demonstrated that LU domains of Negaly6 have 10 position-specific conserved cysteines (Fig. 1b), which form five disulfide bonds typical of known Ly-6 proteins

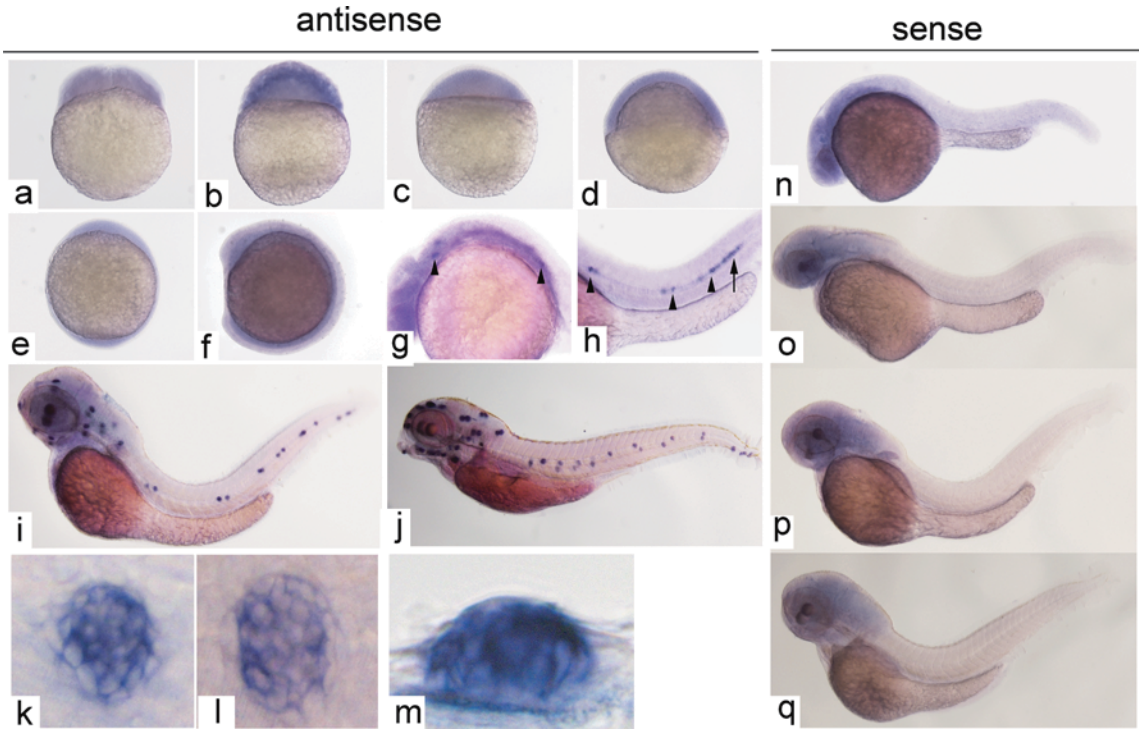

Fig. 4 Expression of *negaly6* during embryonic development detected by WISH. Expression of *negaly6* was not detected before somite stage (**a** 4 cell, **b** 128 cell, **c** 4 hpf, **d** 50 % epiboly, **e** bud, and **f** 10 somites). At 24 hpf (**g**), *negaly6* was expressed in anterior lateral line primordium (aLLp) and posterior lateral line primordium (pLLp) (*black arrowhead*). At 36 hpf (**h**), the expression of *negaly6* appeared in deposited neuromasts (*black arrowhead*) and migrating pLLp (*black arrow*). Expression of *negaly6* in the mature neuromasts in embryos at 2 dpf (**i**, **k**, **m**) and 5 dpf (**j**, **l**). A single neuromast is enlarged in graph k and l; sectioned neuromast is showed in graph m. No signal was detected with sense probe (**n** 24 hpf, **o** 36 hpf, **p** 48 hpf, and **q** 72 hpf)

Developmental and Comparative Immunology 49 (2015) 249–258

Contents lists available at ScienceDirect

Developmental and Comparative Immunology

journal homepage: www.elsevier.com/locate/dci

Molecular cloning, expression, purification and characterization of vitellogenin in scallop *Patinopecten yessoensis* with special emphasis on its antibacterial activity

Biao Wu [a,b], Zhihong Liu [b], Liqing Zhou [b], Guangdong Ji [a,*], Aiguo Yang [b,**]

[a] *Laboratory for Evolution & Development, Institute of Evolution & Marine Biodiversity, Department of Marine Biology, Ocean University of China, Qingdao 266003, China*

[b] *Key Laboratory of Sustainable Development of Marine Fisheries, Ministry of Agriculture, Yellow Sea Fisheries Research Institute, Chinese Academy of Fishery Sciences, Qingdao 266071, China*

ARTICLE INFO

Article history:
Received 1 August 2014
Revised 4 December 2014
Accepted 4 December 2014
Available online 11 December 2014

Keywords:
Scallop
Patinopecten yessoensis
Vitellogenin
Antibacterial activity
Pattern recognition receptor

ABSTRACT

Vitellogenin (Vg), the major precursor of the egg-yolk proteins, has been found to play an immune role in fish and protochordate amphioxus, however, no study on the immune function of Vg in invertebrates has ever been studied before. In this study, the complete cDNA of Vg was identified from the scallop *Patinopecten yessoensis* (termed *PyVg*). The cDNA contained an open reading frame (ORF) of 6888 bp, encoding a polypeptide of 2295 amino acid protein, which had an N-terminal signal peptide followed by the mature Vg. The mature Vg had the domains Vitellogenin_N, domain of unknown function 1943 (DUF1943) and von Willebrand factor type D domain (VWD) as well as the consensus cleavage site (R-X-R/K-R) and conserved motif (KTIGNAG). Tissue distribution assay revealed that *PyVg* transcripts were predominantly present in the ovary and hepatopancreas, and its expression profile in ovary well reflected the annual cycle of vitellogenesis. Interestingly, bacterial challenge caused a significant change in *PyVg* expression, hinting an involvement of PyVg in the acute phase response in *P. yessoensis*. Consistently, recombinant DUF1943 and VWD domains both could interact with LTA and LPS on bacterial wall, and purified native PyVg displayed a broad-spectrum antibacterial activity against both Gram-negative (*Escherichia coli* and *Vibrio anguillarum*) and Gram-positive bacteria (*Staphylococcus aureus*). Overall, these data indicate that Vg is a pattern recognition molecule with bacterial growth-inhibiting activity in the scallop.

1. Introduction

Vitellogenin (Vg), the major precursor of the egg-yolk proteins, is firstly discovered in *Cecropia moth*, which has been shown to be present in all metazoan ranging from the placozoa to the bilateria (Hayward et al., 2010; Matozzo et al., 2008; Zhang et al., 2011). Vg is usually synthesized in extraovarian tissues such as the liver in non-mammalian vertebrates (Anderson and Hinton, 1996), the fat body in insects (Sappington and Raikhel, 1998), and the hepatopancreas in crustaceans (Jeon et al., 2010; Tseng et al., 2001), and the intestine in sea urchin (Shyu et al., 1986), and eventually accumulated in the ovary. The primary function of Vg is to form yolk protein which provides nutrients for the developing embryos and larvae. However, many other biological functions, such as temporal division of labor and foraging specialization, regulation of hormonal dynamics and change in gustatory responsiveness were also reported (Amdam et al., 2003, 2006; Guidugli et al., 2005; Nelson et al., 2007). In particular, Vg has recently been reported to possess a novel function linking with host immune defense in fish (Garcia et al., 2010; Liu et al., 2009; Shi et al., 2006; Zhang et al., 2005). It is shown to play an important immune role as a pattern recognition molecule capable of recognizing bacteria, and an opsonin capable of enhancing macrophage phagocytosis (Li et al., 2008). Moreover, Vg is reported to be directly bactericidal capable of killing *E. coli* and *S. aureus* whole cells via interaction with LPS and LTA existing in the bacterial cell walls, rather than attacking their plasma membranes (Li et al., 2009). It is clear that the immune defense function and mechanism of Vg have been well defined in fish. However, if Vg from invertebrate species is also an immune-competent molecule remains open, although amphioxus Vg has been shown to have hemagglutinating and antibacterial activities (Zhang et al., 2005).

* Corresponding author. Laboratory for Evolution & Development, Institute of Evolution & Marine Biodiversity and Department of Marine Biology, Ocean University of China, Qingdao 266003, China. Tel.: +86 532 82031665; fax: +86 532 82032787.
E-mail address: jamesdong@ouc.edu.cn (G. Ji).
** Corresponding author. Key Laboratory of Sustainable Development of Marine Fisheries, Ministry of Agriculture, Yellow Sea Fisheries Research Institute, Chinese Academy of Fishery Sciences, Qingdao 266071, China. Tel.: +86 532 85811982; fax: +86 532 85803375.
E-mail address: yangag@ysfri.ac.cn (A. Yang).

http://dx.doi.org/10.1016/j.dci.2014.12.004
0145-305X/

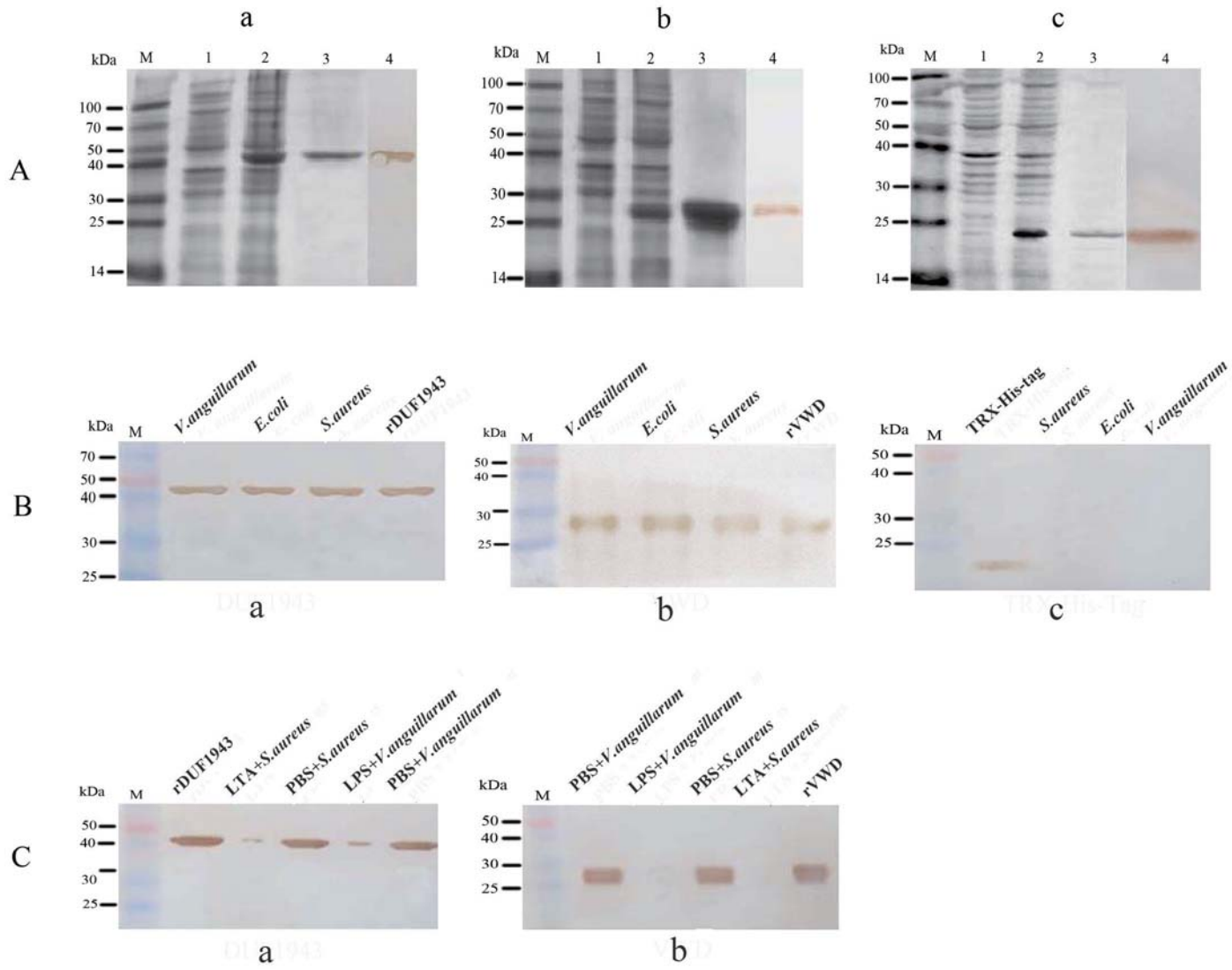

Fig. 4. Binding of rDUF1943 and rVWD domains to bacteria. (A) SDS–PAGE and Western blotting of recombinant proteins rDUF1943(a), rVWD(b) and TRX-His-tag peptide(c). Lane 1, negative control for recombinant proteins without induction; lane 2, IPTG-induced recombinant proteins; lane 3, purified recombinant proteins; lane 4, Western blot of purified recombinant proteins. (B) Binding of rDUF1943 (a), rVWD (b) and TRX-His-tag peptide (c) to bacteria. For a and b, lane 1, *V. anguillarum* incubated with recombinant proteins; lane 2, *E. coli* incubated with recombinant proteins; lane 3, *S. aureus* incubated with recombinant proteins; lane 4, purified recombinant proteins; For c, the sample loaded in reserved order. (C) Binding of rDUF1943, rVWD to LTA and LPS. Binding of rDUF1943 (a) and rVWD (b) to *S. aureus* and *V. anguillarum* was inhibited by the presence of LTA and LPS respectively. For a, lane 1, purified recombinant proteins; lane2, *S.aureus* incubated with recombinant proteins which were pre-incubated with LTA; lane 3, *S. aureus* incubated with recombinant proteins which were pre-incubated with PBS; lane 4, *V. anguillarum* incubated with recombinant proteins which were pre-incubated with LPS; lane 5, *V. anguillarum* incubated with recombinant proteins which were pre-incubated with PBS; For b, the sample loaded in reserved order. Lane M, molecular weight standards (kDa).

protein formed a single band. MALDI TOF/TOF MS analysis proved that the purified protein was indeed Vg from scallop ovary (Fig. 5D).

Next we examined the antibacterial activities of purified Vg against the Gram-negative bacteria *V. anguillarum* and *E. coli* and the Gram-positive bacterium *S. aureus*. As shown in Fig. 6, the growth of all three strains of bacteria was inhibited by purified scallop Vg in a dose-dependent manner. This suggested that like fish Vg, scallop Vg also showed a broad-spectrum antibacterial activity against both Gram-negative and Gram-positive bacteria.

4. Discussion

In the present study, a full-length cDNA of Vg 7707 bp was isolated and characterized from *P. yessoensis*. Primary structure analysis showed that the protein contained the domains Vitellogenin_N, DUF1943 and VWD, and the domain Vitellogenin_N possessed an amino acid motif KTIGNAG, and the cleavage site (R-X-R/K-R), which were both highly conserved in Vg proteins from both vertebrates and invertebrates (Hayward et al., 2010; Zhang et al., 2011). The molecular mass of deduced Vg was 265.14 kDa, in agreement with the previous report showing that the size of the female-specific protein in *P. yessoensis* was approximately 270 kDa (Osada et al., 1992). All these data showed that the isolated cDNA was coded for a canonical Vg in *P. yessoensis*. Phylogenetic analysis showed that all mollusc Vg proteins were all grouped together, suggesting they were monophyletic. Of note, in the genus of Pectinidae, *P. yessoensis* and *C. farreri* were clustered together, then with *P. maximus*, that are temperate species, and finally with *M. nobillis*, which is a tropical and subtropical species. This different geographic distribution has been suggested to an environment factor which may contribute to Vg evolution process (Zheng et al., 2012).

ZOOLOGICAL SCIENCE **32**: 571–578 (2015)

DNA Taxonomy of *Paranemertes* (Nemertea: Hoplonemertea) with Spirally Fluted Stylets

Yue Hao[1], Hiroshi Kajihara[2], Alexei V. Chernyshev[3,4], Robert K. Okazaki[5], and Shi-Chun Sun[1]*

[1]*Institute of Evolution & Marine Biodiversity, Ocean University of China, 5 Yushan Road, Qingdao 266003, China*
[2]*Faculty of Science, Hokkaido University, Sapporo 060-0810, Japan*
[3]*A.V. Zhirmunsky Institute of Marine Biology, Vladivostok 690041, Russia*
[4]*Far Eastern Federal University, Vladivostok, Russia*
[5]*Department of Zoology, Weber State University, 1415 Edvalson Street, Dept 2505, Ogden, UT 84408-2505, USA*

Of the 14 nominal species that are now or have ever been assigned to the genus *Paranemertes* Coe, 1901, four have been reported to have stylets with a spirally fluted or braided appearance. Although differentiation in color patterns has been documented among species/populations, these nemerteans share similar external characters. Using the sequence datasets of mitochondrial cytochrome *c* oxidase subunit I (COI), 16S rRNA, and nuclear 28S rRNA genes of specimens from 14 localities of Canada, USA, Russia, Japan, and China, we analyzed the genetic differentiation and reconstructed the phylogenetic trees for these nemerteans. In conjunction with the external characters, we discuss their taxonomy and species delimitation. An analysis based on COI dataset showed high genetic variations among populations and even among worms from the same geographic area. The analyzed 111 individuals were assigned into seven networks by statistical parsimony analysis. The inter-network uncorrected *p*-distances ranged from 0.044 to 0.172 and the mean intra-network uncorrected *p*-distances varied from 0.001 to 0.005. With the exception of two networks that contain specimens from the East China Sea, all networks were well-supported by the results of Bayesian and neighbor-joining analyses on the COI data. Phylogenetic trees based on 16S rRNA and 28S rRNA datasets were basically similar to the COI trees, but specimens in some networks were merged into larger clades. Present molecular analyses support the validity of *P. sanjuanensis* and the synonymization of *P. cylindracea* with *P. peregrina*. Nemerteans previously recorded as *P. peregrina* may contain several species and sympatric speciation might have been occurred in this nemertean group.

Key words: DNA taxonomy, statistical parsimony network, sibling species, genetic variation, species delimitation, phylogeny, spirally fluted stylets, *Paranemertes*, Nemertea

INTRODUCTION

The genus *Paranemertes* Coe, 1901 (Nemertea: Enopla: Monostilifera) was once classified in the family Emplectonematidae, but was recently transferred to the family Neesiidae (Chernyshev, 2005). This genus has not been definitively diagnosed, and has generally been regarded as comprising hoplonemerteans with numerous eyes, a rhynchocoel extending posteriorly not beyond 3/4 of the body length, the body wall longitudinal musculature anteriorly divided into an outer and an inner portions, an intestinal caecum bearing paired diverticula, the cerebral organs being small and situated in front of brain, and subepithelial glands being well developed (Coe, 1901; Corrêa, 1964; Gibson, 1982). Fourteen nominal species and two varieties have once been assigned to this genus, with two of them being now placed in other genera and one regarded as a junior synonym of other species. Most *Paranemertes* species possess normal (smooth) stylets, but four were reported to have stylets with braided/spirally fluted ornamentation, which is not common in other monostiliferous hoplonemerteans. These four include: *Paranemertes peregrina* Coe, 1901, the type species of the genus, originally described based on specimens from Victoria, British Columbia, Canada to Unalaska Island, Alaska, USA (Coe, 1901); *Paranemertes katoi* Yamaoka, 1947 described from Shimoda, Japan (Yamaoka, 1947); *Paranemertes cylindracea* Korotkevitsch, 1977 described from Paramushir, North Kuril Islands, Russia (Korotkevitsch, 1977); and *Paranemertes sanjuanensis* Stricker, 1982 described from San Juan Island, Washington, USA (Stricker, 1982). The spirally fluted stylets were not reported for *P. peregrina* in the original description, but were subsequently confirmed by the same author (Coe, 1904: p. 144 footnote

* Corresponding author. Tel. : +86-532-82032216;
Fax : +86-532-82301982;
E-mail: sunsc@ouc.edu.cn
doi:10.2108/zs140275

1; pl. XX, figs. 14, 15). It was originally reported that *P. cylindracea* lacked eyes and its stylets were smooth (Korotkevitsch, 1977), whereas later studies revealed that the holotype of this species had eyes and fluted stylets (Chaban and Chernyshev, 2008; AV Chernyshev, personal observation) and the species was synonymized with *P. peregrina* (see Chaban and Chernyshev, 2008). In addition to sharing sculptured stylets, these species (mentioned as "*Paranemertes peregrina* complex" below) are more or less similar in the external appearance and color: dorsally brown, orange brown, dark brown, chestnut-brown, purple brown, orange-tan or overripe cherry colored and ventrally opaque white, yellow, whitish yellow or fleshy (Coe, 1901, 1905; Yamaoka, 1947; Korotkevitsch, 1977; Stricker 1982; Crandall et al., 2001; see also Fig. 1). Among these nemerteans, *P. peregrina* has been reported to have a wide distribution along both eastern and western Pacific coasts and the Arctic coasts by many studies (e.g., Coe, 1901, 1904, 1905, 1940, 1952; Yamaoka, 1940; Iwata, 1954; Corrêa, 1964; Yin et al., 1986; Sun, 1995; Chernyshev, 1997, 2014). Apparent morphological variations have been found for the nemerteans recorded under this name. For instance, Coe (1901, 1905) recognized two color patterns from the northwestern American coasts, namely the "brown variety" and the "purple variety". Later, Coe (1940) proposed the names *Paranemertes peregrina* var. *alaskensis* Coe, 1940 for the "common and of large size northward" form and *Paranemertes peregrina* var. *californiensis* Coe, 1940 for the "less abundant and smaller southward" form. Moreover, the difference between *P. katoi* and *P. peregrina* was questioned by some researchers (Crandall et al., 2001), and some populations (e.g., those from Qingdao and Shengsi, China) that were recorded as *P. peregrina* (Yin et al., 1986; Sun, 1995) looked more similar to *P. katoi* (S-C Sun, personal observation). Therefore, further comparative studies, particularly to check the non-morphological differentiations among different geographic populations and/or color patterns of these nemerteans are worthwhile to pursue.

DNA taxonomy (Tautz et al., 2002) and DNA barcoding (Hebert et al., 2003), based on the analysis of sequence diversity in small segments of DNA with the mitochondrial COI gene being the most widely used in animals, have provided whole new approaches for taxonomists. Although they have been the subject of much discussion and inquiry (Barrett and Hebert, 2005; Meyer and Paulay, 2005; Hickerson et al., 2006), these analyses have been demonstrated to be powerful in identifying and delimiting species, as well as in discovering cryptic species in various animal groups (e.g., Ball et al., 2005; Johnson et al., 2008; Schlei et al., 2008). In addition to the widely used genetic distance comparison and phylogenetic tree analysis methods, some new approaches, such as the statistical parsimony analysis implemented in

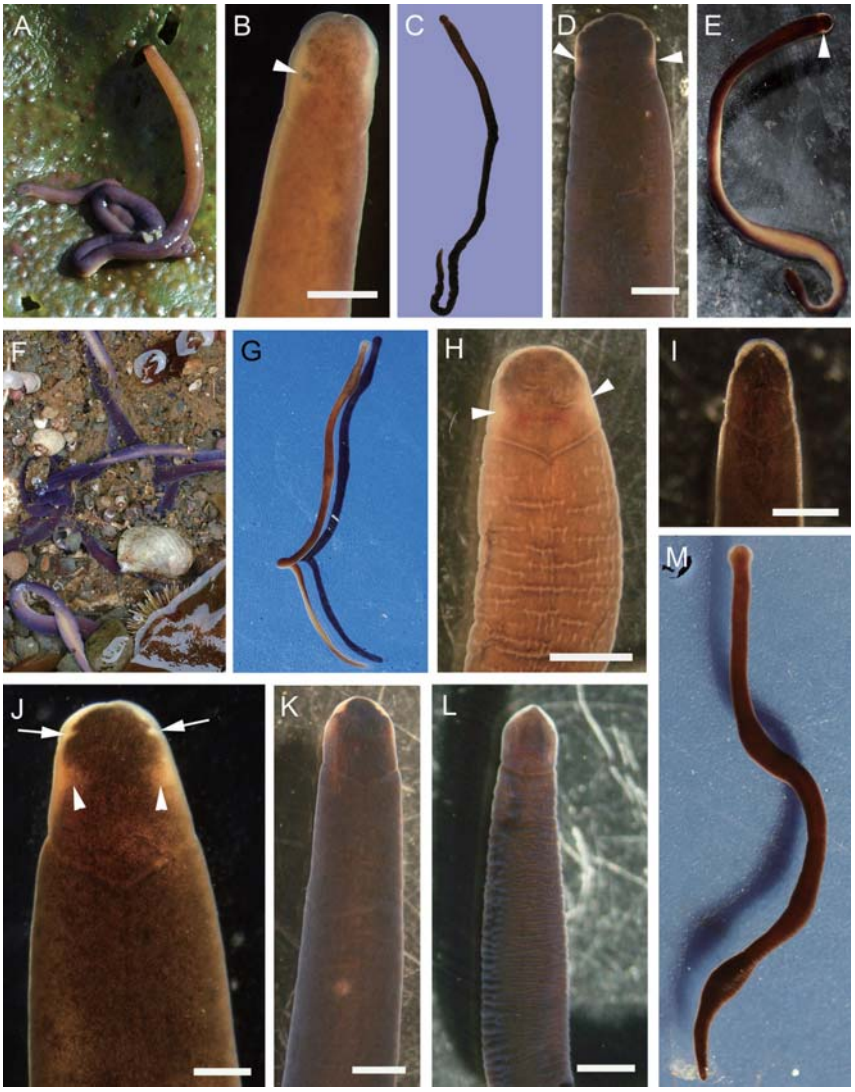

Fig. 1. Photographs of *Paranemertes* specimens collected from different localities. **(A, B)** From Bodega Bay, California, USA; intertidal, rocky shore (among algae). **(C)** From Nanaimo, British Columbia, Canada; intertidal, among oysters and barnacles. **(D)** From Victoria, British Columbia, Canada; intertidal, among algae and barnacles. **(E, F)** From Simushir Island, Kuril Islands, Russia; intertidal, under stones. **(G, H)** From Dalian, Liaoning, China; intertidal, under stone **(G)** or among oysters **(H)**. **(I)** From Changdao, Shandong, China; intertidal, among algae. **(J)** From Bodega Bay, California, USA; intertidal, mudflat. **(K)** From Qingdao, Shandong, China; under stones. **(L, M)** From Pingtan, Fujian, China; intertidal, among algae. Arrow heads indicate the paired, light color spots (the "yellowish spots, continuously with the color of ventral surface" of Coe, 1905). Arrows point to the whitish marks located at the place of the first pair of cephalic grooves. These marks were observed to be conspicuous only in specimens from the harbor mudflat of Bodega Bay, and may refer to the "delicate, whitish, transverse grooves lie on the lateral margins of the head" (Coe, 1905: 220). Scale bars (only given for micrographs): **(B, I, J)** = 0.5 mm; **(D, H, K, L)** = 1.0 mm.

ZOOLOGICAL SCIENCE **32**: 579–589 (2015)

Species Diversity of *Ramphogordius sanguineus/Lineus ruber*-like Nemerteans (Nemertea: Heteronemertea) and Geographic Distribution of *R. sanguineus*

Xing-Xing Kang[1], Fernando Ángel Fernández-Álvarez[2,3†], José E. F. Alfaya[2,4,5], Annie Machordom[2], Malin Strand[6], Per Sundberg[7], and Shi-Chun Sun[1*]

[1]*Institute of Evolution & Marine Biodiversity, Ocean University of China, 5 Yushan Road, Qingdao 266003, China*
[2]*Museo Nacional de Ciencias Naturales (MNCN-CSIC), José Gutiérrez Abascal, 2 28006 Madrid, Spain*
[3]*Departamento de Biología de Organismos y Sistemas (Zoología), Universidad de Oviedo, Catedrático Valentín Andrés, 33006 Oviedo, Asturias, Spain*
[4]*LARBIM-IBIOMAR, Centro Nacional Patagónico (CENPAT-CONICET), Bvd. Brown 2915, U9120ACV Puerto Madryn, Chubut, Argentina*
[5]*Facultad de Ciencias Naturales, Universidad Nacional de la Patagonia San Juan Bosco (UNPSJB), Bvd. Brown, U9120ACV Puerto Madryn, Chubut, Argentina*
[6]*Swedish Species Information Centre, Swedish University of Agricultural Sciences, 75007 Uppsala, Sweden*
[7]*Department of Marine Sciences, University of Gothenburg, Gothenburg, Sweden*

Heteronemerteans, such as *Lineus ruber*, *L. viridis*, *Ramphogordius sanguineus*, *R. lacteus*, *Riseriellus occultus*, and *Micrura varicolor*, share many similar external characters. Although several internal characters useful for distinguishing these nemertean species have been documented, their identification is based mostly on coloration, the shape of the head, and how they contract, which may not be always reliable. We sequenced the mitochondrial COI gene for 160 specimens recently collected from 27 locations around the world (provisionally identified as the above species, according to external characters and contraction patterns, with most of them as *R. sanguineus*). Based on these specimens, together with sequences of 16 specimens from GenBank, we conducted a DNA-based species delimitation/identification by means of statistical parsimony and phylogenetic analyses. Our results show that the analyzed specimens may contain nine species, which can be separated by large genetic gaps; heteronemerteans with an external appearance similar to *R. sanguineus*/*Lineus ruber*/*L. viridis* have high species diversity in European waters from where eight species can be discriminated. Our 42 individuals from Vancouver Island (Canada) are revealed to be *R. sanguineus*, which supports an earlier argument that nemerteans reported as *L. ruber* or *L. viridis* from the Pacific Northwest may refer to this species. We report *R. sanguineus* from Chile, southern China, and the species is also distributed on the Atlantic coast of South America (Argentina). In addition, present analyses reveal the occurrence of *L. viridis* in Qingdao, which is the first record of the species from Chinese waters.

Key words: "*Lineus ruber*" complex, *Ramphogordius sanguineus*, cytochrome *c* oxidase subunit I (COI), statistical parsimony network, phylogeny, geographic distribution, Nemertea

INTRODUCTION

The phylum Nemertea is a poorly characterized metazoan taxa. In addition to the ~1300 described species (Gibson, 1995; Kajihara et al., 2008), numerous species that are new to science have been collected, but not described or nominated, and our knowledge of nemertean biodiversity remains uneven across different parts of the world. For example, about 300 species have been recorded from the Pacific coasts of Asia, but it has been conjectured that the number of species in these areas is probably much higher (Chernyshev, 2014). In a much smaller sea area, the waters off Hong Kong, 39 species have been recorded (including inadequately described species), but many more species of nemerteans as yet unidentified have been collected from the region (Gibson and Sundberg, 2003). The slow pace of

* Corresponding author. Tel. : +86-532-82032216;
Fax : +86-532-82031982;
E-mail: sunsc@ouc.edu.cn
† Current address: Institut de Ciències del Mar (CSIC), Passeig Maritim, 37-49 08003 Barcelona, Spain
doi:10.2108/zs150064

as reference sequences for DNA taxonomy. However, two specimens of *R. lacteus* (RL1/KF935519 and RL2/HQ848583; Table 1) were classified into two different networks with high genetic distance (12.21%) and sister to each other in phylogenetic trees (Figs. 1, 2; Table 3). Since the location (northwestern France) of RL2 (as well as NemBar961, from Wales, UK, see further) (Table 1), is near the type locality of *R. lacteus* (Norwegian waters) (Rathke, 1843), it is likely that Network 4 refers to *R. lacteus* while Network 5/RL1 (from the Mediterranean coast of Spain) represents an unknown cryptic species. This is congruent with the result of an unpublished work that identified a cryptic lineage from *L. lacteus* specimens (Nicolas Bierne, pers. comm.).

Of the 151 specimens provisionally identified as *R. sanguineus*/*sanguineus*(?), 149 specimens, which were considerably variable in coloration (Fig. 3A–H), were confirmed to be *R. sanguineus* by statistical parsimony and phylogenetic analyses (Figs. 1, 2). However, the specimens DGD27 (from Qingdao, China) and NemBar961 (*R. sanguineus*?, from Wales, UK) were assigned to the clades of Network 2 (*L. viridis*) and Network 4 (*R. lacteus*?), respectively (Figs. 1, 2). Two (NemBar1444a, 1444b) of the five individuals formerly identified as *M. varicolor* are revealed to be *L. viridis*. These further indicate that it may not be always possible to correctly identify these nemerteans based solely on external morphology and/or behavior.

The specimen NemBar411, which was provisionally identified as *L. ruber*/*viridis*, forms a mono-individual network/clade in our analyses (Figs. 1, 2). This specimen was collected from Saltö, Sweden. Two obscure forms, *L. pseudoruber* (from Kiel Bay, Germany; Friedrich, 1935) and the cryptic "aberrant type" (from Britain and France waters; Rogers et al., 1995), were reported from adjacent seas. Whether they belong to the same species remains to be determined by future studies. Similarly, the Chile specimen NemBar889 (*L. ruber*?), which has the external appearance and contraction pattern of *L. ruber*, constitutes another mono-individual network/clade (Figs. 1, 2), indicating that there are at least two externally similar species around the coast of Coquimbo, Chile. The NemBar889 may be phylogenetically distant from the other forms analyzed (NCBI blast shows the most similar species (sequence identities 84–85%) are *Dendrorhynchus sinensis* Yin and Zeng, 1985, *Lineus longissimus* (Gunnerus, 1770) and *Cerebratulus leucopsis* (Coe, 1901)), but this must await further study.

The specimen DGD27 was collected among algae from the intertidal zone of Qingdao, China, in August 2010. It was a young individual about 8.0 mm long and 0.8 mm wide after being relaxed, and showed a greenish color (Fig. 3I). This is the first record of *L. viridis* from Chinese waters. Given that the collection site is very close to the port of Qingdao, one of the busiest international ports in the world, there is a possibility that *L. viridis* is a recently introduced species in this region. In other Asian waters, Takakura (1898) reported a form with a greenish or dark brown color from Koajiro Bay, Japan, under the name *Lineus gesserensis* (Müller, 1788), which has been applied to what are now known as *L. viridis* and *L. ruber* (Gibson, 1994, 1995). According to Takakura's (1898) brief description on external features, it was also possible that his specimens referred to *R. sanguineus* (see further).

Ramphogordius sanguineus and its various synonyms

Fig. 3. Photographs for some specimens of the present study. **(A–H)** *Ramphogordius sanguineus* (Rathke, 1799), each from: **(A)** Lingshan Dao, Shandong, China; **(B)** Nanchangshan Dao, Shandong, China; **(C)** Dagong Dao, Qingdao, Shandong, China; **(D)** Los Chalanos beach, Muros de Nalón, Asturias, Spain; **(E)** Dachangshan Dao, Liaoning, China; **(F)** Los Chalanos beach, Muros de Nalón, Asturias, Spain; **(G)** Nanaimo, British Columbia, Canada; **(H)** Cerro Avanzado beach, Nuevo Gulf, Patagonia, Argentina. **(I)** *Lineus viridis* (Müller, 1774), a young specimen from Dagong Dao, Qingdao, Shandong, China. Scale bars (for micrographs only) = 1.0 mm.

International Journal of Biological Macromolecules 73 (2015) 58–64

Contents lists available at ScienceDirect

International Journal of Biological Macromolecules

journal homepage: www.elsevier.com/locate/ijbiomac

Phycoerythrins in phycobilisomes from the marine red alga *Polysiphonia urceolata*

Mingri Zhao[a,b], Li Sun[b,*], Shichun Sun[a], Xueqin Gong[b], Xuejun Fu[b], Min Chen[b]

[a] Institute of Evolution and Marine Biodiversity, Ocean University of China, Qingdao, Shandong 266003, PR China
[b] College of Life Sciences, Yantai University, Shandong 264005, PR China

ARTICLE INFO

Article history:
Received 12 March 2014
Received in revised form 24 August 2014
Accepted 6 November 2014
Available online 13 November 2014

Keywords:
Phycoerythrin
Phycobilisome
γ subunit

ABSTRACT

Phycoerythrins (PE) in phycobilisomes from *Polysiphonia urceolata* were studied in this research. Dissociative products of phycobilisomes were analyzed by sucrose density gradient centrifugation and native-PAGE. At least three types of PEs were found in the dissociative products of phycobilisomes. According to their molecular weights, absorption spectra and subunit components, they should be PE hexamer containing γ_1 subunit, PE hexamer containing γ_2 subunit and PE monomer containing no γ subunit. PEs bigger than hexmer were also found in the dissociative products of phycobilisomes in 200 mM phosphate buffer when dissociated phycobilisomes were analyzed by sucrose density gradient centrifugation. PE trimers containing no γ subunits were also found in products of dissociated phycobilisomes in deionized water when dissociated phycobilisomes were analyzed by native-PAGE. This is the first time that pure PE hexamers containing γ_2 subunits were isolated from *P. urceolata*. The PE monomers containing no γ subunits should come from PE trimers or hexamers containing no γ subunits in the "rod" of phycobilisomes. It can be concluded that there are three types of PEs in "rod" of phycobilisomes from *P. urceolata*: PE containing γ_1 subunit, PE containing γ_2 subunit and PE containing no γ subunit.

1. Introduction

Phycobiliproteins are water soluble proteins and major light-harvesting pigments widely found in red algae, cyanobacteria and some cryptophycean algae [1–4]. Phycobiliproteins are divided into four classes on the basis of their absorption properties: phycoerythrin (PE, λ_{max} ~ 565 nm), phycocyanin (PC, λ_{max} ~ 620 nm), phycoerythrocyanin (PEC, λ_{max} ~ 575 nm) and allophycocyanin (AP, λ_{max} ~ 650 nm) [5–8]; Phycobiliproteins and linker polypeptides are assembled into the light harvesting antenna complexes named phycobilisomes [4,7]. Phycoerythrins are divided into four main classes on the basis of their absorption spectra: B-phycoerythrin (B-PE, peaks at 545, 565 nm and a shoulder at 499 nm), R-phycoerythrin (R-PE, peaks at 499, 565 nm and a shoulder/peak at ~545 nm), C-phycoerythrin (C-PE, peak at 565 nm) and CU-phycoerythrin (CU-PE, peaks at about 498 nm, 540 nm and/or 565 nm) [3,4,9,10]. R-PE and B-PE are found in red algae while C-PE and CU-PE is found in cyanobacteria. R-PE is found in most red macro algae; B-PE is found in some red micro algae such as *Porphyridium* and *Rhodella violacea* [3,4,11]. R-PE and B-PE usually consist of three subunits: α, β and γ, and their structures are generally described as hexameric aggregates $(\alpha\beta)_6\gamma$ or $(\alpha\beta)_3\gamma(\alpha\beta)_3$ [2,8,12].

Each subunit of phycobiliprotiens contains one or more chromophores (phycobilins) bound to specific cysteines in apoprotein chains by thioether bonds [3,4]. The outstanding absorption and fluorescence properties of phycobiliproteins in the visible region originate from phycobilins and their interactions within polypeptide chains [13,14]. Four phycobilins found in phycobiliprotiens from red algae and cyanobacteria are phycoerythrobilin (PEB), phycourobilin (PUB), phycocyanobilin (PCB) and phycobiliviloin (PXB). PEB is found in C-PE, R-PE, B-PE and R-phycocyanin (R-PC), PUB is found in R-PE, CU-PE and B-PE, PCB is found in PC, AP and PEC, while PXB is found in PEC [13–15]. CU-PE has similar chromophores and absorption properties as R-PE, and used to be classified as R-PE [3,10]. Types of phycobiliproteins in organisms and types of phycobilins they carry depend on species, but the phycobilin-binding sites are quite conserved [13–15]. The α subunit of R-PE contains two PEB chromophores which are linked to specific cysteine residues in the polypeptide chain by single thioether bonds; the β subunit of R-PE contains three chromophores: two PEBs are linked to cysteine residues by single thioether bonds, and one PUB is linked to two cysteine residues by double thioether bonds; PEB and PUB are isomeric compounds.

* Corresponding author. Tel.: +86 535 6902638; fax: +86 535 6902638.
E-mail address: sunlwang@public.ytptt.sd.cn (L. Sun).

http://dx.doi.org/10.1016/j.ijbiomac.2014.11.004
0141-8130/

Two kinds of γ subunits were often found in R-PE: the γ_1 subunit contains three PUBs and one PEB and the γ_2 subunit contains two PEBs and two PUBs [4,16–18]. The amounts of R-PEs containing two different γ subunits are usually approximately equal in most reported red algae (e.g. R-PE from *Heterosiphonia japonica*, *Aglaothamnion neglectum* and *Callithamnion*) [18–21]. Only one kind of R-PE which contained γ_1 subunit was reported in the early researches on *Polysiphonia urceolata* [17]. In our research, we found a faint band whose molecular weight and fluorescence property were similar to γ_2 subunit in SDS-PAGE of R-PE from *P. urceolata*, and we think it should be γ_2 subunit [22]; but because the abundance of this faint band was much lower than the abundance of γ_1 subunit, it cannot be ruled out that the faint band at the position of γ_2 subunits was degradation product of γ_1 subunits during the treatment of samples before SDS-PAGE. Because one R-PE hexamer only has one γ subunit, different γ subunits should be in different R-PE hexamers [3,4,16–18]. If R-PE from *P. urceolata* only containing one γ_2 subunit can be separated, the γ_2 subunit can be proved to exist in R-PE from *P. urceolata*. But R-PE hexamers from *P. urceolata* only containing one γ_2 subunit cannot be separated from R-PE hexamers containing one γ_1 subunit in our early researches; neither in other reports on R-PE from *P. urceolata* [17,22]. In this research, phycobilisomes were isolated from *P. urceolata*, and then phycobilisomes were dissociated into phycobiliproteins to study types of PEs in phycobilisomes.

2. Materials and methods

2.1. Sample preparation and purification

Phycobilisomes were prepared and purified according to the methods described by Sun et al. [23]. Macroalgae were obtained from tidelands of Yantai in spring (March), and the fresh algae were milled to break cells in 1 M phosphate buffer solution (PBS, pH 7.0). Surfactant NP-40 (2% v/v) was used to help phycobilisomes dissociate from the thylakoid membrane. The crude extractions of phycobilisomes were obtained after centrifuged at 18,000 × *g* for 20 min at 4 °C. Then the phycobilisomes were prepared and purified by sucrose density gradient centrifugations. All gradient sucrose solutions contained 1 M PBS; and the purple zones between 0.8 M and 1 M sucrose were phycobilisomes. The density gradient centrifugations were performed by a centrifuge Optima L-100XP (Beckman) at 138,000 × *g*, 20 °C for 20 h. The analysis of dissociated phycobilisomes in 200 mM PBS (for about 1 h before centrifugation) by sucrose density gradient centrifugation was also performed at the same conditions.

Phycoerythrins used as control were prepared and purified according to the methods described by Sun et al. [19]. The purified R-PEs showed a single band in native-PAGE examination; in the absorption spectrum of the purified R-PE, the ratio of the absorption peak height at 568 nm to that at 280 nm was 4.92, and there were almost no absorbance at 620 nm and 650 nm.

2.2. SDS-PAGE

According to our previous works, a SDS-PAGE system which is proper to subunit separation of R-PE was used [21]; and the separating gel had a gel concentration of 14% (*C* = 3%), pH 9.0 and 0.275 M Tris–HCl in this system.

2.3. Native-PAGE

The gel concentration of native-PAGE system was 7% and pH was 7.5. Electrophoresis was carried out in a vertical slab gel apparatus (Beijing Liuyi Instrument Factory, DYCZ-24EN) with gel volume of 130 mm × 100 mm × 1 mm.

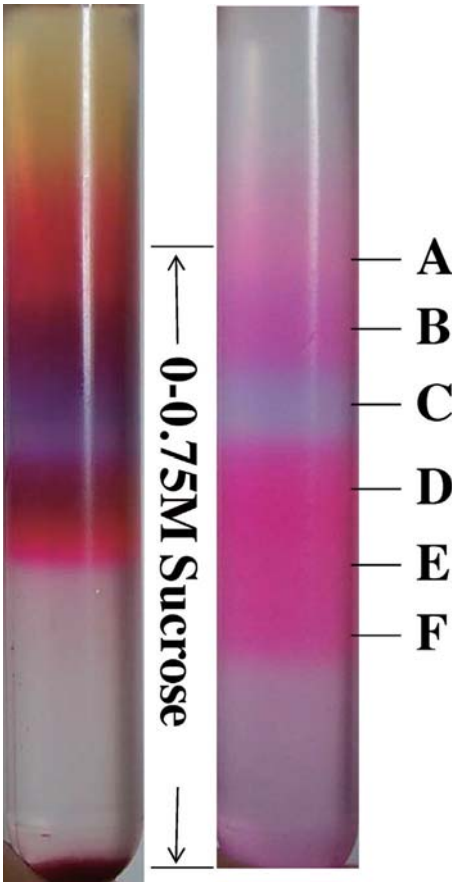

Fig. 1. Continuous sucrose density gradient centrifugation of phycobiliproteins from *Polysiphonia urceolata*. Left: algae extracts by 50 mM phosphate buffer (pH 7.0). Right: phycobiliproteins from phycobilisomes dissociated in 200 mM phosphate buffer (pH 7.0) for 1 h. The sucrose gradient solution contained 1 M phosphate buffer (pH 7.0).

2.4. Staining of gels

Imidazole-SDS-zinc reverse staining of separating gels as described by Fernandez-Patron et al. [24] was performed after electrophoresis; and then the gels were put in UVP Bioimaging systems (Biospectrum-AC) to be observed of fluorescence induced by UV (365 nm). Afterwards, the reverse stained gels were soaked in acetic acid for 30 s to be clarified, then the gels were stained with 0.2% (m/v) Coomassie Brilliant Blue G-250 containing 40% methanol (v/v) and 7.5% (v/v) acetic acid for 2 h, finally the gels were destained in 0.5 M NaCl solution.

3. Results

3.1. Sucrose density gradient centrifugation of dissociated phycobilisomes

Phycobilisomes are relatively stable in high concentrations (≥750 mM) of PBS (pH 7.0), and dissociate into multicomponent mixtures of subcomplexes in 50–200 mM PBS [25]. Dissociated phycobilisomes in 200 mM PBS (for about 1 h before centrifugation) were analyzed by sucrose density gradient centrifugation, and six fractions were obtained (Fig. 1A–F). Crude algae extracts by 50 mM PBS (mainly phycobiliproteins) were used as control. In our research on Sephadex G-150 chromatography of crude extracts

Mitochondrial DNA

http://informahealthcare.com/mdn
ISSN: 1940-1736 (print), 1940-1744 (electronic)

Mitochondrial DNA, Early Online: 1–2
 DOI: 10.3109/19401736.2015.1060429

informa
healthcare

MITOGENOME ANNOUNCEMENT

Mitochondrial genome of *Micrura bella* (Nemertea: Heteronemertea), the largest mitochondrial genome known to phylum Nemertea

Chunyang Shen and Sun Shi-Chun

Institute of Evolution & Marine Biodiversity, Ocean University of China, Qingdao, China

Abstract

The complete mitochondrial genome (mitogenome) of *Micrura bella* was sequenced and analyzed. Being the largest mitogenome known to phylum Nemertea, the genome is 16 847 bp in length. It encodes 37 genes typical to metazoan mitogenomes and has the same gene arrangement with the other Heteronemertea mitogenomes sequenced to date. The genome has the maximal number of non-coding nucleotides (2037 bp at 25 sites) in Nemertea mitogenomes, among which two large non-coding regions were found (507 and 508 bp, respectively).

Keywords

Micrura bella, mitochondrial genome, Nemertea

History

Received 16 May 2015
Revised 18 May 2015
Accepted 30 May 2015
Published online 9 July 2015

Among the 17 nemertean mitogenomes deposited in GenBank, only five were determined for heteronemerteans. In this study, we describe one new mitogenome of the heteronemertean *Micrura bella* (Stimpson, 1857), a species known from Russian, Japanese and Chinese waters.

The specimen of *M. bella* was collected from the coast of Qingdao, Shandong, China. Total DNA was extracted using the SQ Tissue DNA Kit (D6032-01, OMEGA, Norcross, GA). The mitogenome was determined by primer-walking method. Four short fragments (*cox1*, *cox3*, *cob,* and *rrnL*) were amplified first by universal primer pairs (Chen et al., 2012). Then four pairs of specific primers were designed to amplify the remaining fragments of the mitogenome.

The complete mitogenome of *M. bella* is 16 847 bp in length (GenBank accession number: KR703629), which is the longest mitogenome known to phylum Nemertea. The genome encodes 13 protein-coding genes, two ribosomal RNA genes, and 22 transfer RNA genes, and contains 25 intergenic regions. The gene order is the same with all other heteronemertean mitogenomes published to date (Chen et al., 2012; Gonzalez-Cueto et al., 2015; Podsiadlowski et al., 2009; Shen et al., 2014). Two overlappings were found in this genome, situated between *nad4* and *nad4L* (7 bp) and between *cox3* and *trnK* (3 bp), respectively. It is worth noting that the former 7-bp overlapping also exists in other 12 nemertean mitogenomes (Chen et al., 2009, 2011, 2012; Gonzalez-Cueto et al., 2015; Podsiadlowski et al., 2009; Shen et al., 2014; Sun & Sun, 2014; Sun et al., 2014).

Most protein-coding genes employ ATG as start codon, while *cox2* is initiated by GTG. Twelve protein-coding genes are terminated by the typical stop codon TAG or TAA, whereas *nad1* ends with the incomplete stop codon T. *RrnS* (864 bp) and *rrnL* (1318 bp) are located between *tRNA-Met* and *tRNA-Leu* (CUN) and separated by *trnV*. Lengths of 22 tRNA genes vary from 64 to 71 bp. The total length of 25 non-coding regions is 2037 bp, which is considerably longer than those of other nemertean mitogenomes (110–1526 bp) and is the major reason that the genome is significantly larger than the others. Unlike other nemertean mitogenomes which have a ''major non-coding region'' significantly longer than the other non-coding regions, the largest two non-coding regions (507 and 508 bp, respectively) have only single base pair difference in length.

Phylogenetic analysis based on the amino acid dataset of 12 protein-coding genes (*ATP8* is excluded due to nucleotide substitution saturation) of five heteronemertean species shows that *M. bella* is the closest to *Iwatanemertes piperata* (Stimpson, 1855), while *Micrura ignea* Schwartz & Norenburg, 2005 locates at a quite different position in the tree (Figure 1). This further indicates the non-monophyly of genus *Micrura* (Ehrenberg, 1871), as having been shown in previous studies (e.g. Andrade et al., 2012; Kvist et al., 2014). Obviously, data available is not sufficient to gain an overall understanding of the phylogenetic relationship of Heteronemertea taxa, denser taxon sampling is necessary in future studies.

Correspondence: Shi-Chun Sun, Institute of Evolution & Marine Biodiversity, Ocean University of China, 5 Yushan Road, Qingdao 266003, China. Tel: +86 532 82032216. E-mail: sunsc@ouc.edu.cn

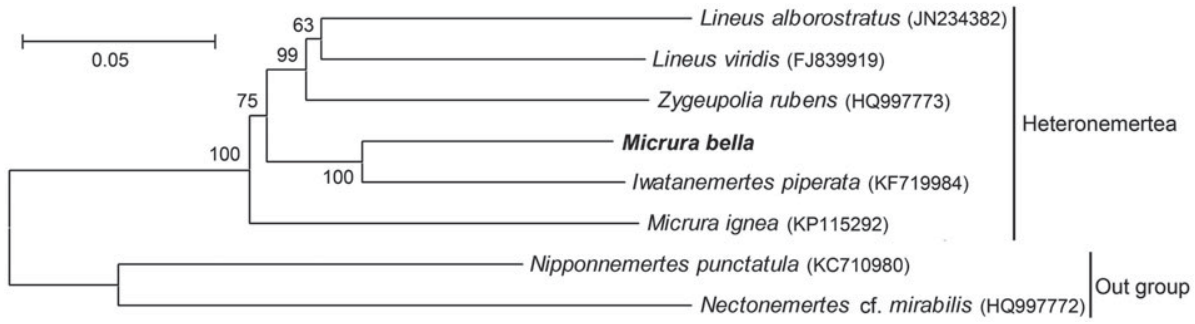

Figure 1. Neighbor-joining (NJ) tree of five Heteronemertea species based on amino acid sequences of 12 protein-coding genes. The tree was constructed using MEGA5 (MEGA Inc., Englewood, NJ) and evaluated with 1000 bootstrap replicates. Two Hoplonemertea species, *Nipponnemertes punctatula* (Coe, 1905) and *Nectonemertes* cf. *mirabilis* Verrill, 1892, are served as outgroups. GenBank accession numbers for data from GenBank are indicated in parentheses. Bootstrap values are shown at nodes.

Declaration of interest

The authors report no conflicts of interest. The authors are responsible for the content and writing of the paper. This study was supported by the National Natural Science Foundation of China (30970333 and 31172046).

References

Andrade S, Strand M, Schwartz M, Chen H, Kajihara H, von Döhren J, Sun S, et al. (2012). Disentangling ribbon worm relationships: Multi – locus analysis supports traditional classification of the phylum Nemertea. Cladistics 28:141–59.

Chen H-X, Sun S-C, Sundberg P, Ren W-C, Norenburg JL. (2012). A comparative study of nemertean complete mitochondrial genomes, including two new ones for Nectonemertes cf. mirabilis and Zygeupolia rubens, may elucidate the fundamental pattern for the phylum Nemertea. BMC Genomics 13:139.

Chen H-X, Sundberg P, Norenburg JL, Sun S-C. (2009). The complete mitochondrial genome of *Cephalothrix simula* (Iwata) (Nemertea: Palaeonemertea). Gene 442:8–17.

Chen H-X, Sundberg P, Wu H-Y, Sun S-C. (2011). The mitochondrial genomes of two nemerteans, Cephalothrix sp. (Nemertea: Palaeonemertea) and Paranemertes cf. peregrina (Nemertea: Hoplonemertea). Mol Biol Rep 38:4509–25.

Gonzalez-Cueto J, Escarraga-Fajardo ME, Lagos AM, Quiroga S, Castro LR. (2015). The complete mitochondrial genome of Micrura ignea Schwartz & Norenburg 2005 (Nemertea: Heteronemertea) and comparative analysis with other nemertean mitogenomes. Marine Genomics 20:33–7.

Kvist S, Laumer CE, Junoy J, Giribet G. (2014). New insights into the phylogeny, systematics and DNA barcoding of Nemertea. Invertebr Syst 28:287–308.

Podsiadlowski L, Braband A, Struck TH, von Dohren J, Bartolomaeus T. (2009). Phylogeny and mitochondrial gene order variation in Lophotrochozoa in the light of new mitogenomic data from Nemertea. BMC Genomics 10:364.

Shen C-Y, Sun W-Y, Sun S-C. (2014). The complete mitochondrial genome of *Iwatanemertes piperata* (Nemertea: Heteronemertea). Mitochondrial DNA, early online. DOI: 10.3109/19401736.2013.855922.

Sun W-Y, Shen C-Y, Sun S-C. (2014). The complete mitochondrial genome of *Tetrastemma olgarum* (Nemertea: Hoplonemertea). Mitochondrial DNA, early online. DOI: 10.3109/19401736.2014.930834.

Sun W-Y, Sun S-C. (2014). A description of the complete mitochondrial genomes of *Amphiporus formidabilis*, *Prosadenoporus spectaculum* and *Nipponnemertes punctatula* (Nemertea: Hoplonemertea: Monostilifera). Mol Biol Rep 41:5681–92.

Xu D-L, Chen H-X, Shi W, Sun S-C. (2012). Complete mitochondrial genome of the nemertean *Lineus alborostratus* (Nemertea: Heteronemertea). Period Ocean Univ China 42:85–92 (in Chinese with English summary).

Available online at www.sciencedirect.com

ScienceDirect

Current Opinion in Genetics & Development

Shaping of biological tubes by mechanical interaction of cell and extracellular matrix

Bo Dong[1,2,3] and Shigeo Hayashi[1,4]

The shape of biological tubes is optimized for supporting efficient circulation of liquid and gas and to maintain organismal homeostasis. Maintaining a constant tube diameter and fitting tube length to body size are two requirements for proper tube function. The tracheal system of the *Drosophila* embryo is established through branching of ectodermal epithelia in the absence of environmental air, and the branching pattern and geometry of this system are genetically specified. Recent studies identified apical extracellular matrix (aECM) as a crucial regulator of tube expansion and elongation. Evidence suggests that aECM coordinates apical membrane growth and cell contractility to control tube growth at the tissue level. In the present review, we will discuss the physical mechanisms underlying this interaction.

Addresses
[1] Laboratory for Morphogenetic Signaling, RIKEN Center for Developmental Biology, 2-2-3 Minatojima-minamimachi, Chuo-ku, Kobe, Hyogo 650-0047, Japan
[2] College of Marine Life Sciences, Ocean University of China, No. 5 Yushan Road, Qingdao 266003, China
[3] Institute of Evolution & Marine Biodiversity, Ocean University of China, No. 5 Yushan Road, Qingdao 266003, China
[4] Department of Biology, Kobe University Graduate School of Science, 1-1 Rokkodai-cho, Nada-ku, Kobe, Hyogo 657-8051, Japan

Corresponding author: Hayashi, Shigeo (shayashi@cdb.riken.jp)

Current Opinion in Genetics & Development 2015, **32**:129–134

This review comes from a themed issue on **Developmental mechanisms, patterning and organogenesis**

Edited by **Deborah J Andrew** and **Deborah Yelon**

http://dx.doi.org/10.1016/j.gde.2015.02.009

Introduction

Explication of the biophysical mechanisms behind organ size and shape regulation is a fundamental challenge in developmental biology. Recent studies using three-dimensional organoid culture of pluripotent stem cells have generated tissue-like and organ-like structures, including intestinal crypt–villus system [1], optic cup [2] and 'mini-brain' [3]. These studies demonstrated that ordered multicellular structures and local extracellular environments can be formed through the autonomous organizing activity of organ precursor cells [4]. In this review, we address the questions of how organ precursor cells create and modulate their extracellular environments, and how the extracellular environment influences tissue morphogenetic processes. We focus our discussion on recent progress in the study of embryonic tracheal tube morphogenesis in *Drosophila*, with special emphasis on the mechanical properties of tracheal apical extracellular matrix (aECM) and their role in controlling tube geometry.

Drosophila trachea is a network of epithelial tubules that takes up air from epidermal openings (spiracles) and delivers it to the internal organs to sustain proper gas exchange (Figure 1a) [5,6]. Tracheal development initiates from the invagination of ten tracheal placodes. After completing the final embryonic cell division, tracheal precursors undergo a tubular branching process induced by the fibroblast growth factor (FGF) signaling pathway. After the establishment of branch-specific cell arrangements, tracheal branches undergo diametric expansion and axial growth to reach their final size, which is unique to each branch type [7]. The dorsal trunk of the trachea tubular system, which has the largest diameter, has been most extensively studied in the context of tube size control and geometry regulation (Figure 1a,b) [8].

Tracheal tube maturation: expansion and elongation

The embryonic tracheal tube comprises a single layer of epithelial cells, which surround the luminal cavity with their apical side facing the intraluminal space. The tracheal lumen is filled with aECM, consisting of various proteins and polysaccharide secreted from the tracheal cells (Figure 1b,c) [9]. Components of aECM that have been identified to date include chitin, chitin deacetylation domain proteins (serpentine/Serp and vermiform/Verm), chitin associated proteins (2A12/Gasp and Obstructor-A/Obst-A), and zona pellucida (ZP) domain proteins (Dumpy/Dp and Piopio/Pio) (Table 1). These components span a wide range of molecular sizes and are distributed in unique patterns, suggesting that aECM is a complex of various structural elements. The deposition of chitin, the major component of aECM and other matrix proteins in the luminal space, is associated with the onset of diametric expansion [10–12]. The secretion process is associated with materials present in the tracheal cell cytoplasm that are released as a bolus into the lumen, via COP I-mediated and COP II-mediated vesicle trafficking between the endoplasmic reticulum (ER) and Golgi apparatus [13–19], and the Diaphanous-dependent

Figure 1

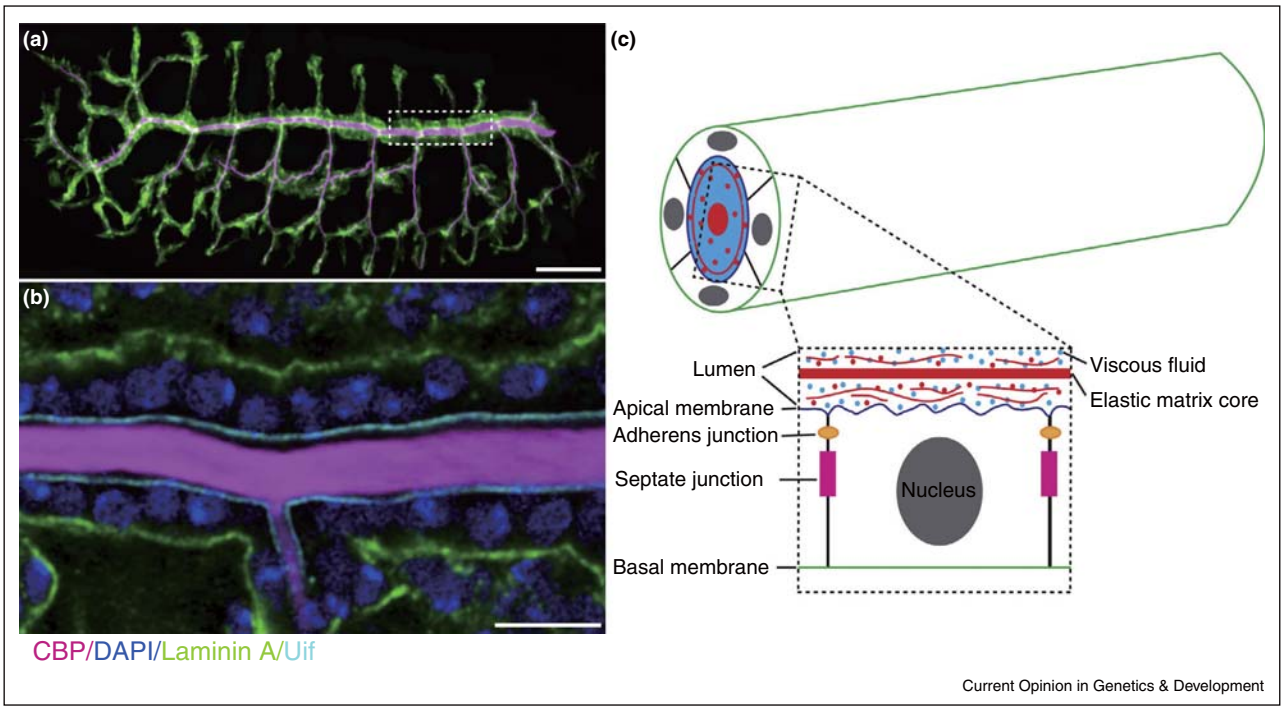

Drosophila tracheal system. **(a)** Embryonic trachea tubular network. Trachea epithelial cells are labeled by cytoplasmic GFP (green). Magenta represents the lumen of the tracheal tube surrounded by the epithelial cells. **(b)** Median confocal section of tracheal dorsal trunk labeled with the markers for apical membrane (Uif), basement membrane (Laminin A), lumen (CBP) and nuclei (DAPI). **(c)** Top: schematic representation of trachea epithelial cells and apical extracellular matrix. Bottom: cross section of the tracheal epithelium facing apical extracellular matrix consisting of viscous fluid and elastic core. Scale bars: 50 μm in a and 10 μm in b.

secretory pathway [20]. These general secretory pathways are required for deposition of aECM components and the addition of membranes into the apical surface, which expands the luminal space. Chitin forms a long fibrous structure along the tube lumen, and is thought to coordinate uniform tube expansion. In the absence of chitin synthesis, lumen expansion occurs, but in an irregular manner associated with dilations [11].

Diametric expansion is followed by axial growth. A series of studies of tube elongation defective mutants [8,21] have shown that axial growth requires the septate junction [22–29], subapical protein complex [20,30,31], planar cell polarity proteins [32], and Src kinase [33••,34••]. With the exception of Src kinases, all known tube length mutants show over-elongation phenotypes. The detailed molecular signaling pathways for driving tube over-elongation in the above mutants remain uncharacterized. For example, it is not clear why an intact septate junction is essential for tube elongation control. Recent works have shown that the apical membrane protein Crumbs appears to play a key regulatory role. Its activity state correlates with the amount of apical cell membrane territory, and mutations (such as ESCRT III) that elevate Crumbs activity cause tube over-elongation [30,35••]. How overproduction of apical membrane in such mutants is partitioned to the axial, but not diametric, dimension is unclear. Circumferential actin organization and taenidial fold formation regulated by Src42 may be involved in restricting diametric expansion and driving axis elongation [33••,34••,36]. After full maturation of tracheal tube and cuticle formation, aECM is removed and the lumen is replaced with a gas in preparation for eclosion.

aECM: component and function

Proper organization and modification of the aECM is also required to restrict tube over-elongation. When the remodeling of chitin polymer is compromised due to loss of function of the secreted chitin deacetylases (Serp and Verm) [25,37] and chitin binding protein Obst-A [38], the tracheal tubules exceed their normal length and show convoluted patterning (Figure 2a). Such over-elongated tube phenotypes suggest that an axial elongation force is present in the tracheal cells and that aECM restricts excess elongation.

Characterizing the physical property of aECM is extremely difficult due to its complexity and inaccessibility to

Xu et al. BMC Genomics (2015) 16:772
DOI 10.1186/s12864-015-2005-3

BMC Genomics

RESEARCH ARTICLE Open Access

Genomic insight into *Aquimarina longa* SW024^T: its ultra-oligotrophic adapting mechanisms and biogeochemical functions

Tingting Xu[1†], Min Yu[1†], Heyu Lin[1], Zenghu Zhang[1], Jiwen Liu[1] and Xiao-Hua Zhang[1,2*]

Abstract

Background: South Pacific Gyre (SPG) is the largest and clearest gyre in the world, where the concentration of surface chlorophyll *a* and primary production are extremely low. *Aquimarina longa* SW024^T was isolated from surface water of the SPG center. To understand how this bacterium could survive in this ultra-oligotrophic oceanic environment and its function in biogeochemical cycle, we sequenced the genome of *A. longa* SW024^T and performed extensive genomic analyses.

Methods: Genomic DNA was extracted and sequenced using Illumina Hiseq 2000 and Miseq platform. Genome annotation, genomic comparison and phylogenetic analyses were performed with the use of multiple bioinformatics tools like: BLAST+ 2.2.24, Glimmer3.0, RAST server, Geneious 4.8.5, ClustalW2 and MEGA5. Physiological and morphological features were tested by bacterial culture, electron microscopy, fluorescence microscopy and exopolysaccharides extraction.

Results: Analysis of seven *Aquimarina* genomes and 30 other genomes of *Flavobacteriaceae* isolated from seawater showed that most of the strains had low DNA G + C contents, and *Aquimarina* had larger genomes than other strains. Genome comparison showed varying genomic properties among seven *Aquimarina* genomes, including genome sizes and gene contents, which may warrant their specific adaptive strategies. Genome of *A. longa* SW024^T was further compared with the genomes of two other *Aquimarina* species which were also isolated from the SPG and *A. longa* SW024^T appeared to have much more genes related to replication, recombination and repair. As a copiotroph, *A. longa* SW024^T is long in length, and possesses large genome size and diverse transporters. However, it has also evolved many properties to survive in the oligotrophic marine environment. This bacterium grew better on solid medium than in liquid medium, suggesting it may be liable to attach to particle surfaces in order to survive in the nutrient-limiting environment. Gliding motility and the capacity to degrade various polymers possibly allow the bacterium to grow on detritus particles and use polymeric substances as carbon and energy sources. Moreover, genes related to carbon, nitrogen, and sulfur metabolisms were identified, which showed that *A. longa* SW024^T might be involved in various elemental cycles.

Conclusions: Genomic comparison of *Aquimarina* genus exhibits comprehensive capabilities of the strains to adapt to diverse marine environments. The genomic characteristics of *A. longa* SW024^T reveal that it evolves various strategies to cope with both copiotrophic and ultra-oligotrophic marine environment, which provides a better understanding of the survival abilities of bacteria in prevalent and even extreme oceanic environments. Furthermore, carbon, nitrogen and sulfur utilization of *A. longa* SW024^T may represent its potential functions in the global biogeochemical cycle.

Keywords: *Aquimarina longa*, Genome analysis, Genome comparison, Oligotrophic bacterium

* Correspondence: xhzhang@ouc.edu.cn
†Equal contributors
[1]College of Marine Life Sciences, Ocean University of China, 5 Yushan Road, Qingdao 266003, P. R. China
[2]Institute of Evolution & Marine Biodiversity, Ocean University of China, Qingdao 266003, China

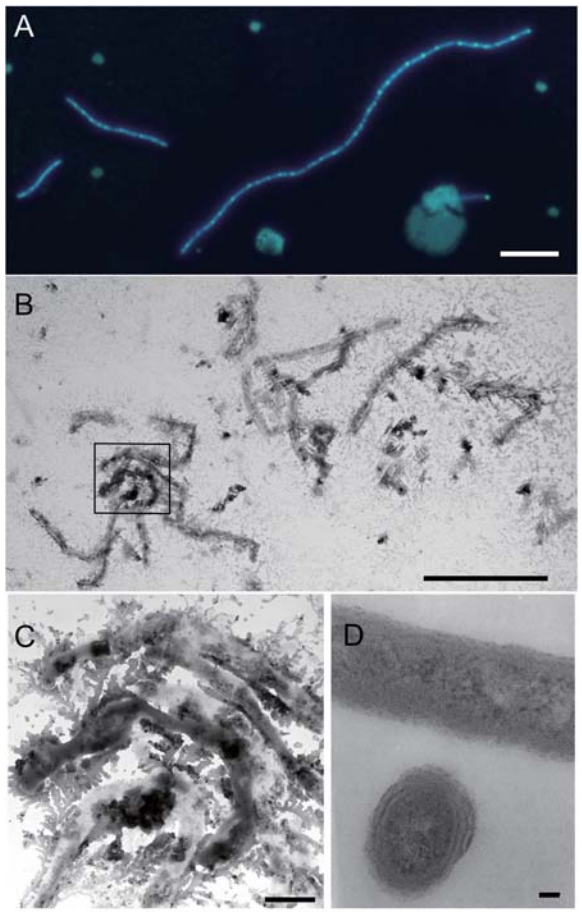

Fig. 6 Bacterial shape of *A. longa* SW024^T. Fluorescence microscopy of *A. longa* SW024^T stained with DAPI, bar = 5 μm (**a**). Transmission electron microscopy of *A. longa* SW024^T culturing in MB medium without staining, bar = 10 μm (**b**) and magnification of aggregate section in the boxed area, bar = 1 μm (**c**). Transmission electron microscopy of *A. longa* SW024^T using ultramicrotomy, including transections and longitudinal section, bar = 50 nm (**d**)

the target proteins interacting with P_{II} protein perform or regulate crucial reactions in nitrogen assimilatory pathways [47]. In addition, ammonium assimilation in this bacterium is mediated via glutamine synthetase and glutamate synthase. Nitrate is the most abundant N species in ocean environments, a complete pathway of denitrification exists in *A. longa* SW024^T, helping the bacterium acquire energy by this process.

P starvation may limit growth, and potentially constrain nitrogen fixation. Four genes in the genome are involved in P acquisition, and all of them encode putative alkaline phosphatases, which are necessary for hydrolysis of dissolved organic phosphorus [48]. Two-component system PhoR/PhoP in the genome may play a role in sensing and responding to changes in external/internal P levels prior to activating components of the P acquisition tool kit.

Although the classical ABC-type sulfate transport system is missing in *A. longa* SW024^T, it encodes two proteins, *i.e.*, a homolog of CysZ and a putative sulfate permease, both of which could serve as a sulfate transporter. Iron uptake mechanisms include TonB-dependent siderophore receptor, ABC-type iron transporter, ferrous iron transport protein, and ferric enterobactin receptor.

Like other marine bacteria, *A. longa* SW024^T encodes a primary Na^+ pump, the Na^+-translocating NADH/ubiquinone oxidoreductase, and probably uses a sodium ion gradient as the source of energy for nutrient uptake. In addition, it encodes primary H^+ pumps, namely, cytochrome bd complex, and cytochrome c oxidase. Salt acclimation includes several ion transporters which serve as exporters for sodium and chloride, the main toxic ions in seawater, and importers for potassium, which is essential for many cellular processes. Exporting of Na^+ ions at the expense of the proton gradient is performed by a variety of Na^+/H^+ antiporters, including NhaA, NhaB, NhaC and NhaP. In addition, *A. longa* SW024^T harbors Na^+/proline symporter, Na^+/phosphate symporter, cation/acetate symporter, Na^+/dicarboxylate symporter, Na^+/nucleoside permease, Na^+/iodide cotransporter, $Na^+/K^+/Ca^{2+}$ exchanger, Na^+/bile acid transporter, Na^+/multivitamin transporter, Na^+/glucose cotransporter, and proton/Na^+-glutamate symporter. Besides, three aquaporins AqpZ could help the bacterium to withstand dramatic changes in extracellular osmolarity and adapt to salinity stress [49].

Resistance to adverse effects

Oxidative DNA damage is a major source of mutation load in living organisms by means of damaging DNA, proteins and membranes of cells [50]. To avoid oxidative damage, *A. longa* SW024^T has set up several antioxidant defense mechanisms comprising antioxidant enzymes as well as antioxidative compounds. Three types of superoxide dismutase (SOD, *i.e.*, Cu-Zn SOD, Mn-SOD, Fe-SOD) which catalyze the dismutation of O_2^- to O_2 and H_2O_2, have been identified in the *A. longa* SW024^T genome. Genes encoding for two catalase-peroxidases, KatG and KatE, catalyzing the decomposition of hydrogen peroxide to water and oxygen are present in the genome. Moreover, it was reported that translation of the quinone-binding proteins was protected by the *katE* gene in tobacco leaves during exposure to light stress [51]. These antioxidants might also be crucial for bacteria survival during exposure to other stresses such as UV radiation. The reactive oxygen species-scavenging system in *A. longa* SW024^T also contains three peroxiredoxins (Prx), termed thioredoxin peroxidases, including one PrxQ and two 2-Cys Prx, which catalyze the reduction of various

1

Leucothrix pacifica sp. nov., isolated from seawater, and emended description of the genus *Leucothrix*

Zenghu Zhang,[1]† Xin Gao,[1]† Long Wang[1] and Xiao-Hua Zhang[1,2]

[1]College of Marine Life Sciences, Ocean University of China, Qingdao, PR China

[2]Institute of Evolution & Marine Biodiversity, Ocean University of China, Qingdao 266003, PR China

Correspondence
Xiao-Hua Zhang
xhzhang@ouc.edu.cn

A Gram-stain-negative, strictly aerobic, non-flagellated, non-gliding, oxidase- and catalase-positive, white-pigmented and rod-shaped bacterium, designated strain XH122^T, was isolated from a surface seawater sample collected from the South Pacific Gyre (45° 58′ E 163° 11′ S) during Integrated Ocean Drilling Program Expedition 329.Phylogenetic analysis based on 16S rRNA gene sequences indicated that strain XH122^T belonged to the genus Leucothrix and showed highest 16S rRNA gene sequence similarity to Leucothrix mucor DSM 2157^T (94.3 %). It showed lower sequence similarities (<90.7 %) with all other representatives of the class *Gammaproteobacteria*. Optimal growth occurred in the presence of 2 % (w/v) NaCl, at pH 8.0 and at 28 °C. The DNA G+C content of strain XH122^T was 46.2 mol%. The major fatty acids were $C_{16:0}$, $C_{16:1}\omega9c$ and $C_{18:1}\omega9c$. The major respiratory quinone was ubiquinone-8 (Q-8). The major polar lipids were phosphatidylethanolamine, phosphatidylglycerol and diphosphatidylglycerol. On the basis of data from this polyphasic study, strain XH122^T is considered to represent a novel species of the genus *Leucothrix*, for which the name *Leucothrix pacifica* sp. nov. is proposed. The type strain is XH122^T (=DSM 25984^T=JCM 18388^T).

The genus *Leucothrix*, a member of the class *Gammaproteobacteria*, was first described by Oersted (1844) and the description was emended by Harold & Stanier (1955). The genus *Leucothrix* was classified in the family Leucotrichaceae proposed by Buchanan (1957). Recently, the taxonomy of the genus *Leucothrix* was changed to the combined family *Thiotrichaceae* (Garrity *et al.*, 2005); however, the polyphyletic family designation should no longer be used because the *Thiotrichaceae* comprised physiologically and phylogenetically divergent bacteria and the genus *Leucothrix* should belong to the family *Leucotrichaceae* (Teske & Salman, 2014). Only one validated species of the genus *Leucothrix*, a large-diameter, morphologically distinct, marine bacterium, is currently recognized, *Leucothrix mucor* (Brock, 1974), and another invalidated species, '*Leucothrix thiophila*', which was capable of lithotrophic growth with reduced sulfur compounds (Grabovich *et al.*, 2002) was lost, and there is no information in GenBank relating to the latter taxon (Dul'tseva *et al.*, 1996). *L. mucor* can be identified mainly on the basis of morphological examination under the light microscope (Brock, 2006). A novel bacterial strain, designated XH122^T, was isolated from surface seawater of the South Pacific Gyre at station U1371 (45° 58′ E 163° 11′ S) during Integrated Ocean Drilling Program (IODP) Expedition 329. The present study describes the phenotypic and phylogenetic characteristics of strain XH122^T, on the basis of which it is considered to represent a novel species of the genus *Leucothrix*.

Surface water of the South Pacific Gyre was collected in November 2010 and spread on marine agar 2216 (MA; Becton Dickinson). Strain XH122^T, which formed opaque, circular (0.3–0.7 mm in diameter) and convex colonies with entire margins on MA after culture at 28 °C for 3 days, was picked and purified by streaking three times on MA. The culture was maintained on MA plates at 28 °C, and stocks were preserved in sterile 0.85 % (w/v) saline supplemented with glycerol at a final concentration of 15 % (v/v) at −80 °C. *L. mucor* DSM 2157^T was used as a reference strain, which was cultured under the same conditions as strain XH122^T [MA/marine broth 2216 (MB; BD), at 28 °C], unless otherwise specified.

Gram-staining and flagellum staining were tested using standard methods (Beveridge *et al.*, 2007). Cell morphology was

†These authors contributed equally to this work.

Abbreviations: IODP, Integrated Ocean Drilling Program.

The GenBank/EMBL/DDBJ accession number for the draft genome sequence of *Bacillus methylotrophicus* KACC 13105^T is JTKJ00000000.

One supplementary figure is available with the online Supplementary Material.

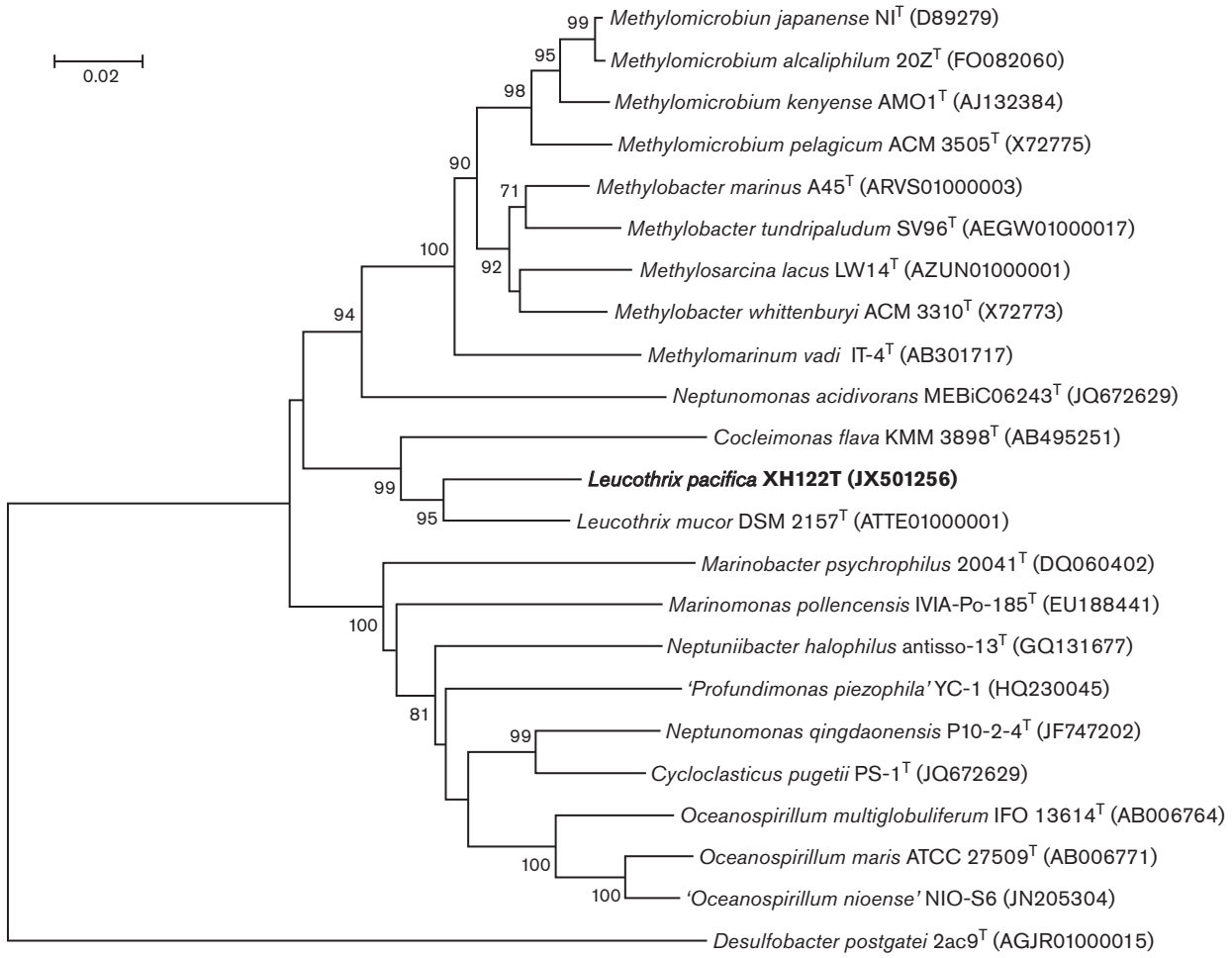

Fig. 2. Neighbour-joining phylogenetic tree based on 16S rRNA gene sequences showing the positions of strain XH122^T and other closely related members of the class *Proteobacteria*. Percentage bootstrap values above 70 (1000 replicates) are shown at branch nodes. *Desulfobacter postgatei* 2ac9^T (GenBank accession no. AGJR01000015) was used as an outgroup. Bar, 0.02 substitutions per nucleotide position.

L. mucor DSM 2157^T by forming a tight phylogenetic cluster with it (Fig. 2; see also Figs S2 and S3). However, the relatively low level of sequence similarity to *L. mucor* DSM 2157^T implied that it may represent a novel species in the genus *Leucothrix*.

The major features of strain XH122^T including the pH range that supports growth, hydrolysis of Tweens 20, 40 and 80, hydrolysis of starch and gelatin, the presence of oxidase and catalase activity, and the absence of indole and H_2S production are closely in line with those of *L. mucor* DSM 2157^T. In particular, the major respiratory quinone was Q-8 and the major profile of polar lipids was phosphatidylethanolamine, phosphatidylglycerol and diphosphatidylglycerol in both strain XH122^T and the reference strain. In addition, the DNA G+C content (46.2 mol%) of strain XH122^T was in the range reported for the genus *Leucothrix* (46–51 mol%) (Brock, 2006) and the major amounts of hexadecanoic acid, hexadecenoic acid and octadecenoic acid in strain XH122^T were similar to those of the reference strain, which indicated that strain XH122^T should be placed within the genus *Leucothrix*. Although strain XH122^T and the reference strain *L. mucor* DSM 2157^T shared many common features, they showed differences in some phenotypic characteristics including the temperature and NaCl ranges that support growth, DNase activity and hydrolysis of casein (Table 1), and in the compositions and proportions of some fatty acids (Table 2). On the basis of phenotypic characteristics and phylogenetic inference, strain XH122^T is assigned to the genus *Leucothrix* as a representative of a novel species, for which the name *Leucothrix pacifica* sp. nov. is proposed.

Emended description of the genus *Leucothrix* Brock 2006

The following description includes characteristics taken from the original description (Brock, 2006) as well as

International Journal of Systematic and Evolutionary Microbiology ijsemijs000270.3d 18/5/2015 15:30:20

Note

Muricauda pacifica sp. nov., isolated from seawater of the South Pacific Gyre

Zenghu Zhang,[1]† Xin Gao,[1]† Yanlu Qiao,[1] Yanan Wang[1] and Xiao-Hua Zhang[1,2]

Correspondence
Xiao-Hua Zhang
xhzhang@ouc.edu.cn

[1]College of Marine Life Sciences, Ocean University of China, Qingdao, PR China

[2]Institute of Evolution & Marine Biodiversity, Ocean University of China, Qingdao 266003, PR China

A Gram-stain-negative, strictly aerobic, non-flagellated, non-gliding, oxidase- and catalase-positive, rod-shaped and orange-pigmented bacterium with appendages, designated strain SW027^T, was isolated from a surface seawater sample collected from the South Pacific Gyre (26° 29′ S 137° 56′ W) during the Integrated Ocean Drilling Program (IODP) Expedition 329. Phylogenetic analysis based on 16S rRNA gene sequences indicated that strain SW027^T shared the highest sequence similarity with members of the genus *Muricauda* (94.3–92.7 %), exhibiting 94.3 % sequence similarity to *Muricauda flavescens* SW-62^T. Optimal growth occurred in the presence of 3 % (w/v) NaCl, at pH 7.0 and at 37 °C. The DNA G+C content of strain SW027^T was 42.7 mol%. The major fatty acids were iso-$C_{15:0}$, iso-$C_{15:1}$ G and iso-$C_{17:0}$ 3-OH. The major respiratory quinone was menaquinone-6. The major polar lipids were phosphatidylethanolamine and two unidentified lipids. Enzymic activity profiles, cell morphology and DNA G+C content differentiated the novel bacterium from the most closely related members of the genus *Muricauda*. On the basis of the polyphasic analyses, strain SW027^T is considered to represent a novel species of the genus *Muricauda*, for which the name *Muricauda pacifica* sp. nov. is proposed. The type strain is SW027^T (=JCM 17861^T=LMG 26637^T).

The genus *Muricauda* was proposed by Bruns *et al.* (2001) and its description was emended by Yoon *et al.* (2005) and Hwang *et al.* (2009); the genus is a member of the family *Flavobacteriaceae* in the class *Flavobacteriia*. At the time of writing, the genus *Muricauda* comprised ten species: *Muricauda ruestringensis* (Bruns *et al.*, 2001), *M. flavescens* and *M. aquimarina* (Yoon *et al.*, 2005), *M. lutimaris* (Yoon *et al.*, 2008), 1 *M. olearia* (Hwang *et al.*, 2009), *M. lutaonensis* (Arun *et al.*, 2009), *M. beolgyonensis* (Lee *et al.*, 2012), *M. taeanensis* (Kim *et al.*, 2013), *M. antarctica* (Wu *et al.*, 2013) and *M. zhangzhouensis* (Yang *et al.*, 2013). All members of the genus *Muricauda* were isolated from saline environments including a salt lake, coastal hot spring, intertidal sediment and tidal flat sediment as well as crude-oil-contaminated seawater and Antarctic seawater. Members of the genus *Muricauda* are Gram-staining-negative, rod-shaped cells, facultatively anaerobic or strictly aerobic. They do not produce flexirubin-type pigment. Optimal growth occurs between 20 and 30 °C or between 30 and 37 °C. All strains are positive for oxidase and catalase activities and hydrolysis of Tween 20. The fatty acid profile is characterized by large amounts of branched- and straight-chain fatty acids. The DNA G+C content is 41–51 mol%. The major isoprenoid quinone is MK-6. In this study, a novel bacterial strain, designated SW027^T, was isolated from surface seawater of the South Pacific Gyre at station U1367 (26° 29′ S 137° 56′ W) during the Integrated Ocean Drilling Program (IODP) Expedition 329. The aim of the present study was to determine the exact taxonomic position of strain SW027^T by a polyphasic taxonomy approach. In this work, we described the phenotypic and phylogenetic characteristics of strain SW027^T.

A surface seawater sample of the South Pacific Gyre was collected in November 2010 and spread on marine agar 2216 (MA; Becton Dickinson). Strain SW027^T, which formed transparent, circular (0.8–1.0 mm in diameter) and convex colonies with entire margins on MA after culturing at 28 °C for 3 days, was picked and purified by streaking three times on MA. The culture was maintained on MA plates at 28 °C, and stocks were preserved in sterile 0.85 % (w/v) saline supplemented with 15 % (v/v) glycerol at −80 °C. According to the initial phylogenetic analysis, strain SW027^T shared the highest sequence similarity with *M. flavescens* JCM 11812^T and formed a monophyletic

†These authors contributed equally to this work.

The GenBank/EMBL/DDBJ accession number for the 16S rRNA gene sequence of *Muricauda pacifica* SW027^T is JN118551.

Four supplementary figures are available with the online Supplementary Material.

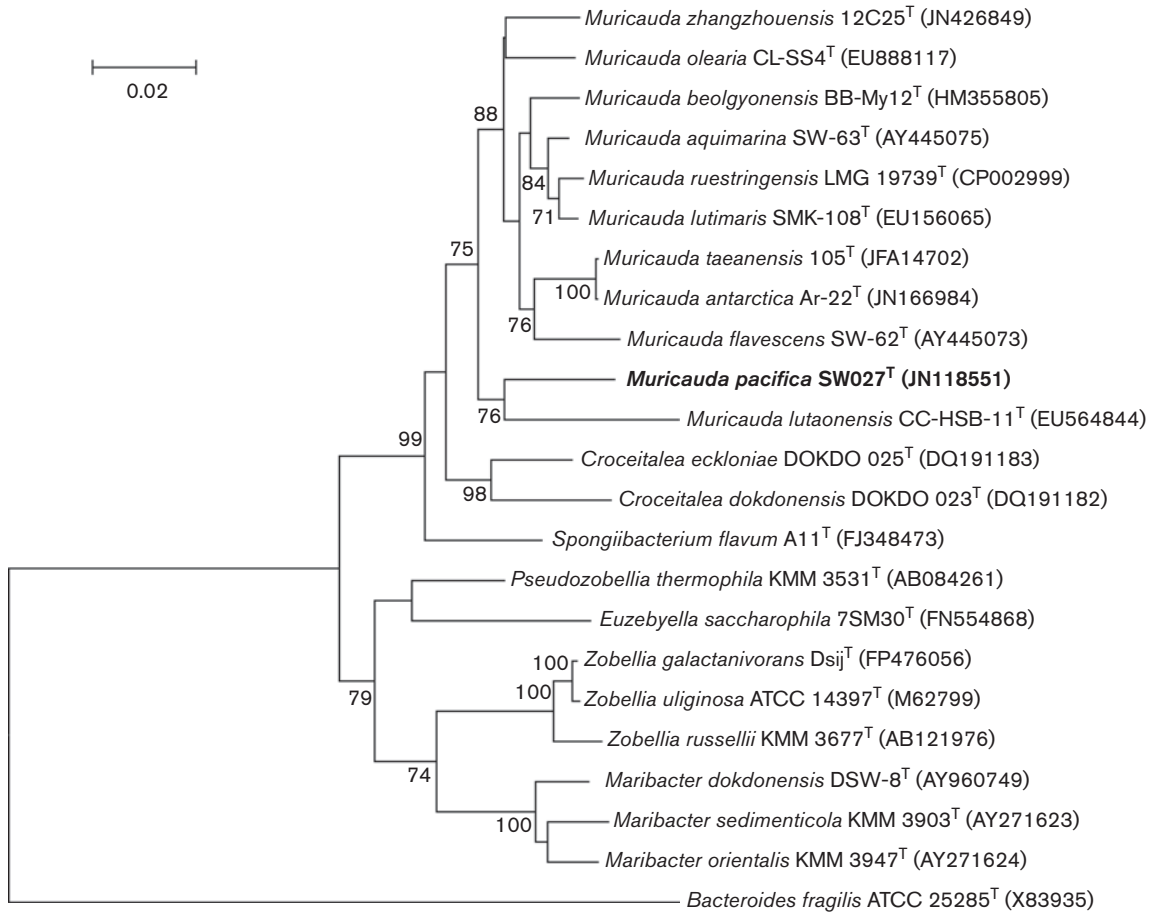

Fig. 1. Neighbour-joining phylogenetic tree based on 16S rRNA gene sequences showing the phylogenetic positions of strain SW027^T and other closely related species of the genus *Muricauda*. Percentage bootstrap values above 70 % (1000 replicates) are shown at branch nodes. *Bacteroides fragilis* ATCC 25285^T (GenBank accession no. X83935) was used as an outgroup. Bar, 0.02 substitutions per nucleotide position.

Pairwise alignment according to the nearly complete 16S rRNA gene sequence (1437 bp) of strain SW027^T showed that this strain shared the highest sequence similarity with members of the genus *Muricauda* (94.3–92.7 %), exhibiting 94.3 % sequence similarity to *M. flavescens* SW-62^T (=JCM 11812^T). Phylogenetic analysis based on 16S rRNA gene sequence comparison showed that strain SW027^T belonged to the genus *Muricauda* in the family *Flavobacteriaceae*. The phylogenetic trees using neighbour-joining, maximum-parsimony and maximum-likelihood methods showed that SW027^T fell within the cluster comprising species of the genus *Muricauda* and formed a monophyletic cluster with *M. lutaonensis* CC-HSB-11^T (Figs. 1, S3 and S4). However, the relatively low level of sequence similarity to the type strains of recognized species in the genus *Muricauda* implied that it may represent a novel species (Stackebrandt & Goebel, 1994).

The major features of strain SW027^T including the major respiratory quinone, the predominant cellular fatty acids (>10 %), the presence of the appendage, the optimum temperature range, hydrolysis of Tweens 20 and 40, hydrolysis of cellulose and starch and the presence of catalase and oxidase activity were significantly in line with those of the three reference strains of the genus *Muricauda*, and the phylogenetic analysis based on 16S rRNA gene sequences showed that strain SW027^T fell within the cluster comprising species of the genus *Muricauda* and formed a monophyletic cluster with *M. lutaonensis* CC-HSB-11^T. The DNA G+C content of strain SW027^T, 42.7 mol%, fell within the range (41–51 mol%) reported for members of the genus *Muricauda* (Arun *et al.*, 2009; Hwang *et al.*, 2009). The major polar lipids detected in strain SW027^T were phosphatidylethanolamine and two unidentified lipids. A similar polar lipid profile was seen in *M. flavescens* 11812^T (Fig. S2). The pigment of strain SW027^T had absorption maxima at 448 and 472 nm, similar to the carotenoid pigment of *M. antarctica* Ar-22^T (Wu *et al.*, 2013). However, strain SW027^T could be clearly distinguished from the reference strains of related species of the genus *Muricauda* by some differences in phenotypic

Celeribacter manganoxidans sp. nov., a manganese-oxidizing bacterium isolated from deep-sea sediment of a polymetallic nodule province

Long Wang,[1]† Yan Liu,[1]† Yanan Wang,[1] Xiaofeng Dai[1] and Xiao-Hua Zhang[1,2]

[1]College of Marine Life Sciences, Ocean University of China, Qingdao 266003, PR China
[2]Institute of Evolution & Marine Biodiversity, Ocean University of China, Qingdao 266003, PR China

Correspondence
Xiao-Hua Zhang
xhzhang@ouc.edu.cn

A Gram-stain-negative, strictly aerobic, non-motile, rod-shaped, manganese-oxidizing bacterial strain, designated DY2–5^T, was isolated from surface sediment of Pacific Clarion-Clipperton Fracture Zone (CCFZ). Growth occurred at 0–37 °C (optimum 28 °C), pH 6.5–9.0 (optimum pH 7.0–7.5) and in the presence of 1–11 % (w/v) NaCl (optimum 3–4 %). Phylogenetic analysis based on 16S rRNA gene sequences revealed that the novel strain was most closely related to *Celeribacter halophilus* ZXM137^T with 96.13 % sequence similarity, and had 16S rRNA gene sequence similarities in the range 93.89–95.87 % with other species of the genus *Celeribacter*. The dominant fatty acids were summed feature 8 ($C_{18:1}\omega7c$ and/or $C_{18:1}\omega6c$) and $C_{16:0}$.The polar lipids of strain DY2–5^T comprised phosphatidylglycerol, phosphatidylcholine, two unknown aminolipids, two unknown glycolipids and one unknown lipid. The major respiratory quinone was ubiquinone–10 (Q–10). The DNA G+C content of strain DY2–5^T was 64.8 mol%. On the basis of the phenotypic, genotypic and physiological evidence, strain DY2–5^T represents a novel species of the genus *Celeribacter*, for which the name *Celeribacter manganoxidans* sp. nov. is proposed. The type strain is DY2–5^T (=JCM 19384^T=KCTC 32473^T).

The genus *Celeribacter*, a member of the family *Rhodobacteraceae*, was first proposed by Ivanova *et al.* (2010). Following reclassification of *Huaishuia halophila* as a member of the genus *Celeribacter* by Lai *et al.* (2014), this genus comprised five species at the time of writing: *Celeribacter neptunius* (Ivanova *et al.*, 2010), *Celeribacter baekdonensis* (Lee *et al.*, 2012), *Celeribacter halophilus* (Wang *et al.*, 2012), *Celeribacter marinus* (Baek *et al.*, 2014) and *Celeribacter indicus* (Lai *et al.*, 2014). While the first four species were isolated from coastal surface seawater, *C. indicus* was isolated from deep-sea sediment. Members of the genus *Celeribacter* are characterized as being Gram-stain-negative, non-spore-forming, chemo-organotrophic with rod-shaped cells that contain ubiquinone-10 (Q-10) as the major respiratory quinone and summed feature 8 ($C_{18:1}\omega7c$ and/or $C_{18:1}\omega6c$) as the most abundant fatty acids. In this study, a manganese-oxidizing bacterial strain, designated DY2–5^T, was isolated from sediment of a polymetallic nodule province and was proposed to be a novel species of the genus *Celeribacter* based on phenotypic and genotypic characterization.

Strain DY2–5^T, isolated from surface sediment of a polymetallic nodule province of Clarion-Clippert Fracture Zone (CCFZ) in the eastern equatorial Pacific Ocean, was picked as a single colony on marine agar 2216 (MA; Becton Dickinson) after incubation for 3 days at 28 °C. *C. neptunius* H 14^T obtained from the Marine Culture Collection of China (MCCC) and *C. halophilus* ZXM137^T obtained from our own laboratory were used as reference strains, and were cultured as for strain DY2–5^T [MA/marine broth 2216 (MB; BD), 28 °C], unless otherwise specified.

For 16S rRNA gene sequencing, genomic DNA was extracted and purified using standard methods (Ausubel *et al.*, 1995). The 16S rRNA gene was amplified by PCR using two universal primers (B8F, 5′-AGAGTTTGATCCTGGCTCAG-3′; B1510, 5′-GGTTACCTTGTTACGACTT-3′; Weisburg *et al.*, 1991). The PCR product was

†These authors contributed equally to this work.

Abbreviation: LBB, leucoberbelin blue.

The GenBank/EMBL/DDBJ accession number for the 16S rRNA gene sequence of strain DY2–5^T is KF356415.

Two supplementary figures are available with the online Supplementary Material.

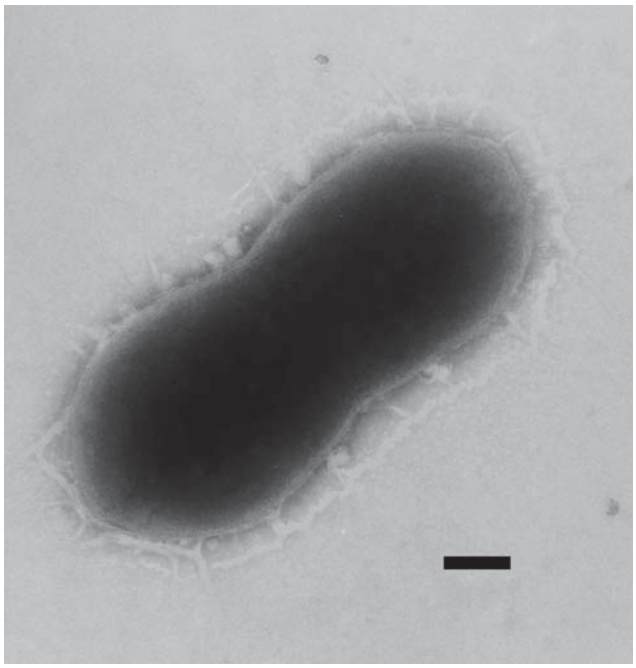

Fig. 2. Transmission electron micrographs of negatively stained cells of strain DY2−5^T cultured on MA at 28 °C for 24 h. Bar, 200 nm.

$NaHCO_3$ (pH 9.0–10.0). The presence of gliding motility and the production of flexirubin-type pigments were investigated using the methods described by Bernardet *et al.* (2002). Standard protocols (Tindall *et al.*, 2007) were used to assess catalase and oxidase activities, degradation of casein, starch, gelatin, agar corrosion, cellulose and Tweens 20, 40 and 80. DNase activity was examined by using DNase agar (Qingdao Hope Bio-technology) according to the manufacturer's instructions. Activities of constitutive enzymes, the fermentation/oxidation profile, acid production and substrate utilization as sole carbon and energy source were performed using API 20E, API 20NE, API 50CH and API ZYM strips (bioMérieux) and the GN2 MicroPlate kit (Biolog) according to the manufacturers' instructions except that sterile seawater was used to prepare the inoculum. The detailed morphological, physiological and biochemical characteristics of strain DY2–5^T are given in the species description, Table 1 and Fig. 2.

The extracellular accumulation of manganic oxide during growth of strains DY2–5^T, *C. neptunius* H 14^T and *C. halophilus* ZXM137^T were examined on K agar plates (Boogerd & de Vrind, 1987) supplemented with 100 mM Mn^{2+} (as $MnCl_2$). The plates were incubated at 28 °C and the presence of brownish manganic oxide deposits in the colonies could be confirmed by the addition of leucoberbelin blue (LBB) reagent (Ghiorse & Hirsch, 1979). After 20 days, small manganic oxide deposits could be observed in the colonies of strain DY2–5^T under the microscope, and these deposits turned blue with the addition of LBB reagent. However, the results of *C. neptunius* H 14^T and *C. halophilus* ZXM137^T were negative.

Table 2. Cellular fatty acid contents (%) of strain DY2−5^T and related species of genus *Celeribacter*

Strains: 1, DY2−5^T; 2, *C. halophilus* ZXM137^T; 3, *C. neptunius* H 14^T; 4, *C. baekdonensis* L-6^T; 5, *C. marinus* IMCC12053^T; 6, *C. indicus* P73^T. Data for strains 1−3 were from this study under the same conditions; data for strains 4−6 were obtained from original references. TR, Trace amount (<1 %); –, not detected.

Fatty acid	1	2	3	4	5	6
$C_{10:0}$ 3-OH	–	6.95	–	2.8	2.6	1.8
$C_{16:0}$	10.68	3.01	2.80	2.4	5.0	7.9
$C_{16:0}$ 3-OH	–	TR	1.21	–	–	–
$C_{18:0}$	1.67	1.85	2.54	1.3	2.2	6.0
$C_{18:0}$ 3-OH	–	TR	1.97	1.5	–	–
$C_{15:1}\omega8c$	–	–	–	–	–	2.5
$C_{18:1}\omega9c$	–	–	–	–	–	2.6
$C_{18:1}\omega7c$ 11-methyl	3.82	6.99	7.22	9.7	9.5	–
$C_{19:0}$ 10-methyl	–	7.21	6.27	3.3	1.3	1.3
$C_{20:4}\omega6,9,12,15c$	–	–	5.98	1.4	–	–
cyclo-$C_{19:0}\omega8c$	7.33	–	–	–	–	17.4
Summed features*						
3	2.90	TR	–	–	–	–
8	72.63	71.58	71.40	73.0	76.3	58.6

*Summed features are groups of two or three fatty acids that are treated together for the purpose of evaluation in the MIDI system and include both peaks with discrete equivalent chain-lengths (ECLs) as well as those where the ECLs are not reported separately, as indicated by Montero-Calasanz *et al.* (2013). Summed feature 3 contains $C_{16:1}\omega7c$ and/or $C_{16:1}\omega6c$; summed feature 8 contains $C_{18:1}\omega6c$ and/or $C_{18:1}\omega7c$.

For fatty acid analysis, cell masses of strain DY2–5^T, *C. neptunius* H 14^T and *C. halophilus* ZXM137^T were obtained after cultivation on MA at 28 °C for 2–3 days when each of the communities reached the late exponential stage of growth. Extraction of fatty acid methyl esters and separation by GC were performed by using the Instant FAME method of the Microbial Identification System (MIDI) version 6.1 and the RTSBA6 6.10 database (Sasser 1990). Polar lipids were analysed by using standard procedures (Minnikin *et al.*, 1984). Extracted lipids were separated by two-dimensional TLC and identified by spraying with appropriate detection reagents. Spraying with 5 % ethanolic molybdophosphoric acid followed by charring at 150 °C revealed the presence of all lipids. Ninhydrin spray was applied to determine most of the lipids with free amino groups, while spraying the plate with the lipid phosphate reagent of Dittmer and Lester after the ninhydrin spray revealed the presence of phospholipids. Spraying with α-naphthol/sulphuric acid determined the presence of glycolipids. The periodate-Schiff reagent spray was applied to reveal lipids with a terminal CH_2OH group, such as glycerol (Minnikin *et al.*, 1984). The respiratory quinone of strain DY2–5^T was extracted with chloroform/methanol (2 : 1, v/v), separated

International Journal of Systematic and Evolutionary Microbiology ijsem000558.3d 28/9/2015 18:13:0

Jiella aquimaris gen. nov., sp. nov., isolated from offshore surface seawater

Jing Liang,[1] Ji Liu[1] and Xiao-Hua Zhang[1,2]

[1]College of Marine Life Sciences, Ocean University of China, Qingdao 266003, PR China

[2]Institute of Evolution & Marine Biodiversity, Ocean University of China, Qingdao 266003, PR China

Correspondence
Xiao-Hua Zhang
xhzhang@ouc.edu.cn

A Gram-stain-negative, strictly aerobic and rod-shaped motile bacterium with peritrichous flagella, designated strain LZB041^T, was isolated from offshore surface seawater of the East China Sea. Phylogenetic analysis based on 16S rRNA gene sequences indicated that strain LZB041^T formed a lineage within the family '*Aurantimonadaceae*' that was distinct from the most closely related genera *Aurantimonas* (96.0–96.4 % 16S rRNA gene sequence similarity) and *Aureimonas* (94.5–96.0 %). Optimal growth occurred in the presence of 1–7 % (w/v) NaCl, at pH 7.0–8.0 and at 28–37 °C. Ubiquinone-10 was the predominant respiratory quinone. The major fatty acids (>10 % of total fatty acids) were $C_{18:1}\omega7c$ and/or $C_{18:1}\omega6c$ (summed feature 8) and cyclo-$C_{19:0}\omega8c$. The major polar lipids were phosphatidylglycerol, diphosphatidylglycerol, phosphatidylcholine, phosphatidylethanolamine, phosphatidylmonomethylethanolamine, one unknown aminolipid, one unknown phospholipid and one unknown polar lipid. The DNA G+C content of strain LZB041^T was 71.3 mol%. On the basis of polyphasic analysis, strain LZB041^T is considered to represent a novel species of a new genus in the class *Alphaproteobacteria*, for which the name *Jiella aquimaris* gen. nov., sp. nov. is proposed. The type strain of the type species is LZB041^T (=JCM 30119^T=MCCC 1K00255^T).

Over recent decades, many novel taxa within the class *Alphaproteobacteria* have been described, and at the time of writing, this class comprises 13 orders. The order *Rhizobiales* is a phenotypically heterogeneous assemblage within the class *Alphaproteobacteria*, and is divided into 13 families based on 16S rRNA gene sequence analyses. The family '*Aurantimonadaceae*' is affiliated to the order *Rhizobiales* (Kuykendall, 2005) and, at the time of writing, comprises the genera *Aurantimonas*, *Aureimonas*, *Fulvimarina* and *Martelella*. The genus *Aurantimonas* was originally described by Denner *et al.* (2003) with *Aurantimonas coralicida* as the type species. Subsequently, five species have been characterized. However, based on the evident heterogeneity to other species in the genus *Aurantimonas*, Rathsack *et al.* (2011) reclassified *Aurantimonas altamirensis*, *Aurantimonas frigidaquae* and *Aurantimonas ureilytica* into a novel genus named *Aureimonas* as *Aureimonas altamirensis*, *Aureimonas frigidaquae* and *Aureimonas ureilytica*, respectively, with *Aureimonas altamirensis* as the type species. The genus *Fulvimarina* was first proposed for a novel bacterium isolated from the Atlantic Ocean (Cho & Giovannoni, 2003), and subsequently emended by Rathsack *et al.* (2011). The genus *Martelella* was proposed by Rivas *et al.* (2005) with a single species, *Martelella mediterranea*, and at the time of writing comprises four species.

Members of the family '*Aurantimonadaceae*' were isolated from various sources including diverse marine environments, water, soil, air, tidal flats, plant tissues and rusty iron plates. In the course of identifying dimethylsulfoniopropionate (DMSP)-utilizing bacteria in the marine environment, a peritrichously flagellated bacterial strain, designated LZB041^T, was isolated from the offshore surface seawater of the East China Sea at station ME3 (28° 43.931′ N 122° 34.904′ E) during the expedition of the R/V 'Dong Fang Hong 2' in July 2013. The aim of the present study was to determine the exact taxonomic position of strain LZB041^T by using a polyphasic characterization that included the determination of chemotaxonomic and phenotypic properties, and detailed phylogenetic investigation based on 16S rRNA gene sequences.

Strain LZB041^T was isolated by the standard dilution spreading method on marine agar 2216 (MA; Becton Dickinson) incubated at 28 °C for up to 1 week. A yellow colony, designated strain LZB041^T, was isolated and subsequently purified three times on MA at 28 °C. Working cultures were routinely maintained on MA at 28 °C and

Abbreviations: DMSP, dimethylsulfoniopropionate; DPG, diphosphatidylglycerol; ML, maximum-likelihood; MP, maximum-parsimony; NJ, neighbour-joining; PC, phosphatidylcholine; PE, phosphatidylethanolamine; PG, phosphatidylglycerol; PME, phosphatidylmonomethylethanolamine.

The GenBank/EMBL/DDBJ accession number for the 16S rRNA gene sequence of strain LZB041^T is KJ620984.

Three supplementary figures are available with the online Supplementary Material.

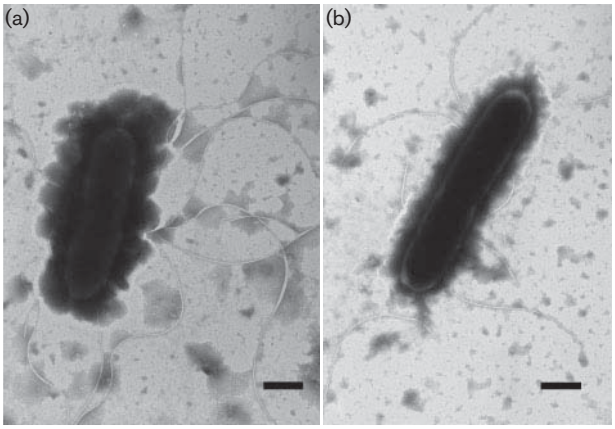

Fig. 2. Transmission electron micrographs of negatively stained cells of strain LZB041^T cultured on MA at 28 °C for 24 h. Bar, 0.5 μm.

total fatty acids) of strain LZB041^T was summed feature 8 ($C_{18:1}\omega7c$ and/or $C_{18:1}\omega6c$). However, in strain LZB041^T, the amount of the second predominant cellular fatty acid, cyclo-$C_{19:0}\omega8c$, was significantly higher than that observed in members of the genera *Aurantimonas* and *Aureimonas*. Differences in fatty acid composition and the proportion of some components were identified between strain LZB041^T and the reference strains (Table 2). The predominant isoprenoid quinone detected in strain LZB041^T was ubiquinone-10 (Q-10), which is consistent with its placement in the family '*Aurantimonadaceae*'. The major polar lipids detected in strain LZB041^T were phosphatidylglycerol (PG), diphosphatidylglycerol (DPG), phosphatidylcholine (PC), phosphatidylethanolamine (PE), phosphatidylmonomethylethanolamine (PME), one unknown aminolipid, one unknown phospholipid and one unknown polar lipid (Fig. S3). This polar lipid profile was mostly similar to the reference strains (Rathsack *et al.*, 2011) but there were some differences in strain LZB041^T including the absence of sulfoquinovosyldiacylglycerol (SQDG) and the unidentified lipids. The DNA G+C content of strain LZB041^T was 71.3 mol%, which falls within the range for members of the genus *Aureimonas* (63.9–71.8 mol%; Lin *et al.*, 2013; Madhaiyan *et al.*, 2013).

The conclusion drawn from phylogenetic analysis that strain LZB041^T represents a novel genus of the family '*Aurantimonadaceae*' was supported by morphological and physiological characteristics that distinguished the novel strain from other bacteria in the family '*Aurantimonadaceae*' including: (i) the presence of peritrichous flagella; (ii) the high tolerance of NaCl for growth; (iii) the proportion of cyclo-$C_{19:0}\omega8c$ was significantly high among total fatty acids; (iv) the evident different results in citrate assimilation, valine arylamidase, α-chymotrypsin and α-glucosidase tests. Other characteristics that differentiate strain LZB041^T from members of related genera are shown in Table 1. It can be concluded after combining phenotypic, phylogenetic and genetic data, strain LZB041^T should be classified as representing a novel species of a new genus in the family '*Aurantimonadaceae*', for which the name *Jiella aquimaris* gen. nov., sp. nov. is proposed.

Table 2. Cellular fatty acid contents (%) of strain LZB041^T and the reference strains

Strains: 1, LZB041^T; 2, *Aurantimonas coralicida* DSM 14790^T; 3, *Aureimonas altamirensis* DSM 21988^T. All data are from this study. Only fatty acids >1 % of the total fatty acids of at least one of the strains are shown. Major fatty acids (>10 %) are indicated in bold type. TR, Trace amount (<1 % of total); −, not detected.

Fatty acid	1	2	3
Straight chain			
$C_{16:0}$	5.91	**13.71**	**11.41**
$C_{18:0}$	1.54	5.31	5.1
Hydroxy			
$C_{18:1}$ 2-OH	−	2.71	−
Unsaturated			
$C_{20:1}\omega7c$	−	TR	1.08
cyclo-$C_{19:0}\omega8c$	**21.44**	3.48	**10.44**
11-methyl $C_{18:1}\omega7c$	Tr	−	−
Summed feature*			
2	1.13	−	1.09
5	TR	1.18	1.14
8	**64.07**	**68.4**	**60.73**

*As indicated by Montero-Calasanz *et al.* (2013), summed features are groups of two or three fatty acids that are treated together for the purpose of evaluation in the MIDI system, and include both peaks with discrete equivalent chain-lengths (ECLs) as well as those where the ECLs are not reported separately. Summed feature 5 was listed as $C_{18:2}\omega6,9c$ and/or anteiso-$C_{18:0}$; summed feature 8 was listed as $C_{18:1}\omega7c$ and/or $C_{18:1}\omega6c$. Summed feature 2 was listed as $C_{12:0}$ aldehyde, unknown 10.928, $C_{14:0}$ 3-OH and iso-$C_{16:1}$ I.

Description of *Jiella* gen. nov.

Jiella (Ji.el′la. N.L. dim. fem. n. *Jiella* of Ji, in honour of the marine microbiologist Weishang Ji from Ocean University of China).

Cells with peritrichous flagella are Gram-stain-negative, strictly aerobic rods. Oxidase-, catalase- and urease-positive. The major respiratory quinone is Q-10. Predominant cellular fatty acids are summed feature 8 ($C_{18:1}\omega7c$ and/or $C_{18:1}\omega6c$) and cyclo-$C_{19:0}\omega8c$. The major polar lipids are PG, DPG, PC, PE, PME, one unknown aminolipid, one unknown phospholipid and one unknown polar lipid. Phylogenetically, the genus belongs to the family '*Aurantimonadaceae*' in the class *Alphaproteobacteria*. The type species is *Jiella aquimaris*.

Description of *Jiella aquimaris* sp. nov.

Jiella aquimaris (a.qui.ma′ris. L. n. *aqua* water; L. gen. n. *maris* of the sea; N.L. gen. n. *aquimaris* of the water of the sea).

International Journal of Systematic and Evolutionary Microbiology (2015), **65**, 154–158 **DOI** 10.1099/ijs.0.069906-0

Spongiibacterium pacificum sp. nov., isolated from seawater of South Pacific Gyre and emended description of the genus *Spongiibacterium*

Xin Gao,[1] Zenghu Zhang,[1] Xiaofeng Dai[1] and Xiao-Hua Zhang[1,2]

Correspondence
Xiao-Hua Zhang
xhzhang@ouc.edu.cn

[1]College of Marine Life Sciences, Ocean University of China, Qingdao, PR China

[2]Institute of Evolution & Marine Biodiversity, Ocean University of China, Qingdao 266003, PR China

A Gram-stain-negative, strictly aerobic, non-flagellated, non-gliding, oxidase-positive and yellow-pigmented rod-shaped bacterium, designated strain SW169^T, was isolated from a surface seawater sample collected from the South Pacific Gyre (27° 55′ S 123° 10′ W) during the Integrated Ocean Drilling Program (IODP) Expedition 329. Phylogenetic analysis based on 16S rRNA gene sequences indicated that strain SW169^T belonged to the genus *Spongiibacterium* and showed the highest 16S rRNA gene sequence similarity with *Spongiibacterium flavum* A11^T (95.9 %). It showed 16S rRNA gene sequence similarities of 93.2–94.8 % with members of the genera *Croceitalea* and *Flagellimonas* in the family *Flavobacteriaceae*. Optimal growth occurred in the presence of 3–4 % (w/v) NaCl, at pH 8.0 and at 28 °C. The DNA G+C content of strain SW169^T was 43.3 mol%. The major fatty acids were iso-$C_{15:1}$ G, iso-$C_{15:0}$, iso-$C_{17:0}$ 3-OH, iso-$C_{15:0}$ 3-OH and summed feature 3 (comprising $C_{16:1}\omega7c$ and/or $C_{16:1}\omega6c$,). The major respiratory quinone was menaquinone-6. The major polar lipids were phosphatidylethanolamine, one unidentified aminolipid and one unidentified lipid. On the basis of the polyphasic analyses, strain SW169^T is considered to represent a novel species of the genus *Spongiibacterium*, for which the name *Spongiibacterium pacificum* sp. nov. is proposed. The type strain is SW169^T (=JCM 18379^T=LMG 26997^T). An emended description of the genus *Spongiibacterium* is also provided.

The genus *Spongiibacterium*, a member of the family *Flavobacteriaceae*, was first proposed by Yoon & Oh (2012) with the description of *Spongiibacterium flavum*, which is the type and only recognized species of the genus at the time of writing. *S. flavum* is a heterotrophic, Gram-negative, non-gliding, yellow-pigmented marine bacterium, which was isolated from marine sponge. A novel bacterial strain, designated SW169^T, was isolated from surface seawater of the South Pacific Gyre at station U1368 (27° 55′ S 123° 10′ W) during the Integrated Ocean Drilling Program (IODP) Expedition 329. The aim of the present study was to investigate the possibility that strain SW169^T may represent a novel species of the genus *Spongiibacterium*. In this work, we describe the phenotypic and phylogenetic characteristics of strain SW169^T.

Abbreviations: IODP, Integrated Ocean Drilling Program; PE, phosphatidylethanolamine.

The GenBank/EMBL/DDBJ accession number for the 16S rRNA gene sequence of strain SW169^T is JX501249.

Three supplementary figures are available with the online Supplementary Material.

Surface water of the South Pacific Gyre was collected in November 2010 and spread on marine agar 2216 (MA; Becton Dickinson). Strain SW169^T, which formed transparent, circular (0.3–0.5 mm in diameter), convex colonies with entire margins on MA after culturing at 28 °C for 3 days, was picked and purified by streaking three times on MA. The culture was maintained on MA at 28 °C, and stocks were preserved in sterile 0.85 % (w/v) saline supplemented with 15 % (v/v) glycerol at −80 °C. *Spongiibacterium flavum* DSM 22638^T was used as a reference strain, which was cultured under the same conditions as strain SW169^T [MA/marine broth 2216 (MB; BD), 28 °C], unless otherwise specified.

Gram-staining and flagellum staining were investigated using standard methods (Beveridge *et al.*, 2007). Cell morphology was determined by transmission electron microscopy (JEM-1200EX; JEOL) after cells had been negatively stained with 1 % (w/v) phosphotungstic acid. The presence of gliding motility and the production of flexirubin-type pigments were investigated using the methods described by Bernardet *et al.* (2002). To test anaerobic growth, bacterial strains were cultured on MA with resazurin (0.02 %, w/v) as an indicator of anaerobic

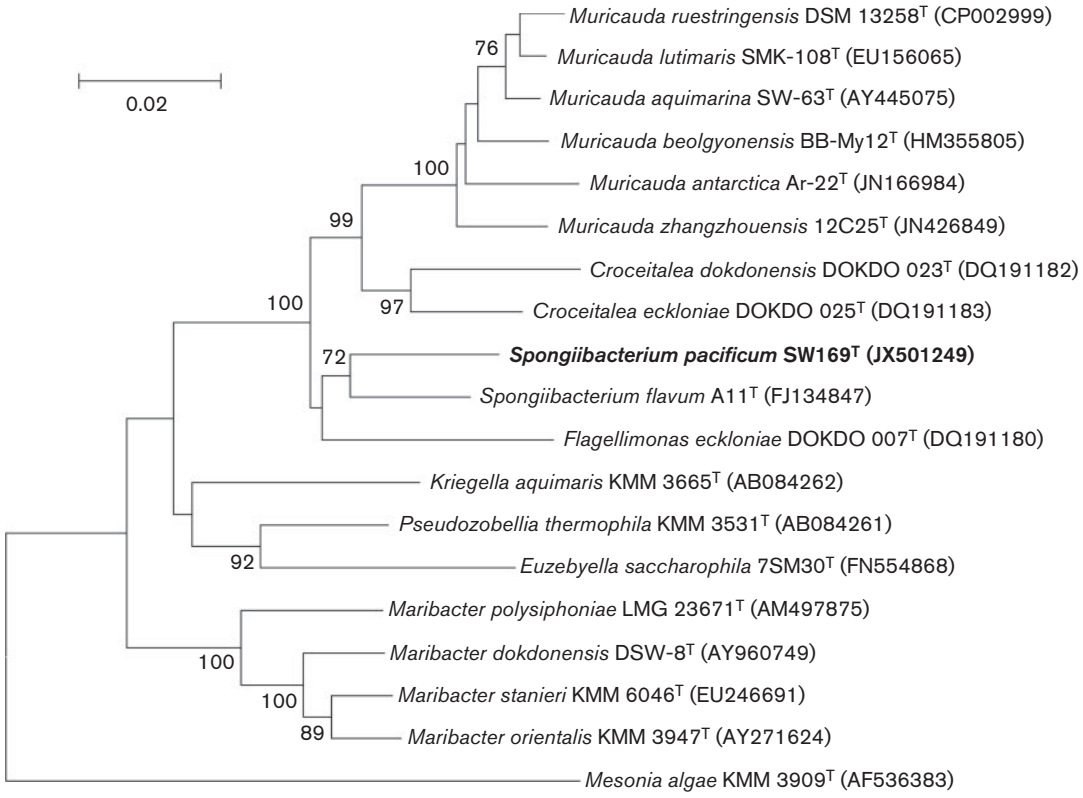

Fig. 1. Neighbour-joining phylogenetic tree based on 16S rRNA gene sequences showing the phylogenetic positions of strain SW169^T and other closely related members of the family *Flavobacteriaceae*. Numbers at nodes are bootstrap values (% of 1000 replicates); only values >70 % are shown. *Mesonia algae* KMM 3909^T (GenBank accession no. AF536383) was used as an out-group. Bar, 0.02 substitutions per nucleotide position.

detected in some strains. The DNA G+C content is 41.7–43.3 mol%.

Description of *Spongiibacterium pacificum* sp. nov.

Spongiibacterium pacificum (pa.ci′fi.cum. L. neut. adj. *pacificum* peaceful, pertaining to the Pacific Ocean).

Cells are Gram-stain-negative, aerobic, non-gliding rods (1.9–2.6 μm in length, 0.2–0.3 μm in width after culturing on MA for 24 h at 28 °C) without any flagella. Colonies are transparent, yellow, circular (0.3–0.5 mm in diameter) and convex on MA after 3 days at 28 °C. Growth occurs at 10–35 °C (optimum 28 °C). The salinity range for growth is 1–6 % (w/v) NaCl (optimum 3–4 %), and the pH range is 7.0–9.0 (optimum pH 8.0). Flexirubin-type pigments are not formed. Oxidase-positive but catalase-negative. DNA, starch and aesculin can be degraded; urea, gelatin, casein and Tweens 20, 40 and 80 are not hydrolysed. Acetoin is produced, but indole and H_2S are not. Nitrate is reduced to nitrite. Lysine decarboxylase, ornithine decarboxylase, tryptophan deaminase and arginine dihydrolase activities are absent. Positive for β-galactosidase activity and citrate utilization. Acid is produced from glucose, sucrose, melibiose, amygdalin and arabinose, but not from mannitol, inositol, sorbitol or rhamnose. Glucose, mannose, mannitol, *N*-acetylglucosamine, gluconate, malate and citrate are assimilated, but arabinose, maltose, capric acid, adipic acid and phenylacetic acid are not. In the API ZYM strip, alkaline phosphatase, esterase (C4), esterase lipase (C8), leucine arylamidase, valine arylamidase, cystine arylamidase, trypsin, acid phosphatase, α-galactosidase, β-galactosidase, naphthol-AS-BI-phosphohydrolase, α-glucosidase and *N*-acetyl-β-glucosaminidase activities are present; lipase (C14), α-chymotrypsin, β-glucuronidase, β-glucosidase, α-mannosidase and α-fucosidase activities are absent. There are positive reactions in the Biolog GN2 MicroPlate system for Tween 40, acetic acid, propionic acid, hydroxy-L-proline, L-proline, inosine, uridine and thymidine. The dominant fatty acids are iso-$C_{15:1}$ G, iso-$C_{15:0}$, iso-$C_{17:0}$ 3-OH, iso-$C_{15:0}$ 3-OH and summed feature 3 ($C_{16:1}\omega7c$ and/or $C_{16:1}\omega6c$). The major respiratory quinone is MK-6. The major polar lipids are PE, an unidentified aminolipid and one unidentified lipid.

The type strain, SW169^T (=JCM 18379^T=LMG 26997^T), was isolated from a seawater sample collected from the South Pacific Gyre (27° 55′ S 123° 10′ W). The DNA G+C content of the type strain is 43.3 mol%.

Hyunsoonleella pacifica sp. nov., isolated from seawater of South Pacific Gyre

Xin Gao,[1] Zenghu Zhang,[1] Xiaofeng Dai[1] and Xiao-Hua Zhang[1,2]

[1]College of Marine Life Sciences, Ocean University of China, Qingdao, PR China

[2]Institute of Evolution & Marine Biodiversity, Ocean University of China, Qingdao 266003, PR China

Correspondence
Xiao-Hua Zhang
xhzhang@ouc.edu.cn

A Gram-stain-negative, strictly aerobic, non-flagellated, non-gliding, oxidase- and catalase-positive and rod-shaped yellow-pigmented bacterium, designated strain SW033^T was isolated from a surface seawater sample collected from the South Pacific Gyre (GPS position: 26° 29′ S 137° 56′ W) during the Integrated Ocean Drilling Program, expedition 329. Phylogenetic analysis based on 16S rRNA gene sequences indicated that strain SW033^T belonged to the genus *Hyunsoonleella* and showed the highest 16S rRNA gene sequence similarity with *Hyunsoonleella jejuensis* CNU004^T (96.8 %). It showed 94.7–95.8 % 16S rRNA gene sequence similarity with respect to members of the genera *Jejuia, Arenitalea* and *Algibacter* in the family *Flavobacteriaceae*. Optimal growth occurred in the presence of 2–3 % (w/v) NaCl, at pH 8.0 and at 28 °C. The genomic DNA G+C content of strain SW033^T was 36.1 mol%. The major fatty acids were iso-$C_{15:1}$ G, iso-$C_{15:0}$, iso-$C_{17:0}$ 3-OH, iso-$C_{15:0}$ 3-OH and summed feature 3 (comprising $C_{16:1}\omega7c$ and/or $C_{16:1}\omega6c$). The major respiratory quinone was menaquinone-6. The major polar lipids were phosphatidylethanolamine, two unidentified aminolipids and four unidentified lipids. On the basis of the polyphasic analyses, strain SW033^T is considered to represent a member of a novel species in the genus *Hyunsoonleella*, for which the name *Hyunsoonleella pacifica* sp. nov. is proposed. The type strain is SW033^T (=CGMCC 1.11009^T=JCM 17860^T).

The genus *Hyunsoonleella*, a member of the family *Flavobacteriaceae*, was first proposed by Yoon *et al.* (2010) with the description of *Hyunsoonleella jejuensis* as the type and only recognized species of the genus so far. *H. jejuensis* is a heterotrophic, Gram-stain-negative, non-gliding and yellow-pigmented marine bacterium, which was isolated from a seawater sample collected along the coastline of Jeju Island, Republic of Korea. A novel bacterial strain, designated SW033^T, was isolated from surface seawater of the South Pacific Gyre at station U1367 (GPS position: 26° 29′ S 137° 56′ W) during the Integrated Ocean Drilling Progra, expedition 329. The aim of the present study was to determine the exact taxonomic position of the strain SW033^T using a polyphasic taxonomic approach.

Surface water of the South Pacific Gyre was collected in November 2010 and spread on marine agar 2216 (MA; Becton Dickinson). Strain SW033^T, which formed translucent, circular (0.6–0.8 mm in diameter) and convex colonies with entire margins on MA after culturing at 28 °C for 3 days, was picked and purified by streaking three times on MA. The cultures were maintained on MA plates at 28 °C, and stocks were preserved in sterile 0.85 % (w/v) saline supplemented with 15 % (v/v) glycerol at −80 °C. *H. jejuensis* DSM 21035^T and *Jejuia pallidilutea* DSM 21165^T were used as the reference strains, which were cultured under the same conditions as SW033^T, unless otherwise specified.

Gram and flagellum staining were investigated using standard methods (Beveridge *et al.*, 2007). Cell morphology was determined by transmission electron microscopy (JEM-1200EX; JEOL) after cells had been negatively stained with 1 % (w/v) phosphotungstic acid. The presence of gliding motility and the production of flexirubin-type pigments were investigated using the methods described by Bernardet *et al.* (2002). To test anaerobic growth, bacterial strains were cultured on MA with resazurin (0.02 %, w/v) as an indicator of anaerobic condition in an anaerobic jar filled with nitrogen and a packet of AneroPack-Anaero (Mitsubishi Gas Chemical) at 28 °C for 1 month. The temperature range for growth was determined on MA by incubating cultures at 4–37 °C (4, 10, 16, 28, 32, 35 and 37 °C) for 7 days and at 0 °C on MA for 30 days. Salinity

Four figures are available as supplementary materials with the online version of this paper.

Abbreviation: PE, phosphatidylethanolamine.

The GenBank/EMBL/DDBJ accession number for the 16S rRNA gene sequence of SW033^T is JX501247.

Four supplementary figures are available with the online Supplementary Material.

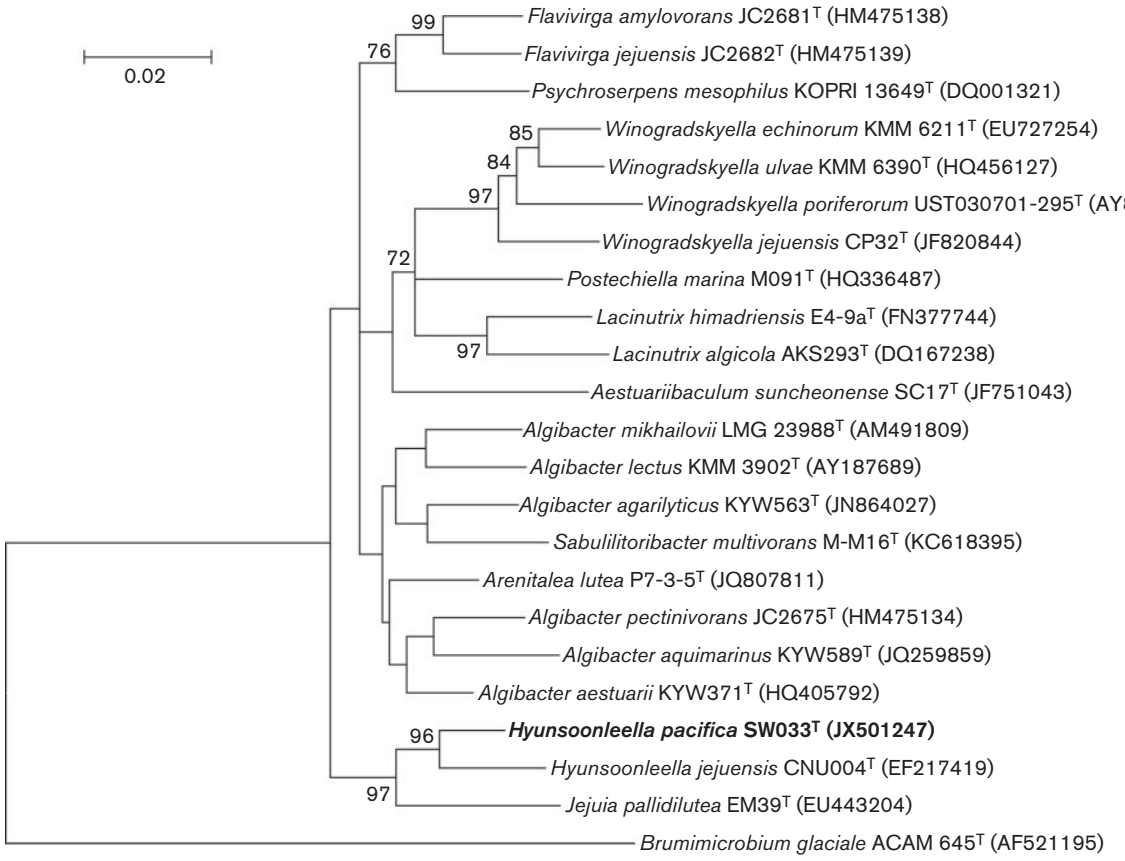

Fig. 1. Neighbour-joining phylogenetic tree based on 16S rRNA gene sequences showing the phylogenetic positions of the type strain SW033^T and other closely related members of the family *Flavobacteriaceae*. Percentage bootstrap values above 70 (1000 replicates) are shown at branch nodes. *Brumimicrobium glaciale* ACAM 645^T (GenBank accession no. AF521195) was used as an outgroup. Bar, 0.02 substitutions per nucleotide position.

α-chymotrypsin, acid phosphatase, naphthol-AS-BI-phosphohydrolase and α-glucosidase activities are present. However, lipase (C14), cystine arylamidase, trypsin, α-galactosidase, β-galactosidase, β-glucuronidase, β-glucosidase, *N*-acetyl-β-glucosaminidase, α-mannosidase and α-fucosidase activities are absent. The following substrates are utilized in the GN2 Microplate: α-cyclodextrin, dextrin, cellobiose, D-galactose, α-D-glucose, maltose, succinic acid monomethyl-ester, acetic acid, citric acid, α-ketobutyric acid, α-ketoglutaric acid, α-ketovaleric acid, L-alaninamide, L-alanine, L-glutamic acid, hydroxy-L-proline, L-ornithine, L-proline, L-serine, L-threonine, inosine, uridine and thymidine; the other substrates are not utilized. The dominant fatty acids are iso-$C_{15:1}$ G, iso-$C_{15:0}$, iso-$C_{17:0}$ 3-OH, iso-$C_{15:0}$ 3-OH and summed feature 3 ($C_{16:1}\omega7c$ and/or $C_{16:1}\omega6c$). The major respiratory quinone is MK-6. The major polar lipids are PE, two unidentified aminolipids and four unidentified lipids.

The type strain, SW033^T (=CGMCC 1.11009^T=JCM 17860^T), was isolated from a seawater sample collected from the South Pacific Gyre (GPS position: 26° 29′ S 137° 56′ W). The genomic DNA G+C content of the type strain is 36.1 mol%.

Acknowledgements

This research used samples provided by the Integrated Ocean Drilling Program (IODP). We thank all of the crews and technical staffs on the *JOIDES Resolution* during the IODP, expedition 329 for their great efforts and help in sample collection. This work was supported by projects from the National Natural Science Foundation of China (grant no. 41276141), the China Ocean Mineral Resources Research & Development Association (COMRA, grant no. DY125-15-R-03), and the National High Technology Research & Development Program of China (863 Programs, grant no. 2012AA091605).

References

Ausubel, F. M., Brent, R., Kingston, R. E., Moore, D. D., Seidman, J. G., Smith, J. A. & Struhl, K. (editors) (1995). *Short Protocols in Molecular Biology: a Compendium of Methods from Current Protocols in Molecular Biology*, 3rd edn. New York: Wiley.

Bernardet, J. F., Nakagawa, Y., Holmes, B. & Subcommittee on the taxonomy of Flavobacterium and Cytophaga-like bacteria of the

JOURNAL OF NATURAL PRODUCTS

Article

pubs.acs.org/jnp

Chromone Derivatives from a Sponge-Derived Strain of the Fungus *Corynespora cassiicola*

Dong-Lin Zhao,[†] Chang-Lun Shao,[†] Li-She Gan,[‡] Mei Wang,[†] and Chang-Yun Wang*[,†,§]

[†]Key Laboratory of Marine Drugs, The Ministry of Education of China, School of Medicine and Pharmacy, and [§]Institute of Evolution & Marine Biodiversity, Ocean University of China, Qingdao 266003, People's Republic of China

[‡]Institute of Modern Chinese Medicine, College of Pharmaceutical Sciences, Zhejiang University, Hangzhou 310058, People's Republic of China

Supporting Information

ABSTRACT: Twelve new chromone derivatives, corynechromones A–L (**1**–**12**), were isolated from the sponge-derived fungus *Corynespora cassiicola* XS-200900I7. Among them, **1**/**2**, **3**/**4**, **5**/**6**, and **7**/**8** were pairs of epimers. The planar structures were determined by extensive NMR spectroscopic data. The absolute configurations of **1**–**10** were assigned by the modified Mosher's method and TDDFT ECD calculations together with comparison of their CD spectra. These are the first chromone derivatives reported from the genus *Corynespora*. A possible rule to determine the absolute configurations at C-2 in chromone derivatives by CD was proposed.

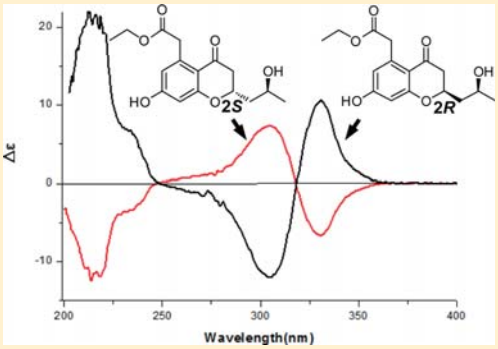

Marine-derived fungi play an important role in the discovery and development of drugs used to treat various diseases and are widely recognized as prolific sources of biologically active and structurally unique natural products.[1,2] During the past several decades, the secondary metabolites of hundreds of species of marine-derived fungi have been investigated; however, the chemical constituents of fungi belonging to the genus *Corynespora* from the marine environment have received scant attention. A literature survey showed that there are only two reports on the secondary metabolites from marine-derived *Corynespora cassiicola*, including decalactones, depsidones, naphthoquinones, and octalactone derivatives.[3] During our ongoing search for new bioactive secondary metabolites from marine-derived fungi in the South China Sea,[4] a sponge-derived fungus, *Corynespora cassiicola* XS-200900I7, collected from the Xisha Islands coral reef, attracted our attention because the HPLC profile of the extract of the fungal culture showed different UV absorption from those of *Corynespora* sp. reported in the literature.[3,5] Chemical investigation on the EtOAc extract led to the isolation of 12 new chromone derivatives, corynechromones A–L (**1**–**12**). Herein we report the isolation, structure elucidation, and biological activities of these compounds.

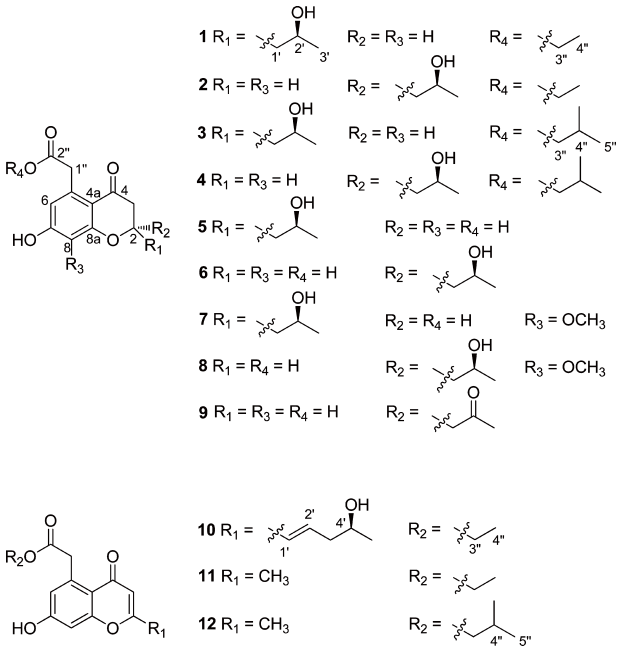

RESULTS AND DISCUSSION

Corynechromone A (**1**) was obtained as a white, amorphous powder and assigned the molecular formula $C_{16}H_{20}O_6$ by HRESIMS, indicating seven degrees of unsaturation. The ^{1}H NMR spectrum (Table 1) displayed signals for two aromatic protons at δ_H 6.38 (d, J = 2.0 Hz) and 6.35 (d, J = 2.0 Hz), two oxymethines at δ_H 4.63 (m) and 4.04–4.10 (m), one oxymethylene at δ_H 4.04–4.10 (m), three sets of nonequivalent methylene protons at δ_H 3.91 (d, J = 17.0 Hz) and 3.87 (d, J =

Received: November 17, 2014
Published: January 16, 2015

DOI: 10.1021/np5009152
J. Nat. Prod. 2015, 78, 286–293

Table 1. ^{1}H NMR Data of 1−6 (500 MHz, acetone-d_6, δ in ppm, J in Hz)

position	1	2	3	4	5	6
2	4.63, m	4.59, m	4.62, m	4.59, m	4.64, m	4.59, m
3	2.51−2.61, m	2.55−2.65, m	2.50−2.60, m	2.58−2.65, m	2.53−2.63, m	2.60−2.67, m
6	6.38, d, 2.0	6.38, d, 2.0	6.38, d, 2.0	6.40, d, 2.5	6.41, d, 2.5	6.41, d, 2.5
8	6.35, d, 2.0	6.36, d, 2.0	6.34, d, 2.0	6.36, d, 2.5	6.36, d, 2.5	6.36, d, 2.5
1′	1.89, m	2.01, m	1.83−1.93, m[a]	2.00, m	1.90, m	2.03, m
	1.64, m	1.78, m	1.63, m	1.78, m	1.64, m	1.78, m
2′	4.04−4.10, m[a]	4.01, m	4.08, m	4.01, m	4.09, m	4.01, m
3′	1.20, d, 6.0	1.22, d, 5.5	1.19, d, 6.0	1.21, d, 6.0	1.20, d, 6.0	1.22, d, 6.0
1″	3.91, d, 17.0	3.91, d, 17.0	3.93, d, 16.5	3.94, d, 16.5	3.96, d, 16.5	3.95, d, 16.5
	3.87, d, 17.0	3.87, d, 17.0	3.88, d, 16.5	3.90, d, 16.5	3.91 d, 16.5	3.91, d, 16.5
3″	4.04−4.10, m[a]	4.07, q, 7.0	3.79, d, 6.5	3.79, d, 6.5		
4″	1.20, t, 7.0	1.20, t, 7.0	1.83−1.93, m[a]	1.88, m		
5″			0.89, d, 6.5	0.89, d, 6.5		
6″			0.89, d, 6.5	0.89, d, 6.5		

[a]Overlapping signals.

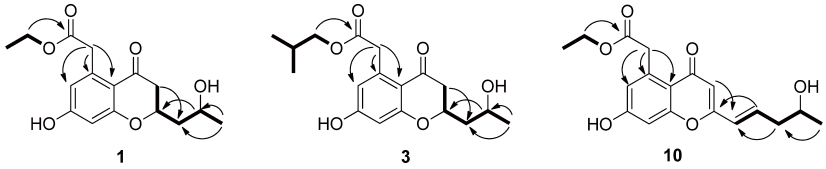

Figure 1. COSY and key HMBC correlations of **1**, **3**, and **10**.

Table 2. ^{1}H NMR Data of 7−12 (500 MHz, acetone-d_6, δ in ppm, J in Hz)

position	7	8	9	10	11	12
2	4.71, m	4.65, m	4.85, m			
3	2.54−2.68, m	2.60−2.71, m	2.58−2.67, m	5.97, s	5.92, s	5.92, s
6	6.47, s	6.47, s	6.43, d, 2.0	6.74, d, 2.0	6.73, brs	6.75, d, 2.5
8			6.32, d, 2.0	6.88, d, 2.0	6.78, brs	6.78, d, 2.5
1′	1.98, m	2.04−2.07, m	3.06, dd, 17.0, 7.0	6.30, d, 16.0	2.30, s	2.30, s
	1.70, m	1.85, m	2.89, dd, 17.0, 5.5			
2′	4.20, m	4.08, m		6.87, dt, 16.0, 7.5		
3′	1.24, d, 6.0	1.24, d, 6.0	2.21, s	2.41, t, 7.5		
4′				3.93, m		
5′				1.19, d, 5.5		
1″	3.92, d, 16.5	3.92, d, 16.5	3.93, s	4.10, s	4.10, s	4.13, s
	3.88, d, 16.5	3.87, d, 16.5				
3″				4.07, q, 7.0	4.07, q, 7.0	3.79, d, 6.5
4″				1.19, t, 7.0	1.20, t, 7.0	1.87, m
5″						0.88, d, 7.0
6″						0.88, d, 7.0
8-OCH_3	3.82, s	3.81, s				

17.0 Hz), δ_H 1.89 (m) and 1.64 (m), and δ_H 2.51−2.61 (m), and two methyl groups at δ_H 1.20 (d, J = 6.0 Hz) and 1.20 (t, J = 7.0 Hz). The ^{13}C NMR and DEPT spectra showed resonances for two carbonyl groups including one α,β-unsaturated ketone (δ_C 192.1) and one ester carbonyl (δ_C 171.2), six aromatic carbon atoms (δ_C 165.4, 163.8, 140.2, 115.0, 113.7, and 103.1), two oxymethines (δ_C 75.5 and 63.5), one oxymethylene (δ_C 60.5), three methylenes (δ_C 45.1, 44.8, and 41.5), and two methyl groups (δ_C 24.6 and 14.6). These spectroscopic features suggested that **1** belongs to the family of chromones and is very similar to aposphaerin B, which was isolated from an endophytic *Aposphaeria* sp. fungus cultured from a birch tree growing in a forest in Lower Saxony, Germany.[6] The only difference between **1** and aposphaerin B was the substituent at C-2. The COSY cross-peaks of H-1′/H-2′/H-3′, together with the HMBC correlations from H-3′ to C-1′ and C-2′, suggested the presence of a 2-hydroxypropyl [$-CH_2CH(OH)CH_2$] moiety (Figure 1). The COSY cross-peaks of H-1′/H-2/H-3 in addition to the HMBC correlations from H-2′ to C-2, from H-1′ to C-2 and C-3, and from H-3 to C-1′ indicated that the 2-hydroxypropyl moiety was located at C-2. Detailed analysis of the HMQC, COSY, and HMBC spectra allowed the assignment for all carbon and proton resonances of **1**, and the planar structure of **1** was elucidated.

Corynechromone B (**2**) was also isolated as a white, amorphous powder, possessing the same molecular formula $C_{16}H_{20}O_6$ as **1**. Comparison of the ^{1}H and ^{13}C NMR spectra of **2** with those of **1** showed strong similarities except that the carbon resonances of **2** at C-2 (δ_C 76.4 in **2** vs 75.5 in **1**), C-3 (δ_C 44.1 in **2** vs 44.8 in **1**), C-1′ (δ_C 44.6 in **2** vs 45.1 in **1**), and

DOI: 10.1021/np5009152
J. Nat. Prod. 2015, 78, 286−293

Mar Biotechnol (2015) 17:99–109
DOI 10.1007/s10126-014-9598-4

ORIGINAL ARTICLE

Phylogenetic Diversity and Antibacterial Activity of Culturable Fungi Derived from the Zoanthid *Palythoa haddoni* in the South China Sea

Xiao-Yan Qin · Kai-Lin Yang · Jing Li · Chang-Yun Wang · Chang-Lun Shao

Received: 14 March 2014 / Accepted: 25 July 2014 / Published online: 13 August 2014

Abstract Investigation on diversity of culturable fungi mainly focused on sponges and corals, yet little attention had been paid to the fungal communities associated with zoanthid corals. In this study, a total of 193 culturable fungal strains were isolated from the zoanthid *Palythoa haddoni* collected in the South China Sea, of which 49 independent isolates were identified using both morphological characteristics and internal transcribed spacer (ITS) sequence analyses. Thirty-five strains were selected for phylogenetic analysis based on fungal ITS sequences. The results indicated that 18 genera within eight taxonomic orders of two phyla (seven orders of the phylum Ascomycota and one order of the phylum Basidiomycota) together with one unidentified fungal strain have been achieved, and *Cladosporium* sp. represented the dominant culturable genus. Particularly, 14 genera were isolated from a zoanthid for the first time. The antibacterial activities of organic extracts of mycelia and fermentation broth of 49 identified fungi were evaluated, and 29 (59.2 %) of the isolates displayed broad-spectrum or selective antibacterial activity. More interestingly, more than 60 % of the active fungal strains showed strong activity against two aquatic pathogenic bacteria *Nocardia brasiliensis* and *Vibrio parahaemolyticus*, compared with other pathogenic bacteria, indicating that zoanthid-derived fungi may protect its host against pathogens. This is the first report of systematically phylogenetic diversity and extensively antibacterial activity of zoanthid-derived fungi.

Keywords Cnidaria · Zoanthid · *Palythoa haddoni* · Marine fungi · Phylogenetic diversity · Antibacterial activity

Introduction

The biodiversity of the marine environment and the associated chemical diversity constitute a practically unlimited resource of new active substances in the field of the development of marine bioactive products (Carté 1996; Kobayashi and Tsuda 2004; Simmons et al. 2005; Strobel 2003). Fungi, as an important composition of marine microorganisms, have attracted more attention in recent years. Secondary metabolites from marine-derived fungi have proved to be rich sources of structurally novel and biologically active compounds that have become significant chemical entities for drug discovery (Blunt et al. 2014; Newman and Cragg 2012).

Marine fungi grow on a wide variety of substrata ranging from wood, sediments, soils, algae, corals, and calcareous tubes of mollusks to decaying leaves of mangroves, intertidal grasses, and living animals (Kohlmeyer and Kohlmeyer 1979; Hyde 1996). About 800–1,000 taxa of marine fungi representing a wide range of pathogens and symbionts had been identified from the complex inhabitants in coral reefs (Herndl and Weinbauer 2003). It has been reported that many marine invertebrates are marine filter feeders that can filter large volumes of surrounding water through a unique aquiferous system (Rohwer et al. 2001; Rohwer et al. 2002; Nithyanand et al. 2011). As a result, they become a rich

Xiao-Yan Qin and Kai-Lin Yang contributed equally to this work.

X.-Y. Qin · K.-L. Yang · C.-Y. Wang · C.-L. Shao (✉)
Key Laboratory of Marine Drugs, The Ministry of Education of China, School of Medicine and Pharmacy, Ocean University of China, 5 Yushan Road, Qingdao 266003, People's Republic of China
e-mail: shaochanglun@163.com

J. Li
College of Marine Life Sciences, Ocean University of China, 5 Yushan Road, Qingdao 266003, People's Republic of China

C.-Y. Wang (✉)
Institute of Evolution & Marine Biodiversity, Ocean University of China, 5 Yushan Road, Qingdao 266003, People's Republic of China
e-mail: changyun@ouc.edu.cn

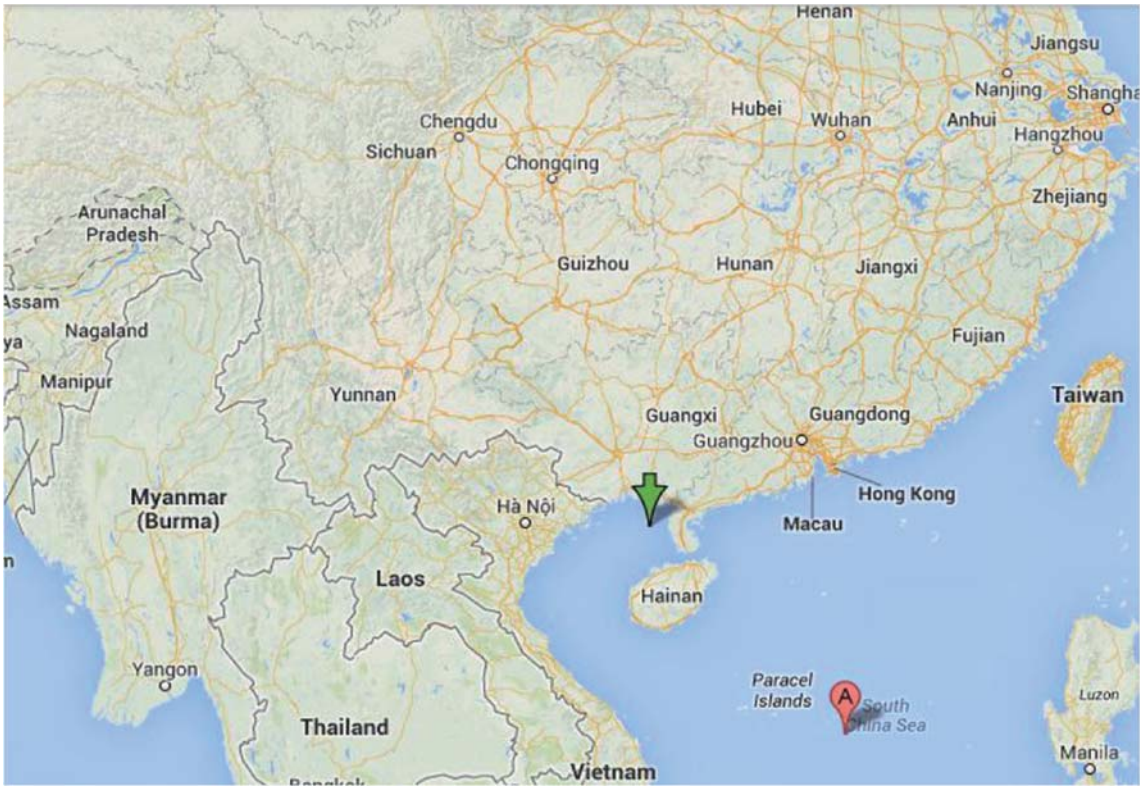

Fig. 1 Map of the South China Sea (*red arrow*) and location of the sampling site (*green arrow*)

DNA Extraction, PCR Amplification, and Sequencing

About 100 mg of fresh fungal mycelium was collected in an Eppendorf tube (1.5 mL) to extract genomic DNA from the fungus using the Fungal DNA kits (50) (E.Z.N.A., Omega) according to the manufacturer's protocol. The resulting genomic DNA was used as template to amplify the fungal ITS-rDNA gene fragment, and nearly full-length ITS sequences were amplified by polymerase chain reaction using primers ITS1F (5′-CTTGGTCATTTAGAGGAAGTAA-3′) (Gardes and Bruns 1993) and ITS4 (5′-TCCTCCGCTTATTGATATGC-3′) (White et al. 1990). The PCR reactions were performed in a final volume of 50 μL, which was composed of template DNA (2 μL), 5 μL 10X PCR buffer, 1 μL dNTP, 0.5 μL ITS1F, 0.5 μL ITS4 (20 μmol/mL each), 0.25 μL Taq polymerase, and appropriate ultrapure water. Amplification reaction was carried out with the following thermal cycles profiles: 1 cycle for 5 min at 94 °C; then 30 cycles of 40 s at 94 °C, 40 s at 52 °C, and 60 s at 72 °C; and followed by a final extension at 72 °C for 10 min. Then, PCR products (5 μL) were loaded onto an agarose gel (1.2 % agarose in 0.5×TAE, 5 μL of ethidium bromide 1 %*m*/*v* solution per 100 mL of gel); then, they were isolated from a gel extraction kit (E.Z.N.A., Omega) according to the manufacturer's protocol after electrophoresis at 100 V for 35 min. PCR products were submitted for sequencing (Invitrogen, Shanghai) with the primer ITS4 or ITS1F. The sequence results were compared in GenBank using the Basic Local Alignment Search Tool.

Table 1 Composition of media used for fungal isolation

Medium	Composition (L^{-1})
Potato dextrose agar (PDA) medium	200 g potato extract[a], 20 g dextrose, 1 g peptone, 3 g K_2HPO_4, 15 g agar
Rose bengal medium (RBM)	5 g peptone, 10 g glucose, 0.033 g rose bengal, 1 g K_2HPO_4, 0.5 g $MgSO_4$, 15 g agar
Czapek-Dox medium	30 g sucrose, 15 g agar, 3 g $NaNO_3$, 0.5 g KCl, 1 g K_2HPO_4, 1.5 g $MgSO_4 \cdot 7H_2O$, 0.01 g $FeSO_4$, 0.5 g KCl
Luria Bertani (LB) agar medium[b]	10 g peptone, 5 g yeast extract, 10 g NaCl, 15 g agar

All media were prepared with artificial sterile seawater (ASW; Li and Liu 2006), and adjusted to pH 7.2 prior to autoclaving at 121 °C for 20 min

[a] The unpeeled potato (200 g) was washed, cut into pieces, and boiled in seawater for 30 min

[b] The LB medium was used in antibacterial activity test

SCIENTIFIC REPORTS

OPEN

Received: 25 November 2014
Accepted: 15 April 2015
Published: 21 May 2015

Bioinformatical Analysis of the Sequences, Structures and Functions of Fungal Polyketide Synthase Product Template Domains

Lu Liu[1], Zheng Zhang[2], Chang-Lun Shao[1], Jin-Lan Wang[3], Hong Bai[1] & Chang-Yun Wang[1,4]

The product template (PT) domains, specifically in fungal non-reducing polyketide synthases (NR-PKSs), mediate the regioselective cyclization of polyketides dominating the final structures. However, up to date, the systematic knowledge about PT domains has been insufficient. In present study, the relationships between sequences, structures and functions of the PT domains were analyzed with 661 NR-PKS sequences. Based on the phylogenetic analysis, the PT domains were classified into prominent eight groups (I–VIII) corresponding with the representative compounds and cyclization regioselectivity (C2-C7, C4-C9, and C6-C11). Most of the cavity lining residue (CLR) sites in all groups were common, while the regional CLR site mutations resulted in the appearance of finger-like regions with different orientation. The cavity volumes and shapes, even the catalytic dyad positions of PT domains in different groups were corresponding with characteristic cyclization regioselectivity and compound sizes. The conservative residues in PT sequences were responsible for the cyclization functions and the evolution of the key residues resulted in the differentiations of cyclization functions. The above findings may help to better understand the cyclization mechanisms of PT domains and even predict the structural types of the aromatic polyketide products.

One hallmark of fungi is their capacity to synthesize diverse biological polyketide natural products with structural variation during synthesis by polyketide synthase (PKSs)[1–3]. With a few exceptions, a majority of fungal PKSs are iterative type I PKSs[1,4]. Fungal PKSs are intrinsically more difficult to be studied than the dissociated bacterial PKSs due to their large sizes (in excess of 200 kDa) and the difficulties with genetic manipulation[5]. In the past decade, more knowledge about biosynthesis mechanisms of fungal polyketide synthases has been acquired. It is generally recognized that most biosynthetic gene clusters including PKSs are silent or expressed at very low levels according to global transcriptomic profile[6]. Fungi have the potential to produce a far greater number of polyketides than the known polyketides isolated from fungi up to date. Therefore, it is essential to investigate and characterize fungal PKSs for enzymatic mechanism elucidation and genetic manipulation to obtain more new metabolites.

The fungal PKSs can be divided into three major classes according to the function and phylogeny, i.e., the non-reducing (NR), the highly-reducing (HR), and the partial-reducing (PR) PKSs[1]. The NR-PKSs synthesize aromatic polyketides, such as carcinogenic mycotoxin aflatoxin[7]. Besides the basic

[1]Key Laboratory of Marine Drugs, the Ministry of Education of China, School of Medicine and Pharmacy, Ocean University of China, Qingdao 266003, China. [2]State Key Laboratory of Microbial Technology, Shandong University, Jinan 250100, China. [3]School of Life Science, Shandong University, Jinan 250100, China. [4]Institute of Evolution & Marine Biodiversity, Ocean University of China, Qingdao 266003, China. Correspondence and requests for materials should be addressed to Z.Z. (email: zhzhang.sdu@gmail.com) or C.Y.W. (email: changyun@ouc.edu.cn)

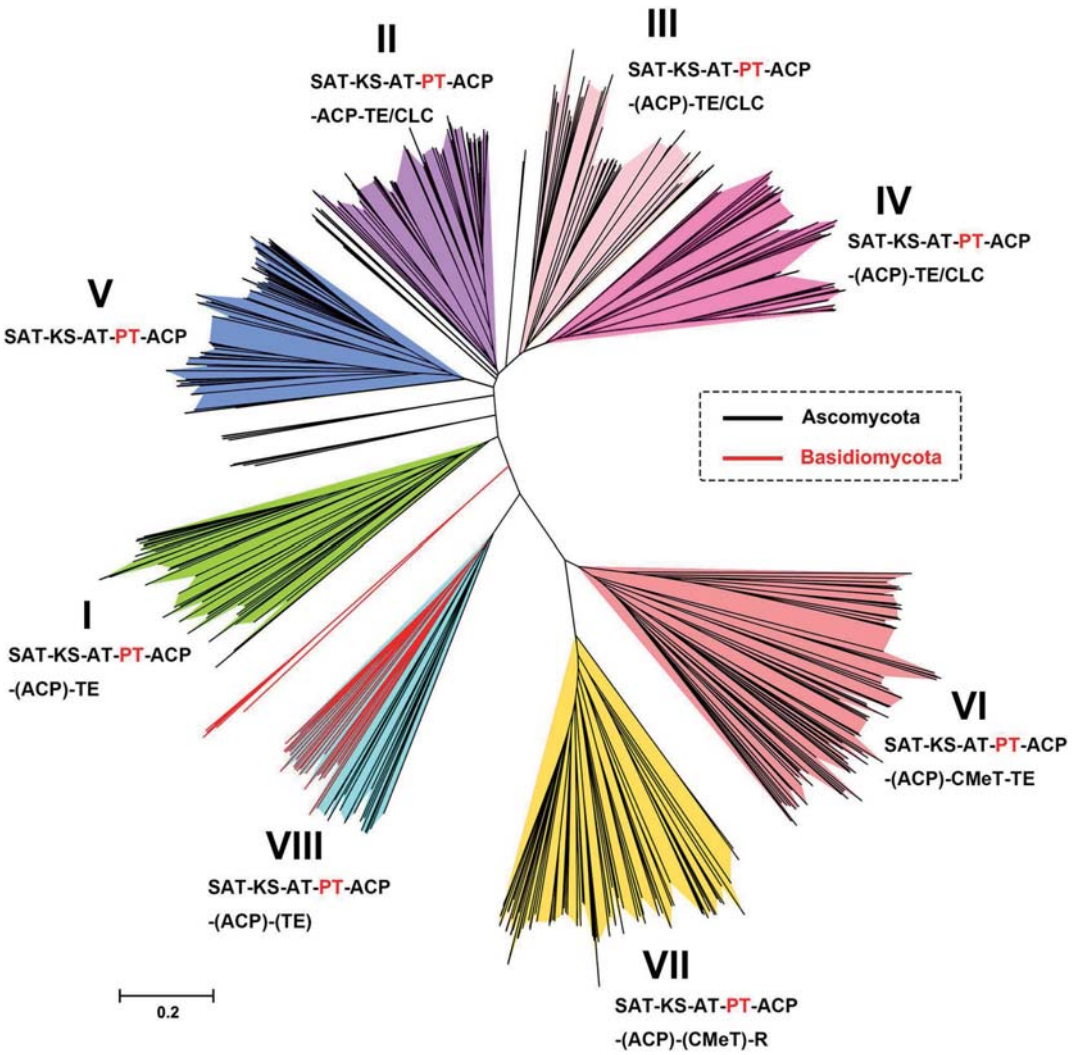

Figure 1. NR-PKS phylogenetic tree of 661 sequences from ascomycetes and basidiomycetes. The branches of eight groups have been colored, each of which shares a common organization of domains (those in parentheses are variable in their presence/absence within that group). Domain abbreviations: SAT = starter unit-ACP transacylase, KS = ketosynthase, AT = acyl transferase, PT = product template, ACP = acyl carrier protein, TE = thioesterase, TE/CLC = thioesterase/Claisen cyclase, CMeT = C-methyltransferase, R = reductase. The tree is drawn to scale, with branch lengths in the same units as those of the evolutionary distances used to infer the phylogenetic tree.

via C2-C7 aldol condensation. The main NR-PKSs in this group are involved in the biosynthesis of aromatic portions in the resorcylic acid lactones, exemplified by hypothemycin Hpm3[14], radicicol RDC1[14]/RADS2[15], and zearalenone PKS13[16]. Group I also includes a single aromatic ring synthase, the orsellinic acid OrsA from *Aspergillus nidulans*[17]. As an exception, the dehydrocurvularin AtCURS2 from *Aspergillus terreus* forms the first rings *via* C3-C8 rather than C2-C7[18].

In group II, the NR-PKSs include the most known THN synthases from a variety of genera responsible for the synthesis of 1,3,6,8-tetrahydroxynaphthalene (THN) analogues[19]. The PT domains of this group catalyze the aldol condensation *via* C2-C7 with pentaketide backbones. The TE/CLC domains in this group are in charge of cyclizing the second rings.

The NR-PKSs in group III synthesize longer polyketide chains *via* C2-C7 cyclization, such as naphthopyrone heptaketide synthase Alb1[20] and bikaverin nonaketide synthase PKS4[21]. Interestingly, the WA synthase from *A. nidulans* also generates pentaketide THN with shorter polyketide chains[11]. The previously biochemical analysis showed that THN is a result of shortening of the heptaketide YWA1, a common metabolite in group III synthesized by WA synthase [11,22].

All the PT domains in group IV cyclize the first ring *via* C4-C9 regiospecificity. The only one crystal structure of PT domain in PksA from *A. parasiticus*[12] is classified into group IV. The NR-PKSs of this group contain the analogues of decaketide synthase PksA, such as aflatoxin/sterigmatocystin

Steroids 94 (2015) 7–14

Contents lists available at ScienceDirect

Steroids

journal homepage: www.elsevier.com/locate/steroids

Subergorgiaols A–L, 9,10-secosteroids from the South China Sea gorgonian *Subergorgia rubra*

Xue-Ping Sun [a,b,1], Fei Cao [a,1], Chang-Lun Shao [a], Min Chen [a], Hai-Juan Liu [b], Cai-Juan Zheng [c], Chang-Yun Wang [a,d,*]

[a] Key Laboratory of Marine Drugs, The Ministry of Education of China, School of Medicine and Pharmacy, Ocean University of China, Qingdao 266003, China
[b] Guangxi Key Laboratory of Marine Biotechnology, Guangxi Institute of Oceanology, Beihai 536000, China
[c] Key Laboratory of Tropical Medicinal Plant Chemistry of Ministry of Education, Hainan Normal University, Haikou 571158, China
[d] Institute of Evolution & Marine Biodiversity, Ocean University of China, Qingdao 266003, China

ARTICLE INFO

Article history:
Received 10 May 2014
Received in revised form 19 November 2014
Accepted 3 December 2014
Available online 17 December 2014

Keywords:
9,10-Secosteroids
Subergorgia rubra
Cytotoxicity
Subergorgiaols A–L

ABSTRACT

Twelve new 9,10-secosteroids designated as subergorgiaols A–L (**1**–**12**), along with four known analogues (**13**–**16**), were isolated from the gorgonian *Subergorgia rubra* collected from the South China Sea. Their planar structures and the relative configurations were elucidated by comprehensive spectroscopic methods including NOESY spectra. The absolute configuration of **1** was established by a dimolybdenum tetraacetate [$Mo_2(AcO)_4$] induced circular dichroism (ICD) procedure and the modified Mosher's method. Compounds **1**–**12** represent the first series of 9,10-secosteroids characterized with a hydroxy group at C-8, which are 8-OH derivatives of astrogorgiadiols/calicoferols. Compound **4** exhibited cytotoxicity against the cervical carcinoma cell line (CaSki) with an IC_{50} value of 2.4 μM, and **6** showed toxicity toward brine shrimp *Artemia salina* with an LC_{50} value of 2.0 μM.

1. Introduction

Secosteroids are a class of secondary metabolites with unusual skeletons that are highly oxidized metabolites with bond cleavage in tetracyclic steroid nucleus, including 5,6-, 9,11-, 9,10-, 8,9-, 8,14-, and 13,17-secosteroids [1]. Among them, 9,10-secosteroids are steroids with B-ring cleavage of the steroid nucleus, which are naturally occurring vitamin D analogues [1]. The first described marine 9,10-secosteroid was obtained from a gorgonian *Astrogorgia* sp. in 1989 [2]. A literature search revealed that twenty-six 9,10-secosteroids have been isolated from the gorgonians of the genus *Muricella*, *Calicogorgia* and *Astrogorgia* so far [2–6]. These compounds possess various biological activities such as antiviral [2,3], cytotoxic [4], brine shrimp lethal [5] and protein kinase inhibitory activities [6]. Due to their biological potential, there has been some synthetic interest in these secosteroids, such as astrogorgiadiols [7] and calicoferols [8].

As part of our ongoing research on bioactive natural products from marine invertebrates and their symbiotic microorganisms in the South China Sea [9–14], the gorgonian coral *Subergorgia rubra* attracted our attention because the EtOAc extract showed lethal activity toward brine shrimps *Artemia salina*. Chemical investigation on the active extract led to the isolation of twelve new 9,10-secosteroids (**1**–**12**) and four known 9,10-secosteroids, astrogorgiadiol (**13**) [2], calicoferol C (**14**) [3], calicoferol F (**15**) [4], and calicoferol A (**16**) [5]. These compounds are all 8-OH derivatives of astrogorgiadiol and calicoferols. Herein, we report the isolation, structural elucidation and biological activities of these compounds.

2. Experimental

2.1. General methods

The optical rotations were measured on a JASCO digital polarimeter. UV spectra were recorded using a Milton-Roy spectrophotometer. CD spectra were acquired on a J-810 Circular Dichroism Spectrometer. IR spectra were recorded on a Nicolet-Nexus-470 spectrophotometer using KBr pellets. NMR spectra were recorded on a JEOL JEM-ECP NNR spectrometer (600 MHz for ^1H and 150 MHz for ^{13}C), using TMS as internal standard. ESIMS and HRESIMS were measured on a Micromass Q-TOF spectrophotometer, and EIMS spectra were measured on a Thermo DSQ EI-mass spectrometer. HPLC separation was performed using a Hitachi

* Corresponding author at: Key Laboratory of Marine Drugs, The Ministry of Education of China, School of Medicine and Pharmacy, Ocean University of China, Qingdao 266003, China. Tel./fax: +86 532 82031536.
E-mail address: changyun@ouc.edu.cn (C.-Y. Wang).

[1] These authors contributed equally.

http://dx.doi.org/10.1016/j.steroids.2014.12.001
0039-128X/

2.6. Biological assays

The isolated compounds were evaluated for their cytotoxicities *in vitro*. Seven cell lines, human hepatoma HepG2, human erythroleukemia K562, human promyelocytic leukemia HL-60, human lung carcinoma A549, human colon carcinoma HCT-116, human cervical carcinoma CaSki, and human cervical carcinoma HeLa cell lines, were used. The cytotoxicities against HepG2, K562, HL-60, and CaSki were determined by MTT [3-(4,5-dimethylthiazol-2-yl)-2,5-diphenyl-2-*H*-tetrazolium bromide], colorimetric assay [18]; and the cytotoxicities against A549, HCT-116 and HeLa were measured by SRB (sulforhodamine B) assay [19]. Adriamycin (ADM) was used as a positive control. Lethal activities to brine shrimp *A. salina* of the compounds were conducted according to literature procedures [20].

3. Results and discussion

An EtOH extract from the gorgonian *S. rubra* was suspended in H_2O and extracted successively with EtOAc. The light yellow oil portion separated from EtOAc extract was subjected to HPLC presenting a series of peaks with similar UV absorptions at 218 and 281 nm, which implied a group of analogues structurally closely related to 9,10-secosteroid bearing an aromatic moiety in ring A [2]. Sixteen compounds (**1**–**16**, Fig. 1) were isolated from this oily portion by using chromatographic techniques including column chromatography and semi-preparative HPLC.

Subergorgiaol A (**1**) was isolated as a colorless oil. Its molecular formula $C_{27}H_{44}O_3$ (six degrees of unsaturation) was determined by HRESIMS combined with ^{1}H NMR and ^{13}C NMR data. The IR absorption suggested the presence of a hydroxy (3515 cm^{-1}) and an aromatic ring (1621–1539 cm^{-1}). Five methyl proton signals were shown in the ^{1}H NMR spectrum at δ_H 2.21 (3H, s), 0.92 (3H, s), 0.90 (3H, d, J = 6.6 Hz), 0.87 (3H, d, J = 6.6 Hz), and 0.86 (3H, d, J = 6.6 Hz) (Table 1). Three aromatic proton signals at δ_H 6.96 (1H, d, J = 8.4 Hz), 6.64 (1H, d, J = 2.4 Hz) and 6.58 (1H, dd, J = 8.4, 2.4 Hz), and six aromatic carbon signals in the region of δ_C 112.9–154.0 (Table 2) indicated the existence of a 3-hydroxy-10-methylphenyl moiety [6]. Careful comparison of the ^{1}H and ^{13}C NMR spectra as well as the MS data of **1** with those of astrogorgiadiol (**13**) [2], revealed that **1** shared the same nucleus structure as **13**. The most obvious difference in the ^{13}C NMR spectra was the presence of an oxygenated quaternary carbon signal at δ_C 76.2 assignable to C-8 in **1**, instead of a tertiary carbon signal at δ_C 41.2 in **13** [2]. HMBC correlations from H_2-6, Hb-7 and H-9 to C-8 confirmed this assignment (Fig. 2). Therefore, a hydroxy group attached to C-8 in **1** was deduced. Detailed analysis of the HMQC, ^{1}H–^{1}H COSY, and HMBC spectra allowed the assignment for all carbon and proton resonances of **1**. Therefore, **1** was assigned as the 8-hydroxy-derivative of **13**.

The relative configuration of **1** was determined by analysis of NOESY experiment (Fig. 2), which showed correlations between H-14 and Hα-11, and H-14 and H-17. These observations suggested that all of these protons have the same α-orientation. Additionally, NOESY correlations between H_3-18 and H-9, H_3-18 and Hβ-11, and H_3-18 and H-20 indicated that these protons have a β-orientation.

The absolute configuration of **1** was established by a dimolybdenum tetraacetate [$Mo_2(AcO)_4$] induced circular dichroism (ICD) procedure and the modified Mosher's method. In order to assign the relative configuration of 8-OH, we used different deuterated solvents including DMSO-d_6 and C_5D_5N in ^{1}H NMR and NOESY experiments for **1**, however the signal of 8-OH was still not observed. Therefore, it is a challenge to determine the absolute configuration of C-8. Molecular modeling study showed that the C ring of **1** should adopt a boat conformation and the dihedral angle between two hydroxy groups of 8,9-diol in **1** was about 60°, suggesting that the Snatzke's method [16,17] with a $Mo_2(AcO)_4$ ICD procedure could be applied to determine the absolute configuration of *vic*-diol in **1**. Compound **1** was mixed with $Mo_2(OAc)_4$ followed by the measurement for the ICD spectrum of Mo-complexes of **1** subtracted from the inherent CD of **1**. The negative diagnostic Cotton effect around 310 nm in the ICD spectrum of Mo-complexes of **1** (Fig. 3) evidenced the absolute configuration of the *vic*-diol as 8*R*,9*R* based on the rule described in literature [16,17]. The absolute configuration of C-9 of **1** was further confirmed by the modified Mosher's method [21]. When reacted with (*R*)- and (*S*)-MTPACl, **1** gave the corresponding (*S*)- and (*R*)-MTPA esters, **1s** and **1r**, respectively. The observed chemical shift differences $\Delta\delta_{H(S-R)}$ (Fig. 4) clearly defined the *R* configuration at C-9. Therefore, the absolute configuration of **1** was defined as 8*R*,9*R*,13*R*,14*R*,17*R*,20*R*.

Subergorgiaols A–G (**1**–**7**) possess an identical steroidal nucleus revealed by the common and highly conserved NMR signals of the steroidal nuclei (Tables 1–4). The difference between these compounds lay only within the respective aliphatic side chains.

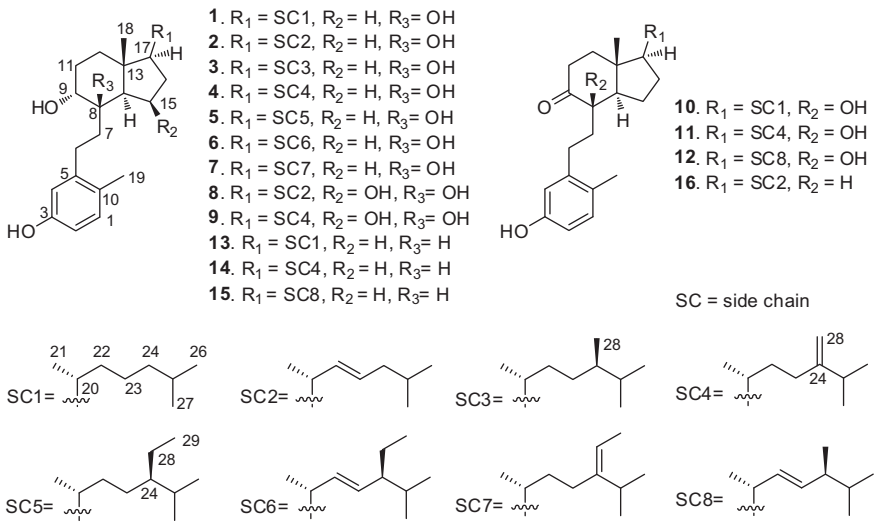

Fig. 1. Structures of compounds (**1**–**16**).

Zhang et al. BMC Genomics (2015) 16:189
DOI 10.1186/s12864-015-1371-1

BMC Genomics

RESEARCH ARTICLE Open Access

Construction of a high density SNP linkage map of kelp (*Saccharina japonica*) by sequencing *Taq* I site associated DNA and mapping of a sex determining locus

Ning Zhang[1,2,3†], Linan Zhang[4†], Ye Tao[5†], Li Guo[1,2,3], Juan Sun[4], Xia Li[4], Nan Zhao[4], Jie Peng[4], Xiaojie Li[4*], Liang Zeng[5], Jinsa Chen[5] and Guanpin Yang[1,2,3*]

Abstract

Background: Kelp (*Saccharina japonica*) has been intensively cultured in China for almost a century. Its genetic improvement is comparable with that of rice. However, the development of its molecular tools is extremely limited, thus its genes, genetics and genomics. Kelp performs an alternative life cycle during which sporophyte generation alternates with gametophyte generation. The gametophytes of kelp can be cloned and crossed. Due to these characteristics, kelp may serve as a reference for the biological and genetic studies of *Volvox*, mosses and ferns.

Results: We constructed a high density single nucleotide polymorphism (SNP) linkage map for kelp by restriction site associated DNA (RAD) sequencing. In total, 4,994 SNP-containing physical (tag-defined) RAD loci were mapped on 31 linkage groups. The map expanded a total genetic distance of 1,782.75 cM, covering 98.66% of the expected (1,806.94 cM). The length of RAD tags (85 bp) was extended to 400–500 bp with Miseq method, offering us an easiness of developing SNP chips and shifting SNP genotyping to a high throughput track. The number of linkage groups was in accordance with the documented with cytological methods. In addition, we identified a set of microsatellites (99 in total) from the extended RAD tags. A gametophyte sex determining locus was mapped on linkage group 2 in a window about 9.0 cM in width, which was 2.66 cM up to marker_40567 and 6.42 cM down to marker_23595.

Conclusions: A high density SNP linkage map was constructed for kelp, an intensively cultured brown alga in China. The RAD tags were also extended so that a SNP chip could be developed. In addition, a set of microsatellites were identified among mapped loci, and a gametophyte sex determining locus was mapped. This map will facilitate the genetic studies of kelp including for example the evaluation of germplasm and the decipherment of the genetic bases of economic traits.

Keywords: Kelp, *Saccharina japonica*, SNP, RAD, Linkage map, Sex determining locus

* Correspondence: yeslxj@sina.com; yguanpin@mail.ouc.edu.cn
†Equal contributors
[4]National Engineering Science Research & Development Center of Algae and Sea Cucumbers of China; Provincial Key Laboratory of Genetic Improvement & Efficient Culture of Marine Algae of Shandong, Shandong Oriental Ocean Sci-tech Co., Ltd, Yantai, Shandong 264003, China
[1]Laboratory of Marine Genetics and Breeding, Ocean University of China, Qingdao 266003, China
Full list of author information is available at the end of the article

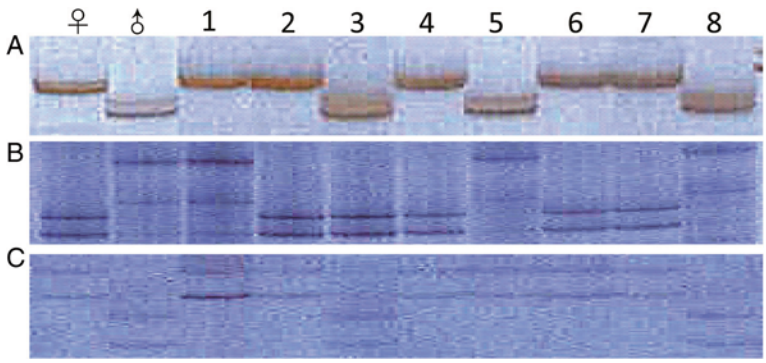

Figure 1 Microsatellite segregation pattern of mapping panel. Eight randomly selected gametophyte clones from mapping panel were genotyped with *D5* **(A)**; *H45* **(B)** and *H123* **(C)**. The gametophyte clones of mapping panel segregate as expected.

cutting gametophyte clone DNA. A total of 24 multiplex sequencing libraries were constructed, in which each gametophyte clone DNA was prefixed with a unique nucleotide multiplex identifier as a barcode. *Taq* I end (101 bp in length) sequencing was performed on Illumina HiSeq2500 platform. Illumina Miseq PE250 was used to extending *Taq* I site associated DNA of two parental gametophyte clones. Raw RAD reads were trimmed to 85 nucleotide tags, which ensured > 97.5% of nucleotides have a quality value > Q30 (<0.1% sequencing error). These tags were aligned into *Taq* I site associated tag piles by their sequence similarity using Stacks [75]. Unique tags, *i.e.* the non-redundant with a maximum of one base difference from others, were screened out of a tag pile and used as the candidate alleles occupying a corresponding physical RAD locus. Physical RAD loci are sequence tagged while genetic loci are linkage determined. All candidate alleles were then collapsed into clusters using Stacks under default parameters for SNP calling [76]. Genotype calling, a process of determining the SNP genotype of physical RAD loci of each gametophyte clone after SNP calling, followed the philosophy of Hohenlohe *et al.* [76]. The customized perl scripts were applied then to generate a ".loc" file as the input of Joinmap 3.0 [77,78] with SNP linkage map calculated at a log of odds (LOD) value of 6.0 and a maximum recombination of 0.400 with regression algorithm. The linkage distances between loci were exported into MapChart [79] for map drawing.

The expected length of map (Ge) was the average of Ge1 and Ge2, where Ge1 was the sum of the lengths of all linkage groups, each revised by adding 2 s (s is the average space between loci, 2 s accounts for the two chromosome ends) to the observed [80], and Ge2 was the sum of the lengths of linkage groups, each revised by multiplying the observed with (m + 1)/(m - 1), where m is the number of genetic loci [81]. The genome coverage was calculated by dividing the observed map length with that of the expected as we did early [82].

Results

Gametophyte clone genotyping

Trimming the raw HiSeq2500 reads yielded the quality tags for gametophyte clones each, which ranged from 341,797 to 4,028,160 with an average of 1,905,908. For parental female and male gametophyte clones, 5,886,795 and 5,634,477 quality tags were generated, respectively (Figure 2). The quality tags of a gametophyte clone were aligned into RAD-tag piles with those covering only one tag discarded in order to ensure sequencing reliability. The remaining RAD-tag piles were considered as physical RAD loci from which unique candidate alleles were picked up. All candidate alleles identified among gametophyte clones of mapping panel were clustered for SNP and SNP genotype calling. Of 153 gametophyte clones, 14 were deleted in linkage map calculation as they were either genotype heterozygous or genotype absent at a large portion of physical RAD loci. The remaining 139 gametophyte clones were used for map calculation.

Construction and characterization of SNP linkage map

In total, 4,994 physical RAD loci survived testing against 1:1 segregation expectation, grouping and map calculation, which were assigned onto 31 linkage groups finally

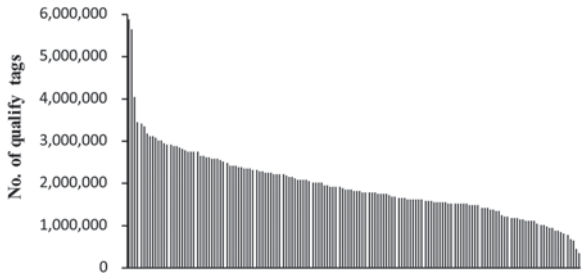

Figure 2 The decreasing number of quality tags. These tags were generated for parental female and male gametophyte clones (bar 1 and 2, respectively) and 140 gametophyte clones of mapping panel (bar 3 through 143).

Developmental and Comparative Immunology 52 (2015) 166–171

Contents lists available at ScienceDirect

Developmental and Comparative Immunology

journal homepage: www.elsevier.com/locate/dci

Short communication

Molecular cloning and expression studies of the adapter molecule myeloid differentiation factor 88 (MyD88) in turbot (*Scophthalmus maximus*)

Jing-Yun Lin [a], Guo-Bin Hu [a,b,*], Chang-Hong Yu [c], Song Li [a], Qiu-Ming Liu [a], Shi-Cui Zhang [a,b]

[a] College of Marine Life Sciences, Ocean University of China, Qingdao 266003, China
[b] Institute of Evolution & Marine Biodiversity, Ocean University of China, Qingdao 266003, China
[c] College of Medicine, Qingdao University, Qingdao 266071, China

ARTICLE INFO

Article history:
Received 12 March 2015
Revised 22 May 2015
Accepted 23 May 2015
Available online 27 May 2015

Keywords:
MyD88
Scophthalmus maximus
LPS
CpG-ODN
TRBIV
Gene expression

ABSTRACT

Myeloid differentiation factor 88 (MyD88) is an adapter protein involved in the interleukin-1 receptor (IL-1R) and Toll-like receptor (TLR)-mediated activation of nuclear factor-kappaB (NF-κB). In this study, a full length cDNA of MyD88 was cloned from turbot, *Scophthalmus maximus*. It is 1619 bp in length and contains an 858-bp open reading frame that encodes a peptide of 285 amino acid residues. The putative turbot (*Sm*)MyD88 protein possesses a N-terminal death domain and a C-terminal Toll/IL-1 receptor (TIR) domain known to be important for the functions of MyD88 in mammals. Phylogenetic analysis grouped *Sm*MyD88 with other fish MyD88s. *SmMyD88* mRNA was ubiquitously expressed in all examined tissues of healthy turbots, with higher levels observed in immune-relevant organs. To explore the role of *SmMyD88*, its gene expression profile in response to stimulation of lipopolysaccharide (LPS), CpG oligodeoxynucleotide (CpG-ODN) or turbot reddish body iridovirus (TRBIV) was studied in the head kidney, spleen, gills and muscle over a 7-day time course. The results showed an up-regulation of *SmMyD88* transcript levels by the three immunostimulants in all four examined tissues, with the induction by CpG-ODN strongest and initiated earliest and inducibility in the muscle very weak. Additionally, TRBIV challenge resulted in a quite high level of *SmMyD88* expression in the spleen, whereas the two synthetic immunostimulants induced the higher levels in the head kidney. These data provide insights into the roles of *Sm*MyD88 in the TLR/IL-1R signaling pathway of the innate immune system in turbot.

1. Introduction

The innate immunity in fish, as in all vertebrates, is the first line of defense and provides crucial signals for activation of adaptive immune responses (Akira et al., 2001). Detection and clearance of invading pathogens by the innate immune system are associated with plenty of signaling pathways that are evolutionarily conserved throughout vertebrates. It works through the way of being triggered when pathogen-associated molecular patterns (PAMPs) come into contact with host-expressed pattern recognition receptors (PRRs) (Medzhitov and Janeway, 2000). One of the well-characterized PRRs is the family of Toll-like receptors (TLRs) that detects microbial PAMPs such as bacterial lipopolysaccharides (LPS), peptidoglycans (PGN) and flagellin, viral RNA, unmethylated CpG DNA of viruses, bacteria and protozoa, β-glycan of fungi and lipoproteins of various pathogens (Akira et al., 2006; Mogensen, 2009). The signaling pathways mediated by TLRs are broadly classified into the myeloid differentiation factor 88 (MyD88)-dependent and -independent ones. The former uses MyD88 as an adapter molecule to activate the signaling cascades and produces inflammatory mediators.

Although MyD88 was first found in mice in 1990 as a myeloid differentiation primary response gene induced during terminal differentiation of M1D$^+$ myeloid precursor cells in response to interleukin (IL)-6 treatment (Lord et al., 1990), its function as a key adapter molecule in the interleukin-1 receptor (IL-1R)/TLR-mediated signaling remains unknown until 1997 (Wesche et al., 1997). MyD88 has a bipartite structure composed of an N-terminal death domain and a C-terminal Toll/IL-1 receptor (TIR) domain with a short intervening linker segment. Upon activation by PAMPs, all of TLRs except TLR3 recruit MyD88 through the TIR domain; the death domain interacts with the corresponding domain in IL-1R-associated kinases (IRAKs), leading to recruitment of downstream tumor necrosis factor receptor (TNFR)-associated factor 6 (TRAF6); these events eventually result in activation of NF-κB and interferon

* Corresponding author. College of Marine Life Sciences, Ocean University of China, Qingdao 266003, China. Tel.: +86 532 82032583; fax: +86 532 82032583.
E-mail address: huguobin@mail.ouc.edu.cn (G.-B. Hu).

http://dx.doi.org/10.1016/j.dci.2015.05.013
0145-305X/

mediator, functioning as a signal transduction adapter downstream of multiple TLRs that are expressed ubiquitously. This may explain the ubiquitous expression of *SmMyD88* in turbot tissues. The higher expression levels were observed in the leukocyte-rich organs, indicating an important role of *Sm*MyD88 in immune system. Interestingly, *SmMyD88* was also strongly expressed in non-immune tissues such as the brain, suggesting that its function is not limited to the immune system. Additionally, MyD88 has been reported to participate in the activation of several members of interferon regulatory factor (IRF) family transcription factors, namely, IRF3, -5 and -7 (Yamamoto et al., 2002). Since these *IRFs* were constitutively expressed also in most tissue types of turbots with higher levels in the leukocyte-rich organs (Hu et al., 2011a, 2011b; Xia et al., 2012), it can be inferred that *Sm*MyD88 has a close relationship with them.

To explore the potential role of *Sm*MyD88 in immune responses of turbot, its gene expression profile was studied over a 7-day time course in the gills, head kidney, spleen and muscle following stimulation with LPS, CpG-ODN or TRBIV. The up-regulation of *SmMyD88* was observed in all four tested tissues after treatment with each stimulant (Fig. 2), suggesting its general inducibility in the immune and non-immune organs by bacterial or viral infections.

The gram-negative endotoxin LPS has been reported to be a powerful stimulator of innate immunity in diverse eukaryotic species (Lemaitre et al., 1996; Ulevitch and Tobias, 1995). Here, its effect on *SmMyD88* expression was investigated (Fig. 2 A1–4). Upon LPS stimulation, *SmMyD88* was markedly induced in the head kidney with a peak transcript level of 5.6-fold over control arising at day 1 post-injection and less induced in the gills and spleen with a peak level of 4.2- and 3.2-fold arising at hour 6 and day 1, respectively. The induction in the muscle was weak with a peak level of 1.5-fold arising at day 3, suggesting a weak Toll/IL-1R signal pathway response taking place in this tissue where lymphomyeloid cells are scarce. This expression pattern generally agrees with the reports for MyD88s from Japanese flounder, rock bream and scallop upon LPS treatment (Qiu et al., 2007; Takano et al., 2006; Whang et al., 2011). In mammals, stimulation with LPS leads to a cellular response where TLR4 in membrane recruits MyD88 that acts as an adapter to propagate the downstream signaling after binding to LPS (Netea et al., 2004; Takano et al., 2006). However, fish TLR4 does not recognize LPS (Sepulcre et al., 2009) and some fish species lack a TLR4 ortholog. Further, the results from zebrafish demonstrated that LPS was signaled through a TLR4- and MyD88-independent pathway (Sepulcre et al., 2009). Thus, the up-regulation of *SmMyD88* is probably mediated independently of *SmMyD88* activation, *i.e.*, via a TLR4- and MyD88-independent pathway. Additionally, some studies suggested that fugu TLR23 may participate in LPS recognition and alternative signaling receptors like beta-2 integrins may play a pivotal role in the activation of piscine leukocytes by LPS (Iliev et al., 2005). These findings

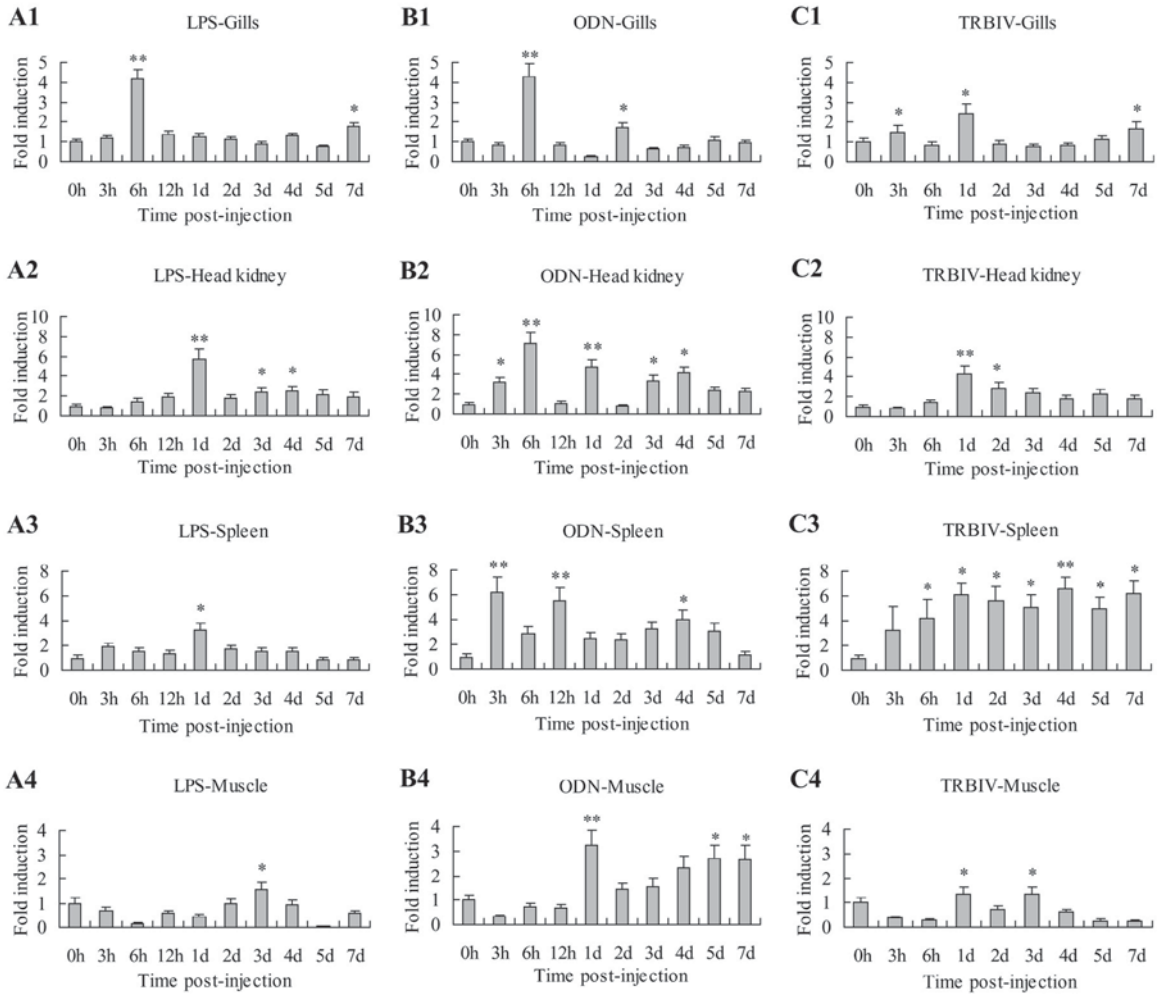

Fig. 2. Time-course expression profiles of *SmMyD88* gene in gills, head kidney, spleen and muscle of turbots injected with 280 ng LPS, 14.25 ng CpG-ODN 2395 or 2.4×10^5 $TCID_{50}$ TRBIV per fish. A1–4 show fold changes of *SmMyD88* expression with LPS stimulation, B1–4 with CpG-ODN 2395 stimulation and C1–4 with TRBIV infection. Values are means ± standard error (S.E.), n = 5. The level of significance of the comparison to the control is indicated by $^*P < 0.05$ and $^{**}P < 0.01$.

Fish & Shellfish Immunology 45 (2015) 895–900

Contents lists available at ScienceDirect

Fish & Shellfish Immunology

journal homepage: www.elsevier.com/locate/fsi

Short communication

Molecular cloning and expression analysis of interferon stimulated gene 15 (ISG15) in turbot, *Scophthalmus maximus*

Jing-Yun Lin [a], Guo-Bin Hu [a, b, *], Da-Hai Liu [b], Song Li [a], Qiu-Ming Liu [a], Shi-Cui Zhang [a, b]

[a] College of Marine Life Sciences, Ocean University of China, Qingdao 266003, China
[b] Institute of Evolution & Marine Biodiversity, Ocean University of China, Qingdao 266003, China

ARTICLE INFO

Article history:
Received 8 March 2015
Received in revised form
17 May 2015
Accepted 24 May 2015
Available online 18 June 2015

Keywords:
ISG15
Scophthalmus maximus
TRBIV
Poly I:C
Gene expression

ABSTRACT

The interferon stimulated gene 15 (ISG15) is strongly induced in many cell types by double-stranded RNA (polyinosinic: polycytidylic acid, poly I:C) and viral infection. In this study, we described the nucleotide, mRNA tissue distribution and regulation of an *ISG15* gene from turbot, *Scophthalmus maximus* (*SmISG15*). *SmISG15* gene is 862 bp in length, composed of two exons and one intron, and encodes 158 amino acids. The deduced protein exhibits the highest homology (44.7–71.2% identity) with ISG15s from other fishes and possesses two conserved tandem ubiquitin-like (UBL) domains and a C-terminal RLRGG conjugating motif known to be important for the functions of ISG15s in vertebrates. Phylogenetic analysis grouped *Sm*ISG15 into fish ISG15. *SmISG15* mRNA was constitutively expressed in all tissues examined, with higher levels observed in immune organs. Gene expression analysis was performed for *SmISG15* in the spleen, head kidney, gills and muscle of turbots challenged with poly I:C or turbot reddish body iridovirus (TRBIV) over a 7-day time course. The result showed that *SmISG15* was upregulated by both stimuli in all four tissues, with induction by poly I:C apparently stronger and initiated more quickly. A two-wave induced expression of *SmISG15* was seen in the spleen, head kidney and gills, suggesting an induction of *SmISG15* either by IFN-dependent or -independent pathway. These results provide insights into the roles of fish ISG15 in antiviral immunity.

1. Introduction

Type I interferons (IFN α/β), a group of proteins with antiviral, antiproliferative and immunomodulating activities, were first discovered in 1957 [1], since then they have been widely used as clinical drugs [2]. All vertebrate groups from fish to mammals possess type I IFNs. They play a crucial role in the innate antiviral response by inducing hundreds of interferon stimulated genes (ISGs) through the JAK-STAT pathway [3], among which the double-stranded RNA (dsRNA)-activated protein kinase (PKR), Myxovirus resistance (Mx) and 2′-5′ oligoadenylate synthetase (OAS) are most studied [4], while other ISGs have not been well functionally characterized [5].

ISG15 is one of the first identified ISGs with molecule weight (MW) of 15 kDa and belongs to a small class of ubiquitin-like proteins (UBLs) that includes SUMO, FAT10, Nedd8 and Ubl1 [6]. It is also called ubiquitin cross-reactive protein (UCRP) because of cross-reactivity with ubiquitin antibodies [7]. Structurally, ISG15 contains two tandem ubiquitin-like domains and a conserved C-terminal RLRGG motif. Like ubiquitin, it can conjugate to target cellular proteins with the motif of RLRGG in a process called ISGylation, but it does not appear to target proteins for degradation, instead influences binding to other molecules, affects enzymatic degradation and subcellular localization, and may also determine the half-life of proteins [8]. ISG15 plays an important role in host response to pathogens. Its expression is a primary response to IFN α/β induction and a marker of viral or bacterial infection in many cell types [9]. It exists in conjugated or free form in cells. The conjugated ISG15 exerts antiviral activity through ISGylation of both host and viral proteins that impact viral replication [10]. However, there is currently no evidence that IFN-α/β-inducible human intracellular ISG15 exerts antiviral effects on documented viral infections via ISGylation. On the contrary, a recent literature has shown that IFN-α/β-inducible ISG15 is essential to negatively regulate IFN-α/β responses via stabilizing USP18, a potent negative regulator of IFN-α/β signalling, thereby preventing auto-

* Corresponding author. College of Marine Life Sciences, Ocean University of China, Yushan Road 5#, Qingdao 266003, China.
E-mail address: huguobin@mail.ouc.edu.cn (G.-B. Hu).

http://dx.doi.org/10.1016/j.fsi.2015.05.050
1050-4648/

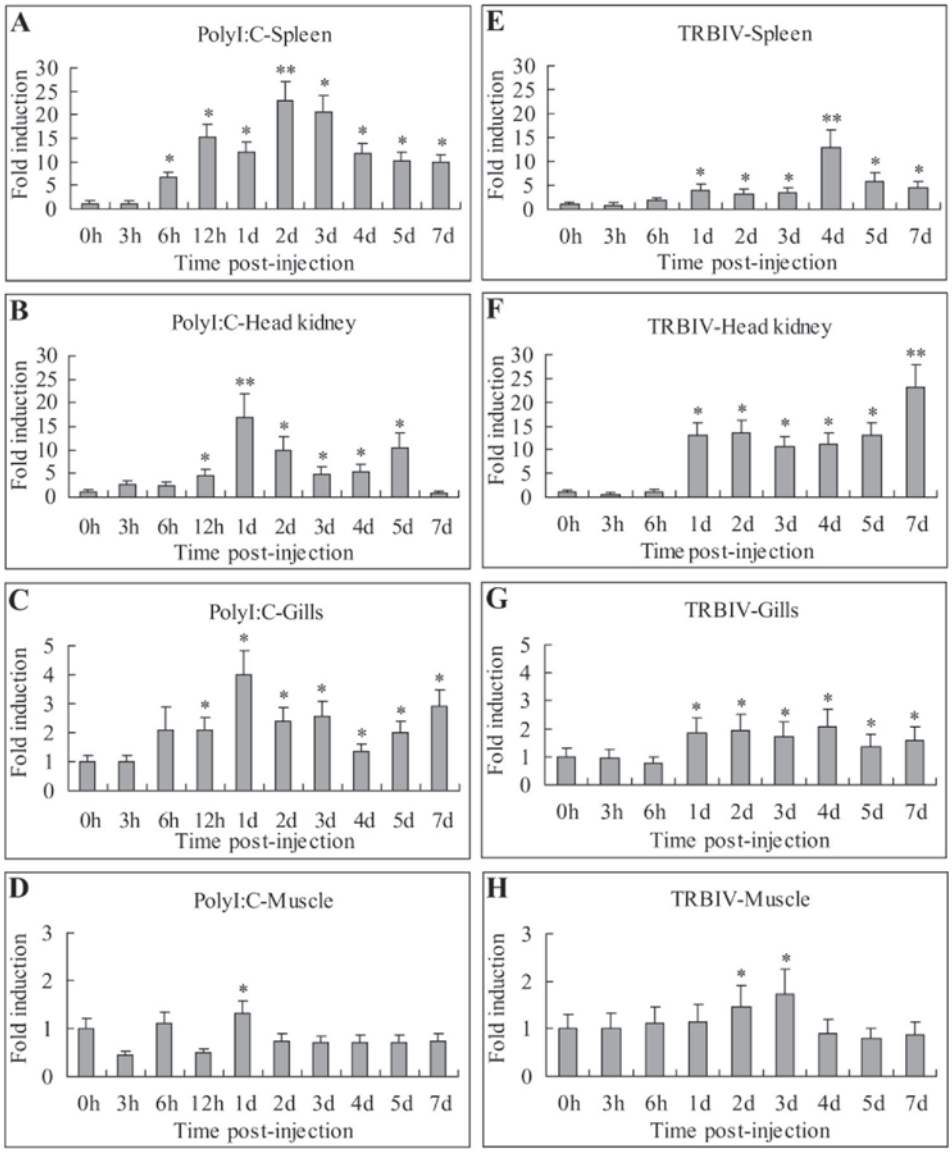

Fig. 5. Induced expression of *SmISG15* gene upon challenge with 1.0 mg poly I:C or 2.4 × 10^5 $TCID_{50}$ TRBIV per fish during a 7-day time course. A–D shows fold changes of *Sm*ISG15 expression upon poly I:C challenge in the spleen, head kidney, gills and muscle, respectively; E–H shows fold changes of *SmISG15* expression upon TRBIV challenge in the spleen, head kidney, gills and muscle, respectively. Values are means ± standard error (S.E.), n = 5. The level of significance of the comparison to the control is indicated by $^*P < 0.05$ and $^{**}P < 0.01$.

SmISG15 transcripts were constitutively expressed in all tested tissues (Fig. 4), suggesting its relation to diverse cellular pathways including those involved in RNA splicing, translation, chromatin remodeling, cytoskeleton organization and stress responses [30]. The strong expression of *Sm*ISG15 was detected in leukocyte-rich organs, such as head kidney, kidney and spleen, a tissue expression pattern similar to Japanese flounder ISG15 [13]. A high level of *Sm*ISG15 was also detected in skin, which may be explained by the finding of macrophages and lymphocytes in skin of rainbow trout, Atlantic salmon and coho [31]. These results indicate that *Sm*ISG15 is synthesized predominantly in leukocytes and may have a role in leukocyte proliferation which has been proved in human [32]. Meanwhile, the *ISG15* is a target gene of a number of IRF family transcription factors like IRF3, -5 and -7 that are constitutively expressed in most tissue and cell types with a strong expression in leukocyte-rich organs in turbot [33–35]. Such a similar tissue expression pattern indicates a close contact of *Sm*ISG15 with IRFs.

The upregulation of *SmISG15* was observed in all four tested tissue types after treatment with poly I:C or TRBIV (Fig. 5), suggesting its general inducibility in the immune and non-immune organs by RNA and DNA viruses. Also, the enhanced expression of *ISG15* followed poly I:C or virus treatments has been observed in other fish species, such as Japanese flounder, black rockfish, Atlantic salmon and Atlantic cod [13–16]. Further, studies with mammalian models have demonstrated that ISG15 possesses a broad spectrum of antiviral activity [36], supporting the induction of *SmISG15* by the two different viral stimuli. The induction of *SmISG15* were found stronger in lymphatic tissues (head kidney and spleen), followed by mucosa-associated lymphatic tissue (gills) and quite weak in muscle that lacks lymphocytes, suggesting a positive correlation between *SmISG15* inducibility and leukocyte content in the tested organs. Compared to TRBIV, the induction by poly I:C was apparently stronger and initiated more quickly, indicating that it acts as a highly pure and concentrated PAMP to activate host's immune response directly. In contrast, TRBIV has to go through replication cycles to produce PAMPs before triggering a detectable response.

Fish & Shellfish Immunology 44 (2015) 399–409

Contents lists available at ScienceDirect

Fish & Shellfish Immunology

journal homepage: www.elsevier.com/locate/fsi

Short communication

Cloning and expression analysis of a Toll-like receptor 22 (*tlr22*) gene from turbot, *Scophthalmus maximus*

Guo-Bin Hu [a, b, *], Shou-Feng Zhang [a], Xi Yang [a], Da-Hai Liu [c], Qiu-Ming Liu [a], Shi-Cui Zhang [a, b]

[a] College of Marine Life Sciences, Ocean University of China, Qingdao 266003, China
[b] Institute of Evolution & Marine Biodiversity, Ocean University of China, Qingdao 266003, China
[c] First Institute of Oceanography, State Oceanic Administration of China, Qingdao 266061, China

ARTICLE INFO

Article history:
Received 9 June 2014
Received in revised form
21 February 2015
Accepted 1 March 2015
Available online 11 March 2015

Keywords:
Scophthalmus maximus
Tlr22
Structural characteristics
Gene expression
PAMPs

ABSTRACT

Toll-like receptor 22 (TLR22) exists exclusively in aquatic animals and recognizes double stranded RNA (dsRNA). In the present study, a *tlr22* gene and its 5′-flanking sequence were cloned from turbot, *Scophthalmus maximus*, its immune responsive expression was subsequently studied *in vivo*. The turbot (*sm*)*tlr22* gene spans over 5.6 kb with a structure of 4 exon-3 intron and encodes 962 amino acids. The deduced protein shows the highest sequence identity (76.7%) to Japanese flounder Tlr22 and possesses a signal peptide sequence, a leucine-rich repeat (LRR) domain composed of 27 LRR motifs, a transmembrane region and a Toll/interleukin-1 receptor (TIR) domain. Phylogenetic analysis grouped it with other teleost Tlr22s. The interferon-stimulated response element (ISRE) and signal transducer and activator of transcription (STAT) binding site important for the basal transcriptional activity of *TLR3* were predicted in the 5′-flanking sequence of *smtlr22* gene. Quantitative real-time PCR (qPCR) analysis demonstrated the constitutive expression of *smtlr22* mRNA in all examined tissues with higher levels in the head kidney, kidney and spleen. Further, *smtlr22* expression was significantly up-regulated following challenge with polyinosinic: polycytidylic acid (poly I:C), lipopolysaccharide (LPS) or turbot reddish body iridovirus (TRBIV) in the gills, head kidney, spleen and muscle, with maximum increases ranging from 2.56 to 6.24 fold upon different immunostimulants and organs. These findings suggest a possible role of Smtlr22 in the immune responses to the infections of a broad range of pathogens that include DNA and RNA viruses and Gram-negative bacteria.

1. Introduction

The innate immune system provides the host's first line of defense against invading microbial pathogens, acting before the adaptive immune system is fully functional. The pattern recognition receptors (PRRs) expressing on cellular/endosomal membrane or in cytoplasm of host cells recognize the specific conserved microbial features called pathogen-associated molecular patterns (PAMPs), such as lipopolysaccharide (LPS) and peptidoglycan (PG) from bacteria, single- and double-stranded RNA (ss-, dsRNA) from viruses, unmethylated CpG DNA found in the genomes of the both pathogens, etc [1,2]. One of important PRR classes is the Toll-like receptors (TLRs) that belong to the type I transmembrane proteins and characterized by two conserved structures, an extracellular leucine-rich repeat (LRR) domain responsible for recognizing and binding PAMPs and a cytoplasmic Toll/interleukin (IL)-1 receptor (TIR) domain for downstream signaling [3,4]. To date, thirteen TLRs (TLR1-13) have been found in mammals since the first TLR, TLR4, was identified in humans in 1997 [5]. In fish, at least 18 Tlrs have been identified, including eight mammalian TLR orthologs, Tlr1-5 and Tlr7-9, and ten non-mammalian Tlrs, soluble Tlr5, Tlr14, Tlr18-23, Tlr25 and Tlr26 [6,7].

TLR-mediated signaling pathways have been well studied in mammals. They are triggered upon the binding of PAMPs to TLRs and arise from intracytoplasmic TIR domain that recruits correlative adaptor proteins and transfers stimulatory signals to the cytosol. Myeloid differentiation factor 88 (MyD88) and TIR domain-containing adaptor inducing interferon-β (TRIF) are the two key adaptors mediating two individual TLR signaling cascades, the

* Corresponding author. College of Marine Life Sciences, Ocean University of China, Yushan Road, 5#, Qingdao 266003, China. Tel./fax: +86 532 82032583.
E-mail address: huguobin@mail.ouc.edu.cn (G.-B. Hu).

http://dx.doi.org/10.1016/j.fsi.2015.03.001
1050-4648/

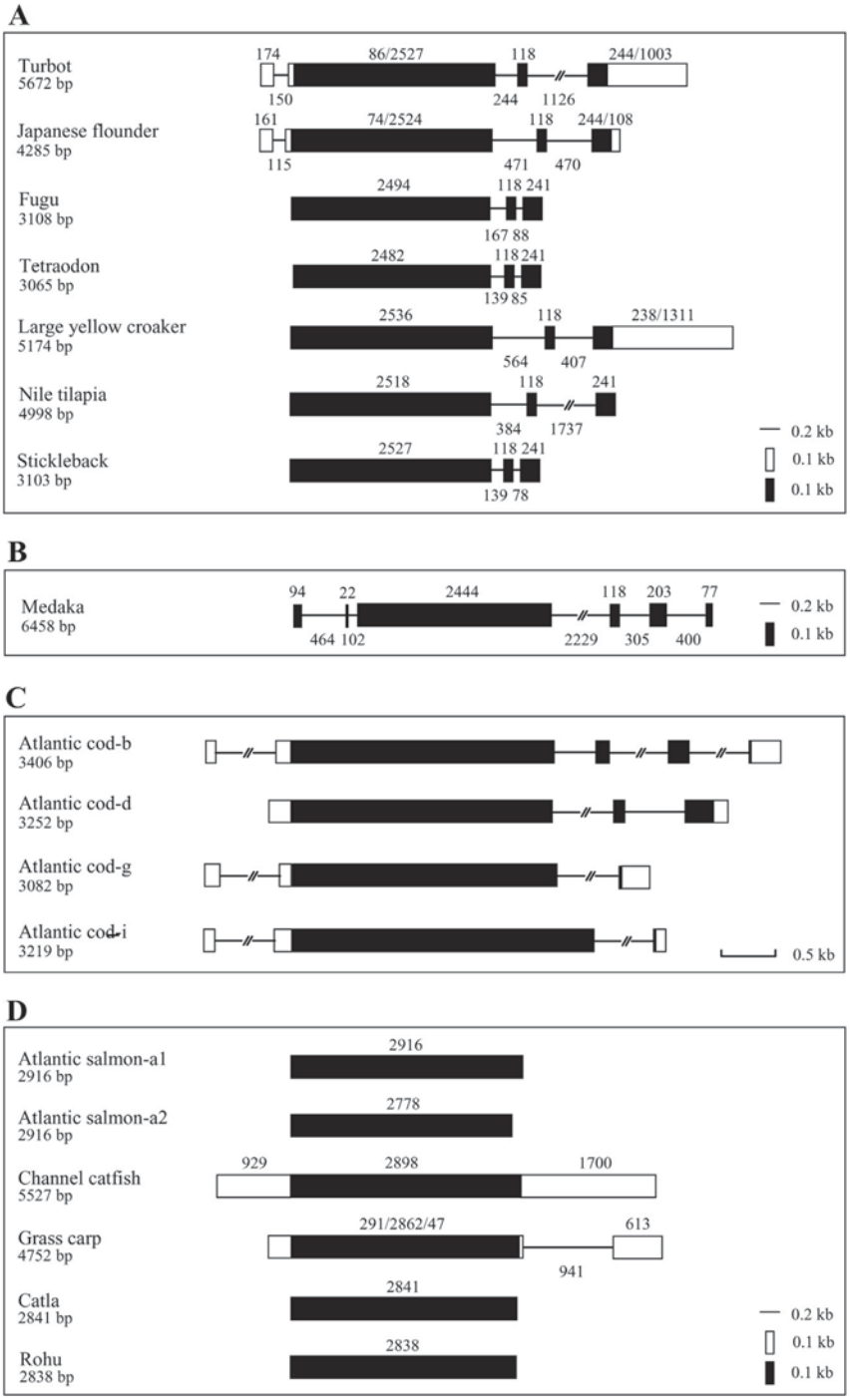

Fig. 4. Comparison of genomic organization of *tlr22* genes in species of percomorpa (A), atherinomorpha/adrianichthyidae (B), paracanthopterygii (C) and protacanthopterygii and ostariophysi (D). Exons are indicated with boxes (untranslated regions with white boxes) and introns with horizontal lines. The numbers showing the length of exons and introns are marked above and below the corresponding elements, respectively. GenBank accession numbers or references: turbot, KJ606345; Japanese flounder, AB109396; large yellow croaker, GU576983/Xiao et al., 2011; fugu, AC156434; tetraodon, ENSTNIG00000013627; stickleback, ENSGACG00000005449; Nile tilapia, KJ010825; medaka, ENSORLG00000020413; Atlantic cod-b/d/g/i, Sundaram et al., 2012; Atlantic salmon-a1/a2, AM233509/FM206383; channel catfish, HQ677725; grass carp, Su et al., 2012; rohu, Panda et al., 2014; catla, Panda et al., 2014.

kidney and muscle, respectively, and 3.12-fold arising at hour 6 in the spleen (Fig. 7).

4. Discussion

In the present study, we report the structure and expression profile of a Tlr22 homologue from turbot (Smtlr22). The full-length *smtlr22* cDNA comprises a 2889-bp open reading frame (ORF) that encodes a 962-aa protein. Five mRNA instability motifs (ATTTA) were found in the 1034-bp 3′-UTR (Fig. 1A), suggesting that *smtlr22* may be transiently expressed. The putative protein possesses the four typical structures of the TLR families, a signal peptide, an extracellular LRR domain, a transmembrane region and an intracellular TIR domain (Fig. 1A and B). The LRR domain, responsible for

Journal of FISH BIOLOGY

fsbi An International Society for Fish Biology

Journal of Fish Biology (2015) **86**, 431–447
doi:10.1111/jfb.12559, available online at wileyonlinelibrary.com

A toll-like receptor 3 homologue that is up-regulated by poly I:C and DNA virus in turbot *Scophthalmus maximus*

G.-B. Hu*†‡, X.-P. Li*, D.-H. Liu§, Q.-M. Liu* and S.-C. Zhang*†

*College of Marine Life Sciences, Ocean University of China, Qingdao 266003, China, †Institute of Evolution & Marine Biodiversity, Ocean University of China, Qingdao 266003, Chinaand §First Institute of Oceanography, State Oceanic Administration of China, Qingdao 266061, China

(Received 25 March 2014, Accepted 21 September 2014)

In this study, the gene and promoter sequences of turbot *Scophthalmus maximus* (Sm) toll-like receptor 3 (Tlr3) were cloned and its mRNA tissue distribution and gene expression in response to polyinosinic:polycytidylic acid (poly I:C) and turbot reddish body iridovirus (TRBIV) challenges were studied *in vivo*. The *smtlr3* gene spans over 4·4 kb with a structure of five exons–four introns and encodes a peptide of 916 amino acids. The putative protein shares the highest sequence identity of 52·8–78·5% with fish Tlr3 and contains a signal peptide sequence, 13 leucine-rich repeat (LRR) motifs, a transmembrane region and a toll/interleukin-1 receptor (TIR) domain. Phylogenetic analysis grouped it with other teleost Tlr3s. A number of transcription factor binding sites were identified in the 1538 bp 5′ flanking region of *smtlr3*, including interferon-stimulated response element (ISRE) and those for interferon regulatory factors (IRF) and signal transducer and activator of transcriptions (STATs) *smtlr3* transcripts were expressed ubiquitously with higher levels in the head kidney, heart and digestion organs. They were up-regulated by both poly I:C and TRBIV in immune and non-immune organs, but most strongly in the head kidney. Finally, the *smtlr3* exhibited a two-wave induced expression during a five day time course when exposure of *S. maximus* to poly I:C. These findings provide insights into the role of SmTlr3 in antiviral response.

Key words: antiviral response; gene expression; promoter characteristics; scophthalmid; Tlr3 signalling.

INTRODUCTION

Toll-like receptors (TLR), belonging to the type I transmembrane (TM) proteins, are at the front line in the fight against invading microorganisms, and they are key mediators of innate immunity in both vertebrates and invertebrates (Gay *et al.*, 2006). The responses of TLRs to pathogen-associated molecular patterns (PAMP) serve as a universal trigger for the immune system, the most crucial result of which is the induction of inflammation response factors and interferons (IFNs) *via* myeloid differentiation factor 88 (MyD88)-dependent or MyD88-independent signalling

‡Author to whom correspondence should be addressed. Tel.: +86 532 82032583; email: huguobin@mail.ouc.edu.cn

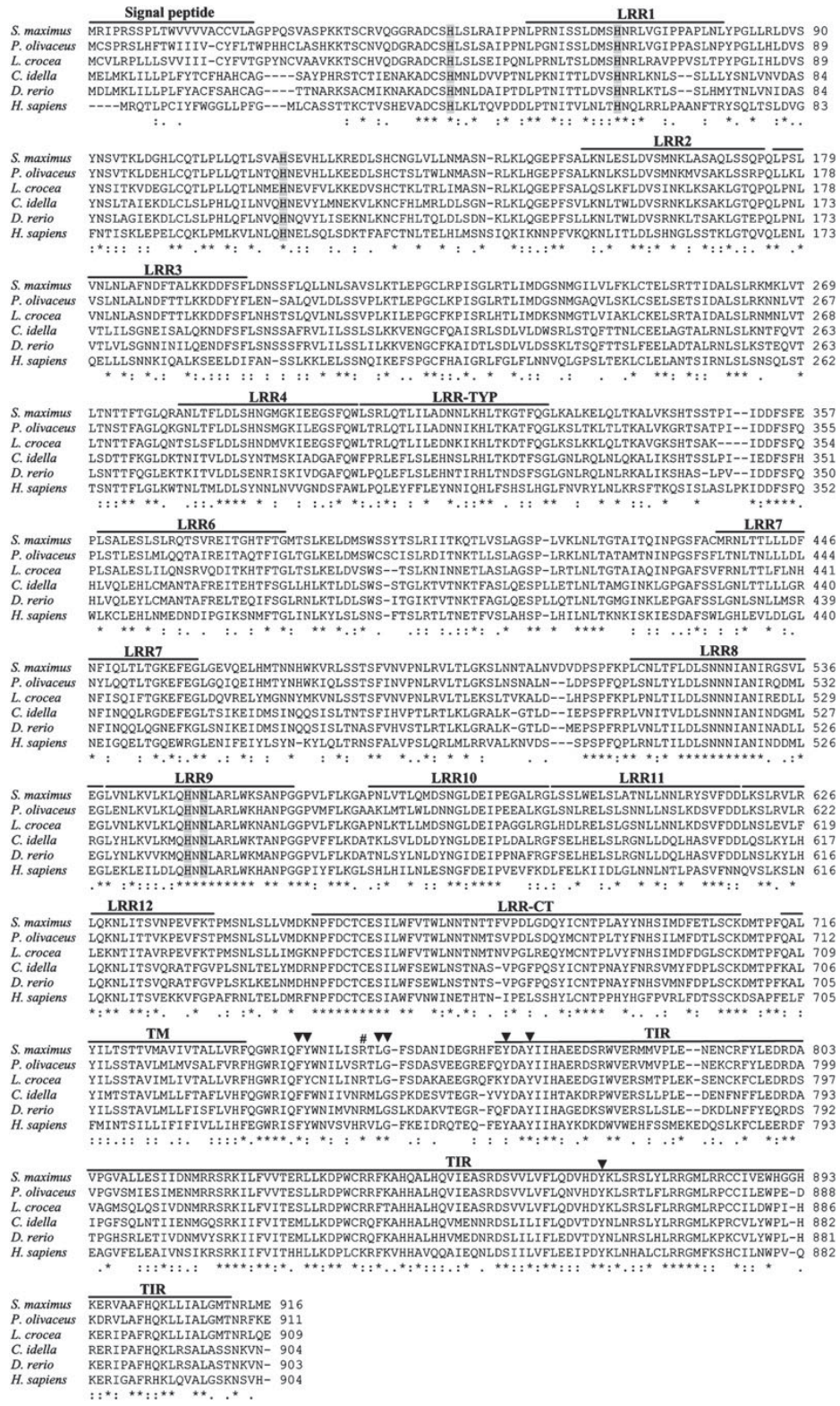

FIG. 1. Alignment of *Scophthalmus maximus* Tlr3 amino-acid sequence with those of Tlr3s from other teleosts, *Paralichthys olivaceus*, *Larimichthys crocea*, *Ctenopharyngodon idella* and *Danio rerio*, and *Homo sapiens*. The signal peptide, leucine-rich repeat (LRR) domains, transmembrane (TM) domain and toll–interleukin-1 receptor (TIR) domain are shown by overbars. Amino acid residues important for ligand binding are shaded, for signalling marked by ▼, and one important for intracellular localization is marked by #. The identical residues (*), conserved substitutions (:) and semi-conserved substitutions (.) identified by the Clustal W programme are indicated. The GenBank accession numbers are shown in Table III.

J. Ocean Univ. China (Oceanic and Coastal Sea Research)
DOI 10.1007/s11802-015-2433-3
ISSN 1672-5182, 2015 14 (2): 362-374
http://www.ouc.edu.cn/xbywb/
E-mail:xbywb@ouc.edu.cn

Evaluation of Cytotoxicity and Genotoxicity of Insecticide Carbaryl to Flounder Gill Cells and Its Teratogenicity to Zebrafish Embryos

PANDEY Manish Raj[1)], and GUO Huarong[2), *]

1) *Laboratory of Evolution & Development*, *Institute of Evolution & Marine Biodiversity*, *Ocean University of China*, *Qingdao* 266003, *P. R. China*
2) *Key Laboratory of Marine Genetics and Breeding of Ministry of Education*, *College of Marine Life Sciences*, *Ocean University of China*, *Qingdao* 266003, *P. R. China*

(Received July 4, 2013; revised December 15, 2013; accepted January 19, 2015)

Abstract In this study, we determined the cytotoxicity and genotoxicity of carbamate insecticide carbaryl to flounder gill (FG) cells and its teratogenicity to zebrafish embryos. The cytotoxicity of carbaryl to FG cells was determined with methods including MTT and neutral red uptaking (NRU), lactate dehydrogenase (LDH) releasing and Hoechst 33342 and propidium idodide (PI) double staining. Moderate cytotoxicity in a concentration-dependent manner was observed. The 24 h-IC_{50} value of 53.48 ± 1.21, 59.13 ± 1.19 and 46.21 ± 1.24 mg L^{-1} carbaryl was obtained through MTT, NRU and LDH assays, respectively. Double fluorescence staining demonstrated that carbaryl induced the death of FG cells mainly through necrosis. There was no significant genotoxicity found in the FG cells exposed to the highest testing concentration of carbaryl (20 mg L^{-1}, $P > 0.05$) as was demonstrated by Comet assay. Zebrafish embryos exposed to carbaryl at concentrations ≥10 mg L^{-1} displayed moderate toxic effects on the survival, spontaneous movement, hatching, heart rates of the embryos and their development, which were evidenced by yolk and pericardial sac edemas, body length reduction and tail flexure in time- and concentration-dependent manners at specific stages. The 24 h-, 48 h- and 96 h-LC_{50} values of carbaryl to zebrafish embryos were 41.80 ± 1.10, 17.80 ± 1.04 and 14.46 ± 1.05 mg L^{-1}, respectively. These results suggested that carbaryl is moderately toxic to FG cells cultured *in vitro* and zebrafish embryos, and the FG cells were similar to zebrafish embryos in their sensitivity to carbaryl as 24 h-IC_{50} and LC_{50} indicated.

Key words carbaryl; cytotoxicity; genotoxicity; teratogenicity; flounder gill cell; zebrafish

1 Introduction

Carbaryl (1-naphthyl-N-methylcarbamate) is the most frequently used carbamate insecticide because of its relatively low mammalian oral and dermal toxicity and broad control spectrum (Agrawal and Sharma, 2010; Kuhr and Dorough, 1976). It has been widely used to the control of a variety of pests on fruits, vegetables, cereals, forage, cotton, forests, lawns, ornamentals and many other crops as well as poultry, livestock and pets in China. It is also used as a molluscicide and an acaricide as well as insecticide against the ectoparasites of humans and animals (Tomlin, 2000; USEPA, 2012). Carbaryl, along with other carbamates for animals, functions to inhibit the activity of acetylcholinesterase (AChE) at synaptic junctions in nervous system, resulting in the accumulation of acetylcholine in nerve synapses, thus uncontrolled movement, paralysis, convulsions and tetany, and possible death (Cox, 1993; Gruber and Munn, 1998; Gunasekara *et al*., 2008; Tomlin, 2000). As was classified by the World Health Organization (WHO), carbaryl is moderately hazardous (WHO, 2002). Carbaryl is not persistent in environment but is more stable in seawater than in freshwater (Pelletier *et al*., 2006; Xu, 2000). Its wide use also increased the risk of being leached into groundwater thus imposing adverse effects on human health (Schock *et al*., 2012; Todd and van Leeuwen, 2002).

The toxicity of carbaryl to fish is species-specific, high to slight to freshwater fish species, and moderate to ocean and estuary fish species on an acute basis (Beyers *et al*., 1994; McKim *et al*., 1987; Sinha *et al*., 1991). Salmon, trout, and perch are reported as the most sensitive species, which will die when the concentration of carbaryl varies between 250 and 970 ng mL^{-1} (USEPA, 2002). The 96 h-LC_{50} value indicated that the acute toxicity of carbaryl was 9.26 mg L^{-1} to zebrafish (*Danio rerio*), 2.52 mg L^{-1} to guppy (*Poecilia reticulata*), 6.4 mg L^{-1} to Indian carp (*Catla catla*), 5.5 mg L^{-1} to climbing perch (*Anabas testudineus*), 4.6 mg L^{-1} to Gangetic mystus (*Mystus cavasius*) and 2.4 mg L^{-1} to striped catfish (*Mystus vittatus*) (Gallo

* Corresponding author. Tel: 0086-532-82031932
E-mail: huarongguo@ouc.edu.cn

shrink and distort into irregular shape, and eventually detached from the substrate surface and lysed.

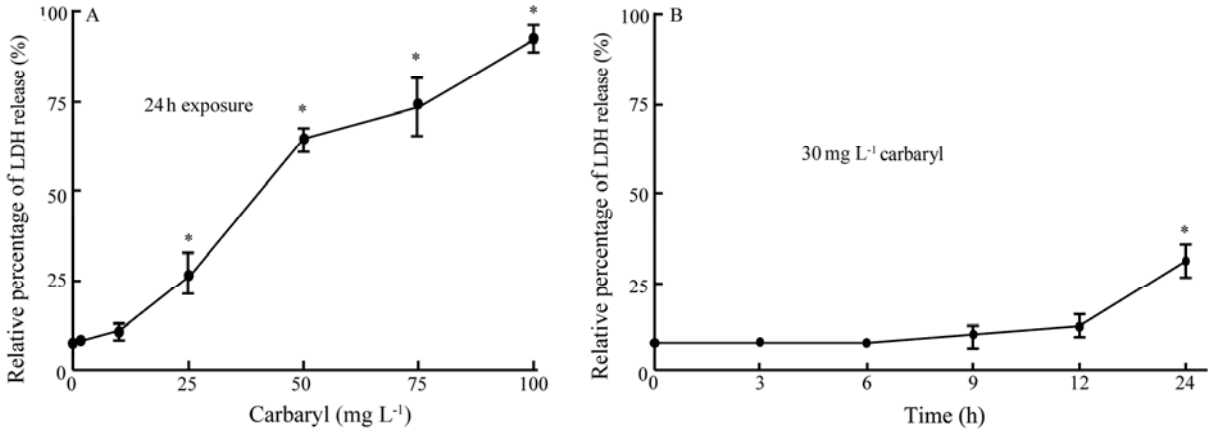

Fig.2 Effects of carbaryl on LDH release in FG cells. (A) Concentration-dependent *in vitro* cytotoxicity of carbaryl to FG cells. (B) Time-course cytotoxicity of carbaryl at a sublethal concentration (30 mg L^{-1}) to FG cells within 24 h exposure period. The values are expressed as mean ± SEM (n=3; *, P < 0.05).

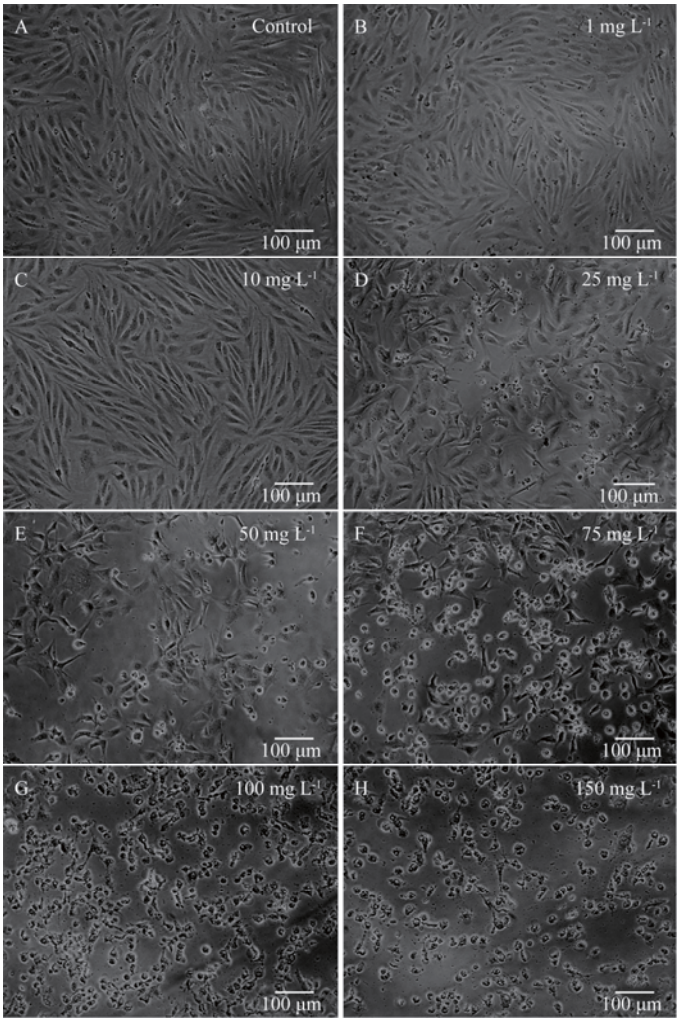

Fig.3 Morphological changes of FG cells after being exposed to carbaryl at various concentrations for 24 h. A through H correspond to 0 (control), 1, 10, 25, 50, 75, 100 and 150 mg L^{-1} carbaryl, respectively.

3.1.3 Carbaryl induced necrosis rather than apoptosis of FG cells

In order to investigate the toxicological mechanism of carbaryl, living, necrotic and apoptotic FG cells were discriminated by Hoechst 33342 and PI double fluorescence staining after the cells were exposed to various concentrations of carbaryl for 24 h. The morphology and the intensity of blue and red fluorescence of the nuclei (Figs.4 and 5, respectively) indicated that carbaryl caused

BRILL

Crustaceana 88 (12-14) 1351-1365

CRUSTACEANA

PROBLEMS WITH THE USE OF LIPOSOME- AND RETROVIRUS-MEDIATED GENE TRANSFER METHODS IN THE PRIMARY LYMPHOID CELLS OF THE OKA ORGANS OF THE GREASYBACK SHRIMP, *METAPENAEUS ENSIS* (DE HAAN, 1844)

BY

QIAN HAN[1]), DANDAN DONG[1]), XIAOJUAN ZHANG[1]), CUICUI LIANG[1]), QIONGXUAN LU[1]) and HUARONG GUO[1,2,3])

[1]) Key Laboratory of Marine Genetics and Breeding, Ministry of Education, Qingdao 266003, P. R. China

[2]) Institute of Evolution and Marine Biodiversity, Ocean University of China, Qingdao 266003, P. R. China

ABSTRACT

In this study, both liposome- and retrovirus-mediated gene transfer methods were examined for their potential to transfer and express two retroviral vectors containing the mouse *c-Myc* or the green fluorescent protein (*GFP*) gene into the primary lymphoid cell cultures (OKA) derived from "Oka" organs (= organs of the lymphoid system) of the greasyback shrimp *Metapenaeus ensis* (De Haan, 1844). It was found that the *c-Myc* gene could be delivered into OKA cells by the liposome-mediated method, but the introduced *c-Myc* gene could not be effectively transcribed into mRNA. In contrast, the pantropic retrovirus-mediated method failed to introduce the *c-Myc* gene into OKA cells, and GFP was not detected in the transformed cells, either. This work inferred two problems for the use of the two above-mentioned gene transfer methods in the non-dividing OKA cells: (1) the viral promoter of long terminal repeats (LTRs) had low activity in shrimp cells; (2) the pantropic retrovirus-mediated gene transfer system had a low tropism to shrimp lymphoid cells.

Key words. — Shrimp cells, gene transfer, liposome, retrovirus, promoter, tropism

ZUSAMMENFASSUNG

In der vorliegenden Studie wurden sowohl Liposomen- als auch Retrovirus-vermittelte Gentransfermethoden hinsichtlich ihres Potentials untersucht, zwei retrovirale Vektoren mit Maus *c-Myc* oder Grün-fluoreszierendes-Protein (*GFP*) Gene in primäre Lymphoidzellkulturen (OKA) abgeleitet von den „Oka"organen [= Organe des lymphoiden Systems] der Sandgarnele *Metapenaeus ensis* zu transferieren und exprimieren. Es wurde gefunden, dass das *c-Myc* Gen zwar in OKA-Zellen durch die Liposomen-vermittelte Methode eingebracht, das eingeschleuste *c-Myc* Gen jedoch nicht effektiv in mRNA transcribiert werden konnte. Im Gegensatz dazu versagte die durch das pantropische

[3]) Corresponding author; e-mail: huarongguo@ouc.edu.cn

DOI 10.1163/15685403-00003498

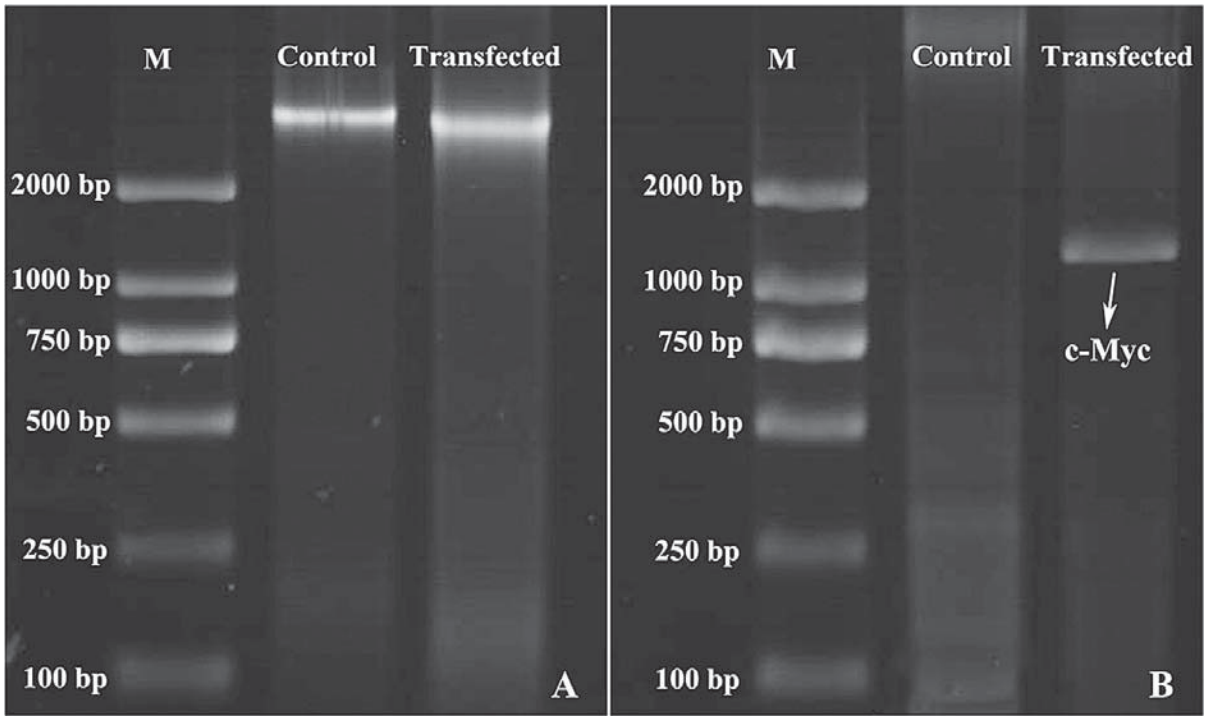

Fig. 1. PCR detection of the delivery of the *c-Myc* gene into the OKA cells by lipofection. Panel A shows the genomic DNAs extracted from the control and transfected OKA cells. Panel B shows the PCR products amplified from the genomic DNA of control and transfected OKA cells using *c-Myc*-specific primers.

vectors. However, the same plasmid pMCs-GFP could be efficiently expressed in mammalian Plat-GP cells, as shown by the packaging of pMCs-GFP retrovirus delivered using the lipofection method (fig. 5A-2). Also, the packaged GFP retrovirus could infect intact Plat-GP cells and express the GFP proteins successfully (fig. 5B-2); the percentage of GFP-positive cells was 39.3 ± 6%. Thus,

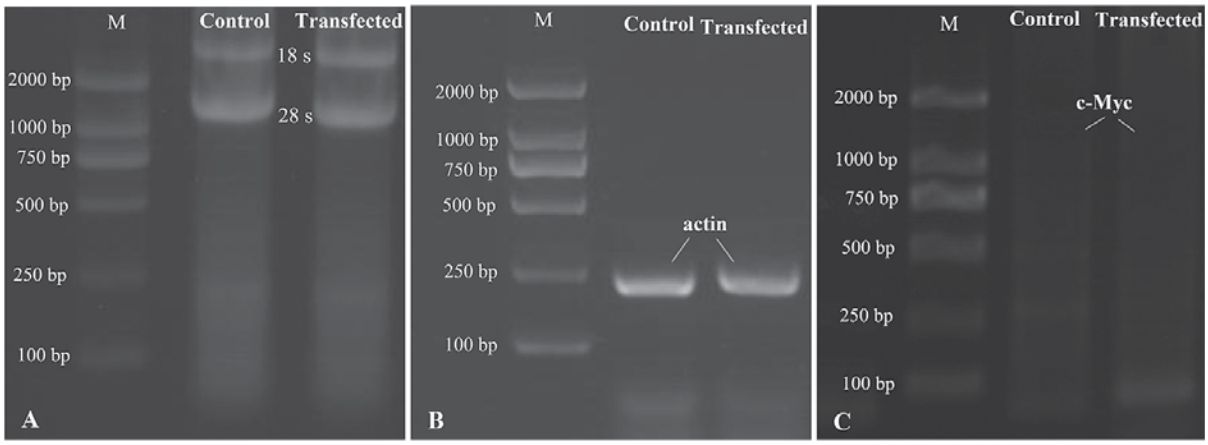

Fig. 2. RT-PCR detection of the mRNA expression of exogenous *c-Myc* gene delivered into the OKA cells by lipofection. Panel A shows the total RNA extracted from the control and transformed OKA cells. Panel B shows the RT-PCR products of the actin gene. Panel C shows that no RT-PCR products for exogenous *c-Myc* gene were amplified from the control and transformed OKA cells.

Curr Microbiol
DOI 10.1007/s00284-015-0919-2

Complete Genome of a Novel *Pseudoalteromonas* Phage PHq0

Duo-bing Wang[1] · Yan Li[1] · Meng-qi Sun[1] · Jin-peng Huang[1] · Hong-bing Shao[1] · Qi-lin Xin[1] · Min Wang[1,2]

Received: 28 May 2015 / Accepted: 23 August 2015

Abstract We isolated and purified a novel virulent *Pseudoalteromonas* bacteriophage PHq0 and the host bacterium *Pseudoalteromonas* BQ0 from seawater collected in a coastal area of the Yellow Sea of China. (36°06′N, 120°32′E). Transmission electron microscopy revealed that the phage had an icosahedral head of 50 nm in diameter with a long tail of 100 nm. The one-step growth curve showed the latent period of about 15 min, a rise period of 15 min, and a burst size of about 363 virions. The genome of phage PHq0 was found to consist of a linear, double-stranded 33,399-bp DNA molecule with a GC content of 40.29 % and 56 putative open reading frames (ORFs). Among these genes, 23 conserved domains were detected by BLASTP, 17 were functionally known, leaving 39 unknown putative genes, BLASTP results show that 57.14 % of the 56 predicted ORFs were not found to have any matches of putative functions or conserved domains in the BLASTP database which should be classified as a new member of the *Siphoviridae* family. The phage PHq0 genome adds a new *Siphoviridae-family* phage genome for marine bacteriophages which will provide useful basic information for further molecular research on interaction mechanism between bacteriophages and their hosts.

✉ Min Wang
mingwang@ouc.edu.cn

[1] College of Marine Life Science, Ocean University of China, Qingdao 266003, People's Republic of China

[2] Institute of Evolution and Marine Biodiversity, Ocean University of China, Qingdao 266003, People's Republic of China

Introduction

Phages are highly abundant and have very high genetic diversity in marine ecosystems [21]; they are powerfully affecting genetic changes in the oceans, regulating nutrient cycle and evolution [20]. The interactions between phages and bacteria are complex processes in marine ecosystems, which is a key factor dominating the mortality of microorganisms [4]. For a comprehensive investigation of the impact on the bacterial physiological and biochemical process, we need isolation, propagation, and purification of phage-host systems (PHS). The genus *Pseudoalteromonas* is a marine group of bacteria belonging to the class *Gammaproteobacteria*, displaying a widespread distribution in the marine environment and significant ecological roles which are ecologically and evolutionarily influenced by phages [4, 15, 18]. To date, six *Pseudoalteromonas* phage genomes have been issued in public datasets (*Pseudoalteromonas phage PM2, Pseudoalteromonas phage H105/1, Pseudoalteromonas phage RIO-1, Pseudoalteromonas phage pYD6-A, Pseudoalteromonas phage TW1, Pseudoalteromonas phage B8b*) [3, 4, 7, 11, 13, 16]. Heterotrophic bacteria infection is the basic knowledge of future development in understanding the role of viruses in aquatic systems, and this study requires the isolation, propagation, and purification of PHS. To the better understanding of *Pseudoalteromonas* phage diversity, the genomic features of marine phages, as well as the phage-host infection/interaction mechanisms in the marine environment, we isolated and characterized the *Pseudoalteromonas* phage PHq0 from the Yellow Sea of China. Although several bacteriophages have been isolated from *Pseudoalteromonas*, previous studies have tended to focus on assessing the diversity and genetic characteristics of the marine bacteriophage in the Yellow Sea of China. The

Published online: 14 October 2015

codons GTG (3 ORFs). Phage ORFs were identified by BlastP searches using the NCBI database. PHq0 has 56 putative open reading frames (ORFs), most ORFs were relatively short, with small intergenic spaces. Among these genes, 17 were functionally known, leaving 39 unknown putative genes (Fig. 4); in all of these 56 ORFs, 23 conserved domains were detected (Table 1). Phages with common genes with *Pseudoalteromonas* phage PHq0 by BLASTP were detected (Table 2).

Discussion

A new bacteriophage, PHq0, specifically infecting *Pseudoalteromonas* BQ0 strains was isolated and characterized. The identity of host bacteria strain to the most related species is only 97.6 % (*Pseudoalteromonas shioyasakiensis SE3 (T)*), and shows that it might be a new species of *Pseudoalteromonas.* The phage PHq0 genome adds a new *Siphovirus* genome for marine bacteriophages. BLASTP analysis of the complete genome sequence showed that there are 56 ORFs in phage PHq0. In total of 32 (57.14 %) of the 56 predicted ORFs, they were not found to have any matches of putative functions or conserved domains in the BLASTP database. Of the 17 (30.36 %) ORFs with predicted functions, they could be classified into four functional groups, including phage structure, adsorption, terminase, DNA binding and regulation. Only one of them (ORF 5: Phage tail length tape-measure protein 1) was not assigned to a conserved domain. Of the 23 (41.07 %) ORFs with conserved domains, 6 of them (HK97 gp 10 like superfamily, AP2 superfamily, Nin B superfamily, KilA-N superfamily, GIY YIG SF superfamily, Spo VR superfamily, SGNH hydrolase superfamily) were not associated with any function. These results indicate that *Pseudoalteromonas* phage PHq0 is a novel bacteriophage.

BLASTP ($e < 10^{-5}$) results of bacteriophage origin were considered, and *Idiomarinaceae* phage Phi1M2-2 was found to have 12 common genes (21.43 %) with *Pseudoalteromonas* phage PHq0, including 9 conserved domains (phage capsid superfamily, HK97 gp 10 like superfamily, phage H T join superfamily, AFD class I superfamily, Peptidase U35 superfamily, phage Mu F superfamily, phage portal superfamily, DUF 3168 superfamily, and phage tail 2 superfamily), 1 putative function protein (phage tail length tape-measure protein 1), and 2 hypothetical proteins (ORF10 and ORF56). An unclassified dsDNA phage *Marinomonas* phage P12026 was found to have 9 common genes (16.07 %) with *Pseudoalteromonas* phage PHq0, including 2 hypothetical proteins (ORF10 and ORF55) and 7 conserved domains (phage capsid superfamily, HK97 gp 10 like superfamily, phage H T join superfamily, AFD class I superfamily, Peptidase U35 superfamily, phage Mu F superfamily, and phage portal superfamily), of which all of the conserved domains are shared with *Idiomarinaceae* phage Phi1M2-2. These common conserved domains suggest that *Pseudoalteromonas* phage PHq0 is closely related to

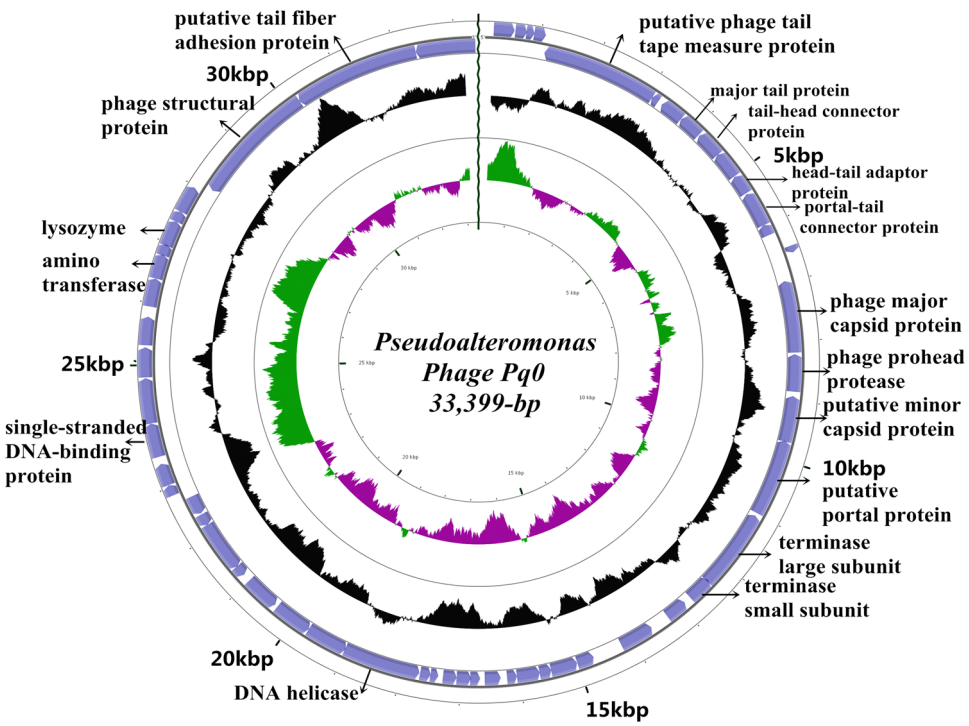

Fig. 4 Cycle graph of the signed genomes phage PHq0